From Stress to Acclimation

A Systems Biology Look on the Life of *Saccharomyces cerevisiae* in Industrial Bioreactors

DISSERTATION

A dissertation accepted by the Faculty of Energy-, Process- and Bio-Engineering of the University of Stuttgart in partial fulfillment of the requirements for the degree of Doctor of Natural Sciences (Dr. rer. nat.)

By:

Steven Minden

from Luxembourg, Luxembourg

Supervisor:	Prof. Dr.-Ing. Ralf Takors
Co-examiner:	Prof. Dr. Aljoscha Wahl
Date of oral examination:	April 18, 2024

University of Stuttgart
Germany

ibvt

University of Stuttgart   Institute of Biochemical Engineering

2024

Titel in deutscher Sprache:

Vom Stress zur Akklimatisierung

Eine Systembiologische Betrachtung des Lebens von *Saccharomyces cerevisiae* in Industriellen Bioreaktoren

Für Sonja

Fir Yves

Für Karuna

Acknowledgments

First and utmost, I want to express gratitude to my promoter Prof. Dr.-Ing. Ralf Takors. Not only for the opportunity but also for the trust I felt when starting as a PhD-student coming from a non-academic phase in my professional life. I sincerely do not take my admission to this project for granted. Thank you for enabling, supervising, discussing, and approving this work!

I thank Prof. Dr. Aljoscha Wahl for taking the time to co-examine this dissertation and Prof. Dr. Björn Voß to take the chair of my defense.

To all ComRaDes: I thank you for every scientific discussion and instructive feedback from the many online and the too few pre-pandemic in-person meetings. I thank Prof. Dr. Ir. Frank Delvigne, Dr. Amit Deshmukh, Dr. Cees Haringa, Dr. Ágnes Jánoska, Prof. Dr. Walter van Gulik, Dr. Peng Wei, and Dr. Boris Zacchetti for discussing my results and considerably improving my understanding of scale-down experimentation. To Prof. Dr. Henk Noorman, I am deeply grateful for your invaluable one-on-one sessions during the decisive phase of my dissertation — it has been a privilege.

None of this would have been possible without two other ComRaDes: Maria Aniolek and Christopher Sarkizi. Maria, I am not sure if anyone else would have been able to pull off the sampling routine we choreographed. You are a big part of this! Chris, your footprint on this thesis goes beyond words — and this is a compliment, for the likely case you cannot read me.

I thank Andreas Freund for enabling precise fermentations. I thank Björn Voß for providing the infrastructure and statistical feedback for all transcriptomic analysis in this project. I thank Attila Teleki for teaching me mass spectrometry and supervising the 'metabolomics task force' for countless hours until the job was done. Martin Siemann-Herzberg, thank you for never declining any urge to discuss findings. And thank you for your support in the time of bringing this thesis to paper!

A special thank-you goes to all technical staff of the IBVT. Alexander Dietrich, Maren Lösch, Silke Reu, Martina Schweikert, and Andrea Seipel are pivotal parts of this thesis. I would have had a hard time without you!

It may not come as a surprise, but I am still amazed at how many great colleagues along the way positively influenced the outcome of this work. Inspiration was absorbed during numerous occasions with Andreas Ankenbauer, Marius Braakmann, Carlos Castillo-Saldarriaga, Adrian

Funding and Scientific Output

Peer-reviewed publications

Research article I

Minden S, Aniolek M, Sarkizi Shams Hajian C, Teleki A, Zerrer T, Delvigne F, van Gulik W, Deshmukh A, Noorman H & Takors R. Monitoring Intracellular Metabolite Dynamics in *Saccharomyces cerevisiae* during Industrially Relevant Famine Stimuli. *Metabolites*. 2022; 12 (263); 1−26.

https://doi.org/10.3390/metabo12030263.

Research article II

Minden S, Aniolek M, Noorman H & Takors R. Performing in spite of starvation: How *Saccharomyces cerevisiae* maintains robust growth when facing famine zones in industrial bioreactors. *Microbial Biotechnology*. 2023; 1 (1); 1−21.

https://doi.org/10.1111/1751-7915.14188

Research article III

Minden S, Aniolek M, Noorman H & Takors R. Mimicked Mixing-Induced Heterogeneities of Industrial Bioreactors Stimulate Long-Lasting Adaption Programs in Ethanol-Producing Yeasts. *Genes*. 2023; 14 (5); 1−23.

https://doi.org/10.3390/genes14050997

Conference contributions

<u>Talk</u>

Minden S, Aniolek M, Sarkizi Shams Hajian C, Takors R. (09/2021)

Adaption efforts of eukaryotic host systems during industrial-scale production scenarios.

13th European Congress of Chemical Engineering and 6th European Congress of Applied Biotechnology, Berlin (online), Germany

<u>Poster</u>

Minden S, Aniolek M, Sarkizi Shams Hajian C, Takors R. (05/2021)

Adaption efforts of eukaryotic host systems experiencing industrial scale substrate gradients (P 62)

Himmelfahrtstagung on Bioprocess Engineering 2021 New Bioprocesses, New Bioproducts, Virtual edition), Germany

Other

<u>Application note</u>

Feith A, **Minden S**, Teleki A, Takors R. (03/2022)

Improved Metabolomic Analysis Using an Iron-Free Flow Path.

Free-to-access application note from Agilent Technologies, incorporated. The document addresses a problem encountered during the work of research article I concerning HILIC-specific peak tailing effects in iron-based LC systems (see chapter 4.1.5).

Declaration of Originality

I hereby declare that the submitted work has been written by me. I clearly marked resources from other authors with references according to scientific standards. All statements taken literally from other writings or referred to by analogy are marked and the source is always given. The presented results are based on my own research activities or on joint activities in which case I have indicated the individual contributions.

_____

Place, Date   *Steven Minden*

Table of Contents

Table of Contents

List of Figures

Figure titles are partially reproduced in an abbreviated form.

List of Tables

Table titles are partially reproduced in an abbreviated form.

List of Symbols and Abbreviations

Symbols

$\$$	Dollar
%	Per cent
D_i	Impeller diameter (m)
ND_i	Impeller tip speed (m·s^{-1})
$k_L a$	Volumetric mass transfer coefficient (h^{-1})
€	Euro
Ø	Diameter
D	Dilution rate (h^{-1})
F	Feed rate (m^3·h^{-1}; kg^3·h^{-1})
K	Affinity constant (mmol$_C$·L^{-1})
N	Stirrer speed (s^{-1}, rotations per minute)
O	Oxygen
P	Product, Phosphate
P/O	ATP yield of respiration
P/V	Power input per volume (W·L^{-1})
Q	Volumetric rate (mmol·L^{-1}·h^{-1})
Re	Reynolds number
S	Substrate
T	Temperature (°C)
V	Volume (m^3; L)
X	Biomass
Y	Yield coefficient (mol$_C$·mol$_C^{-1}$; g·g^{-1})
c	Concentration (mg·L^{-1}; g·L^{-1}; mmol·L^{-1}; mmol$_C$·L^{-1}; µmol·L^{-1}; mg·L^{-1}; mmol·g^{-1}; mmol$_C$·g^{-1}; mg·g^{-1})
i	Number of impellers
k	Reaction rate (s^{-1})
m	Maintenance coefficient (mmol·g^{-1}·h^{-1})
n	Absolute number
p	Probability
q	Biomass specific rate (mmol·g^{-1}·h^{-1}; mmol$_C$·g^{-1}·h^{-1})
t	Time (s; h)

Greek letters

μ	Growth rate (h^{-1})
ρ	Density ($kg \cdot m^{-3}$)
τ	Residence time (s)

Indices

in	Inflow
L	Liquid
M	Michaelis-Menten
max	Maximum value
out	Outflow
P	Product
P/S	Product from substrate
S	Substrate
X	Biomass
X/S	Biomass from substrate
c	Circulation
depl	Depletion
r	Reaction

Abbreviations

2/3PG	Merged 2 and 3 phosphoglycerate
6PGA	6-phosphogluconic acid
ADP	Adenosine diphosphate
AEC	Adenylate energy charge
AIBA	α-amino isobutyric acid
AMP	Adenosine monophosphate
AMPK	AMP-activated protein kinase
ATP	Adenosine triphosphate
ave	Available electrons
AxP	ATP + ADP + AMP
BIC	Built-in component
bp	Base pair
C	Carbon, Celsius
C. glutamicum	*Corynebacterium glutamicum*
CAGR	Compound annual growth rate (%)
cAMP	Cyclic adenosine monophosphate

Cas	CRISPR associated protein
CCR	Carbon catabolite repression
CER	Carbon dioxide emission rate ($mmol \cdot g^{-1} \cdot h^{-1}$)
CFD	Computational Fluid Dynamics
CFU	Colony forming unit
CHO	Chinese hamster ovary
CIT	Citric acid
CO_2	Carbon dioxide
ComRaDes	Computation for Rational Design: From Lab to Production with Success
CRD	Cellular reaction dynamics
CRISPR	Clustered regularly interspaced short palindromic repeats
CTR	Carbon dioxide transfer rate ($mmol \cdot g^{-1} \cdot h^{-1}$)
DBTL	Design, build, test, learn
DEG	Differential gene expression
DMB	Dry matter of biomass ($g \cdot L^{-1}$)
DNA	Deoxyribonucleic acid
DS	Dynamic steady state
E. coli	*Escherichia coli*
e.g.	For example (latin: *exempli gratia*)
ESI	Electrospray ionization
ESR	Environmental stress response
ESRi	ESR induced
et al.	And others (latin: *et alii*)
EU	European Union
F2,6BP	Fructose-2,6-bisphosphate
FBP	Fructose-1,6-bisphosphate
FDR	False discovery rate
fig.	Figure
G6P	Glucose-6-phosphate
Gdh	Glutamate dehydrogenase
GDP	Guanosine diphosphate
GO	Gene ontology
GPCR	G-protein-coupled receptor
GRAS	Generally Recognized as Safe
GSEA	Gene set enrichment analysis
GTP	Guanosine triphosphate

h	Hours
Hex6P	Merged glucose-1-phosphate/fructose-6-phosphate
HOG1	High Osmolarity Glycerol response 1
HYX	Hypoxanthine
i.e.	That is (latin: *id est*)
IFFL	Incoherent feedforward loop
IMP	Inosine monophosphate
INO	Inosine
ISOCIT	Isocitric acid
KDPG	2-keto-3-deoxy-6-phosphogluconate
lab	Laboratory
LC-MS	Liquid chromatography - mass spectrometry
LSL	Limitation-starvation-limitation transition
MAPK	Mitogen activated protein kinase
MDS	Metric multidimensional scaling
MGF	Minimum genome factory
min	Minutes
MINR	MultIplex Navigation of global Regulatory networks
MRM	Multiple reaction monitoring
mRNA	messenger RNA
N	Nitrogen, Normliter (standard temperature and pressure)
NADH	Nicotinamide adenine dinucleotide
NADPH	Nicotinamide adenine dinucleotide phosphate
NGS	Next-generation sequencing
nt	Nucleotides
O_2	Oxygen
–omics	Neologism summarizing disciplines of systems biology ending with the suffix *-omics* (genomics, transcriptomics, …)
ORF	Open reading frame
OTR	Oxygen transfer rate ($mmol \cdot g^{-1} \cdot h^{-1}$)
OUR	Oxygen uptake rate ($mmol \cdot g^{-1} \cdot h^{-1}$)
p	Partial pressure
p-body	Processing body
P. chrysogenum	*Penicillium chrysogenum*
P. pastoris	*Pichia pastoris*
P. putida	*Pseudomonas putida*
P5P	Merged ribose-5-phosphate and ribulose-5-phosphate

Pde2	Phosphodiesterase 2
PEP	Phosphoenolpyruvic acid
Pfk	Phosphofructokinase
PFR	Plug-flow reactor
pH	Logarithmic and inverse activity of hydrogen ions in solution
PKA	Protein kinase A
PKB	Protein kinase B
Pky	Pyruvate kinase
PPP	Pentose phosphate pathway
PRE	Pheromone response element
PRPP	Phosphoribosyl pyrophosphate
PSP	Purine salvage pathway
PTM	Post-translational modification
QQQ	Triple quadrupole
R1P	Ribose-1-phosphate
RiBi	Ribosome biogenesis
r-LSL	Repeated limitation-starvation-limitation transitions
RNA	Ribonucleic acid
RP	Ribosomal protein
RPLC	Reverse phase liquid chromatography
rpm	Revolutions per minute
rRNA	Ribosomal RNA
RS	Reference steady state
s	Seconds
S. cerevisiae	*Saccharomyces cerevisiae*
s.d.	Standard deviation
ScER	Ethanol Red™
SDR	Scale-down reactor
s-LSL	Single limitation-starvation-limitation transition
SNF1	Sucrose Non-Fermenting 1
SRE	Stimulus-response experiment
STR	Stirred tank reactor
STRE	Stress-responsive element
T6P	Trehalose-6-phosphate
TCA	Tricarboxylic acid cycle
TF	Transcription factor
TORC1	Taget of rapamycin kinase complex I

TORC2	Taget of rapamycin kinase complex II
tRNA	Transfer RNA
TRY	Titer, rate, yield
U	Unit
UDP	Uridindiphosphate
UK	United Kingdom
USA	United States of America
v	Volume
vvm	Volume per volume per minute
ZIC-pHILIC	Zwitterionic hydrophilic interaction chromatography
αKG	α-ketoglutaric acid

Abstract

Carbon limitation is a fundamental feeding strategy in commercial fermentations guaranteeing efficient substrate-to-product conversion. However, industrial reaction volumes often prevent a microbe from performing optimally. One common source of interference is insufficient mixing resulting in the formation of concentration gradients. For instance, faster microbial consumption *versus* convective supply depletes the highly diluted limiting substrate locally. The industrial workhorse *Saccharomyces cerevisiae* (*S. cerevisiae*) naturally possesses adaptive mechanisms to cope with substrate depletion. Whether triggered response mechanisms benefit strain performance is doubtful, given that enough substrate is present in an industrial carbon-limited process on average. On the contrary, unnecessary or futile adaptation mechanisms often cause unexpected microbial behavior on large scales. Exploring and elucidating this behavior is the focal point of this thesis.

The presented case study employs a stimulus-response approach mimicking a baker's yeast fermentation snapshot featuring non-ideal starvation zones. In brief, glucose-limited chemostats with two-minute intervals of stopped feeding induce transitions between limitation and starvation. Metabolomic and transcriptomic measurements enable a systems biology analysis of either non-adapted or stimulus-adapted yeasts. One part of this study investigates the haploid laboratory strain CEN.PK113-7D under aerobic conditions. Another part reports gene expression dynamics of the diploid industrial strain Ethanol Red^{TM} under anaerobic conditions.

Both strains display robust growth under the tested conditions at the cost of tactic and strategic investments. The laboratory yeast responds to a 110 µmol·L^{-1} glucose gradient with a modified energy and redox homeostasis. Non-adapted cells perceive this stimulus as a threat, as evidenced by a futile triggering of the environmental stress response causing transient growth rate reduction and increased maintenance demand. Complete adaptation evokes a distinct 'bioreactor phenotype' characterized by increased growth capacities and repressed stress response. Results obtained with Ethanol Red^{TM} confirm this stress defense−growth trade-off to be a conserved implication in bioprocesses with fluctuating carbon supply.

Altogether, the findings presented in this thesis contribute to a fundamental understanding of how *S. cerevisiae* operates in heterogeneous commercial-scale fermentations. Finally, the gained knowledge reveals optimization targets for both strain engineering and bioprocess development.

Zusammenfassung

Die Kohlenstofflimitierung ist eine grundlegende Fütterungsstrategie bei kommerziellen Fermentationen um eine effiziente Umwandlung vom Substrat zum Produkt zu gewährleisten. Allerdings verhindern industrielle Reaktionsvolumina oft, dass ein Mikroorganismus seine optimale Leistung erbringt. Eine häufige Störquelle ist eine unzureichende Durchmischung, die zur Bildung von Konzentrationsgradienten führt. Beispielsweise wird das stark verdünnte limitierende Substrat lokal erschöpft, wenn sein mikrobieller Verbrauch schneller als seine konvektive Zufuhr ist. Der industrielle Standardorganismus *Saccharomyces cerevisiae* (*S. cerevisiae*) verfügt von Natur aus über adaptive Mechanismen, um mit der Erschöpfung des Substrats umzugehen. Es ist jedoch zweifelhaft ob ausgelöste Anpassungsvorgänge die mikrobielle Leistung verbessern, wenn man bedenkt, dass in einem industriellen kohlenstofflimitierten Prozess im Durchschnitt genügend Substrat vorhanden ist. Im Gegenteil, unnötige Adaptionsmechanismen verursachen im großen Maßstab oft unerwartetes mikrobielles Verhalten. Die Erforschung und Charakterisierung dieses Verhaltens ist der Schwerpunkt dieser Arbeit.

Die vorgestellte Fallstudie verwendet einen *stimulus-response* Ansatz, der eine Momentaufnahme der Bäckerhefeproduktion mit nicht idealen Hungerzonen nachahmt. Kurz gesagt simulieren glukoselimitierte kontinuierliche Fermentationen mit zweiminütigen Fütterungsstopps Übergänge zwischen Substratlimitierung und -hunger. Metabolom- und Transkriptommessungen ermöglichen letztendlich eine systembiologische Analyse von nicht-adaptierten und stimulus-adaptierten Hefen. Ein Teil dieser Studie untersucht den haploiden Laborstamm CEN.PK113-7D unter aeroben Bedingungen. Ein weiterer Teil berichtet über die Genexpressionsdynamik des diploiden Industriestamms Ethanol Red[TM] unter anaeroben Bedingungen.

Beide Stämme zeigen robustes Wachstum unter den getesteten Bedingungen auf Kosten taktischer und strategischer Investitionen. Die Laborhefe reagiert auf einen Glukosegradienten von 110 µmol·L^{-1} mit einer veränderten Energie- und Redoxhomöostase. Nicht angepasste Zellen nehmen diesen Reiz als eine Gefahr war, was sich in einer vergeblichen Auslösung der generellen Stressantwort zeigt. Diese führt zu einer vorübergehenden Verringerung der Wachstumsrate und einem erhöhten Erhaltungsstoffwechsel. Die vollständige Anpassung ruft einen ausgeprägten ‚Bioreaktor-Phänotyp' hervor, der durch erhöhte Wachstumskapazitäten und eine unterdrückte Stressantwort gekennzeichnet ist. Die mit Ethanol Red[TM] erzielten

Ergebnisse bestätigen, dass dieser Kompromiss zwischen Stressabwehr und Wachstum eine konservierte Auswirkung auf Bioprozesse mit einer fluktuierenden Kohlenstoffversorgung hat.

Insgesamt tragen die in dieser Arbeit präsentierten Ergebnisse zu einem grundlegenden Verständnis über das Wachstumsverhalten von *S. cerevisiae* in heterogenen Fermentationen im kommerziellen Maßstab bei. Letztlich lassen sich aus den gewonnenen Erkenntnissen Optimierungsziele sowohl für die Stamm- als auch für die Bioprozessentwicklung ableiten.

1 Motivation

Industrial biotechnology, at the core of its definition, applies microorganisms or their subsystems as catalysts for the production of desired compounds. In contrast to the chemical industry, biotechnological processes adopt mild reaction conditions, while cellular capabilities reduce the number of technical conversion steps toward the product. Ergo, the biotech industry benefits from natural microorganic diversity. However, tools from synthetic biology, metabolic and genetic engineering are required to foster advancements in the field (Straathof *et al.*, 2019). For instance, by enabling the usage of energy from renewables and non-valorized industrial or agricultural material streams, the bio-based industry currently bids to lead the transition to a sustainable, circular, and climate-friendly economy. Thus, it does not surprise that biotechnological solutions disrupt the heavy crude oil-dependent plastic and fuel industries, here expressed as 2−3 fold increased 7-year CAGRs of the respective sectors in table 1.

Table 1. Economic data and forecast of individual biotech sectors compared to the total industry.

sector	market size in billion €		7-year CAGR in %	
	total	biotechnology	total	biotechnology
transportation fuels	1200 [a]	141 [d]	3.8 [a]	10.1 [d]
fine chemicals	184 [b]	75 [e]	9.5 [b]	7.9 [e]
plastics	566 [c]	6 [d]	3.7 [c]	10.0 [d]
pharmaceuticals	1430 [c]	438 [d]	5.4 [c]	9.1 [d]

When applicable, market size values were converted to Euro with a rate of 0.93 € (06/02/2023) per \$. Values for the market size were collected for either 2021 or 2022. CAGR, compound annual growth rate.

[a] (DataIntelo, 2022)

[b] (MarketResearch.com, 2022)

[c] (Statista, 2022, 2023)

[d] (Market Research Future, 2021, 2022a, 2022b)

[e] (Precedence Research, 2022)

Political decision-makers recognize the potential of the biotech industry for meeting socioeconomic targets as well and thus incentivize research projects through increased governmental funding. One example is the European Union's Horizon 2020 program, which embedded this thesis in the ComRaDes project under grant number 722361 (European Comission, 2022). This 7-year, 80 billion € program declared biotechnology one of four key-

enabling technologies to empower sustainable and industrial growth in Europe. Still, the biotech industry faces several challenges before unlocking its full potential. Industrial players remain hesitant with dedicated investments given the high failure rate when new products or processes are brought to commercialization (Kampers *et al.*, 2022). Overcoming this so-called 'valley of death' is key to ramping up the trailing CAGR of the biochemical industry or increasing the market share of biotech in general.

But why is the commercialization step so fragile? The short answer is scale-up. A more detailed explanation involves the systematic difference between innovative strain and process engineering on the one hand and comparatively inert process deployment strategies on the other hand. More specifically, several technological advancements that converge on the 'synthetic biology revolution' allow rapid strain and product engineering. This revolution, in turn, is rooted in several micro-revolutions from which the *–omics* disciplines emerged that lay the ground for a deep understanding of biology through data generation, a field known as systems biology. Metabolic engineering approaches, nowadays complemented by machine learning algorithms, harness this data to provide guidelines and ideas for strain construction (Chen *et al.*, 2020). Last, ideas come to life via a plethora of genetic engineering tools, of which the CRISPR/Cas system is a prominent representative of the high density of innovation in the field (Jeong, Lee and Lee, 2023).

Ironically, this innovative force seems to lag behind for the subsequent commercialization step (de Lorenzo and Couto, 2019), even though the related costs range several orders of magnitude above the investments made during lab-scale development (Crater and Lievense, 2018). Sequential thinking, at present, dominates classical scale-up as the production host is developed first before handing it over for testing in increasing fermentation volumes. Here, the strain might encounter one or several environmental changes that were not anticipated during early development stages since they are characteristic of large volumes. Examples of such scale-dependent variables are spatial nutritional gradients due to mass transfer limitations, the choice of raw material, shear stress, or the number of populations in the seed train (Junker, 2004; Takors, 2012; Crater and Lievense, 2018). Consequentially, failing to deliver on promised TRY (titer, rate, yield) metrics while scaling up often turns out to be the deal-breaker in process development endeavors (Takors, 2016; Crater and Lievense, 2018).

The industry is well aware of this problem. Yet, implementing the so-often proclaimed 'begin with the end in mind' attitude seems challenging (Covey, 1991; Takors, 2012; Crater and

Lievense, 2018; Straathof *et al.*, 2019; Hill *et al.*, 2020). Why is that? Beginning with the end in mind means considering the above scale-dependent variables in their final peculiarity already in the lab. For this rational scale-down, again, data is the key but was not readily accessible from the commercial scale in the past either due to the inaccessibility of quantitative data from production tanks or the lack of computational power for predictive simulations. The latter comes in the form of computational fluid dynamics (CFD), a discipline that currently gains momentum, promising to close this knowledge gap (Wang, Haringa, Noorman, *et al.*, 2020). As computational power increased over time, CFD engineers became more and more empowered to couple hydrodynamic simulations with biokinetic models to estimate scale-dependent variables, for instance, glucose gradients in a baker's yeast production (Haringa *et al.*, 2017) or pH gradients in prokaryotic fermentations (Spann *et al.*, 2019).

Finally, the availability of process-relevant data enables the push of rational scale-down from promise to reality. In essence, research has to iterate over several 'design, build, test, and learn (DBTL)'-cycles to catch up with the speed of synthetic biology that employs the same strategy (Campbell, Xia and Nielsen, 2017). Scale-down guidelines are 'designed' by CFD studies and subsequently used to 'build' experimental setups to then 'test' production hosts under the investigated conditions. Systems biology methods are employed to 'learn' about relevant genomic, metabolic, regulatory, or phenotypic traits in the industrial setting to unravel targets for process-adapted strain engineering. The gained knowledge drives the next DBTL iteration and finally allows the construction of realistic scale-down simulators to replace empirical scale-up.

In the case of the industrial workhorse *Saccharomyces cerevisiae*, rational downscaling already produced significant research output. Dated back to 1993, Noorman and colleagues published the first spatial glucose gradients derived from CFD simulations of a 30 m^3 baker's yeast fed-batch process (Noorman *et al.*, 1993). The fed-batch design is a common strategy in the industry to avoid spillage of the primary nutrient, *e.g.* due to overflow metabolism. This advantage, however, makes the process prone to gradient formation due to highly diluted limiting nutrients. Especially when the cell densities are high, the microbial substrate consumption times may be shorter relative to the convective supply of said substrate (Lara *et al.*, 2006). Thus, it may not surprise that CFD studies identified the existence of several metabolic regimes in typical carbon-limited fed-batch processes, including metabolic overflow close to the feed inlet, the limitation sweet-spot in the bulk, and starvation far away from the feed inlet (Haringa *et al.*, 2017; Sarkizi Shams Hajian *et al.*, 2020; Nadal-Rey *et al.*, 2021; Ho *et al.*, 2022). In this context,

the mentioned simulation studies highlighted that second-to-minute exposure to carbon starvation is a dominant scale-up effect.

This thesis aimed to study the behavior of the platform organism *S. cerevisiae* on a systems biology level when encountering industrially relevant starvation zones in large-scale bioreactors. In doing so, metabolic and transcriptomic datasets were generated and analyzed to provide valuable insight into the yeast's metabolic, gene regulatory, and phenotypic behavior at the intersection of limitation and starvation.

2 Introduction

2.1 Industrial fermentation

Fermentation is a core unit operation of the biotechnological industry. Microbial hosts originate from all domains of life, opening up a spectrum of operational modes. Autotrophic and heterotrophic organisms enable the use of feedstocks from defined inorganic gases to complex, organic solids. The valorization might depend on the degradation or fixation of the feedstock, the production of a desired compound from the feedstock — or a combination of the two. In its broadest sense, an industrial fermentation can be as rudimental as compost works or as complex as a tightly controlled bioreactor environment with balanced material streams. Possible products mirror the cellular composition ranging from low molecular primary metabolites over functional enzymes to active microbial biomass. Hence, the fermentation process is indispensable for all domains of industrial biotechnology.

At present, the industry predominantly deploys submerged heterotrophic fermentation in cylindrical vessels (de Lorenzo and Couto, 2019). These vessels, or bioreactors, define the reaction space with the primary task of providing adequate nutrients and environmental conditions for microbial catalysis. Several geometric and operational parameter specifics keep the production host close to its physiological optimum. The task, however, is not trivial due to the complex interplay of multiple physical, chemical and biological state variables (Chmiel, Takors and Weuster-Botz, 2018). Typical fermentation state variables encompass stirrer speed, temperature, pH, pressure, gassing rate, diverse concentrations from substrate to product, and cellular status. In addition, state variables may be converted to calculated variables to qualify the process further. For instance, the oxygen transfer rate (OTR) quantifies the oxygen dislocation from the gas to the liquid phase, a common rate-limiting factor for microbial growth in aerobic processes (Garcia-Ochoa and Gomez, 2009). Titer, rate, and yield, commonly referred to as the TRY criteria, are critical benchmarks from an economic point of view (Crater and Lievense, 2018). Their maximization — and maintenance during scale-up toward commercialization — is the core task of any fermentation process development. The titer describes the product concentration at the end of a process and weighs in on downstream processing considerations. The rate expresses the volumetric production per time and determines the overall process duration. The yield puts a number on the effectiveness of material substrate-to-product conversion. Hence, any ambitious fermentation development

should operate as an optimization function for the combined TRY metrics. Accessible input variables to tune TRY optimization are numerous. Increasing biomass concentration also increases volumetric productivity and titer of a growth-coupled production (Von Kamp and Klamt, 2017). Stoichiometric boundaries limit the maximum theoretical yield (Verduyn, 1991), which can be approximated by metabolic engineering approaches and operational choices, such as carbon-limited growth to avoid by-product formation. Decoupling growth from production can be an attractive strategy, as well. In theory, the absence of proliferation allows channeling the growth-dedicated fraction of substrate toward the product to increase the yield. Furthermore, timely separation of both modes de-risks loss of productivity due to the selection pressure on growth over production (Wehrs *et al.*, 2019).

Accordingly, developing a viable fermentation process displays an interdisciplinary venture, from fundamental systems biology research to steelwork. Common concepts of fermentation technology with emphasis on scale-dependent considerations are introduced in this chapter. Subsequently, the influence of scale will be elaborated in-depth based on the example of *Saccharomyces cerevisiae*, the model organism of this dissertation.

2.1.1 Fundamentals of microbial growth and the impact on bioprocess development

Heterotrophic bioreactor cultivations operate in batch, fed-batch, or continuous mode with respect to the biotic phase and organic reactants (figure 1A). The reaction space V_L is the liquid volume of the culture medium inside the bioreactor, where suspended biomass catalyzes the conversion of substrate to product (figure 1B). Accordingly, reaction rates may be expressed as biomass-specific reaction rates (q_i) and self-replication of the catalyst is expressed as the growth rate μ. These rates, in turn, are functions of all environmental state variables that influence the activity of the cultivated microorganism. Essential variables such as temperature or pH are kept constant at optimal levels in the bioreactor yielding reactant concentrations as the rate-determining factors. In this regard, μ is commonly approximated as a hyperbolic function of the growth-limiting substrate S (equation 1) for a specific concentration range (Monod, 1949):

$$\mu = \frac{\mu_{max} \cdot c_S}{K_S + c_S} \tag{1}$$

In this equation, μ_{max} is the upper growth rate limit and K_S is the substrate concentration c_S at which μ equals half of μ_{max} and can be interpreted as the organism's affinity toward the

substrate. The negative substrate uptake rate q_S can be expressed analogously (2) as it relates to the growth rate via the proportionality factor $Y_{X/S}$ (3).

$$q_S = \frac{q_{S,max} \cdot c_S}{K_S + c_S} \tag{2}$$

$$Y_{X/S} = \frac{\mu}{q_S} \tag{3}$$

Modeling the product is more case-sensitive, as it may be biomass itself or a product of cellular metabolism, which might be growth-coupled or growth-decoupled. Furthermore, a cellular product can turn into a substrate under specific conditions, rendering the biomass-specific production rate q_P negative (figure 1C, first plot). In any case, productivity is proportional to substrate uptake in one way or another (4).

$$Y_{P/S} = \frac{q_P}{q_S} \tag{4}$$

In principle, the intracellular volume of an individual cell opens a second reaction space, which is far more complex than anticipated by the above equations. A network of 1078 reported enzymes and transporters control the levels of $1.6 \cdot 10^4$ metabolites in twice as many reactions in *S. cerevisiae* (Ramirez-Gaona *et al.*, 2017). Fortunately, this complex system can be decomposed into functional modules to describe phenomenological behavior that, in turn, dictates the values of said rates and yields.

The basic design of any microbial cell constitutes a catabolic and an anabolic module. Catabolism oxidizes imported carbohydrates toward a small number of precursor metabolites, a total of twelve in yeast (Nielsen and Keasling, 2016). In the process, free energy is conserved, *e.g.* in the form of the carrier molecule ATP. The reductive anabolism is fueled by catabolically gained free energy to convert the precursors into cellular components and enable self-replication. Inherent thermodynamic and resource allocation constraints submit microbes to a trade-off between the rate and the yield of self-replication. By obeying the second law of thermodynamics, the open, non-equilibrium biological system dissipates a proportion of its catabolic free energy as heat (Westerhoff, Hellingwerf and Van Dam, 1983; Lipson, 2015). This energetic loss scales with μ due to a positively correlated trend described by Calabrese *et al.* (2021): Energy dissipation in the anabolic module tends to increase more with the electron donor uptake rate compared to the dissipation in the catabolic module ultimately leading to decreasing availability of free energy for anabolic demands. Further contributing to the $\mu-Y_{X/S}$

trade-off are growth-unrelated investments of free energy for cellular maintenance, such as futile cycling, chemotaxis, nutrient storage, osmoregulation, macromolecular repair, and stress defense (Hoehler and Jørgensen, 2013). Artificially introduced production pathways may also contribute to maintenance demands in the form of metabolic burden in the bio-production context (G. Wu *et al.*, 2016). Empirically, this partition of energy was formulated by Pirt in 1965 by introducing the maintenance coefficient to discriminate between growth-coupled and growth-decoupled substrate usage (5).

$$\mu = \frac{\mu_{max} \cdot c_S}{K_S + c_S} - m_S \cdot Y_{X/S} \tag{5}$$

Microorganisms are evolutionarily hardwired to maximize their growth rate when nutrient abundance and external conditions are optimal. In any other case, all priority directs to survival (Bachmann *et al.*, 2013). While the latter manifests in raising maintenance demands, the first unfolds as an optimization problem. Constraints of intracellular space limit the total pool allocation for catalytic enzymes as it competes with, *e.g.* the pool allocated for anabolic enzymes (Nilsson and Nielsen, 2016). In other words, the proportion of catabolic protein decreases while the demand for free energy to support growth maximization increases. The microbe finds itself in a situation to prioritize the catabolic configuration with the highest enzyme-specific ATP productivity over that displaying the highest ATP yield (Molenaar *et al.*, 2009). On a biochemical level, more ATP per protein mass and time is gained through substrate-level versus oxidative phosphorylation (Nilsson and Nielsen, 2016). The reason is simple: Complete substrate oxidation requires the enzymatic machinery of the citric acid cycle and electron transfer chain, while *e.g.* ethanol fermentation in yeast only requires additional pyruvate decarboxylase and alcohol dehydrogenase activity. Hence, a gradual shift from respiratory to fermentative energy production occurs when μ increases, leading to the production of incompletely oxidized overflow metabolites, such as lactic acid, acetic acid, or ethanol in *Lactococcus lactis*, *Escherichia coli*, and *Saccharomyces cerevisiae*, respectively. Other phenotypes besides overflow metabolism follow the same rationale of maximizing μ, such as carbon catabolite repression (Harder *et al.*, 1997) or the switch to mixed carbon source utilization (Zeng *et al.*, 2021).
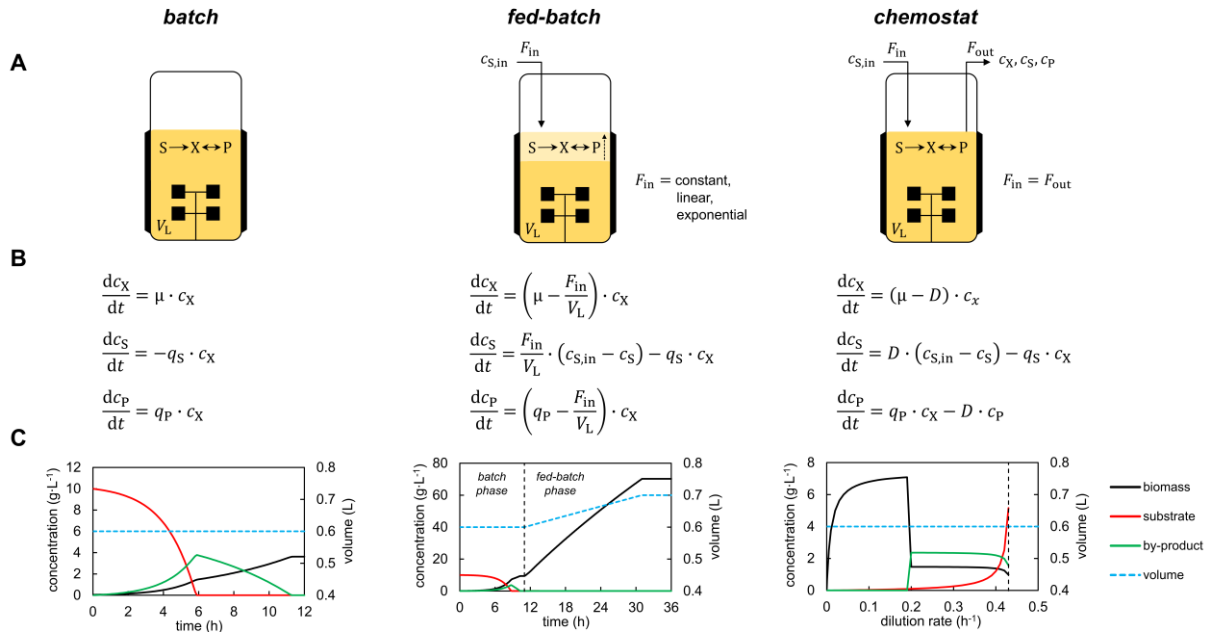
Figure 1. Overview of three common modes of operation for submerged fermentations in stirred tank reactors. The schematic reaction space V_L for each mode is given in the upper panel A. Model equations for substrate (S), biomass (X) and (by)-product (P) were derived from Chmiel, Takors and Weuster-Botz (2018). Examples of characteristic variable levels over time (batch, fed-batch) and dilution rate (chemostat) are given for arbitrary and simplified diauxic reaction rate kinetics in aerobic cultivations (C). The legend key to the differential equations is given in the nomenclature section of this thesis.

The above considerations regarding the biological $\mu-Y_{X/S}$ trade-off play a pivotal role in bioprocess development. A batch process is the simplest design choice. Here, the reaction space is loaded with the culture medium containing the primary substrate. Upon sterilization, the environmental variables are set to the optimal conditions for the microorganism, which is subsequently inoculated to start the reaction. In theory, biomass should accumulate close to its maximum rate since nutrients are present in excess. In reality, the batch process follows a sequence of specific phases (1. lag, 2. acceleration, 3. exponential growth, 4. deceleration, 5. stationary, 6. decline; neglected in figure 1) as cells need to adapt to changing environmental conditions, *e.g.* during inoculation and substrate depletion (Vrabl *et al.*, 2019). Typical batch effects such as substrate inhibition due to high initial concentrations or negative effects of by-products may further limit the productivity of this mode. Thus, cultivations are operated in batch mode when biomass or product yields are less important. For instance, during early screening studies in shake flasks or during alcoholic beverage production when the by-product is valuable. The batch mode further deploys an easy method to assess physiological strain properties such as the maximum growth rate, by-product formation, or diauxic behavior.

Energy and substrate spillage at high growth rates is unfavorable from a commercial standpoint and not compliant with TRY optimization. Controlled feeding of a limiting nutrient source in

the fed-batch mode keeps the microorganism in a phenotypic sweet spot of maximal conversion yield at the highest rate possible. Fed-batch processes differ from batch only in the time-varying supply of at least one essential nutrient source to gain control over μ via the feeding rate F_{in} and the feed concentration $c_{S,in}$. High cell densities > 100 g·L^{-1} are attained and often restricted on the upside by physico-technical limitations, such as oxygen supply in aerobic processes (Riesenberg and Guthke, 1999). Industrially sophisticated bioreactor configurations for aerobic fed-batch processes are stirred tank reactors (STRs), bubble columns, or airlift reactors. Anaerobic fed-batches are less common but may be attractive to prevent negative effects related to batch-loading of the substrate, *e.g.* substrate inhibition or high viscosity (Tomás-Pejó *et al.*, 2010).

A continuous process with constant volume is achieved through equal feed and harvest flow rates resulting in the dilution rate D. On the one hand, continuous fermentations are the ideal mode in terms of run-time and operating costs. Some continuous processes even exist in the biotech industry (Kopp *et al.*, 2019). However, several barriers remain to be overcome, such as compatible downstream processing, long-term sterility, or genomic stability (Wortel *et al.*, 2016; Khanal and Lenhoff, 2021). Continuous fermentations, or chemostats, are most appreciated in the laboratory to enable steady state observations. Time-independency is attained when the dilution rate and all other fermentation variables are kept constant and below μ_{max} resulting in equation 6.

$$\mu = D \tag{6}$$

The inverse of D yields the residence time τ and is an important parameter as the experimenter has to choose the optimal residence time window for steady state observations. Late enough to assume the removal of reactant levels and biological states from pre-equilibrium. Early enough to avoid genomic instability due to the ongoing selective pressure. In this thesis, according to prior experiences in the yeast chemostat community, experimental observations were limited to the window of 5 to 15 τ. Five residence times dilute the culture volume by a factor of 243, while genomic stability is proven for less than 20 generations in the chemostat (Ferea *et al.*, 1999). However, any results derived from chemostat experiments must be carefully evaluated. For instance, on the metabolic level, ten generations suffice to significantly reduce pool sizes of central metabolites by 20 % (Mashego *et al.*, 2005). Furthermore, it does not surprise that glucose affinity increases in the course of a glucose-limited chemostat considering the biological compulsion toward growth rate maximization and the link to substrate affinity

(equations 1 and 5). Jansen *et al.*, (2005) observed a reduction of the extracellular glucose concentration from 20 to 8 mg·L^{-1} after 200 generations. Our own control experiment shown in figure 2 confirmed this trend to initiate already after five τ.
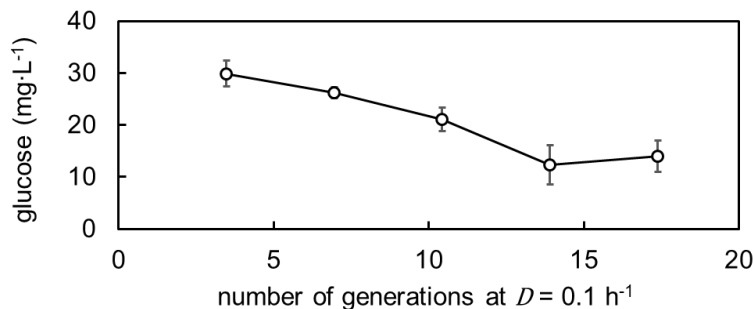
Figure 2. Residual glucose concentration during glucose-limited steady state conditions. The control experiment was performed in the same bioreactor system and under the same conditions as the experiments from the main publications in this thesis. The strain *S. cerevisiae* CEN.PK113-7D was used in the control with a feed concentration of 10 g·L^{-1}glucose. Results show the average ± standard deviation of technical triplicates.

Steady state data derived from chemostats is invaluable to bioprocess developers as it helps identify the mentioned sweet spot of a production host in so-called $D-X$ diagrams (figure 1C, right). Another broad application for chemostats is the study of isolated perturbations on a biological system — the stimulus-response approach (Rizzi *et al.*, 1997; Mashego *et al.*, 2006). This final use case for chemostats is the focal point of this thesis and will be further elaborated in chapter 2.1.3.

2.1.2 Process transfer from lab to production – Scale-up

Meeting economic targets during process development, by far, does not guarantee a successful transfer to the production scale. A plethora of scale-dependent phenomena emerges and the consequences for strain productivity are often unpredictable. These scale-up effects occur on several systematic levels and thorough surveys from different angles exist on the topic (Schmidt, 2005; Lara *et al.*, 2006; Garcia-Ochoa and Gomez, 2009; Hewitt and Nienow, 2010; Takors, 2012; Delvigne and Goffin, 2014; Formenti *et al.*, 2014; Crater and Lievense, 2018).

Multiple operation variables including the volumetric power input P/V, the impeller tip speed ND_i, and the circulation time t_c do not scale linearly with V_L. Equation 7 illustrates the proportionality between V_L and P/V while aiming for equal t_c from the small (subscript 1) to the large (subscript 2) scale assuming equal reactor and impeller aspect ratios (Uhl and Von Essen, 1986).

$$\frac{(P/V)_2}{(P/V)_1} \propto \left(\frac{V_{L,2}}{V_{L,1}}\right)^{\frac{2}{3}} \tag{7}$$

In numbers, the gassed P/V of the perfectly mixed bioreactor system with $V_L = 1.7$ L used in this thesis is 7.1 W·kg^{-1} or ~W·L^{-1} (see appendix B). Any scale-up attempt to maintain t_c in the 22 m^3 demonstration reactor investigated in the ComRaDes project (*e.g.* characterized by Sarkizi Shams Hajian *et al.*, 2020) would yield a P/V of $3.9 \cdot 10^3$ W·L^{-1}. Further increase to an industrially relevant volume of 150 m^3 worsens the picture to a staggering $1.4 \cdot 10^4$ W·L^{-1}. Such values are, of course, not realistic. Several constraints regarding cellular robustness against shear stress, limited heat removal (Votruba and Sobotka, 1992), and energy costs preserve commercial-scale P/V values in the same order of magnitude as on the lab scale. This compromise inevitably increases circulation times on larger scales. In this example, from 0.1 s at the benchtop-scale to 47 s in 22 m^3 (Haringa *et al.*, 2017) up to 250 s in 150 m^3 (Lara *et al.*, 2006). Extending circulation times induce reactant gradients when the respective inversed reaction rates (k in equation 8) are much smaller. In this regard, the dimensionless Damköhler number presented in equation 8 can also be expressed as ratio of circulation time to reaction time t_r (Zlokarnik, 2006)

$$Da = k \cdot \tau \triangleq \frac{t_c}{t_r} \tag{8}$$

$$t_r = \frac{c_S}{q_S \cdot c_x} \tag{9}$$

$$t_r \triangleq t_{depl} = \frac{K_S}{q_{S,max} \cdot c_x} \text{ , for } c_S \to 0 \tag{10}$$

Thus, gradients arise when $Da > 1$. For example, the reaction time may be expressed as the local substrate depletion time at half-saturation levels expressed as t_{depl} in equation 10 (Haringa, 2017). The depletion time would yield 35 s under the experimental conditions chosen in this thesis ($c_x = 11$ g·L^{-1}, $K_S = 1$ mmol·L^{-1} and $q_{S,max} = 9.3$ mmol·g$_{DMB}^{-1}$·h^{-1}). While gradients are avoided in the lab with $Da = 3 \cdot 10^{-3}$, the respective numbers account for 1 and 7 from demonstration to production tank sizes for a relatively low biomass concentration of 11 g·L^{-1}. Industrial-sized C-limited fed-batch tanks suffer from this scale-up effect since the substrate is highly diluted in the fermentation bulk and proliferating cells further decrease t_{depl} over the process time (Nadal-Rey *et al.*, 2021). Spatial dependence aggravates as the limiting substrate is fed locally, usually from the top of the reactor at a high concentration. By analogy,

oxygen supplied from the bottom of the tank via spargers often becomes the limiting factor at the end of high cell density processes causing vertical gradients from aerobiosis to anaerobiosis. Consequentially, gradients of growth-limiting compounds are acknowledged as the main cause of culture performance losses on the large *versus* laboratory scale (Enfors *et al.*, 2001; Hewitt and Nienow, 2010).

Unpredictable strain behavior in a production tank becomes evident as several scale-up effects are often superimposed. Besides mixing limitations, some prevalent shortcomings are the removal of heat or CO_2 accumulation (Noorman, 2011). Space-independent factors might be different media preparation protocols or genetic instability since more generations are necessary to reach the final biomass concentration in production *versus* testing scales (Takors, 2012). Even sterility issues can be considered a scale-up effect. Bioethanol production tanks often resemble more of a mixed culture with bacterial contamination up to $1 \cdot 10^8$ CFU per milliliter, reducing the product yield by 1–5 % (Brexó and Sant'Ana, 2017).

In summary, the industrial fermentation environment is timely and spatially heterogeneous. However, operational modes and fermentation variables are optimized and tested in ideally mixed liquid volumes up to tens of liters, neglecting scale-dependent considerations due to a lack of experimental design parameters. Subsequently, processes are scaled to production empirically, often by sequential 1:10 or even 1:5 increases (Junker, 2004). A limiting operating variable, such as P/V or $k_L a$, is kept constant during each scale translation while compromising on other variables. The limiting variable may be predicted by regime analysis, that is, comparing the time constants of all relevant technical and biological dynamic processes (Oosterhuis, 1984). More often, historic rules of thumb rather than process- and strain-specific knowledge are employed (Junker, 2004; Marques, Cabral and Fernandes, 2010; Böhm *et al.*, 2019). This strictly engineering-driven approach is motivated by preventing critical variable levels rather than exploring a microbe's reaction to non-optimal conditions. The latter can be addressed by scale-down studies.

2.1.3 Process transfer from production to lab – Scale-down

The capital investment concerning scale-up falls in the range of $1 \cdot 10^8 - 1 \cdot 10^9$ € for pilot- to demo-scale testing and the construction of the final production line (Crater and Lievense, 2018). In view of these numbers, prior knowledge of the production host's performance as scale-dependent bottlenecks emerge is highly desirable. Scale-down experiments enable such considerations by mimicking these bottlenecks through specific bioreactor configurations.

Figure 3 illustrates reported designs of scale-down reactors (SDRs). One has to consider several factors for an appropriate SDR selection, including i) the number of scale-up effects, ii) dwell time and frequency of environmental changes, iii) discrete or transient environmental changes, iv) level of observation (*e.g.* population average *versus* single cell or process performance *versus* specific snapshot), or v) experimental bias introduced by the setup (Neubauer and Junne, 2010; Takors, 2012; Papagianni, 2015; Delvigne and Noorman, 2017; Lemoine *et al.*, 2017; Olughu *et al.*, 2019).
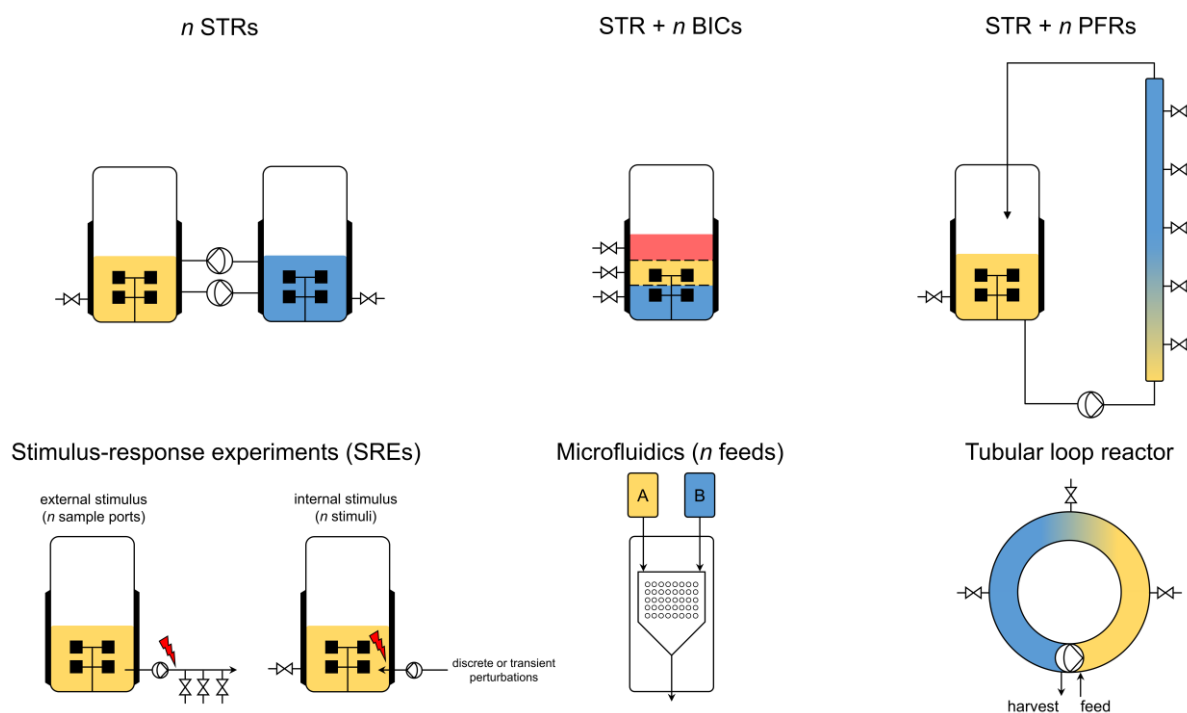
Figure 3. Examples of scale-down reactor configurations. BIC, built-in component; PFR, plug-flow reactor; STR, stirred tank reactor; *n*, number.

Most SDRs partition the reaction space into multiple compartments that reflect mixing-induced heterogeneities (Neubauer and Junne, 2010). For instance, the interconnection of two STRs allows controlled circulation of cells between two discrete conditions through peristaltic pumps. Different bulk effects were successfully tested with this setup for *S. cerevisiae*, *E. coli*, *P. chrysogenum*, and *C. glutamicum* by Sweere *et al.* (1988), Baez *et al.* (2011), Wang *et al.* (2018) and Limberg *et al.* (2017), respectively. Multiple parameter inconstancies were investigated with two STRs representing the feeding (high substrate, low O_2) and a bulk zone (high O_2, low substrate) more holistically (Heins *et al.*, 2015; Wright, Rønnest and Thykaer, 2016). Further increase of representative power can be realized by applying more than two STRs as shown by Buchholz *et al.* (2014) in a cascade of three interconnected STRs.

STRs are coupled to plug-flow reactors (PFRs) to assess the transient change between two environmental conditions and the temporal response of the microorganism. Multiple sample ports over the PFR length represent a distinct residence time in the established condition. In addition, sampling the STR allows to observe adaptation of the culture average against the new, dynamic environment. For instance, the works of Löffler *et al.* (2016) and Ankenbauer *et al.* (2020) uncovered kinetic strategies of *E. coli* and *P. putida* when traveling through glucose starvation zones represented by a PFR loop. By analogy, different residence times in anaerobic PFRs uncovered the resilience of *P. chrysogenum* against short-term oxygen depletion (Larsson et al., 1988). George *et al.*, (1998) used a configuration with static mixing in order to simulate the high sugar concentration close to the feeding point in an aerobic ethanol-fed-batch fermentation with *S. cerevisiae*. Simple solutions, such as unaerated silicon tube loops to test oxygen limitations, are also feasible (Abel, Hübner and Schügerl, 1994). On the contrary, technically challenging systems include two PFRs with multiple gradients. The STR can, for instance, represent an aerated bulk zone while PFR 1 simulates an oxygen-depleted carbon feeding zone and PFR 2 an oxygen-depleted carbon starvation zone (Lemoine *et al.*, 2015; Marbà-Ardébol *et al.*, 2018).

Tubular loop reactors were initially developed for investigating the scale-up effects of vicious, non-Newtonian fermentation cultures. However, yeast processes were scaled down successfully with this method, as well (McNeil and Kristiansen, 1990; Papagianni, Mattey and Kristiansen, 2003). The design of this setup possesses the inherent advantage of establishing continuous environmental shifts without a bulk zone. For this reason, tubular loop reactors are attractive for the scale-down on microalgae cultivations in tubular photobioreactors (Fernández *et al.*, 2023).

The investigator has to control for any potential experimental bias introduced by the technical setup. Nienow and colleagues (2013) identified that the shear stress introduced by the peristaltic pump connecting the STR to the PFR masked any anticipated effect of pH and nutrient gradients on Chinese hamster ovary (CHO) cells. Thus, a single STR with built-in components (BICs) does the job for shear-sensitive CHO cells. In the form of specific perforated discs, these BICs can hamper mixing while forgoing a peristaltic pump (Schilling *et al.*, 1999). Recently, Gaugler *et al.* (2023) reported a guideline for combining geometric disk design and P/V to match the commercial-scale mixing time.

The above configurations introduce heterogeneity by spatial partitioning. As cells fluctuate between compartments, the culture average is in a mixed state of stimulation. While this reflects reality in a large-scale reactor, this SDR concept reduces the ability to track a biological response over time. Stimulus-response experiments (SREs), in turn, enable the observation of isolated perturbations on a population average by introducing stress on a steady-state culture in a single STR. The sampling of time series then allows studying the response of the microbial system to a deviation from the reference condition. Elucidation of biological scale-up phenomena is finally enabled by the combination of rapid sampling techniques and *–omics* analysis (Oldiges and Takors, 2005). Hence, SREs provide quantitative, situation-specific insight rather than a mirror of the commercial-scale environment. A popular experiment is the pulsed addition of the otherwise limiting carbon source to study the onset of overflow metabolism in the vicinity of the substrate inlet point (Kresnowati *et al.*, 2006; Wu, Schipper, Kresnowati, Angela M Proell, *et al.*, 2006; de Jonge *et al.*, 2011; Suarez-Mendez *et al.*, 2014; Vasilakou, Van Loosdrecht and Wahl, 2020). Prolonged environmental shifts, such as the temporal emergence of oxygen shortage in filamentous high-cell-density processes, are introduced by ramp-down or ramp-up experiments (Tang *et al.*, 2017). Observations on the population level are enabled by a new technology called the segregostat (Sassi *et al.*, 2019). This chemostat setup controls phenotypic diversification via frequency-controlled stimulation and online feedback from a flow cytometer. Even though this experiment is not a SDR *per se*, it identifies critical frequencies of environmental shifts causing population dynamics in bioprocesses. In addition, the perturbation may also be imposed on an external sample stream as the STR-culture remains in steady state to investigate several different stimuli. One such device is the Bioscope, which was employed to study *in vivo* kinetics of *S. cerevisiae* against glucose pulses (Visser *et al.*, 2002).

Microfluidics display an attractive methodology to study environmental feedback on the single-cell level (Ho *et al.*, 2022). In contrast to bioreactor experiments, single-cell cultivations in microfluidic chambers rely on using either reporter strains or time-lapse imaging of cellular proliferation. Täuber *et al.* (2020) introduced the 'dynamic microfluidic single-cell cultivation' SDR, which enables fluctuations between two media down to the scale of seconds. This advancement complements bioreactor SDRs by imposing high frequencies of environmental shifts on time scales previously not feasible in bioreactor approaches.

2.1.4 Rationalizing both worlds through bidirectional knowledge transfer

To a large degree, up- and downscaling the fermentation process was and still is a speculative discipline. The missing link to turn from speculation to knowledge is the accessibility of large-scale data. However, probing technology for heterogeneities in commercial tanks is either in early-stage development or considered too invasive for fully operating plants (Formenti *et al.*, 2014). One promising approach uses sterilizable flow-following sensors that reside in the fermentation broth throughout the process and log data at frequencies up to 1 s^{-1} (Bisgaard *et al.*, 2022). Further development is required to capture the entire picture of industrial fermentations since state-of-the-art sensors are still limited to monitoring fluid velocities. Besides, companies are highly incentivized to keep large-scale data proprietary. This reasoning in conjunction with the ideal case to consider potential scale-up effects *a priori* led industrial and academic researchers to turn to computational simulations.

CFD methods simulate the Eulerian flow field of the liquid phase in the fermentation tank using either Lattice-Boltzmann or Navier-Stokes equations (Haringa, 2023). The virtual microorganism is introduced as a second, massless phase in the form of Lagrangian particles (Lapin, Müller and Reuss, 2004). Last, biocatalytic activity is computed *e.g.* by adding unstructured kinetic models to the biotic phase that enable the computation of time- and space-dependent exchange rates (Haringa *et al.*, 2017; Kuschel, Siebler and Takors, 2017). Bioreactor heterogeneities were successfully computed via this framework in the past. Several gradient estimations gave valuable insight into industrial fermentation, including pH (Spann *et al.*, 2019), substrate (Noorman *et al.*, 1993), by-product (Sarkizi Shams Hajian *et al.*, 2020), O_2 (Kuschel and Takors, 2020) and even CO gradients in synthesis gas fermentations (Siebler, Lapin and Takors, 2020). Biological scale-up effects are estimated by implementing structured cell models, albeit their execution is more demanding on the computational side. For instance, Pigou and Morchain (2015) successfully predicted yield reduction during the scale-up of an *E. coli* process by coupling metabolic and population balance models. The structured model allowed pinning the performance loss to locally distributed acetate formation and consumption dynamics.

Thus, CFD coupled to cellular reaction dynamics (CRD) aims to close the above data gap. Post-processing of CFD−CRD simulations in the form of lifeline analysis provides design principles for scale-down experiments. In brief, a lifeline registers the experienced environmental conditions of each virtual cell over time. Statistical analysis of the trajectories from a significant

number of cells allows us to deduce dwell times, frequencies, and amplitudes regarding different fermentation environments (reviewed in Blöbaum, Haringa and Grünberger, 2023). Self-evidently, lifeline analysis can further uncover biological scale-up effects when the trajectories of structured models are investigated (Zieringer, Wild and Takors, 2021).

With a tool such as CFD−CRD modeling at hand, and this is the core of the ComRaDes project, empirical up and downscaling of bioprocesses eventually becomes replaced. *In silico* prediction of the large-scale environment opens up the possibility to enter development cycles following the 'design, build, test, and learn (DBTL)' concept of synthetic biology depicted in figure 4 (Nielsen and Keasling, 2016). It is a common practice to initiate this rational scale-up cycle by investigating the rate-limiting mechanism first. An easy method to identify bottlenecks is regime analysis by comparing time constants of transport and conversion mechanisms as introduced in chapter 2.1.2 (Pollard *et al.*, 2007). For instance, Oosterhuis (1984) identified that oxygen transfer and consumption time constants were on the same order of magnitude. Thus, scaling down oxygen gradients of gluconic acid fermentation with *Gluconobacter oxydans* was the motivation for his doctoral thesis. In the thesis presented here, glucose gradients are considered the first bottleneck in a 22 m^3 pilot process. Next, CFD−CRD simulations based on hyperbolic kinetic equations estimate the environmental gradients to design scale-down experiments. The first iteration of the DBTL cycle may involve SRE experiments to gather metabolomics data from process-relevant perturbations to parametrize CRD models for the next DBTL-cycle (Wang, Haringa, Tang, *et al.*, 2020; Puiman *et al.*, 2023). The lumped '9-pool model' describing the metabolism of *P. chrysogenum* exemplifies this development step as it was developed on the basis of SRE-derived metabolomic data with the aim to integrate it into CFD models (Tang *et al.*, 2017). Moreover, through integrating other *–omics* methodologies, such as transcriptomics, key regulatory elements might be uncovered that allow rational strain engineering (Hewitt and Nienow, 2010). Recently, Ziegler *et al.* (2021) constructed an *E. coli* strain with reduced maintenance demands based on engineering propositions derived from STR-PFR experiments considering periodic carbon and nitrogen starvation (Löffler *et al.*, 2016; Simen *et al.*, 2017).
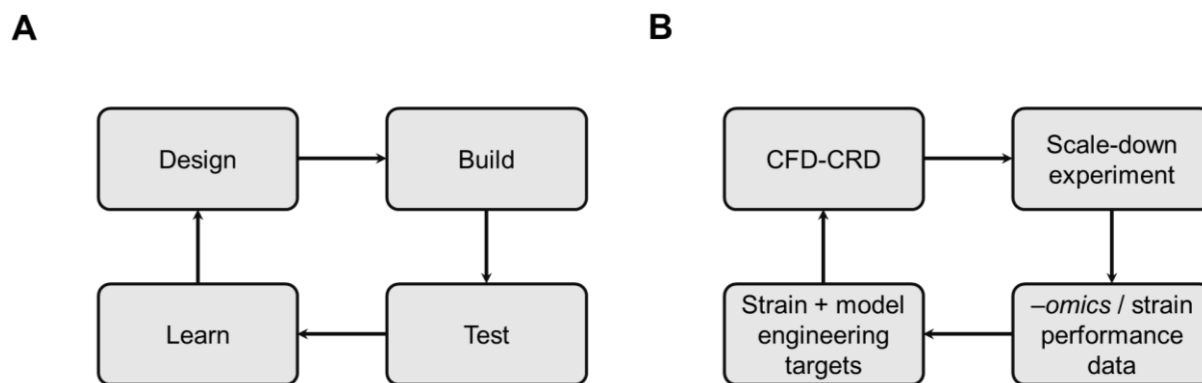
Figure 4. (A) Classical DBTL-cycle employed in synthetic biology. (B) DBTL interpretation in the context of rational scale-up/scale-down engineering. CFD, computational fluid dynamics; CRD, cellular reaction dynamics; DBTL, design, build, test, learn.

Further iterations over this development cycle ultimately result in more realistic wet- and dry lab mirrors of the large scale (Kerssemakers *et al.*, 2023). The ideal rational scale-up/scale-down framework serves a twofold purpose: (i) design of adequate SDRs and (ii) engineering of large-scale adapted strains. In all fairness, a perfect mirror of the large scale remains a fantasy as the SDR design needs to compromise on either dwell time, amplitude, or frequency of a mixing-induced perturbation. However, the different SDR configurations introduced earlier do complement each other in this regard. Furthermore, typically more than one scale-up effect influences TRY output. While most CFD−CRD investigations focus on environmental heterogeneities, other scale-up effects should not be neglected. Plasmid instability due to increased generation times during the industrial seed train, for instance, can be easily contemplated in scale-down studies by adjusting the pre-culture accordingly (Schmidt, 2005). Several strategies exist regarding large-scale adaptation of industrial strains. The mentioned work by Ziegler and colleagues follows the idea of producing a minimal genome. Here, successive knockouts of genomic traits that are triggered but futile under industrial conditions (e.g. chemotaxis) save valuable resources for productive pathways. Currently, this bottom-up strategy is successfully employed for *E. coli* and *P. putida* (Lieder *et al.*, 2015; Ziegler *et al.*, 2021). Examples of top-down approaches encompass dampening the stringent response in *E. coli* (Michalowski, Siemann-Herzberg and Takors, 2017) or introducing genetic switches to control phenotypic stability in industrial processes. The latter prevents loss-of-production mutations *e.g.* by repressing heterologous production during the biomass accumulation phase on maltose through the maltose-inducible repressor protein Gal80 in yeast (Chua, Jiang and Meadows, 2020).

This thesis pursues a contribution to the first DBTL iteration toward rational scale-up of *S. cerevisiae* fed-batch processes. The starting point is the insight from lifeline analysis of a 22 m^3 fed-batch process derived from the simulations of Sarkizi *et al.* (2020) which are reported in this thesis. These lifelines indicate that transitions between glucose limitation and starvation dominate the process at biomass concentrations ranging between 10 and 25 g·L^{-1}. Recently, Nadal-Rey *et al.* (2023) independently concluded a widespread occurrence of carbon starvation zones industrial fed-batch processes with *E.coli* and *S. cerevisiae*. Consequentially, the examination of yeasts transitioning between carbon limitation and starvation is the focal point of this thesis.

2.2 *Saccharomyces cerevisiae*

The budding yeast *S. cerevisiae* is the model organism in this thesis. Attributes including GRAS (Generally Recognized as Safe) status, absence of ethical concerns, extensive biological and analytical knowledge, and adequate eukaryotic representativeness entrenched the organism in the scientific world (Karathia *et al.*, 2011). Its natural ability to convert sugar to ethanol put yeast in the center of our daily lives in the form of alcoholic beverages and fuel. Genetic engineering extended the microorganisms product portfolio to virtually any biotechnological compound, from fine chemicals such as *S*-adenosyl-L-methionine to heterologous proteins like insulin (Nielsen, 2013; Hayakawa, Matsuda and Shimizu, 2016).

The prototrophic, laboratory *S. cerevisiae* strain CEN.PK113-7D was chosen as one of two model strains. This choice is rooted in a comparative study from van Dijken *et al.* (2000), who proclaimed that the CEN.PK lineage fulfills the requirements to serve as a research platform. Traits such as fast growth on defined media, genetic stability, high heterologous protein productivity, and high transformation stability led to this conclusion. As a result, many protocols to conduct *–omics* studies were developed based on the CEN.PK-background. Particularly relevant for this work were the rapid metabolic quenching methods using cold methanol (Canelas *et al.*, 2008) and the reference data from numerous glucose-pulse experiments with this strain (Kresnowati *et al.*, 2006; Wu, Schipper, Kresnowati, Angela M. Proell, *et al.*, 2006; Suarez-Mendez *et al.*, 2014). In addition, the genome of the haploid strain CEN.PK113-7D is sequenced, assembled, and annotated, enabling transcriptomic analyses using next-generation sequencing (NGS) (Nijkamp *et al.*, 2012).

Nevertheless, metabolic and gene regulatory observations derived from haploid lab strains should not be extrapolated offhandedly to the genetically more complex industrial strains (Van Hoek, Van Dijken and Pronk, 1998; Steensels *et al.*, 2014). Di-, poly- and aneuploid chromosome sets are more commonly found in the commercial setting as they improve the organism's chance to adapt to harsh industrial conditions (Borneman *et al.*, 2011; Storchova, 2014). Lineages with *e.g.* high fermentation rates, superior inhibitor and product tolerance, or improved flocculation characteristics emerged from the age-long domestication of *S. cerevisiae* and the historically more recent mutagenic strain improvement programs (de Vries, Pronk and Daran, 2017). In this regard, the diploid yeast Ethanol Red™ (ScER) was selected as a second model organism in this thesis. ScER is currently marketed by Fermentis (Lesaffre, Marcq-en-

Barśul, France) as a state-of-the-art first-generation bioethanol producer with acquired tolerance against several industrial stressors (Mukherjee *et al.*, 2017; Gronchi *et al.*, 2022).

2.2.1 Physiology

The chemo-organotrophic ascomycete *S. cerevisiae* is a member of the fungal kingdom with a facultative-fermentative and Crabtree-positive phenotype. Its ellipsoid appearance is specified by 5–10 µm and 5 µm in length and width, respectively (Walker and White, 2005). *S. cerevisiae* proliferates on a well-characterized palette of essential macro- and micronutrients enabling growth experiments on minimal media. A sophisticated medium composition is that reported by Verduyn *et al.* (1992), a scalable medium to control desired biomass levels during aerobic glucose limitation at 30 °C and pH 5.0. The biomass yield, $Y_{X/S}$, of CEN.PK113-7D accounts for 0.57 $mol_C \cdot mol_C^{-1}$ under said conditions (Canelas *et al.*, 2010), owed to maximum ATP generation via oxidative phosphorylation. Assuming a P/O ratio of 1.0, one mol of glucose yields 16 mol ATP (Verduyn *et al.*, 1991). This yield reduces to 2 mol of ATP from substrate-level phosphorylation when oxygen is absent. Ethanol and CO_2 are the main anaerobic products bound to a stoichiometric ratio of 1:1 and glucose-limited conversion yields of 0.55 and 0.29 $mol_C \cdot mol_C^{-1}$, respectively (Lip *et al.*, 2020). In consequence, anaerobic yeasts channel only one fifth of the assimilated carbon to biomass. Most yeast species require oxygen apart from respiration to synthesize essential structural membrane compounds such as sterols and unsaturated fatty acids (Piškur and Compagno, 2014). Thus, anaerobic growth experiments with the Verduyn medium rely on supplementing *e.g.* ergosterol and polysorbate 80 as a substitution for oleic acid (Tai, 2007).

Both haploid and diploid *S. cerevisiae* proliferates by budding at maximum rates of roughly 0.6 h^{-1} under optimal conditions (Hartwell, 1974). The mechanistic driver behind cellular multiplication is the mitotic cell cycle (Herskowitz, 1988). In brief, cells undergo four morphologically distinct intervals during mitosis, abbreviated with G_1 (first gap), S (synthesis), G_2 (second gap), and M (mitosis) (Hartwell, 1974). The G_1 interval acts as a gatekeeper phase during which adequate nutrient levels and a critical cell size are essential for cell cycle progression. Otherwise, cells transition to a state of quiescence called G_0 under any severe nutrient limitation (de Virgilio, 2012). START initiates at the end of G_1 under resource-rich conditions marking the irreversible entry into the proliferation cycle with bud emergence. The twelve-mega base genome distributed over 16 chromosomes replicates during the subsequent

S-phase (Goffeau *et al.*, 1996). Cells continue to inflate in size during G_2 and divide into one mother and one daughter cell in the M-phase.

S. cerevisiae can escape the asexual, budding reproduction cycle by sporulation through meiosis, as shown in figure 5. Meiosis can only be performed by diploid cells carrying both mating types *MAT*a and *MAT*α under the prerequisite of a nutrient limitation (Haber, 2012). In nature, 95–99 % of all diploid cell cycles are still mitotic (Ruderfer *et al.*, 2006; Zörgö *et al.*, 2012). Meiotic exit of the vegetative cell cycle occurs during the late G_1-phase (Neiman, 2011). The haploid model strain CEN.PK113-7D possesses the *MAT*a allele and is thus neither able to mate nor undergo meiosis in monoseptic cultures (Nijkamp *et al.*, 2012). On the contrary, Ethanol Red™ has the ability to form spores, even though the efficiency to do so is often reduced in industrial strains (Steensels *et al.*, 2014; da Silva Fernandes *et al.*, 2022).
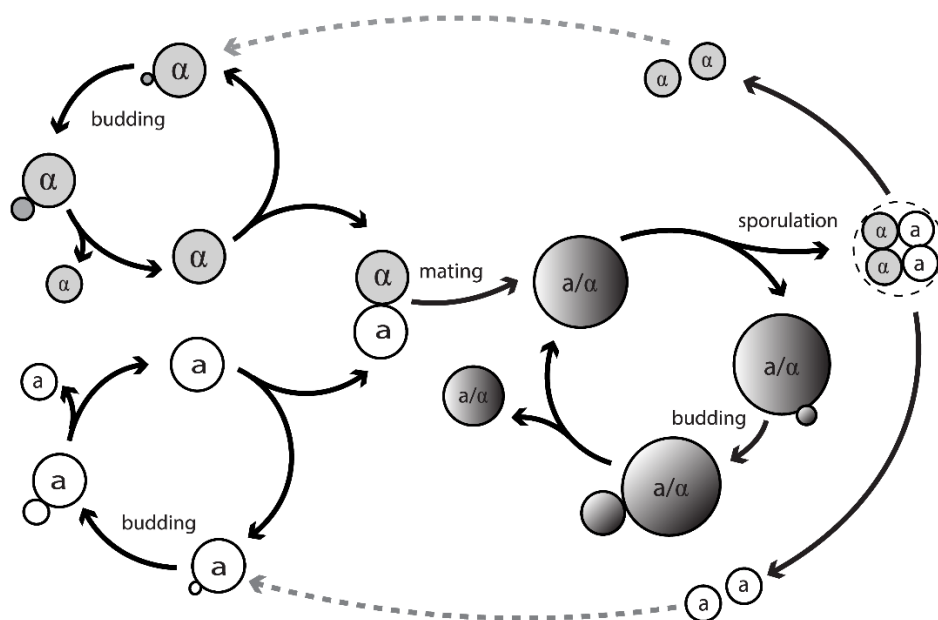
Figure 5. Graphic summary of mitotic and meiotic yeast proliferation. Mitotic haploid yeasts of opposed mating types (*MAT*) a or α can conjugate and form diploid yeasts carrying both *MAT*a/α alleles. Certain nutrient limitations, such as nitrogen, may induce a meiotic cycle resulting in a spore carrying four haploid nuclei. The tetrad divides into two haploid cells of each mating type when an optimal nutrient environment is restored. (from Wang, Lo and Chou, 2017)

Another morphological peculiarity is the stress-induced pseudohyphal growth, occurring when nitrogen is depleted from the environment (Gimeno *et al.*, 1992). The terminology reads pseudohyphal growth for diploids and invasive growth for haploids. During the process, cells spatially scavenge for nutrients by elongating, adhering, and even invading a solid matrix, *e.g.* on agar plates (Gimeno *et al.*, 1992; Pothoulakis and Ellis, 2018). Closely related is a reversible phenomenon called flocculation that is associated with submerged cultures. Here, cells form

agglomerates that drive biomass out of suspension through increased surface hydrophobicity (Soares, 2011). This trait is particularly relevant in brewing processes as it eases the cell harvest at the end of the fermentation *e.g.* for re-pitching the next batch (Walker and White, 2005).

2.2.2 Glucose catabolism and important metabolic crossroads

Organic carbon is the primary electron donor to fuel the metabolism of the eukaryotic cell. Even though *S. cerevisiae* is able to consume a palette of carbohydrates as nutrients, ranging from polyols to alcohols, organic and amino acids we focus on its preferred substrate: glucose (Rodrigues, Ludovicio and Leao, 2006).

Glucose is imported via facilitated diffusion mediated a family of 20 hexose transporter genes (*HXT*). Of those, *HXT1–HXT17* express characterized glucose transporters, *GAL2* encodes a galactose transporter and *SNF3* and *RGT2* are sensory genes for high and low affinity, respectively (Kruckeberg, 1996). However, to products of *HXT1*, *HXT2*, *HXT3*, *HXT4*, *HXT6* and *HXT7* exert the main glucose translocation function. The expression configuration of these glucose transporter genes yields three distinct affinity-phenotypes: i) low-affinity mainly enabled through *HXT1* and *HXT3* with $K_M = 100$ and 60 mmol·L^{-1}, respectively, ii) moderate affinity (*HXT2/4*) with $K_M = 10$ mmol·L^{-1} and iii) high affinity (*HXT6/7*) with $K_M = 1–2$ mmol·L^{-1} (Reifenberger, Boles and Ciriacy, 1997). *HXT3* is the only transporter that is expressed independently of the extracellular glucose concentration (Bisson, Fan and Walker, 2016). The maximum glucose uptake rate of CEN.PK113-7D under glucose limitation is 9.3 and 13.3 mmol·g$_{DMB}$$^{-1}$·h^{-1} under aerobic and anaerobic conditions, respectively (Diderich *et al.*, 1999). Results from this thesis locate the anaerobic $q_{S,max}$ of Ethanol Red^{TM} at 11.4 mmol·g$_{DMB}$$^{-1}$·h^{-1}.

Cytoplasmic glucose is instantly phosphorylated by hexokinase (Hxk) enzymes marking the entry into glycolysis (figure 6). The produced glucose-6-phosphate (G6P) displays an important metabolic branch point. For the purpose of energy storage, futile cycling, flux regulation and stress response G6P is channeled toward glycogen and trehalose (reviewed in François and Parrou, 2001). G6P dehydrogenase (Zwf1) catalyzes the first reaction step of the pentose phosphate pathways (PPP). The PPP (reviewed in Bertels, Murillo and Heinisch, 2021) irreversibly catabolizes G6P to ribulose-5-phosphate producing two NADPH to fuel anabolic reactions such as lipid and fatty acid synthesis. G6P is isomerized to fructose-6-phosphate by phosphoglucose isomerase further down glycolysis. Thus, it is not surprising that both source and sink reactions of G6P are allosterically regulated as they determine the fate of carbon flux

early in the central carbon pathway. For instance, Hxk activity is feedback inhibited by trehalose-6-phosphate (Blázquez *et al.*, 1993) and Zwf1 is feedback inhibited by NADPH (Saliola *et al.*, 2012). The relative flux distribution at the G6P branch point between glycolysis, PPP and trehalose/glycogen under aerobic glucose limitation at a growth rate of 0.1 h^{-1} is 15:1:3 (Suarez-Mendez *et al.*, 2016).

Another important key reaction step is that catalyzed by the phosphofructokinases Pfk1 and Pfk2 delivering fructose-1,6-bisphosphate (FBP). Glycolytic flux on the Pfk level is allosterically inhibited by ATP and citrate or activated by ADP, AMP, and fructose-6-phosphate (Teusink *et al.*, 2000; Bárcena *et al.*, 2007). Furthermore, 6-phosphofructo-2-kinase (Pfk26/27) catalyzes the synthesis fructose-2,6-bisphosphate which, in turn, imposes another feed-forward activation of Pfk1/2 (Tripodi *et al.*, 2015).

Pyruvate displays the central furcation point not only is yeast, but in the metabolism of virtually any microorganism (Pronk, Steensma and Van Dijken, 1996). In *S. cerevisiae*, phosphoenolpyruvate is irreversibly converted to pyruvate under the regeneration of ATP via two pyruvate kinases Cdc19 and Pyk2 of which only the former is allosterically activated by FBP (Boles *et al.*, 1997). Absent oxygen routes the flux from pyruvate to CO_2 and acetaldehyde before alcohol dehydrogenases (Adh) form the end-product ethanol. Redox homeostasis is maintained during anaerobic catabolism through the NADH-dependence of the Adhs. The main fermentation by-product and osmo-regulator glycerol acts as an additional redox sink through the glycerol-3-phosphate dehydrogenase reaction step (Weusthuis *et al.*, 1994). Under aerobiosis, NADH is efficiently kept at low levels though oxidative phosphorylation leading to catabolic reduction charges below 0.2 (Zhang *et al.*, 2015). Mitochondrially located pyruvate enters the tricarboxylic acid cycle through direct dehydrogenation to acetyl coenzyme A catalyzed by Pda1 and Pdb1. Pyruvate may also enter the TCA indirectly via the fermentative bypass through decarboxylation (Pdc1/5/6) to acetaldehyde which is further converted to acetic acid and acetyl coenzyme A (Boubekeur *et al.*, 1999). However, the direct route is favored by aerobic, glucose-limited *S. cerevisiae* as the substrate affinity of Pda1/Pdb1 is one order of magnitude higher than that of the Pdc reaction (Kresze and Ronft, 1981). The bypass on the other hand, is linked to the Crabtree effect as Pdc possesses a higher flux capacity during high pyruvate levels compared to Pda1/Pdb1 (Vemuri *et al.*, 2007). A third alternative route is the metabolic channel through the only known anaplerotic reaction in yeast, which is a cytosolic carboxylation yielding oxaloacetate (Moreira Dos Santos *et al.*, 2004).

Figure 6. Central glucose catabolism. Reaction pathways (solid arrows) and allosteric control (negative: red dashed arrows, positive: green dashed arrows) are derived from the KEGG PATHWAY database (Release 107.0) and Tripodi *et al.* (2015). Values for adenylate energy, catabolic and anabolic reduction charge are reported in Ball and Atkinson (1975), Ask *et al.* (2013), and Zhang *et al.* (2015).

Besides the mentioned allosteric regulations within the central glucose catabolism, most fluxes are further controlled via phosphorylation of metabolic enzymes. A comprehensive study conducted by Oliveira an colleagues in 2012 confirmed that phosphorylation inhibits the activity of Pda1 and Pfk1 *in vivo*. Furthermore, regulatory impacts by phosphorylation are known for Hxk2, Pfk26, Cdc19, and several enzymes involved in glycogen and trehalose metabolism.

2.2.3 Hierarchy of transcription regulation against environmental change

Coordination of gene expression against environmental change is a multilevel process. First, receptor proteins sense internal feedback or external signals (figure 7). Second, a transduction pathway converts the signal through relay molecules allowing downstream cellular mechanisms to react adequately. Third, a response is executed that can be virtually any cellular mechanism — here, we focus on changes in gene expression. Initiation, termination, acceleration, and deceleration of the reaction steps from gene to protein may occur in the stages of chromatin modification, transcription, RNA processing, mRNA degradation, translation, protein processing, and protein degradation (Campbell *et al.*, 2008). This thesis measured cellular adaptation on the level of differential mRNA expression in part supported by a high degree of correlation with differential protein expression (Lee *et al.*, 2011; Lahtvee *et al.*, 2017).
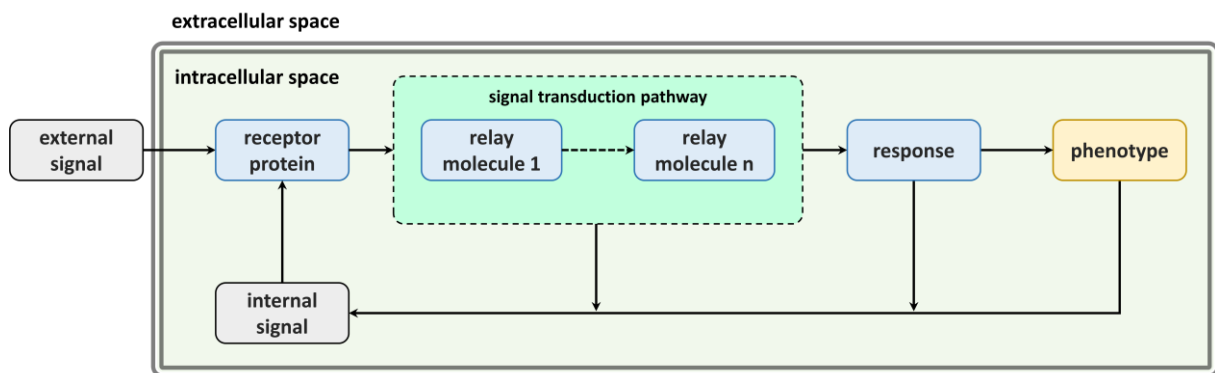
Figure 7. Coordination of gene expression against internal and external stimuli. This graphical representation is based on literature from Levy *et al.* (2007) and Campbell *et al.* (2008).

Internal signals typically arise from feedback mechanisms to fine-tune gene expression for optimal cellular resource management (Levy *et al.*, 2007). External feedforward signals may originate from various environmental variables such as nutrients, oxygen, water, pH, osmosis, temperature, or turgor pressure. In any case, said signals are sensed at levels ranging from physiological optimality to lethality (Giannattasio *et al.*, 2013). Molecular signals, often called first messengers, are received as ligands binding to the receptor protein to cause its activation

through conformational change. For instance, external nutrients are sensed by three classes of membrane receptors, namely: GTP-binding protein (G-protein) coupled receptors (GPCRs, class I), transporters with receptor function (class II), and transporter homologs with receptor but without transporter function (class III) (reviewed in Holsbeeks *et al.*, 2004). In addition, intracellular feedback integrates through a plethora of characterized mechanisms involving GPCRs. The mechanisms of some other signal integration modes is not yet entirely understood, such as the sensory role of Hxk2 for glycolytic flux (Vega *et al.*, 2016). Others are more intertwined, such as the internal growth rate feedback, where the protein homeostasis system senses non-assembled ribosomes (Shore, Zencir and Albert, 2021).

The subsequent signal transduction phase is a multistep pathway. A common theme is the combined action of second messenger molecules and a signal relay via sequential protein de-/phosphorylation (Campbell *et al.*, 2008). Second messengers are molecules connecting the signal from the receptor protein with a specific phosphorylation cascade. In these reaction networks, serine/threonine kinases relay information via the transfer of phosphate groups from ATP to the next kinase until a final protein is phosphorylated to trigger a cellular response. Protein phosphatases catalyze the reverse reaction to close the signaling circuit and enable on/off switching. *S. cerevisiae* employs several signaling cascades, for instance, the three-step mitogen-activated protein kinase (MAPK) systems (Chen and Thorner, 2007). MAPKs are involved in several pathways, such as the responses to pheromones and osmotic shock or filamentous growth (Gustin *et al.*, 1998). Nutrient sensory pathways often employ one-step kinase reactions acting as gatekeepers, such as SNF1, PKA, TORC1, TORC2, Sch9, Yak1, Hap2/3/4/5, and Pho85/Pho80 (Smets *et al.*, 2010; Broach, 2012). A phosphorylation cascade that regulates mRNA expression ends by modulating a transcription factor (TF). Currently, 183 yeast TFs are reported (Teixeira *et al.*, 2018). TFs, in turn, bind upstream activation or repression DNA sequences to exhibit the respective regulatory function via the recruitment of either transcription activator or repressor complexes (Hahn and Young, 2011). More precisely, transcription initiates through TF-guided recruitment of the transcription machinery or co-activator complexes, such as mediator, SAGA, or TFIID, that may further be involved in chromatin remodeling (Drobna, Bialkova and Šubík, 2008; Hahn and Young, 2011). Phosphorylation and other modifications, including ubiquitination, acetylation, and sumoylation, drive TF activity through DNA binding, protein stability, subcellular localization, and protein-protein interaction (Holmberg *et al.*, 2002).

One of the best-studied signaling pathways in yeast is the pheromone response pathway during mating (see figure 5). Sexual reproduction starts with the reception of the pheromone factor of a cell from the opposing mating type by a GPCR system. The receptor proteins Ste2/3 sense either a- or α-factors and are coupled to the G-protein Gpa1, which activates a MAPK cascade comprising four kinases. Their targets are the TF-complex-associated proteins Ste12/Dig1/Dig2 and the TF Far1. The concerted action of this pathway ultimately causes 200 upregulated and 100 downregulated genes via binding of the activator Ste2 to the pheromone response element (PRE) and the repressor Far1 via an unknown mechanism. Dig1 and Dig2 repress Ste12 binding to terminate the response (Bardwell, 2005).

Nutrient signaling is often far more complex and intertwined in comparison to the above-mentioned example. A high degree of kinase crosstalk, protein-protein interactions, and feedback/feedforward regulatory nodes allow a coordinated and fine-tuned gene expression response toward environmental input (Schneper, Düvel and Broach, 2004; Pawson and Scott, 2010; Broach, 2012). Kawakami *et al.* (2016) estimated that signal transduction of glucose and nitrogen stimuli alone comprises 256 proteins and 110 complexes. In this regard, the following paragraph will give an overview of our current understanding of glucose signaling to underline the motivation of this thesis to investigate regulatory effects induced by glucose sensing in industrial bioreactors.

2.2.4 Glucose as an effector in the yeast signaling network

Glucose is the primary nutrient of *S. cerevisiae*. As such, the hexose is not only sensed in the extracellular space but, as it is combusted within the cell, several mechanisms stimulate secondary signaling pathways. Feedback may emerge on the levels of metabolic fluxes or pool sizes, energy homeostasis, or the growth rate, to name a few. Figure 8 summarizes signaling hubs and their interactions with relevance for glucose concentrations that prevail in industrial fermentation processes.
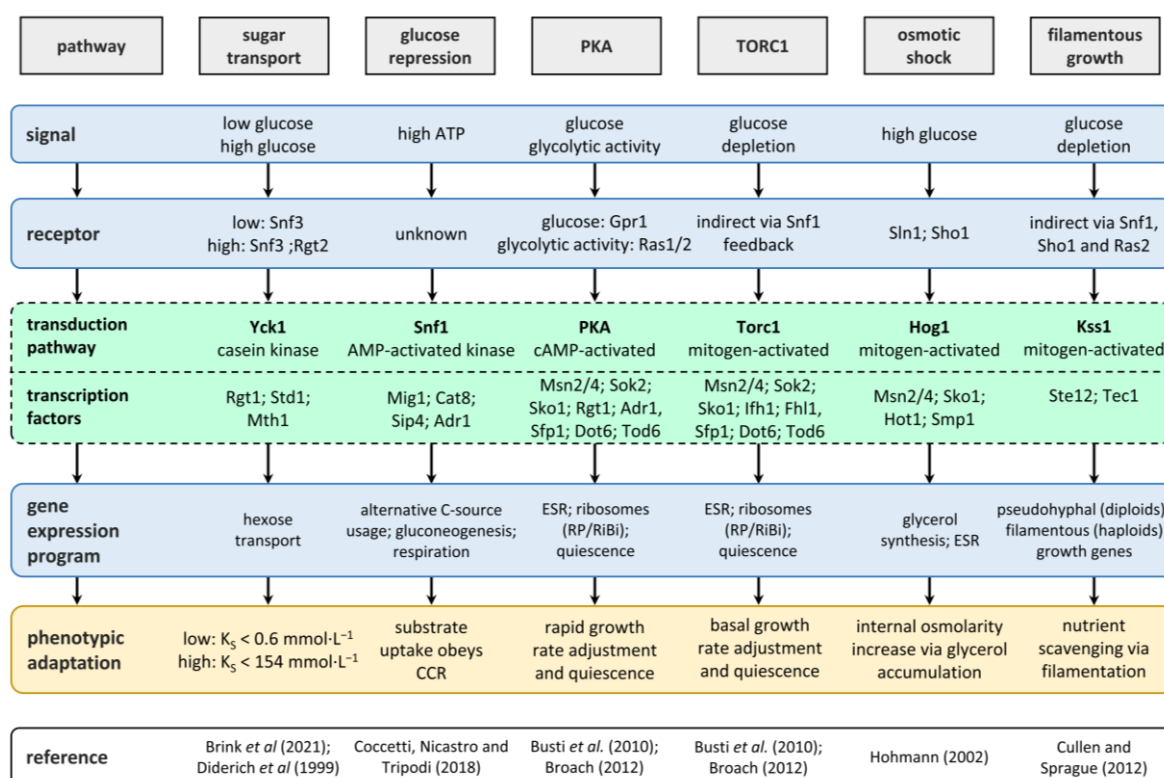
Figure 8. Glucose-responsive signaling pathways in *S. cerevisiae*. The information used to generate this graphic representation is gathered from the references indicated in the bottom tile. Gene expression programs and involved transcription factors are limited to selected examples from the references. CCR, carbon catabolite repression; ESR, environmental stress response; K_S, affinity constant; PKA, protein kinase A; RiBi, ribosome biogenesis; RP, ribosomal protein; TORC1, target of rapamycin kinase 1

Class I and III membrane-bound receptors sense extracellular glucose. Rgt2 and Snf3 belong to the class III of transporter homologs with receptor but without transporter function. Both sensors regulate the expression of the hexose transporters via the membrane-bound casein kinase I (Yck1), which controls the phosphorylation of the TFs Mth1, Rgt1, and Std1. The absence of glucose causes de-phosphorylation of all three TFs, which recruit the repressor complex Tup1-Ssn6 to ramp down the transcription of both low and high-affinity transporters. Rgt1 is phosphorylated at low glucose levels, acting as an inducer of the moderate-affinity transporter genes *HXT2/4*, while high glucose levels induce low-affinity transport. (Ozcan and Johnston, 1999; Brink *et al.*, 2021)

The latter case of glucose excess is further co-regulated by repressive elements of the carbon catabolite repression pathway (CCR) (Johnston, 1999). This pathway ensures strict glucose catabolism even in the presence of other carbon sources. Its main component is the AMP-activated kinase SNF1. Glucose repression occurs when SNF1 is inactive at a low AMP:ATP ratio via an unknown receptor system, leaving the main transcriptional repressor Mig1 de-phosphorylated (Conrad *et al.*, 2014). Under such conditions, Hxk2 interacts with Mig1 to form

a nucleus-located complex that represses genes involved alternative carbon source utilization and high-affinity *HXT* genes (Sanz, Viana and Garcia-Gimeno, 2016). Furthermore, inactive SNF1 maintains the transcriptional activators Cat8, Sip4, and Adr4 inactive, causing the additional repression of genes involved in gluconeogenesis, fatty acid oxidation, and respiration (Busti *et al.*, 2010). Besides its specific role in CCR, SNF1 is a general internal feedback sensor of energy homeostasis. As such, SNF1 aligns stress response mechanisms, DNA damage, aging, endocytosis, and the cell cycle with the energetic status of the cell (Coccetti, Nicastro and Tripodi, 2018).

Protein kinase A (PKA) coordinates 90 % of glucose-induced transcriptional change (Zaman *et al.*, 2009). This central hub exerts a feedforward role of extracellular glucose stimuli via the class I receptor Gpr1 and an internal feedback role by sensing glycolytic activity via the GPCR Ras1/2. Both sensors converge on the level of adenylate cyclase Cyr1, which converts ATP to cAMP (Conrad *et al.*, 2014). The concentration of this second messenger spikes up to 50-fold within 2 min after a glucose pulse to activate PKA (Santangelo, 2006). It is important to note that the strain CEN.PK113-7D possesses a point mutation in Cyr1 (Nijkamp *et al.*, 2012). However, Kümmel *et al.* (2010) compared cAMP concentrations in CEN.PK113-7D and the same strain with a repaired Cyr1 mutation and found no significant difference. In its active form, PKA promotes several processes involved in proliferation while repressing stress-related genes (Busti *et al.*, 2010; Broach, 2012). On the transcriptional level, PKA favors growth by phosphorylating, amongst others, the activator TF Sfp1, which then stimulates the transcription of ribosomal protein (RP) and ribosomal biogenesis (RiBi) genes (Plank, 2022). Repressed programs involve the general stress response, glycogen accumulation and gluconeogenesis, or quiescence via the TFs Msn2/4, Adr1, and Rim15, respectively (Busti *et al.*, 2010; Brink *et al.*, 2021).

Several crosstalking nodes additionally characterize the PKA network. Especially the adjustment of the growth rate relies on monitoring more parameters than just glucose alone. The target of rapamycin kinase complex 1 (TORC1) fulfills this role by integrating information about the quality and quantity of extracellular nitrogen (Broach, 2012). Furthermore, TORC1 is energy sensitive as it is feedback inhibited by active SNF1 (Caligaris *et al.*, 2022). Crosstalk between TORC1 and PKA manifests in the same TFs targeted by both kinases, partially directed through the kinase Sch9. For instance, the RP and RiBi stimulons are under TORC1/PKA-concerted control through the shared TFs Rap1, Stb3, Crf1, Dot6, Tod6, and Sfp1 (Kunkel, Luo and Capaldi, 2019; Plank, 2022). Kunkel and colleagues (2019) could show that both kinases

act cooperatively. While TORC1 primarily adjusts the base growth rate in alignment with internal and external nutrients, the PKA pathway quickly adjusts the ribosome machinery when sudden changes occur. PKA shares downstream targets in a similar fashion with the energy sensor SNF1, such as the TFs Adr1 and Msn2/4 (Coccetti, Nicastro and Tripodi, 2018). In addition, falling glucose levels impose negative feedback on the adenylate cyclase via SNF1-mediated phosphorylation (Nicastro et al., 2015). Glucose depletion signals are partially independent of SNF1 and PKA during the diauxic shift. The Hap2/3/4/5 complex regulates this phase, which induces respiratory genes during the transition to respiratory growth (Mao and Chen, 2019). (Mao and Chen, 2019). Yeasts may scavenge for nutrients via filamentation under several nutrient starvation conditions sensed via specific signaling pathways (see chapter 2.2.1). Carbon starvation signals are integrated either via Ras2, SNF1, or Sho1, a component of the osmotic shock response before the Kss1 MAPK pathways is initiated (Ceccato-Antonini and Sudbery, 2004; Cullen and Sprague, 2012). Prolonged exposure to glucose starvation prompts *S. cerevisiae* to enter quiescence (de Virgilio, 2012). Cells transition to this reversible state when PKA and TORC1 are inactive, causing quiescence initiation via the downstream kinases Rim15 (Reinders *et al.*, 1998; de Virgilio, 2012).

Last, glucose can also pose a severe threat to yeast in the form of an osmotic shock, *e.g.* induced by one mol per liter of glucose (Dihazi, Kessler and Eschrich, 2004). The signal is transduced via a HOG1-dependent MAPK pathway resulting in the Hot1-mediated, stress-specific activation of glycerol synthesis to increase internal osmolarity (Hohmann, 2002). HOG1 signaling shares common TF targets with SNF1, TORC1, and PKA, all converging on the level of Msn2/4-mediated regulation of the environmental stress response (ESR) (Mace *et al.*, 2020). This generic program displays a 'first line of defense' in the adaptation of yeasts toward any environmental insult encompassing approximately 900 differentially expressed genes (Gasch, 2007b). Six hundred genes belonging to the RP and RiBi stimulons are repressed to conserve mass and energy during early stress adaptation. The remaining 300 genes fulfill different functions and their induction depends on Msn2/4 activation combined with Sok2/Sko1 de-repression. For instance, genes involved in metabolism, transport, fatty acid degradation, redox homeostasis, detoxification of reactive oxygen species, or autophagy are upregulated to withstand a shift to an unfavorable environment (Hohmann, 2007). Most of the induced genes have no apparent function that allows the cell to cope *e.g.* with acute glucose starvation or osmotic shock. Instead, the wide implication of Msn2/4-mediated ESR stimulon seems to play a role in acquired stress resistance (Berry and Gasch, 2008).

2.3 Mixing-induced scale-up effects of *S. cerevisiae*

Bioethanol and baker's yeast fermentations are two highly sophisticated *S. cerevisiae* processes with a century-long history. Still, conditions mimicking the industrial fermenter indicate that product yield losses of > 10 % are quite expectable (reviewed in Lara *et al.*, 2006). On the other hand, a scale-up effect might not always inhere downside risk. Scale-down studies with yeast systems expressing heterologous proteins, such as β-galactosidase or insulin, reported superior specific productivities under supposedly non-ideal large-scale conditions (Cortés *et al.*, 2005; Wright *et al.*, 2020). Thus, cellular behavior often adopts upfront hidden peculiarities. In this sense, the presented chapter explores documented *S. cerevisiae* scale-up phenomena and their underlying biological mechanisms on metabolic and gene regulatory levels. This chapter is further limited to mixing-induced effects with relevance for carbon-limited fermentations.

2.3.1 Metabolic implications

Biomass yield loss due to unstable substrate supply is frequently pinned to overflow metabolism triggered by locally high sugar concentrations close to the feed point. Bylund *et al.* (1998) reported ethanol production within eight seconds after a glucose upshift, backed by works from others (Theobald *et al.*, 1997; Wu, Schipper, Kresnowati, Angela M. Proell, *et al.*, 2006). Thus, a scenario arises where timely simultaneous but locally separated ethanol production close to and consumption distant from the feed turns into a quasi-futile cycle (Noorman, 2011; Sarkizi Shams Hajian *et al.*, 2020). Respiration of two ethanol molecules yields 20 % less ATP than one glucose molecule due to the hydrolysis of ATP to AMP during the acetyl-CoA synthetase reaction (Kozak *et al.*, 2016). Stimulus-response experiments (SREs) imposing glucose pulses uncovered further scale-dependent metabolic inconveniences. For instance, sudden transitions from glucose limitation to excess trigger the so-called 'ATP paradox' (Theobald *et al.*, 1997; Somsen *et al.*, 2000; Kresnowati *et al.*, 2006). The phenomenon describes a transiently dissipated adenine nucleotide moiety as AMP channels toward the purine salvage pathway (Walther *et al.*, 2010; Verma *et al.*, 2013). Linked downward-sloping ATP levels further de-represses glycolytic flux to enable a respiro-fermentative coping strategy for the excess sugar concentration. While this metabolic configuration potentially accelerates ethanol secretion at local pockets of high glucose, the work of Suarez-Mendez and colleagues (2014) showed that the ATP paradox vanishes after repetitive exposure. In addition, the carbon flux distribution reconfigures at the G6P branch as more carbon is channeled toward PPP and the storage pools and thus drained from glycolysis (Wu, Schipper, Kresnowati, Angela M. Proell, *et al.*, 2006;

Suarez-Mendez, Ras and Wahl, 2017). The reverse case, that is, a transition from glucose limitation to starvation, is still underrepresented in literature, even though especially computational research points to its relevance in carbon-limited fermentations (Haringa *et al.*, 2017; Sarkizi Shams Hajian *et al.*, 2020; Nadal-Rey *et al.*, 2021; Ho *et al.*, 2022). To date, only two studies investigated the short-term starvation response of yeast on a metabolic level. Weber *et al.* (2020) found a rapid spike in the AMP:ATP ratio within 30 seconds after glucose depletion and the onset of fatty acid β-oxidation to sustain cellular maintenance. Additional experiments presented in the dissertation of Suarez-Mendez (2015) observed glycolytic intermediates mirroring the extracellular drop of glucose after a stopped feed during aerobic, glucose-limited growth in a chemostat.

Vertical oxygen gradients in aerobic processes cause cycling between respiration and fermentation. Scale-down studies with the industrial yeast strain H620 could demonstrate that anaerobic phases of > 1 min suffice to produce ethanol (Abel, Hübner and Schügerl, 1994). Ethanol may be taken up in the respiratory compartment diminishing net by-product formation due to the previously described quasi-futile cycle. Consequentially, longer compartment-specific residence times further reduce the ATP yield as the contribution of the ethanol cycle increases Sweere *et al.* (1988). Increased viscosities during high cell densities may further depress oxygen transfer favoring the development of anaerobic zones. This problem caused deterioration of oxidative phosphorylation during the scale-up of an *S. cerevisiae* fed-batch process to 10 m^3 (Fu *et al.*, 2014). Intermediates of the TCA, such as fumarate or malate, leaked into the extracellular space because of impeded NADH oxidation, an effect the authors termed 'extended overflow' (Paczia *et al.*, 2012). Carbon dioxide and bicarbonate accumulate with increasing hydrostatic pressure in industrial tanks (Takors, 2012). Some reported metabolic consequences in this regard encompass inhibition metabolic enzyme inhibition, acetate production, uncoupling of TCA and electron transport chain, and competing intracellular ATP demand (Eigenstetter and Takors, 2017).

Characteristic times of allosteric and metabolic reactions from $1 \cdot 10^{-4}$ to $1 \cdot 10^2$ seconds back the above considerations. Thus, *S. cerevisiae* is well-equipped to respond to rapid environmental fluctuations that prevail in an industrial bioreactor (Delvigne and Goffin, 2014). In this regard, a part of this thesis covers the endometabolomic reaction upon sudden transitions between glucose limitation and starvation.

2.3.2 Insight from gene expression studies

To date, the gene expression level is somewhat underappreciated when investigating mixing-induced scale-up effects in *S. cerevisiae*. Most insight originates from SREs imposing pulsed upshifts of carbon or nitrogen sources. For instance, a one gram per liter glucose pulse onto a respiratory culture sparked a transcriptomic response within 120–210 s. Gene expression changes indicated a re-configuration toward a respiro-fermentative metabolism via activated CCR and a ramp-up of growth capacities in the form of RP and RiBi clusters (Kresnowati *et al.*, 2006). Analogous SRE experiments involving a 20 g·L^{-1} glucose pulse obtained similar results (Dikicioglu *et al.*, 2011). The expected expression shift toward low-affinity glucose uptake was observed by Buziol *et al.* (2008). Work by both Kresnowati *et al.* and Dikicioglu *et al.* observed significant downregulation of Msn2/4 target genes and concomitant upregulation of ribosomal capacities. Remarkably, pulsing 40 µM glutamine on a nitrogen-limited culture provokes RiBi and RP induction within 40–120 s (Airoldi *et al.*, 2016), which is the fastest transcriptional change reported in SREs according to a thorough literature search. The observed transcriptional strategies, thus far, indicate a conserved strategic response to sudden environmental change that strongly resembles ESR onset. In this context, oxygen depletion experiments on glucose-repressed and de-repressed yeasts confirmed Msn2/4-mediated gene regulation (Lai *et al.*, 2005). Lai and colleagues could show that an unspecific program initiated within ten and terminated after 40 minutes following an anoxic shift. According to the authors, oxygen sensing did not trigger this first response but rather the integration of internal metabolic stimuli. Subsequently, specific differential gene expression prepared the cells for anaerobic adaptation. The pioneering works of Audrey Gasch and Helen C. Causton related to the discovery of the ESR characterized this behavior in a variety of stress scenarios, of which many have relevance in industrial processes, such as heat-shock, osmotic shock, or several nutrient depletions (Gasch *et al.*, 2000; Causton *et al.*, 2001). Still, the present literature lacks reports directly linking short-term gradient exposure to triggering the ESR. Involvement of this global program stands to reason as it plays into acquired stress tolerance (Carlquist *et al.*, 2012; Moutsoglou and Dearden, 2020), a phenomenon that is well-documented in association with industrial fermentation (Abbott *et al.*, 2007; Cheng *et al.*, 2009; Xu *et al.*, 2020).

Synthesis and degradation of messenger RNA is a lengthy process with relaxation times from minutes to hours (Delvigne and Goffin, 2014). Extracellular effectors such as glucose concentration, on the other side, may fluctuate on the hydrodynamic circulation timescale or below (Haringa, 2017). Furthermore, intracellular metabolic effectors, including the AMP to

ATP ratio, mirror the temporal fluctuations since their relaxation times are significantly faster (Stephanopoulos, Aristidou and Nielsen, 1998). Theoretically, the transcriptional network remains responsive toward fast effector signal changes through a segmented approach. For instance, the conformational change within the sensory GCPR system operates at timescales of $1 \cdot 10^{-6}$ to $1 \cdot 10^{-3}$ seconds (Tikhonova and Costanzi, 2009). Ma *et al.* (1999) reported cAMP relaxation times following a glucose pulse ranging from 60 to 90 seconds in wild-type yeasts. The relaxation time of phosphorylation networks depends on their number of reaction steps, topology, and other signal-related factors. The corresponding timescales of the PKA and TORC1 pathways involved in nutrient signaling diverge from minutes to tens of minutes (Jalihal *et al.*, 2021). In addition, many stress-responsive TFs act in a bursting manner. That is, TFs such as calcium-responsive Crz1 or Msn2/4 translocate between cytoplasm and nucleus on timescales of 90 to 120 seconds, in part, as a control mechanism for gene expression (Cai, Dalal and Elowitz, 2008; Zadrąg-Tęcza *et al.*, 2018). Thus, understanding gene expression as a segmented system with component-specific time scales opens the possibility of integrating rapidly fluctuating signals. In other words, there is a high chance that mixing inhomogeneities in the industrial setting is constantly propagated through the sensory network of *S. cerevisiae* to establish a process-specific transcriptional phenotype.

At the time of writing this thesis, a plethora of authors reported transcriptomic studies of yeasts under industrially relevant (Boer *et al.*, 2003; Tai *et al.*, 2005) or even industrial conditions (Li *et al.*, 2010; de Lucena *et al.*, 2015; reviewed in Gibson *et al.*, 2007). Often, these studies compared the transcriptional status between two steady states to uncover condition-specific gene expression. For instance, Tai and Boer found sets of strict oxygen-, carbon, nitrogen-, phosphorous, and sulfur-specific genes. Similar experiments characterizing the transcriptional status in a dynamic bioreactor environment are reported for prokaryotic hosts but not for *S. cerevisiae* (Löffler *et al.*, 2016; Simen *et al.*, 2017; Ankenbauer *et al.*, 2020). In the referenced work, an STR-PFR chemostat setup (see chapter 2.1.3) kept prokaryotic hosts under C- or N-limited conditions in the STR while repeatedly exposing a fraction of the culture to uptake-driven starvation for the limiting nutrient in the PFR. Among strain-specific responses, a common theme was repeated on/off switching of the stringent response in the PFR (Levy *et al.*, 2007). Own experiments in the same setup revealed a transient induction of carbohydrate catabolic genes while repressing the RiBi stimulon after connecting the PFR to glucose-limited yeast cultures (Minden *et al.*, 2021). The response was located in the STR, peaked after 30 min, and vanished after six hours. However, the chosen scale-down configuration employing 120 s-

long residence in the PFR unfolded observational drawbacks. For one, no genes were found differentially expressed over the length of the PFR. Presumably, stimulation and execution of transcriptional dynamics separated locally between PFR and STR. In addition, the dynamic STR-PFR conditions did not reveal a new transcriptional phenotype *versus* the reference state. We reasoned that assessing transcriptional adaptation was impeded by the emergence of transcriptional population heterogeneity in the STR. Nevertheless, observed internal resource reallocation, including reduced glycogen pools and increased nitrogen uptake, pointed toward some degree of phenotypic adaptation.

Taken together, two questions arose from the current knowledge of mixing-induced heterogeneities and the yeast transcriptional network. First, how do short-term stimuli propagate through the transcriptional network of *S. cerevisiae*, and on which timescales? Second, does the integration of rapidly fluctuating signals lead to transcriptomic adaptation that helps to understand the 'bioreactor phenotype'?

3 Aims & objectives

This thesis aims to explore the large-scale phenotype of *S. cerevisiae* on a systems biology level. Short-lived transitions between glucose limitation and starvation were chosen as a representative case to study the impact of limited mixing in the industrial, carbon-limited fed-batch bioreactor. From an industrial engineer's point of view, this work also represents a first iteration over the scale-up/scale-down DBTL-cycle starting from an experimental design inspired from CFD-derived lifelines. In this regard, the presented work tries to fulfill two aims. The first aim is to investigate the short-term tactic and the long-term strategic adaptation mechanism toward dynamic substrate supply. Hence, this part of the study tries to characterize the industrial phenotype. The second aim is to condense the gathered knowledge to propose optimization targets for strain- and scale-down engineering.

Stimulus-response experiments (SREs) are the experimental basis of this work. The stimulus encompassed a two-minute stopped feed in otherwise glucose-limited chemostats. Analyses of characteristic process parameters, intracellular metabolites and differential gene expression were employed to achieve the above goals by following the below objectives.

Objective 1: Endometabolomic studies

O.1.1 Monitor intracellular metabolites of the strain CEN.PK113-7D following a single starvation stimulus until metabolic relaxation is attained using liquid chromatography coupled to tandem mass spectrometry (LC-MS/MS).

O.1.2 Compare the endometabolome pattern of the non-adapted culture after a single *versus* a fully adapted culture after repeated stimulation.

Objective 2: Transcriptomic studies

O.2.1 Monitor differential gene expression of the strain CEN.PK113-7D following a single starvation stimulus until transcriptional relaxation is attained using NGS sequencing.

O.2.2 Compare the unperturbed reference against the dynamic steady state of a culture adapted to repeated stimulation.

O.2.3 Reevaluate the result obtained in O.2.1 and O.2.2 with the industrial strain Ethanol Red^{TM}.

Objective 3: Data interpretation

O.3.1 Condense the data from objectives 1 and 2 to a holistic understanding of the 'bioreactor phenotype'.

O.3.2 Translate the data from objectives 1 and 2 to propositions for engineering industrially robust strains and representative scale-down experiments.

4 Research articles

This section reproduces three first-authored research articles that make up the core of this thesis. Objectives 1.1 and 1.2 are addressed in **article I** titled "Monitoring Intracellular Metabolite Dynamics in *Saccharomyces cerevisiae* during Industrially Relevant Famine Stimuli". Objectives 2.1 and 2.2 are addressed in **article II** titled "Performing in spite of starvation: How *Saccharomyces cerevisiae* maintains robust growth when facing famine zones in industrial bioreactors". Objective 2.3 and further evaluation of objectives 2.1 and 2.2 is addressed in **article III** titled "Mimicked Mixing-Induced Heterogeneities of Industrial Bioreactors Stimulate Long-Lasting Adaption Programs in Ethanol-Producing Yeasts". Objectives 3.1 and 3.2 are collectively addressed and discussed in all three research articles and the **discussion chapter** of this dissertation. Furthermore, non-published results presented in **chapter 5** titled "Additional Analysis - Strain Engineering Targets" contribute to objective 3.2. All reproduced manuscripts are limited to their main text body and the layout is harmonized. The original publications, which are all open-access, are attached at the end of this thesis. Important supplementary information is reproduced in the appendix of this thesis and all raw data is accessible in the ComRaDes repository of the online data storage and sharing platform DataverseNL (*https://dataverse.nl/dataverse/comrades*).

4.1 Monitoring intracellular metabolite dynamics in *Saccharomyces cerevisiae* during industrially relevant famine stimuli

The manuscript was written by Steven Minden as first author. Prof. Dr.-Ing. Ralf Takors contributed to the manuscript's content through principal review. Prof. Dr.-Ing. Ralf Takors is the corresponding author. Steven Minden planned and conducted all experiments, collected and analyzed the according primary data. Maria Aniolek, Christopher Sarkizi Shams Hajian and Tobias Zerrer supported during sampling of the fermentation experiments and the endometabolomic analyses, which was supervised by Dr. Attila Teleki. Prof. Dr.-Ing. Ralf Takors supervised the research. Prof. Dr. Ir. Frank Delvigne, Prof. Dr. Walter van Gulik, Dr. Amit Deshmukh and Prof. Dr. Henk Noorman contributed to the manuscript by reading and approving the final version.

This manuscript was accepted by the Multidisciplinary Digital Publishing Institute (MDPI) and published in the journal *metabolites*:

4.1.1 Abstract

Carbon limitation is a common feeding strategy in bioprocesses to enable efficient microbiological conversion of the substrate to the product. However, industrial settings inherently promote mixing insufficiencies creating zones of famine conditions. Cells frequently traveling through such regions repeatedly experience substrate shortages and respond individually but often with deteriorated production performance. *A priori* knowledge of the expected strain performance would enable targeted strain, process, and bioreactor engineering for minimizing performance loss. Today, computational fluid dynamics (CFD) coupled to data-driven kinetic models is a promising route for *in silico* investigation of the impact of the dynamic environment in the large-scale bioreactor on microbial performance. However, profound wet-lab data sets are needed to cover relevant perturbations on realistic time scales. As a pioneering study, we quantified intracellular metabolome dynamics of *Saccharomyces cerevisiae* following an industrially relevant famine perturbation. The stimulus-response experiments were operated as chemostats with intermittent feed and high-frequency sampling. Our results reveal that even mild glucose gradients in the range of 100 µmol·L^{-1} impose significant perturbations in adapted and non-adapted yeast cells altering energy and redox homeostasis. Apparently, yeast sacrifices catabolic reduction charges for the sake of anabolic persistence under acute carbon starvation conditions. After repeated exposure to famine conditions, adapted cells show 2.7 % increased maintenance demands.

4.1.2 Introduction

Microbial catalysis has a pivotal role in realizing the transition from natural resource depletion towards a sustainable and circular economy (Mengal *et al.*, 2018; Singh, Christensen and Panoutsou, 2021). Key factors underlining this status encompass the use of renewable feedstock, mild reaction conditions, vast diversity of products and high potential for improving production efficiency and product quality — all benefitting from biological flexibility (Straathof *et al.*, 2019). Consequentially, the European Horizon 2020 program recognized biotechnology as one of four "Key Enabling Technologies" to maximize sustainability and growth potential of European companies (European Comission, 2022). A prerequisite, but also one of the greatest challenges is the successful transfer of lab results into commercial-scale bioreactors without loss of performance (Noorman, 2011; Takors, 2012; de Lorenzo and Couto, 2019; Wehrs *et al.*, 2019). This scale-up is often hampered by intrinsic drawbacks such as mixing insufficiencies, which ultimately cause a heterogeneous extracellular environment (Schügerl, 1993; Vrábel *et al.*, 2000; Takors, 2016). Numerous factors become increasingly dynamic causing unexpected biological responses that either reduce expected TRY (titer, rate, yield) criteria or even reveal fatal potential for a given process (Takors, 2016; Crater and Lievense, 2018).

To prevent the occurrence of detrimental scale-up effects, inclusion of large-scale considerations into early stage development is gaining more and more recognition in both the industry (Florez, 2018; Hill *et al.*, 2020; Ögmundarson *et al.*, 2020) and academic research (Neubauer and Junne, 2010; Papagianni, 2015; Delvigne and Noorman, 2017; Täuber *et al.*, 2020). Especially during substrate limited operation modes such as fed-batch or chemostat, concentration gradients can easily emerge since volumetric reaction times are often within the same order of magnitude of the mean broth circulation times in an industrial environment (Lara *et al.*, 2006; Haringa, Mudde and Noorman, 2018). Multiple investigations monitored cellular responses upon exposure to industrial conditions aiming to explain the observed performance losses. Industrial hosts were exposed to substrate heterogeneities revealing overflow metabolism (Bylund *et al.*, 1998; George *et al.*, 1998), disturbance of energy management (Pham *et al.*, 2008; de Jonge *et al.*, 2011) and perturbations of regulatory programs mirrored by metabolomics (Kresnowati *et al.*, 2006; Suarez-Mendez, Ras and Wahl, 2017), transcriptomics (Löffler *et al.*, 2016; Zieringer, Wild and Takors, 2021) and proteomics (Nieß *et al.*, 2017; Anane *et al.*, 2019; Wright *et al.*, 2020). Even population heterogeneity was observed (Delvigne and Goffin, 2014; Heins and Weuster-Botz, 2018).

How can scale-down experiments be designed to adequately reflect industrial hydrodynamics and reaction dynamics when large-scale data is usually not available? Modern bioprocess development strategies substitute this knowledge gap with simulations based on computational fluid dynamics (CFD) coupled to biokinetic models (Noorman, 2011; Haringa, Mudde and Noorman, 2018; Nadal-Rey *et al.*, 2021). This setup allows integrating exchange rates with the hydrodynamic environment of the bioreactor. More precisely, the exposure of individual microorganisms to substrate gradients can be recorded during all process phases and expressed as lifelines (Lapin, Müller and Reuss, 2004). Currently, this approach reaches considerable agreement with quantitative data on concentration gradients from pilot to industrial-scale (Haringa *et al.*, 2016, 2017; Kuschel and Takors, 2020; Sarkizi Shams Hajian *et al.*, 2020). An adjacent development goal is to increase the predictive power to uncover biological scale-up effects already at the development stage in the lab via data-driven models. Thus, comprehensive *–omics* data for model development is paramount and can, for instance, be provided by stimulus-response experiments (SRE) that capture relevant large-scale dynamics. Figure 9 demonstrates a conceptual workflow with integrated wet- and dry-lab contributions. Ultimately, the generated knowledge allows both the identification of strain engineering targets and the quantitative design of scale-down simulators to replace physical upscaling. A successful archetype for this strategy has recently resulted in the construction of an *Escherichia coli* strain with reduced maintenance energy demands when subjected to industrial glucose gradients (Ziegler *et al.*, 2021; Zieringer, Wild and Takors, 2021).
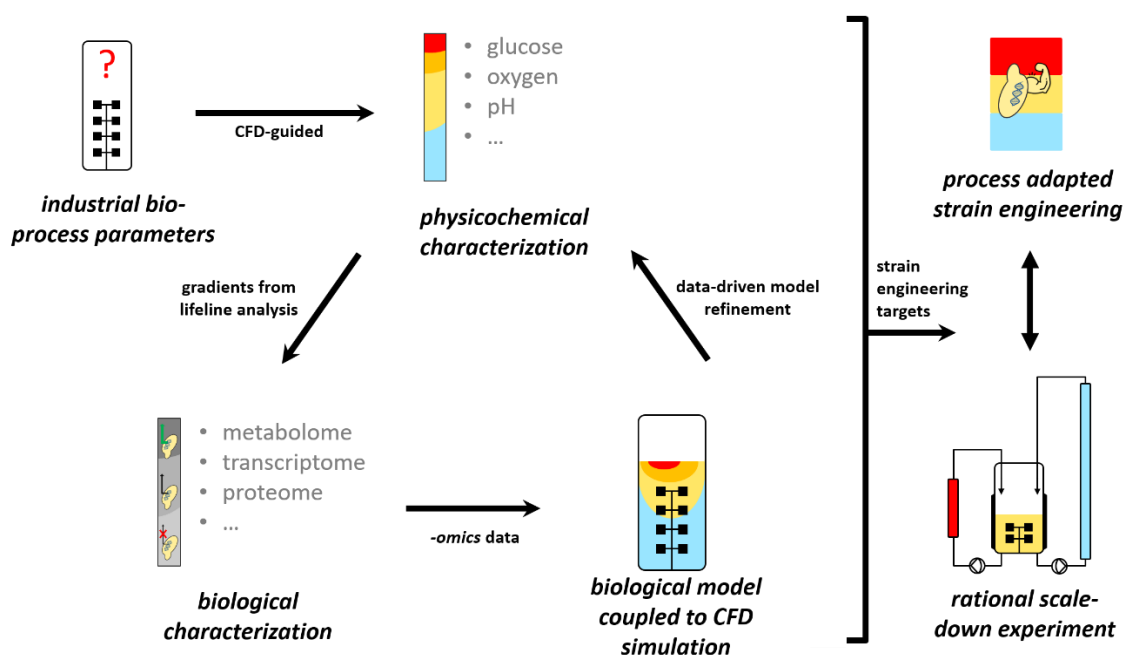
Figure 9. Basic procedure for data-driven scale-up/scale-down development. Concentration gradients are derived from large-scale simulations to design stimulus-response experiments and generate –*omics* datasets. This approach further allows the set-up of biological models to refine large-scale simulations. Ultimately, gained knowledge enables process-adapted strain engineering and the design of realistic scale-down simulators for validation experiments to replace classical scaling up.

This work is part of a case study with the ambition to deploy the aforementioned rational bioprocess engineering approach for a eukaryotic model organism. *Saccharomyces cerevisiae* was chosen due to its broad prevalence in several sectors of the bioprocessing industry comprising foods, fuels, chemicals and pharmaceuticals (Nielsen, 2019; Venturini Copetti, 2019). The industrial setting is derived from a 22 m^3 research bioreactor operated as a glucose-limited fed-batch process for biomass production, which is thoroughly described in the literature (Noorman *et al.*, 1993; Larsson *et al.*, 1996; Haringa *et al.*, 2016). Corresponding CFD investigations and large-scale measurements already identified glucose gradients in the range of 23−460 µmol·L^{-1} (Larsson *et al.*, 1996; Haringa *et al.*, 2017; Sarkizi Shams Hajian *et al.*, 2020). This distinct concentration spectrum favors the emergence of three metabolic regimes: First, the desired operating point in the glucose-limited state to achieve optimal biomass conversion. Second, overflow metabolism due to glucose excess close to the feeding position. Third, starvation regimes far away from the feed where glucose uptake cannot satisfy cellular maintenance demands anymore.

The before mentioned SRE approach represents a proven methodology to provide the necessary ground to set up data-driven models (Rizzi *et al.*, 1997; Mashego *et al.*, 2006; Lao-Martil *et al.*, 2022). For the organism under investigation, several studies quantitatively investigated the

metabolome and transcriptome during a sudden shift from glucose limitation to excess (Theobald *et al.*, 1997; Kresnowati *et al.*, 2006; Mashego *et al.*, 2006; Suarez-Mendez *et al.*, 2014). To the best of our knowledge, the current state of literature is missing complementary data for the opposing transition between limitation and starvation. This study, therefore, set out to close this gap of knowledge, beginning on the metabolic level. On the one hand, quantitative endometabolomic measurements provide a sound database for more detailed model development. On the other hand, interpretation of the dataset uncovers biological mechanisms that can lead to strain performance losses for different production scenarios and guide large-scale adapted strain engineering.

4.1.3 Results

Hyperbolic kinetics overestimate starvation regimes in industrial-scale simulations

Figure 10a presents 24 minutes of a three-hour single-cell lifeline mimicking the late stage of an industrial baker's yeast production scenario. The simulation suggests that cells resided only 39 % of the time in the favored glucose limitation regime delivering planned substrate supply for growth and maintenance. Besides, overflow regimes occurred lasting for 1–10 s and making up 3 % of the lifeline. However, for 58 % of the lifeline, the yeast trajectory was subject to severe starvation conditions, which makes the famine status rather the normality than the exception.

To mimic the dominant role of glucose starvation, we exposed yeast cells to famine conditions (figure 10b). In the glucose depletion experiment, minimal glucose levels of 22 µmol·L^{-1} were found after the feed was stopped for 2 minutes. Interestingly, simulations using the kinetic parameters of Figure 10a predicted residual glucose levels well below 10 µmol·L^{-1}. However, the semi-logarithmic slope of the experimental limitation-starvation transition in figure 10b was only 0.44 s^{-1}, which accounts for 60 % of the anticipated kinetics (0.71 s^{-1}). Apparently, additional impacts occurred that hamper the one-by-one application of said hyperbolic uptake kinetic for the short-term starvation.

Nevertheless, it was concluded that cellular exposure to famine conditions is a dominating scenario in large-scale bioreactors. Accordingly, follow-up studies considered 2 min starvation intervals that allowed the investigation of endo-metabolite dynamics for two scenarios: (i) a single limitation-starvation-limitation (LSL) cycle revealing the non-adapted cellular response and (ii) a representative LSL cycle from an adapted culture.
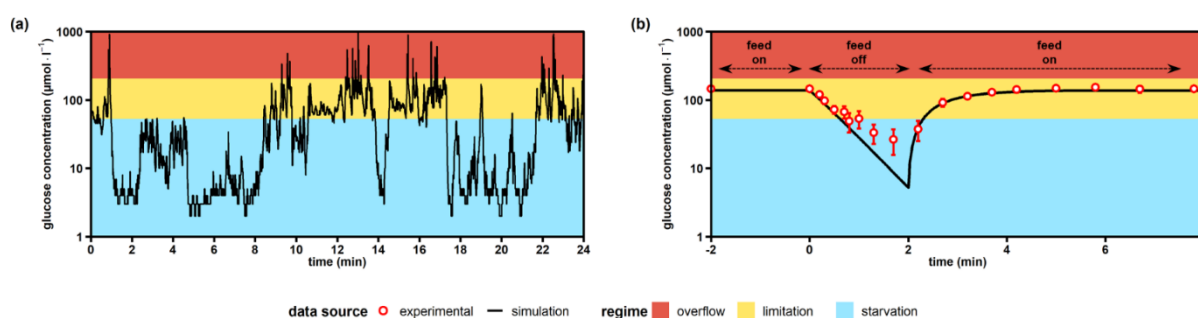
Figure 10. Simulated versus experimental glucose profiles experienced by yeast cells. (a) Exemplary lifeline of a single *S. cerevisiae* trajectory recorded over 24 minutes during an industrial glucose-limited fed-batch process with a biomass concentration of 10 g·L^{-1}. The lifeline was simulated during the work of Sarkizi *et al.* (Sarkizi Shams Hajian *et al.*, 2020), but not published. (b) Stimulus-response experiment as a glucose-limited chemostat with intermittent feed (this work). Extracellular glucose levels are the means ± standard deviation of six biological replicates (merged trends from figure 4). All simulated

values were computed using published glucose uptake kinetics (Diderich *et al.*, 1999). Overflow metabolism is assumed to start at glucose concentrations > 207 µmol·L^{-1} (Marc *et al.*, 2013) and starvation zones develop below 53 µmol·L^{-1} where maintenance demands cannot be covered anymore (Vos *et al.*, 2016).

Process and phenotypic characterization

The haploid *S. cerevisiae* strain CEN.PK113-7D was cultivated in glucose-limited, aerobic chemostats in biological triplicates, each carried out with a dilution rate of 0.1 h^{-1}. Three experimental phases were investigated: (i) The first period operated stably for five residence times serving as reference steady state (RS). (ii) Then, the feed was inactivated once for 120 seconds to install starvation conditions. Subsequently, previous feeds were re-installed and the post-starvation response was tracked for 360 min. (iii) During the third phase, a periodic feed regimen with cycles of 2 min starvation and 7 min limitation was implemented, operating for five residence times to establish a new steady state after dynamic stimuli (DS).

Table 2. Process balances at sample points relevant for this study.

Sample Point	Carbon Recovery (% ± s. d.)	Nitrogen Recovery (% ± s. d.)	Available Electron Recovery (% ± s. d.)
steady state RS	98.8 ± 0.7	102.5 ± 6.5	97.5 ± 0.7
30 min post-stimulus	102.2 ± 1.2	102.8 ± 6.6	100.2 ± 1.2
60 min post-stimulus	97.2 ± 0.6	99.0 ± 3.5	96.4 ± 0.6
120 min post-stimulus	98.6 ± 0.9	98.9 ± 3.5	97.4 ± 0.9
180 min post-stimulus	98.3 ± 0.8	98.9 ± 3.6	97.2 ± 1.0
240 min post-stimulus	98.4 ± 0.5	98.9 ± 3.6	97.3 ± 0.5
360 min post-stimulus	99.0 ± 0.6	101.2 ± 4.6	97.8 ± 0.7
steady state DS	100.7 ± 0.7	101.0 ± 7.8	99.1 ± 1.0

All percentages express means ± standard deviation (s.d.) of three biological replicates. RS, reference steady state; DS, dynamic steady state.

Table 2 lists recoveries of carbon, nitrogen, and available electrons (*ave*) for steady state RS, samples after the first LSL cycle, and for steady state DS. Notably, all balances close within 100 ± 5 %. Except for minor amounts of trehalose and glycerol (data not shown), no by-product formation was detected which agrees with similar studies using CEN.PK113-7D (Suarez-Mendez *et al.*, 2016; Eigenstetter and Takors, 2017). Only acetic acid formation was reported under reference conditions (Suarez-Mendez *et al.*, 2016) which did not occur in our study. The carbon balance of the '30 min post-stimulus' sample is the only significant deviation from the reference steady state (*p*-value < 0.05). In this phase, respiratory dynamics (see next section)

estimated by the mathematical off-gas deconvolution method might have caused a measurement error since both, CO_2 dependent carbon and O_2 dependent *ave* recoveries were affected by the same increase.

Phenotypic characterizations of the steady states RS and DS are presented in table 3. Prominent differences were observed for biomass-specific oxygen demands and carbon dioxide emissions in DS, each rising by 4.3 %. Although $Y_{DMB/glucose}$ and the glucose uptake rate ($q_{glucose}$) remained unchanged in RS and DS, changes of oxygen uptake and carbon dioxide release point towards metabolic re-arrangements. Furthermore, the adapted cells of DS appear to possess a superior cellular integrity, since the leakage of unknown carbon was reduced by 13.4 %, which is an indicator for cell lysis (Roubos *et al.*, 2001).

Summarizing, the comparison of steady state phenotypes hints to elevated ATP needs at DS that are mirrored by increased oxygen uptake and carbon dioxide formation rates. Consequently, time-resolved studies were performed to uncover underlying mechanisms.

Table 3. Yeast kinetics at the steady states RS (reference) and DS (after dynamic perturbation).

Parameter	Dimension	Steady State RS	Steady State DS	Change (%)	Welch Test (p-value)
D	h^{-1}	0.101 ± 0.001	0.100 ± 0.002	n.s.	> 0.05
$Y_{DMB/glucose}$	$g_{DMB} \cdot g_{glucose}^{-1}$	0.494 ± 0.005	0.498 ± 0.002	n.s.	> 0.05
$- q_{glucose}$	$mmol \cdot g_{DMB}^{-1} \cdot h^{-1}$	1.13 ± 0.01	$1.12 \pm 0.02^{*}$	n.s.	> 0.05
$- q_{oxygen}$	$mmol \cdot g_{DMB}^{-1} \cdot h^{-1}$	2.52 ± 0.01	$2.63 \pm 0.04^{*}$	$+ 4.3$	0.03
$q_{carbon\ dioxide}$	$mmol \cdot g_{DMB}^{-1} \cdot h^{-1}$	2.71 ± 0.02	$2.83 \pm 0.04^{*}$	$+ 4.3$	0.02
$Y_{oxygen/glucose}$	$mol \cdot mol^{-1}$	2.23 ± 0.03	$2.34 \pm 0.03^{*}$	$+ 4.9$	0.02
$- q_{ammonia}$	$mmol \cdot g_{DMB}^{-1} \cdot h^{-1}$	0.86 ± 0.04	$0.94 \pm 0.07^{*}$	n.s.	> 0.05
$q_{other\ carbon}$	$mmol_C \cdot g_{DMB}^{-1} \cdot h^{-1}$	0.140 ± 0.008	0.121 ± 0.003	$- 13.4$	0.04

All values represent means $\pm$ standard deviation of three biological replicates. Values marked with an asterisk indicate an averaged parameter over one 9 min perturbation cycle. *DMB*, dry matter of biomass; RS, reference steady state; DS, dynamic steady state; n.s., not significant.

Short-term metabolome relaxation requires 7 minutes after glucose repletion

Metric multidimensional scaling (MDS) plots of the quantified intracellular metabolome and respiratory activity were used as proxy variables to visualize the relaxation pattern of intracellular dynamics in non-adapted and adapted cells. By trend, figure 11a resembles a spiral-type trajectory of metabolites levels converging to the '9 min' spot. Remarkably, late time

points 240 and 360 min do not approximate the reference steady state (0.00 min). This result is rather unexpected since the maximum turnover times for the re-ported metabolites are in the range of $1 \cdot 10^0 - 1 \cdot 10^2$ seconds (Canelas *et al.*, 2008) and thus, two orders of magnitude shorter than the observed time window. Instead, the observation may be taken as a hint on the flexibility of the metabolome enabling similar growth phenotypes with different compositions of intracellular metabolite patterns. Further evidence will be given later. Maybe even more surprising is the continuing phenotype dynamics of oxygen up-take and CO_2 formation during 10–60 min (figure 11c), although the metabolome seems to have already relaxed after converging to the 'attractor' point of the 9-minute sample. Together these results unravel the existence of a first, immediate response to glucose shortage lasting for about 9 minutes and a second, less pronounced dynamic between 10–60 minutes.
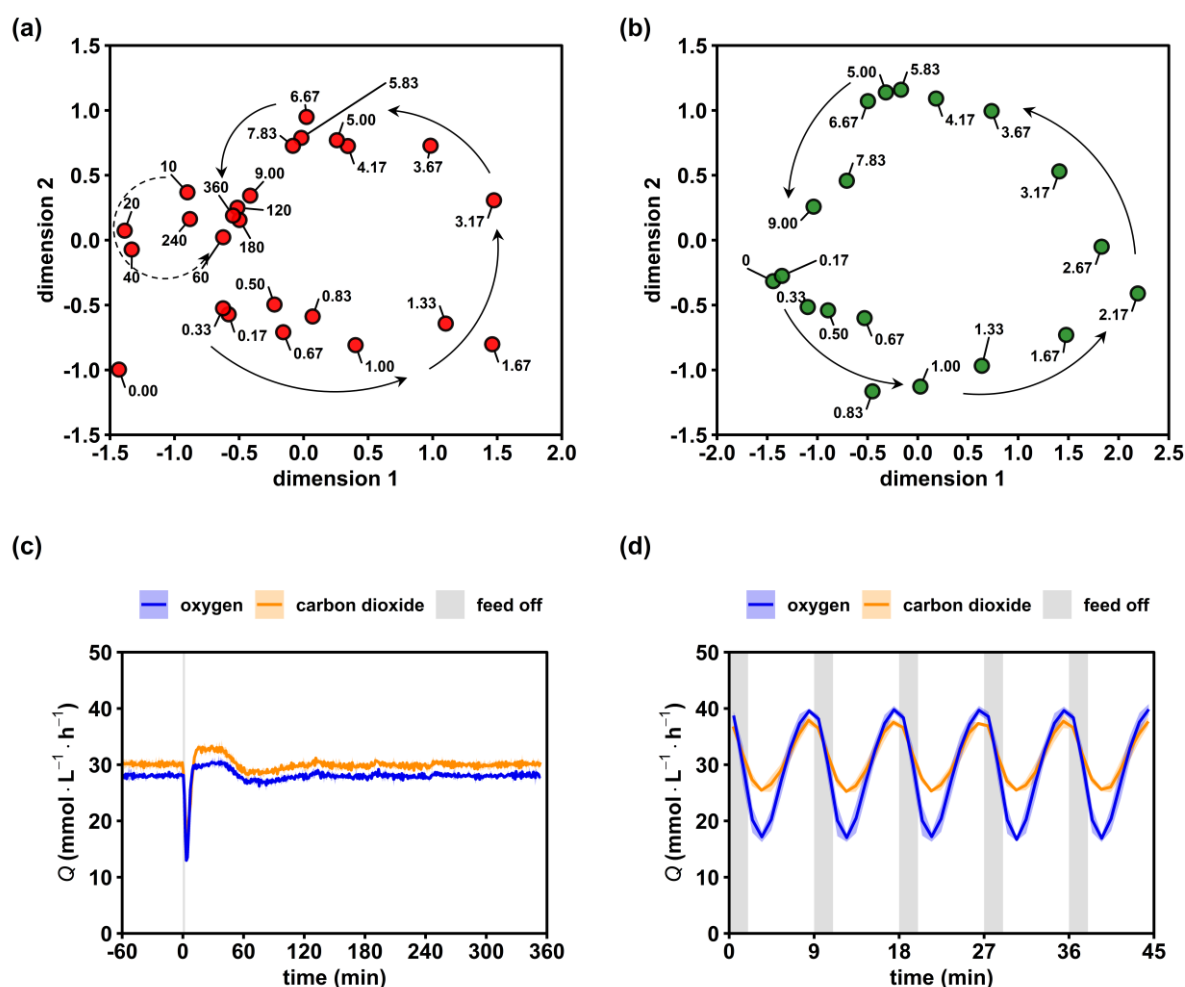
Figure 11. Relaxation of the intracellular metabolome and respiratory activity. (a) Multidimensional scaling (MDS) plot of the non-adapted (red) 6 h time series based on min-max normalized concentrations of 28 intracellular metabolites. Arrows provide a visual aid to follow the short-term (solid) and mid-term (dashed) dynamics (b). Analogous MDS plot of the adapted (green) 9 min time series. (c) Evolutions of the oxygen and carbon dioxide transfer rates after a single starvation transition.

(d) Analogous off gas analysis over 5 perturbation cycles during the dynamic steady state. Text labels in (a) and (b) represent the sample time in minutes. Blue and orange lines in (c) and (d) represent the mean and light areas the respective standard deviation of three biological replicates.

For investigating the adapted response, the final metabolite cycle (figure 11b) after multiple stimulations is expressed in the MDS space. Other than the non-adapted response, we observe no spiral but rather circular 9 min-trajectory without distinct convergence. This reflects the dynamics in the off-gas analysis (figure 11d), showing highly repeatable amplitudes of Q_{oxygen} and $Q_{carbon\ dioxide}$ with 22.8 ± 0.3 mmol·L^{-1}·h^{-1} and 12.3 ± 0.2 mmol·L^{-1}·h^{-1}, respectively. Notably, off-gas dynamics were always observed in biological triplicates lasting for more than 10 cycles (only 5 are shown). The high reproducibility of the phenotype gives rise to the assumption that the metabolite cycles of figure 11b equally repeated in the perturbation series.

Summarizing, results indicate that an observation window of nine minutes covers the first, immediate cellular response on glucose shortage. Differences between the adapted and non-adapted cell response exist that may be elucidated by analysis of intracellular metabolite dynamics.

Short-term dynamics of the central catabolism upon glucose depletion

To elucidate the phenotypic differences shown by non-adapted and adapted cells after exposure to glucose limitation, we investigated the time course of selected intracellular metabolites involved in the glucose catabolism (figure 12).

The central upper glycolysis metabolites glucose-6-phosphate (G6P) and the merged glucose-1-phosphate/fructose-6-phosphate pool (Hex6P) both qualitatively follow the extracellular availability of glucose irrespective of the cellular adaption status. However, a slight overshooting of about 29 % occurred in adapted cells (green) for minimum and maximum G6P compared to the extracellular glucose amplitudes (*p*-value < 0.05). The hexokinase reaction is feedback-inhibited by trehalose-6-phosphate (T6P) (Blázquez *et al.*, 1993; Noubhani *et al.*, 2000) and indeed, on average the T6P pool decreased by 52 % in the adapted yeast population possibly resulting in reduced control over the hexokinase activity. Furthermore, a sharp rise of T6P coincided with peaking G6P levels. Apparently, large G6P pools trigger the carbon drain into the storage compound trehalose via T6P. Interestingly, the total levels of the carbon storage buffers trehalose and glycogen were reduced in adapted versus non-adapted cells by 43 % and 49 %, respectively. As these pool sizes are reported to correlate inversely with the growth rate (Paalman *et al.*, 2003; Francois, Walther and Parrou, 2012), which was kept constant in the

experimental series, the finding was unexpected. Assuming a carbon ratio of 0.04 $mol_C \cdot g_{DMB}^{-1}$ (Canelas *et al.*, 2010), the reduction of the carbohydrate pools should account for a 4 % drop in $Y_{DMB/glucose}$. Because the latter was not observed (table 3), we assume that substantial metabolic re-arrangement should have occurred in adapted cells. Further hints are given by the elevated average concentrations of UDP-glucose (+31 %) in adapted cells. UDP-glucose not only links glycolysis with the carbohydrate storage pools but plays a key role in the anabolism of structural components such as cellulose, β-glucan, glycolipids, and glycoproteins (Yi and Huh, 2015). Consequently, increased UDP-glucose levels may reflect the observed increase in cellular integrity (table 3) of adapted cells.

Regarding the short-term dynamics of the intermediates of the pentose phosphate pathway (PPP), two phases can be observed. Interestingly, they are similar for adapted and non-adapted cells: During the first 2 min of nascent glucose depletion, the trends of 6-phosphogluconic acid (6PGA) and the merged pool of ribose-5-phosphate and ribulose-5-phosphate (P5P) followed the extracellular glucose availability. Then, the recovery to initial pool sizes is delayed and somewhat disconnected from external glucose supply. The observation agrees with findings of Theobald *et al.* and Suarez-Mendez *et al.* who applied glucose pulse experiments (Theobald *et al.*, 1997; Suarez-Mendez *et al.*, 2014). They hypothesized dominating glycolytic flux control over PPP, a conclusion that will be complemented by additional cofactor and sink reaction measurements presented and discussed in figure 13 and figure 14a.

Similar trends of delayed recovery were also observed for fructose-1,6-bisphosphate (FBP). Phosphofructokinase (Pfk) delivering FBP is well known to be inhibited by ATP and citrate (CIT) and activated by ADP, AMP, F6P, and fructose-2,6-bisphosphate (F2,6BP, not quantified) (Teusink *et al.*, 2000; Bárcena *et al.*, 2007). Noteworthy, *in vitro* and *in vivo* studies by van den Brink *et al.* revealed that metabolic regulations of Pfk may be superimposed by upshifting glycolytic fluxes if energy homeostasis is impaired (Brink, 2009). The latter likely occurred during the first 2 min of the experiments (see figure 14a).

Further down in glycolysis, pools of 2- and 3-phosphoglycerate (2/3PG) and phosphoenolpyruvic acid (PEP) showed surprisingly few perturbations irrespective of whether non-adapted or adapted cells were studied. Either related metabolite consumption completely stopped or compensating fluxes occurred. Given the fast turnover rates of said pools typically ranging in seconds, the latter is the likely explanation. Further considering that trehalose and glycogen pool sizes persisted even during the first 2 min of nascent starvation, the start of

gluconeogenesis is a plausible scenario. Pyruvate kinase (Pky) converting PEP+ADP into PYR+ATP is well known to be activated by FBP, which, interesting enough, drops severely by 61 % from 0.36 ± 0.10 µmol·g_{DMB}^{-1} to 0.14 ± 0.02 µmol·g_{DMB}^{-1}. Because of the missing flux downwards, gluconeogenesis is induced (Jurica *et al.*, 1998) causing stable upstream pool sizes.

In the tricarboxylic acid cycle (TCA), intermediates showed similar trends in all conditions. The merged pool of citric acid (CIT) and isocitric acid (ISOCIT) kept constant, whereas the downstream intermediate α-ketoglutaric acid (αKG) mirrored the extracellular glucose shortness of the first 2 min followed by a delayed recovery. This trend is visible in all subsequent TCA-metabolites although dampened with increasing reaction distance to αKG. This finding is in agreement with earlier studies of Mashego *et al.* who performed glucose pulse experiments observing stronger perturbation dynamics of αKG than for CIT (Mashego *et al.*, 2006). Presumably, the trends reflect the mitochondrial export of αKG into the cytosol for oxidative nitrogen fixation in glutamic acid (Gombert *et al.*, 2001). Unfortunately, no dynamic glutamic acid measurements were available in this study.

Taken together, LSL perturbations are propagated on separating time scales through the central metabolic nodes of *S. cerevisiae*. Moreover, the adaption status is most visible in the pool sizes of carbon storage buffers.
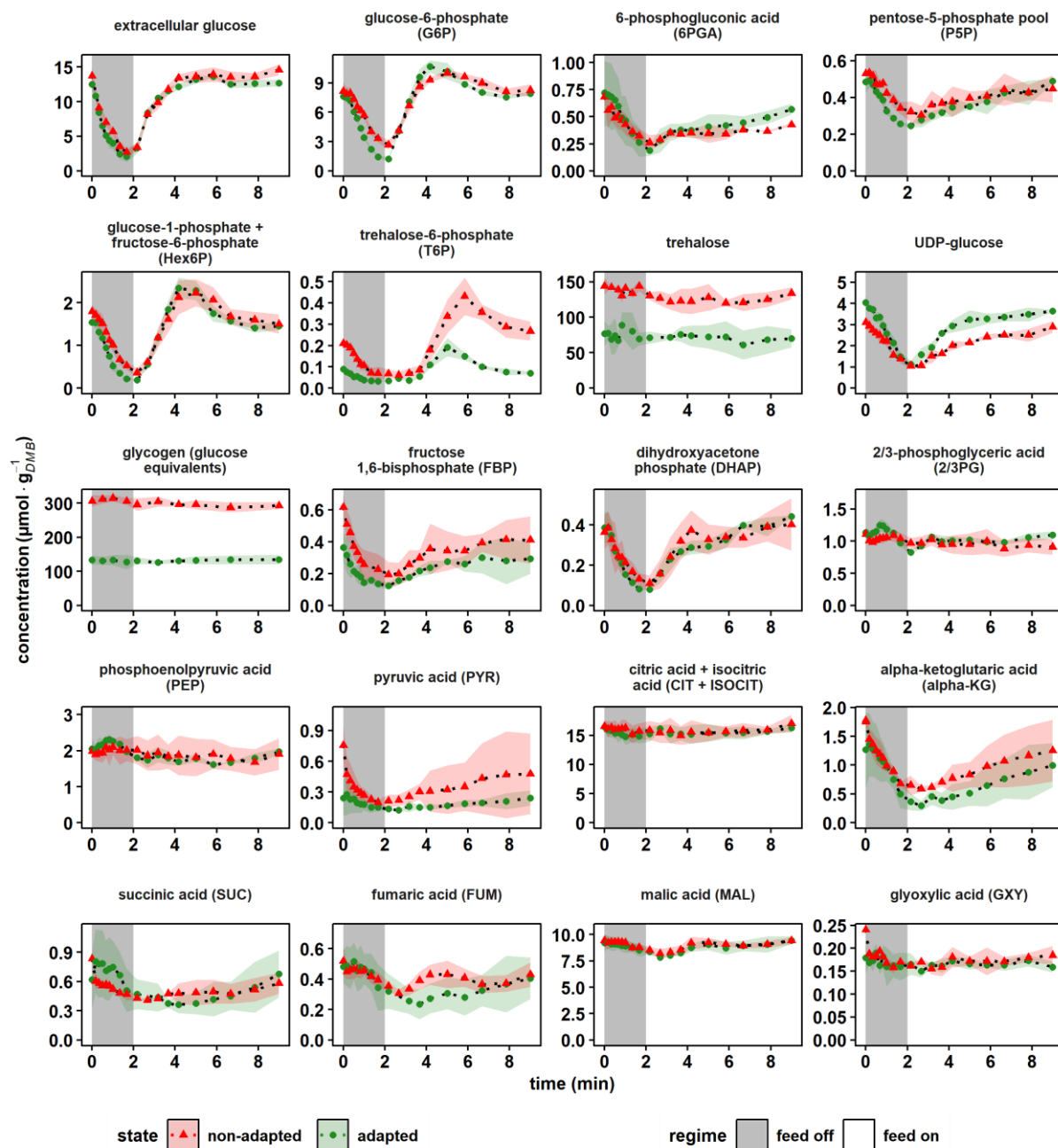
Figure 12. Dynamics of central catabolic metabolites after a 2 min glucose depletion phase. The non-adapted response (red) indicates dynamics following a single transition into a starvation scenario ("feed off" phase) and the adapted response (green) was sampled from representative 9 min cycles during steady state DS. Time point 0 min of the non-adapted response is equal to steady state RS. All values indicate means ± standard deviation of three biological replicates.

Analysis of anabolic and catabolic reduction equivalents

The dynamics of the nicotinamide electron carriers are depicted in figure 13. The upper panel indicates individual concentrations of the anabolic redox pair NADP+, NADPH, their sum and their ratio. By analogy, the catabolic redox state is indicated in the second row.

Regarding anabolic reduction, the total pool size of 0.36 ± 0.00 µmol·g_{DMB}^{-1} and the reductive ratio of 1.28 ± 0.01 measured at reference conditions agree with literature values for CEN.PK113-7D which were observed in glucose-limited chemostat at $D = 0.1\,h^{-1}$ as $0.25-2.17$ µmol·g_{DMB}^{-1} and $0.29-4.86$, respectively (Zhang *et al.*, 2015). By trend, $NADP^+$ pool sizes drop during glucose depletion, both for adapted and non-adapted cells, which leads to rising anabolic reduction charges.

In contrast, NAD^+ concentrations remained virtually unchanged during glucose depletion whereas NADH levels decreased. Interestingly, in the non-adapted scenario, recovery of the NADH pool was not observed within the 9 min time window, but in the adapted case, full relaxation was reached after 5 minutes. However, NADH levelled out at 0.10 ± 0.01 µmol·g_{DMB}^{-1}, which is 43 % less than the reference state at 0.17 ± 0.03 µmol·g_{DMB}^{-1}. The lumped pool size remained stable during the perturbation since only NADH showed dynamics, which only accounts for approximately 4 % of the total pool size. Literature values for the catabolic reduction charge under comparable steady state conditions range from $0.05 - 0.2$ (Visser *et al.*, 2004; Vemuri *et al.*, 2007; Suarez-Mendez *et al.*, 2014) which is somewhat larger than the reference value of 0.046 ± 0.009 measured for the non-adapted yeast. The observation mirrors the 2 fold increased NAD^+ concentrations of this study work versus the respective levels in the cited studies that yielded ratios above 0.1.

Summarizing, the results indicate opposite trends during nascent glucose starvation: While the anabolic reduction state rises, the catabolic drops. Or, in other words: NADPH and NAD^+ levels persist whereas $NADP^+$ and NADH pool sizes drop.
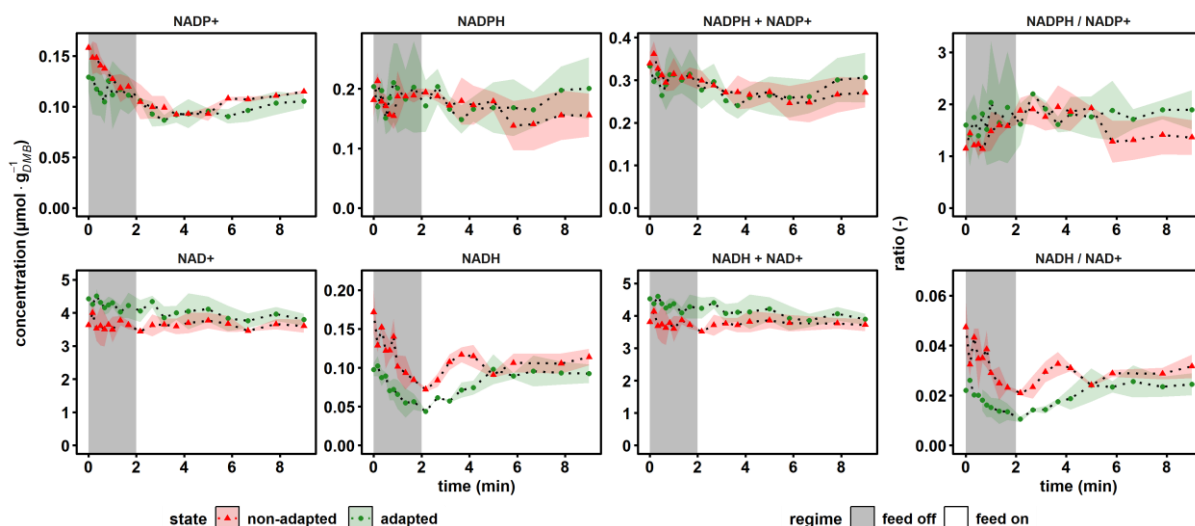
Figure 13. Dynamics of the reduction equivalents, conserved moieties and according ratios. The non-adapted response (red) indicates dynamics following a single transition into a starvation scenario ("feed off" phase) and the adapted response (green) was sampled from representative 9 min cycles during steady state RS. Time point 0 min of the non-adapted response is equal to steady state RS. All values indicate means ± standard deviation of three biological replicates (except for the non-adapted time series, which is derived from two biological replicates).

The adenylate energy charge is quickly regenerated at the cost of total adenylate pool size

Energy carrier homeostasis and nucleotide resource management during dynamic glucose availability were monitored via adenylate and selected purine salvage pathway (PSP) intermediates (figure 14a). The adenylate energy charge (*AEC*) was calculated based on the original approach from Atkinson *et al.* (Ball and Atkinson, 1975). The ATP concentration decreased from 8.12 ± 0.72 µmol·g$_{DMB}^{-1}$ to 3.56 ± 0.16 µmol·g$_{DMB}^{-1}$ and from 5.63 ± 1.54 µmol·g$_{DMB}^{-1}$ to 1.60 ± 0.61 µmol·g$_{DMB}^{-1}$ within 120 s in the non-adapted and adapted scenario, respectively. In the same interval, AMP displayed a sharp 3.9 fold (non-adapted) and 6.6 fold (adapted) peak while ADP first dropped before rising after 30 s with a maximum coinciding with that of AMP. Adenylate energy charges of non-adapted and adapted yeasts showed physiological values of about of 0.90 ± 0.03, which dropped during glucose starvation before recovering again to the initial value. Interestingly, the drop of *AEC* was more pronounced in adapted cells. However, both cells have in common that total AxP pools reduced during glucose starvation and did not fully replenish during the post-starvation period. Apparently, physiological *AEC* values of about 0.9 observed after famine exposure were achieved at the cost of ADP pools that did not recover to the pre-starvation values.

Remarkably, the similar phenotype of *AEC* adjustment at the cost of AxP reduction was reported in glucose pulse studies (Rizzi *et al.*, 1997; Kresnowati *et al.*, 2006; Mashego *et al.*,

2006; Walther *et al.*, 2010). Kresnowati *et al.* and Walther *et al.* hypothesized that nucleotide salvage mechanisms may explain the underlying mechanism of the observation. Adenine nucleotides are shuttled into the PSP via the AMP deaminase (Amd1) reaction yielding inosine monophosphate (IMP), the central intermediate for both, *de novo* and salvage pathways of purines (figure 14b). At this branch point, IMP can either (i) enter a futile cycle where AMP is regenerated at the expense of GTP and aspartate, yielding GDP and fumarate, (ii) be interconverted via inosine (INO) to hypoxanthine (HYX) back to IMP at the expense of Ribose-1-phosphate (R1P) and phosphoribosyl pyrophosphate (PRPP) or (iii) be shuttled towards the guanine salvage branch catalyzed by the NAD^+ dependent IMP dehydrogenase (*Imd2,3,4*) (Walther *et al.*, 2010). Surprisingly, the pattern of IMP under famine conditions rather resembles the oscillatory behavior of ADP than that of the IMP precursor AMP. The IMP levels display a second decline phase after 1 min coinciding with strongly increasing inosine and hypoxanthine levels. The latter accumulated to their maximum concentrations about 1 min later than AMP, their common upstream intermediate. Interestingly, INO pools of non-adapted cells remained 1.6-fold elevated compared to the pre-starvation condition. This may be interpreted as a 'memory' effect that is not shown by adapted cells.
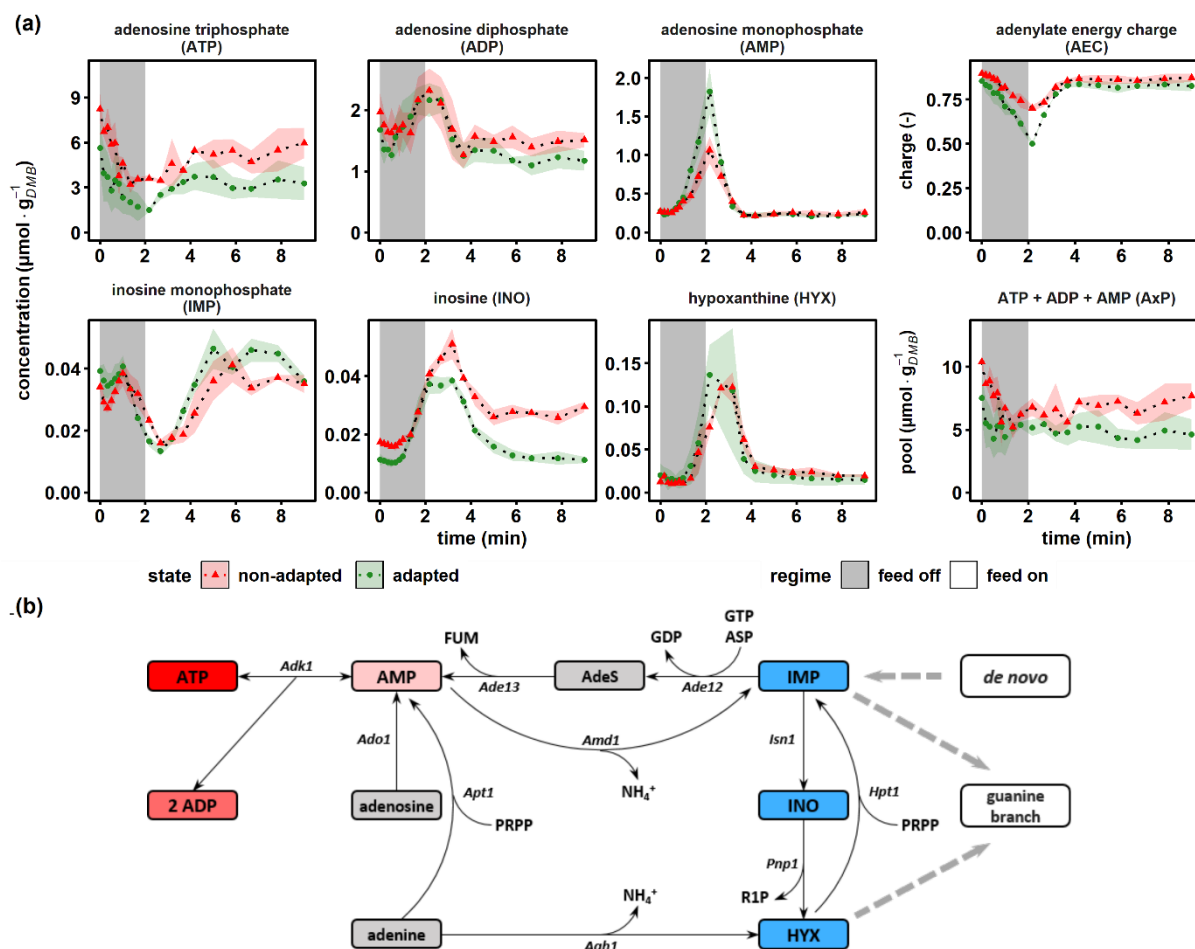
Figure 14. Dynamics of energy carriers and intermediates of the purine salvage pathway. (a) The non-adapted response (red) indicates dynamics following a single transition into a starvation scenario ("feed off" phase) and the adapted response (green) was sampled from representative 9 min cycles during steady state DS. Time point 0 min of the non-adapted response is equal to steady state RS. The adenylate energy charge was calculated according to (Ball and Atkinson, 1975). All values indicate means ± standard deviation of three biological replicates. (b) Schematic representation of the adenylate kinase system attached to the purine salvage pathway, reproduced from (Walther *et al.*, 2010; Pinson *et al.*, 2019). Aah1, adenine deaminase; Ade12, adenylosuccinate synthase; Ade13, adenylosuccinate lyase; AdeS, adenylosuccinate; Adk1, adenylate kinase; Ado1, adenosine kinase; Amd1, AMP deaminase; Apt1, adenine phosphoribosyl transferase; ASP, aspartate; FUM, fumarate; Hpt1, hypoxanthine-guanine phosphoribosyl transferase; Isn1, IMP-specific 50-nucleotidase; Pnp1, purine nucleoside phosphorylase; PRPP, phosphoribosyl pyrophosphate; R1P, Ribose-1-phosphate.

61

4.1.4 Discussion

Decreased glucose uptake kinetics

Several reports have shown that variable substrate availability is a fundamental scale-up effect causing observed strain performance losses in industrial fed-batch processes (Fowler and Dunlop, 1989; Noorman *et al.*, 1993; Bylund *et al.*, 1998; George *et al.*, 1998). The investigated case of glucose limited *S. cerevisiae* CEN.PK113-7D exemplifies the cellular responses at $\mu = 0.1$ h^{-1} when the substrate concentration c_S is 10 fold lower than the affinity constant K_M of the most efficient hexose transporters Hxt6 and Hxt7 (Reifenberger, Boles and Ciriacy, 1997; Diderich *et al.*, 1999). If $c_S \ll K_M$, glucose uptake kinetics are proportional to extracellular concentrations (Boender *et al.*, 2009), which may explain the observed deviation between predictions based on hyperbolic kinetics and the experimental observation in our study (figure 10) and in other works (Suarez-Mendez *et al.*, 2014). This discrepancy could be attributed to the presence of a secondary source of extracellular glucose in the form of exported trehalose. The disaccharide is hydrolyzed in the extracellular space by the free acid trehalase Ath1, which has an optimum at the operated pH of 5.0 (Jules *et al.*, 2008). Comparable fermentation studies investigating ^{13}C labeling patterns traced the presence of unlabeled glucose to trehalose breakdown. Furthermore, there are several other theoretical indications to consider, such as decoupled glucose uptake and sensing (Youk and Van Oudenaarden, 2009) or the inhibition of glucose uptake by intracellular glucose (Teusink *et al.*, 1998) concomitant with glucose secretion due to the reversibility of facilitated diffusion (Bosdriesz *et al.*, 2018). Thus, several aspects of glucose transport and even additional source reactions must be considered for optimal glucose characterization at the boundary of starvation, as they can play an important role in computing realistic large-scale simulations.

Exposure to starvation revealed different tactics of reserve management

Macroscopic observations indicated the emergence of a new growth phenotype of adapted cells compared to non-adapted cells. The first managed to maintain the same biomass/substrate yield while respiratory activity rose and carbon storage pools remained on a lower but constant level. Given that carbon dioxide emission rates of adapted cells increased by about 4.3% while glucose uptake rates kept constant, one may anticipate a likewise dip of $Y_{DMB/\text{glucose}}$ that did not occur. Therefore, the cells should have found alternative resource allocation possibilities targeting proteins. The hypothesis is consistent with strongly reduced amino acid pools (table A2) and an observed 9 % increase of the ammonia uptake rate during the dynamic steady state

(table 3). In general, rearrangement of the cellular composition is a fundamental strategy of *S. cerevisiae* to adjust to new environmental conditions through balancing growth against maintenance (de Alteriis *et al.*, 2018). Fast growth, for instance, is accompanied by high ribosomal contents tapping into storage carbohydrates to ensure anabolic needs (Nissen *et al.*, 1997; Woolford and Baserga, 2013). A similar cellular strategy is revealed in the current study, most likely to support increased maintenance demands rather than to elevate growth. Indeed, estimating q_{ATP} assuming a P/O ratio of 1.08 yields a significant 2.7 % increased ATP demand in adapted cells (Van Den Brink *et al.*, 2008).

Considering intracellular metabolite pool sizes, differences between the adapted and non-adapted states mirror the adaptation of the yeast to cultivation conditions. Prolonged carbon limited chemostat cultivations by Mashego and Jansen *et al.* (Jansen *et al.*, 2005; Mashego *et al.*, 2005) already revealed decreasing pool sizes of max. 20 % after 10 generations that were interpreted as the consequence of selection pressure. The present study also encompassed about 10 generations between steady states RS and DS. Consequently, minor pool size reductions < 20 % should be ignored to separate effects of long-term growth selection from the results of metabolic re-arrangement because of the dynamic stimuli. Still, key findings outlined above should be valid. For instance, trehalose and glycogen pool reductions are likely to be a consequence of the repeated exposure to famine conditions. This makes sense from an economic point of view given the relatively high contribution of both pools towards ATP dissipation via futile cycling (Suarez-Mendez *et al.*, 2016). Another evidence towards a more energy saving mode in adapted cells was derived from the 2-fold increased AMP peak compared to non-adapted yeast. High AMP levels activate the Pfk enzyme while simultaneously inhibiting the reverse reaction catalyzed by FBP and consequentially reduce further ATP dissipation in the F6P-FBP futile cycle (Navas and Gancedo, 1996). Hence, during adaption the non-growth associated ATP usage appeared to be increased and rebalanced for supporting other maintenance components than energy buffering.

There remains the question of which relationship elicits the emerging new phenotype when the same net rates of growth and substrate uptake prevail. As mentioned earlier, glucose uptake and sensing are decoupled processes in *S. cerevisiae* (Youk and Van Oudenaarden, 2009). Zaman *et al.* characterized the transcriptional response of conditional mutants against different glucose sensing scenarios. The authors concluded that extracellular glucose sensing can indeed induce strong phenotypic changes, while the same net influx of glucose prevails (Zaman *et al.*, 2009). Whether decoupled substrate uptake and sensing explains the present observation should be

addressed in future research to fully understand the regulatory mechanisms that shape the industrial phenotype.

The cellular strategy to ensure anabolic demands

The concentration profiles of most intermediates of the upper glycolysis and tightly linked metabolites followed the decline of extracellular glucose levels. However, during the transition from starvation back to the new steady state, time scales of pool relaxation were partially decoupled from glucose availability. The differences of recovery dynamics reflect different flux patterns that apparently mimic cellular needs. For instance, the PPP reaches pre-perturbation levels 4 minutes later than its precursor G6P. Considering that steady state glycolytic flux is about 20 fold larger than the branching flux into PPP (Suarez-Mendez *et al.*, 2016) its pools needed longer to recover. Apparently, this reflects the cellular program to prioritize catabolic over anabolic activity. Saliola and colleagues reported that most eukaryotic G6P dehydrogenases (Zwf1 in *S. cerevisiae*) possess both a catalytic binding site for $NADP^+$ and an allosteric binding site for NADPH (Saliola *et al.*, 2012). This allows the cell to drain fluxes towards glycolytic catabolism, thereby gaining ATP either via Zwf1 inhibition under NADPH excess or via $NADP^+$ limitation. Apparently, the second occurred during the SRE experiments.

Interestingly, neither trehalose nor glycogen pools were degraded during the short-term exposure to glucose starvation. This is in line with previous observations, where short term glucose perturbations on the same time scale did not change glycogen (Suarez-Mendez, Ras and Wahl, 2017; Weber *et al.*, 2020) or trehalose concentrations (Suarez-Mendez, Ras and Wahl, 2017), even though rapid trehalose mobilization is anticipated in the literature (Thevelein, 1984). This disagreement may be explained as follows: cytosolic trehalase is dependent on activation via a cAMP-dependent post-translational modification (PTM) cascade yielding its phosphorylation (Thevelein, 1984). However, the adenylate cyclase Cyr1 in CEN.PK113-7D carries a mutation that causes a delay in trehalose and glycogen mobilization (Nijkamp *et al.*, 2012). Consequentially, the short-term persistence of glycogen and trehalose pools may be a distinct feature of the current strain, and may be different in other genotypes that have not been selected after growth evolution.

Intracellular metabolite dynamics were less pronounced in lower glycolysis and in TCA. In some cases, high variance additionally hindered a statistically sound interpretation (*e.g.* for PYR). However, the quick reduction of the catabolic reduction charge under famine conditions might be the consequence of a reduced flux into the TCA since the onset of gluconeogenesis

was observed. In essence, reactions generating NADH such as oxoglutarate decarboxylase (Ogdc), isocitrate (Idh) and malate dehydrogenases (Mdh) were reduced. With the missing influx, pools of αKG reduced quickly, indicating that the drain into amino acid synthesis and the production of glutamate remained. Notably, αKG may be regarded as an alarmone being at the intersection of oxidative carbon and nitrogen metabolism. The reductive amination to form glutamate is tightly controlled by the redox status of the $NADP^+/NADPH$ couple (Ljungdahl and Daignan-Fornier, 2012). Considering the rising $NADPH/NADP^+$ ratio (figure 13), glutamate formation was likely to continue even during famine conditions. Together with the observation of falling $NADH/NAD^+$ ratios, the conclusion could be drawn that the yeast favors anabolism for the sake of catabolism under short-term carbon starvation.

Ultimately, decreasing catabolic reduction power impaired energy homeostasis due to an imbalance in the electron transport chain. With reducing glycolytic fluxes, ATP gain via respiration got even more important under famine conditions. Consequently, falling NADH supply is proportionally reflected in likewise falling ATP levels. The increasing ADP:ATP ratio pushes the adenylate kinase 1 (Adk1) away from its equilibrium to catalyze the conversion of ADP to ATP and AMP (Hardie, Ross and Hawley, 2012). This correlation might also explain the larger AMP peak in adapted cells since the ADP:ATP ratio is increased by approximately 15 % compared to non-adapted cells. AMP accumulation is prevented via removal towards INO via IMP using the purine salvage pathway. As no obvious regulatory roles could be assigned to IMP and INO so far, Walther and colleagues suggested that AMP is shuttled to PSP to reduce its regulatory impact, which may partially explain the delayed regeneration of the AxP pool after stress relief (Walther *et al.*, 2010).

Consequences for production scenarios with *Saccharomyces cerevisiae*

Dynamic environments in industrial-scale bioreactors can induce manifold cellular responses. Carbon limited fed batch processes typically operate at carefully designed substrate supply optima, which could be easily inferred once cells enter zones of substrate depletion. The latter often occur far away from the feed inlet (Haringa *et al.*, 2017) or in areas with poor mixing. The current study identified a number of intracellular responses that have the potential to impair the yeast performance in large-scale production scenarios. For instance, dynamic extracellular LSL transitions caused the emergence of a new phenotype with possible implications in recombinant protein production. Increased maintenance demands could directly compete with energetic demands for protein production in the form of an added metabolic burden (G. Wu *et*

al., 2016). Another point to consider might be the failure of cellular buffering capacities to counterbalance rapid substrate perturbations. For instance, delayed trehalose or glycogen mobilization to maintain glycolytic flux could result in a dynamic redox state. Celton *et al.* reported a negative impact of aberrant NADPH homeostasis on the production of aromatic molecules (Celton *et al.*, 2012). In addition, a dynamic NAD^+/NADH ratio is constantly monitored via Sir2 in yeasts that can trigger pronounced transcriptional dynamics with possible impacts on different metabolic routes for several production scenarios (Nielsen, 2019). Knowledge concerning dynamics of specific signaling compounds can also shed light on process performance. Alpha-ketoglutaric acid has recently been characterized as a master regulator in *E. coli*, and its role in the yield reduction of recombinant protein production was discussed by Zhang *et al.* (Zhang, Herik and Wahl, 2020).

Thus far, this study has revealed biological feedback of yeast cells on a specific perturbation. Follow-up work will use this finding and complementary datasets to generate models that allow more realistic predictions of the cellular response towards industrial stimuli, with a view to enabling *a priori* identification of biological scale-up effects.

4.1.5   Material and methods

Strain, pre-cultures and medium

The haploid, prototrophic *S. cerevisiae* model strain CEN.PK113-7D (Nijkamp *et al.*, 2012) was used in this study and kindly provided by Royal DSM N.V. (Delft, The Netherlands). Cells were stored at −70 °C in 1 mL aliquots supplemented with 30 % (v/v) glycerol. For each experiment, yeast extract peptone dextrose (YPD) agar plates were prepared by streaking cells directly from the frozen glycerol stock and incubating for two days at 30 °C. Single colonies were picked and suspended with 5 mL YPD broth in a culture glass vial. The vials were mounted at a 45 ° angle on an orbital shaker and incubated for 8 h at 30 °C with 120 revolutions per minute. Subsequently, the cultures were pelleted and inoculated in shake-flask cultures with 110 mL adjusted Verduyn medium (Verduyn *et al.*, 1992) and incubated over night at 30 °C on an orbital shaker with 120 revolutions per minute. To support carbon limited growth in chemostat conditions with 22.5 $g \cdot L^{-1}$ glucose, the medium was designed as follows: ammonium sulfate $((NH_4)_2SO_4)$ 15.0 $g \cdot L^{-1}$, monopotassium phosphate (KH_2PO_4) 9.0 $g \cdot L^{-1}$, magnesium sulfate heptahydrate $(MgSO_4 \cdot 7\ H_2O)$ 1.5 $g \cdot L^{-1}$, ethylenediaminetetraacetic acid $((CH_2N(CH_2CO_2H)_2)_2)$ 38.22 $mg \cdot L^{-1}$, zinc sulfate heptahydrate $(ZnSO_4 \cdot 7\ H_2O)$ 9.00 $mg \cdot L^{-1}$, manganese(II) chloride tetrahydrate $(MnCl_2 \cdot 4\ H_2O)$ 2.00 $mg \cdot L^{-1}$, cobalt(II) chloride hexahydrate $(CoCl_2 \cdot 6\ H_2O)$ 0.60 $mg \cdot L^{-1}$, copper(II) sulfate pentahydrate $(CuSO_4 \cdot 5\ H_2O)$ 0.60 $mg \cdot L^{-1}$, sodium molybdate dihydrate $(NaMoO_4 \cdot 2\ H_2O)$ 0.80 $mg \cdot L^{-1}$, calcium chloride dihydrate $(CaCl_2 \cdot 2\ H_2O)$ 9.00 $mg \cdot L^{-1}$, Iron(II) sulfate heptahydrate $(FeSO_4 \cdot 7\ H_2O)$ 6.00 $mg \cdot L^{-1}$, boric acid (H_3BO_3) 2.00 $mg \cdot L^{-1}$, potassium iodide (KI) 0.20 $mg \cdot L^{-1}$, D-biotin $(C_{10}H_{16}N_2O_3S)$ 0.10 $mg \cdot L^{-1}$, calcium pantothenate $(C_{18}H_{32}CaN_2O_{10})$ 2.00 $mg \cdot L^{-1}$, nicotinic acid $(C_6H_5NO_2)$ 2.00 $mg \cdot L^{-1}$, myo-inositol $(C_6H_{12}O_6)$ 50.00 $mg \cdot L^{-1}$, thiamine HCl $(C_{12}H_{18}Cl_2N_4OS)$ 2.00 $mg \cdot L^{-1}$, pyridoxine HCl $(C_8H_{12}ClNO_3)$ 2.00 $mg \cdot L^{-1}$ and para-aminobenzoic acid $(C_7H_7NO_2)$ 0.40 $mg \cdot L^{-1}$.

Bioreactor and chemostat setup

Aerobic, carbon-limited chemostat cultivations were carried out in a 3 L stainless steel benchtop bioreactor (Bioengineering, Wald, Switzerland) with a working volume of 1.7 L. The reactor was equipped with two six-blade Rushton-type impellers, four baffles, and sensors for pH (Mettler Toledo, Columbus, USA), pO_2 (PreSens, Regensburg, Germany), temperature and pressure (both Bioengineering, Wald, Switzerland). The system was operated with an overpressure of 0.3 bar, pH was controlled at 5.00 with 2 M KOH, the temperature was kept at

$30\,°C$ and aerobic conditions were maintained with bottled, ambient air supplied with $0.8\ NL\cdot min^{-1}$ and bubbles were dispersed with an impeller speed of 800 rpm. Foaming was prevented throughout the process by a continuous supply of Struktol J 674 antifoam (Schill und Seilacher, Hamburg, Germany) with a pump rate of $30\ \mu L\cdot h^{-1}$. Oxygen and carbon dioxide fractions in the off-gas were logged every minute with $BCP-O_2$ and $BCP-CO_2$ sensors (BlueSens, Herten, Germany).

Each process was initiated as a batch fermentation by inoculating 1.6 L adjusted Verduyn medium with 0.1 L of an overnight shake-flask culture. Glucose depletion was monitored based on a sharp increase of the pO_2 signal, which was followed by switching to chemostat conditions. The system was operated at a dilution rate of $0.1\ h^{-1}$ with two U-120 peristaltic pumps (Watson-Marlow, Falmouth, UK). The feed pump was operated continuously at $2.83\ mL\cdot min^{-1}$ and the harvest pump was controlled at a higher speed relative to the feed pump via mass balancing of the bioreactor. The feed medium was continuously stirred with a magnetic stir bar to avoid gradient formation in the feed casket and the dilution rate was monitored based on the mass balance of the feed reservoir.

Stimulus-response experiment

Reference steady state samples were drawn after five residence times with constant off-gas signals. The non-adapted response was induced by a single transition into a non-fed regime by switching off the feed pump for 2 minutes, followed by a continuation of the previous chemostat regime. The biological response was characterized with the below-mentioned methods for up to six hours post-stimulus. Subsequently, the feeding regime was switched to an intermittent feed. The feed pump was switched off for two minutes and switched on for seven minutes repetitively, resulting in nine-minute regime transitioning cycles. During the feed phase of every cycle, the feed rate was adjusted to $3.64\ mL\cdot min^{-1}$ to maintain an average dilution rate of $0.1\ h^{-1}$. After five residence times in the intermittent feeding regime, a dynamic steady state was assumed and samples representing the adapted response were drawn. The whole chemostat process was not operated for more than 15 residence times to avoid the occurrence of laboratory evolution effects (Jansen *et al.*, 2005).

Sampling

The bioreactor was equipped with two custom-made, semi-automated sampling devices. For each sample port, a stainless-steel broach needle (Bioengineering, Wald, Switzerland) was connected via a septum with the bioreactor and the exit was extended with a silicon tube with

an inner diameter of 0.5 mm. The tube was closed with a pinch valve (model: S105, ASCO/Sirai, Bussero, Italy) to allow sampling of precise volumes enabled via time-relay-controlled valve opening (time relay model: FSM10, Tele Haase Steuergeräte, Vienna, Austria). Each sampling device was calibrated during reference steady state conditions for each biological replicate separately and the volume deviation from the set point of five replicates for volumes between 1−5 mL was always below 2 %. All samples were drawn after discarding the dead volume of 300 µL.

Cultivation broth samples for biomass and carbon balancing were briefly chilled on ice for degassing of the broth before distributing adequate volumes for each method.

Extracellular supernatants were obtained by directly sampling into a syringe equipped with a PES filter (Ø 30 mm, 0.22 µm pore size, ROTILABO®, Carl Roth, Karlsruhe, Germany) and the filtrate was collected within 5 s and stored at −70 °C.

Defined biomasses for intracellular metabolic analysis were withdrawn according to an adapted and sequential protocol employing rapid cold-methanol quenching and methanol-chloroform extraction (Koning and Dam, 1992). Following procedure: 1.5 mL cultivation broth was directly injected into 10 mL methanol cooled down to −40 °C and immediately centrifuged at 5000 g for 5 min at −11 °C. Samples were thoroughly decanted, flash-frozen and stored at −70 °C until extraction. During high-frequency sampling periods (initial perturbation phase, up to Δt = 540 sec) quenched cultivation broths were interim stored at −40 °C in a cryostat (RK20, Lauda, Lauda-Königshofen, Germany) for a maximum time of 5 min to prevent metabolite leakage (Canelas *et al.*, 2008). The frozen cell pellets were resuspended in pre-cooled (−20 °C) extraction buffer consisting of 50 % v·v^{-1} aqueous methanol solution, 100 mM ammonium acetate (pH 9.2), 2.5 mM 3-mercaptopropionic acid and 100 µM L-norvaline as internal standard (extraction). Added volumes were adjusted to achieve constant biomass concentrations (8.5 g·L^{-1}) and the sample temperature was kept below −20 °C by rotational mixing (Δt = 30 s) and chilling in a cryostat (−40 °C) during complete resuspension. Next, the same volume of pre-cooled (−20 °C) chloroform was added and the mixed suspension was incubated for 2 h at −20 °C and 1 h at room temperature in a rotary overhead-shaker. Afterwards, the samples were centrifuged at 20000 g for 10 min at 4 °C and the upper aqueous methanol phase containing polar metabolites was carefully removed and stored at −70 °C until measurement.

Off-gas deconvolution

A prerequisite for proper off-gas analysis in stimulus-response experiments is a suitable approach for signal deconvolution. Long tubing lines and foam traps between fermenter and sensors lead to the formation of mixing chambers causing a sensor delay of several minutes and increased apparent time constants versus the reported 55 s for $BCP-O_2$ and $BCP-CO_2$ sensors (Pepper, 2015). Step experiments were carried out under experimental conditions with H_2O as a broth substituent to identify delay times and time constants for each sensor. Correction of the O_2 and CO_2 signals during the stimulus-response experiments was computed based on the methodology by Theobald et al. (Theobald, 1995). For a complete description of the step experiments and mathematical deconvolution approach, the reader is referred to appendix A.

Dry matter of biomass determination

Triplicated 5 mL volumes were vacuum-filtered through dried and tared PES membrane disc filters (Ø 47 mm, Type 154, Sartorius, Göttingen, Germany). Filters were subsequently washed with 15 mL demineralized water and dried at 70 °C until mass constancy was observed. Finally, filters with biomass cakes were brought to room temperature in a desiccator and were weighed again. The calculated weight of the biomass cake was normalized to the sample volume and expressed as dry matter of biomass (*DMB*).

Extracellular metabolite quantification

Frozen supernatant samples were thawed on ice and glucose was measured using a UV-based enzyme test kit (Art. No.: 10716251035, r-biopharm AG, Darmstadt, Germany). The free ammonium concentration was quantified with the LCK302 cuvette test kit (Hach Lange, Düsseldorf, Germany). Each kit was performed according to the manufacturer's instructions on a spectrophotometer (DR 3900, HACH, Colorado, USA). Unknown extracellular carbon was calculated based on an organic carbon balance of broth supernatant using a total carbon analyzer (Multi N/C 2100s, AnalytikJena, Jena, Germany).

Determination of intracellular carbohydrate storage pools

Intracellular glycogen and trehalose levels were determined based on the protocols reported by Parrou *et al.* and Suarez-Mendez *et al.* (Parrou and Francois, 1997; Suarez-Mendez, 2015). Frozen pellets were resuspended in 250 µL 0.25 M sodium carbonate and incubated for 3 h at 95 °C. Subsequently, the pH was adjusted to 5.5 by addition of 150 µL 1 M acetic acid and 600 µL 0.2 M sodium acetate (pH 5.2, adjusted with acetic acid). The sample was split into a

480 µL and a 466 µL aliquot. The first was treated with 20 µL of α-amyloglucosidase (~70 U·mL^{-1}, catalog number: 10115, Merck, Darmstadt, Germany) at 57 °C overnight to determine glycogen expressed as liberated glucose equivalents. For trehalase determination, the pH of the 466 µL aliquot was adjusted slightly upwards by the addition of 30 µL of 0.2 M sodium acetate and trehalose was hydrolyzed to glucose by the addition of 4 µL trehalase (2.27 U·mL^{-1}, catalog number: T8778, Merck, Darmstadt, Germany) and incubated at 37 °C overnight. Glucose equivalents were measured with the UV-based enzyme test kit (Art. No.: 10716251035, r-biopharm AG, Darmstadt, Germany).

Determination of intracellular metabolites measured via LC-MS/MS

Quantitative metabolome analysis of intracellular *S. cerevisiae* extracts were conducted on an Agilent 1200 HPLC system coupled with an Agilent 6410B triple quadrupole (QQQ) mass spectrometer with a classical electrospray ionization (ESI) interface.

Analytical preparation of sample extracts and chromatographic separation of non-derivatized polar metabolites by alkaline polymer-based zwitterionic hydrophilic interaction chromatography (ZIC-pHILIC) were performed as previously described (Feith *et al.*, 2019; Frank, Teleki and Jendrossek, 2020). Defined standard mixtures and samples with adapted dilution containing 50 µM 2-keto-3-deoxy-6-phosphogluconate (KDPG) and α-amino isobutyric acid (AIBA) as global internal standard (measurement) were injected (5 µL) onto a Sequant ZIC-pHILIC column (150 × 2.1 mm, 5 µm, Merck Millipore, Darmstadt, Germany) equipped with a guard column (20 × 2.1 mm, 5 µm, Merck Millipore, Darmstadt, Germany) maintained at 40 °C.

Analogue measurements of previously derivatized (phenylhydrazine) α-keto acids (αKG, PYR, GXY) were performed by an adapted LC-MS/MS protocol (Zimmermann, Sauer and Zamboni, 2014) using 50 µM α-ketovalerate as internal standard (derivatization/measurement). Derivatized analytes were separated under acidic conditions (pH 3.0) by reverse phase liquid chromatography (RPLC) (Junghans *et al.*, 2019). Samples were injected (5 µL) onto a ZORBAX SB-C18 column (150 × 4.6 mm, 5 µm, Agilent Technologies, Waldbronn, Germany) with a guard column (12.5 × 4.6 mm, 5 µm, Agilent Technologies, Waldbronn, Germany) maintained at 40 °C.

Targeted metabolites were detected with high selectivity in multiple reaction monitoring (MRM) mode using established and pre-optimized precursor-to-product transitions and MS/MS parameters with a mass resolution of 0.1 u. Intracellular metabolite pools were absolutely

quantified by a three-fold standard addition of defined amounts of reference standard mixes (internal calibration). Applied amounts were adjusted according to previously estimated concentration levels and linear dynamic ranges of the targeted metabolites (Wijaya *et al.*, 2021). The absolute concentration levels of the AxP species were normalized to results from a reference method (Eigenstetter and Takors, 2017) to compensate for known HILIC-specific peak tailing effects in iron-based LC systems (Wakamatsu *et al.*, 2005). The normalization factors (ATP: 2.71, ADP: 1.88 and AMP: 1.21) were calculated from analogues steady state RS samples and were applied conformably.

Characterization of the endometabolome relaxation pattern

A classical, metric multidimensional scaling approach (Gower, 1966) was chosen to quantify and visualize dissimilarities between the different time points. Concentrations of all 29 intracellular metabolites except pyruvic acid were considered and min-max normalized. In the next step, the Euclidean distance matrix was computed with the function *dist* and used as an input for *cmdscale*, which was limited to a two-dimensional representation of the sample distances ($k = 2$). All computations were executed in the R environment (version 1.4.1106) with the package *stats* (version 4.1.0).

Total carbon and nitrogen determination

One milliliter fermentation broth was mixed with 9 mL 36.84 mM KOH to prevent loss of inorganic carbon in the form of dissolved carbonate. Next, the 1:10 diluted sample was measured in octuplicate and undiluted supernatant (also stabilized with 36.84 mM KOH) was measured in quadruplicate with a multi N/C 2100 S composition analyzer (Analytik Jena, Jena, Germany). The system was calibrated according to the method of Buchholz *et al.* (Buchholz *et al.*, 2014). Nitrogen concentrations were directly measured and organic carbon was determined based on the difference between the total carbon and the inorganic carbon fractions.

4.1.6 Conclusion

This study set out to investigate the response of *S. cerevisiae* during industrially relevant transitions between carbon limitation and starvation, and back. Intracellular metabolite analysis provided a solid dataset for future modeling efforts and revealed distinct phenomena that help to explain biological scale-up effects. The experimental design allowed the observation of several dynamics from allosteric control of specific intermediates to global phenotypic changes as a response to the applied substrate gradient. In particular, a distinct mode was uncovered where yeasts sacrifice catabolic reduction power to sustain ongoing anabolic demands under acute carbon starvation conditions. A natural progression of this work is to expand the obtained knowledge by analyzing gene expression dynamics to investigate (i) if and how metabolic stimuli are propagated in cells exposed to an industrially relevant famine perturbation and (ii) to use the obtained data for setting up data-driven models for rational scale-up/scale-down.

4.2 Performing in spite of starvation: How *Saccharomyces cerevisiae* maintains robust growth when facing famine zones in industrial bioreactors

The manuscript was written by Steven Minden as first author. Prof. Dr.-Ing. Ralf Takors contributed to the manuscript's content through principal review. Prof. Dr.-Ing. Ralf Takors is the corresponding author. Steven Minden planned and conducted all experiments, collected and analyzed the according primary data. Maria Aniolek supported during fermentation experiments. Prof. Dr.-Ing. Ralf Takors supervised the research. Prof. Dr. Henk Noorman contributed to the manuscript by reading and approving the final version.

This manuscript was accepted by Applied Microbiology International and published in the journal *Microbial Biotechnology*.

Citation:

Minden S, Aniolek M, Noorman H, & Takors R. Performing in spite of starvation: How *Saccharomyces cerevisiae* maintains robust growth when facing famine zones in industrial bioreactors. *Microbial Biotechnology*. 2023; 16 (1); 148−168. https://doi.org/10.1111/1751-7915.14188

Data repository:

https://doi.org/10.34894/XAZFCN

4.2.1 Abstract

In fed-batch operated industrial bioreactors, glucose-limited feeding is commonly applied for optimal control of cell growth and product formation. Still, microbial cells such as yeasts and bacteria are frequently exposed to glucose starvation conditions in poorly mixed zones or far away from the feedstock inlet point. Despite its commonness, studies mimicking related stimuli are still underrepresented in scale-up/scale-down considerations. This may surprise as the transition from glucose limitation to starvation has the potential to provoke regulatory responses with negative consequences for production performance. In order to shed more light, we performed gene-expression analysis of *Saccharomyces cerevisiae* grown in intermittently fed chemostat cultures to study the effect of limitation-starvation transitions. The resulting glucose concentration gradient was representative for the commercial scale and compelled cells to tolerate about 76 s with sub-optimal substrate supply. Special attention was paid to the adaptation status of the population by discriminating between first time and repeated entry into the starvation regime. Unprepared cells reacted with a transiently reduced growth rate governed by the general stress response. Yeasts adapted to the dynamic environment by increasing internal growth capacities at the cost of rising maintenance demands by 2.7 %. Evidence was found that multiple protein kinase A (PKA) and SNF1 mediated regulatory circuits were initiated and ramped down still keeping the cells in an adapted trade-off between growth optimization and downregulation of stress response. From this finding, primary engineering guidelines are deduced to optimize both the production host's genetic background and the design of scale-down experiments.

4.2.2 Introduction

S. cerevisiae is a time-tested and widely applied host in the biotech industry. Its central status as a cell-factory is rooted in an extensive knowledge base, advanced and facilitated genetic engineering, unproblematic valorization of biomass as a byproduct and foremost, robustness to diverse industrial conditions (Nielsen, 2019). The latter is based on the yeasts' ability to adapt to a wide array of ecological niches (López-Maury, Marguerat and Bähler, 2008; Goddard and Greig, 2015), which is both a blessing and a curse for bioprocesses development. While ample adaptation mechanisms made the yeast a preferred platform organism for many bioprocesses, its flexibility comes at a price. Bioprocesses are typically developed in a homogeneous environment in lab-scale studies. In contrast, the industrial habitat is characterized by imperfect mixing since maintaining equal mean broth circulation time with increasing tank volume poses an infeasible endeavor (Uhl and Von Essen, 1986; Junker, 2004). Resultant dynamic gradients, *e.g.* of primary nutrients, constantly challenge the adaptive capacity of the cells even leading to non-expected regulation phenomena that may cause the deterioration of expected TRY (titer, rate, yield) criteria (Enfors *et al.*, 2001; Takors, 2016; Crater and Lievense, 2018). This mirrors the interaction of multi-level regulation programs covering allosteric enzymatic control, transcriptional, translational and post-translational responses finally leading to physiological changes. Notably, each regulatory level possesses inherent response and relaxation times which overlap finally creating the integral response on external stimuli (Delvigne and Goffin, 2014; Wehrs *et al.*, 2019). Hence, scale-up effects are the outcome of the complex interactions between production-scale hydrodynamic heterogeneities and multi-level yeast responses.

Carbon-limited fed-batch strategies are widely adopted to ensure efficient conversion of substrate to product, for instance in a baker's yeast production. Feed rates are designed to allow fast growth while avoiding resource spillage through overflow metabolism. As a consequence, consumption times for highly diluted substrates may be shorter than the convective supply of said substrates leading to substrate depletion in poorly mixed zones of the bioreactor or far away from the inlet point (Lara *et al.*, 2006). Inherently, substrate gradients (e.g. for glucose) creating excess and scarcity are likely to occur as confirmed experimentally and by simulation investigating the industrial bioreactor (George *et al.*, 1998; Haringa *et al.*, 2017; Sarkizi Shams Hajian *et al.*, 2020). *S. cerevisiae* senses variable substrate supplies via a plethora of multilayered and interconnected signaling cascades. Extracellular glucose levels are detected via the Gpr1/Ras2-cAMP-dependent protein kinase A (PKA) and Rgt2/Snf3-protein kinase B (PKB) nutrient kinases (Busti *et al.* 2010; Kim *et al.* 2013b). The sensing of intracellular

glucose pools is directly mirrored by hexokinase activity and indirectly by the adenylate energy charge, *AEC,* through the SNF1/AMP-activated protein kinase (AMPK) network (Coccetti, Nicastro and Tripodi, 2018). The status of low ATP availability, i.e. low *AEC*, is transduced via SNF1 to the rapamycin kinase complex I (TORC1) which regulates the growth rate together with PKA (Wullschleger, Loewith and Hall, 2006; Kunkel, Luo and Capaldi, 2019). Further downstream, these regulatory nodes orchestrate the phosphorylation status of central transcription factors (TFs) finally translating external stimuli into well-adjusted microbial responses (Petrenko *et al.*, 2013; Plank, 2022).

What determines the biological output from the above regulatory network is the combination of amplitude, frequency, and dwell time with respect to the exposure to a certain glucose concentration. Responses may be subtle, short-termed but well-buffered energetic imbalances or even fatal growth arrests (Verma *et al.*, 2013; Bisschops *et al.*, 2017). In any case, they are likely to deteriorate the productivity of engineered cells to produce the targeted product. Knowledge-driven downscaling aims to mimic related scenarios already in lab-scale for identifying proper prevention strategies (Delvigne et al., 2017; Straathof et al., 2019; Takors, 2016). As a prerequisite of modern approaches, production-scale information is deduced from computational fluid dynamic (CFD) studies (Lapin, Müller and Reuss, 2004; Haringa *et al.*, 2016). Adding the biological phase to the flow field via cellular reaction dynamics (CRD) models, which are derived from stimulus-response experiments (SRE), enables the *in silico* characterization of relevant environmental stimuli (Kresnowati, Van Winden and Heijnen, 2005; Zieringer and Takors, 2018). Finally, coupled CFD−CRD simulation results govern the quantitative design of both, realistic scale-down reactors and strains with increased process robustness (Haringa *et al.*, 2017; Kuschel and Takors, 2020; Wang, Haringa, Noorman, *et al.*, 2020).

More and more studies highlight the prevalence of starvation zones in bioreactors that are occur distant from the feed zone in fed-batch processes (Haringa *et al.*, 2016; Kuschel and Takors, 2020; Nadal-Rey *et al.*, 2021; Ho *et al.*, 2022). Remarkably, SRE-data covering the transition between carbon limitation and starvation are scarce whereas the opposite, *i.e.* sudden shifts towards glucose excess, were extensively studied in the past (Theobald *et al.*, 1997; Kresnowati *et al.*, 2006; Wu, Schipper, Kresnowati, Angela M Proell, *et al.*, 2006; Suarez-Mendez, Ras and Wahl, 2017; Verhagen *et al.*, 2022). The latter may reflect the fundamental interest in the Crabtree effect and its relevance for multiple metabolic scenarios (de Alteriis *et al.*, 2018). However, such stimuli studies do not mimic the predominant conditions in large-scale

bioreactors. Consequently, we set out to complement the current data base with kinetic studies investigating the endometabolome after glucose shifts from limitation to starvation (Minden *et al.*, 2022). In the referenced work, the metabolome of *S. cerevisiae* revealed a short-term strategy optimized to uphold anabolic needs at the expense of catabolic capacities when entering famine zones. Significantly increased biomass-specific energy demands after repeated exposure to the same glucose gradient raised the question how the stimulus is propagated in the eukaryotic regulatory network. Using next-generation-sequencing data, this study investigates gene-expression dynamics to answer two questions: (i) How does a yeast population respond to the first-time occurrence of glucose scarcity and (ii) how is the regulatory landscape shaped after complete adaptation towards the dynamic production environment?

4.2.3 Experimental procedures

Strain maintenance and seed culture conditions

S. cerevisiae CEN.PK113-7D (Nijkamp *et al.*, 2012) was kindly provided by Royal DSM N.V. (Delft, The Netherlands) and preserved as a 30 % (v/v) glycerol stock at −70 °C and maintained on yeast extract peptone dextrose (YPD) agar plates at +4 °C. Seed cultures were prepared by inoculating 5 mL YPD broth with single colonies in a glass vial followed by an eight-hour incubation at +30 °C on an orbital shaker operated with 120 rpm. The whole culture was pelleted and transferred to 110 mL of a synthetic medium in a 1000 mL baffled shake flask and incubated under identical conditions overnight. The medium was modified from Verduyn *et al.* (1992) to support carbon-limited growth in continuous culture with 22.5 $g \cdot L^{-1}$ glucose. In brief, the referenced salt concentrations were increased threefold and the trace element and vitamin stock solutions were increased twofold.

Bioreactor setup and continuous operation mode

Aerobic, continuous fermentations were carried out in a stainless steel benchtop bioreactor (Bioengineering, Wald, Switzerland) with a liquid working volume of 1.7 L. The culture was supplied with sterile ambient air through a fumigation frit positioned at the reactor bottom with a constant flow rate of 0.5 vvm. Broth homogenization and bubble dispersion were ensured with two six-blade Rushton-type impellers operated constantly at 800 rpm equaling a gassed, volumetric power input of 7.1 $W \cdot kg^{-1}$ to yield a circulation time of 0.1 s (appendix B, tables B1 and B2). The relative dissolved oxygen concentration was determined with an optical pO_2 probe (PreSens, Regensburg, Germany) and never decreased below 70 %. Broth temperature was controlled at +30 °C with electrical heating and water cooling rods and monitored with a Pt100 probe (Bioengineering, Wald, Switzerland). The tank was operated at an absolute pressure of 1.3 bar, which was maintained with a needle valve attached at the off-gas filter element exit. Two molar potassium hydroxide kept the broth pH at 5.00 using a Mettler Toledo probe (Columbus, OH, USA). A continuous supply of Struktol J 674 antifoam agent (Schill und Seilacher, Hamburg, Germany) with a pump rate of 30 $\mu L \cdot h^{-1}$ was realized with a LA-120 syringe pump (IDL GmbH, Nidderau, Germany) to pre-emptively avert foaming. Molar oxygen and carbon dioxide fractions in the off-gas were logged every minute with BCP-O_2 and BCP-CO_2 sensors (BlueSens, Herten, Germany). All in- and outgoing liquid flows were conveyed with U-120 peristaltic pumps (Watson-Marlow, Falmouth, UK). Rapid sampling was enabled

using semi-automated sampling devices based on time-relay controlled opening of a pinch valve (Minden *et al.*, 2022).

Bioreactors were inoculated with 100 mL seed culture and the continuous phase was initiated after a rapid increase of the pO_2 signal marked the end of the batch phase. During continuous operation mode, the medium was fed at a fixed rate of 2.83 mL·min^{-1} to yield a dilution rate of 0.1 h^{-1} via mass balancing of the whole fermenter through the harvest pump. The feed medium was constantly homogenized with a magnetic stirrer to prevent gradient formation.

Experimental design

Both, non-adapted and adapted starvation response experiments were conducted in the same chemostat process according to the process design depicted in figure 15. First, the reference steady state (RS) was sampled after five residence times of constant Q_{O_2} and Q_{CO_2} conjointly marking time point 0 min of the non-adapted time series. Subsequently, the feed was interrupted for 2 min causing a transition from limitation to starvation back to limitation (LSL) and the stimulus-response was monitored for up to six hours (denoted post s-LSL, s for single). Second, the dynamic steady state (DS) was characterized after five residence times of repeated LSL (r-LSL) transitioning. During this phase, the feed was operated in nine-minute LSL-cycles with the feed inactive for two minutes and active for seven minutes equaling a 9 min r-LSL cycle time. The active feed rate was adjusted to 3.64 mL·min^{-1} resulting in a net dilution rate of 0.1 h^{-1}. Samples for the adapted response were drawn over one representative nine-minute cycle and steady state DS was expressed as the average over one cycle.
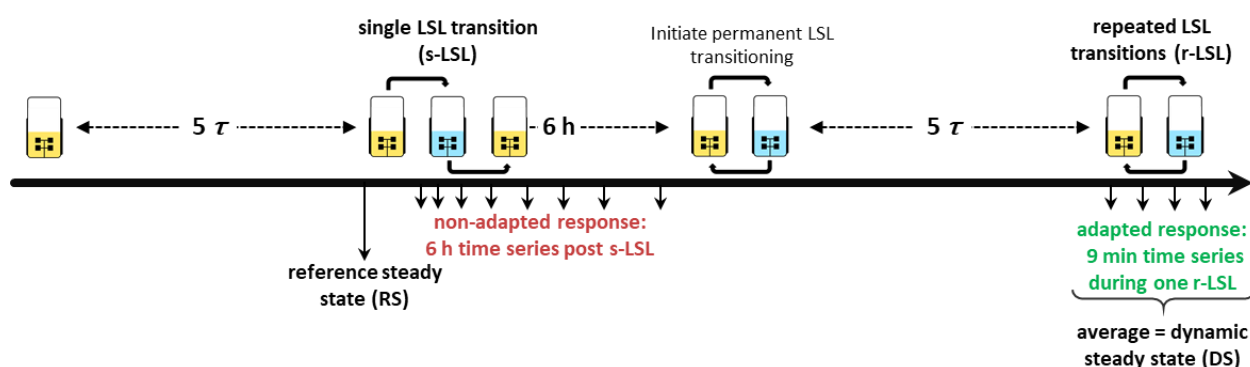
Figure 15. Process design of the chemostat experiment. τ, residence time.

Sample follow-up and analytical procedures

All samples were measured in groups of technical triplicates and values reported in this study are expressed as the arithmetic mean ± standard deviation of technical means from three

independent fermentation experiments. Carbon, nitrogen and available electron balances closed within $\pm$ 3.6 % at any sample point (see appendix B, figure B1).

Dry matter of biomass (*DMB*) was quantified gravimetrically via vacuum-filtration of 5 mL degassed fermentation broth through desiccated and tared membrane filters (Ø 47 mm, Type 154, Sartorius, Göttingen, Germany). The filter cake was washed with 15 mL deionized H_2O and dried in a heating chamber at $+70\,°C$ until mass remained constant after occasional weighing.

To assess extracellular glucose, broth was directly withdrawn into an open syringe and squeezed through a PES filter element (Ø 30 mm, 0.22 µm pore size, ROTILABO®, Carl Roth, Karlsruhe, Germany) within less than five seconds. The supernatant was flash-frozen in liquid nitrogen and stored at $-70\,°C$ until analysis. Glucose was quantified with a UV-based enzyme test kit (art. no. 10716251035, r-biopharm AG, Darmstadt, Germany) without sample dilution according to the manufacturer's instructions.

Intracellular glycogen determination was following the protocol originally published by Parrou and Francois (1997) and modified by Suarez-Mendez (2015) for rapid quenching. In brief, 1.5 mL broth was collected in 10 mL of $< -40\,°C$ methanol and subsequently centrifuged for 5 min at $-11\,°C$ under $5000\,g$. The resulting pellet was flash-frozen and stored at $-70\,°C$. Upon thawing, pellets were rendered permeable in 0.25 mL 0.25 M sodium carbonate heated to $+95\,°C$ for 3 h in a water bath. Next, optimal conditions for enzymatic glycogen conversion to glucose were established by adding 0.15 mL M acetic acid and 0.6 mL 0.2 M sodium acetate (pH 5.2, adjusted with acetic acid). 0.48 mL of the resulting suspension was mixed with 20 µL of α-amyloglucosidase (~70 U/mL, cat. number: 10115, Merck, Darmstadt, Germany) and incubated for $+57\,°C$ for at least 12 h. Finally, the resulting suspension containing liberated glucose was separated from cellular debris via centrifugation ($2 \cdot 10^4\,g$, 1.5 min) and quantified as described above.

Intracellular total RNA levels were assessed based on the method described by Sasano *et al.* (2017). One milliliter of fermentation broth was transferred into a tube containing chilled 0.5 mL 1 M perchloric acid. The sample was immediately homogenized and placed for 20 min in a water bath maintaining $+70\,°C$. Subsequently, the sample was mixed with 0.5 mL of 1 M K_2HPO_4 and the formed precipitate was removed via centrifugation ($2 \cdot 10^4$ g, 1.5 min). The supernatant was flash frozen and stored at $-70\,°C$ until RNA determination with a Nano-Drop

ND-1000 (NanoDrop Technologies, Wilmington, De, USA), which was blanked against a solution containing 0.25 M perchloric acid and 0.25 M K_2HPO_4.

Estimation of q_{ATP}

Biomass-specific ATP formation rate was estimated based on its stoichiometric relationship with oxygen uptake and glucose consumption according to $q_{ATP} = 2 \cdot q_S + 2 \cdot \frac{P}{O} \cdot q_{O_2}$ with an assumed $\frac{P}{O}$ ratio of 1.08 (Van Den Brink *et al.*, 2008). The specific oxygen uptake rate was calculated after deconvolution of the off-gas sensor readout due to the volume of tubing and foam traps causing significant detection delays. The deconvolution method from Theobald (1995) was applied and has been described in detail recently (Minden *et al.*, 2022).

Total RNA extraction

Total RNA extraction was performed using the Quick-RNA Fungal/Bacterial Miniprep Kit (R2014, Zymo Research, Freiburg, Germany) following the manufacturer's instructions with slight modifications. Prior to sampling, ZR BashingBead™ lysis tubes were prepared with 0.4 mL RNA lysis buffer and 0.1 mL DNA/RNA Shield™ agent (Zymo Research, Freiburg, Germany; not provided with the kit). During the experiment, 0.25 mL fermentation broth was instantly added to the prepared lysis tube, vigorously shaken by hand and flash-frozen in liquid nitrogen (all < 10 s). This sampling routine yielded maximally 55 mg wet biomass (assuming a dry:wet matter of biomass correlation of 0.21 estimated from Aon *et al.* (2016)) which is within the range of the recommended upper loading limit of 50−100 mg wet weight. Samples were stored at −70 °C and extracted in batch from all three fermentations. The extraction protocol was started by thawing the samples fifty-fifty and subsequently homogenizing the sample in a Precellys 24 tissue homogenizer (Bertin Technologies, Montigny-le-Bretonneux, France) for two times 20 s at maximum speed with a 10 s break in between. All subsequent steps were performed according to the manufacturer's instructions. At the end of the protocol, total RNA was eluted with 60 µL DNase/RNase-free H_2O and each sample as split in two 30 µL aliquots.

Library preparation and RNA-sequencing

One aliquot from each sample was shipped for mRNA sequencing to GENEWIZ (Leipzig, Germany). Initial quality checks using the Agilent 2100 BioAnalyzer instrument (Agilent, CA, US) revealed high integrity of all samples with uniform RIN (RNA integrity number) values ≥ 9.9. Next, cDNA libraries were synthesized after polyA selection was performed to enrich mRNAs. Libraries were finally sequenced as paired-end reads of 150 base pair length on a

NovaSeq 6000 platform (Illumina, CA, USA) with a sequencing depth of $2 \cdot 10^7$ paired-end reads per sample.

Processing of sequencing data

Sequencing results were received in the *.fastqsanger* format and uploaded on a local galaxy server instance (Afgan *et al.*, 2018). First, the sequencing quality was assessed for each file individually using *FastQC* v. 0.72 (Andrews, 2010). Adapter sequences were removed using *Trimmomatic* v. 0.38.0 (Bolger, Lohse and Usadel, 2014) for paired-end reads with default settings. The trimmed sequence files were then aligned against the *S. cerevisiae* CEN.PK113-7D reference genome (GCA 000269885 – ASM 26988 v1) accessed from the ENSEMBL database (Howe *et al.*, 2021) using the *TopHat* v. 2.1.1 (D. Kim *et al.*, 2013) algorithm for paired-end reads with default settings yielding an overall alignment rate of 86−93 %. Count tables were computed using *featureCounts* v. 1.6.4 (Liao, Smyth and Shi, 2014) together with the strain specific annotation file *Saccharomyces_cerevisiae.R64-1-1.50.gtf*, also obtained from the ENSEMBL database. The generated count tables were merged into a *data.frame* object in the R environment v. 1.4.1106 (R Core Team, 2021) for downstream analysis.

Differential gene expression analysis

Differential gene expression analysis was conducted using the *DESeq2* v. 1.32.0 R-package (Love, Huber and Anders, 2014). After transforming the count table into the homoscedastic $\log_2$-scale with *rlog*, PCA analysis revealed a significant proportion of variance introduced into the dataset via multiple library preparations and sequencing runs (supporting information B, tab 1 and appendix B). Thus, the variables "library run" and "sequencing run" (as a merged variable called "libseq") were introduced into the experimental design matrix. Time series and steady state comparison were analyzed with the likelihood ratio test (`test="LRT"`) and a model reduced by technically introduced variance (for details, see appendix B, figures B2, B3, B4). Genes were considered as differentially expressed with a $|\log_2$-fold change$|$ above 0.322 and a false discovery rate (FDR) (Benjamini and Hochberg, 1995) below $1 \cdot 10^{-3}$. For further analysis, open reading frame identifiers were converted to ENSEMBL gene names using the libraries *AnnotationDBi* v. 1.51.5 and *org.Sc.sgd.db* v. 3.13.0.

Multidimensional scaling

Classical metric multidimensional scaling (Gower, 1966) was performed to visualize global dissimilarities in the gene expression profiles of all samples. First, $\log_2$-scaled count tables were cleaned from technical variance using the function *removeBatchEffect* from the *limma* v. 3.48.3

package (Ritchie *et al.*, 2015). Subsequently, biological replicates were expressed as arithmetic means and only genes with significant differential expression in at least one condition were considered. The resulting table was converted to a Euclidean distance matrix using the *dist* function, transposed and passed to *cmdscale* (k=3) for a three-dimensional representation of the sample distances. The functions *dist* and *cmdscale* were called from the *stats* v. 4.1.0 package.

Cluster and functional enrichment analysis

Time series gene expression data was clustered into groups of genes with similar patterns of $\log_2$-fold changes using the *kmeans* function from the *stats* v. 4.1.0 package. The algorithm was operated with a maximum of $1 \cdot 10^3$ iterations around two centroids for the adapted and six centroids for the non-adapted time series. For each cluster, gene ontology (GO) enrichment was assessed using the YeastEnrichr web interface (Chen *et al.*, 2013; Kuleshov *et al.*, 2019). YeastEnrichr was queried for the "GO_Biological_Process_2018" library (source: http://geneontology.org/; release 2022-03-22) and significant terms (FDR < 0.05) were manually curated to avoid redundancy of GO terms. Up- and downregulated gene lists from the comparison between steady states RS and DS were additionally queried for the "WikiPathways_2018" (source: https://www.wikipathways.org; accessed 2022-04-15) and the "GO_Cellular_Component_2018" (source: http://geneontology.org/; release 2022-03-22). Non-curated enrichment results can be accessed in the (supporting information B, tabs 4–9, 11–12 and 14–19).

Gene set enrichment analysis (GSEA) was performed with the R package *GAGE* v. 2.42.0 (Luo *et al.*, 2009) to investigate significant differential expression of pre-defined gene lists. As described previously, $\log_2$-scaled count tables corrected for technical variance were used as an input for the *gage* function, which was configured to perform paired comparisons (compare="paired"). Two-sample *t*-test values were used as a proxy for the intensity of gene-expression changes of the underlying gene set and converted to heat maps using the *ggplot2* package (version: 3.3.6.9000). Literature gene sets were extracted from various sources and transcription factor target lists were obtained from the Yeastract database (Monteiro *et al.*, 2020). All 183 transcription factors available from Yeastract were queried for genes with documented "DNA binding and expression evidence" and converted to a *.gmt* file as an input for the *gage* function. Only literature gene sets and transcription factor target sets that were enriched significantly (FDR < 0.05) in at least one condition per GSEA analysis were reported.

All input and output tables used in this analysis are accessible in the supporting information B (tabs 20−23; *.gmt* tables were reduced to gene sets which are shown in figure 22).

4.2.4   Results

Characterization of the famine stimulus

Sudden glucose shortages mimicking industrial-scale famine zones were established by periodic stops of the medium feed during carbon-limited growth. The two minutes lasting substrate starvation induced glucose reduction from 150 to 30 µmol·L^{-1} (figure 16A). Afterwards, the glucose limiting feed scenario was re-installed finally creating a limitation-starvation-limitation (LSL) cycle. Interestingly, resulting glucose profiles were similar for non-adapted and adapted cells. The latter resulted from the repeated exposure to said LSL cycles (r-LSL, see Material & Methods). During one LSL-trajectory, biomass-specific glucose uptake rates (q_s) were severely curtailed, not exceeding 5 % of maximum capacities (9.3 mmol·g$_{DMB}$$^{-1}$·h^{-1}, from Diderich *et al.* 1999) for 14 % of cycle duration. Given that large scale CFD simulations assumed CEN.PK113-7D to spend 40 % of the time in sub-5 % $q_{s,max}$ regimes (Haringa *et al.*, 2017), the current experimental approach is qualified as rather mild but still realistic to mimic industrial-scale glucose depletion scenarios. The calculated adenylate energy charge (*AEC*) (previously reported in Minden *et al.* (2022)) was monitored as a possible actuator for initiating regulatory energy sensing cascades (Figure 16B). By trend, *AEC* mirrors the extracellular glucose availability during starvation. The restoration of pre-stimulus values even occurred slightly faster than the recovery of extracellular glucose levels. Non-adapted cells decreased their *AEC* by 0.20 ± 0.03 while amplitudes for adapted cells were almost doubled reaching a minimal value of 0.50 ± 0.01. For a short period, both populations fell below the commonly accepted physiological *AEC* range of 0.7–0.9 (De La Fuente *et al.*, 2014). This is a rather remarkable observation given that long-term glucose starved yeasts can sustain their adenylate energy charge within the physiological range for up to several hours during the stationary phase (Weibel, Mor and Fiechter, 1974; Ball and Atkinson, 1975).

Figure 16. Characterization of the famine stimulus. (A) Extracellular glucose concentration and (B) intracellular adenylate energy charge (*AEC*) during the course of one perturbation cycle. *AEC* was calculated based on the methodology reported by Ball and Atkinson (1975). Red circles indicate dynamics following a single (s) LSL-transition and green triangles depict one representative repeated (r) LSL-cycle during steady state DS. Time point 0 min of s-LSL is the equivalent of steady state RS (yellow squares). All values indicate means ± standard deviation of three biological replicates. The underlying data was previously published in Minden *et al.* (2022).

Short-term starvation evokes macroscopic rearrangements

Figure 17 compares post stimulus data of the unperturbed reference (RS), the steady state after repeated perturbation (DS) and time-series of non-adapted cells. Furthermore, the small plot inside figure 17B depicts two time series that reflect cellular responses during an LSL cycle. This diagram is provided for illustrating that the 'steady-state' after repeated perturbation 'DS' rather represents an average of dynamics than a true steady-state defined by constant state variables.

Notably, the biomass-substrate yield ($Y_{X/S}$) of RS persisted after long-term adaptation to alternating glucose availability as indicated by the similar DS (figure 17A). In part, this was the result of substantial metabolic re-arrangements in adapted versus RS-cells, including a reduction of the glycogen pool by 49 % and increasing internal RNA abundance from 77.0 ± 1.4 mg$\cdot$g$_{DMB}^{-1}$ to 84.9 ± 1.6 mg$\cdot$g$_{DMB}^{-1}$ (figure 17C, D). We quantified total ribonucleic acid as a proxy of ribosomal content, considering that 80 % of total RNA in yeast contributes to the assembly of ribosomes as rRNA (Warner, 1999). Thereof, we hypothesized that the 3 % rise of q_{ATP} ($p < 0.05$, figure 17B) in DS versus RS was necessary to sustain increased translational capacities, which was partially counterbalanced by decreased energy spillage through glycogen-associated futile cycling.

A similar relation was found during the mid-term response of unstressed yeast cells post s-LSL. Within the first 10 min, glycogen pools slightly reduced by 13 % to a minimum of 271 ± 29 μmol$_{glucose}\cdot$g$_{DMB}^{-1}$, followed by a relatively prolonged repletion phase of three hours. In parallel, the population showed 5 % increased q_{ATP} 20–60 min post-stimulus before energy demands relaxed to pre-stimulus levels. Again, RNA ramp-up dynamics seemed tightly linked with the temporally increased ATP demands. Following the peak of this non-adapted response, we found a significant reduction of $Y_{X/S}$ at the one-hour mark ($p < 0.05$) which eventually recovered. Thus, the temporal observation in this phase might reflect the early initiation and retraction of the phenotypic shift, which is completed after long-term adaptation in DS.

Interestingly, the immediate intra-r-LSL q_{ATP} response during the representative cycle in figure 17B revealed a reduction to 4.2 mmol$\cdot$g$_{DMB}^{-1}\cdot$h^{-1} which represents a 44 % larger amplitude than the non-adapted population (figure 17, insert plot). This observation is consistent with the equally larger *AEC* amplitudes within one r-LSL-cycle (figure 17B) and points to a larger ATP drain accounting for the intensified translational capacities in adapted cells.
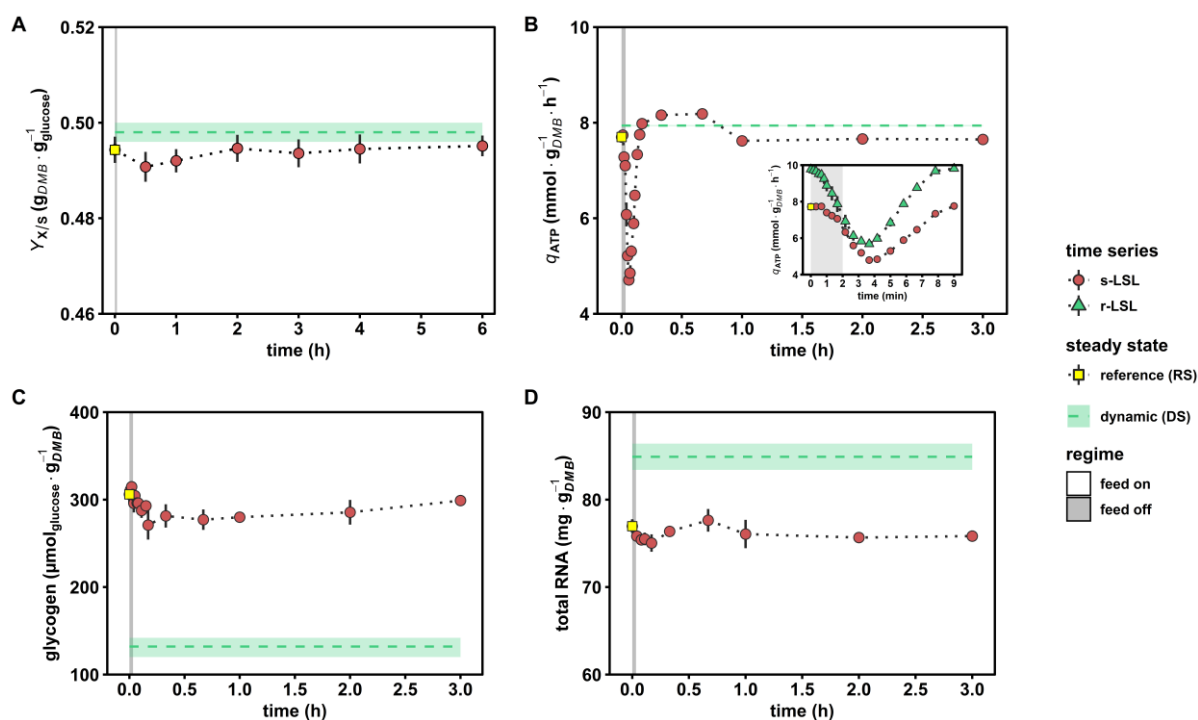
Figure 17. Macroscopic stimulus-response characterization. (A) Biomass-substrate yield. (B) ATP production rate estimated from oxygen and glucose consumption rates assuming a P/O ratio of 1.08 (Van Den Brink *et al.*, 2008). The insert plot depicts the short-term dynamics during one representative LSL-cycle. (C) Intracellular glycogen and (D) total RNA pool dynamics. Red circles indicate dynamics during and up to 6 hours post single (s) LSL and time point 0 min is the equivalent of steady state RS (yellow squares). Green triangles depict one representative repeated (r) LSL cycle during steady state DS. Steady state DS is expressed as the average of dynamic data from r-LSL cycles (green dashed line) ± standard deviation (light area). All time series values indicate means ± standard deviation of three biological replicates.

Next, we set out to elucidate regulatory phenomena on the gene expression level that govern the observed phenotypic shifts. Figure 18 displays the global analysis of Euclidean distances between all investigated samples using classical metric multidimensional scaling over three dimensions. The analysis of the first dimension distinguishes the grouping of adapted and non-adapted cells after their exposure to LSL cycles (figure 18A). The apparent difference in the second dimension is further elucidated if the transcriptional time-series co-consider the third dimension (figure 18B, C). By trend, the s-LSL exposure pushed the cells quickly away from their steady state within the first 4.5 min and it took about 180 min to return on a spiraled course. This pattern entails oscillating transcriptional dynamics, which reinforce until 20 min before complete relaxation after 180 min. In contrast, we observed a rather circular trajectory for adapted cells. The latter anticipates that a fraction of adapted cells always remained transcriptionally stimulated during the entire course of the experiments.
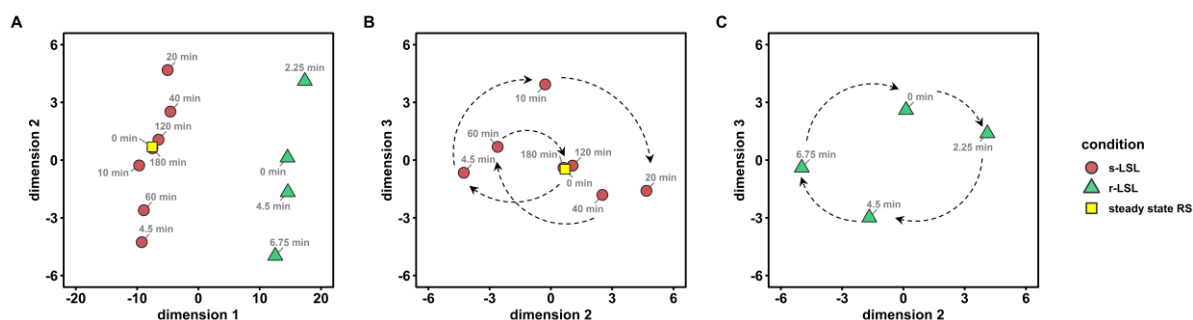
Figure 18. Dissimilarities of significant gene expression patterns in the multidimensional scaling (MDS) space represented by three dimensions. (A) Whole dataset represented by the first two dimensions. (B) MDS plot of the post single (s) LSL time series (red circles + yellow square) based on dimensions 2 and 3. Dashed arrows provide a visual aid to follow the time series (C) Analogous MDS plot of the 9 min repeated (r) LSL time series (green triangles).

S. cerevisiae overloads the strategic response upon first-time glucose deprivation

Differential gene expression analysis uncovered 1065 genes accounting for 16 % of the reference genome all fulfilling the statistical significance ($p < 1 \cdot 10^{-3}$) of differential expression during the 3-hours lasting response upon the s-LSL stimulus. We grouped the differentially expressed genes (DEGs) into six clusters each featuring similar $\log_2$fold changes. Furthermore, we assigned co-regulated genes via the enriched gene ontology (GO) terms (figure 19). In sum, the clusters confirm the dynamics anticipated from the MDS analysis, which comprises an early transcriptional response followed by an amplified mid-term amplitude before slowdown.

Three of six clusters were disproportionately enriched with GO terms related to the translation machinery containing one third of all 135 ribosomal proteins (RPs) in yeast (Gaikwad *et al.*, 2021). Cluster 4 increased steadily over the first 40 minutes. Meanwhile, clusters 1 and 5 highlighted other dynamics that are laterally inversed. Whereas cluster 5 showed the early amplification of gene transcripts as described above, cluster 1 disclosed an opposite trend. The two clusters are particularly interesting as a trade-off between cytoplasmic and mitochondrial translation becomes evident. Several studies outlined that the coordinated redistribution of the costly translation machinery is a crucial feature for building up necessary respiratory capacity under stressful conditions (Bonawitz *et al.*, 2007; Couvillion *et al.*, 2016; Suhm *et al.*, 2018). Further evidence of compartment-specific resource adjustments is provided by the enriched "mitochondrial transport" ontology in cluster 5. However, we did not identify corresponding upregulation of the respiratory chain complex despite our observation of increased ATP dissipation during the observed ramp-up of RNA content and $Y_{X/S}$. In addition, cluster 1 was enriched with transcriptional inducers of rRNA synthesis from polymerase I anticipating a bilateral relationship between regulatory circuits and their provoked strategic responses.

Co-regulated amino acid synthesis genes in cluster 2 followed the trajectory of cluster 1 but with a delayed onset and less pronounced fold changes. Both clusters were significantly enriched for "alpha-amino-acid biosynthesis" activity, reaching a GO-term coverage of 46 %. For some of the comprised genes, *e.g.* those involved in leucine (*LEU2*, *LEU4*, *LEU9*) and aromatic amino acid biosynthesis (*ARO8*, *ARO7*, *TRP2*, *TRP3*, *TRP5*), the intracellular concentrations of their biosynthetic products qualitatively followed the observed cluster dynamics (appendix B, figure B5). On the other hand, absolute glycogen levels appeared detached from the induction-repression dynamic of cluster 6 that comprised the related ontology. Nonetheless, this group contained both genes involved in glycogen mobilization (*GPH1* and *GDB1*) and accumulation (*GLC3* and *GDB1*) which may be taken as a hint towards the dynamic activity of futile cycling (Blomberg, 2000; François and Parrou, 2001). We observed a general tendency for the initial repression of genes involved in primary anabolism, whilst catabolic enzymes from glucose, pentose, and pyruvate metabolic processes followed the opposite trend.

Genes that were annotated to cluster 3 signaled slight activity of stress-responsive mechanisms. For instance, members of the "intracellular protein transport" comprise chaperone activity such as *SSA1* and *CUR1* or were involved in protein recycling, *e.g.* through *VPS29* and *EAR1*. The early induction of transcriptional repressors ("negative regulation of RNA polymerase II promotor transcription") may indicate broader macromolecular savings. Furthermore, the LSL-stimulus triggered changes in cell wall organization and even associated transcription factors (TFs). Taken together, a sudden shift from glucose limitation to starvation prompted *S. cerevisiae* to enter a defensive state preparing for times of scarcity. As this preparatory measure turned out to be premature, a pronounced backlash caused dampened transcriptional bursts up to two hours post-stimulus.
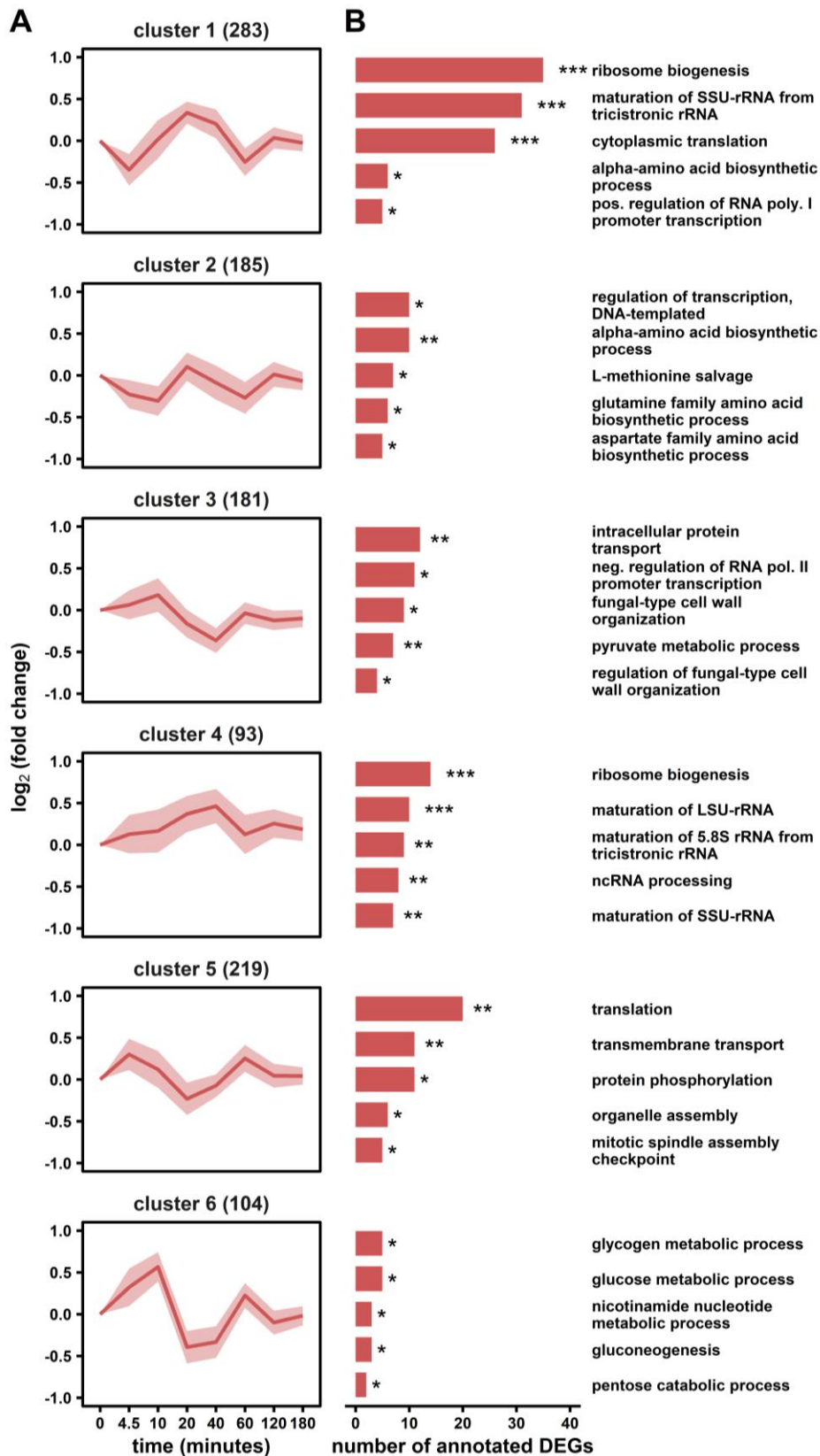
Figure 19. Differential gene expression analysis of the non-adapted s-LSL response. (A) Six clusters with similar gene-expression dynamics are shown with the number of dedicated genes in brackets. (B) Corresponding gene ontology (GO) enrichment analysis. The false discovery rate (FDR) interval is indicated by asterisks for each GO term (* $1 \cdot 10^{-5} \leq \text{FDR} < 5 \cdot 10^{-2}$; ** $1 \cdot 10^{-10} \leq \text{FDR} < 1 \cdot 10^{-5}$; *** FDR $< 1 \cdot 10^{-10}$).

Repeated famine exposure shapes a specialist growth phenotype

The transcriptomic landscape of yeasts adapted to unstable glucose uptake during DS was investigated by 3-level enrichment analysis. Gene ontologies grouping genes according to biological function, pathway affiliation, and compartment-specific localization were used to characterize 728 repressed and 676 induced genes relative to RS (figure 20). The dominant fraction of DEGs was operating in the nucleus, where highlighted reconstructions of the regulatory network and proliferation apparatus occurred. The first is apparent as 20 % of both up- and downregulated mRNAs encoded transcription factors. More specifically, significant downregulation of nuclear protein quality control through ubiquitin-dependent proteolytic activity and upregulation of cell cycle-related DNA metabolic processes was observed.

Regarding the proliferative capabilities, the "cell cycle and cell division" pathway was amplified by increasing expression levels of engaged cyclins, kinases, and transcription factors. Attached were upregulated functional categories on the level of DNA repair and segregation and cell division, represented by the terms "DNA metabolic process" and "mitotic cytokinesis", respectively. Gene expression of the translational machinery was strongly induced at the stage of early ribosome biogenesis (RiBi) in the nucleus, including rRNA processing and the maturation of several ribosomal subunits (Woolford and Baserga, 2013). Induction of RiBi genes was accompanied by the upregulated "nutrient control of ribosomal gene expression" ontology, which involved genes of the cAMP-dependent protein kinase A (PKA) nutrient-signaling network, such as the receptor protein Gpr1 and PKA subunits *TPK1/3*. On the other end of the ribosomal life cycle, downregulation of proteolytic activity was evident from several GO readouts, particularly represented by the term "proteasome-mediated ubiquitin-dependent protein catabolic process". The ubiquitin system predominantly controls the nuclear turnover of ribosomal subunits and its activity must be repressed to allow atypical overexpression of RPs (M. K. Sung *et al.*, 2016; An and Harper, 2020). Additionally, mature ribosomes were adjusted based on their subunit configuration in both the cytosol (16 up, 12 down) and the mitochondrion (7 up, 10 down).

Metabolic enzymes were primarily repressed in the regime-transitioning environment of DS. Especially glycolytic catabolism was subjected to a slowdown as represented by several enriched GO terms. One exception, however, was the non-oxidative branch of the pentose phosphate pathway, possibly a reflection of increased anabolic needs to supply the overproducing translation machinery. Furthermore, *S. cerevisiae* sacrificed activity of various

93

stress-specific programs such as the mentioned MAPK signaling, the "cellular response to oxidative stress" or the nutrient-starvation-specific "lysosomal microautophagy" (Gross and Graef, 2020). In contrast, the upregulated biological function ontology "vesicle mediated transport" involved many endocytic genes. Recently, Johnston *et al.* (2020) reported that under conditions of extracellular nutrient scarcity, yeasts scavenge for alternative nutrients via increased endocytosis activity.
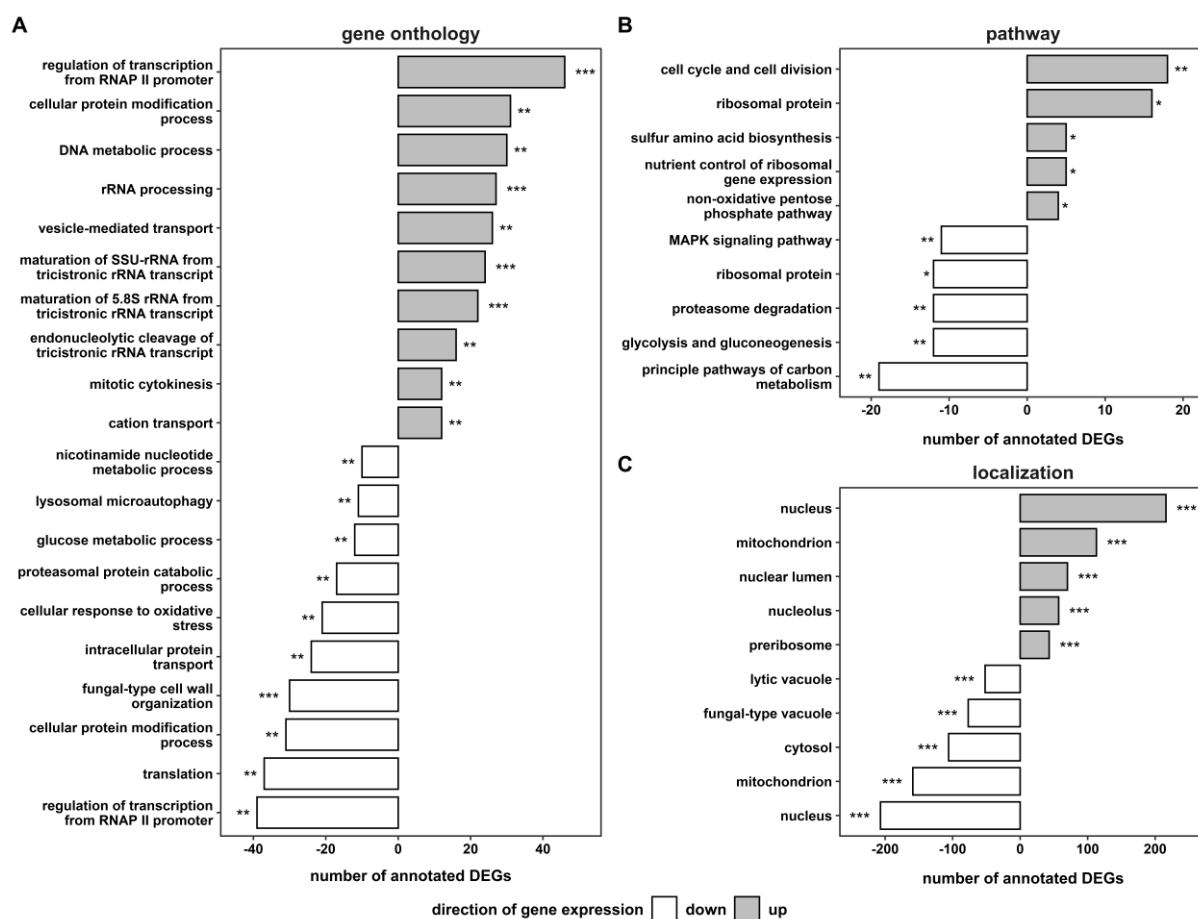
Figure 20. Functional enrichment analysis of steady state DS based on (A) biological function, (B) pathway affiliation and (C) cellular localization annotations. The false discovery rate (FDR) interval is indicated by asterisks for each GO term (* $1 \cdot 10^{-5} \leq$ FDR $< 5 \cdot 10^{-2}$; ** $1 \cdot 10^{-10} \leq$ FDR $< 1 \cdot 10^{-5}$; *** FDR $< 1 \cdot 10^{-10}$).

Complementary to the steady state assessment, we investigated the existence of persistent regulatory dynamics of the DS-population. Accordingly, 251 stimulus-responsive genes in fully adapted cells were identified (figure 21). Two symmetric clusters revealed oscillatory gene expression changes with two inflection points during nine-minute r-LSL cycles. With this short window of observation, the clusters were mainly enriched for fast responding genes with short half-lives < 10 min, such as those involved in stress response, ribosome biogenesis and transcription regulation (Miller *et al.*, 2011). Especially the latter two categories were also

prevalent in the non-adapted response, reflected by 142 overlapping genes accounting for 57 % of the adapted DEG dynamic. Thus, despite pronounced changes in the global transcriptional landscape during steady state DS, *S. cerevisiae* still executes starvation-induced short-term gene expression changes that are independent of its adaptation status.

Cluster 1 revealed regulatory activity of the DNA replication process, represented by the GO terms "sister chromatid segregation" and "mitotic DNA damage checkpoint". The latter involved *RAD53*, the master effector kinase regulating progression through the S-phase of the cell cycle (Branzei and Foiani, 2006). Recently Rad53 revealed additional transcriptional control over several promoters covering 20 % of the whole yeast genome, emphasizing its wide regulatory influence (Sheu *et al.*, 2021). Notably, there was no overlap with "cell cycle and cell division" genes upregulated during steady state DS (figure 20B) despite their involvement in the same signaling cascade of S-phase DNA damage checkpoint, such as the mediator protein *RAD9* (Pardo, Crabbé and Pasero, 2017). The ontology "methionine biosynthetic process" confirms the existence of a tightly regulated crosstalk between glucose sensing and methionine synthesis. Zou *et al.* (2020) linked this relationship to the rate-limiting function of methionine on translation initiation through the formation of methionyl tRNA. More differentially expressed kinase encoding genes were found in the two top GO terms in cluster 2, with no apparent functional connection to the unstable nutrient availability. In contrast, the following two entries contain regulatory proteins involved in the early starvation response (*USV1* and *MTL1*) or glucose catabolite repression, such as transcription factors Adr1 or Mig1 and the SNF1 subunit gene *SIP2* (Stasyk and Stasyk, 2019).

To recapitulate, repeated exposure to glucose shortage in LSL cycles induced pronounced transcriptional reprogramming in *S. cerevisiae*. The strategic response encompassed upregulated growth capacities and downregulated metabolic and stress-responsive pathways. However, full adaptation did not shut down the repeated on-off switching of immediate tactical mechanisms involved in DNA replication and translation initiation control.
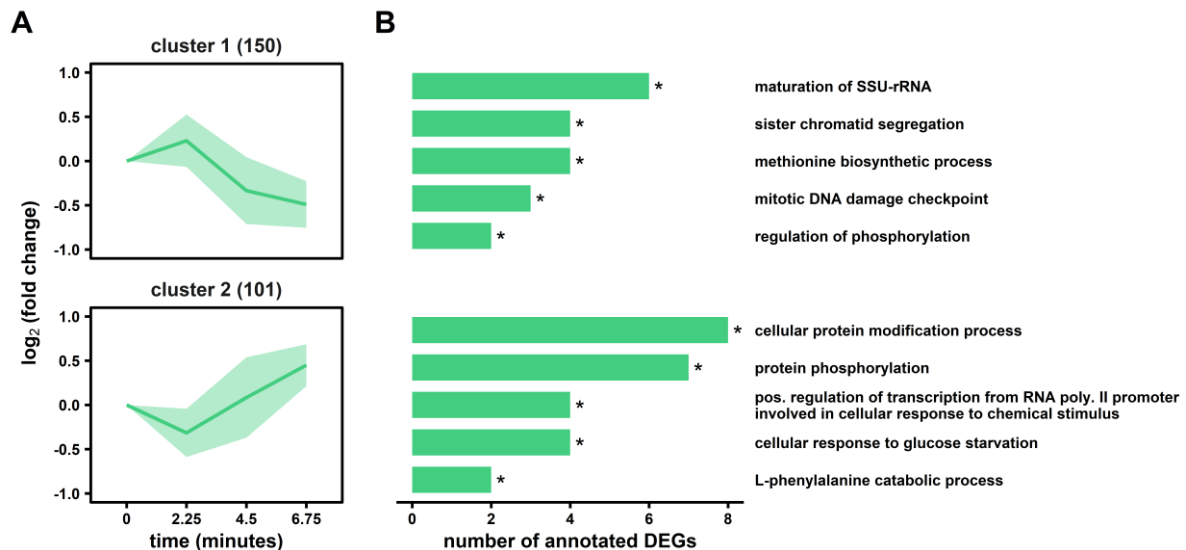
Figure 21. Differential gene expression analysis of the adapted r-LSL time series. (A) Two clusters with similar gene-expression dynamics are shown with the number of dedicated genes in brackets. (B) Corresponding gene ontology enrichment analysis. The false discovery rate (FDR) interval is indicated by asterisks for each GO term (* $1 \cdot 10^{-5} \leq$ FDR $< 5 \cdot 10^{-2}$).

A stress defense–growth trade-off shapes the fate of yeasts in a heterogeneous environment

In the final part of this study, we investigated the presence of global transcriptional programs and their underlying regulatory mediation through gene set enrichment analysis (figure 22). Non-adapted yeast cells showed significant signs of executing the environmental stress response (ESR), a program that initiates a broad spectrum of stress-responsive genes (ESR induced ESRi) while simultaneously repressing ribosomal protein (RP) and biogenesis (RiBi) genes (Brion *et al.*, 2016; Gasch *et al.*, 2017). This well investigated characteristic is clearly visible in Figure 22A and has been observed previously in various stresses (Levy *et al.*, 2007; MacGilvray *et al.*, 2020). The temporal dynamic of the ESR follows the earlier described trend of overshooting as evidenced by matching patterns of gene sets controlled by its master transcription factors Msn4, Sko1, Sok2 (ESRi), Sfp1 (RP and RiBi), and Ifh1 (RP) (Gutin *et al.*, 2015; Gasch *et al.*, 2017; Skoneczny, 2018). Beside common ESR regulators, we identified the activity of non-ESR-associated stress-responsive TFs such as heat shock transcription factor Hsf1, the calcineurin-responsive zinc finger Crz1, and the oxidative stress regulators Cin5 and Skn7. Interestingly, Hsf1 targets seem to operate "out of phase" compared to the overall transcriptional dynamics suggesting divergent signal integration. Indeed, ESR coordination is dominated via target of rapamycin 1 (TORC1) and PKA crosstalk (López-Maury, Marguerat and Bähler, 2008), while glucose starvation induced Hsf1 phosphorylation is dependent on the

SNF1 signaling cascade (Hahn and Thiele, 2004). We further assessed expression changes of 267 strictly growth rate-dependent genes extracted from Fazio *et al.* (2008) which followed the observed transient $Y_{X/S}$ reduction implied by figure 17A. In contrast, the cell cycle gene set was not affected significantly during the non-adapted time series, even though Figure 22B indicated a steady gene expression decline of Swi4 targets. However, this cell cycle regulator reportedly plays a role in the induction of several stress-responsive genes under the control of the Xbp1 promoter (Mai and Breeden, 1997). Altogether, we anticipate that stress-sensing networks dominated the transfer of non-adapted cells to a defensive state. We rule out mere growth rate sensing as an effector since µ correlated genes surged after 4.5 min, whilst the first significant reduction in $Y_{X/S}$ was observed 1 h post-s-LSL stimulus.

Remarkably, the adapted DS-culture predominately followed the same course of transcriptional dynamics of the mid-term s-LSL response after 20–40 min. In this phase, the *S. cerevisiae* transcriptome ramped up growth-associated genes and repressing stress-responsive genes. Regarding metabolic gene sets a pronounced difference emerged: The non-adapted response showed expression changes of gene sets representing glycolysis, gluconeogenesis and fatty acid oxidation coordinated by their respective TFs Adr1 and Cat8 (Young *et al.*, 2003). In contrast, the DS-phenotype showed downregulated glycolytic/gluconeogenic genes, but no sign of Adr1 or Cat8 regulation. Instead, Cat8 targets were constantly differentially expressed within adapted LSL-cycling. Another regulatory program with persistent temporal activity during DS was controlled by Bas1, a control mechanism for ATP homeostasis (Pinson *et al.*, 2019). Figure 22C further indicates additional short-term dynamics of ESR-associated gene expression, although to a lesser extent, compared to the time series after a single famine stimulus. Notably, only RiBi, not RP genes, were differentially expressed in concert with the ESRi group.
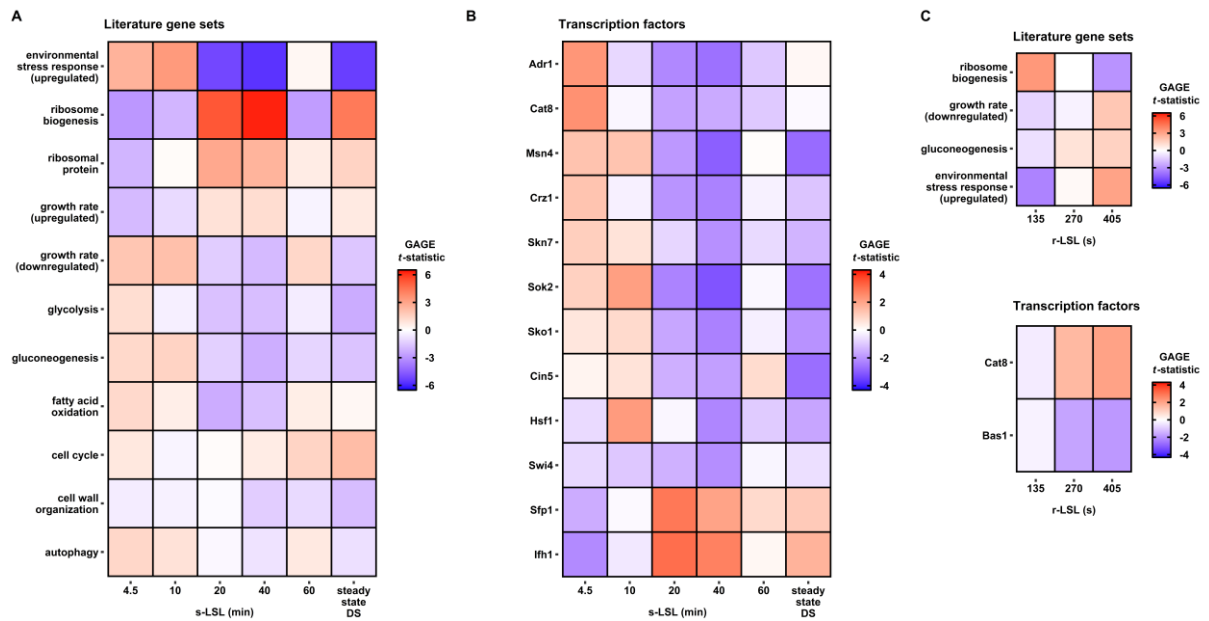
Figure 22. Gene set enrichment analysis (GSEA) of pre-defined gene lists from literature and transcription factor target lists. The reported *t*-statistic implies the strength and direction of coordinated differential gene expression of a given set. GSEA was performed comparing the single (s) LSL time series and steady state DS (A and B) on the one hand, and the dynamics within the repeated (r) LSL cycles (C) on the other hand. Only gene sets with significant enrichment during at least one sample point (FDR < 0.05) are reported in this figure.

4.2.5 Discussion

The impact of famine zones in industrial bioreactors

Gradients of limiting nutrients occur when reaction times of microbial activity match or exceed mean circulation times (Lara *et al.*, 2006; Haringa, Mudde and Noorman, 2018). This correlation causes the appearance of carbon starvation regimes during the growth (Nadal-Rey *et al.*, 2021) or production phase of C-limited fed-batch processes. We imposed a single famine stimulus on steady state yeast cultures to investigate the influence of this scale-up effect on strain performance when starvation zones start to build up. The population which was already adapted to glucose limitation apparently perceived the exposure to glucose starvation as a warning signal, which immediately triggered facets of the ESR (Gasch *et al.*, 2000). Even though optimal conditions were restored within 76 s, *S. cerevisiae* CEN.PK113-7D obviously lacks the regulatory capability to stop the initiated program efficiently. Instead, the stressed cells shifted into a "panic mode" which is characterized by frequent switching on/off of regulatory genes that caused increased ATP expenditure and impaired growth. Understanding the underlying regulatory mechanisms is paramount to engineer robust strains and guided this study.

Several studies anticipate that the initiation of the ESR following acute glucose starvation is dominated by cAMP-dependent PKA signaling (Martínez-Pastor *et al.*, 1996; Görner *et al.*, 2002; De Wever *et al.*, 2005). PKA, in turn, controls the ESRi regulon through activation of the transcriptional inducers Msn2/Msn4 and inactivation of the repressors Sko1 and Sok2 (Gutin *et al.*, 2015). A characteristic property of these and other stress-related TFs such as Crz1 is their oscillating translocation between nucleus and cytoplasm (Zadrąg-Tęcza *et al.*, 2018). Gutin *et al.* (2019) reported that Msn2/Msn4 activate two successive bursts of transcription upon exposure to osmotic stress: First, PKA dephosphorylates Msn2/Msn4 causing their translocation to the nucleus to initiate quick but weak transcriptional changes within ten minutes. Strong transcriptional changes require a pulsatile translocation of Msn2/Msn4 between nucleus and cytoplasm, during which nuclear export is mediated by Msn5. Thus, we reason that the non-adapted response examined in this work displayed the initiation phase but not the second progression phase, potentially explaining the mild log-fold changes compared to others (Causton *et al.*, 2001; Gasch, 2007a). Recently, Wu *et al.* (2021) inferred that Msn4, but not Msn2, is regulated by an incoherent feedforward loop (IFFL), including the intermediate regulator kinase Yak1. Since the purpose of IFFLs is to accelerate response time and execute

oscillatory behavior (Reeves, 2019) we interpret the absence of significant Msn2 regulation (figure 22B) as further support for an early ESR retraction mechanism.

Recent research concerning the ESR identified strong counter-correlated gene expression between the ESRi and RP/RiBi clusters. The latter, sometimes referred to as the ESRr (ESR repressed) cluster, is mediated by the regulatory activity of Sfp1, Ihf1/Fhl1 and the general activator/repressor TF Rap1 (Gasch *et al.*, 2017; MacGilvray *et al.*, 2020). Our experiment confirmed the mutual relationship between ESRi and ESRr, even though transcriptional control of RP and RiBi genes was executed exclusively via Sfp1 and Ifh1. Both TFs are inducers of proliferative capacity as Sfp1 binds the RiBi-associated PAC promoter while Ifh1 positively controls RP gene expression through a currently unknown promoter architecture (Schawalder *et al.*, 2004; Cipollina *et al.*, 2008). Either TORC1 or PKA retains their active state during optimal growth. Sudden downshift of nutrients, however, induces PKA-coordinated ESRr downregulation, which can be explained by cytosolic localization of Sfp1 and Ifh1 alone (Zencir *et al.*, 2020; Shore, Zencir and Albert, 2021). This exclusively stress-specific role of Sfp1 and Ifh1 is mediated through their antagonizing TFs Dot6/Tod6 and Stb3, respectively (Huber *et al.*, 2011; Plank, 2022).

Taken together, the observed retraction and overshooting gene expression originated from the TORC1/PKA circuitry since both nodes tune the temporal and local displacement of overlapping TFs. Acute glucose exhaustion signals PKA to execute its feedforward role to rapidly respond to the stimulus and override the steady state controller TORC1 (Kunkel, Luo and Capaldi, 2019). Similarly, PKA remains dominant when glucose levels elevate, leading to overshooting regulation until TORC1 regains control. It is somewhat surprising that the overshoot amplitude matches the initial response. Combined with the feedforward role of PKA, multiple feedback mechanisms exist with the potential to act as signal amplifiers. For instance, Ashe *et al.* (2000) reported severe inhibition of translation initiation within 30−60 s after glucose depletion, which can induce rapid RiBi and RP mRNA degradation (Huch and Nissan, 2014). In our experiment, ample nutrient conditions 2 min after the start of the s-LSL cycle superimposed the initiated decay of translation-associated genes. The phenotype may be explained by consequent disparate sensing of expected versus actual growth rates that may prompt yeasts to boost transcription of growth associated mRNAs causing the observed overshoot (Shore, Zencir and Albert, 2021). Regarding the regulation of energy homeostasis, the SNF1 kinase is activated upon *AEC* drops by as narrow as 0.1 causing inhibition of TORC1

(Oakhill, Scott and Kemp, 2012; González and Hall, 2017) and co-phosphorylation of stress-responsive PKA targets (De Wever *et al.*, 2005).

Once activated, SNF1 co-activated specific gene expression programs via crosstalk with the TOR/PKA node. Furthermore, the TFs Adr1 and Cat8 are amplified but not Mig1 (Busti *et al.*, 2010). Besides SNF1, Mig1 is dependent on further activation through hexose kinase 2 and represents one branch of dual control over the carbon catabolite repression (CCR) regulon. The second branch integrates extracellular glucose signals through the sensory Rgt2/Snf3-PKB system (Busti *et al.*, 2010; J.-H. Kim *et al.*, 2013). Since we did not observe any differentially expressed CCR genes, we reason that SNF1 regulation is solely *AEC* driven. Consequently, the strictly glucose-related Rgt2/Snf3-PKB pathway was not implicated in the non-adapted response. Short-term energy deprivation further induced changes in mitochondrial translation (see Figure 19 cluster 5). Yi and colleagues (2017) reported that SNF1 associates to the mitochondrial membrane to support respiratory activity for 10 h of glucose starvation – a prerequisite to sustain autophagy during arrested growth. We hypothesize the existence of a preparative program that was aborted in early stage in analogy to the observed ESR dynamics: Genes encoding translational capacities might have been differentially expressed as a preparatory measure to alter mitochondrial respiration. Nevertheless, the cascade was shut down promptly after return to steady state conditions.

The transcriptional response mirroring frequent glucose starvation

Once famine zones are established during industrial fermentations, yeast cells require adaptation to withstand the repeated exposure to the starvation conditions that request regime transitions. Our experimental design enabled the investigation of the growth phenotype and the transcriptional strategy during oscillatory glucose availability by imposing an intermittent feeding regime. On a macroscopic level, the cellular mode of operation mimicked that of a faster-growing population, *i.e.* reduced carbon storage pools, increased rRNA content and ribosomal gene expression, decreased ESR expression levels, downregulated glycolytic genes and upregulated cell cycle genes (Nissen *et al.*, 1997; Silljé *et al.*, 1999; Regenberg *et al.*, 2006; Brauer *et al.*, 2008; Xia *et al.*, 2022).

Processing of dynamic environmental inputs can cause repeated decoupling of the growth rate from the expected μ-specific transcriptome (Levy and Barkai, 2009; Zaman *et al.*, 2009; Zakrzewska *et al.*, 2011). Dedicated studies assigned this dissonance predominantly to high PKA activity, which is in agreement with our DS dataset: Strong ESRi repression and RiBi

induction, backed by increased expression levels of PKA pathway components are opposed to relatively weak RP induction, owing to the TORC1-dependency of the latter (see summarizing figure 23) (Huber *et al.*, 2011). Under the investigated conditions, however, cells did not shut down rapid translation initiation control mechanisms, which is also reflected by dynamic ESRi/RiBi patterns during the adapted time series. This finding may surprise as the yeast's ability to decelerate translation upon glucose scarcity may be regarded as a persistent "first line of defense" (Hershey, Sonenberg and Mathews, 2012). Instead, cells apparently enable growth by benefitting from higher ribosome abundance as it was observed in other studies (Young and Bungay, 1973; Metzl-Raz *et al.*, 2017). This seems to be an evolutionarily conserved principle since bacterial cells elevate ribosome content for accelerating growth after relieving from various stresses (Bergen *et al.*, 2021). However, despite amplifying genes encoding ribosomal proteins, yeasts further backed ribosomal biogenesis and configuration to maximize growth capacities. In this context, Parenteau *et al.* (2015) reported that perturbed growth can induce the expression of different subunits including gene paralogues which increase fitness and which are repressed under normal growth. Likely, de-repressed RP paralogues do not exert stress-specific functions but may enable atypical gene overexpression. In our study, however, we could not draw any conclusion if and to which extent differentially expressed paralogue genes actually contributed to the observed phenotype.

Furthermore, even though still under debate, increased RiBi expression supposedly indirectly promotes progression over START during the cell cycle through Whi5 inactivation (Bernstein *et al.*, 2007; Polymenis and Aramayo, 2015; Schmoller *et al.*, 2015). Eased START passaging leads to reduced time within the G0/G1 phase and decreased trehalose and glycogen pools (Paalman *et al.*, 2003; Brauer *et al.*, 2008). Hence, we argue that the cell cycle aligned with the PKA-guided shaping of the translational machinery following the environmental signal as a feedback mechanism (Müller *et al.*, 2003). Transcriptome analysis revealed added regulatory rearrangements that point towards a preference for PKA activity over TORC1 control. Downregulation of non-relevant stress signaling cascades was observed, such as the osmo-responsive MAPK cascade — a constitutive inhibitor of PKA (Mace *et al.*, 2020). In terms of energy homeostasis, elevated translational capacity is ATP-costly and might have contributed to the increased *AEC* difference during the LSL transition in DS. A more pronounced drop of the *AEC,* in turn, could potentially amplify the earlier discussed SNF1-guided energy signal integration with positive feedback for PKA and repression of TORC1 targets. In conclusion, exposure to recurring regime transitions shifted the regulatory response of *S. cerevisiae* into a

mode of dominating PKA signaling. The kinase constantly overrides the steady state controller TORC1 and is amplified by several feedback mechanisms, the consequence of which is a cellular tuning to enable efficient growth acceleration based on the adapted ribosome portfolio.
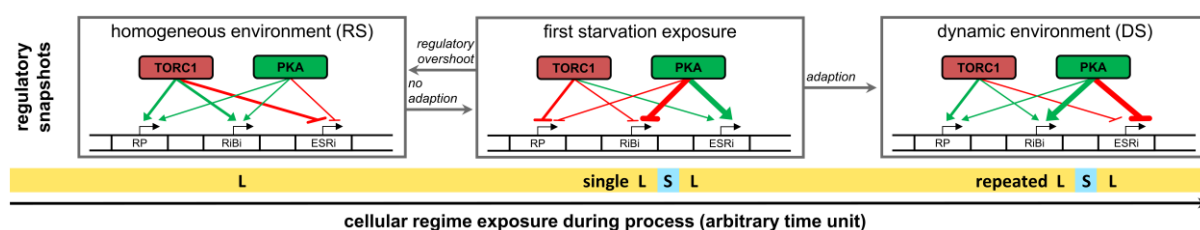
Figure 23. Key regulatory elements comprising target of rapamycin 1 (TORC1) and protein kinase A (PKA) signaling. DS, dynamic steady state; ESRi, induced environmental stress response genes; L, C-limitation; RiBi, ribosome biogenesis genes; RP, ribosome protein genes; RS, reference steady state; S, C-starvation.

Potential transfer of knowledge for industrial strain engineering

Understanding how cells adapt to substrate heterogeneities in industrial bioreactors is important for bioprocess optimization. The trade-off between stress-response and internal growth capacity turned out as a key mechanism to explain cellular performance under recurring glucose starvation. If biomass itself is the product, maintaining a high growth rate is a favorable trait. However, for exploiting metabolic production capacities the priorization of re-installing high growth rates may deteriorate the supply of carbon, reduction factors, and energy for the targeted product formation. This conflict may arise for metabolic products as well as for heterologous proteins. For the latter, ribosome buildup could potentially reduce the product yield and *vice versa* (Birnbaum and Bailey, 1991). Yet, predicting the impact of competing resource allocations influenced by environmental signaling is not a trivial task (Kafri *et al.*, 2016). For instance, Wright *et al.* (2020) reported increased insulin production from *S. cerevisiae* in a two-compartment scale-down approach with a remarkable conformity to the results presented here: Environmental heterogeneity enforced the translational machinery and repressed stress-responsive networks, which proved to be beneficiary for insulin productivity. In consequence, we propose two use cases for our dataset.

First, the deployed scale-down approach can enable strain engineers to streamline industrial hosts. For instance, we observed a presumably unnecessary induction of the ESRi cluster upon first-time glucose withdrawal as it was actively repressed during repeated glucose oscillations. Thus, deleting Msn2/4 could potentially save unwanted resource expenditure. This proposal is supported by the work of Ashe and colleagues (2000), who prove that *msn2/4Δ* strains abolished the induction of the stress response program while maintaining a normal growth phenotype.

Likewise, our dataset suggests wasteful gene expression induced via Hsf1 and Crz1. Indeed, altering nuances of the regulatory response via TF engineering gains popularity as relatively minor changes in the genetic background can improve strain performance significantly (Mohedano, Konzock and Chen, 2022). For instance, several studies achieved increased ethanol yield through the atypical expression of just a single transcription factor (Michael *et al.*, 2016; Watanabe *et al.*, 2017; Samakkarn, Ratanakhanokchai and Soontorngun, 2021).

Second, this and other work supports the finding that glucose availability, but also other industrially relevant heterogeneities, converge mainly on the level of PKA signaling (Norbeck and Blomberg, 2000; Zaman *et al.*, 2009; De Melo *et al.*, 2010; de Lucena *et al.*, 2015; Zhao *et al.*, 2015). To conclude, we would like to formulate a somewhat alternative, maybe even provocative scale-down route. If mere activation/inhibition dynamism of PKA shapes the corpus of adaptation effects during industrial fermentations, wouldn't triggering PKA according to process-relevant stimuli suffice as the most simplistic scale-down experiment? Instead of trying to mimic physicochemical perturbations by wet-lab approaches as close to reality as possible, it might be sufficient to characterize the frequency and amplitude of relevant stimuli *a priori*, for instance, by means of CFD simulations. Consequentially, the simulation output should be translated into an input signal for the PKA hub. Tools to control PKA activity on relevant scales are already available, such as optogenetic switches (Stewart-Ornstein *et al.*, 2017; Hepp *et al.*, 2020). Ultimately, this approach could empower rational scale-down by providing a fast and easy method to estimate the impact of extracellular signal fluctuations on strain performance.

4.2.6 Conclusion

This study revealed that perception of extracellular glucose concentration alone can induce pronounced biological scale-up effects. Industrially relevant glucose gradients with regime transitions between carbon limitation and starvation were set in a chemostat with intermittent feeding. The single most prominent observation, irrespective of the adaptation status, was the adjustment of internal resources following a stress response–growth trade-off. Interpretation of transcriptomic data allowed us to identify the implication of several regulatory circuits, all centered around protein kinase A. In consequence, we were able to define engineering propositions with the potential to (i) improve strain performance in an industrial setting and (ii) simplify classical scale-down. Here, a growth scenario was investigated with the laboratory *S. cerevisiae* strain CEN.PK113-7D. Comparative experiments carried out under the same premise with industrial production hosts, especially considering polyploid strains, could shed further light on the general applicability of the demonstrated approach.

4.3 Mimicked mixing-induced heterogeneities of industrial bioreactors stimulate long-lasting adaption programs in ethanol-producing yeasts

The manuscript was written by Steven Minden as first author. Prof. Dr.-Ing. Ralf Takors contributed to the manuscript's content through principal review. Prof. Dr.-Ing. Ralf Takors is the corresponding author. Steven Minden planned and conducted all experiments, collected and analyzed the according primary data. Maria Aniolek supported during sampling of the fermentation experiments. Prof. Dr.-Ing. Ralf Takors supervised the research.

This manuscript was accepted by the Multidisciplinary Digital Publishing Institute (MDPI) and published in the journal *genes*:

Citation:

Minden S, Aniolek M, Noorman H & Takors R. Mimicked Mixing-Induced Heterogeneities of Industrial Bioreactors Stimulate Long-Lasting Adaption Programs in Ethanol-Producing Yeasts. Genes. 2023; 14 (5); 1−23. https://doi.org/10.3390/genes14050997

Data repository:

https://doi.org/10.34894/6TMJD2

Correction note:

A graphical error was published within figure 7 of the original article as the color scale of the tachometer-representation of the environmental stress response is inverted for the peak s-LSL phase. This misrepresentation is corrected in figure 30 of this thesis.

4.3.1 Abstract

Commercial-scale bioreactors pose an unnatural environment for microbes from an evolutionary point of view. Mixing insufficiencies expose individual cells to fluctuating nutrient concentrations on a second-to-minute scale while transcriptional and translational capacities limit the microbial adaptation time from minutes to hours. This mismatch carries the potential for inadequate adaptation effects, especially considering that nutrients are available at optimal concentrations on average. Consequently, industrial bioprocesses that strive to maintain microbes in a phenotypic sweet spot, during lab-scale development, might suffer performance losses when said adaptive misconfigurations arise during scale-up. Here, we investigated the influence of fluctuating glucose availability on the gene-expression profile in the industrial yeast Ethanol Red^{TM}. The stimulus-response experiment introduced 2-min glucose depletion phases to cells growing under glucose limitation in a chemostat. Even though Ethanol Red^{TM} displayed robust growth and productivity, a single 2-minute depletion of glucose transiently triggered the environmental stress response. Furthermore, a new growth phenotype with an increased ribosome portfolio emerged after complete adaptation to recurring glucose shortages. The results of this study serve a twofold purpose. First, it highlights the necessity to consider the large-scale environment already at the experimental development stage, even when process-related stressors are moderate. Second, it allowed the deduction of strain engineering guidelines to optimize the genetic background of large-scale production hosts.

4.3.2 Introduction

Microbial fitness is determined by the ability to maintain internal homeostasis in view of external heterogeneity. Complex sensory systems allow microorganisms to adapt to the resource availability in a given habitat for survival and enabling growth (López-Maury, Marguerat and Bähler, 2008). Stress-response mechanisms take over if environmental conditions turn for the worse. Depending on the severity of external stress, a growing organism might reduce proliferation, enter a quiescent state or even undergo self-induced cell death (Skoneczny, 2018). Nonetheless, the early response usually involves a transcriptional adjustment that represses growth capacities to save resources for adequate adaptation. This program is a conserved feature across species, commonly referred to as the stringent response or environmental stress response (ESR) in prokaryotes and eukaryotes, respectively (Gasch, 2007b; Boutte and Crosson, 2013). Upon initiation, the transcriptional information propagates towards phenotypic change, which is well-aligned with the environmental shift.

In industrial fermentation development, in the lab the microbial habitat is that of a tightly regulated bioreactor. Several variables, such as pH, temperature, dissolved oxygen and substrate concentration, are kept at optimal levels to maintain the microbial host in the physiological state of optimal productivity. Still, many bioprocesses suffer unforeseen performance losses when engineers transfer a process from the homogeneous lab environment to the industrial scale (Takors, 2016). So-called biological scale-up effects occur when transport limitations in large tanks prevent proper mixing, cooling and mass transfer needs of the broth rendering the environment heterogeneous (Enfors *et al.*, 2001; Crater and Lievense, 2018). Often, limiting substrate concentrations are set during production phases to ensure that microbial activities still cope with the technical limits of aeration, heat exchange, etc. Such limiting substrate supply defines substrate-to-product conversion yields, and cellular and volumetric productivities. Gradients of said substrates evolve as their reaction time is typically shorter than the mean circulation time in industrially-sized tanks (Fowler and Dunlop, 1989). Therefore, a fluctuating physicochemical environment clashes with a complex biological sensory system. Understanding the systematic incompatibility helps to understand why biological scale-up effects occur and guide rational strain engineering efforts (Wehrs *et al.*, 2019).

Saccharomyces cerevisiae, a widely adopted host in the biotech industry, is equipped with the sensory abilities to adapt to the entire spectrum of substrate concentrations it may encounter in

a fermentation process. Backed by large-scale process data, simulation studies confirmed the existence of glucose concentration gradients spanning several metabolic regimes in a glucose-limited fed-batch production of baker's yeast (George *et al.*, 1998; Haringa *et al.*, 2017; Sarkizi Shams Hajian *et al.*, 2020). For instance, highly concentrated feed solutions may locally introduce glucose concentrations above respiratory capacities, potentially triggering carbon catabolite repression. Distant from the feed inlet, in turn, the substrate becomes depleted triggering starvation-like signals. However, minute-to-hour adaptation times typically exceed the second-to-minute exposure times in the stirred bioreactor space (Delvigne and Goffin, 2014). Thus, cells are prompted to initiate adaptive or even stress-responsive programs, and either their execution or trimming causes unnecessary resource expenditure that might even lead to phenotypic heterogeneity (Delvigne and Goffin, 2014; Gutin *et al.*, 2019).

Following the scale-down route, researchers aim to use insights from physical large-scale studies to investigate the physiological response against realistic gradients. Especially in high-cell density processes, the influence of carbon starvation zones draws more and more attention (Kuschel and Takors, 2020; Nadal-Rey *et al.*, 2021; Ho *et al.*, 2022; Minden *et al.*, 2022). Dedicated experiments with prokaryotic hosts revealed redundant induction and repression of the stringent response when cells were repeatedly withheld from the limiting substrate (Löffler *et al.*, 2016; Ankenbauer *et al.*, 2020). Derived knowledge on the gene-regulation level ultimately guided rational strain engineering approaches to increase microbial robustness (Michalowski, Siemann-Herzberg and Takors, 2017; Ziegler *et al.*, 2021). In a recent study, we investigated the transcriptional profile of respiring *S. cerevisiae* against short-term transitions between glucose limitation and starvation in an analogous approach (Minden *et al.*, 2023). First-time exposure to acute glucose depletion elicited the ESR prematurely in a non-adapted culture, while it was globally repressed in a 'stand-by mode' enabling dynamic response once the population was adapted to the signals. We concluded that regulatory elements of the ESR, such as the involved transcriptional activators Msn2/4, might be promising targets for strain engineering approaches. However, both the culture conditions and the applied haploid CEN.PK113-7D strain has little to no relevance in industrial fermentation processes. In addition, this strain harbors several non-synonymous mutations in its cAMP signaling system, the primary mediator of ESR activity (Nijkamp *et al.*, 2012). Consequently, we set out to replicate the experiment with the diploid industrial Ethanol Red^{TM} strain under anaerobic, ethanol-producing conditions.

4.3.3 Material and methods

Strain, maintenance and seed culture

The commercial, MATa/MATα diploid *S. cerevisiae* strain Ethanol Red™, currently marketed by Fermentis (Lesaffre, Marcq-en-Barśul, France), was kindly provided by Royal DSM N.V. (Delft, The Netherlands). Cells were preserved in 30 % (v/v) glycerol at −70 °C and grown on yeast extract peptone dextrose (YPD) agar plates for two days before starting the aerobic seed cultures. First, a 10 mL glass vial with 5 mL of YPD broth was inoculated with a single colony and incubated at + 30 °C on an orbital shaker operated at 120 rpm for 6–8 h. Subsequently, the whole volume was pelleted and used to inoculate 110 mL of a synthetic medium in a 1000 mL baffled shake flask and grown under identical conditions overnight until the stationary phase was reached. The medium was designed to support approximately 5.0 g·L^{-1} biomass during carbon-limited growth with 50 g·L^{-1} glucose and contained 10 g·L^{-1} ammonium sulfate, 6.0 g·L^{-1} monopotassium phosphate, 1.0 mg·L^{-1} magnesium sulfate heptahydrate, 19.1 mg·L^{-1} ethylenediaminetetraacetic, 4.5 mg·L^{-1} zinc sulfate heptahydrate, 1.0 mg·L^{-1} manganese(II) chloride tetrahydrate, 0.3 mg·L^{-1} cobalt(II) chloride hexahydrate, 0.3 mg·L^{-1} copper(II) sulfate pentahydrate, 0.4 mg·L^{-1} sodium molybdate dihydrate, 4.5 mg·L^{-1} calcium chloride, 3.0 mg·L^{-1} iron(II) sulfate heptahydrate, 1.0 mg·L^{-1} boric acid, 0.1 mg·L^{-1} potassium iodide, 0.05 mg·L^{-1} D-biotin, 1.0 mg·L^{-1} calcium pantothenate, 1.0 mg·L^{-1} nicotinic acid, 25.0 mg·L^{-1} myo-inositol, 1.0 mg·L^{-1} thiamine HCl, 1.0 mg·L^{-1} pyridoxine HCl, 0.2 mg·L^{-1} para-aminobenzoic acid, 0.42 g·L^{-1} tween 80, 10 mg·L^{-1} ergosterol and 0.2 g·L^{-1} Struktol J 674 antifoam (Schill und Seilacher, Hamburg, Germany). The same medium was used for seed, batch and continuous cultures.

Chemostat setup

Anaerobic cultivation experiments were carried out in a stainless-steel benchtop bioreactor (Bioengineering, Wald, Switzerland) with a liquid working volume of 1.7 L under a 0.3 bar overpressure. The reactor system and its rapid sampling device were operated as previously described (Minden *et al.*, 2022, 2023) with the following modifications: (i) silicone tubing was replaced by oxygen-impermeable tubing (Norprene, Cole Parmer, Vernon Hills, IL, USA), (ii) anaerobiosis was maintained with a sterile nitrogen supply of 0.425 vvm and (iii) no antifoam agent was supplied as it was already present in the medium. Furthermore, the headspace of the feed casket was kept flushed with sterile nitrogen throughout the experiment.

The reactor was aseptically inoculated with 100 mL of seed culture and operated in batch mode until a decrease in CO_2 emission indicated glucose exhaustion. Subsequently, the chemostat was initiated via continuous medium influx and broth efflux at net rates of 2.83 mL·min^{-1} to yield a dilution rate (D) of 0.10 h^{-1}. During stimulus–response experiments (SREs), the system was operated as an intermittently fed chemostat. The feeding pump was set to 0.00 mL·min^{-1} for two minutes while the harvest pump control was inactive. In the case of repeated perturbation cycles (2 min feed off, 7 min feed on), the feed rate was set to 3.64 mL·min^{-1} to maintain the same net D.

Stimulus–response design

Three biologically independent fermentation experiments were carried out according to the process design depicted in Figure 24. Each chemostat operated for 5 residence times (τ) of constant $q_{carbon\ dioxide}$ to sample the reference steady state (RS). Thereafter, a single limitation–starvation–limitation (s-LSL) stimulus was imposed to track the non-adapted response as a time series of up to six hours. Subsequently, the mode of operation changed to an intermittent feeding regime. After five τ of repeated cycling, the new, dynamic steady state (DS) was established. The adapted response was sampled as a time series during repetitive cycles (r-LSL) and thus limited to one representative nine-minute series. Dynamic steady state values were expressed as cycle averages.
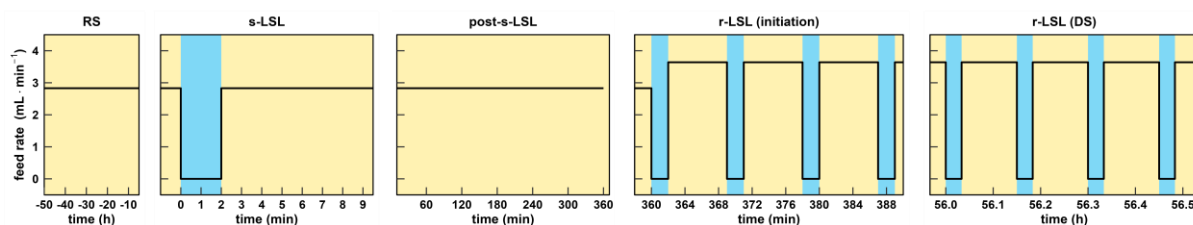
Figure 24. Process design of the chemostat experiment. DS, dynamic steady state; RS, reference steady state; r-LSL, repeated limitation–starvation–limitation transition; s-LSL, single limitation–starvation–limitation transition.

Analytical Procedures

Sample processing and analysis are thoroughly reported in (Minden *et al.*, 2022) and (Minden *et al.*, 2023). In brief, biomass, expressed as dry matter of biomass (*DMB*), was determined gravimetrically. All extracellular metabolites were determined with UV-based enzymatic kits (r-biopharm AG, Darmstadt, Germany). Intracellular carbohydrate and RNA pools were assessed according to the original protocols from Parrou and Sasano, respectively (Parrou and Francois, 1997; Sasano *et al.*, 2017). Unknown carbon in the supernatant was determined by

subtracting the molar carbon concentrations of the antifoam agent and all quantified extracellular metabolites except CO_2 from the total organic carbon concentration in the broth supernatant. We assumed no uptake of the antifoam agent, which has a carbon mass fraction of 61% (*w/w*) (Buchholz, 2015). Total organic carbon was measured indirectly with a multi-N/C 2100 S composition analyzer (Analytik Jena, Jena, Germany) by reducing the inorganic carbon fraction from the total carbon fraction of the supernatant. We estimated a 4.8 % loss of ethanol due to stripping which was accounted for in the carbon balance and parameter calculation ($Y_{ethanol/glucose}$, and $q_{ethanol}$). Ethanol stripping was estimated based on the approach by Löser and colleagues (Löser *et al.*, 2005) and is described in detail in appendix C.

Processing of Next-Generation Sequencing samples

We used the Quick-RNA Fungal/Bacterial Miniprep Kit (R2014, Zymo Research, Freiburg, Germany) for total RNA extraction with the following changes to the manufacturer's instructions: 0.5 mL of the biosuspension was sampled directly into a ZR BashingBead™ lysis tubes, pre-loaded with 0.5 mL of a lysis buffer. After the sample was withdrawn, the whole tube was instantly flash-frozen in liquid nitrogen and stored at −70 °C. The extraction protocol was resumed by thawing the samples halfway (5–10 min at room temperature) before performing the homogenization step in a Precellys 24 tissue homogenizer (Bertin Technologies, Montigny-le-Bretonneux, France) twice for 20 s at maximum speed with a 10 s break in between. At the end of the protocol, total RNA was eluted with 60 µL DNase/RNase-free H_2O and stored at −70 °C.

One 30 µL aliquot from each sample was shipped for mRNA sequencing to AZENTA/GENEWIZ (Leipzig, Germany). The contractor performed an initial quality check using Agilent 2100 BioAnalyzer (Agilent, Santa Clara, CA, USA) which revealed a heterogeneous RIN (RNA integrity number) value distribution ranging from 2.2–9.9 for all samples. After personal communication with the contractor, it was decided that the project would be commenced since the heterogeneous RIN values were a result of non-uniform rRNA peaks, even though the cause for this effect was unknown. Peaks for nucleotides of < 1500 nt including mRNA, however, showed uniform distribution. Next, polyA-selected cDNA libraries were synthesized and sequenced as 150 bp paired-end reads on a NovaSeq 6000 platform (Illumina, CA, USA) with a sequencing depth of $2 \cdot 10^7$ reads.

Gene expression analysis

A sequencing output in the form of *.fastqsanger* files was uploaded on a local Galaxy platform (Afgan *et al.*, 2018) followed by a quality check using *FastQC* v. 0.72 (RTSF - Michigan State University, no date). Sequence files were subsequently aligned with *TopHat* v. 2.1.1 (D. Kim *et al.*, 2013) against the phylogenetically closely related *S. cerevisiae* S288C reference genome (Gronchi *et al.*, 2022) (GCA 000146045.2-2011), which was accessed from the ENSEMBL database (Howe *et al.*, 2021). The overall alignment rate ranged between 83 and 92%. Genes were annotated to *Saccharomyces_cerevisiae.R64-1-1.50.gtf* (from ENSEMBL) and counted using *featureCounts* v. 1.6.4 (Liao, Smyth and Shi, 2014). From here, count tables were extracted from the Galaxy platform and merged into a *data.frame* object for further processing in the R environment v. 1.4.1106 (R Core Team 2021).

Differentially expressed genes (DEGs) were computed using *DESeq2* v. 1.32.0 (Love, Huber and Anders, 2014), applying the likelihood-ratio test with threshold values for $|\log_2$-fold change$|$ and a false discovery rate (FDR) (Benjamini and Hochberg, 1995) of 1.0 and $1 \cdot 10^{-3}$, respectively. More detail is provided in appendix C and the experimental design matrix is reported in supporting information B (tab 1). Time series data was clustered with the *kmeans* function from the *stats* (v. 4.1.0) package and functional annotations were derived from the web implementation of *YeastEnrichr* (Chen *et al.*, 2013; Kuleshov *et al.*, 2019). The raw enrichment analysis output can be accessed in supporting information B. Gene set enrichment analysis (GSEA) was carried out using *GAGE* (v. 2.42.0) (Luo *et al.*, 2009) with $\log_2$-scaled count tables (supporting information B, tab 19) and pre-defined literature data sets (tab 20) or transcription factor (TF) target sets (tab 21), which were downloaded from the *Yeastract* database (Monteiro *et al.*, 2020). The results in figure 6 were reduced to sets showing statistical significance (FDR $< 1 \cdot 10^{-3}$) during at least one condition in the SRE. Multiple set intersections of DEG lists were computed using the package *SuperExactTest* (v 1.1.0) which uses the combinatorial theory to provide the statistical significance of intersections (Wang, Zhao and Zhang, 2015).

4.3.4 Results

Characterization of extracellular glucose profile

The showcasing stimulus–response experiment enabled the observation of transcriptional feedback mechanisms of the industrial yeast Ethanol Red[TM] (ScER) after intermittent carbon supply. After anaerobically growing cells were adapted to strict glucose limitation for five residence times in a chemostat, the glucose feed was stopped for two minutes to establish a single limitation–starvation–limitation (s-LSL) cycle. A sharp, uptake-driven drop of the glucose concentration from 0.86 mmol·L^{-1} to 0.28 mmol·L^{-1} occurred, which restored to previous steady-state levels within eight minutes after feed resumption (figure 25, left panel). The biomass-specific glucose uptake rate (q_{glucose}) ramped down from 45 % to 21 % of the maximum capacities (for $q_{\text{glucose,max}}$, see table 4). Glucose uptake kinetics remained also for cells that were completely adapted to repeated LSL cycling for five residence times (r-LSL, figure 25, right panel). Notably, the perturbation never challenged cellular maintenance demands since the minimum q_{glucose} of 2.5 mmol·g$_{DMB}^{-1}$·h^{-1} stayed 5-fold above the maintenance rate of 0.5 mmol$_{\text{glucose}}$·g$_{DMB}^{-1}$·h^{-1} (Boender *et al.*, 2009).
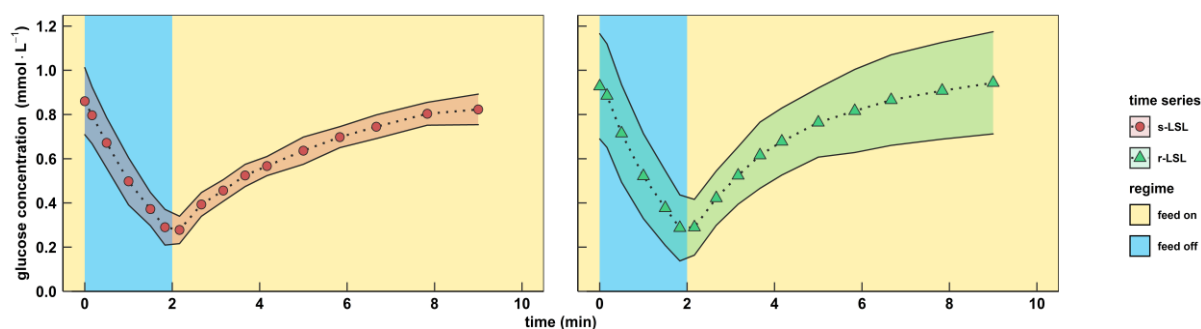
Figure 25. Characterization of the famine stimulus. Extracellular glucose concentrations during the course of one perturbation cycle are shown. Red circles indicate dynamics following a single (s) LSL transition ("feed off" phase) and green triangles indicate trends over a representative repetitive (r) LSL cycle during the DS. Time point 0 min of the s-LSL response is the equivalent of the RS. All values indicate means ± standard deviation of three biological replicates.

Table 4. Process parameters comparing the reference steady state (RS) against the dynamic steady state (DS). RS parameter values are the means ± standard deviation of three biological replicates. Steady state DS indicates averaged parameter values over one 9 min perturbation cycle of three biological replicates. D, dilution rate; DMB, dry matter of biomass; $Y_{i/j}$, yield of compound i from j; q_i, biomass specific rate of compound i; c_i, concentration of compound i; n.a., not applicable; n.s., not significant (p-value > 0.05).

Parameter	Dimension	Steady state RS	Steady state DS	% Change	Welch test (p-value)
D	h^{-1}	0.098 ± 0.003	0.099 ± 0.003	+0.5	n.s.
DMB	$g \cdot l^{-1}$	5.06 ± 0.04	4.72 ± 0.17	−6.8	n.s.
$Y_{DMB/glucose}$	$mol_C \cdot mol_C^{-1}$	0.114 ± 0.001	0.106 ± 0.003	−6.9	0.05
$q_{glucose}$	$mmol_C \cdot g_{DMB}^{-1} \cdot h^{-1}$	32.1 ± 0.8	34.7 ± 1.2	+8.0	0.04
$q_{glucose,max}$ [1]	$mmol_C \cdot g_{DMB}^{-1} \cdot h^{-1}$	71.50	64.80	−9.4	n.a.
K_S [1]	$mmol_C \cdot l^{-1}$	6.19	5.47	−11.6	n.a.
$Y_{ethanol/glucose}$	$mol_C \cdot mol_C^{-1}$	0.488 ± 0.033	0.468 ± 0.026	−4.0	n.s.
$q_{ethanol}$	$mmol_C \cdot g_{DMB}^{-1} \cdot h^{-1}$	16.7 ± 1.3	17.3 ± 1.4	+3.6	n.s.
$q_{carbon\ dioxide}$	$mmol_C \cdot g_{DMB}^{-1} \cdot h^{-1}$	7.68 ± 0.25	8.47 ± 0.18	+10.3	0.01
$q_{glycerole}$	$mmol_C \cdot g_{DMB}^{-1} \cdot h^{-1}$	2.70 ± 0.09	2.99 ± 0.12	+11	n.s.
$q_{acetic\ acid}$	$mmol_C \cdot g_{DMB}^{-1} \cdot h^{-1}$	0.04 ± 0.00	0.04 ± 0.00	−2.1	0.03
$q_{succinic\ acid}$	$mmol_C \cdot g_{DMB}^{-1} \cdot h^{-1}$	$2.9 \cdot 10^{-2} \pm 4.7 \cdot 10^{-3}$	$3.6 \cdot 10^{-2} \pm 1.4 \cdot 10^{-3}$	+25.7	n.s.
$q_{unknown\ carbon}$	$mmol_C \cdot g_{DMB}^{-1} \cdot h^{-1}$	1.06 ± 0.53	1.81 ± 0.91	+71.2	n.s.
$c_{glycogen}$	$mmol_C \cdot g_{DMB}^{-1}$	2.87 ± 0.16	1.65 ± 0.12	−42	$1.0 \cdot 10^{-3}$
$c_{trehalose}$	$mmol_C \cdot g_{DMB}^{-1}$	1.84 ± 0.19	1.25 ± 0.52	−32	n.s.
c_{RNA}	$mg \cdot g_{DMB}^{-1}$	64.3 ± 2.5	80.7 ± 3.1	+25	$2.0 \cdot 10^{-3}$
C-recovery	$mol_C \cdot mol_C^{-1}$	0.98 ± 0.02	0.98 ± 0.02		

[1] estimated parameters (see appendix C, table C1 and figure C1 for details)

The physiology of dynamic and steady state adaptation toward short-lived famine stimuli

The biomass-substrate yield remained for three hours after the s-LSL cycle indicating the absence of growth-arresting measures by the non-adapted yeast culture (figure 26A). Steadiness of growth was backed by constant intracellular RNA levels (figure 26D, p-value > 0.05) that may also serve as a surrogate parameter for ribosomal content (Warner, 1999). Regarding primary metabolism, substrate shortage was propagated through glycolysis causing a transitory reduction of carbon dioxide emission from 7.8 ± 0.2 mmol $\cdot g_{DMB}^{-1} \cdot h^{-1}$ to 5.8 ± 0.2 mmol $\cdot g_{DMB}^{-1} \cdot h^{-1}$ (figure 26B). We reason that the inertness of the off-gas

measurement caused the five-minute delay between both minima of glucose uptake and CO_2 emission. A similar observation was reported in a previous study with the same bioreactor system (Minden *et al.*, 2022). In addition, an acutely decreased glycolytic flux along the s-LSL trajectory caused the short-term mobilization of trehalose (*p*-value 0.06–0.11), but not glycogen, during the first six minutes.
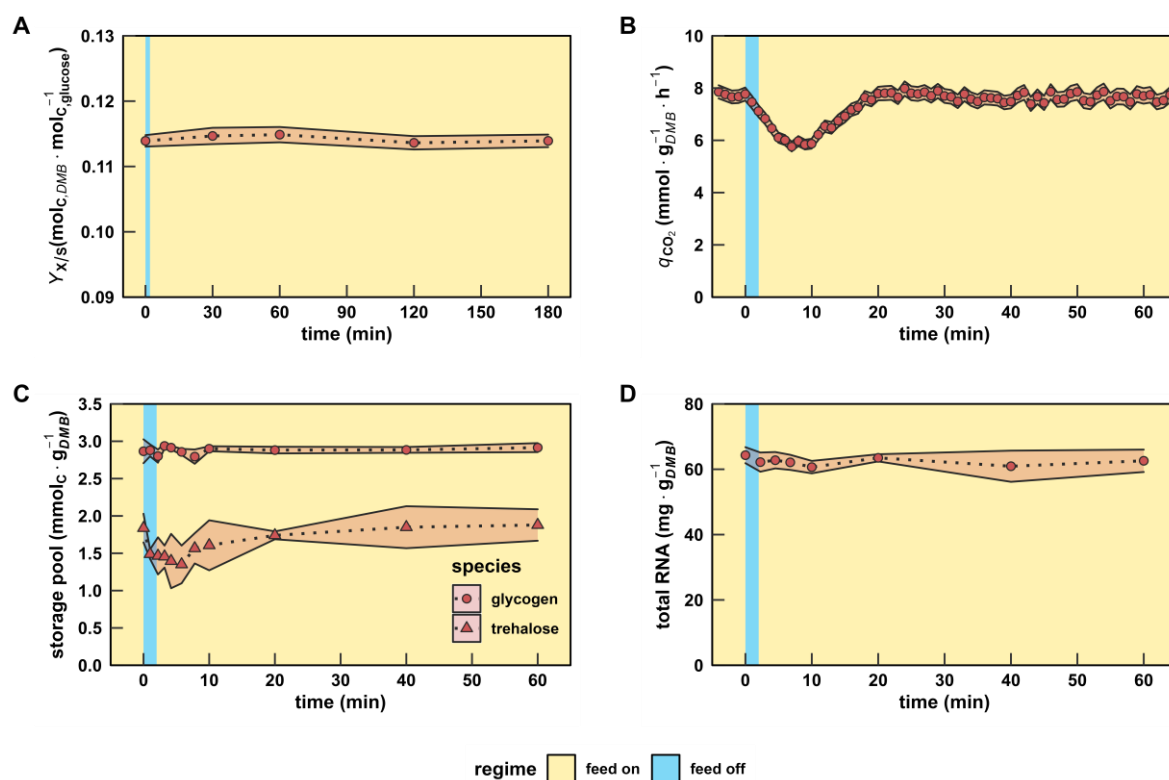
Figure 26. Characterization of macroscopic readouts after a single LSL stimulus. (A) Biomass-substrate yield up to 180 min. (B) Biomass-specific carbon dioxide production rate, (C) intracellular carbon storage, and (D) total RNA pool dynamics up to 60 min. The time series indicates dynamics following a single transition into the starvation phase ("feed off" phase). Time point 0 min is equal to the reference steady state. All values indicate means ± standard deviation of three biological replicates.

After the s-LSL cycle, repeated (r) r-LSL stimuli were performed during the second phase of the experiment. A single r-LSL cycle was analyzed using averaged data, the so-called dynamic steady state (DS). Therewith, distinct adaptations of ScER resource management were unraveled that mimicked cellular efforts to cope with the fluctuating substrate environment (table 4). Supported by closing carbon recoveries, the biomass-substrate yield ($Y_{DMB/\text{glucose}}$) dropped by 6.9 % whereas the net dilution rate and glucose feed remained. Consequentially, an equal rise of biomass-specific glucose uptake occurred. Relative to the reference steady state (RS), the surplus of the glycolytic input was channeled towards CO_2 emission. From the trend, increased ethanol production and glycerol secretion were also found, which agrees with stoichiometric expectations. The DS population released 71.2 % more unknown carbon

products than the reference state. Even though this value possesses low statistical confidence, the trend supports the slightly reduced $Y_{DMB/glucose}$ and might point to elevated cell lysis (Wang, Wu, *et al.*, 2018). Intracellular resource allocation changes made up the most pronounced r-LSL adaptations. We observed glycogen and trehalose pool size reductions of 42 % and 32 %, respectively. They were accompanied by increased intracellular RNA concentrations from 64.3 ± 2.5 mg·g_{DMB}^{-1} to 80.7 ± 3.1 mg·g_{DMB}^{-1}. Even though it is a well-known tendency of *S. cerevisiae* to counterbalance ribosome abundance with the degradation of glycogen reserves, the correlation is anticipated to be growth-rate-dependent only (Nissen *et al.*, 1997).

In consequence, we set out to investigate whether or not the sensing of the dynamic extracellular environment triggered cascading effects that propagated through the ScER regulatory network in a manner that was independent on the growth rate.

The transcriptional response to single starvation exposure (s-LSL)

The post-s-LSL cycle monitoring of ScER cells that operated at the steady state with an industrially representative production rate (Pais *et al.*, 2013) revealed a differential expression of 1053 genes (figure 27). Co-regulated mRNAs were grouped into seven clusters containing 66 to 211 genes before characterizing them through functional enrichment. This non-adapted feedback peaked between 10–20 min and entirely relaxed 60 min after the stimulus added.
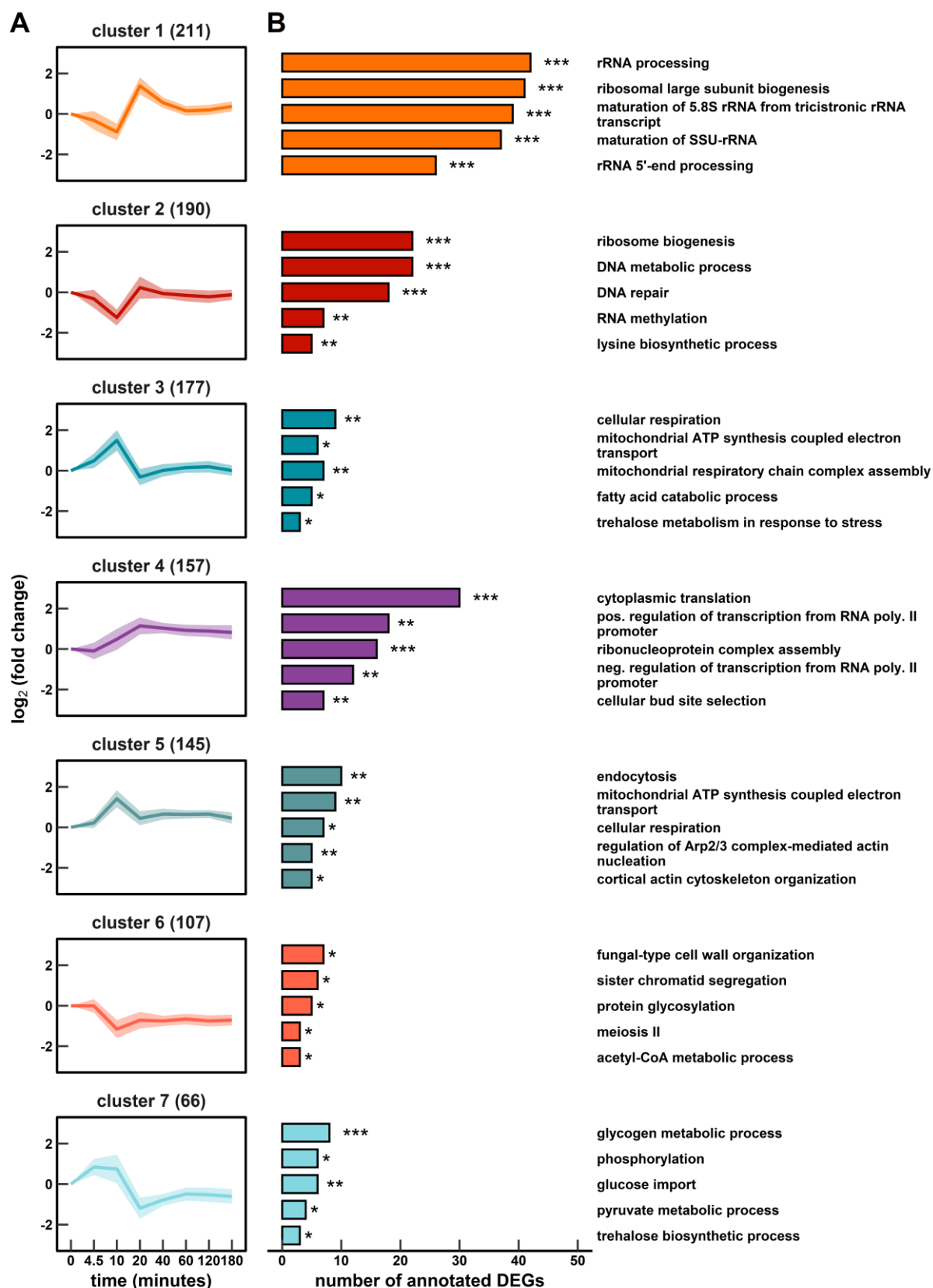
Figure 27. Gene expression dynamics following the single-LSL stimulus up to 180 min. (A) Seven k-means clustered groups of co-expressed genes are shown with the number of corresponding genes in brackets. (B) Corresponding gene ontology (GO) enrichment analysis. The false discovery rate (FDR) is indicated by asterisks for each GO term (* $1 \cdot 10^{-5} \leq$ FDR $< 5 \cdot 10^{-2}$; ** $1 \cdot 10^{-10} \leq$ FDR $< 1 \cdot 10^{-5}$; *** FDR $< 1 \cdot 10^{-10}$).

Clusters 1 and 2 followed a similar repression/de-repression trajectory with a strong amplitude of cluster 1 before RS levels were restored. Both clusters were significantly enriched with genes of the ribosome biogenesis (RiBi) ontology, which were further specified as sub-ontologies such as rRNA processing or subunit maturation. Notably, the observed expression changes did not result in a detectable correlation with total intracellular RNA levels (figure 26D). Cytoplasmic translation was also enriched in the steadily induced cluster 4 opposing the downregulation trend of clusters 1 and 2 during early responses. Cluster 4 contains 29 of 37 differentially expressed ribosome subunits. Thus, the s-LSL response elicited 27 % of all 135 ribosome proteins (RPs). However, the remaining majority responded only in a dampened manner according to the analysis of RiBi-associated gene expressions.

In addition to the well-equilibrated response of protein formation, we observed evidence of the transiently reduced production of cell cycle-related transcripts. Cluster 2 covers DNA metabolic and repair mechanisms while cluster 6 comprises sister chromatid segregation and the term "meiosis II". Even though industrial diploid strains such as ScER should exhibit high mitotic stability (Steensels *et al.*, 2014), meiotic events especially during nutrient starvation are not uncommon (Herskowitz, 1988). In addition, the three genes leading to the significant call of "meiosis II", namely *IRC15*, *IML3* and *IPL1*, are involved in both mitotic and meiotic processes (Cherry *et al.*, 2012).

Clusters 3 and 5 somewhat mirror the trends of clusters 1 and 2 in an opposite manner. As they comprise a significant proportion of genes encoding respiratory capacities, this is unexpected given the strictly anaerobic environment. However, factoring in other functional enrichments, the picture of an acutely energy scavenging population evolves. Upregulated mRNAs coding for both endocytic functions and related regulatory elements such as Arp2/3-mediated actin nucleation are well-studied responses of acute glucose withdrawal (Lang *et al.*, 2014). Furthermore, the joint analysis of clusters 3 and 7 reveals the induced metabolic activity of the major carbon storage compounds glycogen, trehalose, and fatty acids. Rapid trehalose mobilization was accompanied by a 1.2-fold induction of the neutral trehalase encoding transcript *NTH1* in agreement with the literature (Thevelein, 1984). Conversely, glycogen mRNAs in cluster 7 were mainly involved in glycogen buildup (*GAC1*, *GIP2*, *GLC3*, *GLG1*, *GSY1*, *GSY2* and *UGP1*) whereas the respective polymer level remained constant. A functional dependency on the strategic upregulation of the respiratory apparatus becomes evident in genes that make up the "fatty acid catabolic process" ontology. In fact, products of transcripts such as *FOX2*, *ECI1*, *POT1* and *IDP3* catalyze the O_2-dependent β-oxidation of fatty acids (Kohlwein,

Veenhuis and van der Klei, 2013). Glucose import was equally tuned by inducing three high-affinity facilitators (Hxt4/17/13) and two of three hexokinases (Hxk1 and Glk1) (Herrero *et al.*, 1995).

In essence, the cellular transcriptional program prepared the population for carbon scarcity. The reset occurred after the glucose availability improved again. Interestingly, even though the transcriptome was deemed to be fully relaxed after 60 min, clusters 4, 6, and 7 did not re-install RS levels.

The transcriptional response to r-LSL

Next, we set out to investigate the adaptation status of ScER in the permanently dynamic environment. We assessed the steady-state gene expression profile of the DS versus RS. Thereof, we uncovered 332 induced and 265 repressed genes that were characterized using gene ontology and pathway enrichment (figure 28A, B). In addition, 141 transcripts remained responsive, as they were repeatedly upregulated and downregulated within r-LSL cycles (figure 28C, D).
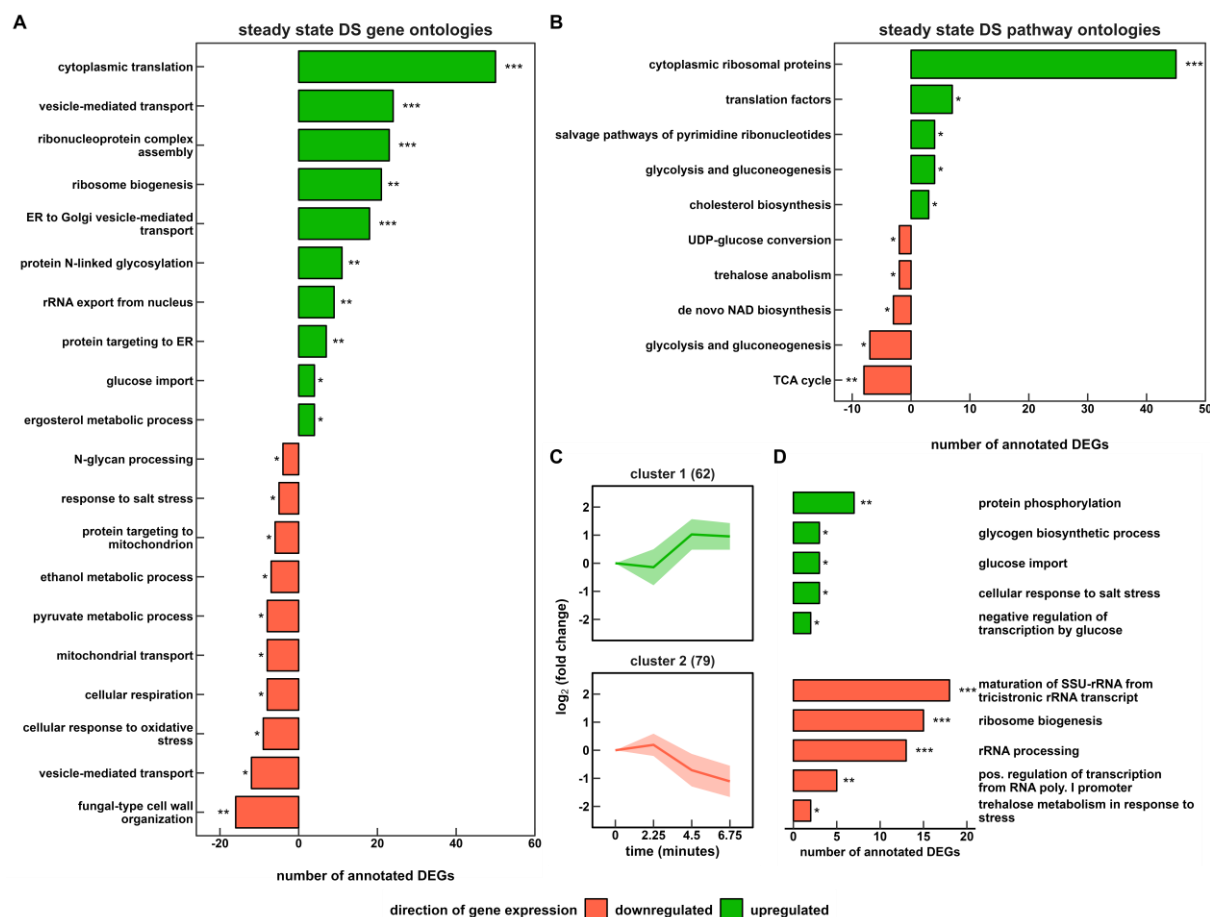
Figure 28. Functional enrichment analysis of DS based on (A) biological function and (B) pathway annotations. Short-term gene expression changes during the repeated (r) LSL cycles are shown in (C). Two k-means clustered groups of co-expressed genes are shown with the number of corresponding genes in brackets (D) representing the corresponding enrichment analysis of biological function. The false discovery rate (FDR) is indicated by asterisks for each category (* $1 \cdot 10^{-5} \leq$ FDR $< 5 \cdot 10^{-2}$; ** $1 \cdot 10^{-10} \leq$ FDR $< 1 \cdot 10^{-5}$; *** FDR $< 1 \cdot 10^{-10}$).

Completely DS-adapted yeast cells revealed a strategy of increasing their internal translation capacities against recurring starvation signals. Significant overrepresentation of related gene ontologies such as "cytoplasmic translation" and "ribosome biogenesis" further indicated that this strategy occurred for two sub-groups: transcripts coding for ribosome subunits and their maintenance apparatus. Notably, 45 RPs of the total 57 RPs revealed permanent amplification. In contrast to the observations for the s-LSL cycle, r-LSL gene expression changes were backed by a 25% increase in the intracellular RNA content (table 4). Pathway ontologies further indicated the marked upregulation of "translation factors" including the initiation factors eIF1, eIF2β, eIF4A, eIF4E, and eIF6. Notably eIF4A (also known as TIF2), which was induced 2.2-fold, plays a pivotal role in the early response of yeast towards acute glucose shortage by dissociating from the 48S pre-initiation complex (Castelli *et al.*, 2011). Dissociated eIF4A caused the instant stalling of translation initiation, which appeared to be alleviated through its

upregulation under the given conditions. Figure 28C, D further indicates the persistent short-term regulatory responses of gene products involved in ribosome biogenesis and more particular, rRNA processing in cluster 2. This functional group accounts for 25% of the steadily upregulated and downregulated portion of the transcriptome.

In addition to protein synthesis, we observed a highly significant differential expression of several genes annotated to protein modification and trafficking. The upregulated group "protein targeting to the endoplasmic reticulum (ER)" contains all four subunits of the signal peptidase complex (SPC), which is involved in cleaving signal peptides of secretory and membrane proteins during translocation into the ER (Antonin, Meyer and Hartmann, 2000). Regarding protein processing activity in the ER, significant upregulation of *N*-linked glycosylation genes occurred, such as the asparagine-linked glycosylation (ALG) group (*alg5/6/8*) and the oligosaccharyltransferase (OST) complex (*ost2/4/5/6*). Induction of genes that are involved in the formation of GPI anchors was observed, too (see supporting information B, tab 12).

Next, anterograde transport from the ER to the Golgi apparatus was stimulated through the induction of several coat protein complex II (COPII) elements, such as the GTPase Sar1 and the ER vesicle genes *erv29*, *erv41*, *erv14,* and *erv15*. COPII-coated vesicles transport membrane-bound proteins to the Golgi apparatus for the maturation of *N-* and *O*-linked glycosylation (Sutterlin *et al.*, 1997). Despite the strong upregulation of 22 Golgi-transport genes, downregulated mannosyltransferase transcripts, represented by the ontology "N-glycan processing", were the only significantly enriched DEGs with a Golgi-located protein modification function. At the end of the secretory pathway, we found upregulated sterol biosynthetic genes in both the gene ontology and pathway enrichment. This observation, however, seems rather counter-intuitive given that sterol synthesis is oxygen-dependent, rendering *S. cerevisiae* auxotrophic for this essential cell membrane component in anaerobic cultivations. In addition, a pronounced repression of "fungal-type cell wall organization" occurred, which included a set of genes such as the cell wall mannoproteins *cwp1*, *cwp2*, *tip1*, *tir3,* and *ccw12* — all functionally related to the downregulated mannosyltransferase capacities.

Yeast cells reportedly maintain branched tricarboxylic acid cycle (TCA) activity under anaerobic conditions to supply building blocks for growth (Rodrigues, Ludovicio and Leao, 2006), which was reflected by the small amounts of extracellular succinic acid (Table 1). Moreover, respiratory abilities are preserved in the absence of oxygen, too (David and Poyton, 2005; Helbig *et al.*, 2009). Here, we observed a significant downregulation of these auxiliary

functions of respiratory pathways, such as mRNAs involved in the reductive (*MDH1, MDH2,* and *FUM1*) and oxidative (*ACO1*) TCA branches and repressed "cellular respiration", "mitochondrial transport", and "TCA cycle" ontologies. Regarding central carbon metabolism, repression also occurred on the level of pyruvate and ethanol metabolism. Gene-level investigation revealed that TCA influx mainly was hampered through pyruvate dehydrogenase (*PDA1*), pyruvate decarboxylase (*PDC6*), and aldehyde dehydrogenase (*ALD4*). This coincided with amplified fluxes towards fermentative pathways upstream of TCA. For instance, *ADH5*, which supports ethanol production (Sazegari *et al.*, 2022), was induced 5.2-fold. Glucose uptake was also re-arranged to cope with decreasing extracellular availability through increased expression levels of the high-affinity transporter mRNA *HXT2/6/7* and the hexokinase 2. Non-glucose hexose transporters, such as mannitol and sorbitol scavenging Hxt13/17 were found to be dynamically expressed/repressed in cluster 1 during r-LSL transitioning.

Taken together, the adaption towards short-term limitation–starvation cycling encompassed the marked restructuring measures taken to aim at fostering growth. Translation-related genes were amplified at the expense of sacrificing reserve respiratory abilities and some non-specific stress response mechanisms, such as the "cellular response to oxidative stress" and the "response to salt stress". As indicated in the gene expression profiles, the ATP-demanding formation of ribosomes was additionally supported by fostering ATP generation through ethanol fermentation.

Comparing transcriptional responses of s-LSL and r-LSL

Regulatory information was deduced from gene set enrichment analysis (GSEA) to uncover the dynamics of literature-derived sets (Fazio *et al.*, 2008; Gasch *et al.*, 2017) (figure 29A) and more nuanced transcription factor (TF)-mediated regulons (figure 29B). The analysis was conducted on s-LSL, r-LSL and DS data while restricting the output to gene sets with statistically significant enrichment in at least one sample point across all conditions. Figure 30 serves as a visual summary of the involved regulatory elements and reported interactions.
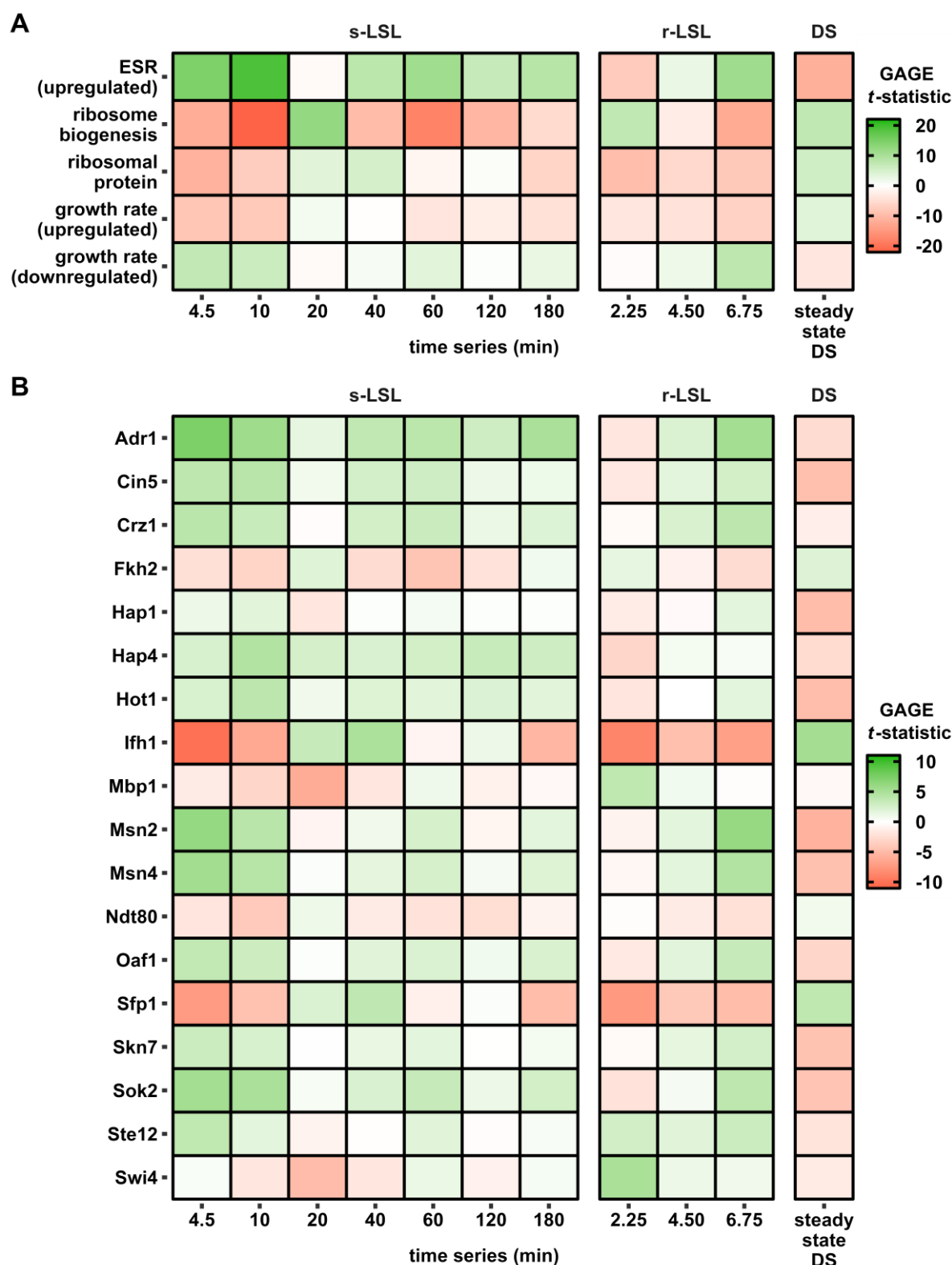
Figure 29. Gene set enrichment analysis (GSEA) of pre-defined gene lists from the literature (A) and transcription factor target lists (B). The reported *t*-statistic implies the strength and direction of the coordinated differential gene expression of a given set. GSEA was performed comparing the single (s) LSL time series against the reference steady state. Furthermore, the repeated (r) LSL time series was compared against its internal time point 0 min. The DS is a contrast between the reference steady state and all r-LSL sample points. Only gene sets with significant enrichment in at least one sample point (FDR < 1 · 10⁻³) are shown.
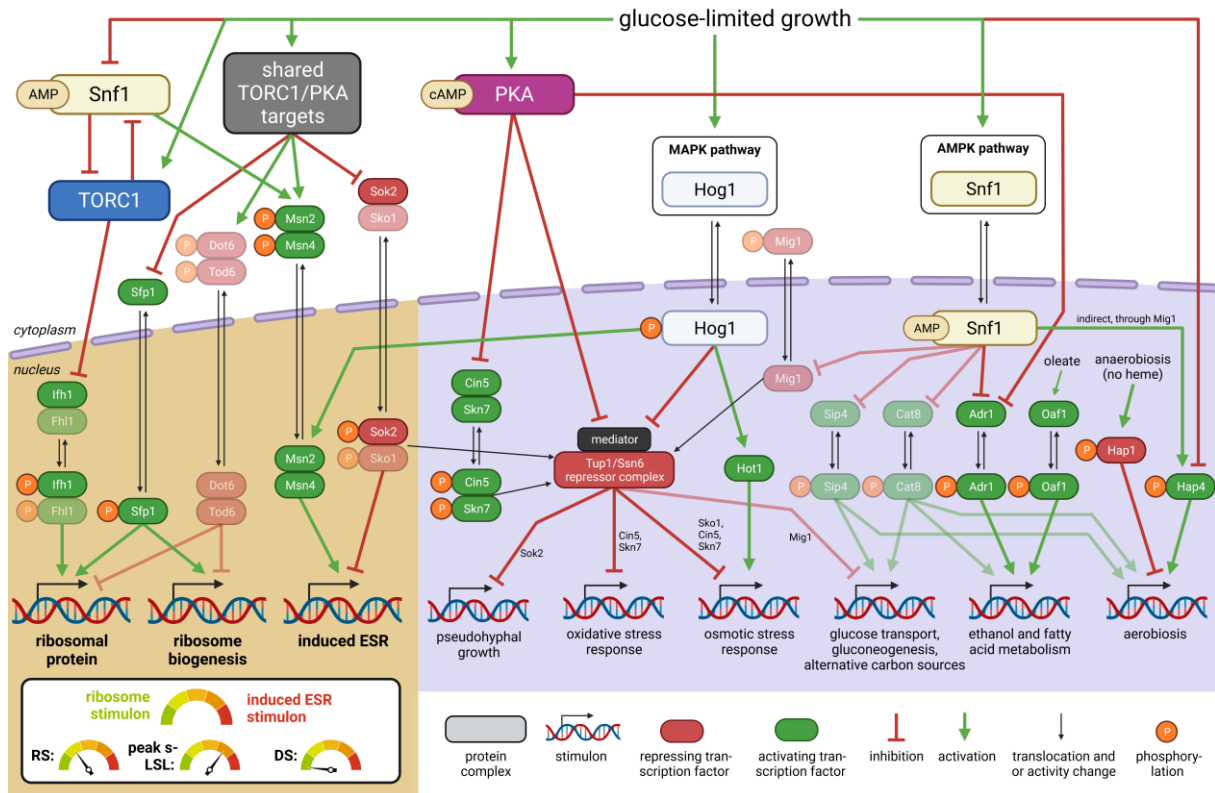
Figure 30. Regulatory kinase and transcription factor network active under the given experimental conditions. The brown background highlights the main ESR-associated stimulons. The violet background depicts observed co-induced stimulons. The simplified schematic network is limited to transcription factors (TFs) with significant calls in the GSEA and their known upstream effectors. Transparent TFs were either not significant or not part of the analytical pipeline but still included due to the reported implication in the given network. For simplification, not all pathway components, connections, and alternative functions are illustrated. The shown network is based on (Charizanis *et al.*, 1999; Shenhar and Kassir, 2001; Lempiäinen and Shore, 2009; Ratnakumar *et al.*, 2009; Busti *et al.*, 2010; Huber *et al.*, 2011; Broach, 2012; Gutin *et al.*, 2015; Zhang *et al.*, 2017).

ScER perceived the transient first-time exposure to starvation as an elicitor of the environmental stress response (ESR). As is typical for this program, the early induction of the ESR stimulon coincided with repression of ribosome stimulons represented by the RiBi and RP sets. Strictly growth-rate-dependent sets were considered to discriminate between the onset of the ESR program and mere adjustments of the growth rate. Since amplitudes measured after 10 min of s-LSL exposure of the ESR and RiBi sets showed 2–3-fold larger |*t*-statistic| values than those of the growth-rate-dependent sets, we concluded that the observed response was dominated by the ESR. This was also backed by constant $Y_{DMB/\text{glucose}}$ throughout the non-adapted time-series. Similarly to the responses to the s-LSL cycle, r-LSL transcript dynamics reveal dampened oscillations, which are also visible in TF targets. Examples are the Msn2/Msn4 pair and the de-repression through Sok2 target genes. Further examples are also given regarding the repressed

ESR branch with Ifh1-guided RP repression and Sfp1 control over both RP and RiBi genes (Gutin *et al.*, 2015; Gasch *et al.*, 2017).

Thus, a stress response–growth trade-off emerges, which is primarily balanced via the upstream effector target of rapamycin 1 (TORC1) and the protein kinase A (PKA). Our results further revealed additional signal input through the stress-activated signaling hubs, such as the mitogen activated kinase (MAPK) cascade or the glucose de-repression program (López-Maury, Marguerat and Bähler, 2008). One example is the osmo-responsive mitogen-activated HOG1 kinase as it is involved in both the direct induction of the osmotic stress response and fine-tuning of the ESR (Hohmann, 2002; Gutin *et al.*, 2015). HOG1 activity was confirmed though the significant regulation of Hot1, a mediator of the osmo-specific gene expression program of this kinase. Closely related are the activators Cin5 and Skn7 and the repressor Sok2, which are stress-responsive recruiter molecules for the Tup1-Ssn6 repressor complex (Hanlon *et al.*, 2011). Tup1-Ssn6, in turn, interacts with the mediator complex — a coordinator of PKA and HOG1 signal integration under environmental stress (Gutin *et al.*, 2015). Tup1-Ssn6 recruitment is not the only role of Skn7 as it further stabilizes the calcineurin-dependent transcription factor Crz1 (Hohmann, 2002). Thus, it may not be surprising that both gene sets displayed almost identical expression dynamics. Another TF under MAPK control with a similar profile is Ste12, which regulates mainly mating and filamentous growth clusters (Bardwell *et al.*, 1998). Typical glucose de-repression signatures were observed by the deregulation of SNF1downstream targets, such as TFs Adr1, Hap4 and putatively Oaf1 (Ratnakumar *et al.*, 2009; Livas *et al.*, 2011). Their activity can be observed in the transient induction of cluster 3 in Figure 27 with the enriched ontologies "cellular respiration" and "fatty acid catabolic process".

GSEA further uncovered four active cell cycle-related transcription factors, two of which make up one partner of the heterodimeric SBF (Swi4) and MBF (Mbp1) factors that induce gene expression during the G_1-to-S transition (Iyer *et al.*, 2001). The forkhead homolog Fkh2 co-regulates genes which are active during both the mitotic and meiotic G_2-to-M transition (Murakami *et al.*, 2010). On the other hand, Ndt80 is a strictly meiotic regulator (Tsuchiya, Yang and Lacefield, 2014). Apparently, cell cycle-related regulation followed a repressive pattern following the single stimulus. More precisely, the G_2/M-related regulatory effects were found to be associated with the repressed dynamics of the ESR while regulation during G_1/S took effect in a delayed manner, peaking after 20 min.

126

In conclusion, the transcriptional response to the s-LSL cycle comprised the transient expression of global regulatory programs, including the ESR and growth repression. DS-adapted yeasts showed the opposite gene expression pattern — namely, the repression of stress-induced gene sets and induction of growth-associated genes. Interestingly, there was still residual transcriptional activity of the same regulatory groups during the r-LSL time series. This result suggests that the short-term responsiveness of the regulatory circuitry controlling the adapted and non-adapted phenotypes was not entirely shut down during the DS.

Comparing different strain backgrounds and production scenarios to the same stimulus

Transcriptional responses of ScER were compared to the likewise stimulated haploid MATa strain CEN.PK113-7D (Minden *et al.*, 2023) that was growing under aerobic conditions (figure 31). Except for different |log$_2$-fold change| thresholds, the same analytical pipeline was used in both studies.
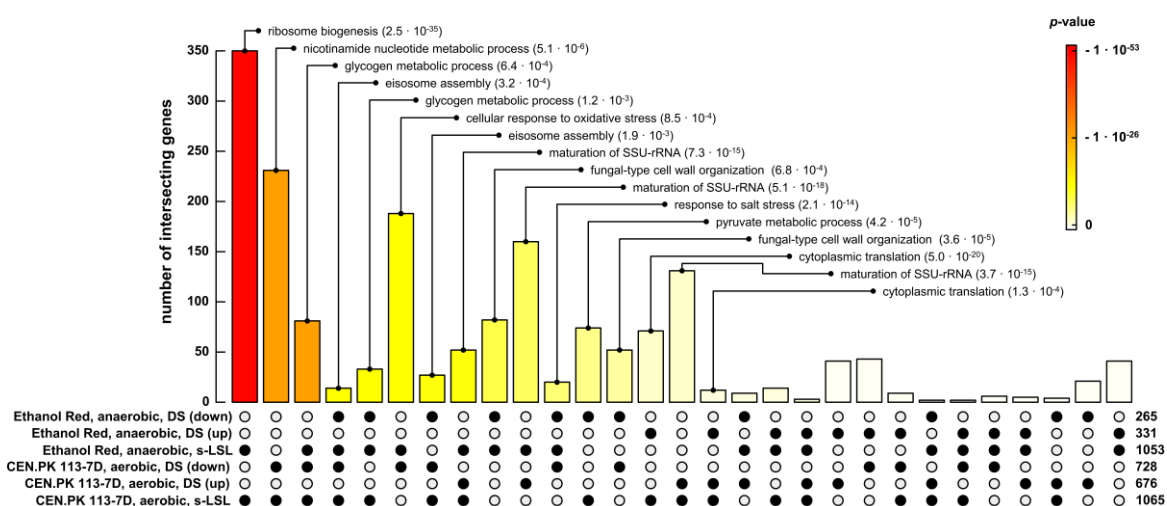
Figure 31. Shared sets of differentially expressed genes under anaerobic (this study) and aerobic (Minden *et al.*, 2023) conditions in LSL-cycling chemostats. Black dots in the matrix indicate the considered DEG sets, the bar above represents the respective intersection size and the color gradient illustrates significance. The number of genes included in each set is reported on the right. Gene ontologies of the intersection sets are only reported if both the intersection and GO enrichment were significant (FDR < $1 \cdot 10^{-3}$).

In essence, commonly found key regulation features are (i) the trade-off between stress response and growth abilities and (ii) the re-allocation of intracellular carbon storage and RNA pools. Whereas CEN.PK113-7D revealed the reduction of $Y_{DMB/\text{glucose}}$ to a single LSL exposure, ScER merely limited responses to the transcriptional level. However, ScER significantly reduced its biomass yield after complete adaptation (r-LSL), which was not the case for CEN.PK113-7D. Other differences were found for transcriptional relaxation times after single perturbation:

ScER restored pre-perturbation conditions almost entirely within one hour. For comparison, the process lasted up to three hours within dampening amplitudes for CEN.PK113-7D.

One-third of differentially expressed genes (350) of the non-adapted response was shared between both strains, indicating the presence of a highly conserved regulatory program. Shared genes in this core response were primarily enriched for RiBi mRNAs during the s-LSL cycle. Moreover, RiBi genes that were repressed initially upon unprecedented glucose exhaustion were upregulated later during the DS. This led to several overlaps of functionally related GO enrichments between the s-LSL cycle and upregulated DS sets of both strains. Eisosome assembly emerged as another conserved mechanism that is positively correlated to the ESR. The finding is in agreement with that of a recent study linking endocytosis to nutrient-scavenging activity in a nutrient-depleted environment (Johnston *et al.*, 2020). As an analogy, "glycogen metabolic process" was found to be significantly enriched in overlapping gene sets of the non-adapted response and repression during DS. Stress programs with an unobvious role in surviving famine exposure, such as the oxidative and salt stress response, were observed to be downregulated during the DS in both strains, but only actively induced during the s-LSL cycle in ScER.

Peculiar CEN.PK113-7D-specific gene expression changes occurred on the metabolic level as the ontology "nicotinamide nucleotide metabolic process" was mainly made up of glycolytic genes. Eighty-two genes were exclusively found in the s-LSL cycle and repressed DS datasets of ER and were functionally enriched for "fungal type cell wall organization". Taken together, we interpret the overall sparsity of common gene sets across conditions per strain as further evidence of a highly conserved transcriptional regulation circuitry, which operates at the glucose limitation–starvation junction.

4.3.5 Discussion

Fluctuating glucose supply — threat or not?

Conditions of limiting glucose availability may frequently occur in large-scale fermentation processes (Haringa *et al.*, 2016; Kuschel and Takors, 2020; Nadal-Rey *et al.*, 2021; Ho *et al.*, 2022) and are not restricted to aerobic cultivations (Bergdahl *et al.*, 2012; Osiro *et al.*, 2018; Saini *et al.*, 2018). In the present study, we cultivated ScER in a tightly controlled steady-state environment to investigate the effect of sudden glucose shortage. Since the stimulus was not strong enough to induce metabolic regime changes or to compete with maintenance demands, the observed signals may have mimicked the immediate cellular response to the environmental perturbations.

Apparently, the rapid ramp-down of the primary substrate supply instantly triggered the defensive transcriptional program, the so-called environmental stress response ESR (Gasch *et al.*, 2000), in the previously unstressed ScER strain. Thus, the first-time occurrence of glucose shortage was perceived as a 'threat'. The primary task of the ESR is to save resources by ramping down growth capacities to invest in defensive precaution measures. Given the absent growth rate reduction and the relatively quick relaxation of the transcriptome changes, we reason that the ER efficiently shut down this program. Otherwise, said consequences would have been much more pronounced (Brauer *et al.*, 2008; López-Maury, Marguerat and Bähler, 2008; De Nadal, Ammerer and Posas, 2011; Minden *et al.*, 2023). Comparing with CEN.PK113-7D, trehalose mobilization, or the lack thereof, might contribute to this difference. The strain ScER instantly mobilized trehalose pools when the glucose influx decreased, likely to support energetic homeostasis (Thevelein, 1984). Contrarily, CEN.PK113-7D failed to maintain glycolytic flux as trehalose and glycogen pools remained stable during the stimulation (see appendix C, figure C5). As a consequence, ATP reduction occurred in CEN.PK113-7D, which further induced the ESR signaling cascade (De Wever *et al.*, 2005; Minden *et al.*, 2023) through the energy-sensory SNF1 kinase. However, the role of trehalose in preventing energetic imbalances still remains somewhat elusive, though divergent short-term metabolic reactions to rapid changes in glucose concentration seem to cause strain-specific adaptation mechanisms. Glucose pulse experiments with *Escherichia coli*, *S. cerevisiae*, *Aspergillus niger* and *Penicillium chrysogenum* showcased this dependency (Wang *et al.*, 2019).

Recurring glucose shortages did negatively affect the biomass-substrate yield. Even though biomass-specific ethanol production seemed to increase, the overall reduction in $Y_{DMB/glucose}$

superimposed this effect and caused a net loss of the ethanol yield on glucose. Apparently, the regulatory modules involved during the peak ESR also controlled the DS phenotype since the same regulatory targets were affected in an inverse manner. Interestingly, these results showed high conformity with the operational mode of fast-growing yeasts, in which decreased carbon reserve pools enable increased anabolic demands to sustain enforced ribosomal machinery (Nissen *et al.*, 1997; Woolford and Baserga, 2013). In an independent study, Metzl-Raz and colleagues confirmed that environmental sensing rather than internal feedback from the actual growth rate controls ribosome abundance (Metzl-Raz *et al.*, 2017). Increased resource allocation for translation finally helps to accelerate growth after stress relief — a mechanism that displays an evolutionary advantage (Remigi *et al.*, 2019), especially in the selective environment of a chemostat.

Taken together, transient glucose depletion did not prove to be detrimental to the productivity of ScER. Nevertheless, we observed the presence of conserved regulation phenomena, such as increased transcriptional activity during ESR execution, which may cause unnecessary metabolic investments when stressful conditions arise (Mattanovich *et al.*, 2004; Gasch, 2007b). Moreover, sustained transcriptional stimulation–repression dynamics after adaptation identifies a non-optimally operating biocatalytic host, and enables an understanding of the underlying regulatory mechanisms that motivated this study.

Not a threat, but still a new habitat — How LSL transitions induce a new growth phenotype

The environmental stress response is a highly conserved gene expression program in *S. cerevisiae* (Gasch, 2007a; Brion *et al.*, 2016). Thus, it may not come as a surprise that different yeasts operating in different environments elicit strikingly conforming differential gene expression patterns when exposed to the same stimulus. The corpus of the induced ESR branch under acute stress, including glucose depletion, is driven by the feed-forward role of cAMP-dependent PKA signaling against the same targets primarily controlled by TORC1 under steady-state conditions (Martínez-Pastor *et al.*, 1996; Görner *et al.*, 2002; De Wever *et al.*, 2005; Kunkel, Luo and Capaldi, 2019; Minden *et al.*, 2023). When cAMP levels drop, PKA de-phosphorylates of the paralogue TFs Msn2 and Msn4 cause their nuclear translocation, during which they bind the so-called stress response elements within promoters to induce downstream expression (Görner *et al.*, 2002). In addition to the dual TORC1–PKA circuit, Msn2/4 regulation is fine-tuned in a condition-specific manner either upstream by the concerted activity

of cross-talking kinases, such as PCK, Pho85, HOG1, and SNF1 or intersecting TFs, such as the repressors Sko1 and Sok2 (Gutin *et al.*, 2015; Plank, 2022).

Indeed, our transcriptomic analysis revealed the involvement of HOG1 through the significant activity of its osmo-specific transcription activator Hot1. This mitogen-activated kinase induces various mechanisms that converge for Msn2/4 regulation, including protection against temperature (Winkler *et al.*, 2002; Panadero *et al.*, 2006) and oxygen (Bilsland *et al.*, 2004) shifts. The latter, especially, displays a high degree of coaction with the program induced by HOG1, even under anaerobic conditions (James *et al.*, 2003; Krantz *et al.*, 2004). Krantz et al. observed a dampened transcriptional response of osmotic and oxidative stress genes following a 0.5 M NaCl shock in anaerobic versus aerobic yeast cultures (Krantz *et al.*, 2004). The authors inferred from their experiments that the glycerol production necessary to maintain NADH redox homeostasis in anaerobic cultures is the main driver of negative feedback for HOG1 phosphorylation. Conversely, this negative feedback does not exist in respiring, glucose-limited yeast cultures. Thus, the more stringent regulation of HOG1 during anaerobic growth might partially explain the more efficient ESR shutdown of non-adapted ScER compared to the dampened dynamic of CEN.PK113-7D during the s-LSL cycle. Consistent with this line of reasoning is the occurrence of overshooting HOG1 activity under aerobic conditions upon transient glucose withdrawal reported in an independent study (Sharifian *et al.*, 2015).

The AMP-activated SNF1 cross-talk could not be characterized based on the dynamics of its actuating parameter, the adenylate energy charge, even though a rapid decrease was described under experimental conditions (Ball and Atkinson, 1975). Upon glucose depletion, however, the SNF1 kinase acts as a cooperative modulator of the PKA pathway, with shared targets such as Msn2/4 and Adr1 (Busti *et al.*, 2010), a direct regulator of glucose de-repression (Zaman *et al.*, 2009; Busti *et al.*, 2010; Caligaris *et al.*, 2022). The role of SNF1 in the latter is thoroughly described in the literature to be involved during the diauxic shift when glucose is depleted in batch cultures (Hardie, Ross and Hawley, 2012; Nicastro *et al.*, 2015; Shashkova, Welkenhuysen and Hohmann, 2015). During the s-LSL response, we observed a significant regulation of Adr1 and genes involved in ethanol metabolism and fatty acid degradation, a typical feature of the diauxic shift. Moreover, this transitionary phase usually encompasses the induction of respiratory, high-glucose-affinity, and alternative carbon assimilation activities (Busti *et al.*, 2010). Although we observed a differential expression of genes involved in said activities, our data lacked statistical significance for the strictly SNF1-dependent TFs Cat8, Sip4, and Mig1 (Busti *et al.*, 2010; Coccetti, Nicastro and Tripodi, 2018). A potential

explanation might be the presence of SNF1 bypassing regulation through either PKA in the case of Adr1 or the heme-activated protein (Hap) complex. The Hap complex is also involved in glucose de-repression (Knijnenburg *et al.*, 2007; Zampar *et al.*, 2013) but displays SNF1- and PKA-independent transcriptional regulation of respiratory genes (Zaman *et al.*, 2009; Zhang *et al.*, 2017).

Past studies concluded the same negative correlation between the induced ESR and repressed ribosome stimulons observed in this study during a s-LSL cycle (Gasch *et al.*, 2017; MacGilvray *et al.*, 2020). Regarding the regulatory hierarchy, both stimulons are controlled by the overriding PKA activity under acute stress and both RiBi and RP genes are repressed through the de-phosphorylation of the master repressor pair Dot6/Tod6. A study by Lippman and Broach suggested that only Dot6 is a substrate of PKA under carbon source stress (Zaman *et al.*, 2009). We were, however, not able to test for significant Dot6/Tod6 regulation as the target gene sets available from the Yeastract database were not rich enough to include the TFs in our analytical pipeline. Nonetheless, we identified significant regulation of the Dot6-antagonizing activators Sfp1 and Ifh1 (Shore, Zencir and Albert, 2021). The somewhat weakened response of the RP versus RiBi sets creates room for speculation as several potentially overlapping mechanisms might become relevant during the investigated perturbation. Both the Sfp1 and Ihf1 TFs target different promoter architectures. Nuclear exit causes Sfp1 release from RiBi-associated RRPE and PAC promoter elements while Ifh1 dissociates from an as-yet-unknown RP-specific promoter (Cipollina *et al.*, 2008; Shore, Zencir and Albert, 2021). Acute glucose withdrawal further post-transcriptionally inhibits translation initiation (Ashe, Long and Sachs, 2000), partly causing mRNAs to aggregate in so-called processing bodies or stress granules. Growth-associated transcripts are withdrawn from translation or actively degraded once located in said agglomerates (Brengues and Parker, 2007; Huch and Nissan, 2014). Bresson *et al.* provide additional evidence that RiBi and RP genes are specifically flagged for TRAMP-mediated mRNA degradation following glucose withdrawal, with both gene sets exhibiting different degradation dynamics (Bresson *et al.*, 2017). High PKA activity reportedly inhibits p-body and stress granule formation (Barraza *et al.*, 2021) and more remarkably, the assembly of these structures is independent of TORC1 or SNF1 signaling (Ramachandran, Shah and Herman, 2011).

The results thus far indicate that cAMP-dependent PKA signaling is at the core of adaption toward dynamic glucose availability. Clearly, specific stress-responsive stimulons and the ESR were repressed while ribosome-associated mRNAs were induced. This emerging "high-

growth" phenotype in the DS showed striking resemblance with the conditions of other experimental scenarios, all having high PKA activity in common (Cannon and Tatchell, 1987; Görner *et al.*, 2002; Müller *et al.*, 2003; De Wever *et al.*, 2005; Zaman *et al.*, 2009; Barraza *et al.*, 2021). Our experimental design, however, involved the same dilution rate during the DS compared to the RS, implying merely transiently downshifting and upshifting signals for protein kinase A. This was indeed reflected by the dynamic fraction of the transcriptome during the r-LSL cycle, especially with respect to the RiBi genes, which possess high transcriptional turnover (Pelechano, Chávez and Pérez-Ortín, 2012). However, the global transcriptional pattern displayed an overall elevated differential expression of PKA targets during the DS. Several feedback mechanisms may play a role when the PKA hub controls transcriptional responses. We recently speculated that during the LSL transition, disparate sensing of internal growth rate feedback and environmental substrate availability causes a boost of growth-related mRNAs at the end of the perturbation, also explaining the regulatory overswing that occurs during a s-LSL cycle (Shore, Zencir and Albert, 2021; Minden *et al.*, 2023). When the population adapts to transitions in a recurring manner, a scenario might occur in which the molecular transmitter, cAMP, accumulates due to an asymmetry in production and decay (Beullens *et al.*, 1988; Botman *et al.*, 2019), finally causing its levels to gradually ramp up during r-LSL adaptation. In conclusion, our data strongly suggest that PKA is the dominant factor that shapes the cellular fate in response to external glucose fluctuations in an industrial bioreactor setting in a highly conserved manner across different strain and bioprocess backgrounds.

Take-away message for industrial strain engineers

We understand the obtained results to be fundamental proof that large-scale insight should be used in early-stage strain development. Here, even moderate environmental oscillations shifted the production host's regulatory configuration. The resulting "large-scale-phenotype" might lead to non-optimal operational decisions given that most growth-coupled production processes are optimized based on the relationship between the biomass-specific production rate and the growth rate (Peebo and Neubauer, 2018). Obviously, an increased ribosome portfolio can impose a substantial metabolic burden on a cell, especially when the product is a heterologous protein (G. Wu *et al.*, 2016). In this specific context, strain performance seems rather unpredictable as neither prokaryotic nor eukaryotic hosts unanimously possess a linear correlation between ribosome content and protein productivity (Birnbaum and Bailey, 1991; Wright *et al.*, 2020).

ScER was proven to be particularly robust under the investigated conditions. Nevertheless, its gene expression profile revealed the presence of futile stress-responsive mechanisms. The induced ESR branch during the s-LSL cycle and the repeatedly triggered RiBi cluster during the r-LSL cycle depict appealing targets for constructing a streamlined universal production chassis. For instance, Msn2/4 deletion could reduce induced ESR expression when cells adapt to emerging famine zones during fed-batch processes, whereas the antagonizing TFs Sko1 and Sok2 still repress the ESR in the adapted state. Likewise, we observed several cross-talking transcription factors activating non-specific stress responses such as the activation of the osmotic stress response or the activation of oxygen-dependent energy scavenging. Hot1 or Hap proteins could be targeted to reduce said expression programs and further enable safe transcriptional expenditures, even though the latter should be restricted to anaerobic production strains. More globally, the stabilization of Tup1/Ssn6-guided repression carries the potential to avoid premature glucose de-repression with possible metabolic impacts. Examples of the beneficial impacts of TF modulation on bioprocesses exist in the literature. For instance, Hap4 deletion increased fermentative capacity during cellobiose fermentation (Lin *et al.*, 2014), and similar results were obtained through Cat8 deletion (Michael *et al.*, 2016). However, the cited studies reasoned that metabolic rerouting rather than gene expression savings caused the boosted productivity.

Here, we propose a valorization of the generated data centered around the idea that the ESR and other transcriptional stress response programs aggravate a variety of production scenarios, all induced by PKA activity (reviewed in (Creamer *et al.*, 2022; Ribeiro, Bourbon-Melo and Sá-Correia, 2022)). In a bottom-up strategy, all TFs that are involved in futile or non-specific transcriptional stress responses such as Msn2/4, Hot1, or Hap4 should be individually tested for their potential to abolish said responses. Finally, such a procedure could lead to a stepwise optimization of the yeast's regulatory landscape and ultimately reduce the maintenance demands made upon the introduction of short-term stimuli.

5 Additional analysis: Transcription factors as strain engineering targets

5.1.1 Introduction

The identification of strain engineering targets surfaced in research articles II and III. The dedicated discussion sections formulate transcription factors such as Msn2/4 as promising candidates to dampen wasteful gene expression programs such as the ESR. Altering global regulatory programs, however, carries the potential to prevent the host from adequate adaptation to the large-scale environment. Furthermore, it is not always a given that fully adapted cells result in reduced productivity (Wright, Rønnest and Thykaer, 2016).

Here, wasteful gene expression is identified conservatively by considering futile regulatory targets that explicitly do not contribute to the scale-down phenotype. Instead, a simplistic approach is presented to find TFs that control transient transcription following the s-LSL or r-LSL trajectories without involvement in DS. The resulting TF target lists in this additional chapter supports the discussion of strategies to derive strain-engineering targets from the SRE experiments in chapter 6.2.2.

5.1.2 Methodology

Data

Lists containing all differentially expressed genes from both strains CEN.PK113-7D and Ethanol Red^{TM} per condition tested (DS, s-LSL, and r-LSL) are accessible from the supporting information of research articles II (https://dataverse.nl/api/access/datafile/314364) and III (https://dataverse.nl/api/access/datafile/354231).

Transcription factor enrichment analysis

Significantly enriched TFs were determined for each DEG list using the Yeastract web interface (Monteiro et al., 2020). All 183 transcription factors available from Yeastract were queried for genes with documented "DNA binding or expression evidence".

Criteria for strain engineering targets

TF targets were identified for each strain separately. Obtained lists with significant TFs (FDR < 0.05) were first reduced to entries with at least 20 % coverage of genes in the queried list (*"% in user set"*) and at least 0.5 % coverage of the whole *S. cerevisiae* genome (*"% in s.*

cerevisiae"). Subsequently, all duplicate TFs between DS and either s-LSL or r-LSL were removed. The remaining TFs from s-LSL and r-LSL were merged and considered potential engineering targets. The hierarchy level of regulation is reported on a scale of three, as proposed by Jothi *et al.* (2009). Regulatory target genes per TF and a brief functional description are reported as documented in the *Saccharomyces* GENOME DATABASE (as of 17/05/2023, (Ramirez-Gaona *et al.*, 2017)).

5.1.3 Results

Seventeen and twenty TFs were found to regulate futile gene expression in CEN.PK113-7D (table 5) and Ethanol Red™ (table 6), respectively. In total, four TFs were identified in both strains, namely Mbp1, Sut1, Yhp1, and Stp1. Even though Mbp1 and Sut1 are regulators of the cell cycle, the four targets show little overlap concerning their regulatory class, action, and function. Furthermore, all target propositions are evenly distributed over the three levels of the regulatory hierarchy.

The entirety of engineering targets for both strains is involved neither in the induced branch of the environmental stress response nor in the regulation of RiBi and RP genes. Thus, the approach apparently fulfills the premise to exclude regulatory phenomena that control the DS phenotype. In line with this statement is the outcome that many TFs reported here for Ethanol Red™ (ScER) are involved in recruiting the Tup1-Ssn6 repressor complex, which integrates PKA and HOG1 signaling on ESR-independent downstream targets (see summarizing figure 30 in chapter 4.3.4). Examples of Tup1-Ssn6 recruiter TFs are Nrg1, Phd1, Mot3, and Rfx1, which are all stress-responsive regulators.

In general, the identified targets for both strains include some apparently stimulus-independent mechanisms, such as resistance to arsenic, activation of amino acid permeases, or regulation of phosphate metabolism for CEN.PK113-7D. In the case of ScER, these examples encompass repression of nitrogen catabolic gene expression, activation of copper genes, and activation of amino acid permeases. Different regulators for respiratory genes, such as Hap1 (ScER) and Hap4 (CEN.PK113-7D) were found in both strains. Similarly, both strains showed active elements of the filamentous growth pathway. In ScER, the targets Tec1 and Ste12 activate filamentation genes. In CEN.PK113-7D, Sut1 represses filamentation under physiological conditions. A unique feature of the ScER target profile indicates futile triggering of the carbon catabolite repression pathway via Adr1, Mig1, Mig2, and Nrg1.

Table 5. Transcription factors as strain engineering targets for CEN.PK113-7D. Levels 1 – 3 categorize the regulation hierarchy of TFs according to the notation of Jothi *et al.* (2009) (1: top, 2: core, 3: bottom). State shows the experimental condition in which the TF was identified. Paralogues and target genes in brackets were not identified through the analytical pipeline. TF family categories were obtained from (Drobna, Bialkova and Šubík, 2008; Hahn and Young, 2011; Ramirez-Gaona *et al.*, 2017). cI-Zn, class I (Cys$_2$His$_2$) Zn finger; cIII-Zn, class III (Cys$_6$) Zn finger; HMG box, high mobility group box domain; βHLH, helix–loop–helix motif; HTH, helix–turn–helix motif; MADS box, Mcm1p, agamous, deficiens, serum response factor; n.d., not determined; r-LSL, repeated limitation-starvation-limitation transition; RI, N-terminal regulatory motif; s-LSL, single limitation-starvation-limitation transition; SAGA, Spt-Ada-Gcn5-acetyltransferase; βZip, leucine zipper motif.

Level	State	Name	Para-logue	Class	Target genes	Function
1	both	Arr1		βZip	16	activator of genes involved in resistance to arsenic
		Mbp1		HTH	116	regulator of gene expression during G1/S cell cycle transition
	r-LSL	Oaf1	(Pip2)	cIII-Zn	21/(49)	activator of β-oxidation of fatty acids, peroxisome organization and biogenesis
2	both	Sut1	(Sut2)	cIII-Zn	4/(10)	activator of sterol uptake under anaerobic conditions
		Hap4		CCAAT complex	50	activator of respiratory gene expression
		Yhp1	Yox1	MADS box	16/17	repressor of gene expression during M/G1 cell cycle phase
	s-LSL	Rox1		HMG box	83	repressor of hypoxic genes
		Cup9	(Tos8)	HTH	13/(0)	repressor of peptide transport
		Gal4		cIII-Zn	44	activator of galactose utilization
3	both	Crz1		cI-Zn	21	activator of stress response genes
		Hms1		βHLH	32	regulator of pseudohyphal growth
	r-LSL	Stp1	(Stp2)	RI	617/(14)	activator amino acid permeases
n.d.	both	Mga2	(Stp23)	n.d.	2/(0)	activator of OLE1 transcription
	s-LSL	Pho2		HTH	142	regulator of phosphate metabolism
		Spt3		SAGA complex	523	regulator of chromatin modification

[1]βZip domains are only documented for Hap4 orthologues. Hap4 itself is known to exert the activation activity of the Hap2p/3p/4p/5p CCAAT-binding complex (Kim *et al.*, 2020)

Table 6. Transcription factors as strain engineering targets for Ethanol Red™. Levels 1 – 3 categorize the regulation hierarchy of TFs according to the notation of Jothi *et al.* (2009) (1: top, 2: core, 3: bottom). State shows the experimental condition in which the TF was identified. Paralogues and target genes in brackets were not identified through the analytical pipeline. TF family categories were obtained from (Drobna, Bialkova and Šubík, 2008; Hahn and Young, 2011; Ramirez-Gaona *et al.*, 2017). cI-Zn, class I (Cys$_2$His$_2$) Zn finger; cII-Zn, class II (Cys$_4$) Zn finger; cIII-Zn, class III (Cys$_6$) Zn finger; βHLH, helix–loop–helix motif; HTH, helix–turn–helix motif; MADS box, Mcm1p, agamous, deficiens, serum response factor; n.d., not determined; PRE, pheromone response element domain; r-LSL, repeated limitation-starvation-limitation transition; RFX, RFX-binding domain; RI, N-terminal regulatory motif; s-LSL, single limitation-starvation-limitation transition; TEAD, TEA domain; βZip, leucine zipper motif.

Level	State	Name	Para-logue	Class	Target genes	Function
1	both	Mbp1		HTH	116	regulator of gene expression during G1/S cell cycle transition
	r-LSL	Nrg1	(Nrg2)	cI-Zn	95/(0)	repressor in response to glucose
		Flo8		multiple targets	34	activator involved in regulation of cell adhesion, flocculation, invasive growth, and starch catabolism
2	both	Ste12		PRE	199	activator involved in mating or pseudohyphal/invasive growth
		Tec1		TEAD	165	regulator of pseudohyphal growth
		Sut1	(Sut2)	cIII-Zn	4/(10)	activator of sterol uptake under anaerobic conditions
		Yhp1	(Yox1)	MADS box	16/(17)	repressor of transcription during mitotic cell cycle
		Adr1		cI-Zn	20	activator of glucose-repressed genes
	r-LSL	Mig2	(Mig3)	cI-Zn	4/(11)	repressor in response to glucose
		Mig1		cI-Zn	49	repressor in response to glucose
		Hap1		cIII-Zn	75	regulator of heme and oxygen responsive genes
		Gzf3	(Dal80)	cII-Zn	17/(15)	repressor of nitrogen catabolic gene expression
		Phd1	(Sok2)	βHLH	87/(71)	activator of pseudohyphal growth
3		Cup2	Haa1	cII-Zn (Cu^{+2}-stabilized)	34/31	activator of copper genes

		Mot3		multiple targets	59	activator of osmotic stress genes / repressor of ergosterol biosynthetic genes
		Stp1	(Stp2)	RI	617/(14)	activator amino acid permeases
n.d.	both	Rlm1	(Smp1)	MADS box	36/(11)	activator of cell wall stress genes
	r-LSL	YLR-278C		cIII-Zn	0	uncharacterized
		Rfx1		RFX	598	repressor of DNA-damage-regulated genes

6 Discussion

6.1 From stress to acclimation

Carbon source depletion elicits different stress-responsive adaptations in proportion to the insult. Early tactic response mechanisms of *S. cerevisiae* are exclusively defensive and not mechanistically linked to stress survival. For instance, translation initiation completely but reversibly stalls during the first minute of glucose depletion (Ashe, Long and Sachs, 2000; Castelli *et al.*, 2011), followed by nuclear translocation of ESR-inducing TFs after the two-minute mark (Görner *et al.*, 2002). Prolonged exposure to a lack of carbon causes strategic investments into adaptive programs from the scavenging modes of autophagy and filamentation to growth escape via quiescence or sporulation (Broach, 2012). This chapter discusses the gained insight of the cellular tactic and strategy against glucose starvation in the context of the fluctuating environment in industrial bioreactors to fulfill objective 3.1.

6.1.1 Stress — the cellular tactic between glucose limitation and starvation

The first aim of this thesis sought to characterize the response against first-time glucose withdrawal through objectives 1.1, 2.1, and 2.3 (see chapter 3). In this regard, the most obvious finding reveals that the stimulus was perceived as an external insult worthy of triggering tactic responses without inducing strategic adaptation in *S. cerevisiae* CEN.PK113-7D. Complete metabolic and transcriptional reversion to the pre-stimulus steady state after seven minutes and two hours of starvation relief underlines this conclusion. Specifically, the ESR shapes the transcriptional tactic, as confirmed by analogous experiments with the industrial strain ScER.

Quantitative metabolomics reported in chapter 4.1 broadly supports reported studies investigating the transition of exponentially growing yeasts to glucose-depleted medium. Common themes are metabolites of upper glycolysis and the oxidative PPP following the decreasing trend of extracellular glucose (Brauer *et al.*, 2006; Weber *et al.*, 2020). Consistent with the referenced literature is the finding that lower glycolysis and the TCA decouple from this dynamic. Inevitably, a stopped supply of the primary carbon source drags down the adenylate energy charge (Ball and Atkinson, 1975; Weber *et al.*, 2020). Under such conditions, most eukaryotes, including yeast, stop translation as a first measure to dampen anabolic expenditure (Castelli *et al.*, 2011; Zhang, Hardie and Lin, 2020). Yet, the presented study indicates ongoing drainage of αKG toward anabolic build-up of amino acids. A possible explanation is the absent regulatory leverage to allosterically shut down glutamate

dehydrogenase (Gdh) activity due to stable NADPH availability (Mara *et al.*, 2018). The data at hand cannot sufficiently explain the persistence of the NADPH pool during the famine phase. Ongoing dehydrogenase activity in the oxidative PPP might compensate for the NADPH sink of the Gdh reaction, as evidenced by falling $NADP^+$ concentrations. The non-conserved NADP(H) moiety during this phase begs the question of whether aggregate sinks are present. Net loss of the NADP(H) pool could hypothetically arise from specific phosphatase activity. Whether phosphatase activity antagonizes the NADP(H) generating kinases Utr1, Yef1, and Pos5, similar to other eukaryotes, has not been demonstrated in *S. cerevisiae* to date (Agledal, Niere and Ziegler, 2010; Estrella *et al.*, 2019). However, it stands to reason that the rapidly contracting TCA pacemaker αKG (N. Wu *et al.*, 2016), together with the reduced feedforward activation of the pyruvate kinase via FBP (Jurica *et al.*, 1998), represent an efficient catabolic break when glucose depletes rapidly.

Yeast cells fluctuating in a bioreactor inevitably transition from starving to limiting or excessive conditions. While the former case was subject to this work, Suarez and colleagues investigated the latter in glucose pulse experiments. The concentration of the glycolytic entry metabolite, G6P, was the same at the start of the glucose pulse cycle (Suarez-Mendez *et al.*, 2014) and at the end of the starvation stimulus (figure 12). In essence, the transition from glucose starvation to excess agrees with several metabolic patterns observed during the relief from starvation toward limitation. One shared trait is the delayed replenishment of oxidative PPP intermediates and relatively mild changes in lower glycolysis and TCA intermediates. Another is the regeneration of the *AEC* and *CRC* following the extracellular glucose availability. Given the chaotic reality of a bioreactor, one obvious limitation of this study is the smooth s-LSL trajectory, where cellular uptake controls the glucose concentration. Still, the conformity of metabolic dynamics between this and analogous studies with abrupt regime transitions (Bergdahl *et al.*, 2012; Suarez-Mendez *et al.*, 2014; Weber *et al.*, 2020) allows a tentative mitigation of this concern.

Metabolic data revealed transient adjustments of several regulatory effectors, including extracellular glucose and the intracellular adenylate, catabolic, and anabolic energy charges. Other potential, but not directly observed, triggers might include cAMP, hexokinase activity, and even the putative alarmone αKG (N. Wu *et al.*, 2016). Transcriptional analysis in chapters 4.2 and 4.3 attempted to answer the adjacent research question formulated in the introduction on how said stimuli propagate through the yeast transcriptional network. Remarkably, the single stimulation initiated neither strategic adaptation nor glucose-specific expression changes in

hexose transport or catabolite repression in CEN.PK113-7D. Instead, the dominant mechanism driving the observed gene expression changes upon glucose withdrawal is the ESR. This study presents the first proof of ESR activity during mixing-induced heterogeneities. Since this defensive program displays a highly conserved response to changing environments in eukaryotes (Hackley and Schmid, 2019), its general relevance during industrial-scale fermentations seems likely. Scale-down studies with prokaryotes already highlighted the importance of an analogous program — the stringent response (Neubauer *et al.*, 1995; Löffler *et al.*, 2016; Ankenbauer *et al.*, 2020). The current advancement in engineering strains for increasing industrial robustness via mitigating the stringent response may serve as a blueprint for optimizing the performance of *S. cerevisiae* (further explored in chapter 6.2.2).

One important characteristic is that initial gene expression changes peaked at 4.5–40 minutes along the s-LSL trajectory in CEN.PK113-7D and 4.5–20 minutes in ScER. The signaling mechanisms of ligand-binding, phosphorylation cascades, and TF–DNA interaction operate on time scales in the sub-second to second range (De Nadal, Ammerer and Posas, 2011; Alon, 2019). For instance, model-supported time-lapse imaging studies reported instant nuclear translocation of HOG1, Msn2, and Crz1 following external cues of osmosis, glucose, and calcium, respectively (Jiang *et al.*, 2017; Chen *et al.*, 2019; Wosika and Pelet, 2020). The activity of antagonizing kinases or karyopherins, such as the Msn5 phosphatase, ensures symmetric import–export rates of TFs (Yoshida and Blobel, 2001; Görner *et al.*, 2002; De Wever *et al.*, 2005). From this linear signal transduction point of view, promoter activity is directly proportional to the stimulus in a timely manner. This view is far too simplistic to explain the observed transcriptional behavior. For one, the kinetics of promoter activation–inactivation rates are often neither uniform nor symmetric, decoupling promoter-specific transcriptional time windows from environmental signals. For instance, gene expression upon pulsatile nuclear Crz1 translocation relies on fast promoter activation and slow promoter inactivation rates owed to chromatin remodeling mechanisms (Chen *et al.*, 2019). Indeed, nucleosome-remodeling complexes such as SWI/SNF and modifiers of histone acetylation such as Rpd3, mediator, and SAGA substantially contribute to transcriptional regulation (De Nadal, Ammerer and Posas, 2011). Differential RP and RiBi expression dynamics are also probably owed to specific histone acetylation patterns (Weiner *et al.*, 2012). On the other hand, internal feedback mechanisms add regulatory levels that are not obvious from the external considerations. Chapter 4.2.5 discussed internal kinase feedback in an attempt to elucidate the oscillatory overswing in CENPK113-7D. As an addendum, internal sensing of metabolic rearrangements following

nutrient shifts may add a layer of sensory input for nutrient-specific signaling cascades (Jalihal *et al.*, 2021). Even though the quantified endometabolome fully relaxed after seven minutes, metabolic feedback cannot be ruled out, especially since regulatory effectors, such as the second messenger cAMP, were not monitored.

There remains the question concerning the more efficient shutdown of the ESR in ScER *versus* CEN.PK113-7D. Efficient ESR termination can be viewed as a favorable industrial trait, considering ScER maintained robust μ post-stimulus. One potential explanation might be the mentioned delayed trehalose mobilization in CEN.PK113-7D, causing additional energetic feedback through SNF1. On another note, said delayed trehalose mobilization upon glucose stimuli points toward impaired signaling dynamics despite cAMP levels being seemingly unaffected by the Cyr1 mutation during unlimited growth (Kümmel *et al.*, 2010). The adenylate cyclase, in turn, displays an integral point of PKA–SNF1 crosstalk mediating Msn2/4 activity (Nicastro *et al.*, 2015; Coccetti, Nicastro and Tripodi, 2018). Thus, aberrant feed-forward and feedback signal integration at this decisive node should be considered when interpreting the strain-specific regulatory behavior.

Last, the above-mentioned experimental limitation concerning the smoothness of the LSL trajectory potentially limits the general validity of the presented gene expression response given real-life conditions. In this regard, a study from Nisamedtinov *et al.* concluded that sudden *versus* gradual environmental shifts of several stressors impose 2–20-fold higher expression of the stress marker gene Hsp12 (Nisamedtinov *et al.*, 2008). Hence, the presented results may be interpreted as a conservative estimate of industrially relevant regulation phenomena.

6.1.2 Acclimation — How tactics turn to strategy during repetitive stimulation

Objectives 1.2, 2.2, and 2.3 (see chapter 3) explored strategic adaptation toward repeated exposure to starvation zones. In this regard, both aerobic and anaerobic experiments revealed an overall robustness of TRY parameters. Yet, the cellular metabolic and transcriptional landscape required strategic investments to sustain strain performance. The strategy includes increasing growth capacities via ramping up RP and RiBi expression, concomitant with deceased carbon storage, and dampened ESR transcription. While chapters 4.1.4, 4.2.5, and 4.3.5 characterize this adapted state in detail, this chapter adds perspective to potential adaptive elicitors and consequences for the commercial-scale setup.

The dynamic feeding phase of the SRE experiment mirrored the situation in a commercial tank where the supply of the limiting nutrient is variable, but its average meets the set point. In other

words, once famine zones emerge, optimal growth is not supported throughout the bioreactor space. Take the investigated r-LSL cycle: From an oversimplified, binary point of view, the lifeline supports a growth rate of $\mu = 0.13$ h^{-1} for seven minutes and no growth for two minutes to average μ of 0.10 h^{-1}. Of course, *S. cerevisiae* cannot control its growth rate as a function of available carbon within nine minutes. The required μ adjustment would rather fall in the range of five hours, given that ribosome production limits its adjustment (Young and Bungay, 1973; Warner, 1999). Given the yeast's evolutionary compulsion to maximize μ, the only feasible option is to raise translation capacities above the average requirement (Metzl-Raz *et al.*, 2017). This presents an internal optimization problem as maintenance demands increase to sustain the boosted translation machinery. Here, CEN.PK113-7D liberated ATP by reducing futile cycling and increasing cell-specific aerobic respiration. Increasing respiratory activity is also a strategy to reduce lag phases in yeasts adapted to frequent glucose–maltose or –galactose shifts (Cerulus *et al.*, 2018; Perez-Samper *et al.*, 2018). Reducing carbon storage pools was one employed strategy to cover these demands under the investigated conditions. Anaerobic ScER employs the same strategy except that the fermentation rate, instead of the respiration rate, increases. Further macromolecular savings were necessary during the anaerobic experiment, as evidenced by a reduced $Y_{X/S}$.

The herein-reported metabolic and transcriptional data could not provide an unequivocal mediating mechanism behind this strategic adaptation. In particular, the two quantified regulatory effectors are no viable candidates. Extracellular glucose dynamics remained unchanged from s-LSL to r-LSL and the increased *AEC* amplitude is the consequence, not the cause, of adaptation. Instead, two aspects render the ESR and its underlying regulatory landscape a hypothetical elicitor of adaptation. First, the stress response–growth trade-off shapes both the non-adapted s-LSL response and the adapted DS phenotype. Second, the ESR promotes acquired stress resistance via chromatin state, long-lasting protein inheritance, and regulatory memory effects (Berry and Gasch, 2008; Guan *et al.*, 2012). The two former can be ruled out as said effects last for several generations via epigenetic factors, while the s-LSL experiment revealed complete transcriptomic relaxation within one doubling time (Vermeersch *et al.*, 2022). Regulatory memory relies on characteristic timescales of individual components of the involved network. In brief, memory develops transiently when the relaxation time of an initiated response outlasts the stress phase (Bheda, 2020). Recently, Jiang and colleagues proposed a biphasic model for the memory effects of the ESR (Jiang *et al.*, 2020). First, short-lived memory is mediated by PTMs through PKA phosphorylation. In the referenced work,

short-term memory of osmotic stress was gained via the regulation of trehalose degradation. The TFs Msn2/4 and Yap1, as well as downstream mRNA stabilization in P-bodies, mediate long-term memory. Similar transcriptional memory occurs during fluctuating osmotic stress (Mettetal *et al.*, 2008). Applying this model to the LSL adaptation in this thesis seems straightforward. For instance, asymmetric cAMP production and decay mechanisms may represent the short-term memory component (Beullens et al., 1988; Botman et al., 2019). On another note, strain-specific short-term memory may entail the previously discussed divergent ESR shutdown in CEN.PK113-7D *versus* Ethanol Red^{TM}. The involvement of cAMP signaling, thus, remains elusive in this work. Long-term transcriptional memory is indeed obvious since the transcriptional tactics following the s-LSL transition exceeded one LSL cycle time in the dynamic steady state. Hence, induction and repression dynamics of the ESR stimulons, together with potential metabolic memory effects, propagate through several LSL cycles toward new basal expression states. This interpretation agrees with our observation that induced and repressed ESR stimulons are still dynamic during the r-LSL cycle.

What happens if we extrapolate the proposed LSL adaptation strategy to the actual environment of large-scale fermentations? Amplitudes, frequencies, and dwell times in starvation are certainly not uniform in industrial processes. Starvation zones will grow in relative size during high-cell-density operations as biomass concentrations approach > 100 g·L^{-1} (Nadal-Rey *et al.*, 2021). In consequence, the compartment supporting active growth shrinks raising the required growth capacities to sustain the average growth rate even further. Expanding starvation exposure potentially amplifies the above-discussed adaptation strategies. For instance, cAMP levels follow the so-called Weber-Fechner law. Accordingly, cAMP peak heights scale with relative, not absolute, glucose concentration changes (Botman *et al.*, 2019). Amplitudes of extracellular glucose exposure will likely rise throughout a C-limited process. Thus, excess zones close to the feed and growing famine zones impose positive feedback for putative short-term memory effects. The fixed ratio of limitation to starvation in the herein-reported experimental design supposedly prompted the transcriptional memory to repress the ESR and induce the RiBi and RP stimulons. Considering dynamic ratios of metabolic regimes in the industrial process, follow-up research questions could include "Is metabolic and transcriptional memory the limiting factor controlling the phenotype against mixing-induced heterogeneities?" and "Can we model memory effects adequately to predict the 'bioreactor phenotype' *a priori*?"

In summary, exploring the strategic adaptation of *S. cerevisiae* toward mild starvation stimuli delivered a systematic understanding of the industrial phenotype. Whether the yeast's

compulsion toward optimizing self-replication displays a benefit or not seems intuitively case-specific. While biomass production might not suffer from this cellular trait, more metabolically burdensome production systems might face deterioration. Some other open questions, *e.g.* related to metabolic and transcriptional memory, require further experimental or computational exploration. Likewise, further approximation toward realistic mirrors of the industrial environment is necessary. In this regard, the next chapter discusses how the next iteration over the DBTL cycle can satisfy these needs.

6.2 Enabling the next 'DBTL' cycle

One focal point of this thesis is the exploration of the *S. cerevisiae* phenotype within the famine-prone industrial fermentation environment. The lessons learned and the questions that arose provide a rich base for the next DBTL cycle. This chapter discusses the outcome of this thesis in a forward-looking manner from the scale-down and strain-engineering perspective to address objective 3.2.

6.2.1 Scale-down engineering

Scale-down studies are a powerful tool to uncover mixing-induced scale-up effects in carbon-limited processes. Ethanol formation resulting from overflow metabolism or anaerobic transitions is a prominent example (see chapter 2.3.1). On the gene regulatory level, several studies reported clues implying the presence of a stress response–growth trade-off in yeast (Lai *et al.*, 2005; Kresnowati *et al.*, 2006; Airoldi *et al.*, 2016; Wright *et al.*, 2020). On the contrary, the impact of a trade-off between the stringent response and growth in prokaryotes is well established in a heterogeneous bioreactor environment (Neubauer *et al.*, 1995). This research shows for the first time that industrially relevant extracellular glucose and intracellular energy fluctuations converge on the ESR–growth trade-off ultimately shaping the industrial phenotype.

Early bioprocess development may miss severe risks when process optimization is done based on a non-representative phenotype. For instance, the key parameter for carbon-limited fed-batch processes, the feed rate, controls growth-coupled product formation. The feed rate, in turn, is optimized based on empirical chemostat data in the form of $D–q_P$ diagrams. Especially metabolically burdensome products display distinct q_P maxima guiding decision-making (Mendoza-Vega, Hebert and Brown, 1994; Peebo and Neubauer, 2018). Such tight q_P-optima are most likely to shift when the underlying growth phenotype is not stable on the commercial scale, either for the better or the worse (Cortés *et al.*, 2005; Wright *et al.*, 2020). Follow-up research should invest in decreasing this phenotypic uncertainty in view of mixing-induced limitation–starvation transitioning. To do so, realistic dwell times, amplitudes, and frequencies characterizing commercial-scale glucose gradients are essential. Subsequently, the 'bioreactor phenotype' can be further explored in a relevant environmental parameter space using complementary SDR approaches.

The identification of realistic environmental parameters requires refined biokinetic models capable of CFD integration. Ideal CFD-assisted scale-down provides insight into the

extracellular environment and the intracellular state (Blöbaum, Haringa and Grünberger, 2023), calling for integrating cellular reaction dynamics (CRD). Wang, Haringa, Tang, *et al.* (2020) categorized several model structures for their ability to satisfy CFD−CRD requirements. In their review, lumped kinetic models, such as the ''9-pool model' by Tang *et al.* (2017), showed the best feature set in terms of its ability to capture metabolic dynamics on relevant time scales, computational burden, and parameter identifiability. However, mechanistic models rely on *a priori* defined kinetic formulations of the individual reactions, often derived from *in vitro* assays under reference conditions. This dependence often hampers the development of a portable and scalable CRD framework as non-reference conditions or adaptation effects may challenge anticipated kinetic formulations. For example, results presented in chapter 4.1 unveiled that hyperbolic uptake kinetics overestimate glucose uptake at $c_S \ll K_M$. In this regard, approximative kinetic modeling provides an alternative by applying unified model formulations. Heijnen proposed the so-called *linlog* model structure reproduced in equation 11 (Heijnen, 2005). Here, the *linlog* model is briefly discussed for valorizing the herein-presented metabolome dataset (RS, s-LSL, and r-LSL).

$$\frac{v}{j^0} = \left[\frac{e}{e^0}\right]\left(i + E_x^0 \times ln\frac{x}{x_0} + E_c^0 \times ln\frac{c}{c_0}\right) \tag{11}$$

First, the model parameters are normalized toward their reference state (superscript 0) to avoid weighing problems. The flux-normalized (j^0) vector of reaction rates v is proportional to the square diagonal matrix of enzyme concentrations $\left[\frac{e}{e^0}\right]$, linear to the logarithm of the dependent intracellular ($\frac{x}{x_0}$) and independent extracellular ($\frac{c}{c_0}$) metabolite concentration vectors, and (iii) linear to the kinetic parameters expressed as elasticity coefficients (here contained in matrices E_x^0 and E_c^0). For further information, refer to Visser and Heijnen (2003). To put it simply, the *linlog* model can be parametrized based on the reference data from RS and the s-SLS time series with fixed enzyme levels $\frac{e}{e^0} = 1$. In theory, fitting $\frac{e}{e^0}$ of the parametrized model to r-LSL data enables phenotype-specific simulations. Whether this approach yields superior simulation output to mechanistic models is an ongoing topic in the aftermath of the ComRaDes project and will be addressed in dedicated follow-up studies (Sarkizi *et al.* manuscript in preparation).

Even when realistic intra- and extracellular lifelines are enabled, to be blunt, a perfect experimental mirror of the commercial bioreactor remains an experimental fantasy. One has to compromise on several aspects, including operational constraints preventing short fluctuation time scales in bioreactor SDRs or the level of observation in smaller volumes, such as

microfluidics (Haringa, 2017; Wei *et al.*, 2023). Therefore, valorization of scale-down experiments may follow two rationales: first, critical parameters are derived to de-risk industrial bioreactor operation *a priori*. Second, biological knowledge is used to construct more robust strains withstanding the heterogeneous environment (Delvigne *et al.*, 2017).

The earlier stipulated predictable bioreactor phenotype enables the definition of design parameters for bioprocess development. However, more data concerning how industrially relevant glucose fluctuations control the phenotype is required. The uncovered determinant role of the ESR–growth trade-off under the tested conditions opens the possibility of harnessing the benefits of microfluidic experimentation. Fluorescent reporter strains monitoring the status between stress and growth can be constructed based on submitting fluorescent reporter genes to PAC and STRE promoter activity as a proxy for RiBi and ESRi expression, respectively. Others already demonstrated the feasibility of similar reporter systems for *S. cerevisiae* (Delvigne *et al.*, 2015; Heins *et al.*, 2015; Gutin *et al.*, 2019; Torello Pianale, Rugbjerg and Olsson, 2022). Microfluidic SDRs impose glucose fluctuations as a function of amplitudes and frequencies on relevant time scales guided by CFD−CRD-derived lifeline analysis (Blöbaum, Haringa and Grünberger, 2023). The gained data provides valuable feedback to CFD−CRD output by annotating growth phenotypic peculiarities to lifelines representing distinct operational modes or process phases. A framework like this could provide early estimates of whether an anticipated phenotype remains intact in large-scale processes — or define tailored operating conditions keeping the growth phenotype within an acceptable range *a priori*. One aspect to consider is the boundary of starvation exposure in which the observed stress–growth balance controls the phenotype. Extending the exposure time to starvation will, at one point, trigger adaptation programs beyond the ESR, such as quiescence or sporulation. Critical values for starvation exposure can be easily determined using the here-employed SRE methodology with increasing stopped feed intervals.

6.2.2 Strain engineering

Freely adapted from Lara *et al.* (2006), we have to *"live with heterogeneities in bioreactors"* to a certain extent. Hence, tailoring the production host biology toward fluctuating conditions seems a valid strategy. The literature contains several examples of engineering prokaryotic production hosts toward large-scale heterogeneities. For instance, in a bottom-up approach, the genomes of *E. coli* and *P. putida* were systematically reduced by the genes that displayed futile triggering in SDR experiments (Martínez-García *et al.*, 2014; Ziegler *et al.*, 2021). Top-down

approaches yielded strains with decreased stringent response to render strains blind toward gradients (Michalowski, Siemann-Herzberg and Takors, 2017) or altered glucose uptake and sensory systems to enable C-limited growth during excess (Velazquez *et al.*, 2022). Along with its century-long domestication process, *S. cerevisiae* strains were engineered either evolutionarily or genetically to withstand a plethora of industrial stressors, such as ethanol toxicity, inhibitor compounds, high temperature, and genetic instability, to name a few (Çakar *et al.*, 2012; Deparis *et al.*, 2017; Chua, Jiang and Meadows, 2020). Remarkably, modified yeast constructs streamlined toward substrate fluctuations in large tanks are not reported as of today. Of course, we cannot know whether such strains circulate in the non-disclosed industrial world. In any case, the herein-presented data opens the potential to follow strategies from bottom-up to top-down approaches, bringing fluctuation-robust strains to life.

The 'minimum genome factory' (MGF) proposes the reduction of maintenance demands by removing industrially irrelevant genes (B. H. Sung *et al.*, 2016; Xu *et al.*, 2023). Approximately 80 % of the yeast genome is considered non-essential, and more than half of its open reading frames (ORFs) can be individually deleted without impairing the growth phenotype under laboratory conditions (Winzeler *et al.*, 1999; Giaever *et al.*, 2002). Accordingly, the feasibility of large-scale genome reduction was later shown in two independent studies via reducing the genomic sequence by 5 % (Murakami *et al.*, 2007) and 8 % (Luo *et al.*, 2021), even though the former resulted in impaired growth abilities. Yet, deleting non-essential genes in the pursuit of an MGF only benefits strain performance if they add to maintenance under process-relevant conditions in the first place (Ziegler and Takors, 2020). Even though this thesis uncovered the futile triggering of hundreds to thousands of genes in CEN.PK113-7D and ScER, most of those genes fulfill essential tasks and are thus no deletion candidates. Furthermore, the success of reducing prokaryotic genomes relies on the knockout of complete cellular functions, such as the biosynthetically expensive flagellar apparatus triggered by chemotaxis in famine zones (Schavemaker and Lynch, 2022). Manual curation of our data did not yield such promising candidates. Thus, the expected benefit of deleting single non-essential genes would be minor, especially since these genes are often expressed at lower levels compared to essential genes (Cohen *et al.*, 2016). Another concomitant risk is owed to the decision strategy toward defining knockout candidates. The choice is made based on futile differential expression but complete gene removal might disrupt unrealized functions, causing severely deteriorated strain behavior (de Lorenzo and Couto, 2019). In the end, deleting single eukaryotic genes toward a minimized

genome is a lengthy and resource-intensive process, and the benefits, in an industrial setting, probably do not outweigh the means and risks associated with its construction (Xu *et al.*, 2023).

Transcription factor (TF) engineering offers the mitigation potential some of the above drawbacks concerning monogenic manipulations (Mohedano, Konzock and Chen, 2022). Due to the high degree of redundancy and interconnectivity, a rational choice of TF engineering candidates is usually not trivial (Wu *et al.*, 2021). However, condition-specific transcriptomic data like that presented in chapters 4.2.4 and 4.3.4 allows the definition of TF targets by two rationales. By rationale A, the TF landscape is streamlined toward the adapted phenotype. For instance, knocking out the ESRi inducers Msn2/4 or the RiBi and RP repressors Dot6 and Tod6 may prevent adaptation efforts through transient triggering of the ESR (Wagner and Gasch, 2023). Chapters 4.2.5 and 4.3.5 discuss this approach, which relies on previous mechanistic knowledge of the respective TF network. Rationale B follows the school of the MGF by reducing futile gene expression derived from scale-down data. Accordingly, we define all transient regulatory events that explicitly do not contribute to the bioreactor phenotype as futile. A decision-based, data-driven approach is presented in chapter 5 and yielded 17 (CEN.PK113-7D) and 20 (ScER) TFs that induce expendable stimulon expression. Subsequent genetic engineering of these targets toward dampened gene regulation displays a far greater challenge since each TF candidate requires an individual genetic engineering strategy to achieve the desired gene regulatory output. Promising strategies include high throughput tools, such as MINR (MultIplex Navigation of global Regulatory networks), to enable the screening of tens of thousands of random mutations in a small set of TFs (Liu *et al.*, 2019). However, while MINR applies growth competition experiments in vials or shake flasks with elevated stressor concentrations, scale-adapted strain selection requires high throughput SDRs. Future advancements in the field of microfluidics might alleviate this technical bottleneck (Blöbaum, Haringa and Grünberger, 2023).

The central role of the PKA and adjacent regulatory hubs for integrating short-term glucose fluctuations as stress signals is discussed in chapter 4.2.5. Its feedforward function to fulfill the fast-responding component toward external and internal stimuli (Kunkel, Luo and Capaldi, 2019) offers an attractive engineering target from a top-down perspective. Based on the observed mismatch between the time scales of substrate fluctuations and biological adaptation abilities, one can doubt the usefulness of the latter. Therefore, instead of screening for dispensable regulatory subsystems, it seems plausible to render the entire system blind toward non-compatible environmental signals. Dampening the responsiveness of PKA activity would

be the obvious goal. Slowing the kinetics of its activation is a rational strategy. In this regard, Van Dijck *et al.* (2000) used a similar approach to remedy the loss of yeast viability that occurs during the production of freeze dough. PKA becomes rapidly activated as glycolytic flux increases when exposed to the high sugar content of the dough. The result is almost instant activation of growth and inactivation of the stress response, and thus, yeasts are freeze-dried at the point of their highest vulnerability. A point mutation in Cyr1 led to a tenfold drop in its cyclase activity, causing a delayed PKA activation, which, in turn, kept stress resistance at a high level at the critical process step. In the context of acute starvation, PKA deactivation can be decelerated by removing the cAMP hydrolyzing phosphodiesterase Pde2. Indeed, Pde2-knockout strains result in a significant loss of ESRi induction and RiBi and RP repression upon acute salt stress (Chasman *et al.*, 2014). However, the rational engineering of an industrial chassis with dampened PKA kinetics faces the obstacle of pathway redundancy in *S. cerevisiae* (Wu *et al.*, 2021). For instance, as discussed earlier, potential SNF1 crosstalk alleviates the effects of the point mutation in Cyr1 in CEN.PK113-7D on the transcriptional level. Unfortunately, in the case of SNF1–PKA crosstalk, the connecting components are not yet characterized (Shashkova, Welkenhuysen and Hohmann, 2015). Hence, while altering PKA activation kinetics seems promising, the lack of essential mechanistic insight currently limits the applicability of this approach.

In summary, scale-down and strain engineering strategies are offered based on the data generated in this thesis. Still, following up on these strategies comes with certain limitations requiring the concerted effort of subdisciplines from molecular biology, computational science, bioprocess development, and process engineering.

6.3 Limitations of this study

This thesis has limitations considering the employed experimental strategy. First, as introduced in chapter 2.1.1, chemostat experiments are performed under a steady-state assumption. As discussed in chapter 4.1.4, some biological processes do not satisfy this assumption. While these aspects are characterized for CEN.PK113-7D (Jansen *et al.*, 2005; Mashego *et al.*, 2005) and own reference chemostats (figure 2), analog reference data is not available for ScER. Literature research yielded tree chemostat studies with ScER that all kept the observational window below 15 generations and did not report any implications considering the validity of the steady state assumption (Lip *et al.*, 2020; Pinheiro *et al.*, 2020; García-Ríos *et al.*, 2022).

The transcriptomic analysis presented in chapter 4.3 suffers from the lack of a ScER reference genome. Using the reference of the phylogenetically closely related haploid strain S288C (Gronchi *et al.*, 2022) harbors limitations concerning strain-specific gene expression. A study by Borneman and colleagues identified five industry-specific ORFs present in six industrial wine and brewing strains but not in S288C (Borneman *et al.*, 2011). Hence, it is possible that the herein-reported results missed gene expression dynamics of ScER-specific genes or gene clusters.

The nutrient-limited chemostat fermentation figuratively operates as a μ-dependent selection device. Consequentially, the adjusted growth phenotype observed during the dynamic steady state DS could be subjected to selection bias. For instance, perturbation times falling below adaptation times can prompt stochastic switching, also called bet-hedging, rather than a uniform adaptive response (Acar, Mettetal and Van Oudenaarden, 2008; Vermeersch *et al.*, 2022). Hypothetical growth-arrested subpopulations would wash out under the given experimental conditions. However, bet-hedging typically comprises several non-redundant strategic measures with potential fitness increases (Wright *et al.*, 2022). The cellular response toward a single two-minute feed interruption (s-LSL) is limited to the ESR tactic without executing starvation-specific strategies such as quiescence or pseudohyphal growth. In this regard, the involvement of population segregation strategies seems unlikely. Still, its presence cannot be ruled out, especially under repetitive LSL stimulation. One recommendation for follow-up experiments to overcome this analytical shortcoming is the use of specific reporter strains and flow cytometry, for example, as applied by Heins *et al.* or Sassi *et al.* (Heins *et al.*, 2015; Sassi *et al.*, 2019).

7 Conclusion

This study set out to explore how famine zones in industrial bioreactors impact glucose-limited *S. cerevisiae* fermentations. Stimulus-response experiments found that yeasts maintain robust growth while fluctuating between glucose limitation and starvation. Yet, the observed growth preservation demanded intracellular resource re-allocations arising from a stress response–growth trade-off. This work shows for the first time that the regulatory network centered around the environmental stress response controls the yeast phenotype during industrially relevant mixing-induced substrate fluctuations. Furthermore, the ESR–growth trade-off is a conserved feature across the genetic backgrounds of the haploid laboratory strain CEN.PK113-7D and the industrial diploid Ethanol Red^{TM} strain. Annotated increased maintenance demands finally underline the relevance of considering even mild environmental perturbations early during process development.

Comprehensive metabolic and transcriptomic data was generated and interpreted during this research project. Despite attaining the above conclusion, the presented data provides a sound basis for enabling upcoming iterations over the scale-up/scale-down DBTL cycle. While CFD−CRD modelers may use the metabolomic time series to parametrize models under process-relevant conditions, our transcriptomic analysis uncovered several potential targets for engineering scale-adapted strains. The discussed considerations revealed a true need for more sophisticated SDR setups, such as microfluidics, to investigate the bioreactor phenotype under more realistic environmental conditions.

In the end, this work explored mechanisms controlling the bioreactor phenotype under non-producing conditions. The phenotypic changes, although subtle, still possess the potential to cause severe deteriorations of valuable compounds with tight productivity optima. Thus, subsequent research could explore the economic impact of the bioreactor phenotype on real-world production scenarios.

Taken together, the results reported here significantly contribute to our understanding of the bioreactor phenotype under non-perfectly mixed conditions in carbon-limited processes. What hopefully emerges from this thesis is the impulse to push toward new DBTL iterations to turn rational scale-up/scale-down engineering from promise to reality.

Bibliography

Abbott, D. A. *et al.* (2007) 'Generic and specific transcriptional responses to different weak organic acids in anaerobic chemostat cultures of *Saccharomyces cerevisiae*', *FEMS Yeast Research*, 7(6), pp. 819–833. doi: 10.1111/j.1567-1364.2007.00242.x.

Abel, C., Hübner, U. and Schügerl, K. (1994) 'Transient behaviour of Baker's yeast during enforced periodical variation of dissolved oxygen concentration', *Journal of Biotechnology*, 32(1), pp. 45–57. doi: 10.1016/0168-1656(94)90119-8.

Acar, M., Mettetal, J. T. and Van Oudenaarden, A. (2008) 'Stochastic switching as a survival strategy in fluctuating environments', *Nature Genetics*, 40(4), pp. 471–475. doi: 10.1038/ng.110.

Afgan, E. *et al.* (2018) 'The Galaxy platform for accessible, reproducible and collaborative biomedical analyses: 2018 update', *Nucleic Acids Research*, 46(W1), pp. W537–W544. doi: 10.1093/nar/gky379.

Agledal, L., Niere, M. and Ziegler, M. (2010) 'The phosphate makes a difference: Cellular functions of NADP', *Redox Report*, 15(1), pp. 2–10. doi: 10.1179/174329210X12650506623122.

Airoldi, E. M. *et al.* (2016) 'Steady-state and dynamic gene expression programs in *Saccharomyces cerevisiae* in response to variation in environmental nitrogen', *Molecular Biology of the Cell*, 27(8), pp. 1383–1396. doi: 10.1091/mbc.E14-05-1013.

Alon, U. (2019) 'An introduction to systems biology: design principles of biological circuits', *CRC press*.

de Alteriis, E. *et al.* (2018) 'Revisiting the Crabtree/Warburg effect in a dynamic perspective: a fitness advantage against sugar-induced cell death Elisabetta', *Cell Cycle*. Nature Publishing Group, 17(6), pp. 688–701. doi: https://doi.org/10.1080/15384101.2018.1442622.

An, H. and Harper, J. W. (2020) 'Ribosome Abundance Control Via the Ubiquitin–Proteasome System and Autophagy', *Journal of Molecular Biology*. Elsevier Ltd, 432(1), pp. 170–184. doi: 10.1016/j.jmb.2019.06.001.

Anane, E. *et al.* (2019) 'Modelling concentration gradients in fed-batch cultivations of *E. coli* – towards the flexible design of scale-down experiments', *Journal of Chemical Technology and Biotechnology*, 94(2), pp. 516–526. doi: 10.1002/jctb.5798.

Andrews, S. (2010) 'Babraham Bioinformatics – FastQC: a quality control tool for high throughput sequence data', http://www.bioinformatics.babraham.ac.uk/projects/fastqc/.

Ankenbauer, A. *et al.* (2020) '*Pseudomonas putida* KT2440 is naturally endowed to withstand industrial-scale stress conditions', *Microbial Biotechnology*, 13(4), pp. 1145–1161. doi: 10.1111/1751-7915.13571.

Antonin, W., Meyer, H.-A. and Hartmann, E. (2000) 'Interactions between Spc2p and Other Components of the Endoplasmic Reticulum Translocation Sites of the Yeast *Saccharomyces cerevisiae* *', *Journal of Biological Chemistry*, 275(44), pp. 34068–34072. doi: https://doi.org/10.1074/jbc.M006126200.

Aon, J. C. *et al.* (2016) 'Hypoxia-elicited impairment of cell wall integrity, glycosylation precursor synthesis, and growth in scaled-up high-cell density fed-batch cultures of

Saccharomyces cerevisiae', *Microbial Cell Factories*. BioMed Central, 15(1), pp. 1–16. doi: 10.1186/s12934-016-0542-3.

Ashe, M. P., De Long, S. K. and Sachs, A. B. (2000) 'Glucose Depletion Rapidly Inhibits Translation Initiation in Yeast', *Molecular Biology of the Cell*, 11(March), pp. 833–848.

Ask, M. *et al.* (2013) 'The influence of HMF and furfural on redox-balance and energy-state of xylose-utilizing *Saccharomyces cerevisiae*', *Biotechnology for Biofuels*, 6(1), pp. 1–13. doi: 10.1186/1754-6834-6-22.

Bachmann, H. *et al.* (2013) 'Availability of public goods shapes the evolution of competing metabolic strategies', *Proceedings of the National Academy of Sciences of the United States of America*, 110(35), pp. 14302–14307. doi: 10.1073/pnas.1308523110.

Baez, A. *et al.* (2011) 'Simulation of dissolved CO_2 gradients in a scale-down system: A metabolic and transcriptional study of recombinant Escherichia coli', *Biotechnology Journal*, 6(8), pp. 959–967. doi: 10.1002/biot.201000407.

Ball, W. J. and Atkinson, D. E. (1975) 'Adenylate energy charge in *Saccharomyces cerevisiae* during starvation', *Journal of Bacteriology*, 121(3), pp. 975–982.

Bárcena, M. *et al.* (2007) 'The structure of the ATP-bound state of *S. cerevisiae* phosphofructokinase determined by cryo-electron microscopy', *Journal of Structural Biology*, 159(1), pp. 135–143. doi: 10.1016/j.jsb.2007.03.004.

Bardwell, L. *et al.* (1998) 'Repression of yeast Ste12 transcription factor by direct binding of unphosphorylated Kss1 MAPK and its regulation by the Ste7 MEK', *Genes and Development*, 12(18), pp. 2887–2898. doi: 10.1101/gad.12.18.2887.

Bardwell, L. (2005) 'A walk-through of the yeast mating pheromone response pathway', *Peptides*, 26(2), pp. 339–350. doi: 10.1016/j.peptides.2004.10.002.

Barraza, C. E. *et al.* (2021) 'A prion-like domain of Tpk2 catalytic subunit of protein kinase A modulates P-body formation in response to stress in budding yeast', *Biochimica et Biophysica Acta - Molecular Cell Research*. Elsevier, 1868(1), p. 118884. doi: 10.1016/j.bbamcr.2020.118884.

Bates, R. L., Fondy, P. L. and Corpstein, R. R. (1963) 'An examination of some geometric parameters of impeller power', *Industrial and Engineering Chemistry Process Design and Development*, 2(4), pp. 310–314. doi: 10.1021/i260008a011.

Benjamini, Y. and Hochberg, Y. (1995) 'Controlling the False Discovery Rate : A Practical and Powerful Approach to Multiple Testing Author (s): Yoav Benjamini and Yosef Hochberg Source : Journal of the Royal Statistical Society . Series B (Methodological), Vol . 57 , No . 1 (1995), Publi', *Journal of the Royal Statistical Society*, 57(1), pp. 289–300.

Bergdahl, B. *et al.* (2012) 'Dynamic metabolomics differentiates between carbon and energy starvation in recombinant *Saccharomyces cerevisiae* fermenting xylose', *Biotechnology for Biofuels*, 5, pp. 1–19. doi: 10.1186/1754-6834-5-34.

Bergen, A. C. *et al.* (2021) 'Integrating multiple single-cell phenotypes links stress acclimation to prior life history in yeast', *bioRxiv*, p. 2021.09.08.459442. doi: https://doi.org/10.1101/2021.09.08.459442.

Bernstein, K. A. *et al.* (2007) 'Ribosome Biogenesis Is Sensed at the Start Cell Cycle Checkpoint', *Molecular biology of the cell*, 18(March), pp. 953–964. doi: 10.1091/mbc.E06–06–0512.

Berry, D. B. and Gasch, A. P. (2008) 'Stress-activated Genomic Expression Changes Serve a Preparative Role for Impending Stress in Yeast', 19(November), pp. 4580–4587. doi: 10.1091/mbc.E07.

Bertels, L.-K., Murillo, L. F. and Heinisch, J. (2021) 'The Pentose Phosphate Pathway in Yeasts – More Than a Poor Cousin of Glycolysis', *Biomolecules*, 11(725). doi: https://doi.org/10.3390/biom11050725.

Beullens, M. *et al.* (1988) 'Studies on the mechanism of the glucose-induced cAMP signal in glycolysis and glucose repression mutants of the yeast *Saccharomyces cerevisiae*', *European Journal of Biochemistry*, 172(1), pp. 227–231. doi: 10.1111/j.1432-1033.1988.tb13877.x.

Bheda, P. (2020) 'Metabolic transcriptional memory', *Molecular Metabolism*. Elsevier GmbH, 38(February), p. 100955. doi: 10.1016/j.molmet.2020.01.019.

Bilsland, E. *et al.* (2004) 'Rck1 and Rck2 MAPKAP kinases and the HOG pathway are required for oxidative stress resistance.', *Molecular microbiology*. England, 53(6), pp. 1743–1756. doi: 10.1111/j.1365-2958.2004.04238.x.

Birnbaum, S. and Bailey, J. E. (1991) 'Plasmid presence changes the relative levels of many host cell proteins and ribosome components in recombinant *Escherichia coli*', *Biotechnology and Bioengineering*, 37(8), pp. 736–745. doi: 10.1002/bit.260370808.

Bisgaard, J. *et al.* (2022) ' Data-based dynamic compartment model: Modeling of *E. coli* fed-batch fermentation in a 600 m3 bubble column ', *Journal of Industrial Microbiology and Biotechnology*, 49(5). doi: 10.1093/jimb/kuac021.

Bisschops, M. M. M. *et al.* (2017) 'Extreme calorie restriction in yeast retentostats induces uniform non-quiescent growth arrest', *Biochimica et Biophysica Acta - Molecular Cell Research*. Elsevier B.V., 1864(1), pp. 231–242. doi: 10.1016/j.bbamcr.2016.11.002.

Bisson, L. F., Fan, Q. and Walker, G. A. (2016) 'Sugar and Glycerol Transport in *Saccharomyces cerevisiae* BT - Yeast Membrane Transport', in Ramos, J., Sychrová, H., and Kschischo, M. (eds). Cham: Springer International Publishing, pp. 125–168. doi: 10.1007/978-3-319-25304-6_6.

Blázquez, M. A. *et al.* (1993) 'Trehalose-6-phosphate, a new regulator of yeast glycolysis that inhibits hexokinases', *FEBS Letters*, 329(1–2), pp. 51–54. doi: 10.1016/0014-5793(93)80191-V.

Blöbaum, L., Haringa, C. and Grünberger, A. (2023) 'Microbial lifelines in bioprocesses: From concept to application', *Biotechnology advances*, 62(September 2022), p. 108071. doi: 10.1016/j.biotechadv.2022.108071.

Blomberg, A. (2000) 'Metabolic surprises in *Saccharomyces cerevisiae* during adaptation to saline conditions: Questions, some answers and a model', *FEMS Microbiology Letters*, 182(1), pp. 1–8. doi: 10.1016/S0378-1097(99)00531-5.

Boender, L. G. M. *et al.* (2009) 'Quantitative physiology of *Saccharomyces cerevisiae* at near-zero specific growth rates', *Applied and Environmental Microbiology*, 75(17), pp. 5607–5614. doi: 10.1128/AEM.00429-09.

Boer, V. M. *et al.* (2003) 'The genome-wide transcriptional responses of *Saccharomyces cerevisiae* grown on glucose in aerobic chemostat cultures limited for carbon, nitrogen, phosphorus, or sulfur', *Journal of Biological Chemistry*, 278(5), pp. 3265–3274. doi: 10.1074/jbc.M209759200.

Böhm, L. *et al.* (2019) 'Multiphase Stirred Tank Bioreactors – New Geometrical Concepts and Scale-up Approaches', *Chemie-Ingenieur-Technik*, 91(12), pp. 1724–1746. doi: 10.1002/cite.201900165.

Boles, E. *et al.* (1997) 'Characterization of a glucose-repressed pyruvate kinase (Pyk2p) in *Saccharomyces cerevisiae* that is catalytically insensitive to fructose-1,6-bisphosphate.', *Journal of bacteriology*, 179(9), pp. 2987–2993.

Bolger, A. M., Lohse, M. and Usadel, B. (2014) 'Trimmomatic: A flexible trimmer for Illumina sequence data', *Bioinformatics*, 30(15), pp. 2114–2120. doi: 10.1093/bioinformatics/btu170.

Bonawitz, N. D. *et al.* (2007) 'Reduced TOR Signaling Extends Chronological Life Span via Increased Respiration and Upregulation of Mitochondrial Gene Expression', *Cell Metabolism*, 5(4), pp. 265–277. doi: 10.1016/j.cmet.2007.02.009.

Borneman, A. R. *et al.* (2011) 'Whole-genome comparison reveals novel genetic elements that characterize the genome of industrial strains of *Saccharomyces cerevisiae*', *PLoS Genetics*, 7(2). doi: 10.1371/journal.pgen.1001287.

Bosdriesz, E. *et al.* (2018) 'Low affinity uniporter carrier proteins can increase net substrate uptake rate by reducing efflux', *Scientific Reports*, 8(1), pp. 1–9. doi: 10.1038/s41598-018-23528-7.

Botman, D. *et al.* (2019) 'A new FRET biosensor enlightens cAMP signalling in budding yeast', *bioRxiv*, pp. 1–22. doi: https://doi.org/10.1101/831354.

Boubekeur, S. *et al.* (1999) 'A Mitochondrial Pyruvate Dehydrogenase Bypass in the Yeast *Saccharomyces cerevisiae*', *Journal of Biological Chemistry*, 274(30), pp. 21044–21048. doi: https://doi.org/10.1074/jbc.274.30.21044.

Boutte, C. C. and Crosson, S. (2013) 'Bacterial lifestyle shapes stringent response activation', *Trends in Microbiology*. Elsevier Ltd, 21(4), pp. 174–180. doi: 10.1016/j.tim.2013.01.002.

Branzei, D. and Foiani, M. (2006) 'The Rad53 signal transduction pathway: Replication fork stabilization, DNA repair, and adaptation', *Experimental Cell Research*, 312(14), pp. 2654–2659. doi: 10.1016/j.yexcr.2006.06.012.

Brauer, J. M. *et al.* (2008) 'Coordination of Growth Rate, Cell Cycle, Stress Response, and Metabolic Activity in Yeast', *Molecular biology of the cell*, 19(September), pp. 308–317. doi: 10.1091/mbc.E07.

Brauer, M. J. *et al.* (2006) 'Conservation of the metabolomic response to starvation across two divergent microbes', *Proceedings of the National Academy of Sciences of the United States of America*, 103(51), pp. 19302–19307. doi: 10.1073/pnas.0609508103.

Brengues, M. and Parker, R. (2007) 'Accumulation of Polyadenylated mRNA, Pab1p, eIF4E, and eIF4G with P-Bodies in *Saccharomyces cerevisiae*', *Molecular biology of the cell*, 18(July), pp. 2592–2602. doi: 10.1091/mbc.E06–12–1149.

Bresson, S. *et al.* (2017) 'Nuclear RNA Decay Pathways Aid Rapid Remodeling of Gene Expression in Yeast', *Molecular Cell*. Elsevier Inc., 65(5), pp. 787-800.e5. doi: 10.1016/j.molcel.2017.01.005.

Brexó, R. P. and Sant'Ana, A. S. (2017) 'Impact and significance of microbial contamination during fermentation for bioethanol production', *Renewable and Sustainable Energy Reviews*. Elsevier Ltd, 73(November), pp. 423–434. doi: 10.1016/j.rser.2017.01.151.

Brink, D. P. *et al.* (2021) 'D-xylose sensing in *Saccharomyces cerevisiae*: Insights from D-glucose signaling and native D-xylose utilizers', *International Journal of Molecular Sciences*, 22(22). doi: 10.3390/ijms222212410.

Van Den Brink, J. *et al.* (2008) 'Dynamics of glycolytic regulation during adaptation of *Saccharomyces cerevisiae* to fermentative metabolism', *Applied and Environmental Microbiology*, 74(18), pp. 5710–5723. doi: 10.1128/AEM.01121-08.

Van Den Brink, J. (2009) Dynamic response of *Saccharomyces cerevisiae* to fermentative growth conditions, *Applied Sciences*, 1(2), 3.

Brion, C. *et al.* (2016) 'Differences in environmental stress response among yeasts is consistent with species-specific lifestyles', *Molecular Biology of the Cell*, 27(10), pp. 1694–1705. doi: 10.1091/mbc.E15-12-0816.

Broach, J. R. (2012) 'Nutritional control of growth and development in yeast', *Genetics*, 192(1), pp. 73–105. doi: 10.1534/genetics.111.135731.

Buchholz, J. *et al.* (2014) 'CO_2/HCO_3-perturbations of simulated large scale gradients in a scale-down device cause fast transcriptional responses in *Corynebacterium glutamicum*', *Applied Microbiology and Biotechnology*, 98(20), pp. 8563–8572. doi: 10.1007/s00253-014-6014-y.

Buchholz, J. (2015) 'Development, characterization, and application of a novel scale-down apparatus for the investigation of the scale-up dependent CO_2/HCO_3 – stimulus in *Corynebacterium glutamicum*', p. 278.

Busti, S. *et al.* (2010) 'Glucose signaling-mediated coordination of cell growth and cell cycle in *Saccharomyces cerevisiae*', *Sensors*, 10(6), pp. 6195–6240. doi: 10.3390/s100606195.

Buziol, S. *et al.* (2008) 'Dynamic response of the expression of hxt1, hxt5 and hxt7 transport proteins in *Saccharomyces cerevisiae* to perturbations in the extracellular glucose concentration', *Journal of Biotechnology*, 134(3–4), pp. 203–210. doi: 10.1016/j.jbiotec.2008.02.002.

Bylund, F. *et al.* (1998) 'Substrate gradient formation in the large-scale bioreactor lowers cell yield and increases by-product formation', *Bioprocess Engineering*, 18(3), pp. 171–180. doi: 10.1007/s004490050427.

Cai, L., Dalal, C. K. and Elowitz, M. B. (2008) 'Frequency-modulated nuclear localization bursts coordinate gene regulation', *Nature*, 455(7212), pp. 485–490. doi: 10.1038/nature07292.

Çakar, Z. P. *et al.* (2012) 'Evolutionary engineering of *Saccharomyces cerevisiae* for improved industrially important properties', *FEMS Yeast Research*, 12(2), pp. 171–182. doi: 10.1111/j.1567-1364.2011.00775.x.

Calabrese, S. *et al.* (2021) 'Energetic scaling in microbial growth', *Proceedings of the National Academy of Sciences of the United States of America*, 118(47), pp. 1–8. doi: 10.1073/pnas.2107668118.

Caligaris, M. *et al.* (2022) 'SNF1/AMPK fine-tunes TORC1 signaling in response to glucose starvation', *bioRxiv*, p. 2022.10.18.512649. doi: 10.1101/2022.10.18.512649.

Campbell, K., Xia, J. and Nielsen, J. (2017) 'The Impact of Systems Biology on Bioprocessing', *Trends in Biotechnology*. Elsevier Ltd, 35(12), pp. 1156–1168. doi: 10.1016/j.tibtech.2017.08.011.

Campbell, N A *et al.* (2008) 'Biology, 8th edition', San Francisco, USA, *Pearson Benjamin Cummings*. ISBN: 978-0805368444.

Canelas, A. B. *et al.* (2008) 'Leakage-free rapid quenching technique for yeast metabolomics', *Metabolomics*, 4(3), pp. 226–239. doi: 10.1007/s11306-008-0116-4.

Canelas, A. B. *et al.* (2010) 'Integrated multilaboratory systems biology reveals differences in protein metabolism between two reference yeast strains', *Nature Communications*. Nature Publishing Group, 1(9), pp. 145–148. doi: 10.1038/ncomms1150.

Cannon, J. F. and Tatchell, K. (1987) 'Characterization of *Saccharomyces cerevisiae* genes encoding subunits of cyclic AMP-dependent protein kinase', *Molecular and Cellular Biology*, 7(8), pp. 2653–2663. doi: 10.1128/mcb.7.8.2653-2663.1987.

Carlquist, M. *et al.* (2012) 'Physiological heterogeneities in microbial populations and implications for physical stress tolerance', *Microbial Cell Factories*, 11(1), p. 94. doi: 10.1186/1475-2859-11-94.

Castelli, L. M. *et al.* (2011) 'Glucose depletion inhibits translation initiation via eIF4A loss and subsequent 48S preinitiation complex accumulation, while the pentose phosphate pathway is coordinately up-regulated', *Molecular Biology of the Cell*, 22(18), pp. 3379–3393. doi: 10.1091/mbc.E11-02-0153.

Causton, H. C. *et al.* (2001) 'Remodeling of Yeast Genome Expression in Response to Environmental Changes', *Molecular Biology of the Cell*, 12(2), pp. 323–337. doi: 10.1091/mbc.12.2.323.

Ceccato-Antonini, S. R. and Sudbery, P. E. (2004) 'Filamentous growth in *Saccharomyces cerevisiae*', *Brazilian Journal of Microbiology*, 35(3), pp. 173–181. doi: 10.1590/S1517-83822004000200001.

Celton, M. *et al.* (2012) 'A comparative transcriptomic, fluxomic and metabolomic analysis of the response of *Saccharomyces cerevisiae* to increases in NADPH oxidation', *BMC Genomics*, 13(1). doi: 10.1186/1471-2164-13-317.

Cerulus, B. *et al.* (2018) 'Transition between fermentation and respiration determines history-dependent behavior in fluctuating carbon sources', *eLife*. Edited by N. Barkai. eLife Sciences Publications, Ltd, 7, p. e39234. doi: 10.7554/eLife.39234.

Charizanis, C. *et al.* (1999) 'The oxidative stress response mediated via Pos9/Skn7 is negatively regulated by the Ras/PKA pathway in *Saccharomyces cerevisiae*', *Molecular and General Genetics MGG*. Springer, 261, pp. 740–752.

Chasman, D. *et al.* (2014) 'Pathway connectivity and signaling coordination in the yeast stress-activated signaling network', *Molecular Systems Biology*, 10(11), p. 759. doi: 10.15252/msb.20145120.

Chen, E. Y. *et al.* (2013) 'Enrichr: Interactive and collaborative HTML5 gene list enrichment analysis tool', *BMC Bioinformatics*, 14. doi: 10.1186/1471-2105-14-128.

Chen, R. E. and Thorner, J. (2007) 'Function and regulation in MAPK signaling pathways: Lessons learned from the yeast *Saccharomyces cerevisiae*', *Biochimica et Biophysica Acta - Molecular Cell Research*, 1773(8), pp. 1311–1340. doi: 10.1016/j.bbamcr.2007.05.003.

Chen, S. Y. *et al.* (2019) 'Optogenetic control reveals differential promoter interpretation of transcription factor nuclear translocation dynamics', *bioRxiv*, p. 548255. doi: 10.1101/548255.

Chen, Y. *et al.* (2020) 'Systems and synthetic biology tools for advanced bioproduction hosts', *Current Opinion in Biotechnology*, 64, pp. 101–109. doi: 10.1016/j.copbio.2019.12.007.

Cheng, J. S. *et al.* (2009) 'Proteomic insights into adaptive responses of *Saccharomyces cerevisiae* to the repeated vacuum fermentation', *Applied Microbiology and Biotechnology*, 83(5), pp. 909–923. doi: 10.1007/s00253-009-2037-1.

Cherry, J. *et al.* (2012) '*Saccharomyces* Genome Database: the genomics resource of budding yeast', *Nucleic acids research*, 40(D1), pp. D700-D705.

Chmiel, H., Takors, R. and Weuster-Botz, D. (2018) 'Bioprozesstechnik', Berlin/Heidelberg, Germany, *Springer Spektrum*. ISBN: 978-3-662-54041-1.

Chua, P. R., Jiang, H. and Meadows, A. L. (2020) 'Maltose dependent degrons, maltose-responsive promoters, stabilization constructs, and their use in production of non-catabolic compounds'. US Patent number: US10808015B2.

Cipollina, C. *et al.* (2008) '*Saccharomyces cerevisiae* SFP1: At the crossroads of central metabolism and ribosome biogenesis', *Microbiology*, 154(6), pp. 1686–1699. doi: 10.1099/mic.0.2008/017392-0.

Coccetti, P., Nicastro, R. and Tripodi, F. (2018) 'Conventional and emerging roles of the energy sensor SNF1/AMPK in *Saccharomyces cerevisiae*', *Microbial Cell*, 5(11), pp. 482–494. doi: 10.15698/mic2018.11.655.

Cohen, O. *et al.* (2016) 'Essential Genes Embody Increased Mutational Robustness to Compensate for the Lack of Backup Genetic Redundancy', *PLOS ONE*. Public Library of Science, 11(12), p. e0168444. URL: https://doi.org/10.1371/journal.pone.0168444.

Conrad, M. *et al.* (2014) 'Nutrient sensing and signaling in the yeast *Saccharomyces cerevisiae*', *FEMS Microbiology Reviews*, 38(2), pp. 254–299. doi: 10.1111/1574-6976.12065.

Cortés, G. *et al.* (2005) 'Production of β-galactosidase by Kluyveromyces marxianus under oscillating dissolved oxygen tension', *Process Biochemistry*, 40(2), pp. 773–778. doi: https://doi.org/10.1016/j.procbio.2004.02.001.

Couvillion, M. T. *et al.* (2016) 'Synchronized mitochondrial and cytosolic translation programs', *Nature*. 533(7604), pp. 499–503. doi: 10.1038/nature18015.

Covey, S. R. (1991) 'The seven habits of highly effective people', Covey Leadership Center Provo, UT.

Crater, J. S. and Lievense, J. C. (2018) 'Scale-up of industrial microbial processes', *FEMS Microbiology Letters*, 365(13), pp. 1–5. doi: 10.1093/femsle/fny138.

Creamer, D. R. *et al.* (2022) 'Yeast Protein Kinase A Isoforms: A Means of Encoding Specificity in the Response to Diverse Stress Conditions?', *Biomolecules*, 12(7), pp. 1–17. doi: 10.3390/biom12070958.

Cullen, P. J. and Sprague, G. F. (2012) 'The regulation of filamentous growth in yeast', *Genetics*, 190(1), pp. 23–49. doi: 10.1534/genetics.111.127456.

DataIntelo (2022) 'Global Transportation Market by Type'. URL: https://dataintelo.com/report/global-transportation-market/ (Accessed: 7 February 2023).

David, P. S. and Poyton, R. O. (2005) 'Effects of a transition from normoxia to anoxia on yeast cytochrome c oxidase and the mitochondrial respiratory chain: Implications for

hypoxic gene induction', *Biochimica et Biophysica Acta - Bioenergetics*, 1709(2), pp. 169–180. doi: 10.1016/j.bbabio.2005.07.002.

Delvigne, F. *et al.* (2015) 'Dynamic single-cell analysis of *Saccharomyces cerevisiae* under process perturbation: comparison of different methods for monitoring the intensity of population heterogeneity', *Journal of Chemical Technology & Biotechnology*. John Wiley & Sons, Ltd, 90(2), pp. 314–323. doi: https://doi.org/10.1002/jctb.4430.

Delvigne, F. *et al.* (2017) 'Bioprocess scale-up/down as integrative enabling technology: from fluid mechanics to systems biology and beyond', *Microbial Biotechnology*, 10(5), pp. 1267–1274. doi: 10.1111/1751-7915.12803.

Delvigne, F. and Goffin, P. (2014) 'Microbial heterogeneity affects bioprocess robustness: Dynamic single-cell analysis contributes to understanding of microbial populations', *Biotechnology Journal*, 9(1), pp. 61–72. doi: 10.1002/biot.201300119.

Delvigne, F. and Noorman, H. (2017) 'Scale-up/Scale-down of microbial bioprocesses: a modern light on an old issue', *Microbial Biotechnology*, 10(4), pp. 685–687. doi: 10.1111/1751-7915.12732.

Deparis, Q. *et al.* (2017) 'Engineering tolerance to industrially relevant stress factors in yeast cell factories', *FEMS yeast research*, 17(4), pp. 1–17. doi: 10.1093/femsyr/fox036.

Diderich, J. A. *et al.* (1999) 'Glucose uptake kinetics and transcription of HXT genes in chemostat cultures of *Saccharomyces cerevisiae*', *Journal of Biological Chemistry*, 274(22), pp. 15350–15359. doi: 10.1074/jbc.274.22.15350.

Dihazi, H., Kessler, R. and Eschrich, K. (2004) 'High Osmolarity Glycerol (HOG) Pathway-induced Phosphorylation and Activation of 6-Phosphofructo-2-kinase Are Essential for Glycerol Accumulation and Yeast Cell Proliferation under Hyperosmotic Stress*', *Journal of Biological Chemistry*, 279(23), pp. 23961–23968. doi: https://doi.org/10.1074/jbc.M312974200.

Van Dijck, P. *et al.* (2000) 'A baker's yeast mutant (fil1) with a specific, partially inactivating mutation in adenylate cyclase maintains a high stress resistance during active fermentation and growth.', *Journal of molecular microbiology and biotechnology*. Switzerland, 2(4), pp. 521–530.

van Dijken, J. *et al.* (2000) 'An interlaboratory comparison of physiological and genetic properties of four *Saccharomyces cerevisiae* strains', *Enzyme and Microbial Technology*, 26(9), pp. 706–714. doi: 10.1016/S0141-0229(00)00162-9.

Dikicioglu, D. *et al.* (2011) 'How yeast re-programmes its transcriptional profile in response to different nutrient impulses', *BMC Systems Biology*, 5, pp. 1–16. doi: 10.1186/1752-0509-5-148.

Drobna, E., Bialkova, A. and Šubík, J. (2008) 'Transcriptional regulators of seven yeast species: comparative genome analysis', *Folia Microbiologica*. Springer, 53, pp. 275–287.

Eigenstetter, G. and Takors, R. (2017) 'Dynamic modeling reveals a three-step response of *Saccharomyces cerevisiae* to high CO2levels accompanied by increasing ATP demands', *FEMS Yeast Research*, 17(1), pp. 1–11. doi: 10.1093/femsyr/fox008.

EKATO Rühr-und Mischtechnik GmbH (2013) *EKATO. THE BOOK*. Edited by W. Himmelsbach and M. Delbrück. Weinheim: Wiley-VCH Verlag GmbH & Co. KGaA.

Enfors, S. O. *et al.* (2001) 'Physiological responses to mixing in large scale bioreactors', *Journal of Biotechnology*, 85(2), pp. 175–185. doi: 10.1016/S0168-1656(00)00365-5.

Estrella, M. A. *et al.* (2019) 'The metabolites NADP$^+$ and NADPH are the targets of the circadian protein Nocturnin (Curled)', *Nature Communications*. Springer US, 10(1), pp. 1–10. doi: 10.1038/s41467-019-10125-z.

European Comission (2022) 'What is Horizon 2020?' URL: https://wayback.archive-it.org/12090/20220124080448/https://ec.europa.eu/programmes/horizon2020/en/what-horizon-2020 (Accessed: 15 February 2023).

Fazio, A. *et al.* (2008) 'Transcription factor control of growth rate dependent genes in *Saccharomyces cerevisiae*: A three factor design', *BMC Genomics*, 9, pp. 1–14. doi: 10.1186/1471-2164-9-341.

Feith, A. *et al.* (2019) 'Hilic-enabled13c metabolomics strategies: Comparing quantitative precision and spectral accuracy of qtof high- and qqq low-resolution mass spectrometry', *Metabolites*, 9(4). doi: 10.3390/metabo9040063.

Ferea, T. L. *et al.* (1999) 'Systematic changes in gene expression patterns following adaptive evolution in yeast.', *Proceedings of the National Academy of Sciences of the United States of America*, 96(17), pp. 9721–6. doi: 10.1073/pnas.96.17.9721.

Fernández, P. M. *et al.* (2023) 'Scale-down of oxygen and glucose fluctuations in a tubular photobioreactor operated under oxygen-balanced mixotrophy', *Biotechnology and Bioengineering*, (October). doi: 10.1002/bit.28372.

Florez, S. L. (2018) 'Accelerating fermentation process development at Ginkgo using Sartorius' Ambr250 Platform', *BIOworld Congress on Industrial Biotechnology*. URL: https://www.bio.org/sites/default/files/legacy/bioorg/docs/Florez Ginkgo.pdf.

Formenti, L. R. *et al.* (2014) 'Challenges in industrial fermentation technology research', *Biotechnology Journal*, 9(6), pp. 727–738. doi: 10.1002/biot.201300236.

Fowler, J. D. and Dunlop, E. H. (1989) 'Effects of reactant heterogeneity and mixing on catabolite repression in cultures of *Saccharomyces cerevisiae*', *Biotechnology and Bioengineering*, 33(8), pp. 1039–1046. doi: 10.1002/bit.260330813.

Francois, J., Walther, T. and Parrou, J. L. (2012) 'Genetics and Regulation of Glycogen and Trehalose Metabolism in *Saccharomyces cerevisiae*', *Microbial Stress Tolerance for Biofuels*, 22, pp. 29–56. doi: 10.1007/978-3-642-21467-7.

François, J. and Parrou, J. L. (2001) 'Reserve carbohydrates metabolism in the yeast *Saccharomyces cerevisiae*', *FEMS Microbiology Reviews*, 25(1), pp. 125–145. doi: 10.1016/S0168-6445(00)00059-0.

Frank, C., Teleki, A. and Jendrossek, D. (2020) 'Characterization of *Agrobacterium tumefaciens* PPKs reveals the formation of oligophosphorylated products up to nucleoside nona-phosphates', *Applied Microbiology and Biotechnology*. Applied Microbiology and Biotechnology, 104(22), pp. 9683–9692. doi: 10.1007/s00253-020-10891-7.

Fu, Z. *et al.* (2014) 'Exometabolome analysis reveals hypoxia at the up-scaling of a *Saccharomyces cerevisiae* high-cell density fed-batch biopharmaceutical process', *Microbial Cell Factories*, 13(1), pp. 1–22. doi: 10.1186/1475-2859-13-32.

Gaikwad, S. *et al.* (2021) 'Reprogramming of translation in yeast cells impaired for ribosome recycling favors short, efficiently translated mRNAs', *eLife*, 10, pp. 1–38. doi: 10.7554/eLife.64283.

Garcia-Ochoa, F. and Gomez, E. (2009) 'Bioreactor scale-up and oxygen transfer rate in

microbial processes: An overview', *Biotechnology Advances*. Elsevier Inc., 27(2), pp. 153–176. doi: 10.1016/j.biotechadv.2008.10.006.

García-Ríos, E. *et al.* (2022) 'Genome-wide effect of non-optimal temperatures under anaerobic conditions on gene expression in *Saccharomyces cerevisiae*', *Genomics*, 114(4). doi: 10.1016/j.ygeno.2022.110386.

Gasch, A. P. *et al.* (2000) 'Genomic Expression Programs in the Response of Yeast Cells to Environmental Changes', *Molecular Biology of the Cell*, 11(12), pp. 4241–4257. doi: 10.1091/mbc.11.12.4241.

Gasch, A. P. (2007a) 'Comparative genomics of the environmental stress response in ascomycete fungi', *Yeast*, 24(July), pp. 961–976. doi: 10.1002/yea.1512.

Gasch, A. P. (2007b) 'The environmental stress response: a common yeast response to diverse environmental stresses', *Yeast Stress Responses*. Edited by S. Hohmann and W. H. Mager. Berlin, Heidelberg: Springer Berlin Heidelberg, 1, pp. 11–70. doi: 10.1007/3-540-45611-2_2.

Gasch, A. P. *et al.* (2017) 'Single-cell RNA sequencing reveals intrinsic and extrinsic regulatory heterogeneity in yeast responding to stress', *PLoS Biology*, 15(12), pp. 1–28. doi: 10.1371/journal.pbio.2004050.

Gaugler, L. *et al.* (2023) 'Scaling-down biopharmaceutical production processes via a single multi-compartment bioreactor (SMCB)', *Engineering in Life Sciences*. John Wiley & Sons, Ltd, 23(1), p. e2100161. doi: https://doi.org/10.1002/elsc.202100161.

George, S. *et al.* (1998) 'Comparison of the Baker's yeast process performance in laboratory and production scale', *Bioprocess Engineering*, 18, pp. 135–142. doi: 10.1007/PL00008979.

Giaever, G. *et al.* (2002) 'Functional profiling of the *Saccharomyces cerevisiae* genome', *Nature*, 418(6896), pp. 387–391. doi: 10.1038/nature00935.

Giannattasio, S. *et al.* (2013) 'Molecular mechanisms of *Saccharomyces cerevisiae* stress adaptation and programmed cell death in response to acetic acid', *Frontiers in Microbiology*, 4(FEB), pp. 1–7. doi: 10.3389/fmicb.2013.00033.

Gibson, B. R. *et al.* (2007) 'Yeast responses to stresses associated with industrial brewery handling', *FEMS Microbiology Reviews*. doi: 10.1111/j.1574-6976.2007.00076.x.

Gimeno, C. J. *et al.* (1992) 'Unipolar cell divisions in the yeast S. cerevisiae lead to filamentous growth: Regulation by starvation and RAS', *Cell*, 68(6), pp. 1077–1090. doi: 10.1016/0092-8674(92)90079-R.

Goddard, M. R. and Greig, D. (2015) '*Saccharomyces cerevisiae*: A nomadic yeast with no niche?', *FEMS Yeast Research*, 15(3), pp. 1–6. doi: 10.1093/femsyr/fov009.

Goffeau, A. *et al.* (1996) 'Life with 6000 genes', *Science*. American Association for the Advancement of Science, 274(5287), pp. 546–567.

Gombert, A. K. *et al.* (2001) 'Network Identification and Flux Quantification in the Central Metabolism of *Saccharomyces cerevisiae* under Different Conditions of Glucose Repression', 183(4), pp. 1441–1451. doi: 10.1128/JB.183.4.1441.

González, A. and Hall, M. N. (2017) 'Nutrient sensing and TOR signaling in yeast and mammals ', *The EMBO Journal*, 36(4), pp. 397–408. doi: 10.15252/embj.201696010.

Görner, W. *et al.* (2002) 'Acute glucose starvation activates the nuclear localization signal of

a stress-specific yeast transcription factor', *EMBO Journal*, 21(1–2), pp. 135–144. doi: 10.1093/emboj/21.1.135.

Gower, J. C. (1966) 'Some Distance Properties of Latent Root and Vector Methods Used in Multivariate Analysis', *Biometrika*, 53(3/4), p. 325. doi: 10.2307/2333639.

Gronchi, N. *et al.* (2022) 'Natural *Saccharomyces cerevisiae* Strain Reveals Peculiar Genomic Traits for Starch-to-Bioethanol Production: the Design of an Amylolytic Consolidated Bioprocessing Yeast', *Frontiers in Microbiology*, 12(January), pp. 1–19. doi: 10.3389/fmicb.2021.768562.

Gross, A. S. and Graef, M. (2020) 'Mechanisms of Autophagy in Metabolic Stress Response', *Journal of Molecular Biology*. Elsevier Ltd, 432(1), pp. 28–52. doi: 10.1016/j.jmb.2019.09.005.

Guan, Q. *et al.* (2012) 'Cellular memory of acquired stress resistance in *Saccharomyces cerevisiae*', *Genetics*, 192(2), pp. 495–505. doi: 10.1534/genetics.112.143016.

Gustin, M. C. *et al.* (1998) ' MAP Kinase Pathways in the Yeast *Saccharomyces cerevisiae* ', *Microbiology and Molecular Biology Reviews*, 62(4), pp. 1264–1300. doi: 10.1128/mmbr.62.4.1264-1300.1998.

Gutin, J. *et al.* (2015) ' Condition-specific genetic interaction maps reveal crosstalk between the cAMP / PKA and the HOG MAPK pathways in the activation of the general stress response ', *Molecular Systems Biology*, 11(10), p. 829. doi: 10.15252/msb.20156451.

Gutin, J. *et al.* (2019) 'Genetic screen of the yeast environmental stress response dynamics uncovers distinct regulatory phases', *Molecular Systems Biology*, 15(8), pp. 1–16. doi: 10.15252/msb.20198939.

Haber, J. E. (2012) 'Mating-type genes and MAT switching in *Saccharomyces cerevisiae*', *Genetics*, 191(1), pp. 33–64. doi: 10.1534/genetics.111.134577.

Hackley, R. K. and Schmid, A. K. (2019) 'Global Transcriptional Programs in Archaea Share Features with the Eukaryotic Environmental Stress Response', *Journal of Molecular Biology*, 431(20), pp. 4147–4166. doi: https://doi.org/10.1016/j.jmb.2019.07.029.

Hahn, J. S. and Thiele, D. J. (2004) 'Activation of the *Saccharomyces cerevisiae* Heat Shock Transcription Factor under Glucose Starvation Conditions by SNF1 Protein Kinase', *Journal of Biological Chemistry*, 279(7), pp. 5169–5176. doi: 10.1074/jbc.M311005200.

Hahn, S. and Young, E. T. (2011) 'Transcriptional regulation in *Saccharomyces cerevisiae*: Transcription factor regulation and function, mechanisms of initiation, and roles of activators and coactivators', *Genetics*, 189(3), pp. 705–736. doi: 10.1534/genetics.111.127019.

Hanlon, S. E. *et al.* (2011) 'The stress response factors Yap6, Cin5, Phd1, and Skn7 direct targeting of the conserved co-repressor Tup1-Ssn6 in S. cerevisiae', *PLoS ONE*, 6(4). doi: 10.1371/journal.pone.0019060.

Harder, W. *et al.* (1997) 'Strategies of mixed substrate utilization in microorganisms', *Philosophical Transactions of the Royal Society of London. B, Biological Sciences*. Royal Society, 297(1088), pp. 459–480. doi: 10.1098/rstb.1982.0055.

Hardie, D. G., Ross, F. A. and Hawley, S. A. (2012) 'AMPK: A nutrient and energy sensor that maintains energy homeostasis', *Nature Reviews Molecular Cell Biology*, 13(4), pp. 251–262. doi: 10.1038/nrm3311.

Haringa, C. *et al.* (2016) 'Euler-Lagrange computational fluid dynamics for (bio)reactor scale down: An analysis of organism lifelines', *Engineering in Life Sciences*, 16(7), pp. 652–663. doi: 10.1002/elsc.201600061.

Haringa, C. *et al.* (2017) 'Euler-Lagrange analysis towards representative down-scaling of a 22 m3 aerobic *S. cerevisiae* fermentation', *Chemical Engineering Science*. The Author(s), 170, pp. 653–669. doi: 10.1016/j.ces.2017.01.014.

Haringa, C. (2017) 'Through the organisms's eye', Delft, Netherlands: TU Delft University.

Haringa, C. (2023) 'An analysis of organism lifelines in an industrial bioreactor using Lattice-Boltzmann CFD', *Engineering in Life Sciences*. Wiley Online Library, 23(1), p. e2100159.

Haringa, C., Mudde, R. F. and Noorman, H. (2018) 'From industrial fermentor to CFD-guided downscaling: what have we learned?', *Biochemical Engineering Journal*, (September). doi: 10.1016/j.bej.2018.09.001.

Hartwell, L. H. (1974) '*Saccharomyces cerevisiae* cell cycle', *Bacteriological Reviews*, 38(2), pp. 164–198. doi: 10.1128/mmbr.38.2.164-198.1974.

Hayakawa, K., Matsuda, F. and Shimizu, H. (2016) 'Metabolome analysis of *Saccharomyces cerevisiae* and optimization of culture medium for S-adenosyl-l-methionine production', *AMB Express*. Springer Berlin Heidelberg, 6(1). doi: 10.1186/s13568-016-0210-3.

Heijnen, J. J. (2005) 'Approximative kinetic formats used in metabolic network modeling', *Biotechnology and bioengineering*. United States, 91(5), pp. 534–545. doi: 10.1002/bit.20558.

Heins, A. L. *et al.* (2015) 'Experimental and in silico investigation of population heterogeneity in continuous *Saccharomyces cerevisiae* scale-down fermentation in a two-compartment setup', *Journal of Chemical Technology and Biotechnology*, 90(2), pp. 324–340. doi: 10.1002/jctb.4532.

Heins, A. L. and Weuster-Botz, D. (2018) 'Population heterogeneity in microbial bioprocesses: origin, analysis, mechanisms, and future perspectives', *Bioprocess and Biosystems Engineering*. Springer Berlin Heidelberg, 41(7), pp. 889–916. doi: 10.1007/s00449-018-1922-3.

Helbig, A. O. *et al.* (2009) 'A three-way proteomics strategy allows differential analysis of yeast mitochondrial membrane protein complexes under anaerobic and aerobic conditions', *Proteomics*, 9(20), pp. 4787–4798. doi: 10.1002/pmic.200800951.

Hepp, S. *et al.* (2020) 'An Optogenetic Tool for Induced Protein Stabilization Based on the *Phaeodactylum tricornutum* Aureochrome 1a Light–Oxygen–Voltage Domain', *Journal of Molecular Biology*. Elsevier Ltd. doi: 10.1016/j.jmb.2020.02.019.

Herrero, P. *et al.* (1995) 'Transcriptional regulation of the *Saccharomyces cerevisiae* HXK1, HXK2 and GLK1 genes.', *Yeast (Chichester, England)*, 11(2), pp. 137–144.

Hershey, J. W. B., Sonenberg, N. and Mathews, M. B. (2012) 'Principles of translational control: An overview', *Cold Spring Harbor Perspectives in Biology*, 4(12), pp. 1–10. doi: 10.1101/cshperspect.a009829.

Herskowitz, I. (1988) 'Life Cycle of the Budding Yeast *Saccharomyces cerevisiae*', *Microbiological reviews*, 52(4), pp. 536–553. doi: 0146-0749/88/04536-18$02.00/0.

Hewitt, C. and Nienow, A. W. (2010) 'The Scale-Up of microbial batch and fed-batch

fermentation processes', *Comprehensive Bioprocess Engineering*, pp. 295–320. doi: 10.1016/S0065-2164(07)62005-X.

Hill, P. *et al.* (2020) 'Clean manufacturing powered by biology: how Amyris has deployed technology and aims to do it better', *Journal of Industrial Microbiology and Biotechnology*. Springer International Publishing, 47(11), pp. 965–975. doi: 10.1007/s10295-020-02314-3.

Ho, P. *et al.* (2022) 'Microfluidic Reproduction of Dynamic Bioreactor Environment Based on Computational Lifelines', *Frontiers in Chemical Engineering*, 4(March), pp. 1–15. doi: 10.3389/fceng.2022.826485.

Hoehler, T. M. and Jørgensen, B. B. (2013) 'Microbial life under extreme energy limitation', *Nature Reviews Microbiology*. Nature Publishing Group, 11(2), pp. 83–94. doi: 10.1038/nrmicro2939.

Van Hoek, P., Van Dijken, J. P. and Pronk, J. T. (1998) 'Effect of specific growth rate on fermentative capacity of baker's yeast.', *Applied and environmental microbiology*. United States, 64(11), pp. 4226–4233. doi: 10.1128/AEM.64.11.4226-4233.1998.

Hohmann, S. (2002) 'Osmotic Stress Signaling and Osmoadaptation in Yeasts', *MICROBIOLOGY AND MOLECULAR BIOLOGY REVIEWS*, 66(2), pp. 300–372. doi: 1. Hohmann, S. Osmotic Stress Signaling and Osmoadaptation in Yeasts. Microbiol. Mol. Biol. Rev. 2002, 66 (2), 300–372. https://doi.org/10.1007/BF01666364.

Hohmann, S. (2007) 'Yeast stress responses (vol.1)', *Springer Science & Business Media*.

Holmberg, C. I. *et al.* (2002) 'Multisite phosphorylation provides sophisticated regulation of transcription factors', *Trends in Biochemical Sciences*, 27(12), pp. 619–627. doi: 10.1016/S0968-0004(02)02207-7.

Holsbeeks, I. *et al.* (2004) 'The eukaryotic plasma membrane as a nutrient-sensing device.', *Trends in biochemical sciences*. England, 29(10), pp. 556–564. doi: 10.1016/j.tibs.2004.08.010.

Howe, K. L. *et al.* (2021) 'Ensembl 2021', *Nucleic Acids Research*, 49(D1), pp. D884–D891. doi: 10.1093/nar/gkaa942.

Huber, A. *et al.* (2011) 'Sch9 regulates ribosome biogenesis via Stb3, Dot6 and Tod6 and the histone deacetylase complex RPD3L', *EMBO Journal*. Nature Publishing Group, 30(15), pp. 3052–3064. doi: 10.1038/emboj.2011.221.

Huch, S. and Nissan, T. (2014) 'Interrelations between translation and general mRNA degradation in yeast', *Wiley interdisciplinary reviews. RNA*, 5(6), pp. 747–763. doi: 10.1002/wrna.1244.

Iyer, V. R. *et al.* (2001) 'Genomic binding sites of the yeast cell-cycle transcription factors SBF and MBF.', *Nature*. England, 409(6819), pp. 533–538. doi: 10.1038/35054095.

Jalihal, A. P. *et al.* (2021) 'Modeling and analysis of the macronutrient signaling network in budding yeast', *Molecular Biology of the Cell*. American Society for Cell Biology (mboc), 32(21), p. ar20. doi: 10.1091/mbc.E20-02-0117.

James, T. C. *et al.* (2003) 'Transcription profile of brewery yeast under fermentation conditions', *Journal of Applied Microbiology*, 94(3), pp. 432–448. doi: 10.1046/j.1365-2672.2003.01849.x.

Jansen, M. L. A. *et al.* (2005) 'Prolonged selection in aerobic, glucose-limited chemostat

cultures of *Saccharomyces cerevisiae* causes a partial loss of glycolytic capacity', *Microbiology*, 151(5), pp. 1657–1669. doi: 10.1099/mic.0.27577-0.

Jeong, S. H., Lee, H. J. and Lee, S. J. (2023) 'Recent Advances in CRISPR-Cas Technologies for Synthetic Biology', *Journal of Microbiology*, 61(1), pp. 13–36. doi: 10.1007/s12275-022-00005-5.

Jiang, Y. *et al.* (2017) 'Coupled feedback loops control the stimulus-dependent dynamics of the yeast transcription factor Msn2', *Journal of Biological Chemistry*, 292(30), pp. 12366–12372. doi: 10.1074/jbc.C117.800896.

Jiang, Y. *et al.* (2020) 'A protein kinase A–regulated network encodes short- And long-lived cellular memories', *Science Signaling*, 13(632). doi: 10.1126/scisignal.aaw8905.

Johnston, M. (1999) 'Feasting, fasting and fermenting: Glucose sensing in yeast and other cells', *Trends in Genetics*, 15(1), pp. 29–33. doi: 10.1016/S0168-9525(98)01637-0.

Johnston, N. R. *et al.* (2020) 'Genome-Wide Identification of Genes Involved in General Acid Stress and Fluoride Toxicity in *Saccharomyces cerevisiae*', *Frontiers in Microbiology*, 11(June), pp. 1–11. doi: 10.3389/fmicb.2020.01410.

de Jonge, L. P. *et al.* (2011) 'Scale-down of penicillin production in *Penicillium chrysogenum*', *Biotechnology Journal*, 6(8), pp. 944–958. doi: 10.1002/biot.201000409.

Jothi, R. *et al.* (2009) 'Genomic analysis reveals a tight link between transcription factor dynamics and regulatory network architecture', *Molecular Systems Biology*. John Wiley & Sons, Ltd, 5(1), p. 294. doi: https://doi.org/10.1038/msb.2009.52.

Jules, M. *et al.* (2008) 'New Insights into Trehalose Metabolism by *Saccharomyces cerevisiae* NTH2 Encodes a Functional Cytosolic Trehalase, and Deletion of TPS1 Reveals Ath1p-Dependent Trehalose Mobilization.pdf', *APPLIED AND ENVIRONMENTAL MICROBIOLOGY*, 74(3), pp. 605–614. doi: 10.1128/AEM.00557-07.

Junghans, L. *et al.* (2019) 'From nutritional wealth to autophagy: In vivo metabolic dynamics in the cytosol, mitochondrion and shuttles of IgG producing CHO cells', *Metabolic Engineering*. Elsevier Inc., 54(January), pp. 145–159. doi: 10.1016/j.ymben.2019.02.005.

Junker, B. H. (2004) 'Scale-up methodologies for *Escherichia coli* and yeast fermentation processes', *J Biosci Bioeng*, 97(6), pp. 347–364.

Jurica, M. S. *et al.* (1998) 'The allosteric regulation of pyruvate kinase by fructose-1 , 6-bisphosphate', *Structure*, 6(2), pp. 195–210. doi: 10.1016/s0969-2126(98)00021-5.

Jüsten, P. *et al.* (1996) 'Dependence of mycelial morphology on impeller type and agitation intensity', *Biotechnology and Bioengineering*, 52(6), pp. 672–684. doi: 10.1002/(SICI)1097-0290(19961220)52:6<672::AID-BIT5>3.0.CO;2-L.

Jüsten, P. *et al.* (1998) 'Dependence of *Penicillium chrysogenum* Growth, Morphology, Vacuolation, and Productivity in Fed-Batch Fermentations on Impeller Type and Agitation Intensity', *Biotechnology and Bioengineering*, 59(6), pp. 762–775. doi: https://doi.org/10.1002/(SICI)1097-0290(19980920)59:6%3C762::AID-BIT13%3E3.0.CO;2-7.

Kafri, M. *et al.* (2016) 'The Cost of Protein Production', *Cell Reports*. Elsevier Ltd, 14(1), pp. 22–31. doi: 10.1016/j.celrep.2015.12.015.

Von Kamp, A. and Klamt, S. (2017) 'Growth-coupled overproduction is feasible for almost all metabolites in five major production organisms', *Nature Communications*. Nature

Publishing Group, 8(May), pp. 1–10. doi: 10.1038/ncomms15956.

Kampers, L. F. C. *et al.* (2022) 'Navigating the Valley of Death: Perceptions of Industry and Academia on Production Platforms and Opportunities in Biotechnology', *EFB Bioeconomy Journal*. Elsevier B.V., 2(June), p. 100033. doi: 10.1016/j.bioeco.2022.100033.

Karathia, H. *et al.* (2011) '*Saccharomyces cerevisiae* as a model organism: A comparative study', *PLoS ONE*, 6(2). doi: 10.1371/journal.pone.0016015.

Kawakami, E. *et al.* (2016) 'Network analyses based on comprehensive molecular interaction maps reveal robust control structures in yeast stress response pathways', *npj Systems Biology and Applications*. Nature Publishing Group, 2(October 2015). doi: 10.1038/npjsba.2015.18.

Kerssemakers, A. A. J. *et al.* (2023) 'Dynamic Interplay between O_2 Availability, Growth Rates, and the Transcriptome of Yarrowia lipolytica', *Fermentation*, 9(1), pp. 1–18. doi: 10.3390/fermentation9010074.

Khanal, O. and Lenhoff, A. M. (2021) 'Developments and opportunities in continuous biopharmaceutical manufacturing', *mAbs*. Taylor & Francis, 13(1). doi: 10.1080/19420862.2021.1903664.

Kim, D. *et al.* (2013) 'TopHat2: accurate alignment of transcriptomes in the presence of insertions, deletions and gene fusions', *Genome Biology*, 14(1–13), pp. 957–961. doi: 10.1186/gb-2013-14-4-r36.

Kim, J.-E. *et al.* (2020) 'Characterization of the CCAAT-binding transcription factor complex in the plant pathogenic fungus *Fusarium graminearum*.', *Scientific reports*. England, 10(1), p. 4898. doi: 10.1038/s41598-020-61885-4.

Kim, J.-H. *et al.* (2013) 'The glucose signaling network in yeast', *Biochimica et Biophysica Acta*, 1830(11), pp. 5204–5210. doi: doi:10.1016/j.bbagen.2013.07.025.

Knijnenburg, T. A. *et al.* (2007) 'Exploiting combinatorial cultivation conditions to infer transcriptional regulation', *BMC Genomics*, 8(1), p. 25. doi: 10.1186/1471-2164-8-25.

Kohlwein, S. D., Veenhuis, M. and van der Klei, I. J. (2013) 'Lipid droplets and peroxisomes: Key players in cellular lipid homeostasis or a matter of fat-store'em up or burn'em down', *Genetics*, 193(1), pp. 1–50. doi: 10.1534/genetics.112.143362.

Koning, W. de and Dam, K. van (1992) 'A method for the determination of changes of glycolytic metabolites in yeast on a subsecond time scale using extraction at neutral pH', *Analytical Biochemistry*, 204(1), pp. 118–123. doi: 10.1016/0003-2697(92)90149-2.

Kopp, J. *et al.* (2019) 'The Rocky Road From Fed-Batch to Continuous Processing With *E. coli*', *Frontiers in Bioengineering and Biotechnology*, 7(November), pp. 1–16. doi: 10.3389/fbioe.2019.00328.

Kozak, B. U. *et al.* (2016) 'Replacement of the initial steps of ethanol metabolism in *Saccharomyces cerevisiae* by ATP-independent acetylating acetaldehyde dehydrogenase', *FEMS Yeast Research*, 16(2), pp. 1–15. doi: 10.1093/femsyr/fow006.

Krantz, M. *et al.* (2004) 'Anaerobicity prepares *Saccharomyces cerevisiae* cells for faster adaptation to osmotic shock', *Eukaryotic Cell*, 3(6), pp. 1381–1390. doi: 10.1128/EC.3.6.1381-1390.2004.

Kresnowati, M. T. A. P. *et al.* (2006) 'When transcriptome meets metabolome: Fast cellular

responses of yeast to sudden relief of glucose limitation', *Molecular Systems Biology*, 2. doi: 10.1038/msb4100083.

Kresnowati, M. T. A. P., Van Winden, W. A. and Heijnen, J. J. (2005) 'Determination of elasticities, concentration and flux control coefficients from transient metabolite data using linlog kinetics', *Metabolic Engineering*, 7(2), pp. 142–153. doi: 10.1016/j.ymben.2004.12.002.

Kresze, G. B. and Ronft, H. (1981) 'Pyruvate dehydrogenase complex from baker's yeast. 1. Purification and some kinetic and regulatory properties.', *European journal of biochemistry*. England, 119(3), pp. 573–579. doi: 10.1111/j.1432-1033.1981.tb05646.x.

Kruckeberg, A. L. (1996) 'The hexose transporter family of *Saccharomyces cerevisiae*.', *Archives of microbiology*. Germany, 166(5), pp. 283–292. doi: 10.1007/s002030050385.

Kuleshov, M. V. *et al.* (2019) 'modEnrichr: a suite of gene set enrichment analysis tools for model organisms', *Nucleic acids research*. Oxford University Press, 47(W1), pp. W183–W190. doi: 10.1093/nar/gkz347.

Kümmel, A. *et al.* (2010) 'Differential glucose repression in common yeast strains in response to HXK2 deletion', *FEMS Yeast Research*, 10(3), pp. 322–332. doi: 10.1111/j.1567-1364.2010.00609.x.

Kunkel, J., Luo, X. and Capaldi, A. P. (2019) 'Integrated TORC1 and PKA signaling control the temporal activation of glucose-induced gene expression in yeast', *Nature Communications*. Springer US, 10(1), pp. 1–11. doi: 10.1038/s41467-019-11540-y.

Kuschel, M., Siebler, F. and Takors, R. (2017) 'Lagrangian Trajectories to Predict the Formation of Population Heterogeneity in Large-Scale Bioreactors', *Bioengineering*, 4(2), p. 27. doi: 10.3390/bioengineering4020027.

Kuschel, M. and Takors, R. (2020) 'Simulated oxygen and glucose gradients as a prerequisite for predicting industrial scale performance *a priori*', *Biotechnology and Bioengineering*, 117(9), pp. 2760–2770. doi: 10.1002/bit.27457.

De La Fuente, I. M. *et al.* (2014) 'On the dynamics of the adenylate energy system: Homeorhesis vs homeostasis', *PLoS ONE*, 9(10). doi: 10.1371/journal.pone.0108676.

Lahtvee, P. J. *et al.* (2017) 'Absolute Quantification of Protein and mRNA Abundances Demonstrate Variability in Gene-Specific Translation Efficiency in Yeast', *Cell Systems*, 4(5), pp. 495-504.e5. doi: 10.1016/j.cels.2017.03.003.

Lai, L.-C. *et al.* (2005) ' Dynamical Remodeling of the Transcriptome during Short-Term Anaerobiosis in *Saccharomyces cerevisiae* : Differential Response and Role of Msn2 and/or Msn4 and Other Factors in Galactose and Glucose Media ', *Molecular and Cellular Biology*, 25(10), pp. 4075–4091. doi: 10.1128/mcb.25.10.4075-4091.2005.

Lang, M. J. *et al.* (2014) 'Glucose starvation inhibits autophagy via vacuolar hydrolysis and induces plasma membrane internalization by down-regulating recycling', *Journal of Biological Chemistry*, 289(24), pp. 16736–16747. doi: 10.1074/jbc.M113.525782.

Lao-Martil, D. *et al.* (2022) 'Kinetic Modeling of *Saccharomyces cerevisiae* Central Carbon Metabolism : Achievements , Limitations , and Opportunities'.

Lapin, A., Müller, D. and Reuss, M. (2004) 'Dynamic Behavior of Microbial Populations in Stirred Bioreactors Simulated with Euler−Lagrange Methods: Traveling along the Lifelines of Single Cells [†]', *Industrial & Engineering Chemistry Research*, 43(16), pp. 4647–4656. doi: 10.1021/ie030786k.

Lara, A. R. *et al.* (2006) 'Living with heterogeneities in bioreactors', *Molecular Biotechnology*, 34(3), pp. 355–381. doi: 10.1385/mb:34:3:355.

Larsson, G. *et al.* (1996) 'Substrate gradients in bioreactors: origin and consequences', *Bioprocess Engineering*, 14, pp. 281–289. doi: 10.1007/PL00008979.

Lee, M. V. *et al.* (2011) 'A dynamic model of proteome changes reveals new roles for transcript alteration in yeast', *Molecular Systems Biology*. Nature Publishing Group, 7(514), pp. 1–12. doi: 10.1038/msb.2011.48.

Lemoine, A. *et al.* (2015) 'Response of *Corynebacterium glutamicum* exposed to oscillating cultivation conditions in a two- and a novel three-compartment scale-down bioreactor', *Biotechnology and Bioengineering*, 112(6), pp. 1220–1231. doi: 10.1002/bit.25543.

Lemoine, A. *et al.* (2017) 'Tools for the determination of population heterogeneity caused by inhomogeneous cultivation conditions', *Journal of Biotechnology*. Elsevier, 251(April), pp. 84–93. doi: 10.1016/j.jbiotec.2017.03.020.

Lempiäinen, H. and Shore, D. (2009) 'Growth control and ribosome biogenesis', *Current Opinion in Cell Biology*, 21(6), pp. 855–863. doi: 10.1016/j.ceb.2009.09.002.

Levy, S. *et al.* (2007) 'Strategy of transcription regulation in the budding yeast', *PLoS ONE*, 2(2). doi: 10.1371/journal.pone.0000250.

Levy, S. and Barkai, N. (2009) 'Coordination of gene expression with growth rate: A feedback or a feed-forward strategy?', *FEBS Letters*, 583(24), pp. 3974–3978. doi: 10.1016/j.febslet.2009.10.071.

Li, B. Z. *et al.* (2010) 'Genome-wide transcriptional analysis of *Saccharomyces cerevisiae* during industrial bioethanol fermentation', *Journal of Industrial Microbiology and Biotechnology*, 37(1), pp. 43–55. doi: 10.1007/s10295-009-0646-4.

Liao, Y., Smyth, G. K. and Shi, W. (2014) 'FeatureCounts: An efficient general purpose program for assigning sequence reads to genomic features', *Bioinformatics*, 30(7), pp. 923–930. doi: 10.1093/bioinformatics/btt656.

Lieder, S. *et al.* (2015) 'Genome reduction boosts heterologous gene expression in *Pseudomonas putida*', *Microbial cell factories*. BioMed Central, 14(1), pp. 1–14.

Limberg, M. H. *et al.* (2017) 'Metabolic profile of 1,5-diaminopentane producing *Corynebacterium glutamicum* under scale-down conditions: Blueprint for robustness to bioreactor inhomogeneities', *Biotechnology and Bioengineering*, 114(3), pp. 560–575. doi: 10.1002/bit.26184.

Lin, Y. *et al.* (2014) 'Leveraging transcription factors to speed cellobiose fermentation by *Saccharomyces cerevisiae.*', *Biotechnology for biofuels*. England, 7(1), p. 126. doi: 10.1186/s13068-014-0126-6.

Lip, K. Y. F. *et al.* (2020) 'Selection and subsequent physiological characterization of industrial *Saccharomyces cerevisiae* strains during continuous growth at sub- and- supra optimal temperatures', *Biotechnology Reports*, 26. doi: 10.1016/j.btre.2020.e00462.

Lipson, D. A. (2015) 'The complex relationship between microbial growth rate and yield and its implications for ecosystem processes', *Frontiers in Microbiology*, 6(JUN), pp. 1–5. doi: 10.3389/fmicb.2015.00615.

Liu, R. *et al.* (2019) 'Multiplex navigation of global regulatory networks (MINR) in yeast for improved ethanol tolerance and production', *Metabolic Engineering*, 51, pp. 50–58. doi:

https://doi.org/10.1016/j.ymben.2018.07.007.

Livas, D. *et al.* (2011) 'Transcriptional responses to glucose in *Saccharomyces cerevisiae* strains lacking a functional protein kinase A', *BMC Genomics*, 12, pp. 1–12. doi: 10.1186/1471-2164-12-405.

Ljungdahl, P. O. and Daignan-Fornier, B. (2012) 'Regulation of amino acid, nucleotide, and phosphate metabolism in *Saccharomyces cerevisiae*', *Genetics*, 190(3), pp. 885–929. doi: 10.1534/genetics.111.133306.

Löffler, M. *et al.* (2016) 'Engineering *E. coli* for large-scale production – Strategies considering ATP expenses and transcriptional responses', *Metabolic Engineering*, 38, pp. 73–85. doi: 10.1016/j.ymben.2016.06.008.

López-Maury, L., Marguerat, S. and Bähler, J. (2008) 'Tuning gene expression to changing environments: From rapid responses to evolutionary adaptation', *Nature Reviews Genetics*, 9(8), pp. 583–593. doi: 10.1038/nrg2398.

de Lorenzo, V. and Couto, J. (2019) 'The important versus the exciting: reining contradictions in contemporary biotechnology', *Microbial Biotechnology*, 12(1), pp. 32–34. doi: 10.1111/1751-7915.13348.

Löser, C. *et al.* (2005) 'Balancing the ethanol formation in continuous bioreactors with ethanol stripping', *Engineering in Life Sciences*, 5(4), pp. 325–332. doi: 10.1002/elsc.200520084.

Love, M. I., Huber, W. and Anders, S. (2014) 'Moderated estimation of fold change and dispersion for RNA-seq data with DESeq2', *Genome Biology*, 15(12), pp. 1–21. doi: 10.1186/s13059-014-0550-8.

de Lucena, R. M. *et al.* (2015) 'Transcriptomic response of *Saccharomyces cerevisiae* for its adaptation to sulphuric acid-induced stress', *Antonie van Leeuwenhoek, International Journal of General and Molecular Microbiology*, 108(5), pp. 1147–1160. doi: 10.1007/s10482-015-0568-2.

Luo, W. *et al.* (2009) 'GAGE: Generally applicable gene set enrichment for pathway analysis', *BMC Bioinformatics*, 10, pp. 1–17. doi: 10.1186/1471-2105-10-161.

Luo, Z. *et al.* (2021) 'Compacting a synthetic yeast chromosome arm', *Genome Biology*. Genome Biology, 22(1), pp. 1–18. doi: 10.1186/s13059-020-02232-8.

Ma, P. *et al.* (1999) 'The PDE1-encoded low-affinity phosphodiesterase in the yeast *Saccharomyces cerevisiae* has a specific function in controlling agonist- induced cAMP signaling', *Molecular Biology of the Cell*, 10(1), pp. 91–104. doi: 10.1091/mbc.10.1.91.

Mace, K. *et al.* (2020) 'Multi-kinase control of environmental stress responsive transcription', *PLoS ONE*, 15(3), pp. 1–21. doi: 10.1371/journal.pone.0230246.

MacGilvray, M. E. *et al.* (2020) 'Phosphoproteome Response to Dithiothreitol Reveals Unique Versus Shared Features of *Saccharomyces cerevisiae* Stress Responses', *Journal of Proteome Research*, 19(8), pp. 3405–3417. doi: 10.1021/acs.jproteome.0c00253.

Mai, B. and Breeden, L. (1997) 'Xbp1, a stress-induced transcriptional repressor of the *Saccharomyces cerevisiae* Swi4/Mbp1 family', *Molecular and Cellular Biology*, 17(11), pp. 6491–6501. doi: 10.1128/mcb.17.11.6491.

Mao, Y. and Chen, C. (2019) 'The Hap Complex in Yeasts: Structure, Assembly Mode, and Gene Regulation', *Frontiers in Microbiology*. URL:

https://www.frontiersin.org/articles/10.3389/fmicb.2019.01645.

Mara, P. *et al.* (2018) 'The pleiotropic effects of the glutamate dehydrogenase (GDH) pathway in *Saccharomyces cerevisiae.*', *Microbial cell factories*. England, 17(1), p. 170. doi: 10.1186/s12934-018-1018-4.

Marbà-Ardébol, A. M. *et al.* (2018) 'Sterol synthesis and cell size distribution under oscillatory growth conditions in *Saccharomyces cerevisiae* scale-down cultivations', *Yeast*, 35(2), pp. 213–223. doi: 10.1002/yea.3281.

Marc, J. *et al.* (2013) 'Impact of oleic acid as co-substrate of glucose on "short" and "long-term" Crabtree effect in *Saccharomyces cerevisiae*', *Microbial Cell Factories*, 12(1), pp. 1–11. doi: 10.1186/1475-2859-12-83.

Market Research Future (2021) 'Bioplastics Market: Information by Type'. URL: https://www.marketresearchfuture.com/reports/bioplastic-market-1964 (Accessed: 7 February 2023).

Market Research Future (2022a) 'Biofuels Market Research Report Information By Fuel Type'. URL: https://www.marketresearchfuture.com/reports/bio-fuels-market-2933 (Accessed: 7 February 2023).

Market Research Future (2022b) 'Biopharmaceuticals Market Research Report: By Product Type'. URL: https://www.marketresearchfuture.com/reports/biopharmaceuticals-market-8439 (Accessed: 7 February 2023).

MarketResearch.com (2022) 'Fine Chemicals - Global Market Outlook (2021 - 2028)'. URL: https://www.marketresearch.com/Stratistics-Market-Research-Consulting-v4058/Fine-Chemicals-Global-Outlook-31255768/ (Accessed: 7 February 2023).

Marques, M. P. C., Cabral, J. M. S. and Fernandes, P. (2010) 'Bioprocess scale-up: Quest for the parameters to be used as criterion to move from microreactors to lab-scale', *Journal of Chemical Technology and Biotechnology*, 85(9), pp. 1184–1198. doi: 10.1002/jctb.2387.

Martínez-García, E. *et al.* (2014) '*Pseudomonas* 2.0: genetic upgrading of *P. putida* KT2440 as an enhanced host for heterologous gene expression', *Microbial Cell Factories*, 13(1), p. 159. doi: 10.1186/s12934-014-0159-3.

Martínez-Pastor, M. T. *et al.* (1996) 'The *Saccharomyces cerevisiae* zinc finger proteins Msn2p and Msn4p are required for transcriptional induction through the stress response element (STRE).', *The EMBO Journal*, 15(9), pp. 2227–2235. doi: 10.1002/j.1460-2075.1996.tb00576.x.

Mashego, M. R. *et al.* (2005) 'Changes in the metabolome of *Saccharomyces cerevisiae* associated with evolution in aerobic glucose-limited chemostats', *FEMS Yeast Research*, 5(4–5), pp. 419–430. doi: 10.1016/j.femsyr.2004.11.008.

Mashego, M. R. *et al.* (2006) 'In vivo kinetics with rapid perturbation experiments in *Saccharomyces cerevisiae* using a second-generation BioScope', *Metabolic Engineering*, 8(4), pp. 370–383. doi: 10.1016/j.ymben.2006.02.002.

Mattanovich, D. *et al.* (2004) 'Stress in recombinant protein producing yeasts', *Journal of Biotechnology*, 113(1–3), pp. 121–135. doi: 10.1016/j.jbiotec.2004.04.035.

McNeil, B. and Kristiansen, B. (1990) 'Simulated Scale-up of a Yeast Fermentation Using a Loop Bioreactor', *Biotechnologu Letters*, 12(1), pp. 39–44.

De Melo, H. F. *et al.* (2010) 'Physiological and molecular analysis of the stress response of *Saccharomyces cerevisiae* imposed by strong inorganic acid with implication to industrial fermentations', *Journal of Applied Microbiology*, 109(1), pp. 116–127. doi: 10.1111/j.1365-2672.2009.04633.x.

Mendoza-Vega, O., Hebert, C. and Brown, S. W. (1994) 'Production of recombinant hirudin by high cell density fed-batch cultivations of a *Saccharomyces cerevisiae* strain: physiological considerations during the bioprocess design', *Journal of Biotechnology*, 32(3), pp. 249–259. doi: 10.1016/0168-1656(94)90211-9.

Mengal, P. *et al.* (2018) 'Bio-based Industries Joint Undertaking: The catalyst for sustainable bio-based economic growth in Europe', *New Biotechnology*. Elsevier B.V., 40, pp. 31–39. doi: 10.1016/j.nbt.2017.06.002.

Mettetal, J. T. *et al.* (2008) 'The frequency dependence of osmo-adaptation in *Saccharomyces cerevisiae*', *Science (New York, N.Y.)*. United States, 319(5862), pp. 482–484. doi: 10.1126/science.1151582.

Metzl-Raz, E. *et al.* (2017) 'Principles of cellular resource allocation revealed by condition-dependent proteome profiling', *eLife*, 6, pp. 1–21. doi: 10.7554/eLife.28034.

Michael, D. G. *et al.* (2016) 'Model-based transcriptome engineering promotes a fermentative transcriptional state in yeast', *Proceedings of the National Academy of Sciences of the United States of America*, 113(47), pp. E7428–E7437. doi: 10.1073/pnas.1603577113.

Michalowski, A., Siemann-Herzberg, M. and Takors, R. (2017) '*Escherichia coli* HGT: Engineered for high glucose throughput even under slowly growing or resting conditions', *Metabolic Engineering*. Elsevier Inc., 40(December 2016), pp. 93–103. doi: 10.1016/j.ymben.2017.01.005.

Michel, B. J. and Miller, S. A. (1962) 'Power requirements of gas-liquid agitated systems', *AIChE Journal*, 8(2), pp. 262–266. doi: 10.1002/aic.690080226.

Miller, C. *et al.* (2011) 'Dynamic transcriptome analysis measures rates of mRNA synthesis and decay in yeast', *Molecular Systems Biology*, 7(458). doi: 10.1038/msb.2010.112.

Minden, S. *et al.* (2021) 'Poster: Adaption efforts of eukaryotic host systems experiencing industrial-scale substrate gradients', in *Himmelfahrtstagung on Bioprocess Engineering 2021 - New Bioprocesses, New Bioproducts*. online conference.

Minden, S. *et al.* (2022) 'Monitoring Intracellular Metabolite Dynamics in *Saccharomyces cerevisiae* during Industrially Relevant Famine Stimuli', *metabolites*, 12(263), pp. 1–26. doi: https://doi.org/10.3390/metabo12030263.

Minden, S. *et al.* (2023) 'Performing in spite of starvation: How *Saccharomyces cerevisiae* maintains robust growth when facing famine zones in industrial bioreactors', *Microbial Biotechnology*, 16(1), pp. 148–168. doi: 10.1111/1751-7915.14188.

Mohedano, M. T., Konzock, O. and Chen, Y. (2022) 'Strategies to increase tolerance and robustness of industrial microorganisms', *Synthetic and Systems Biotechnology*. KeAi Communications Co, 7(1), pp. 533–540. doi: 10.1016/j.synbio.2021.12.009.

Molenaar, D. *et al.* (2009) 'Shifts in growth strategies reflect tradeoffs in cellular economics', *Molecular Systems Biology*. Nature Publishing Group, 5(323), pp. 1–10. doi: 10.1038/msb.2009.82.

Monod, J. (1949) 'The growth of bacterial cultures', *Annual review of microbiology*, 3(l), pp. 371–394.

Monteiro, P. T. *et al.* (2020) 'YEASTRACT+: A portal for cross-species comparative genomics of transcription regulation in yeasts', *Nucleic Acids Research*, 48(D1), pp. D642–D649. doi: 10.1093/nar/gkz859.

Moreira Dos Santos, M. *et al.* (2004) 'Manipulation of malic enzyme in *Saccharomyces cerevisiae* for increasing NADPH production capacity aerobically in different cellular compartments', *Metabolic Engineering*, 6(4), pp. 352–363. doi: 10.1016/j.ymben.2004.06.002.

Moutsoglou, M. E. and Dearden, A. C. (2020) 'Effect of the respiro-fermentative balance during yeast propagation on fermentation and wort attenuation', *Journal of the Institute of Brewing*. Wiley Online Library, 126(3), pp. 289–297.

Mukherjee, V. *et al.* (2017) 'Phenotypic landscape of non-conventional yeast species for different stress tolerance traits desirable in bioethanol fermentation', *Biotechnology for Biofuels*, 10(1), p. 216. doi: 10.1186/s13068-017-0899-5.

Müller, D. *et al.* (2003) 'Cyclic AMP mediates the cell cycle dynamics of energy metabolism in *Saccharomyces cerevisiae*', *Yeast*, 20(4), pp. 351–367. doi: 10.1002/yea.967.

Murakami, H. *et al.* (2010) 'Regulation of yeast forkhead transcription factors and FoxM1 by cyclin-dependent and polo-like kinases.', *Cell cycle (Georgetown, Tex.)*. United States, 9(16), pp. 3233–3242. doi: 10.4161/cc.9.16.12599.

Murakami, K. *et al.* (2007) 'Large scale deletions in the *Saccharomyces cerevisiae* genome create strains with altered regulation of carbon metabolism', *Applied Microbiology and Biotechnology*, 75(3), pp. 589–597. doi: 10.1007/s00253-007-0859-2.

Nadal-Rey, G. *et al.* (2021) 'Development of dynamic compartment models for industrial aerobic fed-batch fermentation processes', *Chemical Engineering Journal*. Elsevier B.V., 420(P3), p. 130402. doi: 10.1016/j.cej.2021.130402.

Nadal-Rey, G. *et al.* (2023) 'Modelling of industrial-scale bioreactors using the particle lifeline approach', *Biochemical Engineering Journal*, p. 108989. doi: https://doi.org/10.1016/j.bej.2023.108989.

De Nadal, E., Ammerer, G. and Posas, F. (2011) 'Controlling gene expression in response to stress', *Nature Reviews Genetics*. Nature Publishing Group, 12(12), pp. 833–845. doi: 10.1038/nrg3055.

Navas, M. A. and Gancedo, J. M. (1996) 'The regulatory characteristics of yeast fructose-1,6-bisphosphatase confer only a small selective advantage', *Journal of Bacteriology*, 178(7), pp. 1809–1812. doi: 10.1128/jb.178.7.1809-1812.1996.

Neiman, A. M. (2011) 'Sporulation in the budding yeast *Saccharomyces cerevisiae*', *Genetics*, 189(3), pp. 737–765. doi: 10.1534/genetics.111.127126.

Neubauer, P. *et al.* (1995) 'Response of guanosine tetraphosphate to glucose fluctuations in fed-batch cultivations of *Escherichia coli*', *Journal of Biotechnology*, 43(3), pp. 195–204. doi: https://doi.org/10.1016/0168-1656(95)00130-1.

Neubauer, P. and Junne, S. (2010) 'Scale-down simulators for metabolic analysis of large-scale bioprocesses', *Current Opinion in Biotechnology*. Elsevier Ltd, 21(1), pp. 114–121. doi: 10.1016/j.copbio.2010.02.001.

Nicastro, R. *et al.* (2015) 'SNF1 phosphorylates adenylate cyclase and negatively regulates protein kinase A-dependent transcription in *Saccharomyces cerevisiae*', *Journal of Biological Chemistry*, 290(41), pp. 24715–24726. doi: 10.1074/jbc.M115.658005.

Nielsen, J. (2013) 'Production of biopharmaceutical proteins by yeast: advances through metabolic engineering.', *Bioengineered*. United States, 4(4), pp. 207–211. doi: 10.4161/bioe.22856.

Nielsen, J. (2019) 'Yeast Systems Biology: Model Organism and Cell Factory', *Biotechnology Journal*. John Wiley & Sons, Ltd, 14(9), pp. 1–9. doi: 10.1002/biot.201800421.

Nielsen, J. and Keasling, J. D. (2016) 'Engineering Cellular Metabolism', *Cell*. Elsevier Ltd, 164(6), pp. 1185–1197. doi: 10.1016/j.cell.2016.02.004.

Nienow, A. W. *et al.* (2013) 'Scale-down studies for assessing the impact of different stress parameters on growth and product quality during animal cell culture', *Chemical Engineering Research and Design*, 91(11), pp. 2265–2274. doi: https://doi.org/10.1016/j.cherd.2013.04.002.

Nieß, A. *et al.* (2017) 'Repetitive short-term stimuli imposed in poor mixing zones induce long-term adaptation of *E. coli* cultures in large-scale bioreactors: Experimental evidence and mathematical model', *Frontiers in Microbiology*, 8(JUN), pp. 1–9. doi: 10.3389/fmicb.2017.01195.

Nijkamp, J. F. *et al.* (2012) 'De novo sequencing, assembly and analysis of the genome of the laboratory strain *Saccharomyces cerevisiae* CEN.PK113-7D, a model for modern industrial biotechnology', *Microbial Cell Factories*, 11(March). doi: 10.1186/1475-2859-11-36.

Nilsson, A. and Nielsen, J. (2016) 'Metabolic Trade-offs in Yeast are Caused by F1F0-ATP synthase', *Scientific Reports*. Nature Publishing Group, 6(November 2015), pp. 1–11. doi: 10.1038/srep22264.

Nisamedtinov, I. *et al.* (2008) 'The response of the yeast *Saccharomyces cerevisiae* to sudden vs. gradual changes in environmental stress monitored by expression of the stress response protein Hsp12p', *FEMS Yeast Research*, 8(6), pp. 829–838. doi: 10.1111/j.1567-1364.2008.00391.x.

Nissen, T. L. *et al.* (1997) 'Flux distributions in anaerobic, glucose-limited continuous cultures of *Saccharomyces cerevisiae*', *Microbiology*, 143(1), pp. 203–218. doi: 10.1099/00221287-143-1-203.

Noorman, H. *et al.* (1993) 'Measurement and Computational Fluid Dynamics Simulations of *Saccharomyces cerevisiae* production in a 30 m3 Stirred Tank Reactor', *International Symposium on Bioreactor Performance*, (October 2018), pp. 243–263.

Noorman, H. (2011) 'An industrial perspective on bioreactor scale-down: What we can learn from combined large-scale bioprocess and model fluid studies', *Biotechnology Journal*, 6(8), pp. 934–943. doi: 10.1002/biot.201000406.

Norbeck, J. and Blomberg, A. (2000) 'The level of cAMP-dependent protein kinase A activity strongly affects osmotolerance and osmo-instigated gene expression changes in *Saccharomyces cerevisiae*', *Yeast*, 16(2), pp. 121–137. doi: 10.1002/(SICI)1097-0061(20000130)16:2<121::AID-YEA511>3.0.CO;2-A.

Noubhani, A. *et al.* (2000) 'Reconstitution of ethanolic fermentation in permeabilized spheroplasts of wild-type and trehalose-6-phosphate synthase mutants of the yeast *Saccharomyces cerevisiae*', *European Journal of Biochemistry*, 267(14), pp. 4566–4576. doi: 10.1046/j.1432-1327.2000.01511.x.

Oakhill, J. S., Scott, J. W. and Kemp, B. E. (2012) 'AMPK functions as an adenylate charge-regulated protein kinase', *Trends in Endocrinology and Metabolism*. Elsevier Ltd, 23(3), pp. 125–132. doi: 10.1016/j.tem.2011.12.006.

Ögmundarson, Ó. *et al.* (2020) 'Combining Environmental and Economic Performance for Bioprocess Optimization', *Trends in Biotechnology*. The Authors, 38(11), pp. 1203–1214. doi: 10.1016/j.tibtech.2020.04.011.

Oldiges, M. and Takors, R. (2005) 'Applying Metabolic ProfilingTechniques for Stimulus-Response Experiments: Chances and Pitfalls', in Scheper, T. and Kragl, U. (eds) *Advances in Biochemical Engineering/Biotechnology*. Springer-Verlag Berlin Heidelberg, pp. 173–196. doi: 10.1007/b14094.

Oliveira, A. P. *et al.* (2012) 'Regulation of yeast central metabolism by enzyme phosphorylation', *Molecular Systems Biology*. John Wiley & Sons, Ltd, 8(1), p. 623. doi: https://doi.org/10.1038/msb.2012.55.

Olughu, W. *et al.* (2019) 'Insight into the large-scale upstream fermentation environment using scaled-down models', *Journal of Chemical Technology and Biotechnology*, 94(3), pp. 647–657. doi: 10.1002/jctb.5804.

Oosterhuis, N. M. G. (1984) '*Scale-up of bioreactors - A Scale-down approach*', Delft, Netherlands, TU Delft Universtiy.

Osiro, K. O. *et al.* (2018) 'Assessing the effect of D-xylose on the sugar signaling pathways of *Saccharomyces cerevisiae* in strains engineered for xylose transport and assimilation', *FEMS Yeast Research*, 18(1), pp. 1–15. doi: 10.1093/femsyr/fox096.

Ozcan, S. and Johnston, M. (1999) 'Function and regulation of yeast hexose transporters.', *Microbiology and molecular biology reviews : MMBR*, 63(3), pp. 554–69. URL: http://www.ncbi.nlm.nih.gov/pubmed/10477308%0Ahttp://www.pubmedcentral.nih.gov/articlerender.fcgi?artid=PMC103746.

Paalman, J. W. G. *et al.* (2003) 'Trehalose and glycogen accumulation is related to the duration of the G1 phase of *Saccharomyces cerevisiae*', *FEMS Yeast Research*, 3(3), pp. 261–268. doi: 10.1016/S1567-1356(02)00163-0.

Paczia, N. *et al.* (2012) 'Extensive exometabolome analysis reveals extended overflow metabolism in various microorganisms', *Microbial Cell Factories*, 11, pp. 1–14. doi: 10.1186/1475-2859-11-122.

Pais, T. M. *et al.* (2013) 'Comparative Polygenic Analysis of Maximal Ethanol Accumulation Capacity and Tolerance to High Ethanol Levels of Cell Proliferation in Yeast', *PLoS Genetics*, 9(6). doi: 10.1371/journal.pgen.1003548.

Panadero, J. *et al.* (2006) 'A downshift in temperature activates the high osmolarity glycerol (HOG) pathway, which determines freeze tolerance in *Saccharomyces cerevisiae*.', *The Journal of biological chemistry*. United States, 281(8), pp. 4638–4645. doi: 10.1074/jbc.M512736200.

Papagianni, M. (2015) 'Methodologies for Scale-down of Microbial Bioprocesses', *Journal of Microbial & Biochemical Technology*, s5, pp. 1–7. doi: 10.4172/1948-5948.S5-001.

Papagianni, M., Mattey, M. and Kristiansen, B. (2003) 'Design of a Tubular Loop Bioreactor for Scale-up and Scale-down of Fermentation Processes', *Biotechnology Progress*, 19(5), pp. 1498–1504. doi: 10.1021/bp030002y.

Pardo, B., Crabbé, L. and Pasero, P. (2017) 'Signaling pathways of replication stress in yeast',

FEMS Yeast Research, 17(2), pp. 1–11. doi: 10.1093/femsyr/fow101.

Parenteau, J. *et al.* (2015) 'Preservation of Gene Duplication Increases the Regulatory Spectrum of Ribosomal Protein Genes and Enhances Growth under Stress', *Cell Reports*. Elsevier Ltd, 13(11), pp. 2516–2526. doi: 10.1016/j.celrep.2015.11.033.

Parrou, J. L. and Francois, J. (1997) 'A Simplified Procedure for a Rapid and Reliable Assay of both Glycogen and Trehalose in Whole Yeast Cells', *Analytical Biochemistry*, 248, pp. 186–188. doi: 10.1556/aarch.59.2008.2.28.

Pawson, C. T. and Scott, J. D. (2010) 'Signal integration through blending, bolstering and bifurcating of intracellular information.', *Nature structural & molecular biology*. United States, 17(6), pp. 653–658. doi: 10.1038/nsmb.1843.

Peebo, K. and Neubauer, P. (2018) 'Application of continuous culture methods to recombinant protein production in microorganisms', *Microorganisms*, 6(3), pp. 1–12. doi: 10.3390/microorganisms6030056.

Pelechano, V., Chávez, S. and Pérez-Ortín, J. E. (2012) 'A Complete Set of Nascent Transcription Rates for Yeast Genes', *PloS one*, 7(4), pp. 1–10. doi: 10.1371/journal.pone.0015442.

Pepper, M. E. (2015) 'Designing a Minimal-Knowledge Controller to Achieve Maximum Stable Growth for an *Escherichia coli* Bioprocess', *ProQuest Dissertations Publishing*.

Perez-Samper, G. *et al.* (2018) 'The Crabtree Effect Shapes the *Saccharomyces cerevisiae* Lag Phase during the Switch between Different Carbon Sources', *mBio*. American Society for Microbiology, 9(5), pp. 10.1128/mbio.01331-18. doi: 10.1128/mbio.01331-18.

Petrenko, N. *et al.* (2013) 'Noise and interlocking signaling pathways promote distinct transcription factor dynamics in response to different stresses', *Molecular Biology of the Cell*, 24(12), pp. 2045–2057. doi: 10.1091/mbc.E12-12-0870.

Pham, T. H. *et al.* (2008) 'Gaseous environments modify physiology in the brewing yeast *Saccharomyces cerevisiae* during batch alcoholic fermentation', *Journal of Applied Microbiology*, 105(3), pp. 858–874. doi: 10.1111/j.1365-2672.2008.03821.x.

Pigou, M. and Morchain, J. (2015) 'Investigating the interactions between physical and biological heterogeneities in bioreactors using compartment, population balance and metabolic models', *Chemical Engineering Science*. Elsevier, 126(April), pp. 267–282. doi: 10.1016/j.ces.2014.11.035.

Pinheiro, T. *et al.* (2020) 'Differential proteomic analysis by SWATH-MS unravels the most dominant mechanisms underlying yeast adaptation to non-optimal temperatures under anaerobic conditions', *Scientific Reports*. Nature Publishing Group UK, 10(1), pp. 1–17. doi: 10.1038/s41598-020-77846-w.

Pinson, B. *et al.* (2019) 'Dual control of NAD^+ synthesis by purine metabolites in yeast', *eLife*, 8, pp. 1–23. doi: 10.7554/eLife.43808.

Piškur, J. and Compagno, C. (2014) 'Molecular mechanisms in yeast carbon metabolism', *Molecular Mechanisms in Yeast Carbon Metabolism*, pp. 1–326. doi: 10.1007/978-3-642-55013-3.

Plank, M. (2022) 'Interaction of TOR and PKA Signaling in *S. cerevisiae*', *Biomolecules*, 12(2). doi: 10.3390/biom12020210.

Pollard, D. J. *et al.* (2007) 'Scale Up of a Viscous Fungal Fermentation: Application of Scale-Up Criteria With Regime Analysis and Operating Boundary Conditions', *Biotechnology and Bioengineering*, 96(4), pp. 307–317. doi: 10.1002/bit.21112.

Polymenis, M. and Aramayo, R. (2015) 'Translate to divide: control of the cell cycle by protein synthesis', *Microbial Cell*, 2(4), pp. 94–104. doi: 10.15698/mic2015.04.198.

Pothoulakis, G. and Ellis, T. (2018) 'Synthetic gene regulation for independent external induction of the *Saccharomyces cerevisiae* pseudohyphal growth phenotype', *Communications Biology*, 1(1), p. 7. doi: 10.1038/s42003-017-0008-0.

Precedence Research (2022) 'Biochemical Market'. URL: https://www.precedenceresearch.com/biochemical-market (Accessed: 7 February 2023).

Pronk, J. T., Steensma, H. Y. and Van Dijken, J. P. (1996) 'Pyruvate metabolism in *Saccharomyces cerevisiae*', *Yeast*, 12(16), pp. 1607–1633. doi: 10.1002/(SICI)1097-0061(199612)12:16<1607::AID-YEA70>3.0.CO;2-4.

Puiman, L. *et al.* (2023) 'Downscaling Industrial-Scale Syngas Fermentation to Simulate Frequent and Irregular Dissolved Gas Concentration Shocks', *Bioengineering*. doi: 10.3390/bioengineering10050518.

R Core Team (2021) 'R: A language and environment for statistical computing', *R Foundation for Statistical Computing*. URL: https://www.r-project.org/.

Ramachandran, V., Shah, K. H. and Herman, P. K. (2011) 'The cAMP-Dependent Protein Kinase Signaling Pathway Is a Key Regulator of P Body Foci Formation', *Molecular Cell*. Elsevier Inc., 43(6), pp. 973–981. doi: 10.1016/j.molcel.2011.06.032.

Ramirez-Gaona, M. *et al.* (2017) 'YMDB 2.0: a significantly expanded version of the yeast metabolome database', *Nucleic Acids Research*, 45(D1), pp. D440–D445. doi: 10.1093/nar/gkw1058.

Ratnakumar, S. *et al.* (2009) 'SNF1 controls the activity of Adr1 through dephosphorylation of Ser230', *Genetics*, 182(3), pp. 735–745. doi: 10.1534/genetics.109.103432.

Reeves, G. T. (2019) 'The engineering principles of combining a transcriptional incoherent feedforward loop with negative feedback', *Journal of Biological Engineering*. Journal of Biological Engineering, 13(1), pp. 1–11. doi: 10.1186/s13036-019-0190-3.

Regenberg, B. *et al.* (2006) 'Growth-rate regulated genes have profound impact on interpretation of transcriptome profiling in *Saccharomyces cerevisiae*', *Genome Biology*, 7(11). doi: 10.1186/gb-2006-7-11-r107.

Reifenberger, E., Boles, E. and Ciriacy, M. (1997) 'Kinetic Characterization of Individual Hexose Transporters of *Saccharomyces cerevisiae* and their Relation to the Triggering Mechanisms of Glucose Repression', *European Journal of Biochemistry*. Wiley Online Library, 245(2), pp. 324–333. doi: 10.1111/j.1432-1033.1997.00324.x.

Reinders, A. *et al.* (1998) '*Saccharomyces cerevisiae* cAMP-dependent protein kinase controls entry into stationary phase through the Rim15p protein kinase', *Genes and Development*, 12(18), pp. 2943–2955. doi: 10.1101/gad.12.18.2943.

Remigi, P. *et al.* (2019) 'Ribosome Provisioning Activates a Bistable Switch Coupled to Fast Exit from Stationary Phase', *Molecular Biology and Evolution*, 36(5), pp. 1056–1070. doi: 10.1093/molbev/msz041.

Ribeiro, R. A., Bourbon-Melo, N. and Sá-Correia, I. (2022) 'The cell wall and the response

and tolerance to stresses of biotechnological relevance in yeasts', *Frontiers in Microbiology*, 13(July), pp. 1–25. doi: 10.3389/fmicb.2022.953479.

Riesenberg, D. and Guthke, R. (1999) 'High-cell-density cultivation of microorganisms', *Applied Microbiology and Biotechnology*, 51(4), pp. 422–430. doi: 10.1007/s002530051412.

Ritchie, M. E. *et al.* (2015) 'Limma powers differential expression analyses for RNA-sequencing and microarray studies', *Nucleic Acids Research*, 43(7), p. e47. doi: 10.1093/nar/gkv007.

Rizzi, M. *et al.* (1997) 'In vivo analysis of metabolic dynamics in *Saccharomyces cerevisiae*: II. Mathematical model', *Biotechnology and Bioengineering*, 55(4), pp. 592–608. doi: 10.1002/(SICI)1097-0290(19970820)55:4<592::AID-BIT2>3.0.CO;2-C.

Rodrigues, F., Ludovicio, P. and Leao, C. (2006) 'Sugar Metabolism in Yeasts : an Overview of Aerobic and Anaerobic Glucose Catabolism', *Biodiversity and Ecophysiology of Yeasts*, pp. 101–122.

Roubos, J. A. *et al.* (2001) 'A quantitative approach to characterizing cell lysis caused by mechanical agitation of *Streptomyces clavuligerus*', *Biotechnology Progress*, 17(2), pp. 336–347. doi: 10.1021/bp0001617.

RTSF - Michigan State University (no date) 'FastQC Tutorial & FAQ', Tech Note. URL: https://www.bioinformatics.babraham.ac.uk/projects/fastqc/.

Ruderfer, D. M. *et al.* (2006) 'Population genomic analysis of outcrossing and recombination in yeast', *Nature Genetics*, 38(9), pp. 1077–1081. doi: 10.1038/ng1859.

Saini, P. *et al.* (2018) 'Response and tolerance of yeast to changing environmental stress during ethanol fermentation', *Process Biochemistry*. Elsevier, 72(March), pp. 1–12. doi: 10.1016/j.procbio.2018.07.001.

Saliola, M. *et al.* (2012) 'Intracellular NADPH levels affect the oligomeric state of the glucose 6-phosphate dehydrogenase', *Eukaryotic Cell*, 11(12), pp. 1503–1511. doi: 10.1128/EC.00211-12.

Samakkarn, W., Ratanakhanokchai, K. and Soontorngun, N. (2021) 'Reprogramming of the ethanol stress response in *Saccharomyces cerevisiae* by the transcription factor znf1 and its effect on the biosynthesis of glycerol and ethanol', *Applied and Environmental Microbiology*, 87(16), pp. 1–26. doi: 10.1128/AEM.00588-21.

Santangelo, G. M. (2006) 'Glucose Signaling in *Saccharomyces cerevisiae*', 70(1), pp. 253–282. doi: 10.1128/MMBR.70.1.253.

Sanz, P., Viana, R. and Garcia-Gimeno, M. A. (2016) 'AMPK in Yeast: The SNF1 (Sucrose Non-fermenting 1) Protein Kinase Complex BT - AMP-activated Protein Kinase', in Cordero, M. D. and Viollet, B. (eds). Cham: Springer International Publishing, pp. 353–374. doi: 10.1007/978-3-319-43589-3_14.

Sarkizi Shams Hajian, C. *et al.* (2020) 'Predicting By-Product Gradients of Baker's Yeast Production at Industrial Scale: A Practical Simulation Approach', *processes*, 8(1554), p. 19. doi: 10.3390/pr8121554.

Sasano, Y. *et al.* (2017) 'Molecular breeding of *Saccharomyces cerevisiae* with high RNA content by harnessing essential ribosomal RNA transcription regulator', *AMB Express*. Springer Berlin Heidelberg, 7(1). doi: 10.1186/s13568-017-0330-4.

Sassi, H. *et al.* (2019) 'Segregostat: a novel concept to control phenotypic diversification dynamics on the example of Gram-negative bacteria', *Microbial biotechnology*. Wiley Online Library, 12(5), pp. 1064–1075.

Sazegari, S. *et al.* (2022) 'Mining transcriptomic data to identify *Saccharomyces cerevisiae* signatures related to improved and repressed ethanol production under fermentation', *PLoS ONE*, 17(7 July), pp. 1–18. doi: 10.1371/journal.pone.0259476.

Schavemaker, P. E. and Lynch, M. (2022) 'Flagellar energy costs across the tree of life', *eLife*. Edited by A. Michelot, A. M. Walczak, and E. Loiseau. eLife Sciences Publications, Ltd, 11, p. e77266. doi: 10.7554/eLife.77266.

Schawalder, S. B. *et al.* (2004) 'Growth-regulated recruitment of the essential yeast ribosomal protein gene activator Ifh1', *Nature*, 432(7020), pp. 1058–1061. doi: 10.1038/nature03200.

Schilling, B. M. *et al.* (1999) 'A special reactor design for investigations of mixing time effects in a scaled-down industrial L-lysine fed-batch fermentation process', *Biotechnology and Bioengineering*, 64(5), pp. 599–606. doi: 10.1002/(SICI)1097-0290(19990905)64:5<599::AID-BIT10>3.0.CO;2-C.

Schmidt, F. R. (2005) 'Optimization and scale up of industrial fermentation processes', *Applied Microbiology and Biotechnology*, 68(4), pp. 425–435. doi: 10.1007/s00253-005-0003-0.

Schmoller, K. M. *et al.* (2015) 'Dilution of the cell cycle inhibitor Whi5 controls budding-yeast cell size', *Nature*, 526(7572), pp. 268–272. doi: 10.1038/nature14908.

Schneper, L., Düvel, K. and Broach, J. R. (2004) 'Sense and sensibility: Nutritional response and signal integration in yeast', *Current Opinion in Microbiology*, 7(6), pp. 624–630. doi: 10.1016/j.mib.2004.10.002.

Schügerl, K. (1993) 'Comparison of different bioreactor performances', *Bioprocess Engineering*, 9(5), pp. 215–223. doi: 10.1007/BF00369405.

Sharifian, H. *et al.* (2015) 'Parallel feedback loops control the basal activity of the HOG MAPK signaling cascade', *Integrative Biology (United Kingdom)*. Royal Society of Chemistry, 7(4), pp. 412–422. doi: 10.1039/c4ib00299g.

Shashkova, S., Welkenhuysen, N. and Hohmann, S. (2015) 'Molecular communication: Crosstalk between the SNF1 and other signaling pathways', *FEMS Yeast Research*, 15(4), pp. 1–10. doi: 10.1093/femsyr/fov026.

Shenhar, G. and Kassir, Y. (2001) 'A positive regulator of mitosis, Sok2, functions as a negative regulator of meiosis in *Saccharomyces cerevisiae*.', *Molecular and cellular biology*. United States, 21(5), pp. 1603–1612. doi: 10.1128/MCB.21.5.1603-1612.2001.

Sheu, Y.-J. *et al.* (2021) 'Prevalent and Dynamic Binding of the Cell Cycle Checkpoint Kinase Rad53 to Gene Promoters', *bioRxiv*, p. 2021.05.23.445333. URL: https://www.biorxiv.org/content/10.1101/2021.05.23.445333v2%0Ahttps://www.biorxiv.org/content/10.1101/2021.05.23.445333v2.abstract.

Shore, D., Zencir, S. and Albert, B. (2021) 'Transcriptional control of ribosome biogenesis in yeast: Links to growth and stress signals', *Biochemical Society Transactions*, 49(4), pp. 1589–1599. doi: 10.1042/BST20201136.

Siebler, F., Lapin, A. and Takors, R. (2020) 'Synergistically applying 1-D modeling and CFD for designing industrial scale bubble column syngas bioreactors', *Engineering in Life

Sciences, 20(7), pp. 239–251. doi: https://doi.org/10.1002/elsc.201900132.

Silljé, H. H. W. *et al.* (1999) 'Function of trehalose and glycogen in cell cycle progression and cell viability in *Saccharomyces cerevisiae*', *Journal of Bacteriology*, 181(2), pp. 396–400. doi: 10.1128/jb.181.2.396-400.1999.

da Silva Fernandes, F. *et al.* (2022) 'Current Ethanol Production Requirements for the Yeast *Saccharomyces cerevisiae.*', *International journal of microbiology*. Egypt, 2022, p. 7878830. doi: 10.1155/2022/7878830.

Simen, J. D. *et al.* (2017) 'Transcriptional response of *Escherichia coli* to ammonia and glucose fluctuations', *Microbial Biotechnology*, 10(4), pp. 858–872. doi: 10.1111/1751-7915.12713.

Singh, A., Christensen, T. and Panoutsou, C. (2021) 'Policy review for biomass value chains in the European bioeconomy', *Global Transitions*. Elsevier Ltd, 3, pp. 13–42. doi: 10.1016/j.glt.2020.11.003.

Skoneczny, M (2018) 'Stress Response Mechanisms in Fungi', Edited by Marek Skoneczny. Springer Nature Switzerland. doi: 10.1007/978-3-030-00683-9.

Smets, B. *et al.* (2010) 'Life in the midst of scarcity: Adaptations to nutrient availability in *Saccharomyces cerevisiae*', *Current Genetics*. doi: 10.1007/s00294-009-0287-1.

Soares, E. V (2011) 'Flocculation in *Saccharomyces cerevisiae*: a review', *Journal of Applied Microbiology*, 110(1), pp. 1–18. doi: 10.1111/j.1365-2672.2010.04897.x.

Soetaert, K., Petzoldt, T. and Setzer, R. W. (2010) 'Solving differential equations in R: Package deSolve', *Journal of Statistical Software*, 33(9), pp. 1–25. doi: 10.18637/jss.v033.i09.

Somsen, O. J. G. *et al.* (2000) 'Glucose and the ATP paradox in yeast', *Biochemical Journal*, 352(2), pp. 593–599. doi: 10.1042/0264-6021:3520593.

Spann, R. *et al.* (2019) 'CFD predicted pH gradients in lactic acid bacteria cultivations', *Biotechnology and Bioengineering*, 116(4), pp. 769–780. doi: 10.1002/bit.26868.

Stasyk, O. G. and Stasyk, O. V. (2019) 'Glucose Sensing and Regulation in Yeasts, Non-conventional Yeasts: from Basic Research to Application'. doi: 10.1007/978-3-030-21110-3_14.

Statista (2022) 'Market size value of plastics worldwide from 2021 to 2030'. URL: https://www.statista.com/statistics/1060583/global-market-value-of-plastic/ (Accessed: 7 February 2023).

Statista (2023) 'Health Market Insights - Pharmaceuticals'. URL: https://www.statista.com/outlook/hmo/pharmaceuticals/worldwide (Accessed: 7 February 2023).

Steensels, J. *et al.* (2014) 'Improving industrial yeast strains: Exploiting natural and artificial diversity', *FEMS Microbiology Reviews*, 38(5), pp. 947–995. doi: 10.1111/1574-6976.12073.

Stephanopoulos, G., Aristidou, A. A. and Nielsen, J. (1998) 'Metabolic engineering: principles and methodologies', *Academic Press*, Elsevier. ISBN: 978-0126662603

Stewart-Ornstein, J. *et al.* (2017) 'Model-guided optogenetic study of PKA signaling in budding yeast', *Molecular Biology of the Cell*, 28(1), pp. 221–227. doi: 10.1091/mbc.E16-06-0354.

Storchova, Z. (2014) 'Ploidy changes and genome stability in yeast', *Yeast*. Wiley Online Library, 31(11), pp. 421–430.

Straathof, A. J. J. *et al.* (2019) 'Grand Research Challenges for Sustainable Industrial Biotechnology', *Trends in Biotechnology*, 37(10), pp. 1042–1050. doi: 10.1016/j.tibtech.2019.04.002.

Suarez-Mendez, C. A. *et al.* (2014) 'Feast "Feast/Famine" Cycles for Studying Microbial Physiology Under Dynamic Conditions: A Case Study with *Saccharomyces cerevisiae*', *Metabolites*, 4(2), pp. 347–372. doi: 10.3390/metabo4020347.

Suarez-Mendez, C. A. (2015) 'Dynamics of Storage Carbohydrates Metabolism in Saccharomyces cerevisiae: A Quantitative Approach'. Delft, The Netherlands, TU Delft University.

Suarez-Mendez, C. A. *et al.* (2016) 'Interaction of storage carbohydrates and other cyclic fluxes with central metabolism: A quantitative approach by non-stationary 13C metabolic flux analysis', *Metabolic Engineering Communications*. Elsevier, 3(65), pp. 52–63. doi: 10.1016/j.meteno.2016.01.001.

Suarez-Mendez, C. A., Ras, C. and Wahl, S. A. (2017) 'Metabolic adjustment upon repetitive substrate perturbations using dynamic13C-tracing in yeast', *Microbial Cell Factories*. BioMed Central, 16(1), pp. 1–14. doi: 10.1186/s12934-017-0778-6.

Suhm, T. *et al.* (2018) 'Mitochondrial Translation Efficiency Controls Cytoplasmic Protein Homeostasis', *Cell Metabolism*, 27(6), pp. 1309-1322.e6. doi: 10.1016/j.cmet.2018.04.011.

Sung, B. H. *et al.* (2016) 'Construction of a minimal genome as a chassis for synthetic biology', *Essays in Biochemistry*. Edited by V. B. Pinheiro, 60(4), pp. 337–346. doi: 10.1042/EBC20160024.

Sung, M. K. *et al.* (2016) 'Ribosomal proteins produced in excess are degraded by the ubiquitin-proteasome system', *Molecular Biology of the Cell*, 27(17), pp. 2642–2652. doi: 10.1091/mbc.E16-05-0290.

Sutterlin, C. *et al.* (1997) 'Specific requirements for the ER to Golgi transport of GPI-anchored proteins in yeast', *Journal of Cell Science*, 110(21), pp. 2703–2714. doi: 10.1242/jcs.110.21.2703.

Sweere, A. P. J. *et al.* (1988) 'Experimental simulation of oxygen profiles and their influence on baker's yeast production: I. One-fermentor system', *Biotechnology and Bioengineering*, 31(6), pp. 567–578. doi: 10.1002/bit.260310609.

Taghavi, M. (2010) 'Power Consumption and Flow Regime Transition in a Stirred Tank Reactor', pp. 25–28.

Tai, S. L. *et al.* (2005) 'Two-dimensional transcriptome analysis in chemostat cultures: Combinatorial effects of oxygen availability and macronutrient limitation in *Saccharomyces cerevisiae*', *Journal of Biological Chemistry*, 280(1), pp. 437–447. doi: 10.1074/jbc.M410573200.

Tai, S. L. (2007) 'Physiological impact and context dependency of transcriptional responses: A chemostat study in *Saccharomyces cerevisiae*',Delft, The Netherlands, TU Delft Universtiy.

Takors, R. (2012) 'Scale-up of microbial processes: Impacts, tools and open questions', *Journal of Biotechnology*. Elsevier B.V., 160(1–2), pp. 3–9. doi:

10.1016/j.jbiotec.2011.12.010.

Takors, R. (2016) 'Editorial: How can we ensure the successful transfer from lab- to large-scale production?', *Engineering in Life Sciences*, 16(7), p. 587. doi: 10.1002/elsc.201670073.

Tang, W. *et al.* (2017) 'A 9-pool metabolic structured kinetic model describing days to seconds dynamics of growth and product formation by *Penicillium chrysogenum*', *Biotechnology and Bioengineering*, 114(8), pp. 1733–1743. doi: 10.1002/bit.26294.

Täuber, S. *et al.* (2020) 'dMSCC : A microfluidic platform for microbial single-cell cultivation under dynamic environmental medium conditions', bioRxiv (2020): 2020-07

Teixeira, M. C. *et al.* (2018) 'YEASTRACT: An upgraded database for the analysis of transcription regulatory networks in *Saccharomyces cerevisiae*', *Nucleic Acids Research*, 46(D1), pp. D348–D353. doi: 10.1093/nar/gkx842.

Teusink, B. *et al.* (1998) 'Intracellular glucose concentration in derepressed yeast cells consuming glucose is high enough to reduce the glucose transport rate by 50%', *Journal of Bacteriology*, 180(3), pp. 556–562. doi: 10.1128/jb.180.3.556-562.1998.

Teusink, B. *et al.* (2000) 'Can yeast glycolysis be understood terms of vitro kinetics of the constituent enzymes? Testing biochemistry', *European Journal of Biochemistry*, 267(17), pp. 5313–5329. doi: 10.1046/j.1432-1327.2000.01527.x.

Theobald, U. M. (1995) 'Untersuchungen zur Dynamik des Crabtree-Effektes', Reihe 17, Düsseldorf, Germany, Fortschrittberichte / VDI.

Theobald, U. M. *et al.* (1997) 'In vivo analysis of metabolic dynamics in *Saccharomyces cerevisiae*: I. Experimental observations', *Biotechnol Bioeng*, 55, pp. 305–316.

Thevelein, J. M. (1984) 'Regulation of Trehalose Mobilization in Fungi', *MICROBIOLOGICAL REVIEWS*, 48(1), pp. 42–59. doi: 0146-0749/84/010042-18$02.00/0.

Tikhonova, I. G. and Costanzi, S. (2009) 'Unraveling the structure and function of G protein-coupled receptors through NMR spectroscopy.', *Current pharmaceutical design*. United Arab Emirates, 15(35), pp. 4003–4016. doi: 10.2174/138161209789824803.

Tomás-Pejó, E. *et al.* (2010) 'Adaptation of the xylose fermenting yeast *Saccharomyces cerevisiae* F12 for improving ethanol production in different fed-batch SSF processes', *Journal of Industrial Microbiology and Biotechnology*, 37(11), pp. 1211–1220. doi: 10.1007/s10295-010-0768-8.

Torello Pianale, L., Rugbjerg, P. and Olsson, L. (2022) 'Real-Time Monitoring of the Yeast Intracellular State During Bioprocesses With a Toolbox of Biosensors', *Frontiers in Microbiology*, 12(January). doi: 10.3389/fmicb.2021.802169.

Tripodi, F. *et al.* (2015) 'Post-translational modifications on yeast carbon metabolism: Regulatory mechanisms beyond transcriptional control', *Biochimica et Biophysica Acta - General Subjects*. Elsevier B.V., 1850(4), pp. 620–627. doi: 10.1016/j.bbagen.2014.12.010.

Tsuchiya, D., Yang, Y. and Lacefield, S. (2014) 'Positive Feedback of NDT80 Expression Ensures Irreversible Meiotic Commitment in Budding Yeast', *PLOS Genetics*. Public Library of Science, 10(6), p. e1004398. URL: https://doi.org/10.1371/journal.pgen.1004398.

Uhl, V. W. and Von Essen, J. A. (1986) 'Scale-Up of Equipment for Agitating Liquids', *Mixing*, Academic Press, Inc. doi: 10.1016/b978-0-12-706603-5.50007-6.

Vasilakou, E., Van Loosdrecht, M. C. M. and Wahl, S. A. (2020) '*Escherichia coli* metabolism under short-term repetitive substrate dynamics: Adaptation and trade-offs', *Microbial Cell Factories*. BioMed Central, 19(1), pp. 1–19. doi: 10.1186/s12934-020-01379-0.

Vega, M. *et al.* (2016) 'Hexokinase 2 Is an Intracellular Glucose Sensor of Yeast Cells That Maintains the Structure and Activity of Mig1 Protein Repressor Complex.', *The Journal of biological chemistry*. United States, 291(14), pp. 7267–7285. doi: 10.1074/jbc.M115.711408.

Velazquez, D. *et al.* (2022) 'Glucose transport engineering allows mimicking fed-batch performance in batch mode and selection of superior producer strains', *Microbial Cell Factories*, 21(1). doi: 10.1186/s12934-022-01906-1.

Vemuri, G. N. *et al.* (2007) 'Increasing NADH oxidation reduces overflow metabolism in *Saccharomyces cerevisiae*'.

Venturini Copetti, M. (2019) 'Yeasts and molds in fermented food production: an ancient bioprocess', *Current Opinion in Food Science*. Elsevier Ltd, 25, pp. 57–61. doi: 10.1016/j.cofs.2019.02.014.

Verduyn, C. *et al.* (1991) 'A theoretical evaluation of growth yields of yeasts', *Antonie van Leeuwenhoek*, 59(1), pp. 49–63. doi: 10.1007/BF00582119.

Verduyn, C. (1991) 'Physiology of yeasts in relation to biomass yields', *Antonie van Leeuwenhoek*, 60(3–4), pp. 325–353. doi: 10.1007/BF00430373.

Verduyn, C. *et al.* (1992) 'Effect of Benzoic Acid on Metabolic Fluxes in Yeasts':, *Yeast*, 8(1992), pp. 501–517. doi: 10.1007/BF00270792.

Verhagen, K. J. A. *et al.* (2022) 'Predicting Metabolic Adaptation Under Dynamic Substrate Conditions Using a Resource-Dependent Kinetic Model : A Case Study Using *Saccharomyces cerevisiae*', 9(May), pp. 1–12. doi: 10.3389/fmolb.2022.863470.

Verma, M. *et al.* (2013) '"Domino" systems biology and the "A" of ATP', *Biochimica et Biophysica Acta - Bioenergetics*. Elsevier B.V., 1827(1), pp. 19–29. doi: 10.1016/j.bbabio.2012.09.014.

Vermeersch, L. *et al.* (2022) 'Do microbes have a memory? History-dependent behavior in the adaptation to variable environments', *Frontiers in Microbiology*, 13(October), pp. 1–11. doi: 10.3389/fmicb.2022.1004488.

de Virgilio, C. (2012) 'The essence of yeast quiescence', *FEMS Microbiology Reviews*, 36(2), pp. 306–339. doi: 10.1111/j.1574-6976.2011.00287.x.

Visser, D. *et al.* (2002) 'Rapid sampling for analysis of in vivo kinetics using the BioScope: A system for continuous-pulse experiments', *Biotechnology and Bioengineering*, 79(6), pp. 674–681. doi: 10.1002/bit.10328.

Visser, D. *et al.* (2004) 'Analysis of in vivo kinetics of glycolysis in aerobic *Saccharomyces cerevisiae* by application of glucose and ethanol pulses', *Biotechnology and Bioengineering*, 88(2), pp. 157–167. doi: 10.1002/bit.20235.

Vos, T. *et al.* (2016) 'Maintenance-energy requirements and robustness of *Saccharomyces cerevisiae* at aerobic near-zero specific growth rates', *Microbial Cell Factories*. BioMed

Central, 15(1), pp. 1–20. doi: 10.1186/s12934-016-0501-z.

Votruba, J. and Sobotka, M. (1992) 'Physiological similarity and bioreactor scale-up', *Folia Microbiologica: Official Journal of the Institute of Microbiology, Academy of Sciences of the Czech Republic*, 37(5), pp. 331–345. doi: 10.1007/BF02815659.

Vrábel, P. *et al.* (2000) 'Mixing in large-scale vessels stirred with multiple radial or radial and axial up-pumping impellers: Modelling and measurements', *Chemical Engineering Science*, 55(23), pp. 5881–5896. doi: 10.1016/S0009-2509(00)00175-5.

Vrabl, P. *et al.* (2019) 'Fungal Growth in Batch Culture – What We Could Benefit If We Start Looking Closer', *Frontiers in Microbiology*, 10(October), pp. 1–11. doi: 10.3389/fmicb.2019.02391.

de Vries, A. G. R., Pronk, J. T. and Daran, J. M. (2017) 'Industrial Relevance of Chromosomal Copy Number Variation in Saccharomyces Yeasts', *Applied and Environmental Microbiology*. American Society for Microbiology, 83(11), pp. e03206-16. doi: 10.1128/AEM.03206-16.

Wagner, E. R. and Gasch, A. P. (2023) 'Advances in *S*. *cerevisiae* Engineering for Xylose Fermentation and Biofuel Production : Balancing Growth , Metabolism , and Defense'.

Wakamatsu, A. *et al.* (2005) 'A severe peak tailing of phosphate compounds caused by interaction with stainless steel used for liquid chromatography and electrospray mass spectrometry', *Journal of Separation Science*, 28(14), pp. 1823–1830. doi: 10.1002/jssc.200400027.

Walker, G. M. and White, N. A. (2005) 'Introduction to Fungal Physiology, Fungi: Biology and Applications'. doi: 10.1002/0470015330.ch1.

Walther, T. *et al.* (2010) 'Control of ATP homeostasis during the respiro-fermentative transition in yeast', *Molecular Systems Biology*, 6(344). doi: 10.1038/msb.2009.100.

Wang, G., Zhao, J., *et al.* (2018) 'Comparative performance of different scale-down simulators of substrate gradients in *Penicillium chrysogenum* cultures: the need of a biological systems response analysis', *Microbial Biotechnology*, 11(3), pp. 486–497. doi: 10.1111/1751-7915.13046.

Wang, G., Wu, B., *et al.* (2018) 'Power input effects on degeneration in prolonged penicillin chemostat cultures: A systems analysis at flux, residual glucose, metabolite, and transcript levels', *Biotechnology and Bioengineering*, 115(1), pp. 114–125. doi: 10.1002/bit.26447.

Wang, G., Haringa, C., Tang, W., *et al.* (2020) 'Coupled metabolic-hydrodynamic modeling enabling rational scale-up of industrial bioprocesses', *Biotechnology and Bioengineering*. John Wiley & Sons, Ltd, 117(3), pp. 844–867. doi: 10.1002/bit.27243.

Wang, G., Haringa, C., Noorman, H., *et al.* (2020) 'Developing a Computational Framework To Advance Bioprocess Scale-Up', *Trends in Biotechnology*. Elsevier Ltd, 38(8), pp. 846–856. doi: 10.1016/j.tibtech.2020.01.009.

Wang, M., Zhao, Y. and Zhang, B. (2015) 'Efficient Test and Visualization of Multi-Set Intersections', *Scientific Reports*. Nature Publishing Group, 5, pp. 1–12. doi: 10.1038/srep16923.

Wang, S. *et al.* (2019) 'Dynamic response of *Aspergillus niger* to single pulses of glucose with high and low concentrations', *Bioresources and Bioprocessing*. Springer Singapore, 6(1). doi: 10.1186/s40643-019-0251-y.

Wang, Y., Lo, W. C. and Chou, C. S. (2017) 'A modeling study of budding yeast colony formation and its relationship to budding pattern and aging', *PLoS Computational Biology*, 13(11), pp. 1–23. doi: 10.1371/journal.pcbi.1005843.

Warner, J. R. (1999) 'The economics of ribosome biosynthesis in yeast', *Trends in biochemical sciences*, 4(November), pp. 437–440.

Watanabe, D. *et al.* (2017) 'Promoter engineering of the *Saccharomyces cerevisiae* RIM15 gene for improvement of alcoholic fermentation rates under stress conditions', *Journal of Bioscience and Bioengineering*. Elsevier Ltd, 123(2), pp. 183–189. doi: 10.1016/j.jbiosc.2016.08.004.

Weber, C. A. *et al.* (2020) 'β-Oxidation and autophagy are critical energy providers during acute glucose depletion in *Saccharomyces cerevisiae*', *Proceedings of the National Academy of Sciences of the United States of America*, 117(22). doi: 10.1073/pnas.1913370117.

Wehrs, M. *et al.* (2019) 'Engineering Robust Production Microbes for Large-Scale Cultivation', *Trends in Microbiology*. Elsevier Ltd, 27(6), pp. 524–537. doi: 10.1016/j.tim.2019.01.006.

Wei, P. *et al.* (2023) 'Metabolic-fluid dynamics model construction and scale-down design for an industrial penicillin chrysogenum fermentation with combined dissolved oxygen and glucose concentration dynamics', *Chemical Engineering Science*. The Author(s), p. 118770. doi: 10.1016/j.ces.2023.118770.

Weibel, K. E., Mor, J. R. and Fiechter, A. (1974) 'Rapid sampling of yeast cells and automated assays of adenylate, citrate, pyruvate and glucose-6-phosphate pools', *Analytical Biochemistry*, 58(1), pp. 208–216. doi: 10.1016/0003-2697(74)90459-X.

Weiner, A. *et al.* (2012) 'Systematic dissection of roles for chromatin regulators in a yeast stress response', *PLoS Biology*, 10(7), p. 17. doi: 10.1371/journal.pbio.1001369.

Westerhoff, H. V., Hellingwerf, K. J. and Van Dam, K. (1983) 'Thermodynamic efficiency of microbial growth is low but optimal for maximal growth rate.', *Proceedings of the National Academy of Sciences of the United States of America*, 80(1), pp. 305–309. doi: 10.1073/pnas.80.1.305.

Weusthuis, R. A. *et al.* (1994) 'Effects of oxygen limitation on sugar metabolism in yeasts: A continuous-culture study of the Kluyver effect', *Microbiology*, 140(4), pp. 703–715. doi: 10.1099/00221287-140-4-703.

De Wever, V. *et al.* (2005) 'A dual role for PP1 in shaping the Msn2-dependent transcriptional response to glucose starvation', *EMBO Journal*, 24(23), pp. 4115–4123. doi: 10.1038/sj.emboj.7600871.

Wijaya, A. W. *et al.* (2021) 'Compartment-specific metabolome labeling enables the identification of subcellular fluxes that may serve as promising metabolic engineering targets in CHO cells', *Bioprocess and Biosystems Engineering*. Springer Berlin Heidelberg, 44(12), pp. 2567–2578. doi: 10.1007/s00449-021-02628-1.

Winkler, A. *et al.* (2002) 'Heat stress activates the yeast high-osmolarity glycerol mitogen-activated protein kinase pathway, and protein tyrosine phosphatases are essential under heat stress.', *Eukaryotic cell*. United States, 1(2), pp. 163–173. doi: 10.1128/EC.1.2.163-173.2002.

Winzeler, E. A. *et al.* (1999) 'Functional characterization of the *S. cerevisiae* genome by gene

deletion and parallel analysis.', *Science (New York, N.Y.)*. United States, 285(5429), pp. 901–906. doi: 10.1126/science.285.5429.901.

Woolford, J. L. and Baserga, S. J. (2013) 'Ribosome biogenesis in the yeast *Saccharomyces cerevisiae*', *Genetics*, 195(3), pp. 643–681. doi: 10.1534/genetics.113.153197.

Wortel, M. T. *et al.* (2016) 'Evolutionary pressures on microbial metabolic strategies in the chemostat', *Scientific Reports*. Nature Publishing Group, 6(July), pp. 1–11. doi: 10.1038/srep29503.

Wosika, V. and Pelet, S. (2020) 'Single-particle imaging of stress-promoters induction reveals the interplay between MAPK signaling, chromatin and transcription factors', *Nature Communications*. Springer US, 11(1), pp. 1–13. doi: 10.1038/s41467-020-16943-w.

Wright, N. R. *et al.* (2020) 'Fluctuations in glucose availability prevent global proteome changes and physiological transition during prolonged chemostat cultivations of *Saccharomyces cerevisiae*', *Biotechnology and Bioengineering*, 117(7), pp. 2074–2088. doi: 10.1002/bit.27353.

Wright, N. R. *et al.* (2022) 'Emergence of Phenotypically Distinct Subpopulations Is a Factor in Adaptation of Recombinant *Saccharomyces cerevisiae* under Glucose-Limited Conditions', *Applied and Environmental Microbiology*, 88(7). doi: 10.1128/aem.02307-21.

Wright, N. R., Rønnest, N. P. and Thykaer, J. (2016) 'Scale-down of continuous protein producing *Saccharomyces cerevisiae* cultivations using a two-compartment system', *Biotechnology Progress*, 32(1), pp. 152–159. doi: 10.1002/btpr.2184.

Wu, G. *et al.* (2016) 'Metabolic Burden: Cornerstones in Synthetic Biology and Metabolic Engineering Applications', *Trends in Biotechnology*. Elsevier Ltd, 34(8), pp. 652–664. doi: 10.1016/j.tibtech.2016.02.010.

Wu, L., Schipper, D., Kresnowati, P., Proell, Angela M, *et al.* (2006) 'Short-Term Metabolome Dynamics and Carbon, Electron, and ATP Balances in Chemostat-Grown', *Society*, 72(5), pp. 3566–3577. doi: 10.1128/AEM.72.5.3566.

Wu, L., Schipper, D., Kresnowati, P., Proell, Angela M., *et al.* (2006) 'Short-term metabolome dynamics and carbon, electron, and ATP balances in chemostat-grown *Saccharomyces cerevisiae* CEN.PK 113-7D following a glucose pulse', *Applied and Environmental Microbiology*, 72(5), pp. 3566–3577. doi: 10.1128/AEM.72.5.3566.

Wu, N. *et al.* (2016) 'Alpha-ketoglutarate: Physiological functions and applications', *Biomolecules and Therapeutics*, 24(1), pp. 1–8. doi: 10.4062/biomolther.2015.078.

Wu, Y. *et al.* (2021) 'Yeast cell fate control by temporal redundancy modulation of transcription factor paralogs', *Nature Communications*. Springer US, 12(1), pp. 1–13. doi: 10.1038/s41467-021-23425-0.

Wullschleger, S., Loewith, R. and Hall, M. N. (2006) 'TOR signaling in growth and metabolism', *Cell*, 124(3), pp. 471–484. doi: 10.1016/j.cell.2006.01.016.

Xia, J. *et al.* (2022) 'Proteome allocations change linearly with the specific growth rate of *Saccharomyces cerevisiae* under glucose limitation'. Springer US, 13(2819), pp. 1–12. doi: 10.1038/s41467-022-30513-2.

Xu, K. *et al.* (2020) 'Multilevel Defense System (MDS) Relieves Multiple Stresses for Economically Boosting Ethanol Production of Industrial *Saccharomyces cerevisiae*', *ACS Energy Letters*, 5(2), pp. 572–582. doi: 10.1021/acsenergylett.9b02681.

Xu, X. *et al.* (2023) 'Trimming the genomic fat: minimising and re-functionalising genomes using synthetic biology', *Nature Communications*. Springer US, 14(1), pp. 1–11. doi: 10.1038/s41467-023-37748-7.

Yi, C. *et al.* (2017) 'Formation of a SNF1-Mec1-Atg1 Module on Mitochondria Governs Energy Deprivation-Induced Autophagy by Regulating Mitochondrial Respiration', *Developmental Cell*, 41(1), pp. 59-71.e4. doi: 10.1016/j.devcel.2017.03.007.

Yi, D. G. and Huh, W. K. (2015) 'UDP-glucose pyrophosphorylase Ugp1 is involved in oxidative stress response and long-term survival during stationary phase in *Saccharomyces cerevisiae*', *Biochemical and Biophysical Research Communications*. Elsevier Ltd, 467(4), pp. 657–663. doi: 10.1016/j.bbrc.2015.10.090.

Yoshida, K. and Blobel, G. (2001) 'The karyopherin Kap142p/Msn5p mediates nuclear import and nuclear export of different cargo proteins.', *The Journal of cell biology*. United States, 152(4), pp. 729–740. doi: 10.1083/jcb.152.4.729.

Youk, H. and Van Oudenaarden, A. (2009) 'Growth landscape formed by perception and import of glucose in yeast', *Nature*. Nature Publishing Group, 462(7275), pp. 875–879. doi: 10.1038/nature08653.

Young, E. T. *et al.* (2003) 'Multiple pathways are co-regulated by the protein kinase SNF1 and the transcription factors Adr1 and Cat8', *Journal of Biological Chemistry*[©]. 2003 ASBMB. Currently published by Elsevier Inc; originally published by American Society for Biochemistry and Molecular Biology., 278(28), pp. 26146–26158. doi: 10.1074/jbc.M301981200.

Young, T. B. and Bungay, H. R. (1973) 'Dynamic analysis of a microbial process: A systems engineering approach', *Biotechnology and Bioengineering*, 15(2), pp. 377–393. doi: 10.1002/bit.260150212.

Zadrąg-Tęcza, R. *et al.* (2018) 'Stress Response Mechanisms in Fungi: Theoretical and Practical Aspects', *Stress Response Mechanisms in Fungi*. doi: 10.1007/978-3-030-00683-9.

Zakrzewska, A. *et al.* (2011) 'Genome-wide analysis of yeast stress survival and tolerance acquisition to analyze the central trade-off between growth rate and cellular robustness', *Molecular Biology of the Cell*, 22(22), pp. 4435–4446. doi: 10.1091/mbc.E10-08-0721.

Zaman, S. *et al.* (2009) 'Glucose regulates transcription in yeast through a network of signaling pathways', *Molecular Systems Biology*, 5(245), pp. 1–14. doi: 10.1038/msb.2009.2.

Zampar, G. G. *et al.* (2013) 'Temporal system-level organization of the switch from glycolytic to gluconeogenic operation in yeast', *Molecular Systems Biology*, 9(651). doi: 10.1038/msb.2013.11.

Zencir, S. *et al.* (2020) 'Mechanisms coordinating ribosomal protein gene transcription in response to stress', *Nucleic Acids Research*. Oxford University Press, 48(20), pp. 11408–11420. doi: 10.1093/nar/gkaa852.

Zeng, H. *et al.* (2021) 'Understanding and mathematical modelling of cellular resource allocation in microorganisms: a comparative synthesis', *BMC Bioinformatics*. BioMed Central, 22(1), pp. 1–22. doi: 10.1186/s12859-021-04382-3.

Zhang, C.-S., Hardie, D. G. and Lin, S.-C. (2020) 'Glucose Starvation Blocks Translation at Multiple Levels', *Cell Metabolism*, 31(2), pp. 217–218. doi: https://doi.org/10.1016/j.cmet.2020.01.005.

Zhang, J. *et al.* (2015) 'Determination of the Cytosolic NADPH/NADP Ratio in *Saccharo-*

myces cerevisiae using Shikimate Dehydrogenase as Sensor Reaction', *Scientific Reports*. Nature Publishing Group, 5(August), pp. 1–12. doi: 10.1038/srep12846.

Zhang, J., Herik, B. M. Van Den and Wahl, S. A. (2020) 'Alpha - ketoglutarate utilization in *Saccharomyces cerevisiae* : transport , compartmentation and catabolism', *Scientific Reports*. Nature Publishing Group UK, 10, pp. 1–11. doi: 10.1038/s41598-020-69178-6.

Zhang, T. *et al.* (2017) 'Increased heme synthesis in yeast induces a metabolic switch from fermentation to respiration even under conditions of glucose repression', *Journal of Biological Chemistry*. Currently published by Elsevier Inc; originally published by American Society for Biochemistry and Molecular Biology., 292(41), pp. 16942–16954. doi: 10.1074/jbc.M117.790923.

Zhao, H. *et al.* (2015) 'Transcriptome analysis reveals the oxidative stress response in *Saccharomyces cerevisiae*', *RSC Advances*. Royal Society of Chemistry, 5(29), pp. 22923–22934. doi: 10.1039/c4ra14600j.

Ziegler, M. *et al.* (2021) 'Engineering of a robust *Escherichia coli* chassis and exploitation for large-scale production processes', *Metabolic Engineering*, 67(June), pp. 75–87. doi: 10.1016/j.ymben.2021.05.011.

Ziegler, M. and Takors, R. (2020) 'Reduced and Minimal Cell Factories in Bioprocesses: Towards a Streamlined Chassis BT - Minimal Cells: Design, Construction, Biotechnological Applications', in Lara, A. R. and Gosset, G. (eds). Cham: Springer International Publishing, pp. 1–44. doi: 10.1007/978-3-030-31897-0_1.

Zieringer, J. and Takors, R. (2018) '*In Silico* Prediction of Large-Scale Microbial Production Performance: Constraints for Getting Proper Data-Driven Models', *Computational and Structural Biotechnology Journal*. The Authors, 16, pp. 246–256. doi: 10.1016/j.csbj.2018.06.002.

Zieringer, J., Wild, M. and Takors, R. (2021) 'Data-driven *in silico* prediction of regulation heterogeneity and ATP demands of *Escherichia coli* in large-scale bioreactors', *Biotechnology and Bioengineering*, 118(1), pp. 265–278. doi: 10.1002/bit.27568.

Zimmermann, M., Sauer, U. and Zamboni, N. (2014) 'Quantification and mass isotopomer profiling of α-keto acids in central carbon metabolism', *Analytical Chemistry*, 86(6), pp. 3232–3238. doi: 10.1021/ac500472c.

Zlokarnik, M. (2006) 'Scale-up in chemical engineering'. John Wiley & Sons.

Zörgö, E. *et al.* (2012) 'Life History Shapes Trait Heredity by Accumulation of Loss-of-Function Alleles in Yeast', *Molecular Biology and Evolution*, 29(7), pp. 1781–1789. doi: 10.1093/molbev/mss019.

Zou, K. *et al.* (2020) 'Life span extension by glucose restriction is abrogated by methionine supplementation: Cross-talk between glucose and methionine and implication of methionine as a key regulator of life span', *Science Advances*, 6(32). doi: 10.1126/sciadv.aba1306.

Appendix

Appendix A

Appendix A comprises the published supporting material of research article I.

Off-gas Deconvolution

A prerequisite for off-gas analysis in stimulus response experiments is a suitable approach for data deconvolution. Long tubing lines and foam traps between fermenter and sensors lead to the formation of mixing chambers causing a sensor delay of several minutes and increased apparent time constants versus the reported 40 - 55 s for BCP-O_2 and BCB-CO_2 sensors (Pepper, 2015). This can cause misguided readouts, such as strong RQ dynamics that might not be caused by biological effects, at all. To compensate for this system characteristic, step experiments under experimental conditions were carried out to acquire delay times and time constants for the whole "fermenter → sensor" unit as laid out in table A1. Correction of measured off-gas signals was calculated according to the procedure of Theobald *et al.* (Theobald, 1995):

$$\left(Y_{O_2}^{\omega}\right)_F\left(t - \tau_d^{O_2}\right) = \left(Y_{O_2}^{\omega}\right)_A + \tau_1^{O_2} \frac{d\left(Y_{O_2}^{\omega}\right)_A}{dt} \tag{A1}$$

$$\left(Y_{CO_2}^{\omega}\right)_F\left(t - \tau_d^{CO_2}\right) = \left(Y_{CO_2}^{\omega}\right)_A + \tau_1^{CO_2} \frac{d\left(Y_{CO_2}^{\omega}\right)_A}{dt} \tag{A2}$$

, with

$\left(Y_{O_2}^{\omega}\right)_F$ molar fraction of O_2 in the fermenter broth

$\left(Y_{CO_2}^{\omega}\right)_F$ molar fraction of CO_2 in the fermenter broth

$\left(Y_{O_2}^{\omega}\right)_A$ measured molar fraction of O_2 at the sensor

$\left(Y_{CO_2}^{\omega}\right)_A$ measured molar fraction of CO_2 at the sensor

t time of data logging for O_2 and CO_2

$\tau_d^{O_2}$ delay time of O_2 signal

$\tau_d^{CO_2}$ delay time of CO_2 signal

$\tau_1^{O_2}$ time constant of BCP-O_2 sensor and gas line "fermenter → sensor"

$\tau_1^{CO_2}$ time constant of BCP-CO_2 sensor and gas line "fermenter → sensor"

Table A1. Parameters for off-gas deconvolution. Delay times (τ_d) and time constants (τ_1) were derived from step experiments, where the reactor system was operated with water, but otherwise equal to fermentation conditions. Each parameter is derived from two-step experiments, where aeration was switched from a calibration gas mixture (2.00 % O_2, 8.99 % CO_2) to ambient air (20.94 % O_2, 0.04 % CO_2).

Analyte	Sensor	Manufacturer	τ_d (s)	τ_1 (s)
oxygen	BCP-O_2	BlueSens, Herten, Germany	92	381
carbon dioxide	BCP-CO_2	BlueSens, Herten, Germany	155	490

Figure A1 shows an exemplary correction for both, oxygen and carbon dioxide signals against raw signal readouts after a single perturbation (see Figure 11C) indicated by the dashed lines. It becomes obvious that this procedure is essential to compensate for delays and curve flattening due to a total of 3.2 L mixing volume in the off-gas line.
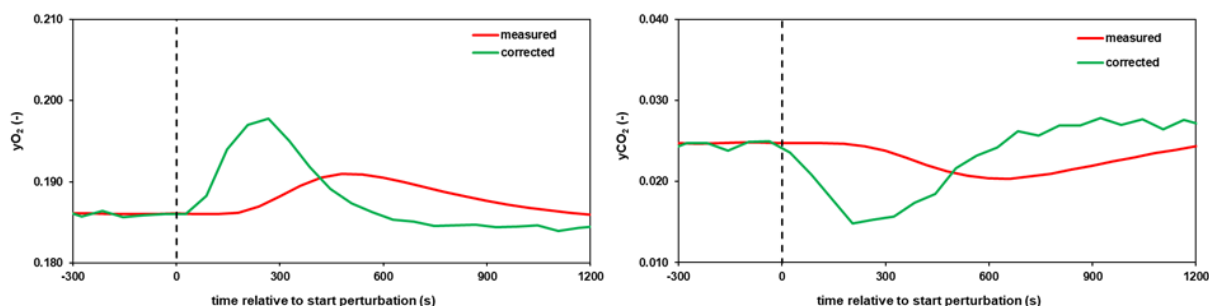
Figure A1. Exemplary deconvolution results for O_2 and CO_2 signals of one replicate after a single perturbation (see figure 3c). Deconvolution of O_2 (left panel) and CO_2 (right panel) signals (green) was calculated based on equations (A1) and (A2), parameters from table A1 and plotted against raw signals (red).

Steady State Amino Acid Concentrations

A total of 18 amino acids were also monitored during the SRE experiment under both conditions. However, due to the absence of significant dynamics during the perturbation, only steady state values are reported in table A2.

Table A2. Amino acid concentrations during reference and dynamic steady state conditions. For the dynamic steady state, average pool concentrations over one perturbation cycle are reported.

Amino Acid	Steady State RS ($\mu mol \cdot g_{DMB}^{-1}$)	Steady State DS ($\mu mol \cdot g_{DMB}^{-1}$)	Change (%)	Welch Test (p-value)
glycine	2.37 ± 0.02	$1.05 \pm 0,28$	- 56	$7.4 \cdot 10^{-5}$
L-methionine	0.18 ± 0.04	0.05 ± 0.01	- 72	$2.9 \cdot 10^{-2}$
L-serine	3.29 ± 0.19	1.29 ± 0.51	- 61	$6.9 \cdot 10^{-5}$
L-proline	6.15 ± 1.12	2.17 ± 1.08	- 65	$7.4 \cdot 10^{-3}$
L-threonine	10.5 ± 4.5	9.8 ± 2.9	- 7	n.s.
L-glutamine	149 ± 10	103 ± 20	- 31	$2.6 \cdot 10^{-3}$
L-asparagine	8.64 ± 1.31	8.7 ± 1.60	+ 1	n.s.
L-glutamic acid	449 ± 26	390 ± 71	- 13	n.s.
L-aspartic acid	22.9 ± 5.7	22.4 ± 5.8	- 2	n.s.
L-lysine	3.79 ± 0.47	4.19 ± 0.12	+ 11	n.s.
L-arginine	17.8 ± 0.3	9.8 ± 0.9	- 45	$5.9 \cdot 10^{-7}$
L-tyrosine	1.92 ± 0.05	0.41 ± 0.05	- 78	$1.5 \cdot 10^{-3}$
L-tryptophane	0.36 ± 0.11	0.11 ± 0.01	- 68	n.s.
L-phenylalanine	0.85 ± 0.09	0.28 ± 0.05	- 66	$4.1 \cdot 10^{-3}$
L-valine	22.1 ± 2.6	12.6 ± 4.1	- 43	$5.0 \cdot 10^{-3}$
L-leucine	0.69 ± 0.09	0.38 ± 0.1	- 46	$6.8 \cdot 10^{-3}$
L-isoleucine	1.45 ± 0.02	0.79 ± 0.19	- 46	$3.1 \cdot 10^{-4}$
L-alanine	84.9 ± 8.0	43.4 ± 16.7	- 49	$1.5 \cdot 10^{-3}$

All values represent means $\pm$ standard deviation (s.d.) of three biological replicates. n.s., not significant.

Appendix B

Appendix B comprises the published supporting information of research article II.

Bioreactor characterization

The ungassed power number N_p was determined based on a Reynolds number of $6\cdot10^4$. Next, the ungassed power input was calculated under the assumption that both Rushton turbines did not influence each other, yielding a value of 18.8 $kg\cdot m^2\cdot s^{-3}$. Michel and Millers correlation was used to estimate the gassed power input of 12.0 $kg\cdot m^2\cdot s^{-3}$, translating to a volumetric gassed power input of 7.1 $W\cdot kg^{-1}$ (Michel and Miller, 1962).

Estimation of the circulation time t_c was based on the approach reported by Jüsten et al. (1996) with an estimated gassed power number $N_{p,g}$ of 48 according to the relation from (EKATO Rühr-und Mischtechnik GmbH 2013, page 52). The approach yielded time $t_c = 0.1$ s allowed to conclude a perfectly mixed environment.

Table B1. Bioreactor operating parameters and physical conditions.

Parameter	Symbol	Value	Dimension	Reference
stirrer speed	N	13.3	s^{-1}	set point
vessel diameter	D_v	0.125	m	measurement
impeller blade width	W	$1.5\cdot10^{-2}$	m	measurement
impeller diameter	D_i	$6\cdot10^{-2}$	m	measurement
number of blades	z	6	-	measurement
Number of impellers	i	2	-	set point
liquid volume	V_l	$1.7\cdot10^{-3}$	m^3	set point
volumetric air flow rate	Q_{air}	$1.42\cdot10^{-5}$	$m^3\cdot s^{-1}$	set point
broth density	ρ	1021	$kg\cdot m^{-3}$	measurement
dynamic broth viscosity	η	$7.97\cdot10^{-4}$	$kg\cdot m^{-1}\cdot s^{-1}$	assumed as H_2O (30 °C)
ungassed power number	N_p	5	-	(Bates, Fondy and Corpstein, 1963)
constant for Po_g	c	0.812	-	(Taghavi, 2010)

Table B2. Calculated parameters and formula.

Parameter	Symbol	Formula	Dimension	Reference
Reynolds number	Re	$N \cdot D_i^2 \cdot \dfrac{\rho}{\eta}$	-	(Bates, Fondy and Corpstein, 1963)
ungassed power input	Po	$i \cdot N_P \cdot \rho \cdot D_i^5 \cdot N^3$	kg·m²·s⁻³	(EKATO Rühr-und Mischtechnik GmbH, 2013)
gassed power input	Po_g	$c \cdot \left(\dfrac{Po^2 \cdot N \cdot D_i^3}{Q_{air}^{0.56}} \right)^{0.43}$	kg·m²·s⁻³	(Michel and Miller, 1962)
Froude number	Fr	$N^2 \cdot \dfrac{D_i}{9.78}$	-	(EKATO Rühr-und Mischtechnik GmbH, 2013)
aeration number	N_{ae}	$\dfrac{Q_{air}}{N \cdot D_i^3}$	-	(EKATO Rühr-und Mischtechnik GmbH, 2013)
gassed power number	$N_{p,g}$	$z \cdot \dfrac{\left[N_p + \left(187 \cdot N_{ae} \cdot Fr^{-0.32} \cdot \left(\dfrac{D_i}{D_v}\right)^{1.53} \right) - \left(4.6 \cdot N_{ae}^{\,1.25}\right) \right]}{\left[1 + \left(136 \cdot N_{ae} \cdot \left(\dfrac{D_i}{D_v}\right)^{1.14}\right)\right]}$	-	(EKATO Rühr-und Mischtechnik GmbH, 2013)
ungassed flow number	N_{Fl}	$\left(0.91 \cdot N_p \cdot \dfrac{W}{D_i}\right)^{0.5}$	-	(Jüsten et al., 1996)
gassed flow number	$N_{Fl,g}$	$N_{Fl} \cdot \left(\dfrac{N_{p,g}}{N_p}\right)$	-	(Jüsten et al., 1998)
circulation time	t_c	$\dfrac{V_l}{N_{Fl,g} \cdot N \cdot D_i^3}$	s	(Jüsten et al., 1998)

Carbon, nitrogen and electron balancing

A

B

C
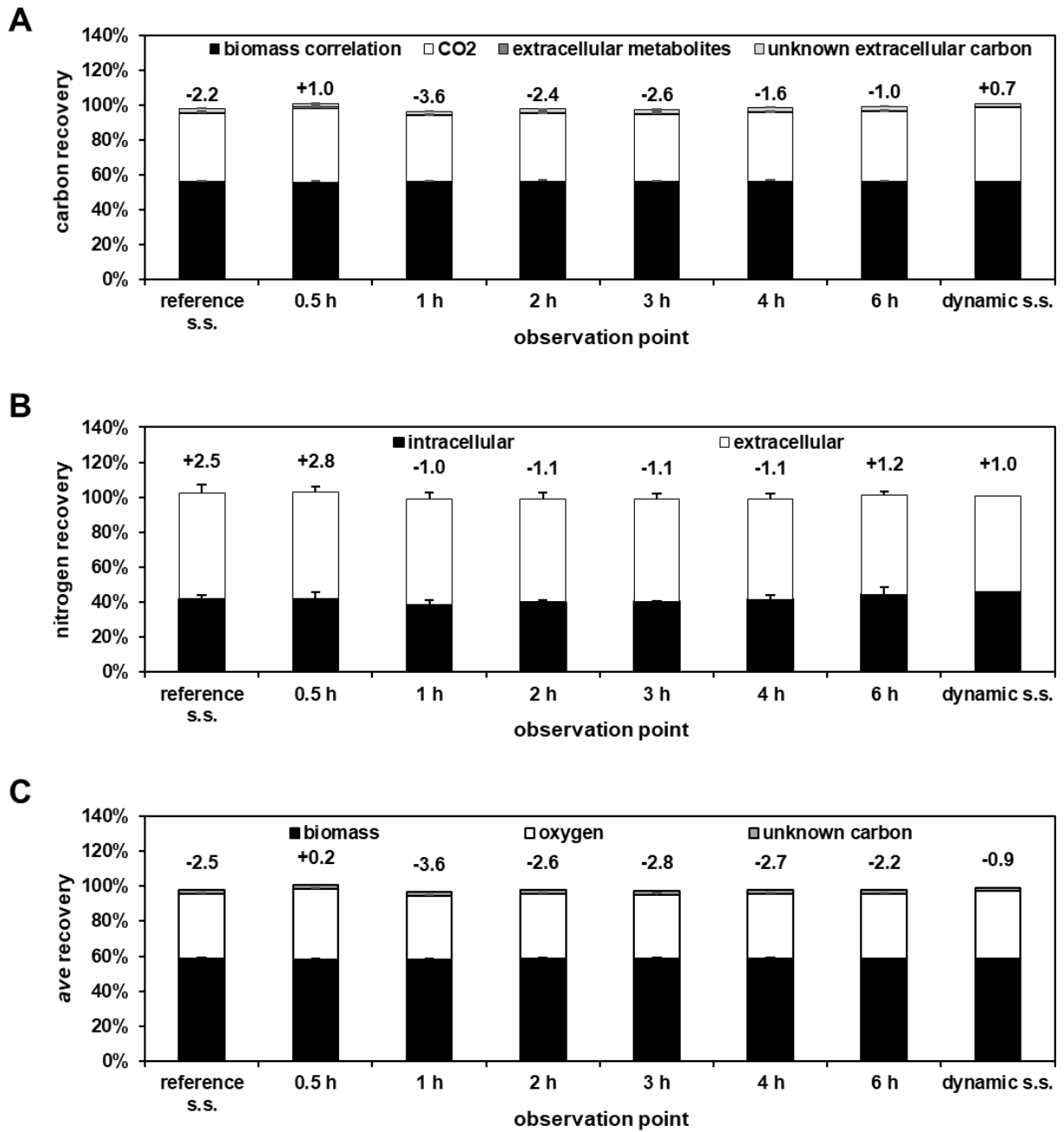
Figure B1. Recoveries of organic carbon (A), nitrogen (B) and available electrons (C) during the reference steady state up to 6 h post stimulus during the non-adapted time series and during the dynamic steady state. Numbers above bars indicate the deviation from complete recovery in percent. *ave*, available electrons.

Differential gene expression analysis

For gene expression analysis, the complete count table was split into three datasets: (i) the post s-LSL time series including the reference steady state (RS) and all time points of the series up to 3 h (figure B2), (ii) the adapted time series with timely equidistant samples within one r-LSL cycle of 9 min with time point 0 s serving as the reference sample (figure B3) and (iii) the characterization of the dynamic steady state (DS) using the grouped samples of RS and relaxed time points 2 h and 3 h as the reference and all samples of the adapted time series representing the adapted steady state. All functions used in the subsequent section were called from the R package DESeq2 v. 1.32.0 (Love, Huber and Anders, 2014). Cook's distances were computed for an initial outlier detection via calling "cooks" from the "DESeqDataSetFromMatrix" object of the respective dataset. In order to discriminate between the introduction of biological and technical variance, we included the variables time (for biological variance), replicate (technical) and libseq (technical, merged variable for different library preparation and sequencing runs, see supporting information B of the original research article; tab 1) into the model. Next, count tables were transformed into the rlog space to stabilize the variance of genes with low counts using "rlog". Principal component analysis (plotPCA) revealed a strong influence of technical variables (figures B2 B+D; B3 B+D and B4 A+C). Thus, we applied a batch correction using "removeBatchEffect" from the limma v. 3.48.3 package (Ritchie *et al.*, 2015) to dampen the technically introduced variance leading to a reduced model, which allowed the investigation of biologically introduced variance (figures B2 C+E; B3 C+E and B4 B+D).

A

B

C

D

E
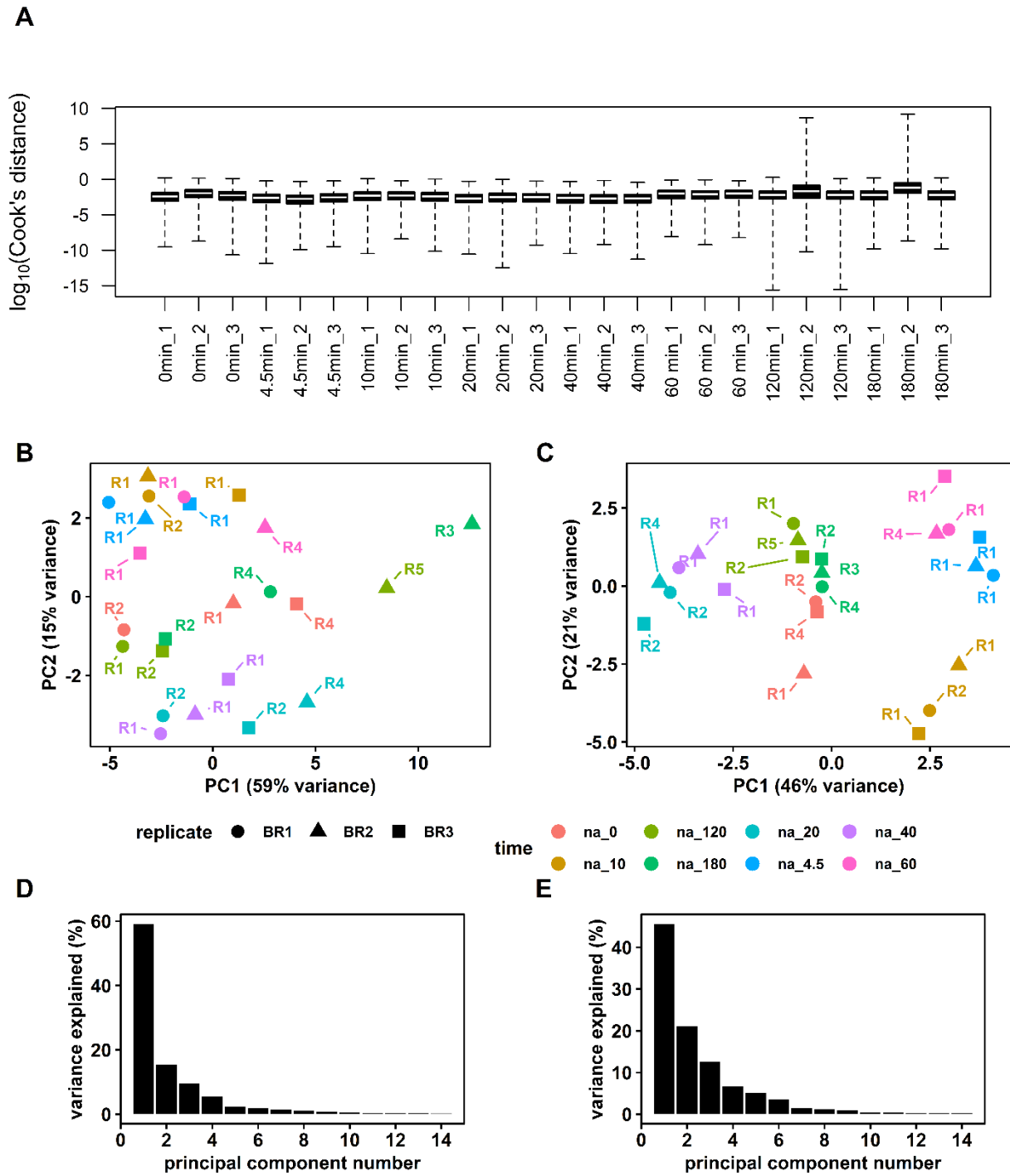
Figure B2. Analysis of all 24 samples from the non-adapted post s-LSL time series. (A) Boxplot of the Cook's distances. Numbers behind the sample time points indicate the biological replicate (B) Individual samples of 8 time points plotted on principal component 1 (PC1) and 2 (PC2). Labels R1 - R5 indicate separate library preparation and/or sequencing runs. (C) Analogue to (B), but with the reduced model. (D) Corresponding scree plot of (B). (E) Corresponding scree plot of (C).
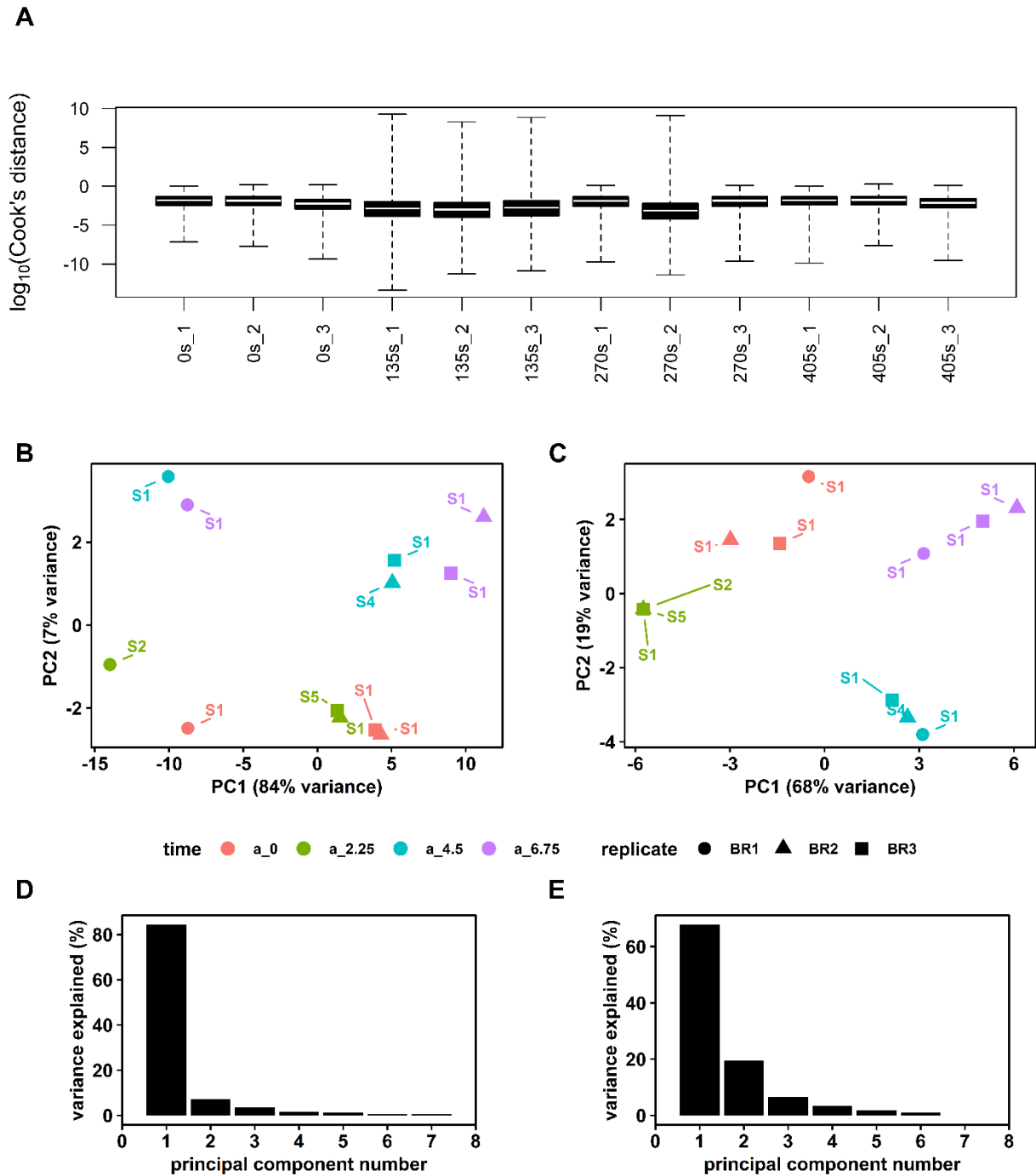
Figure B3. Analysis of all 12 samples from the adapted r-LSL time series. (A) Boxplot of the Cook's distances. Numbers behind the sample time points indicate the biological replicate (B) Individual samples of 4 time points plotted on principal component 1 (PC1) and 2 (PC2). Labels R1 - R5 indicate separate library preparation and/or sequencing runs. (C) Analogue to (B), but with the reduced model. (D) Corresponding scree plot of (B). (E) Corresponding scree plot of (C).
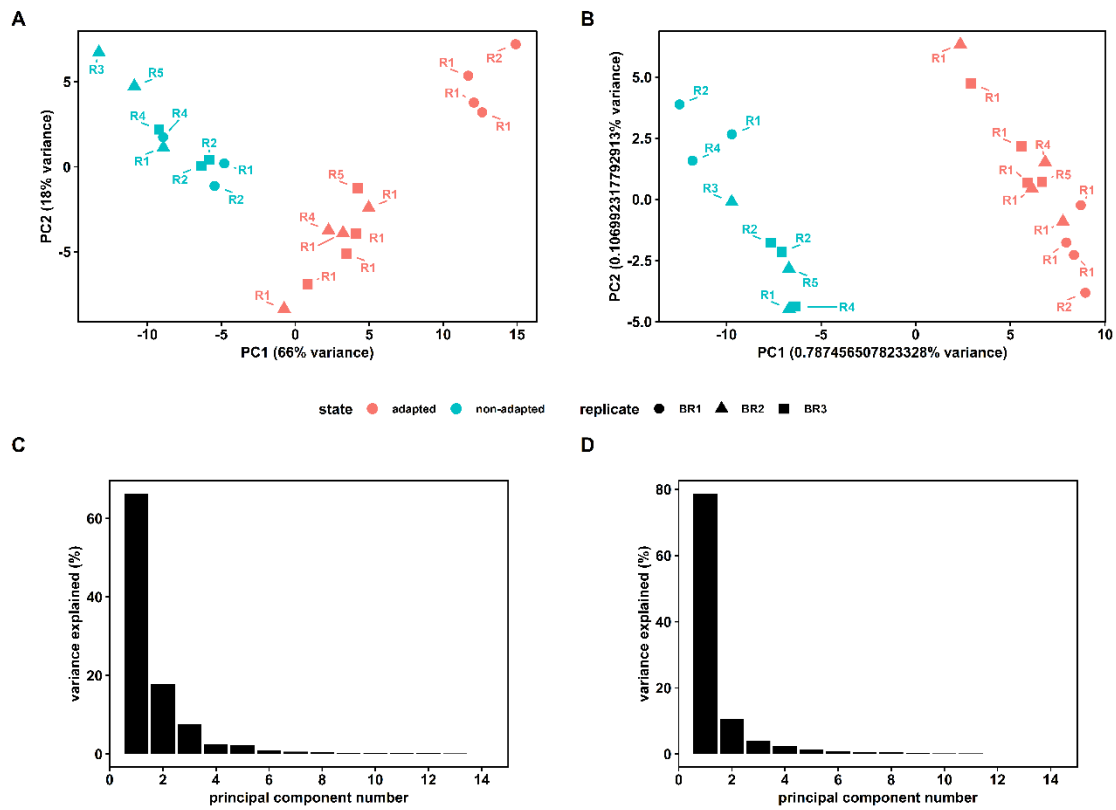
Figure B4. Analysis of all 36 samples generated in this study. (A) Individual samples plotted on principal component 1 (PC1) and 2 (PC2). Labels R1 - R5 indicate separate library preparation and/or sequencing runs. (B) Analogue to (B), but with the reduced model. (C) Corresponding scree plot of (A). (D) Corresponding scree plot of (B).

Temporal dynamics of amino acids during the non-adapted response

Intracellular amino acids were monitored via LC-MS/MS and steady state concentrations in RS versus DS have been published previously (Minden *et al.*, 2022). The time series data for S-LSL was not published in the mentioned work due to the generally large variance in the dataset. However, in order to support the findings of Figure 19 (dynamics of cluster 2) time series data of all measured amino acids is reproduced here. Amino acids where respective biosynthetic genes were found to be significantly enriched in cluster 2 (supporting information B of the original research article, tab 5) are phenylalanine, glutamine, aspartic acid, methionine, leucine, histidine, tryptophan and arginine, all of which were quantified except histidine.
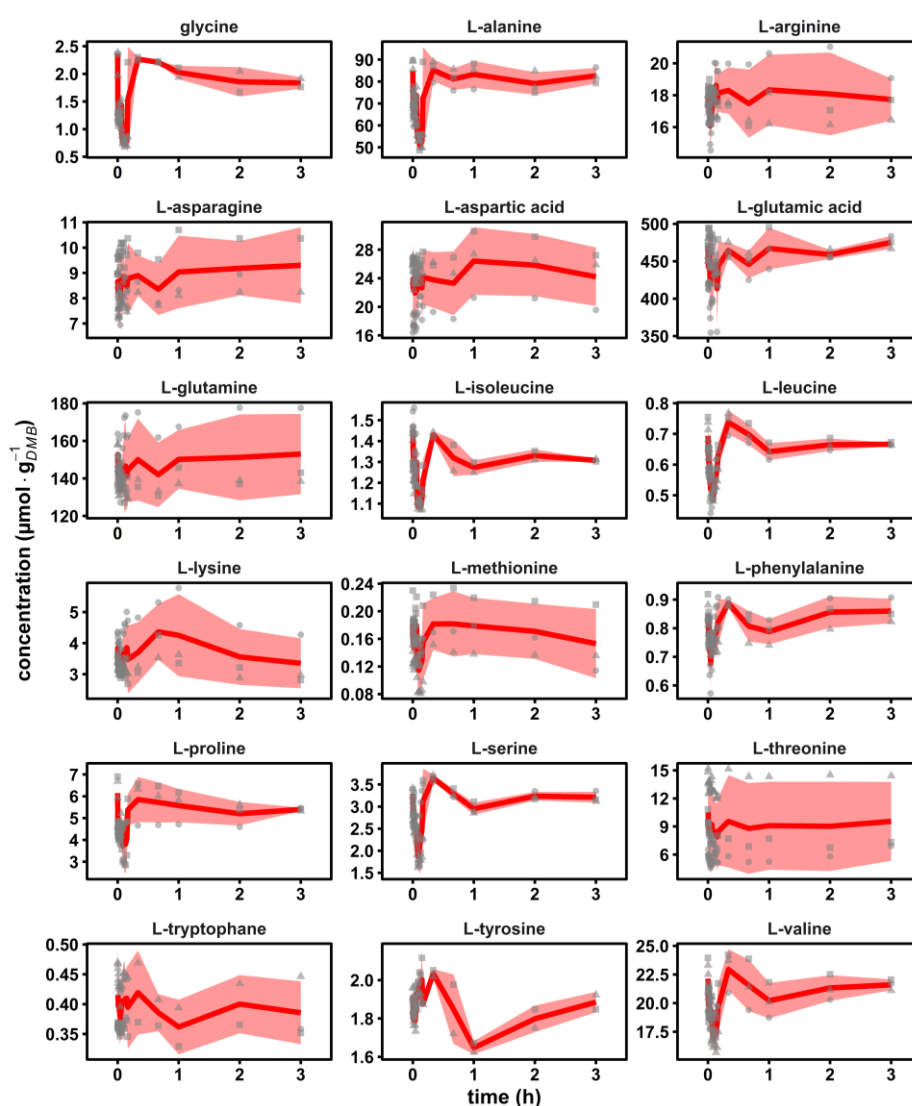
Figure B5. Dynamics of intracellular amino acids for three hours following a single transition into a starvation scenario ("feed off" phase) representing the non-adapted response (post s-LSL). The trends are shown as means (line) ± standard deviation (light area) of three biological replicates. The underlying single replicates are shown as grey symbols, where each symbol (square, triangle, circle) represents one biological replicate.

Appendix C

Appendix C comprises the published supporting information of research article III.

Estimation of ethanol stripping

Ethanol can be partially stripped in gassed fermentation processes leading to underestimated parameters such as $q_{ethanol}$ or the carbon balance. We estimated a 4.8 % loss of ethanol in the liquid phase using the approach reported by Löser *et al.* (2005). First, the millimolar stripping rate from the system was calculated according to equation C1:

$$\dot{m}_{ethanol,G} = \frac{q_{ethanol} \cdot c_{DMB} \cdot \dot{Q}_G}{K_{ethanol,L/G} \cdot D} \tag{C1}$$

, with:

$\dot{m}_{ethanol,G}$ stripping rate of ethanol (3.26 mmol·h^{-1})

$q_{ethanol}$ biomass specific ethanol production rate (7.98 mmol·g$_{DMB}^{-1}$·h^{-1})

c_{DMB} biomass concentration (5 g$_{DMB}$·L^{-1})

$\dot{Q}_G$ volumetric gassing rate (25.5 L·h^{-1})

$K_{ethanol,L/G}$ ethanol partition coefficient between gas and liquid phase (3125 L·L^{-1})

D dilution rate (0.1 h^{-1})

Then, the 4.8 % loss of ethanol in the liquid phase due to stripping was calculated by dividing the ethanol stripping rate by the ethanol production rate:

$$loss \, (\%) = \left[\frac{\dot{m}_{ethanol,G}}{q_{ethanol} \cdot c_{DMB} \cdot V_L} \right] \cdot 100 \tag{C2}$$

, with:

V_L liquid reactor volume (1.7 L)

Estimation of $q_{\text{glucose, max}}$ and K_{glucose}

As of to date, there are no published parameters for hyperbolic glucose uptake kinetics under anaerobic growth conditions available for Ethanol Red™. In order to characterize the stimulus, we conducted a parameter fitting of equation 3 to our experimental data. We repeated the reference steady state value between -600 and 0 seconds in 50 s intervals as a means to increase the weight of the steady state relative to dynamic data. For simulation and parameter fitting, the R packages *deSolve* v. 1.33 and *minpack.lm* v. 1.2.2 were used, respectively (Soetaert, Petzoldt and Setzer, 2010). Glucose uptake was modeled according to:

$$\frac{dc_{glucose}}{dt} = \left(c_{glucose,feed} - c_{glucose}\right) \cdot D - \left(\frac{q_{glucose,max} \cdot c_{glucose}}{K_{glucose} + c_{glucose}} \cdot c_{DMB}\right) \qquad \text{(C3)}$$

, with:

$c_{glucose}$ glucose concentration (initial value: 5.2 mmol$_C$·L^{-1} in s-LSL and 5.6 mmol$_C$·L^{-1} in r-LSL)

$c_{glucose,feed}$ glucose concentration in feed reservoir (1366 mmol$_C$·L^{-1})

c_{DMB} biomass concentration (5.06 g$_{DMB}$·L^{-1} in s-LSL and 4.72 g$_{DMB}$·L^{-1} in r-LSL)

$q_{glucose,max}$ maximum biomass specific glucose uptake rate (initial guess: 65 mmol$_C$·g$_{DMB}^{-1}$·h^{-1})

$K_{glucose}$ glucose half-saturation constant (initial guess: 6 mmol$_C$·L^{-1})

D dilution rate (0.1 h^{-1})

The famine stimulus within each perturbation cycle was implemented using an *ifelse*-loop where the dilution rate was set to zero during the feed-off time. The ordinary differential equation (3) was solved with the *ode()* function of *deSolve* (method = "ode45") and the parameters $q_{glucose,max}$ and $K_{glucose}$ were estimated by curve fitting via a Levenberg-Marquardt routine implemented in *nls.lm()* of the *minpack.lm* package (output and statistics in table C1). The simulated glucose levels versus experimental levels are shown in figure C1 A+C. Furthermore, an estimation of uncertainty was conducted. A random variable within the mean square error between model and experimental values was computed for each data point with

rnorm() to achieve a new simulated dataset. The parameters were then fit to 1000 simulated datasets and a 95 % confidence ellipse was drawn around the resulting parameter tuples (figure C1 B+D).

Table C1. Parameter estimation and statistics output from *nls.lm()*.

parameter	data set	estimate	standard error	*t*-value	Pr > |t|	*p*-value
$q_{glucose,max}$ $(\text{mmol}_C \cdot \text{g}_{DMB}^{-1} \cdot \text{h}^{-1})$	s-LSL	71.50	0.02	$8.9 \cdot 10^4$	$< 2 \cdot 10^{-16}$	< 0.001
	r-LSL	64.80	0.00	$3.5 \cdot 10^5$	$< 2 \cdot 10^{-16}$	< 0.001
$K_{glucose}$ $(\text{mmol}_C \cdot l^{-1})$	s-LSL	6.19	0.03	1.39	$< 2 \cdot 10^{-16}$	< 0.001
	r-LSL	5.47	0.00	106	$< 2 \cdot 10^{-16}$	< 0.001
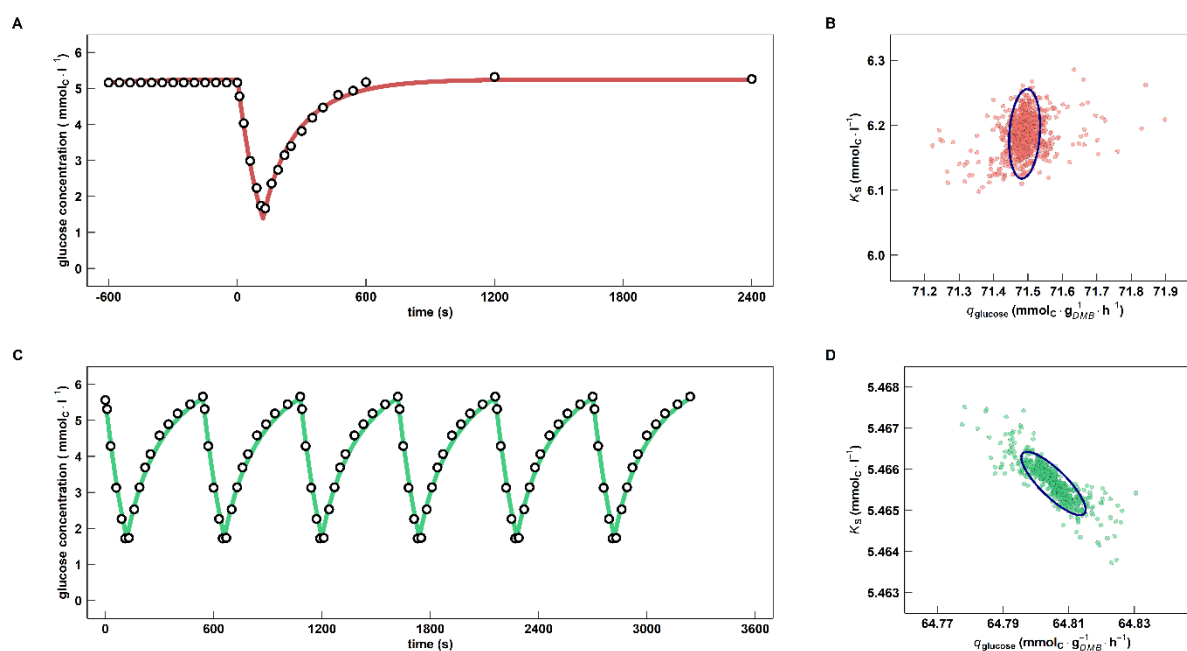
Figure C1. Simulation readouts for determination of glucose uptake kinetic parameters. Simulated data for s-LSL in shown in red (A) and r-LSL in green (C) with the corresponding experimental data as black circles. B and D depict the corresponding estimation of uncertainty. Estimated parameters for 1000 iterations over the curve fitting routine with simulated data, which was randomized within the mean square error of the model. The 95 % confidence interval is shown in blue.

Differential gene expression analysis

For gene expression analysis, the complete count table was split into three datasets: (i) the single-(s)-LSL time series including the reference steady state (RS) and post stimulus time points up to 3 h (figure S1), (ii) the characterization of the dynamic steady state (DS) using RS as the reference and all samples of the repeated-(r)-LSL time series representing DS (figure C2) and (iii) the r-LSL time series with timely equidistant samples within one perturbation cycle of 9 min with time point 0 s serving as the reference (figure C3). Except stated otherwise, all functions used in the subsequent section were called from the R package *DESeq2* v. 1.32.0 (Love, Huber and Anders, 2014). Cook's distances were computed for an initial outlier detection via calling "*cooks*" from the "*DESeqDataSetFromMatrix*" object of the respective dataset. In order to discriminate between the introduction of biological and technical variance, we included the variables time (for biological variance) and intervallic RIN (technical, for RNA integrity number) into the model. Next, count tables were transformed into the rlog space to stabilize the variance of genes with low counts using "*rlog*". Principal component analysis (*plotPCA*) revealed a strong influence of the RIN values (figures C2-C4 B+D). Thus, we applied a batch correction using "removeBatchEffect" from the *limma* v. 3.48.3 package (Ritchie *et al.*, 2015) to dampen the technically introduced variance leading to a reduced model, which allowed the investigation of biologically introduced variance (figures C2-C4 C+E).
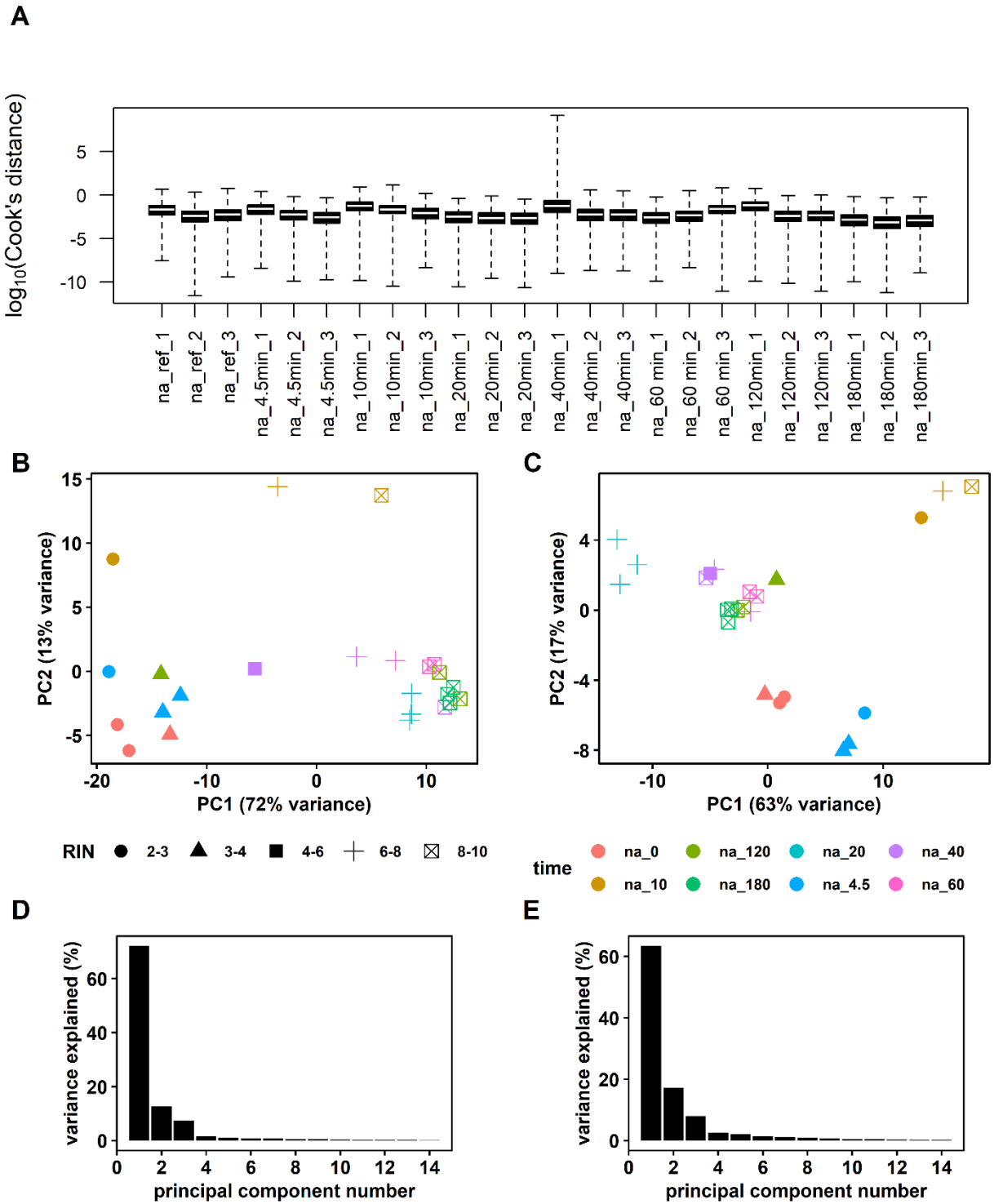
Figure C2. Analysis of all 24 samples from the s-LSL time series. (A) Boxplot of the Cook's distances. (B) Individual samples of 8 time points plotted on principal component 1 (PC1) and 2 (PC2). (C) Analogue to (B), but with the reduced model. (D) Corresponding scree plot of (B). (E) Corresponding scree plot of (C).
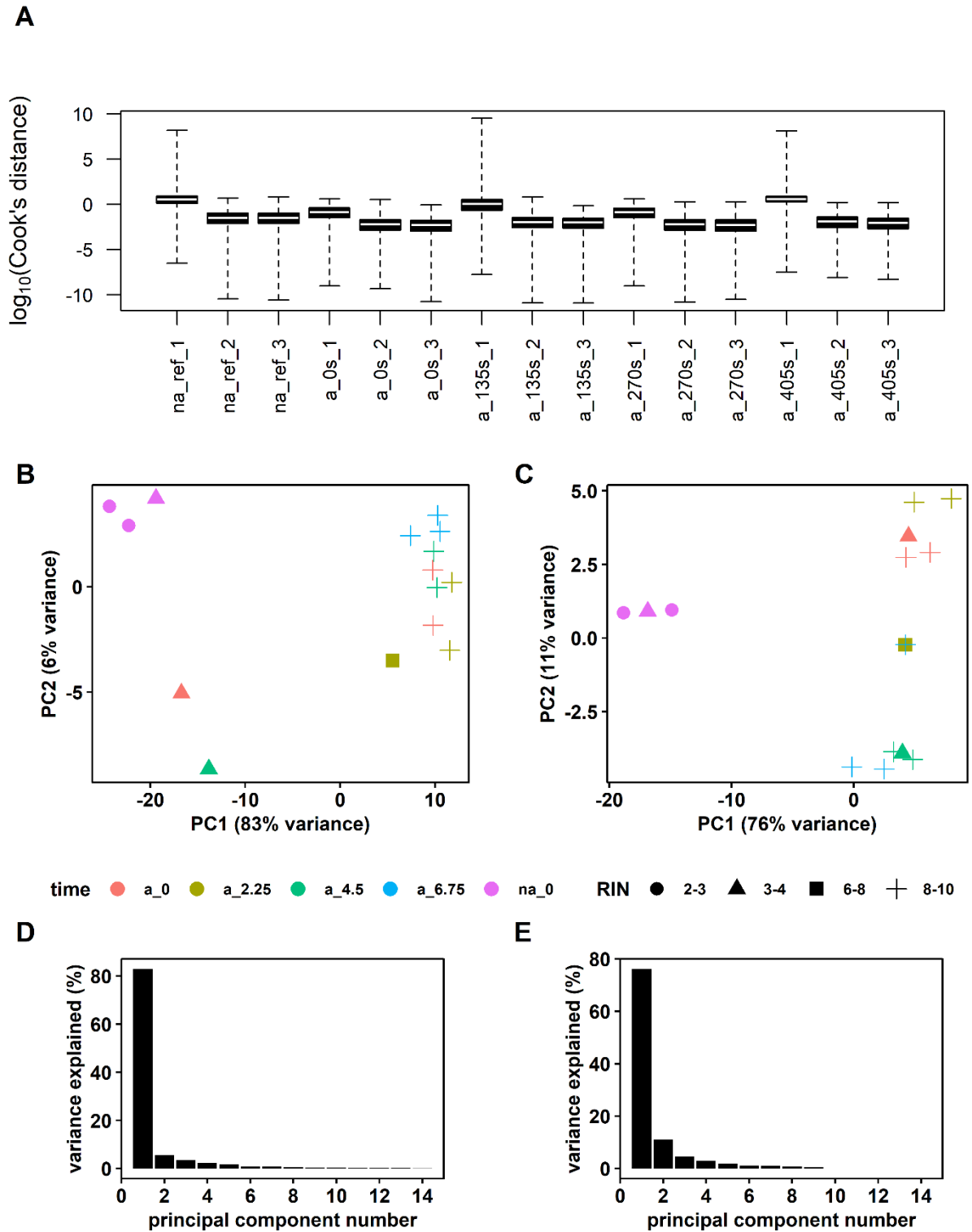
Figure C3 Analysis of 15 samples used for analyzing steady state DS (na_0 samples representing RS). (A) Boxplot of the Cook's distances. (B) Individual samples of 4 time points plotted on principal component 1 (PC1) and 2 (PC2). (C) Analogue to (B), but with the reduced model. (D) Corresponding scree plot of (B). (E) Corresponding scree plot of (C).
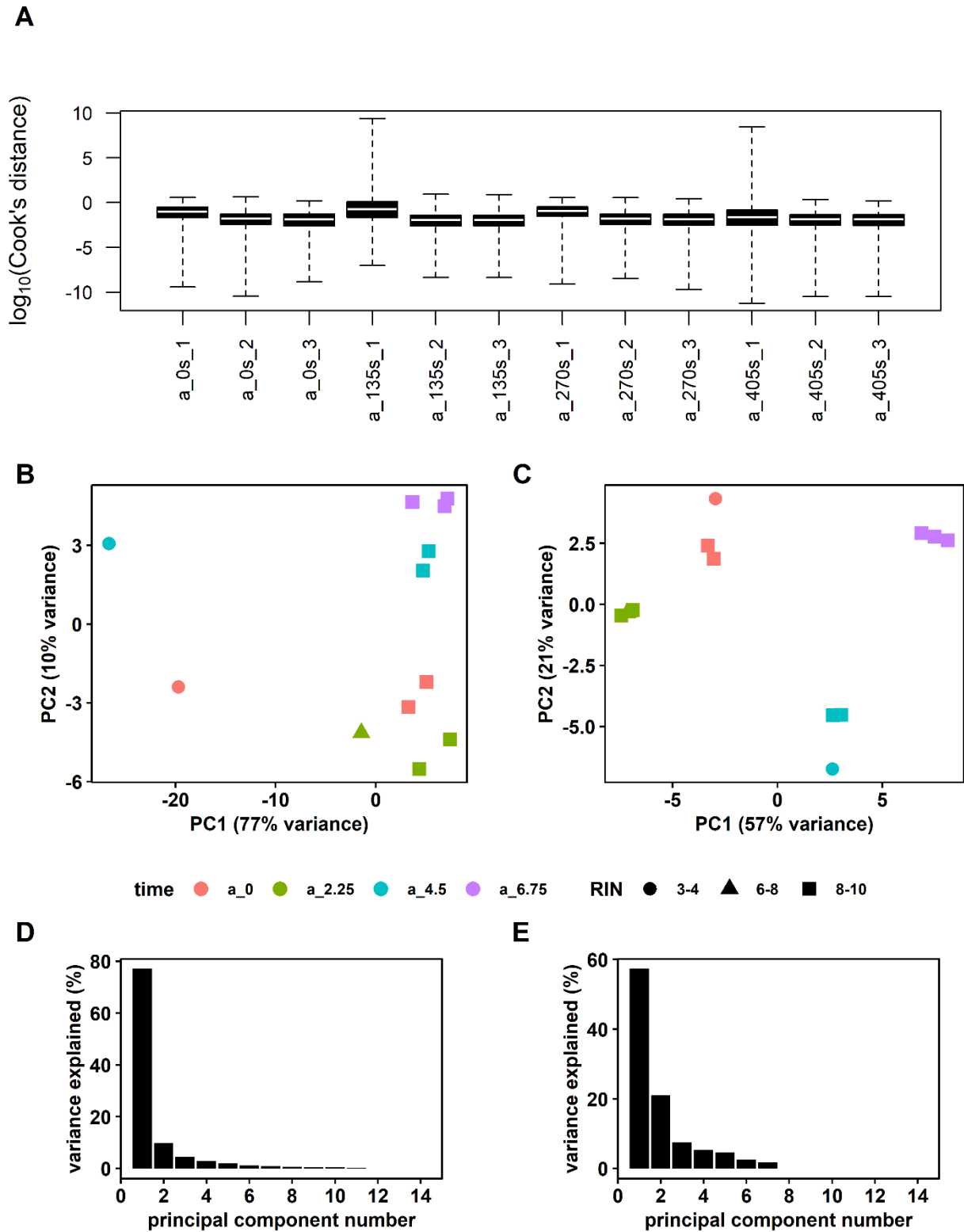
Figure C4. Analysis of all 12 samples from the r-LSL time series. (A) Boxplot of the Cook's distances. (B) Individual samples of 4 time points plotted on principal component 1 (PC1) and 2 (PC2). (C) Analogue to (B), but with the reduced model. (D) Corresponding scree plot of (B). (E) Corresponding scree plot of (C).

Comparison of storage compound liberation between experiments

Differences of trehalose and glycogen dynamics between this and the aerobic experiment with CEN.PK113-7D are visualized in the following figure C5. The comparing plots reproduce data from figure 3 for the 40-minute time window of the main publication and from reference (Minden *et al.*, 2022) to ease comparing the underlying dynamics of the s-LSL response.
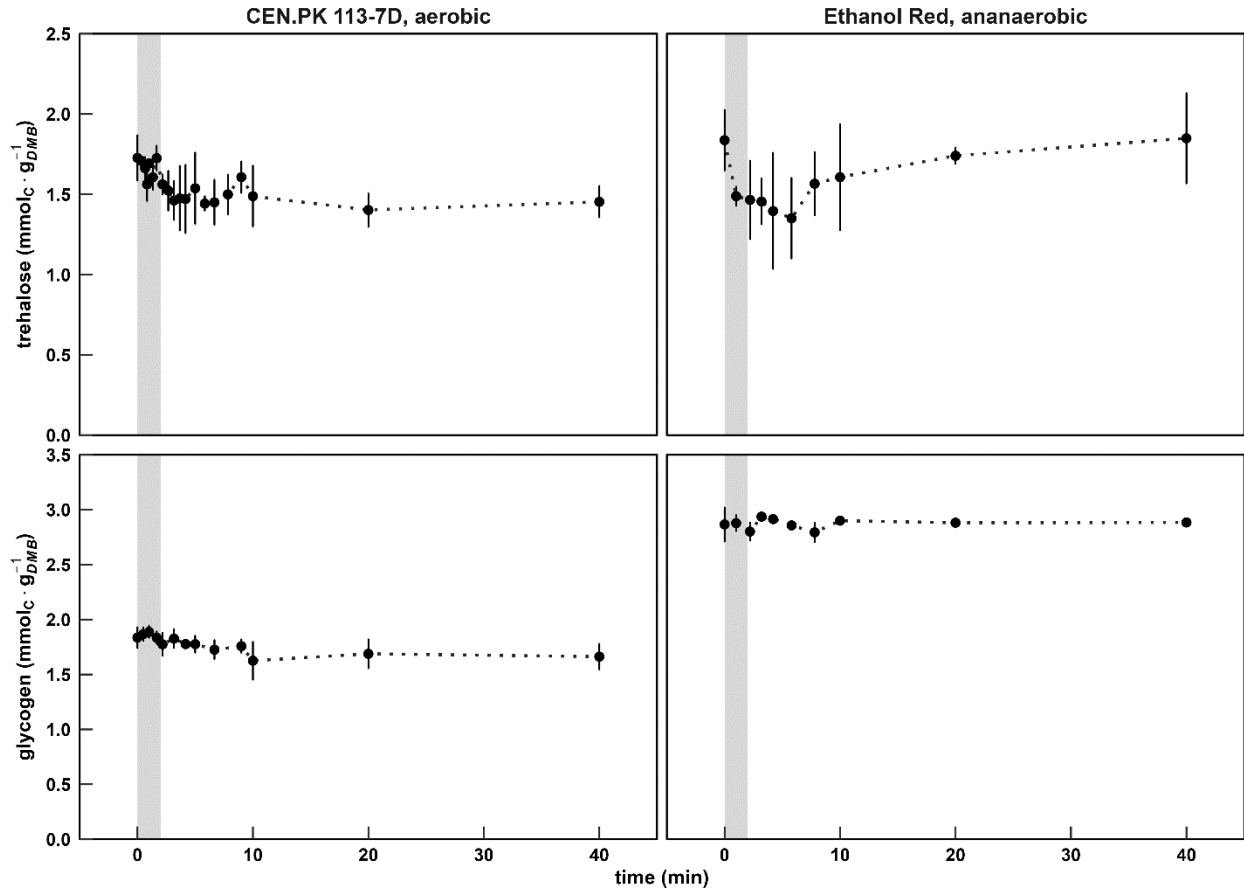
Figure C5. Characterization of intracellular trehalose and glycogen pools during the s-LSL stimulus. The left panel reproduces results from the aerobic stimulus-response experiment with CEN.PK113-7D under otherwise identical experimental conditions (Minden et al., 2022). The right panel reproduces results from the anaerobic experiment with Ethanol RedTM of figure 3 in this publication. The time series indicates dynamics following a single transition into starvation ("feed off" phase in grey). Time point 0 min is equal to the reference steady state. All values indicate means ± standard deviation of three biological replicates.

Appendix D

Appendix D contains the original research articles I − III as a single, non-paginated attachment in the order of appearance in the main text. The publications were downloaded from the according publisher's website as publicly available.

Article

Monitoring Intracellular Metabolite Dynamics in *Saccharomyces cerevisiae* during Industrially Relevant Famine Stimuli

Steven Minden [1], Maria Aniolek [1], Christopher Sarkizi Shams Hajian [1], Attila Teleki [1], Tobias Zerrer [1], Frank Delvigne [2], Walter van Gulik [3], Amit Deshmukh [4], Henk Noorman [4,5] and Ralf Takors [1,*]

[1] Institute of Biochemical Engineering, University of Stuttgart, 70569 Stuttgart, Germany; steven.minden@ibvt.uni-stuttgart.de (S.M.); maria.aniolek@ibvt.uni-stuttgart.de (M.A.); c.sarkizi@ibvt.uni-stuttgart.de (C.S.S.H.); attila.teleki@ibvt.uni-stuttgart.de (A.T.); st163004@stud.uni-stuttgart.de (T.Z.)

[2] Microbial Processes and Interactions (MiPI), TERRA Research and Teaching Centre, Gembloux Agro Bio Tech, University of Liege, 5030 Gembloux, Belgium; f.delvigne@uliege.be

[3] Department of Biotechnology, Delft University of Technology, van der Maasweg 6, 2629 HZ Delft, The Netherlands; w.m.vangulik@tudelft.nl

[4] Royal DSM, 2613 AX Delft, The Netherlands; amit.deshmukh@dsm.com (A.D.); henk.noorman@dsm.com (H.N.)

[5] Department of Biotechnology, Delft University of Technology, 2628 CD Delft, The Netherlands

[*] Correspondence: takors@ibvt.uni-stuttgart.de

Abstract: Carbon limitation is a common feeding strategy in bioprocesses to enable an efficient microbiological conversion of a substrate to a product. However, industrial settings inherently promote mixing insufficiencies, creating zones of famine conditions. Cells frequently traveling through such regions repeatedly experience substrate shortages and respond individually but often with a deteriorated production performance. *A priori* knowledge of the expected strain performance would enable targeted strain, process, and bioreactor engineering for minimizing performance loss. Today, computational fluid dynamics (CFD) coupled to data-driven kinetic models are a promising route for the in silico investigation of the impact of the dynamic environment in the large-scale bioreactor on microbial performance. However, profound wet-lab datasets are needed to cover relevant perturbations on realistic time scales. As a pioneering study, we quantified intracellular metabolome dynamics of *Saccharomyces cerevisiae* following an industrially relevant famine perturbation. Stimulus-response experiments were operated as chemostats with an intermittent feed and high-frequency sampling. Our results reveal that even mild glucose gradients in the range of 100 μmol·L^{-1} impose significant perturbations in adapted and non-adapted yeast cells, altering energy and redox homeostasis. Apparently, yeast sacrifices catabolic reduction charges for the sake of anabolic persistence under acute carbon starvation conditions. After repeated exposure to famine conditions, adapted cells show 2.7% increased maintenance demands.

Keywords: scale-up; scale-down; metabolomics; bioreactor; systems biology; baker's yeast; *Saccharomyces cerevisiae*; stimulus-response experiment; substrate gradient; bioprocess engineering; chemostat

1. Introduction

Microbial catalysis has a pivotal role in realizing the transition from natural resource depletion towards a sustainable and circular economy [1,2]. Key factors underlining this status encompass the use of renewable feedstock, mild reaction conditions, a vast diversity of products and high potential for improving production efficiency and product quality—all benefitting from biological flexibility [3]. Consequently, the European Horizon

2020 program recognizes biotechnology as one of four "Key Enabling Technologies" to maximize the sustainability and growth potential of European companies [4]. A prerequisite, but also one of the greatest challenges, is the successful transfer of lab results into commercial-scale bioreactors without the loss of performance [5–8]. This scale-up is often hampered by intrinsic drawbacks such as mixing insufficiencies, which, ultimately, cause a heterogeneous extracellular environment [9–11]. Numerous factors become increasingly dynamic, causing unexpected biological responses that either reduce the expected TRY (titer, rate and yield) criteria or even reveal a fatal potential for a given process [11,12].

To prevent the occurrence of detrimental scale-up effects, the inclusion of large-scale considerations into early-stage development is gaining more and more recognition in both the industry [13–15] and academic research [16–19]. Especially during substrate limited operation modes such as fed-batch or chemostat, concentration gradients can easily emerge, since volumetric reaction times are often within the same order of magnitude of the mean broth circulation times in an industrial environment [20,21]. Multiple investigations monitored cellular responses upon exposure to industrial conditions, aiming to explain the observed performance losses. Industrial hosts were exposed to substrate heterogeneities, revealing an overflow metabolism [22,23], the disturbance of energy management [24,25] and perturbations of regulatory programs mirrored by metabolomics [26,27], transcriptomics [28,29] and proteomics [30–32]. Even a population heterogeneity was observed [33,34].

How can scale-down experiments be designed to adequately reflect industrial hydrodynamics and reaction dynamics when large-scale data are usually not available? Modern bioprocess development strategies substitute this knowledge gap with simulations based on computational fluid dynamics (CFD) coupled to biokinetic models [6,21,35]. This setup allows integrating exchange rates with the hydrodynamic environment of the bioreactor. More precisely, the exposure of individual microorganisms to substrate gradients can be recorded during all process phases and expressed as lifelines [36]. Currently, this approach reaches considerable agreement with quantitative data on concentration gradients from pilot to industrial scale [37–40]. An adjacent development goal is to increase the predictive power to uncover biological scale-up effects already at the development stage in the lab via data-driven models. Thus, comprehensive *-omics* data for model development are paramount and can, for instance, be provided by stimulus-response experiments (SRE) that capture relevant large-scale dynamics. Figure 1 demonstrates a conceptual workflow with integrated wet- and dry-lab contributions. Ultimately, the generated knowledge allows both the identification of strain engineering targets and the quantitative design of scale-down simulators to replace physical upscaling. A successful archetype for this strategy has recently resulted in the construction of an *E. coli* strain with reduced maintenance energy demands when subjected to industrial glucose gradients [29,41].
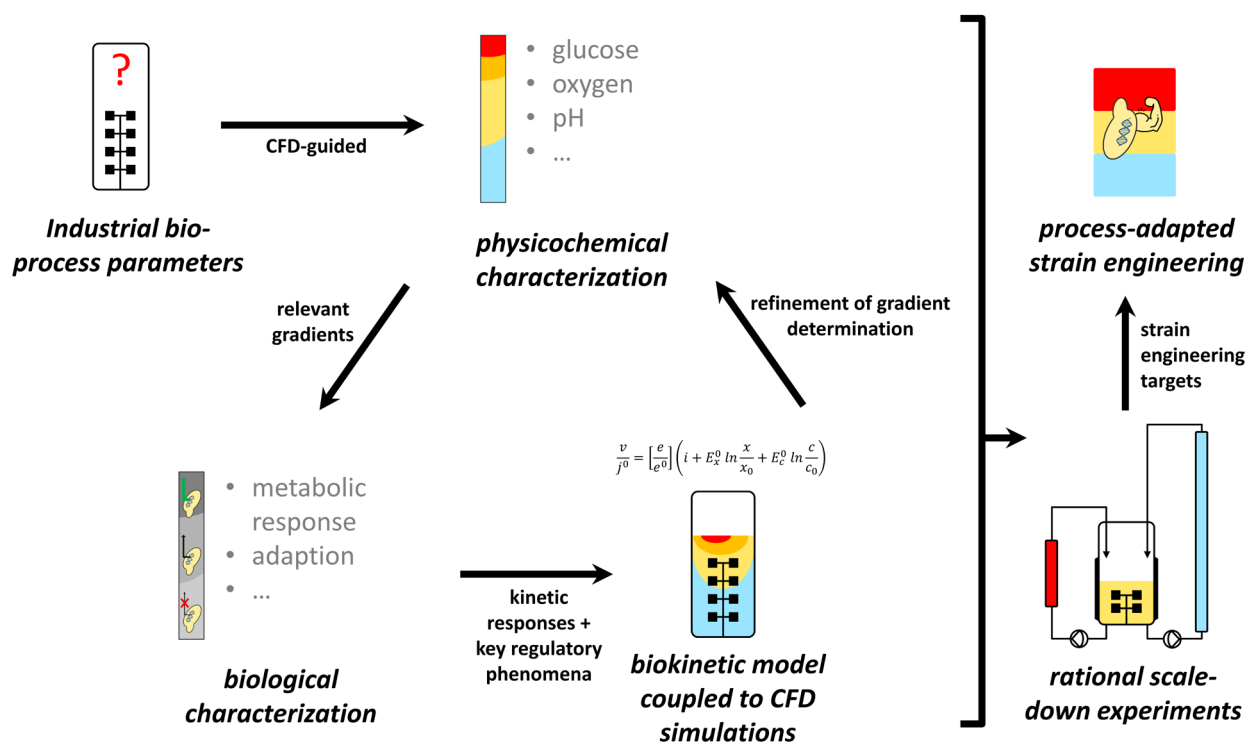
Figure 1. Basic procedure for data-driven scale-up/scale-down development. Concentration gradients are derived from large-scale simulations to design stimulus-response experiments and generate *-omics* datasets. This approach further allows the set-up of biological models to refine large-scale simulations. Ultimately, gained knowledge enables process-adapted strain engineering and the design of realistic scale-down simulators for validation experiments to replace classical scaling-up.

This work is part of a case study with the ambition to deploy the aforementioned rational bioprocess engineering approach for a eukaryotic model organism. *Saccharomyces cerevisiae* was chosen due to its broad prevalence in several sectors of the bioprocessing industry, comprising foods, fuels, chemicals and pharmaceuticals [42,43]. The industrial setting is derived from a 22 m³ research bioreactor operated as a glucose-limited fed-batch process for biomass production, which is thoroughly described in the literature [37,44,45]. Corresponding CFD investigations and large-scale measurements already identified glucose gradients in the range of 23–460 µmol·L⁻¹ [22,38,39]. This distinct concentration spectrum favors the emergence of three metabolic regimes: First, the desired operating point in the glucose-limited state to achieve an optimal biomass conversion. Second, overflow metabolism due to a glucose excess close to the feeding position. Third, starvation regimes far away from the feed, where the glucose uptake cannot satisfy cellular maintenance demands anymore.

The before-mentioned SRE approach represents a proven methodology to provide the necessary ground to set up data-driven models [46–48]. For the organism under investigation, several studies quantitatively investigated the metabolome and transcriptome during a sudden shift from a glucose limitation to excess [26,47,49,50]. To the best of our knowledge, the current state of the literature is missing complementary data for the opposing transition between limitation and starvation. This study, therefore, set out to close this gap of knowledge, beginning on the metabolic level. On the one hand, quantitative endometabolomic measurements provide a sound database for a more detailed model development. On the other hand, the interpretation of the dataset uncovers biological mechanisms that can lead to strain performance losses for different production scenarios and guide large-scale adapted strain engineering.

2. Results

2.1. Hyperbolic Kinetics Overestimate Starvation Regimes in Industrial-Scale Simulations

Figure 2a presents 24 min of a three-hour single-cell lifeline mimicking the late stage of an industrial baker's yeast production scenario. The simulation suggests that cells resided only 39% of the time in the favored glucose limitation regime, delivering the planned substrate supply for growth and maintenance. Moreover, overflow regimes occurred, lasting for 1–10 s and making up 3% of the lifeline. However, for 58% of the lifeline, the yeast trajectory was subject to severe starvation conditions, which caused the famine status to be the normality rather than the exception.

To mimic the dominant role of glucose starvation, we exposed yeast cells to famine conditions (Figure 2b). In the glucose depletion experiment, minimal glucose levels of 22 $\mu mol \cdot L^{-1}$ were found after the feed was stopped for 2 min. Interestingly, simulations using the kinetic parameters of Figure 2a predicted residual glucose levels well below 10 $\mu mol \cdot L^{-1}$. However, the semilogarithmic slope of the experimental limitation-starvation transition in Figure 2b was only 0.44 s^{-1}, which accounted for 60% of the anticipated kinetics (0.71 s^{-1}). Apparently, additional impacts occurred that hampered the one-by-one application of the stated hyperbolic uptake kinetic for the short-term starvation.

Nevertheless, it was concluded that cellular exposure to famine conditions was a dominating scenario in large-scale bioreactors. Accordingly, follow-up studies considered 2 min starvation intervals that allowed the investigation of endo-metabolite dynamics for two scenarios: (i) a single limitation–starvation–limitation (LSL) cycle revealing the non-adapted cellular response and (ii) a representative LSL cycle from an adapted culture.
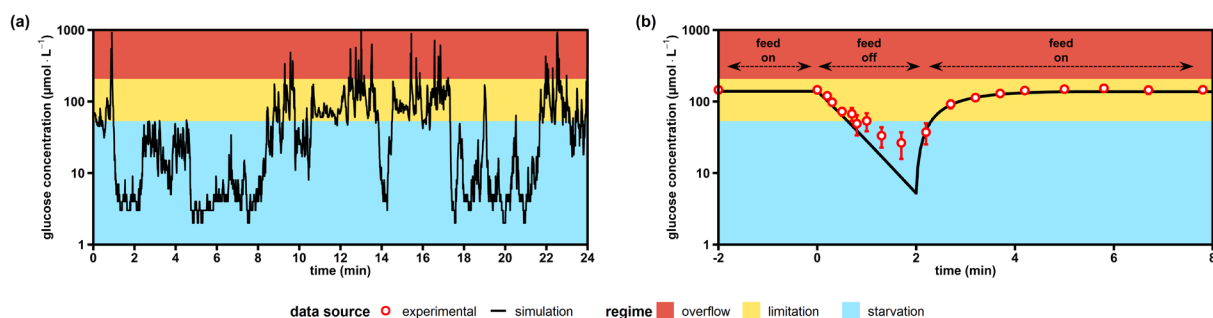
Figure 2. Simulated versus experimental glucose profiles experienced by yeast cells. (**a**) Exemplary lifeline of a single *Saccharomyces cerevisiae* trajectory recorded over 24 min during an industrial glucose-limited fed-batch process with a biomass concentration of 10 $g \cdot L^{-1}$. The lifeline was simulated during the work of Sarkizi et al. [39], but not published. (**b**) Stimulus-response experiment as a glucose-limited chemostat with intermittent feed (this work). Extracellular glucose levels are the means ± standard deviation of six biological replicates (merged trends from adapted and non-adapted time series). All simulated values were computed using published glucose uptake kinetics [51]. Overflow metabolism was assumed to start at glucose concentrations >207 $\mu mol \cdot L^{-1}$ [52] and starvation zones developed below 53 $\mu mol \cdot L^{-1}$, where maintenance demands could not be covered anymore [53].

2.2. Process and Phenotypic Characterization

The haploid *S. cerevisiae* strain CEN.PK 113-7D was cultivated in glucose-limited, aerobic chemostats in biological triplicates, each carried out with a dilution rate of 0.1 h^{-1}. Three experimental phases were investigated: (i) The first period operated stably for five residence times serving as the reference steady state (RS). (ii) Then, the feed was inactivated once for 120 s to install starvation conditions. Subsequently, previous feeds were reinstalled and the post-starvation response was tracked for 360 min. (iii) During the third phase, a periodic feed regimen with cycles of 2 min starvation and 7 min limitation was implemented, operating for five residence times to establish a new steady state after dynamic stimuli (DS).

Table 1 lists recoveries of carbon, nitrogen and available electrons (*ave*) for steady-state RS, samples after the first LSL cycle and for steady-state DS. Notably, all balances closed within 100 ± 5%. Except for minor amounts of trehalose and glycerol (data not shown), no by-product formation was detected, which agreed with similar studies using CEN.PK 113 7D [54,55]. Only acetic acid formation was reported under reference conditions [55], which did not occur in our study. The carbon balance of the '30 min post-stimulus' sample was the only significant deviation from the reference steady state (*p*-value < 0.05). In this phase, respiratory dynamics (see Section 2.3) estimated by the mathematical off-gas deconvolution method might have caused a measurement error, since both the CO_2-dependent carbon and O_2-dependent *ave* recoveries were affected by the same increase.

Table 1. Process balances at sample points relevant for this study.

Sample Point	Carbon Recovery (% ± s.d.)	Nitrogen Recovery (% ± s.d.)	Available Electron Recovery (% ± s.d.)
Steady-state RS	98.8 ± 0.7	102.5 ± 6.5	97.5 ± 0.7
30 min post-stimulus	102.2 ± 1.2	102.8 ± 6.6	100.2 ± 1.2
60 min post-stimulus	97.2 ± 0.6	99.0 ± 3.5	96.4 ± 0.6
120 min post-stimulus	98.6 ± 0.9	98.9 ± 3.5	97.4 ± 0.9
180 min post-stimulus	98.3 ± 0.8	98.9 ± 3.6	97.2 ± 1.0
240 min post-stimulus	98.4 ± 0.5	98.9 ± 3.6	97.3 ± 0.5
360 min post-stimulus	99.0 ± 0.6	101.2 ± 4.6	97.8 ± 0.7
Steady-state DS	100.7 ± 0.7	101.0 ± 7.8	99.1 ± 1.0

All percentages express means ± standard deviation (s.d.) of three biological replicates. RS, reference steady state; DS, dynamic steady state.

The phenotypic characterizations of the steady states RS and DS are presented in Table 2. Prominent differences were observed for biomass-specific oxygen demands and carbon dioxide emissions in DS, each rising by 4.3%. Although $Y_{DMB/glucose}$ and the glucose uptake rate ($q_{glucose}$) remained unchanged in RS and DS, changes in the oxygen uptake and carbon dioxide release pointed towards metabolic rearrangements. Furthermore, the adapted cells of DS appeared to possess a superior cellular integrity, since the leakage of unknown carbon was reduced by 13.4%, which is an indicator for cell lysis [56].

Summarizing, the comparison of steady-state phenotypes hinted to elevated ATP needs at DS that were mirrored by an increased oxygen uptake and carbon dioxide formation rates. Consequently, time-resolved studies were performed to uncover underlying mechanisms.

Table 2. Yeast kinetics at the steady states RS (reference) and DS (after dynamic perturbation).

Parameter	Dimension	Steady-State RS	Steady-State DS	Change (%)	Welch Test (*p*-Value)
D	h^{-1}	0.101 ± 0.001	0.100 ± 0.002	n.s.	>0.05
$Y_{DMB/glucose}$	$g_{DMB} \cdot g_{glucose}^{-1}$	0.494 ± 0.005	0.498 ± 0.002	n.s.	>0.05
$-q_{glucose}$	$mmol \cdot g_{DMB}^{-1} \cdot h^{-1}$	1.13 ± 0.01	1.12 ± 0.02 *	n.s.	>0.05
$-q_{oxygen}$	$mmol \cdot g_{DMB}^{-1} \cdot h^{-1}$	2.52 ± 0.01	2.63 ± 0.04 *	+4.3	0.03
$q_{carbon\ dioxide}$	$mmol \cdot g_{DMB}^{-1} \cdot h^{-1}$	2.71 ± 0.02	2.83 ± 0.04 *	+4.3	0.02
$Y_{oxygen/glucose}$	$mol \cdot mol^{-1}$	2.23 ± 0.03	2.34 ± 0.03 *	+4.9	0.02
$-q_{ammonia}$	$mmol \cdot g_{DMB}^{-1} \cdot h^{-1}$	0.86 ± 0.04	0.94 ± 0.07 *	n.s.	>0.05
$q_{other\ carbon}$	$mmolc \cdot g_{DMB}^{-1} \cdot h^{-1}$	0.140 ± 0.008	0.121 ± 0.003	−13.4	0.04

All values represent means ± standard deviation of three biological replicates. Values marked with an asterisk indicate an averaged parameter over one 9 min perturbation cycle. *DMB*, dry matter of biomass; RS, reference steady state; DS, dynamic steady state; n.s., not significant.

2.3. Short-Term Metabolome Relaxation Requires 7 min after Glucose Repletion

　　　Metric multidimensional scaling (MDS) plots of the quantified intracellular metabolome and respiratory activity were used as proxy variables to visualize the relaxation pattern of intracellular dynamics in non-adapted and adapted cells. By trend, Figure 3a resembles a spiral-type trajectory of metabolite levels converging to the '9 min' spot. Remarkably, late time points 240 and 360 min did not approximate the reference steady state (0.00 min). This result was rather unexpected, since the maximum turnover times for the reported metabolites were in the range of 1×10^{0}–1×10^{2} s [57] and, thus, two orders of magnitude shorter than the observed time window. Instead, the observation may be taken as a hint on the flexibility of the metabolome, enabling similar growth phenotypes with different compositions of intracellular metabolite patterns. Further evidence was provided later. Maybe even more surprising was the continuing phenotype dynamics of the oxygen uptake and CO_2 formation during 10–60 min (Figure 3c), although the metabolome seemed to have already relaxed after converging to the 'attractor' point of the 9 min sample. Together, these results unraveled the existence of a first, immediate response to a glucose shortage lasting for about 9 min, and a second, less pronounced dynamic between 10 and 60 min.
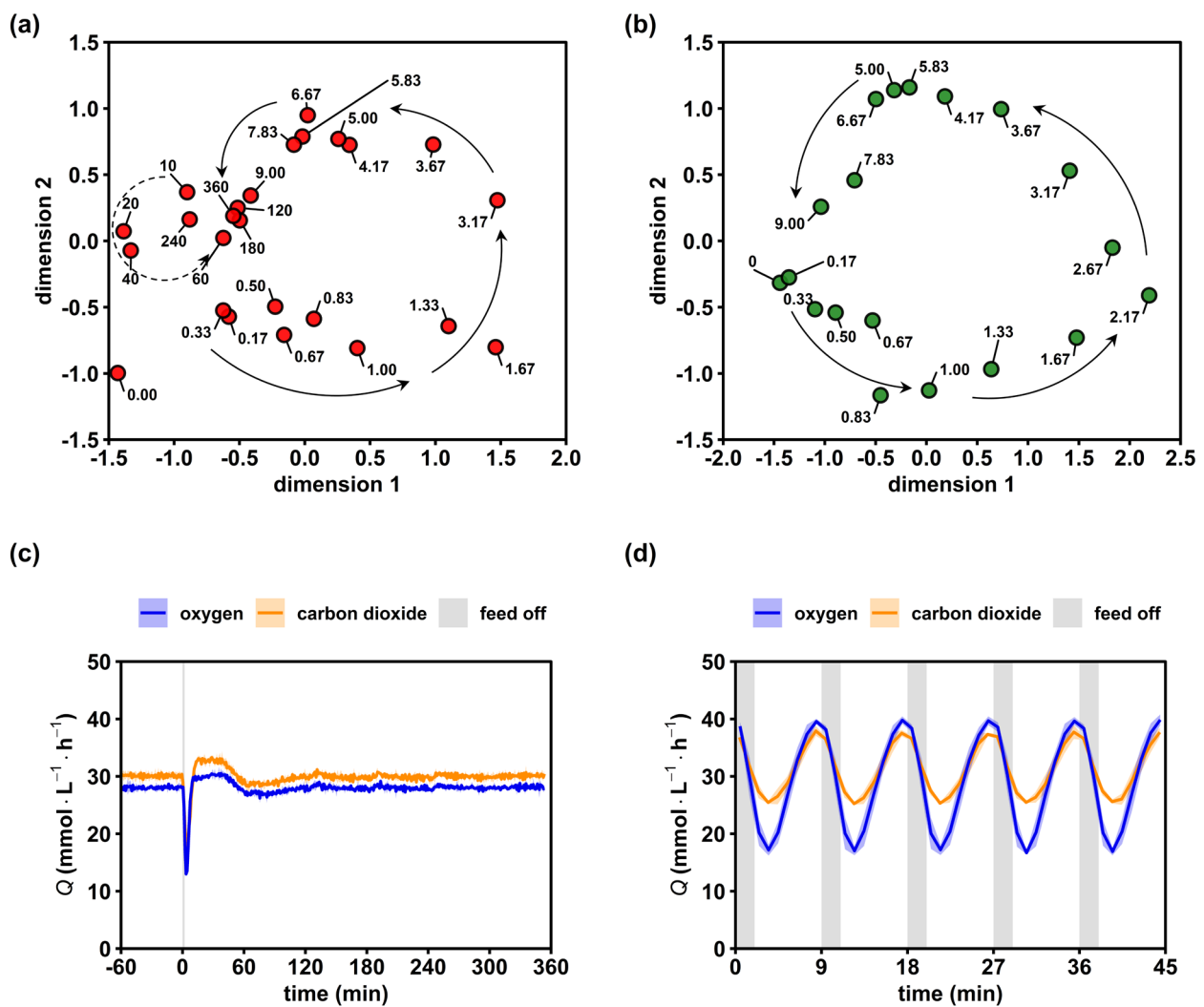
Figure 3. Relaxation of the intracellular metabolome and respiratory activity. (**a**) Multidimensional scaling (MDS) plot of the non-adapted (red) 6 h time series based on min–max normalized concentrations of 28 intracellular metabolites. Arrows provide a visual aid to follow the short-term (solid) and mid-term (dashed) dynamics. (**b**) Analogous MDS plot of the adapted (green) 9 min time series. (**c**) Evolutions of the oxygen and carbon dioxide transfer rates after a single starvation transition. (**d**)

Analogous off gas analysis over 5 perturbation cycles during the dynamic steady state. Text labels in (**a**,**b**) represent the sample time in minutes. Blue and orange lines in (**c**,**d**) represent the mean and light areas represent the respective standard deviation of three biological replicates.

For investigating the adapted response, the final metabolite cycle (Figure 3b) after multiple stimulations was expressed in the MDS space. Other than the non-adapted response, we observed no spiral but rather a circular 9 min trajectory without a distinct convergence. This reflected the dynamics in the off-gas analysis (Figure 3d), showing highly repeatable amplitudes of Q_{oxygen} and $Q_{carbon\ dioxide}$ with 22.8 ± 0.3 mmol·L^{-1}·h^{-1} and 12.3 ± 0.2 mmol·L^{-1}·h^{-1}, respectively. Notably, off-gas dynamics were always observed in biological triplicates lasting for more than 10 cycles (only 5 were shown). The high reproducibility of the phenotype gave rise to the assumption that the metabolite cycles of Figure 3b equally repeated in the perturbation series.

Summarizing, results indicated that an observation window of nine minutes covered the first, immediate cellular response on the glucose shortage. Differences between the adapted and non-adapted cell response existed that may have been elucidated by the analysis of intracellular metabolite dynamics.

2.4. Short-Term Dynamics of the Central Catabolism upon Glucose Depletion

To elucidate the phenotypic differences shown by non-adapted and adapted cells after exposure to a glucose limitation, we investigated the time course of selected intracellular metabolites involved in the glucose catabolism (Figure 4).

The central upper glycolysis metabolites glucose-6-phosphate (G6P) and the merged glucose-1-phosphate/fructose-6-phosphate pool (Hex6P) both qualitatively followed the extracellular availability of glucose, irrespective of the cellular adaption status. However, a slight overshooting of about 29% occurred in adapted cells (green) for the minimum and maximum G6P compared to the extracellular glucose amplitudes (*p*-value < 0.05). The hexokinase reaction was feedback-inhibited by trehalose-6-phosphate (T6P) [58,59] and indeed, on average, the T6P pool decreased by 52% in the adapted yeast population, possibly resulting in reduced control over the hexokinase activity. Furthermore, a sharp rise of T6P coincided with peaking G6P levels. Apparently, large G6P pools triggered the carbon drain into the storage compound trehalose via T6P. Interestingly, the total levels of the carbon storage buffers trehalose and glycogen were reduced in adapted versus non-adapted cells by 43% and 49%, respectively. As these pool sizes are reported to correlate inversely with the growth rate [60,61], which was kept constant in the experimental series, the finding was unexpected. Assuming a carbon ratio of 0.04 mol$_C$·g$_{DMB}$$^{-1}$ [62], the reduction in the carbohydrate pools should account for a 4% drop in $Y_{DMB/glucose}$. Because the latter was not observed (Table 2), we assumed that the substantial metabolic re-arrangement should have occurred in adapted cells. Further hints were provided by the elevated average concentrations of UDP-glucose (+31%) in adapted cells. UDP-glucose not only links glycolysis with the carbohydrate storage pools, but plays a key role in the anabolism of structural components such as cellulose, β-glucan, glycolipids and glycoproteins [63]. Consequently, increased UDP-glucose levels may reflect the observed increase in the cellular integrity (Table 2) of adapted cells.

Regarding the short-term dynamics of the intermediates of the pentose phosphate pathway (PPP), two phases could be observed. Interestingly, they were similar for adapted and non-adapted cells. During the first 2 min of nascent glucose depletion, the trends of 6-phosphogluconic acid (6PGA) and the merged pool of ribose-5-phosphate and ribulose-5-phosphate (P5P) followed the extracellular glucose availability. Then, the recovery to initial pool sizes was delayed and somewhat disconnected from the external glucose supply. The observation agreed with findings of Theobald et al. and Suarez-Mendez et al., who applied glucose pulse experiments [49,50]. They hypothesized a dominating glycolytic flux control over PPP, a conclusion that was complemented by additional cofactor and sink reaction measurements presented and discussed in Figures 5 and 6a.

Similar trends of delayed recovery were also observed for fructose-1,6-bisphosphate (FBP). Phosphofructokinase (PFK) delivering FBP is well known to be inhibited by ATP and citrate (CIT) and activated by ADP, AMP, F6P and fructose-2,6-bisphosphate (F2,6BP, not quantified) [64,65]. Noteworthy are the in vitro and in vivo studies by van den Brink et al., revealing that metabolic regulations of PFK may be superimposed by upshifting glycolytic fluxes if energy homeostasis is impaired [66]. The latter likely occurred during the first 2 min of the experiments (see Figure 6a).

Further down in glycolysis, pools of 2- and 3-phosphoglycerate (2/3PG) and phosphoenolpyruvic acid (PEP) showed surprisingly few perturbations irrespective of whether non-adapted or adapted cells were studied. Either related metabolite consumption completely stopped or compensating fluxes occurred. Given the fast turnover rates of the stated pools typically ranged in seconds, the latter is the likely explanation. Further considering that trehalose and glycogen pool sizes persisted even during the first 2 min of nascent starvation, the start of gluconeogenesis is a plausible scenario. Pyruvate kinase (PKY) converting PEP + ADP into PYR + ATP is well known to be activated by FBP, which, interestingly enough, dropped severely by 61% from 0.36 ± 0.10 µmol·g_{DMB}^{-1} to 0.14 ± 0.02 µmol·g_{DMB}^{-1}. Because of the missing downwards flux, gluconeogenesis was induced [67], causing stable upstream pool sizes.

In the tricarboxylic acid cycle (TCA), intermediates showed similar trends in all conditions. The merged pool of citric acid (CIT) and isocitric acid (ISOCIT) kept constant, whereas the downstream intermediate α-ketoglutaric acid (αKG) mirrored the extracellular glucose shortness of the first 2 min, followed by a delayed recovery. This trend was visible in all subsequent TCA metabolites, although dampened with an increasing reaction distance to αKG. This finding was in agreement with earlier studies of Mashego et al., who performed glucose pulse experiments, observing stronger perturbation dynamics for αKG than for CIT [47]. Presumably, the trends reflect the mitochondrial export of αKG into the cytosol for oxidative nitrogen fixation in glutamic acid [68]. Unfortunately, no dynamic glutamic acid measurements were available in this study.

Taken together, LSL perturbations were propagated on separating time scales through the central metabolic nodes of *S. cerevisiae*. Moreover, the adaption status was most visible in the pool sizes of carbon storage buffers.
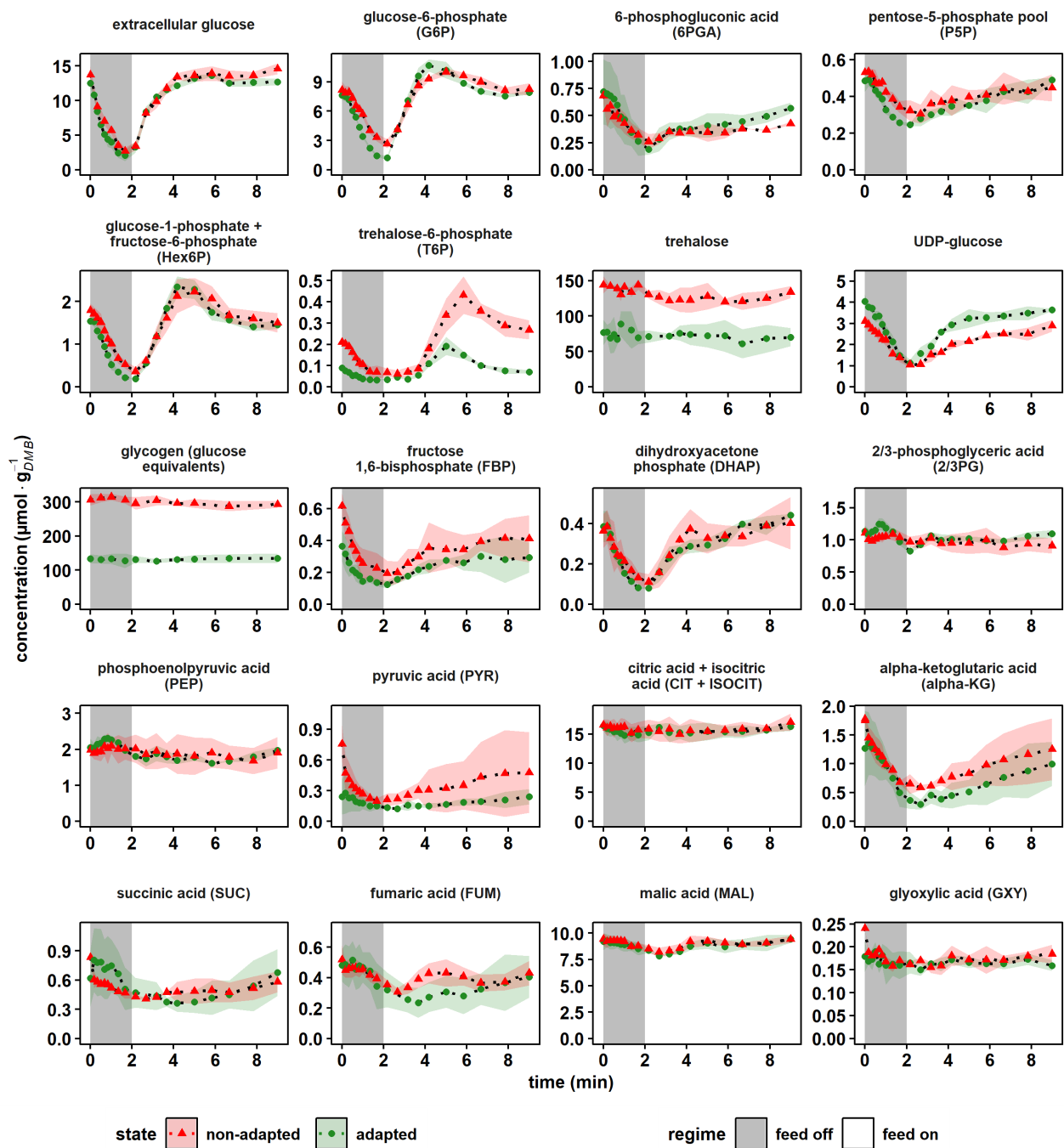
Figure 4. Dynamics of central catabolic metabolites after a 2 min glucose depletion phase. The non-adapted response (red) indicates dynamics following a single transition into a starvation scenario ("feed off" phase) and the adapted response (green) was sampled from representative 9 min cycles during steady-state DS. Time point 0 min of the non-adapted response was equal to steady-state RS. All values indicate means ± standard deviation of three biological replicates.

2.5. Analysis of Anabolic and Catabolic Reduction Equivalents

The dynamics of the nicotinamide electron carriers are depicted in Figure 5. The upper panel indicates individual concentrations of the anabolic redox pair NADP+, NADPH, their sum and their ratio. By analogy, the catabolic redox state is indicated in the second row.

Regarding anabolic reduction, the total pool size of 0.36 ± 0.00 µmol·g_{DMB}^{-1} and the reductive ratio of 1.28 ± 0.01 measured at reference conditions agreed with literature values for CEN.PK113-7D, which were observed in glucose-limited chemostat at $D = 0.1$ h^{-1} as 0.25–2.17 µmol·g_{DMB}^{-1} and 0.29–4.86, respectively [69]. By trend, NADP$^+$ pool sizes dropped during glucose depletion, both for adapted and non-adapted cells, which led to rising anabolic reduction charges.

In contrast, NAD$^+$ concentrations remained virtually unchanged during glucose depletion, whereas NADH levels decreased. Interestingly, in the non-adapted scenario, the recovery of the NADH pool was not observed within the 9 min time window, but in the adapted case, full relaxation was reached after 5 min. However, NADH levelled out at 0.10 ± 0.01 µmol·g_{DMB}^{-1}, which was 43 % less than the reference state at 0.17 ± 0.03 µmol·g_{DMB}^{-1}. The lumped pool size remained stable during the perturbation, since only NADH showed dynamics, which only accounted for approximately 4 % of the total pool size. Literature values for the catabolic reduction charge under comparable steady-state conditions ranged from 0.05 to 0.2 [50,70,71], which was somewhat larger than the reference value of 0.046 ± 0.009 measured for the non-adapted yeast. The observation mirrored the twofold increased NAD$^+$ concentrations of this study work versus the respective levels in the cited studies that yielded ratios above 0.1.

Summarizing, the results indicated opposite trends during nascent glucose starvation: while the anabolic reduction state rose, the catabolic dropped. Or, in other words, NADPH and NAD$^+$ levels persisted, whereas NADP$^+$ and NADH pool sizes dropped.
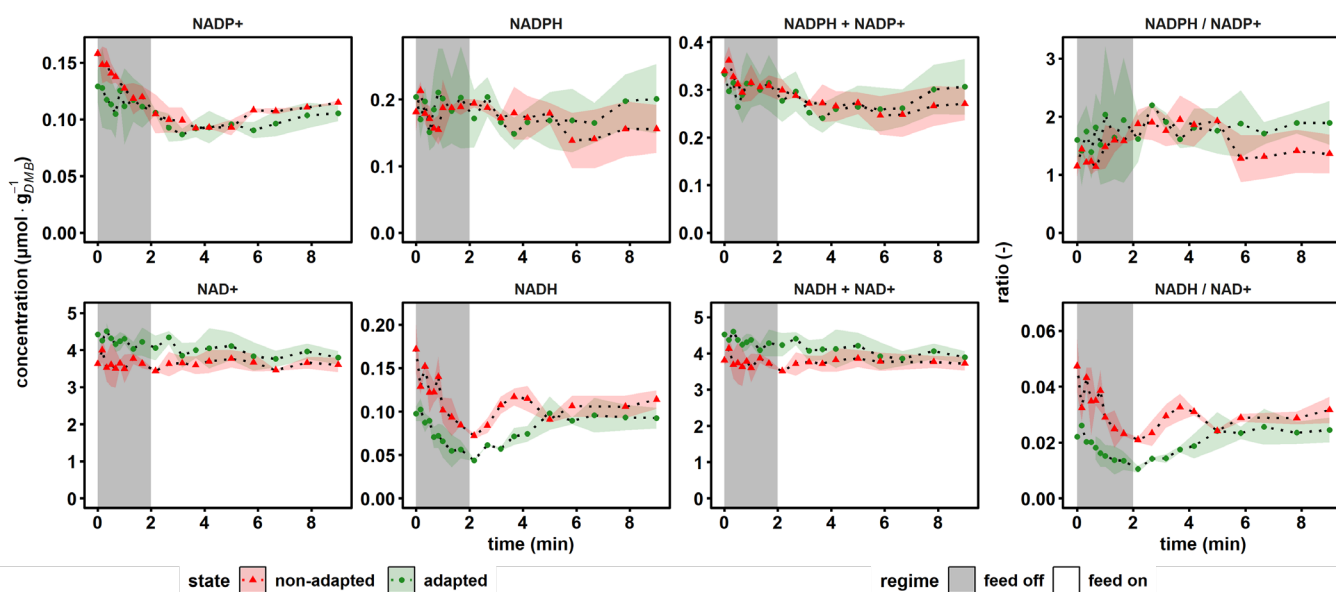
Figure 5. Dynamics of the reduction equivalents, conserved moieties and according to ratios. The non-adapted response (red) indicates dynamics following a single transition into a starvation scenario ("feed off" phase) and the adapted response (green) was sampled from representative 9 min cycles during steady-state RS. Time point 0 min of the non-adapted response was equal to steady-state RS. All values indicate means ± standard deviation of three biological replicates (except for the non-adapted time series, which was derived from two biological replicates).

2.6. The Adenylate Energy Charge Is Quickly Regenerated at the Cost of Total Adenylate Pool Size

Energy carrier homeostasis and nucleotide resource management during dynamic glucose availability were monitored via adenylate and selected purine salvage pathway (PSP) intermediates (Figure 6a). The adenylate energy charge (*AEC*) was calculated based on the original approach from Atkinson et al. [72]. The ATP concentration decreased from 8.12 ± 0.72 µmol·g_{DMB}^{-1} to 3.56 ± 0.16 µmol·g_{DMB}^{-1} and from 5.63 ± 1.54 µmol·g_{DMB}^{-1} to 1.60 ± 0.61 µmol·g_{DMB}^{-1} within 120 s in the non-adapted and adapted scenarios, respectively. In the same interval, AMP displayed a sharp 3.9-fold (non-adapted) and 6.6-fold (adapted) peak, while ADP first dropped before rising after 30 s with a maximum coinciding with that of AMP. Adenylate energy charges of non-adapted and adapted yeasts showed physiological values of about 0.90 ± 0.03, which dropped during glucose starvation before recovering again to the initial value. Interestingly, the drop of *AEC* was more pronounced in adapted cells. However, both cells had in common that total AxP pools reduced during glucose starvation and did not fully replenish during the post-starvation period. Apparently, physiological *AEC* values of about 0.9 observed after famine exposure were achieved at the cost of ADP pools that did not recover to the prestarvation values.

Remarkably, the similar phenotype of the *AEC* adjustment at the cost of AxP reduction was reported in glucose pulse studies [26,46,47,73]. Kresnowati et al. and Walther et al. hypothesized that nucleotide salvage mechanisms may explain the underlying mechanism of the observation. Adenine nucleotides were shuttled into the PSP via the AMP deaminase (AMD1) reaction yielding inosine monophosphate (IMP), the central intermediate for both, de novo and salvage pathways of purines (Figure 6b). At this branch point, IMP could either (i) enter a futile cycle where AMP is regenerated at the expense of GTP and aspartate, yielding GDP and fumarate; (ii) be interconverted via inosine (INO) to hypoxanthine (HYX) back to IMP at the expense of ribose-1-phosphate (R1P) and phosphoribosyl pyrophosphate (PRPP) or (iii) be shuttled towards the guanine salvage branch catalyzed by the NAD$^+$-dependent IMP dehydrogenase (IMD2,3,4) [73]. Surprisingly, the pattern of IMP under famine conditions resembled the oscillatory behavior of ADP rather than that of the IMP precursor AMP. The IMP levels displayed a second decline phase after 1 min, coinciding with strongly increasing inosine and hypoxanthine levels. The latter accumulated to their maximum concentrations about 1 min later than AMP, their common upstream intermediate. Interestingly, INO pools of non-adapted cells remained 1.6-fold elevated compared to the prestarvation condition. This may be interpreted as a 'memory' effect that was not shown by adapted cells.
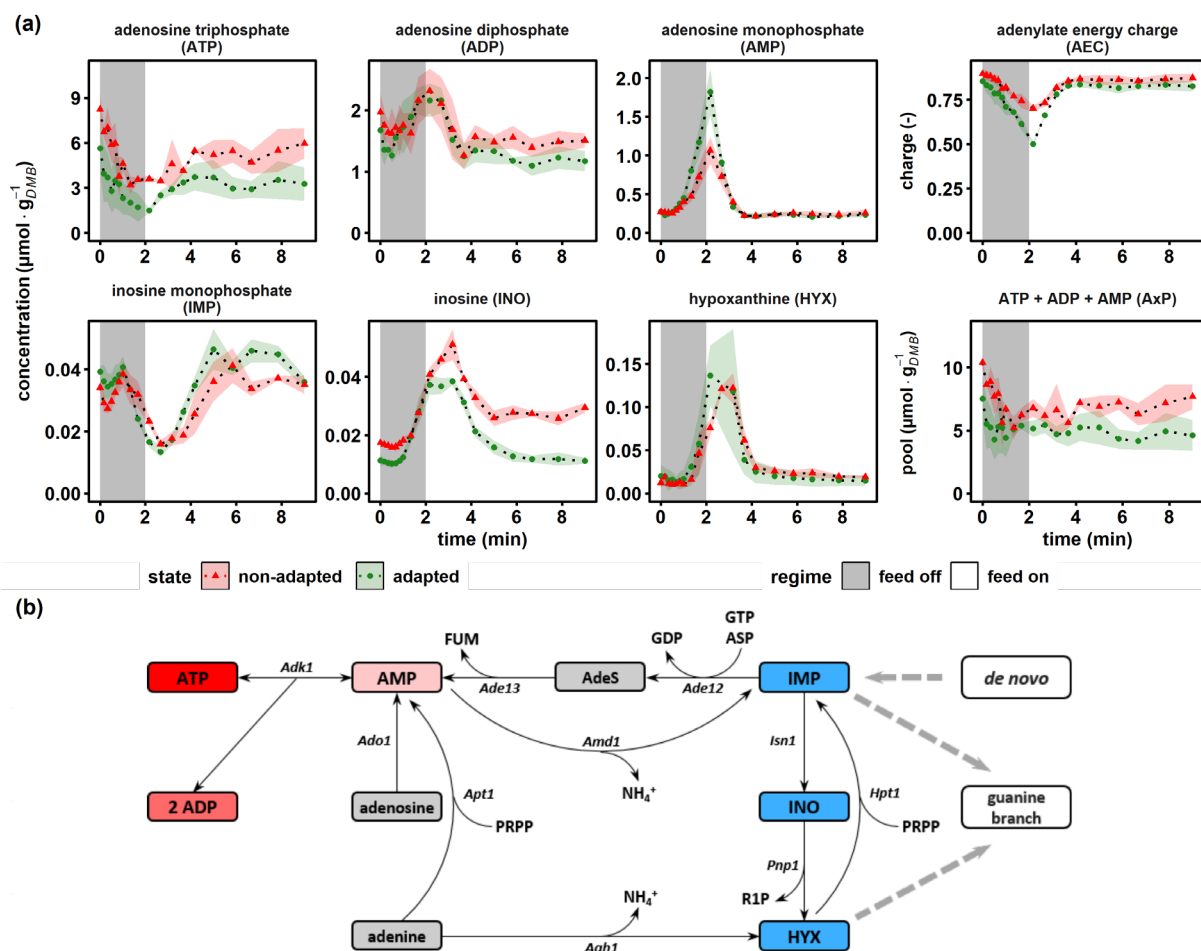
Figure 6. Dynamics of energy carriers and intermediates of the purine salvage pathway. (**a**) The non-adapted response (red) indicates dynamics following a single transition into a starvation scenario ("feed off" phase) and the adapted response (green) was sampled from representative 9 min cycles during steady-state DS. Time point 0 min of the non-adapted response was equal to steady-state RS. The adenylate energy charge was calculated according to [72]. All values indicate means ± standard deviation of three biological replicates. (**b**) Schematic representation of the adenylate kinase system attached to the purine salvage pathway, reproduced from [73,74]. *Aah1*, adenine deaminase; *Ade12*, adenylosuccinate synthase; *Ade13*, adenylosuccinate lyase; AdeS, adenylosuccinate; *Adk1*, adenylate kinase; *Ado1*, adenosine kinase; *Amd1*, AMP deaminase; *Apt1*, adenine phosphoribosyl transferase; ASP, aspartate; FUM, fumarate; *Hpt1*, hypoxanthine-guanine phosphoribosyl transferase; *Isn1*, IMP-specific 50-nucleotidase; *Pnp1*, purine nucleoside phosphorylase; PRPP, phosphoribosyl pyrophosphate; R1P, ribose-1-phosphate.

3. Discussion

3.1. Decreased Glucose Uptake Kinetics

Several reports have shown that a variable substrate availability is a fundamental scale-up effect causing observed strain performance losses in industrial fed-batch processes [22,23,45,75]. The investigated case of glucose limited *S. cerevisiae* CEN.PK113-7D exemplified the cellular responses at $\mu = 0.1$ h^{-1} when the substrate concentration c_S was 10-fold lower than the affinity constant K_M of the most efficient hexose transporters HXT6 and HXT7 [51,76]. If $c_S \ll K_M$, the glucose uptake kinetics are proportional to extracellular concentrations [77], which may explain the observed deviation between predictions based on hyperbolic kinetics and the experimental observation in our study (Figure 2) and in other works [50]. This discrepancy could be attributed to the presence of a secondary source of extracellular glucose in the form of exported trehalose. The disaccharide is hydrolyzed in the extracellular space by the free acid trehalase Ath1, which has an optimum

at the operated pH of 5.0 [78]. Comparable fermentation studies investigating ¹³C labeling patterns traced the presence of unlabeled glucose to trehalose breakdown. Furthermore, there are several other theoretical indications to consider, such as the decoupled glucose uptake and sensing [79] or the inhibition of the glucose uptake by intracellular glucose [80] concomitant with glucose secretion due to the reversibility of facilitated diffusion [81]. Thus, several aspects of glucose transport and even additional source reactions must be considered for optimal glucose characterization at the boundary of starvation, as they can play an important role in computing realistic large-scale simulations.

3.2. Exposure to Starvation Revealed Different Tactics of Reserve Management

Macroscopic observations indicated the emergence of a new growth phenotype of adapted cells compared to non-adapted cells. The first managed to maintain the same biomass/substrate yield, while the respiratory activity rose and carbon storage pools remained on a lower, but constant, level. Given that carbon dioxide emission rates of adapted cells increased by about 4.3% while the glucose uptake rates kept constant, one may anticipate a likewise dip of $Y_{DMB/glucose}$ that did not occur. Therefore, the cells should have found alternative resource allocation possibilities targeting proteins. The hypothesis was consistent with strongly reduced amino acid pools (Table A2) and an observed 9 % increase in the ammonia uptake rate during the dynamic steady state (Table 2). In general, the rearrangement of the cellular composition is a fundamental strategy of *S. cerevisiae* to adjust to new environmental conditions through balancing growth against maintenance [82]. Fast growth, for instance, is accompanied by high ribosomal contents tapping into storage carbohydrates to ensure anabolic needs [83,84]. A similar cellular strategy was revealed in the current study, most likely to support the increased maintenance demands rather than to elevate growth. Indeed, estimating q_{ATP} assuming a P/O ratio of 1.08 yielded a significant 2.7 % increased ATP demand in adapted cells [85].

Considering intracellular metabolite pool sizes, differences between the adapted and non-adapted states mirrored the adaptation of the yeast to cultivation conditions. Prolonged carbon-limited chemostat cultivations by Mashego and Jansen et al. [86,87] already revealed decreasing pool sizes of maximum 20 % after 10 generations that were interpreted as the consequence of selection pressure. The present study also encompassed approximately 10 generations between steady states RS and DS. Consequently, minor pool size reductions <20% should be ignored to separate the effects of long-term growth selection from the results of metabolic rearrangement because of the dynamic stimuli. Still, key findings outlined above should be valid. For instance, trehalose and glycogen pool reductions were likely to be a consequence of the repeated exposure to famine conditions. This made sense from an economic point of view, given the relatively high contribution of both pools towards ATP dissipation via futile cycling [55]. Other evidence towards a more energy-saving mode in adapted cells was derived from the twofold increased AMP peak compared to the non-adapted yeast. High AMP levels activate the PFK enzyme while simultaneously inhibiting the reverse reaction catalyzed by FBP and, consequentially, further reduce ATP dissipation in the F6P–FBP futile cycle [88]. Hence, during adaption, the non-growth-associated ATP usage appeared to be increased and rebalanced for supporting other maintenance components than energy buffering.

There remains the question of which relationship elicited the emerging new phenotype when the same net rates of growth and substrate uptake prevailed. As mentioned earlier, glucose uptake and sensing are decoupled processes in *S. cerevisiae* [79]. Zaman et al. characterized the transcriptional response of conditional mutants against different glucose sensing scenarios. The authors concluded that extracellular glucose sensing could indeed induce strong phenotypic changes, while the same net influx of glucose prevails [89]. Whether the decoupled substrate uptake and sensing explain the present observation should be addressed in future research to fully understand the regulatory mechanisms that shape the industrial phenotype.

3.3. The Cellular Strategy to Ensure Anabolic Demands

The concentration profiles of most intermediates of the upper glycolysis and tightly linked metabolites followed the decline in extracellular glucose levels. However, during the transition from starvation back to the new steady state, time scales of pool relaxation were partially decoupled from glucose availability. The differences of recovery dynamics reflected different flux patterns that apparently mimicked cellular needs. For instance, the PPP reached pre-perturbation levels 4 min later than its precursor G6P. Considering that steady-state glycolytic flux was about 20-fold larger than the branching flux into PPP [55], its pools needed longer to recover. Apparently, this reflected the cellular program to prioritize catabolic over anabolic activity. Saliola and colleagues reported that most eukaryotic G6P dehydrogenases (*Zwf1* in *S. cerevisiae*) possess both a catalytic binding site for NADP+ and an allosteric binding site for NADPH [90]. This allows the cell to drain fluxes towards glycolytic catabolism, thereby gaining ATP either via *Zwf1* inhibition under NADPH excess or via NADP+ limitation. Apparently, the second occurred during the SRE experiments.

Interestingly, neither trehalose nor glycogen pools were degraded during the short-term exposure to glucose starvation. This was in line with previous observations, where short-term glucose perturbations on the same time scale did not change glycogen [27,91] or trehalose concentrations [27], even though rapid trehalose mobilization is anticipated in the literature [92]. This disagreement may be explained as follows: cytosolic trehalase is dependent on activation via a cAMP-dependent prost-translational modification (PTM) cascade yielding its phosphorylation [92]. However, the adenylate cyclase *Cyr1* in CEN.PK113-7D carries a mutation that causes a delay in trehalose and glycogen mobilization [93]. Consequentially, the short-term persistence of glycogen and trehalose pools may be a distinct feature of the current strain, and may be different in other genotypes that were not selected after growth evolution.

Intracellular metabolite dynamics were less pronounced in lower glycolysis and in TCA. In some cases, a high variance additionally hindered a statistically sound interpretation (e.g., for PYR). However, the quick reduction in the catabolic reduction charge under famine conditions might be the consequence of a reduced flux into the TCA, since the onset of gluconeogenesis was observed. In essence, reactions generating NADH, such as oxoglutarate decarboxylase (OGDC), isocitrate (IDH) and malate dehydrogenases (MDH), were reduced. With the missing influx, pools of αKG reduced quickly, indicating that the drain into amino acid synthesis and the production of glutamate remained. Notably, αKG may be regarded as an alarmone, being at the intersection of oxidative carbon and nitrogen metabolism. The reductive amination to form glutamate is tightly controlled by the redox status of the NADP+/NADPH couple [94]. Considering the rising NADPH/NADP+ ratio (Figure 5), glutamate formation was likely to continue even during famine conditions. Together with the observation of falling NADH/NAD+ ratios, the conclusion could be drawn that the yeast favored anabolism for the sake of catabolism under short-term carbon starvation.

Ultimately, decreasing catabolic reduction power impaired energy homeostasis due to an imbalance in the electron transport chain. With reducing glycolytic fluxes, ATP gain via respiration became even more important under famine conditions. Consequently, the falling NADH supply was proportionally reflected in likewise falling ATP levels. The increasing ADP:ATP ratio pushed the adenylate kinase 1 (*Adk1*) away from its equilibrium to catalyze the conversion of ADP to ATP and AMP [95]. This correlation might also explain the larger AMP peak in adapted cells, since the ADP:ATP ratio increased by approximately 15% compared to non-adapted cells. AMP accumulation was prevented via removal towards INO via IMP using the purine salvage pathway. As no obvious regulatory roles could be assigned to IMP and INO thus far, Walther and colleagues suggested that AMP is shuttled to PSP to reduce its regulatory impact, which may partially explain the delayed regeneration of the AxP pool after stress relief [73].

3.4. Consequences for Production Scenarios with Saccharomyces cerevisiae

Dynamic environments in industrial-scale bioreactors can induce manifold cellular responses. Carbon-limited fed-batch processes typically operate at carefully designed substrate supply optima, which could be easily inferred once cells enter zones of substrate depletion. The latter often occur far away from the feed inlet [38] or in areas with poor mixing. The current study identified a number of intracellular responses that have the potential to impair the yeast performance in large-scale production scenarios. For instance, dynamic extracellular LSL transitions caused the emergence of a new phenotype with possible implications in recombinant protein production. Increased maintenance demands could directly compete with energetic demands for protein production in the form of an added metabolic burden [96]. Another point to consider might be the failure of cellular buffering capacities to counterbalance rapid substrate perturbations. For instance, a delayed trehalose or glycogen mobilization to maintain the glycolytic flux could result in a dynamic redox state. Celton et al. reported a negative impact of aberrant NADPH homeostasis on the production of aromatic molecules [97]. In addition, a dynamic $NAD^+/NADH$ ratio is constantly monitored via *Sir2* in yeasts that can trigger pronounced transcriptional dynamics with possible impacts on different metabolic routes for several production scenarios [43]. Knowledge concerning dynamics of specific signaling compounds could also shed light on process performance. Alpha-ketoglutaric acid has recently been characterized as a master regulator in *E. coli*, and its role in the yield reduction in recombinant protein production was discussed by Zhang et al. [98].

Thus far, this study revealed the biological feedback of yeast cells on a specific perturbation. Follow-up work should use this finding and complementary datasets to generate models that would allow more realistic predictions of the cellular response towards industrial stimuli, with a view to enabling the *a priori* identification of biological scale-up effects.

4. Materials and Methods

4.1. Strain, Precultures and Medium

The haploid, prototrophic *Saccharomyces cerevisiae* model strain CEN.PK 113-7D [93] was used in this study and was kindly provided by Royal DSM N.V. (Delft, The Netherlands). Cells were stored at −70 °C in 1 mL aliquots supplemented with 30 % (*v/v*) glycerol. For each experiment, yeast extract peptone dextrose (YPD) agar plates were prepared by streaking cells directly from the frozen glycerol stock and incubating for two days at 30 °C. Single colonies were picked and suspended with 5 mL YPD broth in a culture glass vial. The vials were mounted at a 45° angle on an orbital shaker and incubated for 8 h at 30 °C with 120 revolutions per minute. Subsequently, the cultures were pelleted and inoculated in shake-flask cultures with 110 mL adjusted Verduyn medium [99] and incubated over night at 30 °C on an orbital shaker with 120 revolutions per minute. To support carbon-limited growth in chemostat conditions with 22.5 g·L⁻¹ glucose, the medium was designed as follows: ammonium sulfate ((NH_4)$_2SO_4$) 15.0 g·L⁻¹, monopotassium phosphate (KH_2PO_4) 9.0 g·L⁻¹, magnesium sulfate heptahydrate ($MgSO_4$·7 H_2O) 1.5 g·L⁻¹, ethylenediaminetetraacetic acid (($CH_2N(CH_2CO_2H)_2)_2$) 38.22 mg·L⁻¹, zinc sulfate heptahydrate ($ZnSO_4$·7 H_2O) 9.00 mg·L⁻¹, manganese(II) chloride tetrahydrate ($MnCl_2$·4 H_2O) 2.00 mg·L⁻¹, cobalt(II) chloride hexahydrate ($CoCl_2$·6 H_2O) 0.60 mg·L⁻¹, copper(II) sulfate pentahydrate ($CuSO_4$·5 H_2O) 0.60 mg·L⁻¹, sodium molybdate dihydrate ($NaMoO_4$·2 H_2O) 0.80 mg·L⁻¹, calcium chloride dihydrate ($CaCl_2$·2 H_2O) 9.00 mg·L⁻¹, iron(II) sulfate heptahydrate ($FeSO_4$·7 H_2O) 6.00 mg·L⁻¹, boric acid (H_3BO_3) 2.00 mg·L⁻¹, potassium iodide (KI) 0.20 mg·L⁻¹, D-biotin ($C_{10}H_{16}N_2O_3S$) 0.10 mg·L⁻¹, calcium pantothenate ($C_{18}H_{32}CaN_2O_{10}$) 2.00 mg·L⁻¹, nicotinic acid ($C_6H_5NO_2$) 2.00 mg·L⁻¹, myo-inositol ($C_6H_{12}O_6$) 50.00 mg·L⁻¹, thiamine HCl ($C_{12}H_{18}Cl_2N_4OS$) 2.00 mg·L⁻¹, pyridoxine HCl ($C_8H_{12}ClNO_3$) 2.00 mg·L⁻¹ and para-aminobenzoic acid ($C_7H_7NO_2$) 0.40 mg·L⁻¹.

4.2. Bioreactor and Chemostat Setup

Aerobic, carbon-limited chemostat cultivations were carried out in a 3 l stainless steel benchtop bioreactor (Bioengineering, Wald, Switzerland) with a working volume of 1.7 L. The reactor was equipped with two six-blade Rushton-type impellers, four baffles and sensors for pH (Mettler Toledo, Columbus, OH, USA), pO_2 (PreSens, Regensburg, Germany), temperature and pressure (both Bioengineering, Wald, Switzerland). The system was operated with an overpressure of 0.3 bar, pH was controlled at 5.00 with 2 M KOH, the temperature was kept at 30 °C and aerobic conditions were maintained with bottled, ambient air supplied with $0.8 \; Nl \cdot min^{-1}$ and bubbles were dispersed with an impeller speed of 800 rpm. Foaming was prevented throughout the process by a continuous supply of Struktol J 674 antifoam (Schill und Seilacher, Hamburg, Germany) with a pump rate of 30 $\mu L \cdot h^{-1}$. Oxygen and carbon dioxide fractions in the off-gas were logged every minute with BCP-O_2 and BCP-CO_2 sensors (BlueSens, Herten, Germany).

Each process was initiated as a batch fermentation by inoculating 1.6 L adjusted Verduyn medium with 0.1 L of an overnight shake-flask culture. Glucose depletion was monitored based on a sharp increase in the pO_2 signal, which was followed by switching to chemostat conditions. The system was operated at a dilution rate of $0.1 \; h^{-1}$ with two U-120 peristaltic pumps (Watson-Marlow, Falmouth, UK). The feed pump was operated continuously at $2.83 \; mL \cdot min^{-1}$ and the harvest pump was controlled at a higher speed relative to the feed pump via mass balancing of the bioreactor. The feed medium was continuously stirred with a magnetic stir bar to avoid gradient formation in the feed casket and the dilution rate was monitored based on the mass balance of the feed reservoir.

4.3. Stimulus-Response Experiment

Reference steady-state samples were drawn after five residence times with constant off-gas signals. The non-adapted response was induced by a single transition into a non-fed regime by switching off the feed pump for 2 min, followed by a continuation of the previous chemostat regime. The biological response was characterized with the below-mentioned methods for up to six hours post-stimulus. Subsequently, the feeding regime was switched to an intermittent feed. The feed pump was switched off for two minutes and switched on for seven minutes repetitively, resulting in nine-minute regime transitioning cycles. During the feed phase of every cycle, the feed rate was adjusted to 3.64 $mL \cdot min^{-1}$ to maintain an average dilution rate of $0.1 \; h^{-1}$. After five residence times in the intermittent feeding regime, a dynamic steady state was assumed and samples representing the adapted response were drawn. The whole chemostat process was not operated for more than 15 residence times to avoid the occurrence of laboratory evolution effects [86].

4.4. Sampling

The bioreactor was equipped with two custom-made, semiautomated sampling devices. For each sample port, a stainless steel broach needle (Bioengineering, Wald, Switzerland) was connected via a septum with the bioreactor and the exit was extended with a silicon tube with an inner diameter of 0.5 mm. The tube was closed with a pinch valve (model: S105, ASCO/Sirai, Bussero, Italy) to allow sampling of precise volumes enabled via time-relay-controlled valve opening (time relay model: FSM10, Tele Haase Steuergeräte, Vienna, Austria). Each sampling device was calibrated during reference steady-state conditions for each biological replicate separately and the volume deviation from the set point of five replicates for volumes between 1 and 5 mL was always below 2 %. All samples were drawn after discarding the dead volume of 300 μL.

Cultivation broth samples for biomass and carbon balancing were briefly chilled on ice for degassing of the broth before distributing adequate volumes for each method.

Extracellular supernatants were obtained by directly sampling into a syringe equipped with a PES filter (Ø 30 mm, 0.22 μm pore size, ROTILABO®, Carl Roth, Karlsruhe, Germany) and the filtrate was collected within 5 s and stored at −70 °C.

Defined biomasses for intracellular metabolic analysis were withdrawn according to an adapted and sequential protocol employing rapid cold-methanol quenching and methanol–chloroform extraction [100]. Following procedure: 1.5 mL cultivation broth was directly injected into 10 mL methanol cooled down to −40 °C and immediately centrifuged at 5000× g for 5 min at −11 °C. Samples were thoroughly decanted, flash-frozen and stored at −70 °C until extraction. During high-frequency sampling periods (initial perturbation phase, up to Δt = 540 s), quenched cultivation broths were interim stored at −40 °C in a cryostat (RK20, Lauda, Lauda-Königshofen, Germany) for a maximum time of 5 min to prevent metabolite leakage [57]. The frozen cell pellets were resuspended in precooled (−20 °C) extraction buffer consisting of 50% vv^{-1} aqueous methanol solution, 100 mM ammonium acetate (pH 9.2), 2.5 mM 3-mercaptopropionic acid and 100 µM L-norvaline as internal standard (extraction). Added volumes were adjusted to achieve constant biomass concentrations (8.5 g·L^{-1}) and the sample temperature was kept below −20 °C by rotational mixing (Δt = 30 s) and chilling in a cryostat (−40 °C) during complete resuspension. Next, the same volume of precooled (−20 °C) chloroform was added and the mixed suspension was incubated for 2 h at −20 °C and 1 h at room temperature in a rotary overhead shaker. Afterwards, the samples were centrifuged at 20,000× g for 10 min at 4 °C and the upper aqueous methanol phase containing polar metabolites was carefully removed and stored at −70 °C until measurement.

4.5. Off-Gas Deconvolution

A prerequisite for proper off-gas analysis in stimulus-response experiments is a suitable approach for signal deconvolution. Long tubing lines and foam traps between fermenter and sensors led to the formation of mixing chambers, causing a sensor delay of several minutes and increased apparent time constants versus the reported 55 s for BCP-O_2 and BCP-CO_2 sensors [101]. Step experiments were carried out under experimental conditions with H_2O as a broth substituent to identify delay times and time constants for each sensor. Correction of the O_2 and CO_2 signals during the stimulus-response experiments was computed based on the methodology by Theobald et al. [102]. For a complete description of the step experiments and mathematical deconvolution approach, the reader is referred to Appendix A.

4.6. Dry Matter of Biomass Determination

Triplicated 5 mL volumes were vacuum-filtered through dried and tared PES membrane disc filters (Ø 47 mm, Type 154, Sartorius, Göttingen, Germany). Filters were, subsequently, washed with 15 mL demineralized water and dried at 70 °C until mass constancy was observed. Finally, filters with biomass cakes were brought to room temperature in a desiccator and were weighed again. The calculated weight of the biomass cake was normalized to the sample volume and expressed as dry matter of biomass (*DMB*).

4.7. Extracellular Metabolite Quantification

Frozen supernatant samples were thawed on ice and glucose was measured using a UV-based enzyme test kit (art. no. 10716251035, r-biopharm AG, Darmstadt, Germany). The free ammonium concentration was quantified with the LCK302 cuvette test kit (Hach Lange, Düsseldorf, Germany). Each kit was performed according to the manufacturer's instructions on a spectrophotometer (Hach Lange, Düsseldorf, Germany). Unknown extracellular carbon was calculated based on an organic carbon balance of broth supernatant using a total carbon analyzer (Multi N/C 2100s, AnalytikJena, Jena, Germany).

4.8. Determination of Intracellular Carbohydrate Storage Pools

Intracellular glycogen and trehalose levels were determined based on the protocols reported by Parrou et al. and Suarez-Mendez et al. [103,104]. Frozen pellets were resuspended in 250 μL 0.25 M sodium carbonate and incubated for 3 h at 95 °C. Subsequently, the pH was adjusted to 5.5 by addition of 150 μL^{-1} M acetic acid and 600 μL 0.2 M sodium acetate (pH 5.2, adjusted with acetic acid). The sample was split into a 480 μL and a 466 μL aliquot. The first was treated with 20 μL of α-amyloglucosidase (~70 U/mL, catalog number: 10115, Merck, Darmstadt, Germany) at 57 °C overnight to determine glycogen expressed as liberated glucose equivalents. For trehalase determination, the pH of the 466 μL aliquot was adjusted slightly upwards by the addition of 30 μL of 0.2 M sodium acetate, and trehalose was hydrolyzed to glucose by the addition of 4 μL trehalase (2.27 U/mL, catalog number: T8778, Merck, Darmstadt, Germany) and incubated at 37 °C overnight. Glucose equivalents were measured with the UV-based enzyme test kit (art. no. 10716251035, r-biopharm AG, Darmstadt, Germany).

4.9. Determination of Intracellular Metabolites Measured via LC-MS/MS

Quantitative metabolome analyses of intracellular *S. cerevisiae* extracts (see section 4.4) were conducted on an Agilent 1200 HPLC system coupled with an Agilent 6410B triple-quadrupole (QQQ) mass spectrometer with a classical electrospray ionization (ESI) interface.

Analytical preparation of sample extracts and chromatographic separation of non-derivatized polar metabolites by alkaline polymer-based zwitterionic hydrophilic interaction chromatography (ZIC-pHILIC) were performed as previously described [105,106]. Defined standard mixtures and samples with adapted dilution containing 50 μM 2-keto-3-deoxy-6-phosphogluconate (KDPG) and α-amino isobutyric acid (AIBA) as global internal standard (measurement) were injected (5 μL) into a Sequant ZIC-pHILIC column (150 × 2.1 mm, 5 μm, Merck Millipore, Darmstadt, Germany) equipped with a guard column (20 × 2.1 mm, 5 μm, Merck Millipore, Darmstadt, Germany) maintained at 40 °C.

Analogue measurements of previously derivatized (Phenylhydrazine) α-keto acids (αKG, PYR, GXY) were performed by an adapted LC-MS/MS protocol [107] using 50 μM α-ketovalerate as internal standard (derivatization/measurement). Derivatized analytes were separated under acidic conditions (pH 3.0) by reverse-phase liquid chromatography (RPLC) [108]. Samples were injected (5 μL) onto a ZORBAX SB-C18 column (150 × 4.6 mm, 5 μm, Agilent Technologies, Waldbronn, Germany) with a guard column (12.5 × 4.6 mm, 5 μm, Agilent Technologies, Waldbronn, Germany) maintained at 40 °C.

Targeted metabolites were detected with high selectivity in multiple reaction monitoring (MRM) mode using established and preoptimized precursor-to-product transitions and MS/MS parameters with a mass resolution of 0.1 u. Intracellular metabolite pools were absolutely quantified by a threefold standard addition of defined amounts of reference standard mixes (internal calibration). Applied amounts were adjusted according to previously estimated concentration levels and linear dynamic ranges of the targeted metabolites [109]. The absolute concentration levels of the AxP species were normalized to results from a reference method [54] to compensate for known HILIC-specific peak tailing effects in iron-based LC systems [110]. The normalization factors (ATP: 2.71, ADP: 1.88 and AMP: 1.21) were calculated from analogues steady-state RS samples and were applied conformably.

4.10. Characterization of the Endometabolome Relaxation Pattern

A classical, metric multidimensional scaling approach [111] was chosen to quantify and visualize dissimilarities between the different time points. Concentrations of all 29 intracellular metabolites, except pyruvic acid, were considered and min–max normalized. In the next step, the Euclidean distance matrix was computed with the function *dist* and used as an input for *cmdscale*, which was limited to a two-dimensional representation of the sample distances (k = 2). All computations were executed in the R environment (version 1.4.1106) with the package *stats* (version 4.1.0).

4.11. Total Carbon and Nitrogen Determination

One milliliter of fermentation broth was mixed with nine milliliters of 36.84 mM KOH to prevent loss of inorganic carbon in the form of dissolved carbonate. Next, the 1:10 diluted sample was measured in octuplicate, and undiluted supernatant (also stabilized with 36.84 mM KOH) was measured in quadruplicate with a multi N/C 2100 S composition analyzer (Analytik Jena, Jena, Germany). The system was calibrated according to the method of Buchholz et al. [112]. Nitrogen concentrations were directly measured and organic carbon was determined based on the difference between the total carbon and the inorganic carbon fractions.

5. Conclusions

This study set out to investigate the response of *Saccharomyces cerevisiae* during industrially relevant transitions between carbon limitation and starvation, and vice versa. The intracellular metabolite analysis provided a solid dataset for future modeling efforts and revealed distinct phenomena that helped to explain biological scale-up effects. The experimental design allowed the observation of several dynamics from the allosteric control of specific intermediates to global phenotypic changes as a response to the applied substrate gradient. In particular, a distinct mode was uncovered where yeasts sacrificed catabolic reduction power to sustain ongoing anabolic demands under acute carbon starvation conditions. A natural progression of this work is to expand the obtained knowledge by analyzing gene expression dynamics to investigate (i) if and how metabolic stimuli are propagated in cells exposed to an industrially relevant famine perturbation and (ii) to use the obtained data for setting up data-driven models for a rational scale-up/scale-down.

Appendix A. Off-Gas Deconvolution

A prerequisite for the off-gas analysis in stimulus-response experiments is a suitable approach for data deconvolution. Long tubing lines and foam traps between fermenter and sensors led to the formation of mixing chambers, causing a sensor delay of several minutes and increased apparent time constants versus the reported 40–55 s for BCP-O_2 and BCB-CO_2 sensors [101]. This could cause misguided readouts such as strong RQ dynamics that might not at all be caused by biological effects. To compensate for this system

characteristic, step experiments under experimental conditions were carried out to acquire delay times and time constants for the whole "fermenter → sensor" unit, as laid out in Table A1. A correction of measured off-gas signals was calculated according to the procedure of Theobald et al. [102]:

$$\left(Y_{O_2}^{\omega}\right)_F\left(t - \tau_d^{O_2}\right) = \left(Y_{O_2}^{\omega}\right)_A + \tau_1^{O_2}\frac{d\left(Y_{O_2}^{\omega}\right)_A}{dt} \tag{A1}$$

$$\left(Y_{CO_2}^{\omega}\right)_F\left(t - \tau_d^{CO_2}\right) = \left(Y_{CO_2}^{\omega}\right)_A + \tau_1^{CO_2}\frac{d\left(Y_{CO_2}^{\omega}\right)_A}{dt} \tag{A2}$$

with

$\left(Y_{O_2}^{\omega}\right)_F$ molar fraction of O_2 in the fermenter broth;

$\left(Y_{CO_2}^{\omega}\right)_F$ molar fraction of CO_2 in the fermenter broth;

$\left(Y_{O_2}^{\omega}\right)_A$ measured molar fraction of O_2 at the sensor;

$\left(Y_{CO_2}^{\omega}\right)_A$ measured molar fraction of CO_2 at the sensor;

t time of data logging for O_2 and CO_2;

$\tau_d^{O_2}$ delay time of O_2 signal;

$\tau_d^{CO_2}$ delay time of CO_2 signal;

$\tau_1^{O_2}$ time constant of BCP-O_2 sensor and gas line "fermenter → sensor";

$\tau_1^{CO_2}$ time constant of BCP-CO_2 sensor and gas line "fermenter → sensor".

Table A1. Parameters for off-gas deconvolution. Delay times (τ_d) and time constants (τ_1) were derived from step experiments, where the reactor system was operated with water, but otherwise equal to fermentation conditions. Each parameter was derived from two-step experiments, where aeration was switched from a calibration gas mixture (2.00% O_2, 8.99% CO_2) to ambient air (20.94% O_2, 0.04% CO_2).

Analyte	Sensor	Manufacturer	τ_d (s)	τ_1 (s)
Oxygen	BCP-O_2	BlueSens, Herten, Germany	92	381
Carbon dioxide	BCP-CO_2	BlueSens, Herten, Germany	155	490

Figure A1 shows an exemplary correction for both, oxygen and carbon dioxide signals against raw signal readouts after a single perturbation (Figure 3c), as indicated by the dashed lines. It became obvious that this procedure was essential to compensate for delays and curve flattening due to a total of 3.2 L mixing volume in the off-gas line.
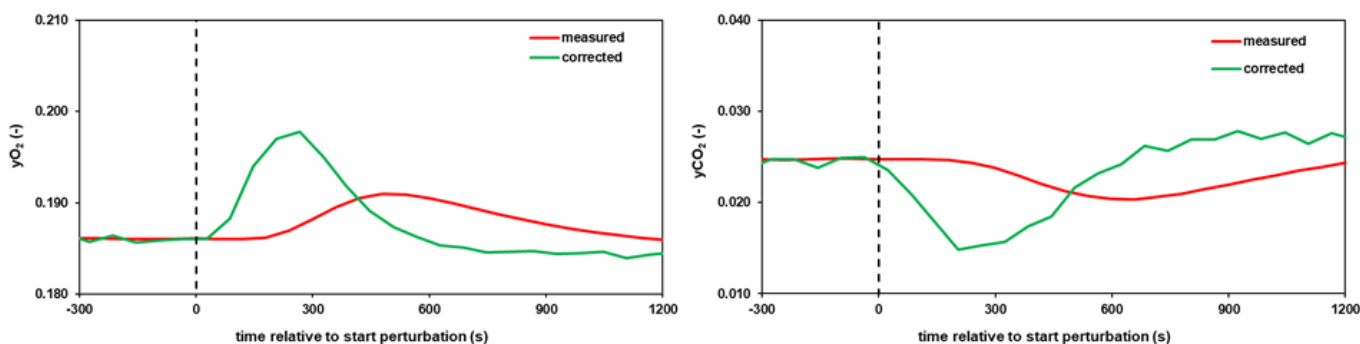

Figure A1. Exemplary deconvolution results for O_2 and CO_2 signals of one replicate after a single perturbation (see Figure 3c). Deconvolution of O_2 (left panel) and CO_2 (right panel) signals (green) was calculated based on equations (A1) and (A2), parameters from table A1 and plotted against raw signals (red).

Appendix B. Steady-State Amino Acid Concentrations

A total of 18 amino acids was also monitored during the SRE experiment under both conditions. However, due to the absence of significant dynamics during the perturbation, only steady-state values were reported in Table A2.

Table A2. Amino acid concentrations during reference and dynamic steady-state conditions. For the dynamic steady state, average pool concentrations over one perturbation cycle were reported.

Amino Acid	Steady-State RS ($\mu mol \cdot g_{DMB}^{-1}$)	Steady-State DS ($\mu mol \cdot g_{DMB}^{-1}$)	Change (%)	Welch Test (*p*-Value)
glycine	2.37 ± 0.02	1.05 ± 0.28	−56	7.4×10^{-5}
L-methionine	0.18 ± 0.04	0.05 ± 0.01	−72	2.9×10^{-2}
L-serine	3.29 ± 0.19	1.29 ± 0.51	−61	6.9×10^{-5}
L-proline	6.15 ± 1.12	2.17 ± 1.08	−65	7.4×10^{-3}
L-threonine	10.5 ± 4.5	9.8 ± 2.9	−7	n.s.
L-glutamine	149 ± 10	103 ± 20	−31	2.6×10^{-3}
L-asparagine	8.64 ± 1.31	8.7 ± 1.60	+1	n.s.
L-glutamic acid	449 ± 26	390 ± 71	−13	n.s.
L-aspartic acid	22.9 ± 5.7	22.4 ± 5.8	−2	n.s.
L-lysine	3.79 ± 0.47	4.19 ± 0.12	+11	n.s.
L-arginine	17.8 ± 0.3	9.8 ± 0.9	−45	5.9×10^{-7}
L-tyrosine	1.92 ± 0.05	0.41 ± 0.05	−78	1.5×10^{-3}
L-tryptophane	0.36 ± 0.11	0.11 ± 0.01	−68	n.s.
L-phenylalanine	0.85 ± 0.09	0.28± 0.05	−66	4.1×10^{-3}
L-valine	22.1 ± 2.6	12.6 ± 4.1	−43	5.0×10^{-3}
L-leucine	0.69 ± 0.09	0.38 ± 0.1	−46	6.8×10^{-3}
L-isoleucine	1.45 ± 0.02	0.79 ± 0.19	−46	3.1×10^{-4}
L-alanine	84.9 ± 8.0	43.4 ± 16.7	−49	1.5×10^{-3}

All values represent means ± standard deviation (s.d.) of three biological replicates. n.s., not significant.

References

1. Mengal, P.; Wubbolts, M.; Zika, E.; Ruiz, A.; Brigitta, D.; Pieniadz, A.; Black, S. Bio-based Industries Joint Undertaking: The catalyst for sustainable bio-based economic growth in Europe. *New Biotechnol.* **2018**, *40*, 31–39. https://doi.org/10.1016/j.nbt.2017.06.002.
2. Singh, A.; Christensen, T.; Panoutsou, C. Policy review for biomass value chains in the European bioeconomy. *Glob. Transit.* **2021**, *3*, 13–42. https://doi.org/10.1016/j.glt.2020.11.003.
3. Straathof, A.J.; Wahl, S.A.; Benjamin, K.R.; Takors, R.; Wierckx, N.; Noorman, H.J. Grand Research Challenges for Sustainable Industrial Biotechnology. *Trends Biotechnol.* **2019**, *37*, 1042–1050. https://doi.org/10.1016/j.tibtech.2019.04.002.
4. What Is Horizon 2020? Available online: https://ec.europa.eu/programmes/horizon2020/en/what-horizon-2020 (accessed on 15 January 2022).
5. Takors, R. Scale-up of microbial processes: Impacts, tools and open questions. *J. Biotechnol.* **2012**, *160*, 3–9. https://doi.org/10.1016/j.jbiotec.2011.12.010.
6. Noorman, H. An industrial perspective on bioreactor scale-down: What we can learn from combined large-scale bioprocess and model fluid studies. *Biotechnol. J.* **2011**, *6*, 934–943. https://doi.org/10.1002/biot.201000406.
7. De Lorenzo, V.; Couto, J. The important versus the exciting: Reining contradictions in contemporary biotechnology. *Microb. Biotechnol.* **2018**, *12*, 32–34. https://doi.org/10.1111/1751-7915.13348.
8. Wehrs, M.; Tanjore, D.; Eng, T.; Lievense, J.; Pray, T.R.; Mukhopadhyay, A. Engineering robust production microbes for large-scale cultivation. *Trends Microbiol.* **2019**, *27*, 524–537. https://doi.org/10.1016/j.tim.2019.01.006.
9. Schügerl, K. Comparison of different bioreactor performances. *Bioprocess Biosyst. Eng.* **1993**, *9*, 215–223. https://doi.org/10.1007/bf00369405.
10. Vrábel, P.; van der Lans, R.G.; Luyben, K.C.; Boon, L.; Nienow, A.W. Mixing in large-scale vessels stirred with multiple radial or radial and axial up-pumping impellers: Modelling and measurements. *Chem. Eng. Sci.* **2000**, *55*, 5881–5896. https://doi.org/10.1016/s0009-2509(00)00175-5.
11. Takors, R. Editorial: How can we ensure the successful transfer from lab- to large-scale production? *Eng. Life Sci.* **2016**, *16*, 587. https://doi.org/10.1002/elsc.201670073.

12. Crater, J.S.; Lievense, J.C. Scale-up of industrial microbial processes. *FEMS Microbiol. Lett.* **2018**, *365*, 1–5. https://doi.org/10.1093/femsle/fny138.

13. Hill, P.; Benjamin, K.; Bhattacharjee, B.; Garcia, F.; Leng, J.; Liu, C.-L.; Murarka, A.; Pitera, D.; Rodriguez Porcel, E.M; da Silva, I.; et al. Clean manufacturing powered by biology: How Amyris has deployed technology and aims to do it better. *J. Ind. Microbiol. Biotechnol.* **2020**, *47*, 965–975. https://doi.org/10.1007/s10295-020-02314-3.

14. Florez, S.L. Accelerating Fermentation Process Development at Ginkgo Using Sartorius' Ambr250 Platform. In Proceedings of the BIO World Congress on Industrial Biotechnology, Des Moines, IA, USA, 8–11 July 2019. https://www.bio.org/sites/default/files/legacy/bioorg/docs/Florez Ginkgo.pdf.

15. Ögmundarson, Ó.; Sukumara, S.; Herrgård, M.J.; Fantke, P. Combining Environmental and Economic Performance for Bioprocess Optimization. *Trends Biotechnol.* **2020**, *38*, 1203–1214. https://doi.org/10.1016/j.tibtech.2020.04.011.

16. Neubauer, P.; Junne, S. Scale-down simulators for metabolic analysis of large-scale bioprocesses. *Curr. Opin. Biotechnol.* **2010**, *21*, 114–121. https://doi.org/10.1016/j.copbio.2010.02.001.

17. Täuber, S.; Golze, C.; Ho, P.; Lieres, E.V. DMSCC: A Microfluidic Platform for Microbial Single-Cell Cultivation under Dynamic Environmental Medium Conditions. *bioRxiv* **2020**, https://doi.org/10.1101/2020.07.10.188938.

18. Delvigne, F.; Takors, R.; Mudde, R.; Van Gulik, W.; Noorman, H. Bioprocess scale-up/down as integrative enabling technology: From fluid mechanics to systems biology and beyond. *Microb. Biotechnol.* **2017**, *10*, 1267–1274. https://doi.org/10.1111/1751-7915.12803.

19. Papagianni, M. Methodologies for Scale-down of Microbial Bioprocesses. *J. Microb. Biochem. Technol.* **2015**, *s5*, 1–7. https://doi.org/10.4172/1948-5948.s5-001.

20. Lara, A. R.; Galindo, E.; Ramírez, O. T.; Palomares, L. A. Living with Heterogeneities in Bioreactors. *Mol. Biotechnol.* **2006**, *34*, 355–381. https://doi.org/10.1385/mb:34:3:355.

21. Haringa, C.; Mudde, R.F.; Noorman, H.J. From industrial fermentor to CFD-guided downscaling: What have we learned? *Biochem. Eng. J.* **2018**, *140*, 57–71. https://doi.org/10.1016/j.bej.2018.09.001.

22. George, S.; Larsson, G.; Olsson, K.; Enfors, S.-O. Comparison of the Baker's yeast process performance in laboratory and production scale. *Bioprocess Biosyst. Eng.* **1998**, *18*, 135–142. https://doi.org/10.1007/pl00008979.

23. Bylund, F.; Collet, E.; Enfors, S.-O.; Larsson, G. Substrate gradient formation in the large-scale bioreactor lowers cell yield and increases by-product formation. *Bioprocess Biosyst. Eng.* **1998**, *18*, 171–180. https://doi.org/10.1007/s004490050427.

24. de Jonge, L.P.; Buijs, N.A.A.; Pierick, A.T.; Deshmukh, A.; Zhao, Z.; Kiel, J.A.K.W.; Heijnen, J.J.; van Gulik, W.M. Scale-down of penicillin production in Penicillium chrysogenum. *Biotechnol. J.* **2011**, *6*, 944–958. https://doi.org/10.1002/biot.201000409.

25. Pham, T.-H.; Mauvais, G.; Vergoignan, C.; De Coninck, J.; Dumont, F.; Lherminier, J.; Cachon, R.; Feron, G. Gaseous environments modify physiology in the brewing yeast *Saccharomyces cerevisiae* during batch alcoholic fermentation. *J. Appl. Microbiol.* **2008**, *105*, 858–874. https://doi.org/10.1111/j.1365-2672.2008.03821.x.

26. Kresnowati, M.T.A.P.; Van Winden, W.A.; Almering, M.J.H.; Pierick, A.T.; Ras, C.; A Knijnenburg, T.; Daran-Lapujade, P.; Pronk, J.T.; Heijnen, J.J.; Daran, J.-M. When transcriptome meets metabolome: Fast cellular responses of yeast to sudden relief of glucose limitation. *Mol. Syst. Biol.* **2006**, *2*, 49. https://doi.org/10.1038/msb4100083.

27. Suarez-Mendez, C.A.; Ras, C.; Wahl, S.A. Metabolic adjustment upon repetitive substrate perturbations using dynamic 13C-tracing in yeast. *Microb. Cell Factories* **2017**, *16*, 161. https://doi.org/10.1186/s12934-017-0778-6.

28. Löffler, M.; Simen, J.D.; Jäger, G.; Schäferhoff, K.; Freund, A.; Takors, R. Engineering *E. coli* for large-scale production-Strategies considering ATP expenses and transcriptional responses. *Metab. Eng.* **2016**, *38*, 73–85. https://doi.org/10.1016/j.ymben.2016.06.008.

29. Zieringer, J.; Wild, M.; Takors, R. Data-driven in silico prediction of regulation heterogeneity and ATP demands of *Escherichia coli* in large-scale bioreactors. *Biotechnol. Bioeng.* **2021**, *118*, 265–278. https://doi.org/10.1002/bit.27568.

30. Wright, N.R.; Wulff, T.; Palmqvist, E.A.; Jørgensen, T.R.; Workman, C.T.; Sonnenschein, N.; Rønnest, N.P.; Herrgård, M.J. Fluctuations in glucose availability prevent global proteome changes and physiological transition during prolonged chemostat cultivations of *Saccharomyces cerevisiae*. *Biotechnol. Bioeng.* **2020**, *117*, 2074–2088. https://doi.org/10.1002/bit.27353.

31. Nieß, A.; Löffler, M.; Simen, J.D.; Takors, R. Repetitive Short-Term Stimuli Imposed in Poor Mixing Zones Induce Long-Term Adaptation of *E. coli* Cultures in Large-Scale Bioreactors: Experimental Evidence and Mathematical Model. *Front. Microbiol.* **2017**, *8*, 1195. https://doi.org/10.3389/fmicb.2017.01195.

32. Anane, E.; Sawatzki, A.; Neubauer, P.; Cruz-Bournazou, M.N. Modelling concentration gradients in fed-batch cultivations of *E. coli*-towards the flexible design of scale-down experiments. *J. Chem. Technol. Biotechnol.* **2019**, *94*, 516–526. https://doi.org/10.1002/jctb.5798.

33. Delvigne, F.; Goffin, P. Microbial heterogeneity affects bioprocess robustness: Dynamic single-cell analysis contributes to understanding of microbial populations. *Biotechnol. J.* **2013**, *9*, 61–72. https://doi.org/10.1002/biot.201300119.

34. Heins, A.-L.; Weuster-Botz, D. Population heterogeneity in microbial bioprocesses: Origin, analysis, mechanisms, and future perspectives. *Bioprocess Biosyst. Eng.* **2018**, *41*, 889–916. https://doi.org/10.1007/s00449-018-1922-3.

35. Nadal-Rey, G.; McClure, D.D.; Kavanagh, J.M.; Cassells, B.; Cornelissen, S.; Fletcher, D.F.; Gernaey, K.V. Development of dynamic compartment models for industrial aerobic fed-batch fermentation processes. *Chem. Eng. J.* **2021**, *420*, 130402. https://doi.org/10.1016/j.cej.2021.130402.

36. Lapin, A.; Müller, D.; Reuss, M. Dynamic Behavior of Microbial Populations in Stirred Bioreactors Simulated with Euler−Lagrange Methods: Traveling along the Lifelines of Single Cells. *Ind. Eng. Chem. Res.* **2004**, *43*, 4647–4656. https://doi.org/10.1021/ie030786k.

37. Haringa, C.; Tang, W.; Deshmukh, A.T.; Xia, J.; Reuss, M.; Heijnen, J.J.; Mudde, R.F.; Noorman, H.J. Euler-Lagrange computational fluid dynamics for (bio) reactor scale down: An analysis of organism lifelines. *Eng. Life Sci.* **2016**, *16*, 652–663. https://doi.org/10.1002/elsc.201600061.

38. Haringa, C.; Deshmukh, A.T.; Mudde, R.F.; Noorman, H.J. Euler-Lagrange analysis towards representative down-scaling of a 22 m 3 aerobic *S. cerevisiae* fermentation. *Chem. Eng. Sci.* **2017**, *170*, 653–669. https://doi.org/10.1016/j.ces.2017.01.014.

39. Sarkizi Shams Hajian, C.; Haringa, C.; Noorman, H.; Takors, R. Predicting By-Product Gradients of Baker's Yeast Production at Industrial Scale: A Practical Simulation Approach. *Processes* **2020**, *8*, 1554. https://doi.org/10.3390/pr8121554.

40. Kuschel, M.; Takors, R. Simulated oxygen and glucose gradients as a prerequisite for predicting industrial scale performance a priori. *Biotechnol. Bioeng.* **2020**, *117*, 2760–2770. https://doi.org/10.1002/bit.27457.

41. Ziegler, M.; Zieringer, J.; Döring, C.-L.; Paul, L.; Schaal, C.; Takors, R. Engineering of a robust *Escherichia coli* chassis and exploitation for large-scale production processes. *Metab. Eng.* **2021**, *67*, 75–87. https://doi.org/10.1016/j.ymben.2021.05.011.

42. Venturini Copetti , M. Yeasts and molds in fermented food production: An ancient bioprocess. *Curr. Opin. Food Sci.* **2019**, *25*, 57–61. https://doi.org/10.1016/j.cofs.2019.02.014.

43. Nielsen, J. Yeast systems biology: Model organism and cell factory. *Biotechnol. J.* **2019**, *14*, 1800421. https://doi.org/10.1002/biot.201800421.

44. Larsson, G.; Törnkvist, M.; Ståhl Wernersson, E.; Trägårdh, C.; Noorman, H.J.; Enfors, S.O. Substrate gradients in bioreactors: Origin and consequences. *Bioprocess Biosyst. Eng.* **1996**, *14*, 281–289. https://doi.org/10.1007/bf00369471.

45. Noorman, H.; Hjertager, B.H.; Morud, K.; Targardh, C.; Enfors, S.-O.; Larsson, G.; Tornkvist, M. Measurement and Computational Fluid Dynamics Simulations of *Saccharomyces cerevisiae* Production in a 30 m³ Stirred Tank Reactor. *Int. Symp. Bioreact. Perform.* **1993**, *150*, 243–263.

46. Rizzi, M.; Baltes, M.; Theobald, U.; Reuss, M. In vivo analysis of metabolic dynamics in *Saccharomyces cerevisiae*: II. Mathematical model. *Biotechnol. Bioeng.* **1997**, *55*, 592–608. https://doi.org/10.1002/(sici)1097-0290(19970820)55:43.3.co;2-1.

47. Mashego, M.R.; van Gulik, W.M.; Vinke, J.L.; Visser, D.; Heijnen, J.J. In vivo kinetics with rapid perturbation experiments in *Saccharomyces cerevisiae* using a second-generation BioScope. *Metab. Eng.* **2006**, *8*, 370–383. https://doi.org/10.1016/j.ymben.2006.02.002.

48. Lao-Martil, D.; Verhagen, K.J.A.; Schmitz, J.P.J.; Teusink, B.; Wahl, S.A.; van Riel, N.A.W. Kinetic Modeling of *Saccharomyces cerevisiae* Central Carbon Metabolism : Achievements, Limitations, and Opportunities. *Metabolites* **2022**, *12*, 74.

49. Theobald, U.M.; Mailinger, W.; Baltes, M.; Rizzi, M.; Reuss, M. In Vivo Analysis of Metabolic Dynamics in *Saccharomyces cerevisiae*: I. Experimental Observations. *Biotechnol. Bioeng.* **1997**, *55*, 305–316.

50. Suarez-Mendez, C.; Sousa, A.; Heijnen, J.J.; Wahl, A. Fast "Feast/Famine" Cycles for Studying Microbial Physiology Under Dynamic Conditions: A Case Study with *Saccharomyces cerevisiae*. *Metabolites* **2014**, *4*, 347–372. https://doi.org/10.3390/metabo4020347.

51. Diderich, J.A.; Schepper, M.; van Hoek, P.; Luttik, M.A.H.; van Dijken, J.P.; Pronk, J.T.; Klaassen, P.; Boelens, H.F.M.; de Mattos, M.J.T.; van Dam, K.; et al. Glucose Uptake Kinetics and Transcription of HXTGenes in Chemostat Cultures of *Saccharomyces cerevisiae*. *J. Biol. Chem.* **1999**, *274*, 15350–15359. https://doi.org/10.1074/jbc.274.22.15350.

52. Marc, J.; Feria-Gervasio, D.; Mouret, J.-R.; E Guillouet, S. Impact of oleic acid as co-substrate of glucose on "short" and "long-term" Crabtree effect in *Saccharomyces cerevisiae*. *Microb. Cell Factories* **2013**, *12*, 83. https://doi.org/10.1186/1475-2859-12-83.

53. Vos, T.; Hakkaart, X.D.V.; De Hulster, E.A.F.; Van Maris, A.J.A.; Pronk, J.T.; Daran-Lapujade, P. Maintenance-energy requirements and robustness of *Saccharomyces cerevisiae* at aerobic near-zero specific growth rates. *Microb. Cell Factories* **2016**, *15*, 111. https://doi.org/10.1186/s12934-016-0501-z.

54. Eigenstetter, G.; Takors, R. Dynamic modeling reveals a three-step response of *Saccharomyces cerevisiae* to high CO2 levels accompanied by increasing ATP demands. *FEMS Yeast Res.* **2017**, *17*, fox008. https://doi.org/10.1093/femsyr/fox008.

55. Suarez-Mendez, C.; Hanemaaijer, M.; Pierick, A.T.; Wolters, J.C.; Heijnen, J.; Wahl, S. Interaction of storage carbohydrates and other cyclic fluxes with central metabolism: A quantitative approach by non-stationary 13 C metabolic flux analysis. *Metab. Eng. Commun.* **2016**, *3*, 52–63. https://doi.org/10.1016/j.meteno.2016.01.001.

56. Roubos, J.A.; Krabben, P.; Luiten, R.G.M.; Verbruggen, H.B.; Heijnen, J.J. A Quantitative Approach to Characterizing Cell Lysis Caused by Mechanical Agitation of *Streptomyces clavuligerus*. *Biotechnol. Prog.* **2001**, *17*, 336–347. https://doi.org/10.1021/bp0001617.

57. Canelas, A.B.; Ras, C.; ten Pierick, A.; van Dam, J.C.; Heijnen, J.J.; van Gulik, W.M. Leakage-free rapid quenching technique for yeast metabolomics. *Metabolomics* **2008**, *4*, 226–239. https://doi.org/10.1007/s11306-008-0116-4.

58. Noubhani, A.; Bunoust, O.; Rigoulet, M.; Thevelein, J. Reconstitution of ethanolic fermentation in permeabilized spheroplasts of wild-type and trehalose-6-phosphate synthase mutants of the yeast *Saccharomyces cerevisiae*. *JBIC J. Biol. Inorg. Chem.* **2000**, *267*, 4566–4576. https://doi.org/10.1046/j.1432-1327.2000.01511.x.

59. Blazquez, M.; Lagunas, R.; Gancedo, C.; Gancedo, J.M. Trehalose-6-phosphate, a new regulator of yeast glycolysis that inhibits hexokinases. *FEBS Lett.* **1993**, *329*, 51–54. https://doi.org/10.1016/0014-5793(93)80191-v.

60. Paalman, J.W.G.; Verwaal, R.; Slofstra, S.H.; Verkleij, A.J.; Boonstra, J.; Verrips, C. Trehalose and glycogen accumulation is related to the duration of the G1 phase of *Saccharomyces cerevisiae*. *FEMS Yeast Res.* **2003**, *3*, 261–268. https://doi.org/10.1016/s1567-1356(02)00163-0.

61. Francois, J.; Walther, T.; Parrou, J.L. Genetics and Regulation of Glycogen and Trehalose Metabolism in *Saccharomyces cerevisiae*. *Microb. Stress Toler. Biofuels* **2012**, *22*, 29–56. https://doi.org/10.1007/978-3-642-21467-7.

62. Canelas, A.B.; Harrison, N.; Fazio, A.; Zhang, J.; Pitkänen, J.-P.; Brink, J.V.D.; Bakker, B.; Bogner, L.; Bouwman, J.; Castrillo, J.I.; et al. Integrated multilaboratory systems biology reveals differences in protein metabolism between two reference yeast strains. *Nat. Commun.* **2010**, *1*, 145–148. https://doi.org/10.1038/ncomms1150.

63. Yi, D.-G.; Huh, W.-K. UDP-glucose pyrophosphorylase Ugp1 is involved in oxidative stress response and long-term survival during stationary phase in *Saccharomyces cerevisiae*. *Biochem. Biophys. Res. Commun.* **2015**, *467*, 657–663. https://doi.org/10.1016/j.bbrc.2015.10.090.

64. Bárcena, M.; Radermacher, M.; Bär, J.; Kopperschläger, G.; Ruiz, T. The structure of the ATP-bound state of S. cerevisiae phosphofructokinase determined by cryo-electron microscopy. *J. Struct. Biol.* **2007**, *159*, 135–143. https://doi.org/10.1016/j.jsb.2007.03.004.

65. Teusink, B.; Passarge, J.; Reijenga, C.A.; Esgalhado, M.; van der Weijden, C.C.; Schepper, M.; Walsh, M.C.; Bakker, B.M.; Van Dam, K.; Westerhoff, H.V.; et al. Can yeast glycolysis be understood in terms of in vitro kinetics of the constituent enzymes? Testing biochemistry. *JBIC J. Biol. Inorg. Chem.* **2000**, *267*, 5313–5329. https://doi.org/10.1046/j.1432-1327.2000.01527.x.

66. van den Brink, J. Dynamic Response of *Saccharomyces cerevisiae* to Fermentative Growth Conditions. Ph.D. Thesis, Technische Universiteit Delft, Delft, The Netherlands, 9 February 2009.

67. Jurica, M.S.; Mesecar, A.; Heath, P.J.; Shi, W.; Nowak, T.; Stoddard, B.L. The allosteric regulation of pyruvate kinase by fructose-1, 6-bisphosphate. *Structure* **1998**, *6*, 195–210. https://doi.org/10.1016/s0969-2126(98)00021-5.

68. Gombert, A.K.; dos Santos, M.M.; Christensen, B.; Nielsen, J. Network Identification and Flux Quantification in the Central Metabolism of *Saccharomyces cerevisiae* under Different Conditions of Glucose Repression. *J. Bacteriol.* **2001**, *183*, 1441–1451. https://doi.org/10.1128/jb.183.4.1441-1451.2001.

69. Zhang, J.; Pierick, A.T.; Van Rossum, H.M.; Seifar, R.M.; Ras, C.; Daran, J.-M.; Heijnen, J.J.; Wahl, S.A. Determination of the Cytosolic NADPH/NADP Ratio in *Saccharomyces cerevisiae* using Shikimate Dehydrogenase as Sensor Reaction. *Sci. Rep.* **2015**, *5*, 12846. https://doi.org/10.1038/srep12846.

70. Vemuri, G.N.; Eiteman, M.A.; McEwen, J.E.; Olsson, L.; Nielsen, J. Increasing NADH oxidation reduces overflow metabolism in *Saccharomyces cerevisiae*. *Proc. Natl. Acad. Sci. USA* **2007**, *104*, 2402–2407. https://doi.org/10.1073/pnas.0607469104.

71. Visser, D.; van Zuylen, G.A.; van Dam, J.C.; Eman, M.R.; Pröll, A.; Ras, C.; Wu, L.; van Gulik, W.M.; Heijnen, J.J. Analysis of in vivo kinetics of glycolysis in aerobic *Saccharomyces cerevisiae* by application of glucose and ethanol pulses. *Biotechnol. Bioeng.* **2004**, *88*, 157–167. https://doi.org/10.1002/bit.20235.

72. Ball, W.J.; E Atkinson, D. Adenylate energy charge in *Saccharomyces cerevisiae* during starvation. *J. Bacteriol.* **1975**, *121*, 975–982. https://doi.org/10.1128/jb.121.3.975-982.1975.

73. Walther, T.; Novo, M.; Rössger, K.; Létisse, F.; Loret, M.-O.; Portais, J.-C.; François, J.M. Control of ATP homeostasis during the respiro-fermentative transition in yeast. *Mol. Syst. Biol.* **2010**, *6*, 344. https://doi.org/10.1038/msb.2009.100.

74. Pinson, B.; Ceschin, J.; Saint-Marc, C.; Daignan-Fornier, B. Dual control of NAD+ synthesis by purine metabolites in yeast. *Elife* **2019**, *8*, 43808. https://doi.org/10.7554/elife.43808.

75. Fowler, J.D.; Dunlop, E.H. Effects of reactant heterogeneity and mixing on catabolite repression in cultures of *Saccharomyces cerevisiae*. *Biotechnol. Bioeng.* **1989**, *33*, 1039–1046. https://doi.org/10.1002/bit.260330813.

76. Reifenberger, E.; Boles, E.; Ciriacy, M. Kinetic Characterization of Individual Hexose Transporters of *Saccharomyces cerevisiae* and their Relation to the Triggering Mechanisms of Glucose Repression. *JBIC J. Biol. Inorg. Chem.* **1997**, *245*, 324–333. https://doi.org/10.1111/j.1432-1033.1997.00324.x.

77. Boender, L.G.M.; de Hulster, E.A.F.; van Maris, A.J.A.; Daran-Lapujade, P.A.S.; Pronk, J.T. Quantitative Physiology of *Saccharomyces cerevisiae* at Near-Zero Specific Growth Rates. *Appl. Environ. Microbiol.* **2009**, *75*, 5607–5614. https://doi.org/10.1128/aem.00429-09.

78. Jules, M.; Beltran, G.; François, J.M.; Parrou, J.L. New Insights into Trehalose Metabolism by *Saccharomyces cerevisiae*: NTH2 Encodes a Functional Cytosolic Trehalase, and Deletion of TPS1 Reveals Ath1p-Dependent Trehalose Mobilization. *Appl. Environ. Microbiol.* **2008**, *74*, 605–614. https://doi.org/10.1128/aem.00557-07.

79. Youk, H.; Van Oudenaarden, A. Growth landscape formed by perception and import of glucose in yeast. *Nature* **2009**, *462*, 875–879. https://doi.org/10.1038/nature08653.

80. Teusink, B.; Diderich, J.; Westerhoff, H.V.; van Dam, K.; Walsh, M.C. Intracellular Glucose Concentration in Derepressed Yeast Cells Consuming Glucose Is High Enough To Reduce the Glucose Transport Rate by 50%. *J. Bacteriol.* **1998**, *180*, 556–562. https://doi.org/10.1128/jb.180.3.556-562.1998.

81. Bosdriesz, E.; Wortel, M.T.; Haanstra, J.R.; Wagner, M.J.; Cortés, P.D.L.T.; Teusink, B. Low affinity uniporter carrier proteins can increase net substrate uptake rate by reducing efflux. *Sci. Rep.* **2018**, *8*, 5576. https://doi.org/10.1038/s41598-018-23528-7.

82. De Alteriis, E.; Cartenì, F.; Parascandola, P.; Serpa, J.; Mazzoleni, S. Revisiting the Crabtree/Warburg effect in a dynamic perspective: A fitness advantage against sugar-induced cell death. *Cell Cycle* **2018**, *17*, 688–701. https://doi.org/10.1080/15384101.2018.1442622.

83. Woolford, J.L.; Baserga, S.J. Ribosome Biogenesis in the Yeast *Saccharomyces cerevisiae*. *Genetics* **2013**, *195*, 643–681. https://doi.org/10.1534/genetics.113.153197.

84. Nissen, T.L.; Schulze, U.; Nielsen, J.; Villadsen, J. Flux Distributions in Anaerobic, Glucose-Limited Continuous Cultures of *Saccharomyces cerevisiae*. *Microbiology* **1997**, *143*, 203–218. https://doi.org/10.1099/00221287-143-1-203.

85. van den Brink, J. Canelas, A.B.; van Gulik, W.M.; Pronk, J.T.; Heijnen, J.J.; de Winde, J.H.; Daran-Lapujade, P. Dynamics of Glycolytic Regulation during Adaptation of *Saccharomyces cerevisiae* to Fermentative Metabolism. *Appl. Environ. Microbiol.* **2008**, *74*, 5710–5723. https://doi.org/10.1128/aem.01121-08.

86. Jansen, M.L.A.; Diderich, J.A.; Mashego, M.; Hassane, A.; de Winde, J.H.; Daran-Lapujade, P.; Pronk, J.T. Prolonged selection in aerobic, glucose-limited chemostat cultures of *Saccharomyces cerevisiae* causes a partial loss of glycolytic capacity. *Microbiology* **2005**, *151*, 1657–1669. https://doi.org/10.1099/mic.0.27577-0.

87. Mashego, M.R.; Jansen, M.L.; Vinke, J.L.; Van Gulik, W.M.; Heijnen, J.J. Changes in the metabolome of *Saccharomyces cerevisiae* associated with evolution in aerobic glucose-limited chemostats. *FEMS Yeast Res.* **2005**, *5*, 419–430. https://doi.org/10.1016/j.femsyr.2004.11.008.

88. A Navas, M.; Gancedo, J.M. The regulatory characteristics of yeast fructose-1, 6-bisphosphatase confer only a small selective advantage. *J. Bacteriol.* **1996**, *178*, 1809–1812. https://doi.org/10.1128/jb.178.7.1809-1812.1996.

89. Zaman, S.; I Lippman, S.; Schneper, L.; Slonim, N.; Broach, J.R. Glucose regulates transcription in yeast through a network of signaling pathways. *Mol. Syst. Biol.* **2009**, *5*, 245. https://doi.org/10.1038/msb.2009.2.

90. Saliola, M.; Tramonti, A.; Lanini, C.; Cialfi, S.; De Biase, D.; Falcone, C. Intracellular NADPH Levels Affect the Oligomeric State of the Glucose 6-Phosphate Dehydrogenase. *Eukaryot. Cell* **2012**, *11*, 1503–1511. https://doi.org/10.1128/ec.00211-12.

91. Weber, C.A.; Sekar, K.; Tang, J.H.; Warmer, P.; Sauer, U.; Weis, K. β-Oxidation and autophagy are critical energy providers during acute glucose depletion in *Saccharomyces cerevisiae*. *Proc. Natl. Acad. Sci. USA* **2020**, *117*, 12239–12248. https://doi.org/10.1073/pnas.1913370117.

92. Thevelein, J.M. Regulation of Trehalose Mobilization in Fungi. *Microbiol. Rev.* **1984**, *48*, 42–59. https://doi.org/0146-0749/84/010042-18$02.00/0.

93. Nijkamp, J.F.; Broek, M.V.D.; Datema, E.; de Kok, S.; Bosman, L.; A Luttik, M.; Daran-Lapujade, P.; Vongsangnak, W.; Nielsen, J.; Heijne, W.H.; et al. De novo sequencing, assembly and analysis of the genome of the laboratory strain *Saccharomyces cerevisiae* CEN.PK113-7D, a model for modern industrial biotechnology. *Microb. Cell Factories* **2012**, *11*, 36. https://doi.org/10.1186/1475-2859-11-36.

94. Ljungdahl, P.; Daignan-Fornier, B. Regulation of Amino Acid, Nucleotide, and Phosphate Metabolism in *Saccharomyces cerevisiae*. *Genetics* **2012**, *190*, 885–929. https://doi.org/10.1534/genetics.111.133306.

95. Hardie, D.G.; Ross, F.A.; Hawley, S.A. AMPK: A nutrient and energy sensor that maintains energy homeostasis. *Nat. Rev. Mol. Cell Biol.* **2012**, *13*, 251–262. https://doi.org/10.1038/nrm3311.

96. Wu, G.; Yan, Q.; Jones, J.A.; Tang, Y.J.; Fong, S.S.; Koffas, M.A. Metabolic Burden: Cornerstones in Synthetic Biology and Metabolic Engineering Applications. *Trends Biotechnol.* **2016**, *34*, 652–664. https://doi.org/10.1016/j.tibtech.2016.02.010.

97. Celton, M.; Sanchez, I.; Goelzer, A.; Fromion, V.; Camarasa, C.; Dequin, S. A comparative transcriptomic, fluxomic and metabolomic analysis of the response of *Saccharomyces cerevisiae* to increases in NADPH oxidation. *BMC Genom.* **2012**, *13*, 317. https://doi.org/10.1186/1471-2164-13-317.

98. Zhang, J.; Herik, B.M.V.D.; Wahl, S.A. Alpha-ketoglutarate utilization in *Saccharomyces cerevisiae*: Transport, compartmentation and catabolism. *Sci. Rep.* **2020**, *10*, 12838. https://doi.org/10.1038/s41598-020-69178-6.

99. Verduyn, C.; Postma, E.; Scheffers, W.A.; van Dijken, J.P. Effect of benzoic acid on metabolic fluxes in yeasts: A continuous-culture study on the regulation of respiration and alcoholic fermentation. *Yeast* **1992**, *8*, 501–517.

100. de Koning, W.; van Dam, K.; de Koning, W. A method for the determination of changes of glycolytic metabolites in yeast on a subsecond time scale using extraction at neutral pH. *Anal. Biochem.* **1992**, *204*, 118–123. https://doi.org/10.1016/0003-2697(92)90149-2.

101. Pepper, M.E. Designing a Minimal-Knowledge Controller to Achieve Maximum Stable Growth for an *Escherichia coli* Bioprocess. *ProQuest Diss. Publ.* **2015**.

102. Theobald, U. *Untersuchungen zur Dynamik des Crabtree-Effektes, Reihe 17*; Fortschrittberichte/VDI: Düsseldorf, Germany, 1995.

103. Parrou, J.L.; Francois, J. A Simplified Procedure for a Rapid and Reliable Assay of Both Glycogen and Trehalose in Whole Yeast Cells. *Anal. Biochem.* **1997**, *248*, 186–188. https://doi.org/10.1556/aarch.59.2008.2.28.

104. Suarez-Mendez, C.A. Dynamics of Storage Carbohydrates Metabolism in *Saccharomyces cerevisiae*: A Quantitative study. *TU Delft Repos.* **2015**.

105. Feith, A.; Teleki, A.; Graf, M.; Favilli, L.; Takors, R. HILIC-Enabled 13C Metabolomics Strategies: Comparing Quantitative Precision and Spectral Accuracy of QTOF High- and QQQ Low-Resolution Mass Spectrometry. *Metabolites* **2019**, *9*, 63. https://doi.org/10.3390/metabo9040063.

106. Frank, C.; Teleki, A.; Jendrossek, D. Characterization of Agrobacterium tumefaciens PPKs reveals the formation of oligophosphorylated products up to nucleoside nona-phosphates. *Appl. Microbiol. Biotechnol.* **2020**, *104*, 9683–9692. https://doi.org/10.1007/s00253-020-10891-7.

107. Zimmermann, M.; Sauer, U.; Zamboni, N. Quantification and Mass Isotopomer Profiling of α-Keto Acids in Central Carbon Metabolism. *Anal. Chem.* **2014**, *86*, 3232–3237. https://doi.org/10.1021/ac500472c.

108. Junghans, L.; Teleki, A.; Wijaya, A.W.; Becker, M.; Schweikert, M.; Takors, R. From nutritional wealth to autophagy: In vivo metabolic dynamics in the cytosol, mitochondrion and shuttles of IgG producing CHO cells. *Metab. Eng.* **2019**, *54*, 145–159. https://doi.org/10.1016/j.ymben.2019.02.005.

109. Wijaya, A.W.; Ulmer, A.; Hundsdorfer, L.; Verhagen, N.; Teleki, A.; Takors, R. Compartment-specific metabolome labeling enables the identification of subcellular fluxes that may serve as promising metabolic engineering targets in CHO cells. *Bioprocess Biosyst. Eng.* **2021**, *44*, 2567–2578. https://doi.org/10.1007/s00449-021-02628-1.

110. Wakamatsu, A.; Morimoto, K.; Shimizu, M.; Kudoh, S. A severe peak tailing of phosphate compounds caused by interaction with stainless steel used for liquid chromatography and electrospray mass spectrometry. *J. Sep. Sci.* **2005**, *28*, 1823–1830. https://doi.org/10.1002/jssc.200400027.

111. Gower, J.C. Some Distance Properties of Latent Root and Vector Methods Used in Multivariate Analysis. *Biometrika* **1966**, *53*, 325. https://doi.org/10.2307/2333639.

112. Buchholz, J.; Graf, M.; Freund, A.; Busche, T.; Kalinowski, J.; Blombach, B.; Takors, R. CO_2/HCO_3-perturbations of simulated large scale gradients in a scale-down device cause fast transcriptional responses in Corynebacterium glutamicum. *Appl. Microbiol. Biotechnol.* **2014**, *98*, 8563–8572. https://doi.org/10.1007/s00253-014-6014-y.

RESEARCH ARTICLE

MICROBIAL BIOTECHNOLOGY | Applied Microbiology International

Performing in spite of starvation: How *Saccharomyces cerevisiae* maintains robust growth when facing famine zones in industrial bioreactors

Steven Minden[1] [ID] | Maria Aniolek[1] | Henk Noorman[2,3] | Ralf Takors[1] [ID]

[1]Institute of Biochemical Engineering, University of Stuttgart, Stuttgart, Germany

[2]Royal DSM, Delft, The Netherlands

[3]Department of Biotechnology, Delft University of Technology, Delft, The Netherlands

Correspondence
Ralf Takors, Institute of Biochemical Engineering, University of Stuttgart, Allmandring 31, 70569 Stuttgart, Germany.
Email: takors@ibvt.uni-stuttgart.de

Abstract

In fed-batch operated industrial bioreactors, glucose-limited feeding is commonly applied for optimal control of cell growth and product formation. Still, microbial cells such as yeasts and bacteria are frequently exposed to glucose starvation conditions in poorly mixed zones or far away from the feedstock inlet point. Despite its commonness, studies mimicking related stimuli are still underrepresented in scale-up/scale-down considerations. This may surprise as the transition from glucose limitation to starvation has the potential to provoke regulatory responses with negative consequences for production performance. In order to shed more light, we performed gene-expression analysis of *Saccharomyces cerevisiae* grown in intermittently fed chemostat cultures to study the effect of limitation-starvation transitions. The resulting glucose concentration gradient was representative for the commercial scale and compelled cells to tolerate about 76 s with sub-optimal substrate supply. Special attention was paid to the adaptation status of the population by discriminating between first time and repeated entry into the starvation regime. Unprepared cells reacted with a transiently reduced growth rate governed by the general stress response. Yeasts adapted to the dynamic environment by increasing internal growth capacities at the cost of rising maintenance demands by 2.7%. Evidence was found that multiple protein kinase A (PKA) and Snf1-mediated regulatory circuits were initiated and ramped down still keeping the cells in an adapted trade-off between growth optimization and down-regulation of stress response. From this finding, primary engineering guidelines are deduced to optimize both the production host's genetic background and the design of scale-down experiments.

INTRODUCTION

Saccharomyces cerevisiae is a time-tested and widely applied host in the biotech industry. Its central status as a cell-factory is rooted in an extensive knowledge base, advanced and facilitated genetic engineering, unproblematic valorization of biomass as a byproduct and foremost, robustness to diverse industrial conditions (Nielsen, 2019). The latter is based on the yeasts' ability to adapt to a wide array of ecological niches (Goddard & Greig, 2015; López-Maury et al., 2008), which is both a blessing and a curse for bioprocesses development. While ample adaptation mechanisms made the yeast a preferred platform organism for many bioprocesses, its flexibility comes at a price. Bioprocesses are typically developed in a homogeneous environment in lab-scale studies. In contrast, the industrial habitat is characterized by imperfect mixing since maintaining

RESEARCH ARTICLE

MICROBIAL
BIOTECHNOLOGY

Applied
Microbiology
International

149

equal mean broth circulation time with increasing tank volume poses an infeasible endeavour (Junker, 2004; Uhl & Von Essen, 1986). Resultant dynamic gradients, *for example*, of primary nutrients, constantly challenge the adaptive capacity of the cells even leading to non-expected regulation phenomena that may cause the deterioration of expected TRY (titre, rate, yield) criteria (Crater & Lievense, 2018; Enfors et al., 2001; Takors, 2016). This mirrors the interaction of multi-level regulation programs covering allosteric enzymatic control, transcriptional, translational and post-translational responses finally leading to physiological changes. Notably, each regulatory level possesses inherent response and relaxation times which overlap finally creating the integral response on external stimuli (Delvigne & Goffin, 2014; Wehrs et al., 2019). Hence, scale-up effects are the outcome of the complex interactions between production-scale hydrodynamic heterogeneities and multi-level yeast responses.

Carbon-limited fed-batch strategies are widely adopted to ensure efficient conversion of substrate to product, for instance, in a baker's yeast production. Feed rates are designed to allow fast growth while avoiding resource spillage through overflow metabolism. As a consequence, consumption times for highly diluted substrates may be shorter than the convective supply of said substrates leading to substrate depletion in poorly mixed zones of the bioreactor or far away from the inlet point (Lara et al., 2006). Inherently, substrate gradients (e.g. for glucose) creating excess and scarcity are likely to occur as confirmed experimentally and by simulation investigating the industrial bioreactor (George et al., 1998; Haringa et al., 2017; Sarkizi Shams Hajian et al., 2020). *Saccharomyces cerevisiae* senses variable substrate supplies via a plethora of multilayered and interconnected signalling cascades. Extracellular glucose levels are detected via the Gpr1/Ras2-cAMP-dependent protein kinase A (PKA) and Rgt2/Snf3-protein kinase B (PKB) nutrient kinases (Busti et al., 2010; Kim, Roy, et al., 2013). The sensing of intracellular glucose pools is directly mirrored by hexokinase activity and indirectly by the adenylate energy charge, AEC, through the Snf1/AMP-activated protein kinase (AMPK) network (Coccetti et al., 2018). The status of low ATP availability, that is, low AEC, is transduced via Snf1 to the rapamycin kinase complex I (TORC1) which regulates the growth rate together with PKA (Kunkel et al., 2019; Wullschleger et al., 2006). Further downstream, these regulatory nodes orchestrate the phosphorylation status of central transcription factors (TFs) finally translating external stimuli into well-adjusted microbial responses (Petrenko et al., 2013; Plank, 2022).

What determines the biological output from the above regulatory network is the combination of amplitude, frequency and dwell time with respect to the exposure to a certain glucose concentration.

Responses may be subtle, short-termed but well-buffered energetic imbalances or even fatal growth arrests (Bisschops et al., 2017; Verma et al., 2013). In any case, they are likely to deteriorate the productivity of engineered cells to produce the targeted product. Knowledge-driven downscaling aims to mimic related scenarios already in lab-scale for identifying proper prevention strategies (Delvigne & Noorman, 2017; Straathof et al., 2019; Takors, 2016). As a prerequisite of modern approaches, production-scale information is deduced from computational fluid dynamic (CFD) studies (Haringa et al., 2016; Lapin et al., 2004). Adding the biological phase to the flow field via cellular reaction dynamics (CRD) models, which are derived from stimulus–response experiments (SRE), enables the in silico characterization of relevant environmental stimuli (Penia Kresnowati et al., 2005; Zieringer & Takors, 2018). Finally, coupled CFD-CRD simulation results govern the quantitative design of both, realistic scale-down reactors and strains with increased process robustness (Haringa et al., 2017; Kuschel & Takors, 2020; Wang et al., 2020).

More and more studies highlight the prevalence of starvation zones in bioreactors that occurred distant from the feed zone in fed-batch processes (Haringa et al., 2016; Ho et al., 2022; Kuschel & Takors, 2020; Nadal-Rey et al., 2021). Remarkably, SRE-data covering the transition between carbon limitation and starvation are scarce, whereas the opposite, that is, sudden shifts towards glucose excess, were extensively studied in the past (Kresnowati et al., 2006; Suarez-Mendez et al., 2017; Theobald et al., 1997; Verhagen et al., 2022; Wu et al., 2006). The latter may reflect the fundamental interest in the Crabtree effect and its relevance for multiple metabolic scenarios (de Alteriis et al., 2018). However, such stimuli studies do not mimic the predominant conditions in large-scale bioreactors. Consequently, we set out to complement the current database with kinetic studies investigating the endometabolome after glucose shifts from limitation to starvation (Minden et al., 2022). In the referenced work, the metabolome of *S. cerevisiae* revealed a short-term strategy optimized to uphold anabolic needs at the expense of catabolic capacities when entering famine zones. Significantly increased biomass-specific energy demands after repeated exposure to the same glucose gradient raised the question how the stimulus is propagated in the eukaryotic regulatory network. Using next-generation-sequencing data, this study investigates gene-expression dynamics to answer two questions: (i) How does a yeast population respond to the first-time occurrence of glucose scarcity and (ii) how is the regulatory landscape shaped after complete adaptation towards the dynamic production environment?
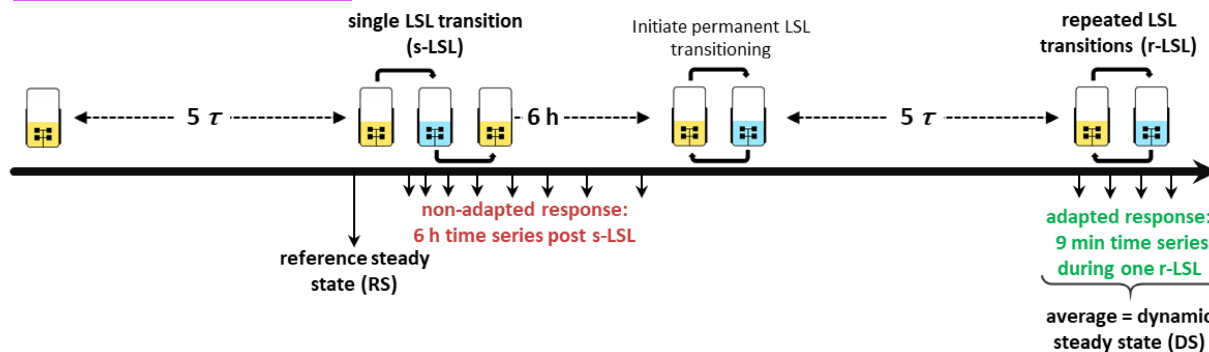
150

MICROBIAL
BIOTECHNOLOGY

Applied
Microbiology
International

RESEARCH ARTICLE

FIGURE 1 Process design of the chemostat experiment. τ, residence time.

EXPERIMENTAL PROCEDURES

Strain maintenance and seed culture conditions

Saccharomyces cerevisiae CEN.PK 113-7D (Nijkamp et al., 2012) was kindly provided by Royal DSM N.V. and preserved as a 30% (v/v) glycerol stock at −70°C and maintained on yeast extract peptone dextrose (YPD) agar plates at +4°C. Seed cultures were prepared by inoculating 5 ml YPD broth with single colonies in a glass vial followed by an 8-h incubation at +30°C on an orbital shaker operated with 120 rpm. The whole culture was pelleted and transferred to 110 ml of a synthetic medium in a 1000 ml baffled shake flask and incubated under identical conditions overnight. The medium was modified from Verduyn et al. (1992) to support carbon-limited growth in continuous culture with 22.5 g L^{-1} glucose. In brief, the referenced salt concentrations were increased threefold and the trace element and vitamin stock solutions were increased twofold.

Bioreactor setup and continuous operation mode

Aerobic, continuous fermentations were carried out in a stainless steel benchtop bioreactor (Bioengineering) with a liquid working volume of 1.7 L. The culture was supplied with sterile ambient air through a fumigation frit positioned at the reactor bottom with a constant flow rate of 0.5 vvm. Broth homogenization and bubble dispersion were ensured with two six-blade Rushton-type impellers operated constantly at 800 rpm equalling a gassed, volumetric power input of 7.1 W kg^{-1} to yield a circulation time of 0.1 s (Appendix S1: Tables S1 and S2). The relative dissolved oxygen concentration was determined with an optical pO$_2$ probe (PreSens) and never decreased below 70%. Broth temperature was controlled at +30°C with electrical heating and water cooling rods and monitored with a Pt100 probe (Bioengineering). The tank was operated at an absolute pressure of 1.3 bar, which was maintained with a

needle valve attached at the off-gas filter element exit. Two molar potassium hydroxide kept the broth pH at 5.00 using a Mettler Toledo probe. A continuous supply of Struktol J 674 antifoam agent (Schill und Seilacher) with a pump rate of 30 μl h^{-1} was realized with a LA-120 syringe pump (IDL GmbH) to pre-emptively avert foaming. Molar oxygen and carbon dioxide fractions in the off-gas were logged every minute with BCP-O$_2$ and BCP-CO$_2$ sensors (BlueSens). All in- and outgoing liquid flows were conveyed with U-120 peristaltic pumps (Watson-Marlow). Rapid sampling was enabled using semi-automated sampling devices based on time-relay controlled opening of a pinch valve (Minden et al., 2022).

Bioreactors were inoculated with 100 ml seed culture and the continuous phase was initiated after a rapid increase in the pO$_2$ signal marked the end of the batch phase. During continuous operation mode, the medium was fed at a fixed rate of 2.83 ml min^{-1} to yield a dilution rate of 0.1 h^{-1} via mass balancing of the whole fermenter through the harvest pump. The feed medium was constantly homogenized with a magnetic stirrer to prevent gradient formation.

Experimental design

Both, non-adapted and adapted starvation response experiments were conducted in the same chemostat process according to the process design depicted in Figure 1. First, the reference steady state (RS) was sampled after five residence times of constant Q_{O_2} and Q_{CO_2} conjointly marking time point 0 min of the non-adapted time series. Subsequently, the feed was interrupted for 2 min causing a transition from limitation to starvation back to limitation (LSL) and the stimulus–response was monitored for up to 6 h (denoted post s-LSL, s for single). Second, the dynamic steady state (DS) was characterized after five residence times of repeated LSL (r-LSL) transitioning. During this phase, the feed was operated in 9-min LSL-cycles with the feed inactive for 2 min and active for 7 min equalling a 9 min r-LSL cycle time. The active feed rate was adjusted to

3.64 ml min^{-1} resulting in a net dilution rate of 0.1 h^{-1}. Samples for the adapted response were drawn over one representative 9-min cycle and steady-state DS was expressed as the average over one cycle.

Sample follow-up and analytical procedures

All samples were measured in groups of technical triplicates and values reported in this study are expressed as the arithmetic mean ± standard deviation of technical means from three independent fermentation experiments. Carbon, nitrogen and available electron balances closed within ±3.6% at any sample point (see Appendix S1: Figure S1).

Dry matter of biomass (DMB) was quantified gravimetrically via vacuum-filtration of 5 ml degassed fermentation broth through desiccated and tared membrane filters (Ø 47 mm, Type 154; Sartorius). The filter cake was washed with 15 ml deionized H$_2$O and dried in a heating chamber at +70°C until mass remained constant after occasional weighing.

To assess extracellular glucose, broth was directly withdrawn into an open syringe and squeezed through a PES filter element (Ø 30 mm, 0.22 μm pore size, ROTILABO®; Carl Roth) within less than five seconds. The supernatant was flash-frozen in liquid nitrogen and stored at −70°C until analysis. Glucose was quantified with a UV-based enzyme test kit (art. no. 10716251035; r-biopharm AG) without sample dilution according to the manufacturer's instructions.

Intracellular glycogen determination was following the protocol originally published by Parrou and Francois (1997) and modified by Suarez-Mendez (2015) for rapid quenching. In brief, 1.5 ml broth was collected in 10 ml of <−40°C methanol and subsequently centrifuged for 5 min at −11°C under 5000 g. The resulting pellet was flash-frozen and stored at −70°C. Upon thawing, pellets were rendered permeable in 0.25 ml 0.25 M sodium carbonate heated to +95°C for 3 h in a water bath. Next, optimal conditions for enzymatic glycogen conversion to glucose were established by adding 0.15 ml M acetic acid and 0.6 ml 0.2 M sodium acetate (pH 5.2, adjusted with acetic acid). 0.48 ml of the resulting suspension was mixed with 20 μl of α-amyloglucosidase (~70 U ml^{-1}, cat. number: 10115; Merck) and incubated for +57°C for at least 12 h. Finally, the resulting suspension containing liberated glucose was separated from cellular debris via centrifugation (2 × 10^4 g, 1.5 min) and quantified as described above.

Intracellular total RNA levels were assessed based on the method described by Sasano et al. (2017). One millilitre of fermentation broth was transferred into a tube containing chilled 0.5 ml 1 M perchloric acid. The sample was immediately homogenized and placed for 20 min in a water bath maintaining +70°C. Subsequently,

the sample was mixed with 0.5 ml of 1 M K$_2$HPO$_4$ and the formed precipitate was removed via centrifugation (2 × 10^4 g, 1.5 min). The supernatant was flash frozen and stored at −70°C until RNA determination with a Nano-Drop ND-1000 (NanoDrop Technologies), which was blanked against a solution containing 0.25 M perchloric acid and 0.25 M K$_2$HPO$_4$.

Estimation of q$_{ATP}$

Biomass-specific ATP formation rate was estimated based on its stoichiometric relationship with oxygen uptake and glucose consumption according to $q_{ATP} = 2 \cdot q_S + 2 \cdot \frac{P}{O} \cdot q_{O_2}$ with an assumed $\frac{P}{O}$ ratio of 1.08 (Van Den Brink et al., 2008). The specific oxygen uptake rate was calculated after deconvolution of the off-gas sensor readout due to the volume of tubing and foam traps causing significant detection delays. The deconvolution method from Theobald (1995) was applied and has been described in detail recently (Minden et al., 2022).

Total RNA extraction

Total RNA extraction was performed using the Quick-RNA Fungal/Bacterial Miniprep Kit (R2014; Zymo Research) following the manufacturer's instructions with slight modifications. Prior to sampling, ZR BashingBead™ lysis tubes were prepared with 0.4 ml RNA lysis buffer and 0.1 ml DNA/RNA Shield™ agent (Zymo Research; not provided with the kit). During the experiment, 0.25 ml fermentation broth was instantly added to the prepared lysis tube, vigorously shaken by hand and flash-frozen in liquid nitrogen (all <10 s). This sampling routine yielded maximally 55 mg wet biomass (assuming a dry:wet matter of biomass correlation of 0.21 estimated from Aon et al., 2016) which is within the range of the recommended upper loading limit of 50–100 mg wet weight. Samples were stored at −70°C and extracted in batch from all three fermentations. The extraction protocol was started by thawing the samples fifty-fifty and subsequently homogenizing the sample in a Precellys 24 tissue homogenizer (Bertin Technologies) for two times 20 s at maximum speed with a 10 s break in between. All subsequent steps were performed according to the manufacturer's instructions. At the end of the protocol, total RNA was eluted with 60 μl DNase/RNase-free H$_2$O and each sample as split in two 30 μl aliquots.

Library preparation and RNA-sequencing

One aliquot from each sample was shipped for mRNA sequencing to GENEWIZ. Initial quality checks using the Agilent 2100 BioAnalyzer instrument (Agilent)

revealed high integrity of all samples with uniform RIN (RNA integrity number) values ≥9.9. Next, cDNA libraries were synthesized after polyA selection was performed to enrich mRNAs. Libraries were finally sequenced as paired-end reads of 150 base pair length on a NovaSeq 6000 platform (Illumina) with a sequencing depth of 2×10^7 paired-end reads per sample.

Processing of sequencing data

Sequencing results were received in the *.fastqsanger* format and uploaded on a local galaxy server instance (Afgan et al., 2018). First, the sequencing quality was assessed for each file individually using *FastQC* v. 0.72 (Andrews, 2010). Adapter sequences were removed using *Trimmomatic* v. 0.38.0 (Bolger et al., 2014) for paired-end reads with default settings. The trimmed sequence files were then aligned against the *S. cerevisiae* CEN.PK113-7D reference genome (GCA 000269885 – ASM 26988 v1) accessed from the ENSEMBL database (Howe et al., 2021) using the *TopHat* v. 2.1.1 (Kim, Pertea, et al., 2013) algorithm for paired-end reads with default settings yielding an overall alignment rate of 86%–93%. Count tables were computed using *featureCounts* v. 1.6.4 (Liao et al., 2014) together with the strain-specific annotation file *Saccharomyces_cerevisiae.R64-1-1.50.gtf*, also obtained from the ENSEMBL database. The generated count tables were merged into a *data.frame* object in the R environment v. 1.4.1106 (R Core Team, 2021) for downstream analysis.

Differential gene expression analysis

Differential gene expression analysis was conducted using the *DESeq2* v. 1.32.0 R-package (Love et al., 2014). After transforming the count table into the homoscedastic $\log_2$-scale with *rlog*, PCA analysis revealed a significant proportion of variance introduced into the dataset via multiple library preparations and sequencing runs (Appendix S2: Table S1 and Appendix S1: Section A3). Thus, the variables 'library run' and 'sequencing run' (as a merged variable called 'libseq') were introduced into the experimental design matrix. Time series and steady-state comparison were analysed with the likelihood ratio test (test = "LRT") and a model reduced by technically introduced variance (for details, see Appendix S1: Figures S2–S4). Genes were considered as differentially expressed with a |$\log_2$-fold change| above 0.322 and a false discovery rate (FDR) (Benjamini & Hochberg, 1995) below 1×10^{-3}. For further analysis, open reading frame identifiers were converted to ENSEMBL gene names using the libraries *AnnotationDBi* v. 1.51.5 and *org.Sc.sgd.db* v. 3.13.0.

Multidimensional scaling

Classical metric multidimensional scaling (Gower, 1966) was performed to visualize global dissimilarities in the gene expression profiles of all samples. First, $\log_2$-scaled count tables were cleaned from technical variance using the function *removeBatchEffect* from the *limma* v. 3.48.3 package (Ritchie et al., 2015). Subsequently, biological replicates were expressed as arithmetic means and only genes with significant differential expression in at least one condition were considered. The resulting table was converted to a Euclidean distance matrix using the *dist* function, transposed and passed to *cmdscale* (k = 3) for a three-dimensional representation of the sample distances. The functions *dist* and *cmdscale* were called from the *stats* v. 4.1.0 package.

Cluster and functional enrichment analysis

Time series gene expression data were clustered into groups of genes with similar patterns of $\log_2$-fold changes using the *kmeans* function from the *stats* v. 4.1.0 package. The algorithm was operated with a maximum of 1×10^3 iterations around two centroids for the adapted and six centroids for the non-adapted time series. For each cluster, gene ontology (GO) enrichment was assessed using the YeastEnrichr web interface (Chen et al., 2013; Kuleshov et al., 2019). YeastEnrichr was queried for the 'GO_Biological_Process_2018' library (source: http://geneontology.org/; release 2022-03-22) and significant terms (FDR < 0.05) were manually curated to avoid redundancy of GO terms. Up- and down-regulated gene lists from the comparison between steady-states RS and DS were additionally queried for the 'WikiPathways_2018' (source: https://www.wikipathways.org; accessed 2022-04-15) and the 'GO_Cellular_Component_2018' (source: http://geneontology.org/; release 2022-03-22). Non-curated enrichment results can be accessed in the Appendix S2, Tables S4–S9, S11, S12 and S14–S19.

Gene set enrichment analysis (GSEA) was performed with the R package *GAGE* v. 2.42.0 (Luo et al., 2009) to investigate significant differential expression of pre-defined gene lists. As described previously, $\log_2$-scaled count tables corrected for technical variance were used as an input for the *gage* function, which was configured to perform paired comparisons (compare = "paired"). Two-sample *t*-test values were used as a proxy for the intensity of gene-expression changes of the underlying gene set and converted to heat maps using the *ggplot2* package (version: 3.3.6.9000). Literature gene sets were extracted from various sources and transcription factor target lists were obtained from the Yeastract database (Monteiro et al., 2020). All 183 transcription factors available from

Yeastract were queried for genes with documented 'DNA binding and expression evidence' and converted to a *.gmt* file as an input for the *gage* function. Only literature gene sets and transcription factor target sets that were enriched significantly (FDR<0.05) in at least one condition per GSEA analysis were reported. All input and output tables used in this analysis are accessible in the Appendix S2 (Tables S20−S23; *.gmt* tables were reduced to gene sets which are shown in Figure 7).

RESULTS

Characterization of the famine stimulus

Sudden glucose shortages mimicking industrial-scale famine zones were established by periodic stops of the medium feed during carbon-limited growth. The 2-min lasting substrate starvation-induced glucose reduction from 150 to $30\,\mu mol\,L^{-1}$ (Figure 2A). Afterwards, the glucose-limiting feed scenario was re-installed finally creating a limitation-starvation-limitation (LSL) cycle. Interestingly, resulting glucose profiles were similar for non-adapted and adapted cells. The latter resulted from the repeated exposure to said LSL cycles (r-LSL, see Experimental Procedures). During one LSL-trajectory, biomass-specific glucose uptake rates (q_s) were severely curtailed, not exceeding 5% of maximum capacities ($9.3\,mmol\,g_{DMB}^{-1}\,h^{-1}$, from Diderich et al., 1999) for 14% of cycle duration. Given that large-scale CFD simulations assumed CEN.PK 113-7D to spend 40% of the time in sub-5% $q_{s,max}$ regimes (Haringa et al., 2017), the current experimental approach is qualified as rather mild but still realistic to mimic industrial-scale glucose depletion scenarios. The calculated adenylate energy charge (AEC) (previously reported in Minden et al., 2022) was monitored as a possible actuator for initiating regulatory energy sensing cascades (Figure 2B). By trend, AEC mirrors the extracellular glucose availability during starvation. The restoration of pre-stimulus values even occurred slightly faster than the recovery of extracellular glucose levels. Non-adapted cells decreased their AEC by 0.20±0.03 while amplitudes for adapted cells were almost doubled reaching a minimal value of 0.50±0.01. For a short period, both populations fell below the commonly accepted physiological AEC range of 0.7–0.9 (De La Fuente et al., 2014). This is a rather remarkable observation given that long-term glucose-starved yeasts can sustain their adenylate energy charge within the physiological range for up to several hours during the stationary phase (Ball & Atkinson, 1975; Weibel et al., 1974).

Short-term starvation evokes macroscopic rearrangements

Figure 3 compares post-stimulus data of the unperturbed reference (RS), the steady state after repeated

FIGURE 2 Characterization of the famine stimulus. (A) Extracellular glucose concentration and (B) intracellular adenylate energy charge (AEC) during the course of one perturbation cycle. AEC was calculated based on the methodology reported by Ball and Atkinson (1975). Red circles indicate dynamics following a single (s) LSL-transition and green triangles depict one representative repeated (r) LSL-cycle during steady-state DS. Time point 0 min of s-LSL is the equivalent of steady-state RS (yellow squares). All values indicate means ± standard deviation of three biological replicates. The underlying data were previously published in Minden et al. (2022).

perturbation (DS) and time-series of non-adapted cells. Furthermore, the small plot inside Figure 3B depicts two time series that reflect cellular responses during an LSL cycle. This diagram is provided for illustrating that the 'steady-state' after repeated perturbation 'DS' rather represents an average of dynamics than a true steady-state defined by constant state variables.

Notably, the biomass-substrate yield ($Y_{X/S}$) of RS persisted after long-term adaptation to alternating glucose availability as indicated by the similar DS (Figure 3A). In part, this was the result of

substantial metabolic re-arrangements in adapted versus RS-cells, including a reduction of the glycogen pool by 49% and increasing internal RNA abundance from $77.0 \pm 1.4\,\mathrm{mg\,g_{DMB}}^{-1}$ to $84.9 \pm 1.6\,\mathrm{mg\,g_{DMB}}^{-1}$ (Figure 3C,D). We quantified total ribonucleic acid as a proxy of ribosomal content, considering that 80% of total RNA in yeast contributes to the assembly of ribosomes as rRNA (Warner, 1999). Thereof, we hypothesized that the 3% rise of q_{ATP} ($p < 0.05$, Figure 2B) in DS versus RS was necessary to sustain increased translational capacities, which was partially counterbalanced by decreased energy spillage through glycogen-associated futile cycling.

A similar relation was found during the mid-term response of unstressed yeast cells post s-LSL. Within the first 10 min, glycogen pools slightly reduced by 13% to a minimum of $271 \pm 29\,\mathrm{\mu mol_{glucose}\,g_{DMB}}^{-1}$, followed by a relatively prolonged repletion phase of 3 h. In parallel, the population showed 5% increased q_{ATP} 20–60 min post-stimulus before energy demands relaxed to pre-stimulus levels. Again, RNA ramp-up dynamics seemed tightly linked with the temporally increased ATP demands. Following the peak of this non-adapted response, we found a significant reduction of $Y_{X/S}$ at the 1-h mark ($p < 0.05$) which eventually recovered. Thus, the temporal observation in this phase might reflect the

early initiation and retraction of the phenotypic shift, which is completed after long-term adaptation in DS.

Interestingly, the immediate intra-r-LSL q_{ATP} response during the representative cycle in Figure 3B revealed a reduction to $4.2\,\mathrm{mmol\,g_{DMB}}^{-1}\,\mathrm{h}^{-1}$ which represents a 44% larger amplitude than the non-adapted population (Figure 3B, insert plot). This observation is consistent with the equally larger AEC amplitudes within one r-LSL-cycle (Figure 2B) and points to a larger ATP drain accounting for the intensified translational capacities in adapted cells.

Next, we set out to elucidate regulatory phenomena on the gene expression level that govern the observed phenotypic shifts. Figure 4 displays the global analysis of Euclidean distances between all investigated samples using classical metric multidimensional scaling over three dimensions. The analysis of the first dimension distinguishes the grouping of adapted and non-adapted cells after their exposure to LSL cycles (Figure 4A). The apparent difference in the second dimension is further elucidated if the transcriptional time-series co-consider the third dimension (Figure 4B,C). By trend, the s-LSL exposure pushed the cells quickly away from their steady state within the first 4.5 min and it took about 180 min to return on a spiralled course. This pattern entails oscillating transcriptional dynamics, which reinforce until 20 min
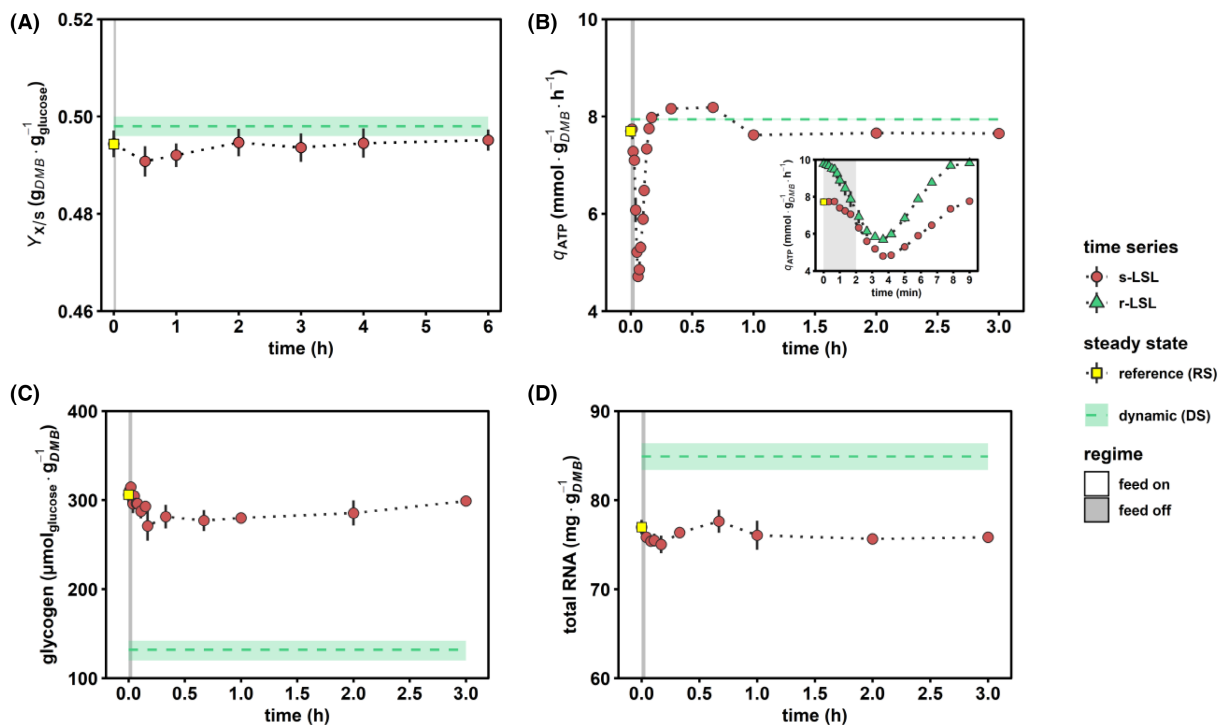

FIGURE 3 Macroscopic stimulus–response characterization. (A) Biomass-substrate yield. (B) ATP production rate estimated from oxygen and glucose consumption rates assuming a *P/O* ratio of 1.08 (Van Den Brink et al., 2008). The insert plot depicts the short-term dynamics during one representative LSL-cycle. (C) Intracellular glycogen and (D) total RNA pool dynamics. Red circles indicate dynamics during and up to 6 h post single (s) LSL and time point 0 min is the equivalent of steady-state RS (yellow squares). Green triangles depict one representative repeated (r) LSL cycle during steady-state DS. Steady-state DS is expressed as the average of dynamic data from r-LSL cycles (green dashed line) ± standard deviation (light area). All time series values indicate means ± standard deviation of three biological replicates.

RESEARCH ARTICLE

MICROBIAL
BIOTECHNOLOGY

Applied
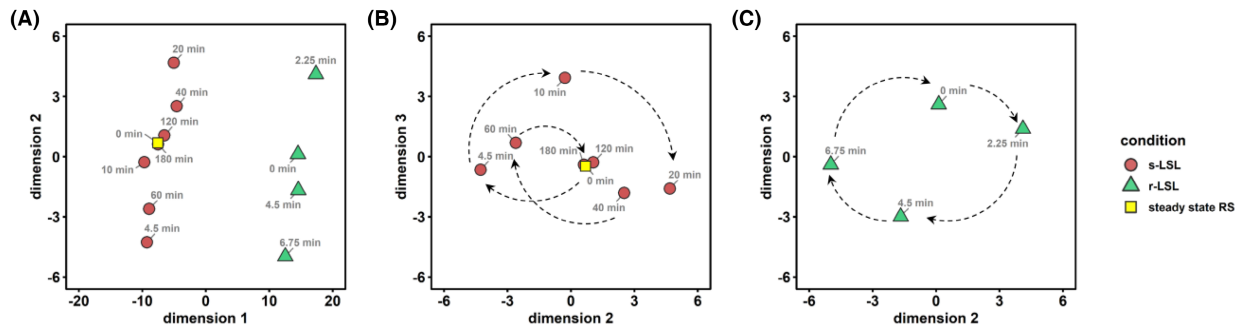Microbiology
International

155

FIGURE 4 Dissimilarities of significant gene expression patterns in the multidimensional scaling (MDS) space represented by three dimensions. (A) Whole dataset represented by the first two dimensions. (B) MDS plot of the post single (s) LSL time series (red circles + yellow square) based on dimensions 2 and 3. Dashed arrows provide a visual aid to follow the time series (C) Analogous MDS plot of the 9 min repeated (r) LSL time series (green triangles).

before complete relaxation after 180 min. In contrast, we observed a rather circular trajectory for adapted cells. The latter anticipates that a fraction of adapted cells always remained transcriptionally stimulated during the entire course of the experiments.

S. cerevisiae overloads the strategic response upon first-time glucose deprivation

Differential gene expression analysis uncovered 1065 genes accounting for 16% of the reference genome all fulfilling the statistical significance ($p < 1 \times 10^{-3}$) of differential expression during the 3-h lasting response upon the s-LSL stimulus. We grouped the differentially expressed genes (DEGs) into six clusters each featuring similar $\log_2$ fold changes. Furthermore, we assigned co-regulated genes via the enriched gene ontology (GO) terms (Figure 5). In sum, the clusters confirm the dynamics anticipated from the MDS analysis, which comprises an early transcriptional response followed by an amplified mid-term amplitude before slowdown.

Three of six clusters were disproportionately enriched with GO terms related to the translation machinery containing one-third of all 135 ribosomal proteins (RPs) in yeast (Gaikwad et al., 2021). Cluster 4 increased steadily over the first 40 min. Meanwhile, clusters 1 and 5 highlighted other dynamics that are laterally inversed. Whereas cluster 5 showed the early amplification of gene transcripts as described above, cluster 1 disclosed an opposite trend. The two clusters are particularly interesting as a trade-off between cytoplasmic and mitochondrial translation becomes evident. Several studies outlined that the coordinated redistribution of the costly translation machinery is a crucial feature for building up necessary respiratory capacity under stressful conditions (Bonawitz et al., 2007; Couvillion et al., 2016; Suhm et al., 2018). Further evidence of compartment-specific resource adjustments is provided by the enriched 'mitochondrial transport' ontology in cluster 5. However, we did not identify corresponding up-regulation of the respiratory chain complex despite our observation of increased ATP dissipation during the observed ramp-up of RNA content and $Y_{X/S}$. In addition, cluster 1 was enriched with transcriptional inducers of rRNA synthesis from polymerase I anticipating a bilateral relationship between regulatory circuits and their provoked strategic responses.

Co-regulated amino acid synthesis genes in cluster 2 followed the trajectory of cluster 1 but with a delayed onset and less pronounced fold changes. Both clusters were significantly enriched for 'alpha-amino-acid biosynthesis' activity, reaching a GO-term coverage of 46%. For some of the comprised genes, for example, those involved in leucine (*LEU2*, *LEU4*, *LEU9*) and aromatic amino acid biosynthesis (*ARO8*, *ARO7*, *TRP2*, *TRP3*, *TRP5*), the intracellular concentrations of their biosynthetic products qualitatively followed the observed cluster dynamics (Appendix S1: Figure S5). On the other hand, absolute glycogen levels appeared detached from the induction-repression dynamic of cluster 6 that comprised the related ontology. Nonetheless, this group contained both genes involved in glycogen mobilization (*GPH1* and *GDB1*) and accumulation (*GLC3* and *GDB1*) which may be taken as a hint towards the dynamic activity of futile cycling (Blomberg, 2000; François & Parrou, 2001). We observed a general tendency for the initial repression of genes involved in primary anabolism, while catabolic enzymes from glucose, pentose, and pyruvate metabolic processes followed the opposite trend.

Genes that were annotated to cluster 3 signalled slight activity of stress-responsive mechanisms. For instance, members of the 'intracellular protein transport' comprise chaperone activity such as *SSA1* and *CUR1* or were involved in protein recycling, *for example*, through *VPS29* and *EAR1*. The early induction of transcriptional repressors ('negative regulation of RNA polymerase II promotor transcription') may indicate broader macromolecular savings. Furthermore, the LSL-stimulus triggered
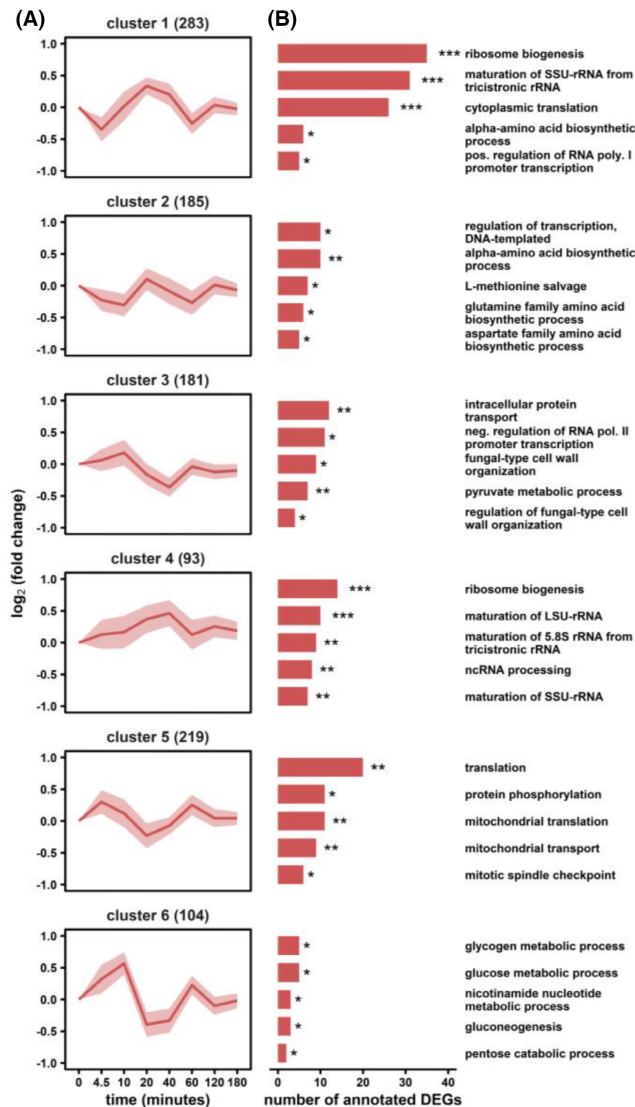
FIGURE 5 Differential gene expression analysis of the non-adapted s-LSL response. (A) Six clusters with similar gene-expression dynamics are shown with the number of dedicated genes in brackets. (B) Corresponding gene ontology (GO) enrichment analysis. The false discovery rate (FDR) interval is indicated by asterisks for each GO term (* $1 \times 10^{-5} \leq FDR < 5 \times 10^{-2}$; ** $1 \times 10^{-10} \leq FDR < 1 \times 10^{-5}$; *** $FDR < 1 \times 10^{-10}$).

changes in cell wall organization and even associated transcription factors (TFs). Taken together, a sudden shift from glucose limitation to starvation prompted *S. cerevisiae* to enter a defensive state preparing for times of scarcity. As this preparatory measure turned out to be premature, a pronounced backlash caused dampened transcriptional bursts up to 2h post-stimulus.

Repeated famine exposure shapes a specialist growth phenotype

The transcriptomic landscape of yeasts adapted to unstable glucose uptake during DS was investigated by three-level enrichment analysis. Gene ontologies grouping genes according to biological function, pathway affiliation, and compartment-specific localization were used to characterize 728 repressed and 676 induced genes relative to RS (Figure 6). The dominant fraction of DEGs was operating in the nucleus, where highlighted reconstructions of the regulatory network and proliferation apparatus occurred. The first is apparent as 20% of both up- and down-regulated mRNAs encoded transcription factors. More specifically, significant down-regulation of nuclear protein quality control through ubiquitin-dependent proteolytic activity and up-regulation of cell cycle-related DNA metabolic processes was observed.

Regarding the proliferative capabilities, the 'cell cycle and cell division' pathway were amplified by increasing expression levels of engaged cyclins, kinases and transcription factors. Attached were up-regulated functional categories on the level of DNA repair and segregation and cell division, represented by the terms 'DNA metabolic process' and 'mitotic cytokinesis' respectively. Gene expression of the translational machinery was strongly induced at the stage of early ribosome biogenesis (RiBi) in the nucleus, including rRNA processing and the maturation of several ribosomal subunits (Woolford & Baserga, 2013). Induction of RiBi genes was accompanied by the up-regulated 'nutrient control of ribosomal gene expression' ontology, which involved genes of the cAMP-dependent protein kinase A (PKA) nutrient-signalling network, such as the receptor protein Gpr1 and PKA subunits *TPK1/3*. On the other end of the ribosomal life cycle, down-regulation of proteolytic activity was evident from several GO readouts, particularly represented by the term 'proteasome-mediated ubiquitin-dependent protein catabolic process'. The ubiquitin system predominantly controls the nuclear turnover of ribosomal subunits and its activity must be repressed to allow atypical overexpression of RPs (An & Harper, 2020; Sung et al., 2016). Additionally, mature ribosomes were adjusted based on their subunit configuration in both the cytosol (16 up, 12 down) and the mitochondrion (7 up, 10 down).

Metabolic enzymes were primarily repressed in the regime-transitioning environment of DS. Especially, glycolytic catabolism was subjected to a slowdown as represented by several enriched GO terms. One exception, however, was the non-oxidative branch of the pentose phosphate pathway, possibly a reflection of increased anabolic needs to supply the overproducing translation machinery. Furthermore, *S. cerevisiae* sacrificed activity of various stress-specific programs such as the mentioned MAPK signalling, the 'cellular response to oxidative stress' or the nutrient-starvation-specific 'lysosomal microautophagy' (Gross & Graef, 2020). In contrast, the up-regulated biological function ontology 'vesicle-mediated transport' involved many endocytic genes. Recently, Johnston et al. (2020)
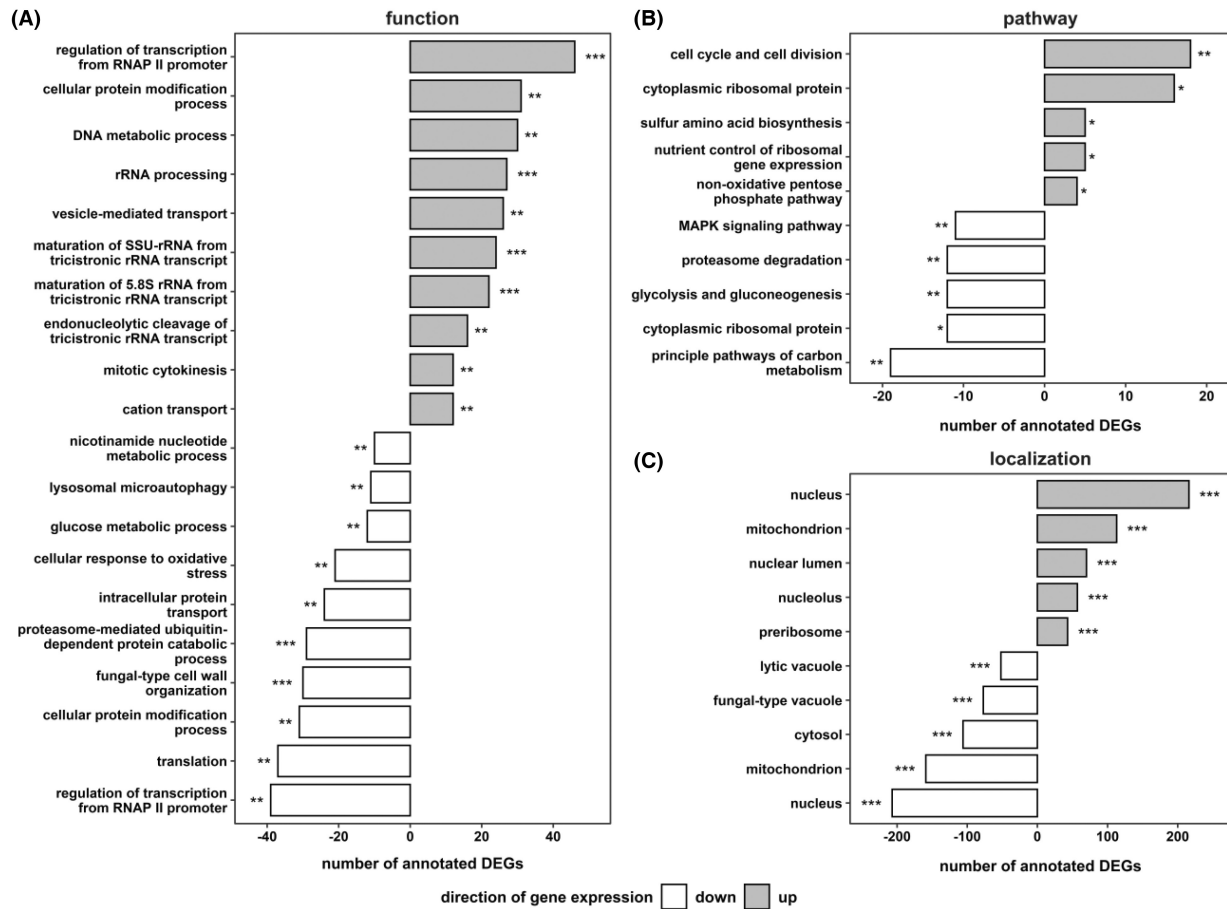
FIGURE 6 Functional enrichment analysis of steady-state DS based on (A) biological function, (B) pathway affiliation and (C) cellular localization annotations. The false discovery rate (FDR) interval is indicated by asterisks for each GO term (* $1 \times 10^{-5} \leq \text{FDR} < 5 \times 10^{-2}$; ** $1 \times 10^{-10} \leq \text{FDR} < 1 \times 10^{-5}$; *** $\text{FDR} < 1 \times 10^{-10}$).

reported that under conditions of extracellular nutrient scarcity, yeasts scavenge for alternative nutrients via increased endocytosis activity.

Complementary to the steady-state assessment, we investigated the existence of persistent regulatory dynamics of the DS-population. Accordingly, 251 stimulus-responsive genes in fully adapted cells were identified (Figure 7). Two symmetric clusters revealed oscillatory gene expression changes with two inflection points during 9-min r-LSL cycles. With this short window of observation, the clusters were mainly enriched for fast-responding genes with short half-lives <10 min, such as those involved in stress response, ribosome biogenesis and transcription regulation (Miller et al., 2011). Especially, the latter two categories were also prevalent in the non-adapted response, reflected by 142 overlapping genes accounting for 57% of the adapted DEG dynamic. Thus, despite pronounced changes in the global transcriptional landscape during steady-state DS, *S. cerevisiae* still executes starvation-induced short-term gene expression changes that are independent of its adaptation status.

Cluster 1 revealed regulatory activity of the DNA replication process, represented by the GO terms 'sister chromatid segregation' and 'mitotic DNA damage checkpoint'. The latter involved *RAD53*, the master effector kinase regulating progression through the S-phase of the cell cycle (Branzei & Foiani, 2006). Recently, *RAD53* revealed additional transcriptional control over several promoters covering 20% of the whole yeast genome, emphasizing its wide regulatory influence (Sheu et al., 2021). Notably, there was no overlap with 'cell cycle and cell division' genes up-regulated during steady-state DS (Figure 6B) despite their involvement in the same signalling cascade of S-phase DNA damage checkpoint, such as the mediator protein *RAD9* (Pardo et al., 2017). The ontology 'methionine biosynthetic process' confirms the existence of a tightly regulated crosstalk between glucose sensing and methionine synthesis. Zou et al. (2020) linked this relationship to the rate-limiting function of methionine on translation initiation through the formation of methionyl tRNA. More differentially expressed kinase encoding genes were found in the two top GO terms in cluster 2, with no apparent functional connection to the
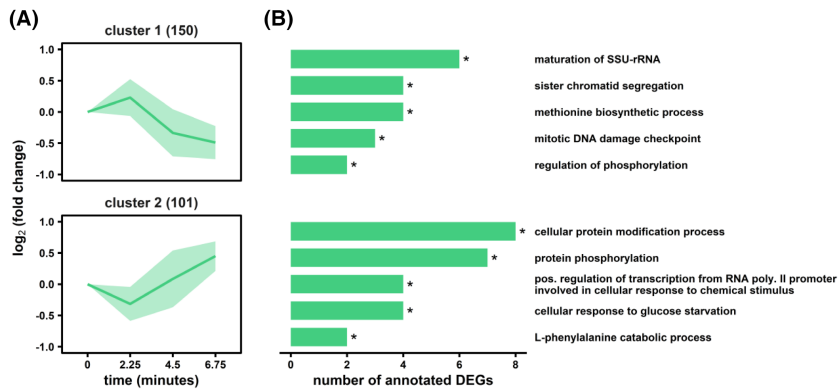
FIGURE 7 Differential gene expression analysis of the adapted r-LSL time series. (A) Two clusters with similar gene-expression dynamics are shown with the number of dedicated genes in brackets. (B) Corresponding gene ontology enrichment analysis. The false discovery rate (FDR) interval is indicated by asterisks for each GO term (* $1 \times 10^{-5} \leq$ FDR $< 5 \times 10^{-2}$).

unstable nutrient availability. In contrast, the following two entries contain regulatory proteins involved in the early starvation response (*USV1* and *MTL1*) or glucose catabolite repression, such as transcription factors Adr1 or Mig1 and the Snf1 subunit gene *SIP2* (Stasyk & Stasyk, 2019).

To recapitulate, repeated exposure to glucose shortage in LSL cycles induced pronounced transcriptional reprogramming in *S. cerevisiae*. The strategic response encompassed up-regulated growth capacities and down-regulated metabolic and stress-responsive pathways. However, full adaptation did not shut down the repeated on–off switching of immediate tactical mechanisms involved in DNA replication and translation initiation control.

A stress defence—growth trade-off shapes the fate of yeasts in a heterogeneous environment

In the final part of this study, we investigated the presence of global transcriptional programs and their underlying regulatory mediation through gene set enrichment analysis (Figure 8). Non-adapted yeast cells showed significant signs of executing the environmental stress response (ESR), a program that initiates a broad spectrum of stress-responsive genes (ESR-induced ESRi) while simultaneously repressing ribosomal protein (RP) and biogenesis (RiBi) genes (Brion et al., 2016; Gasch et al., 2017). This well-investigated characteristic is clearly visible in Figure 8A and has been observed previously in various stresses (Levy et al., 2007; MacGilvray et al., 2020). The temporal dynamic of the ESR follows the earlier described trend of overshooting as evidenced by matching patterns of gene sets controlled by its master transcription factors Msn4, Sko1, Sok2 (ESRi), Sfp1 (RP and RiBi) and Ifh1 (RP) (Gasch et al., 2017; Gutin et al., 2015; Skoneczny, 2018). Besides common ESR regulators, we identified the activity of non-ESR-associated stress-responsive TFs such as heat shock transcription factor Hsf1, the calcineurin-responsive zinc finger Crz1, and

the oxidative stress regulators Cin5 and Skn7. Interestingly, Hsf1 targets seem to operate 'out of phase' compared to the overall transcriptional dynamics suggesting divergent signal integration. Indeed, ESR coordination is dominated via target of rapamycin 1 (TORC1) and PKA crosstalk (López-Maury et al., 2008), while glucose starvation-induced Hsf1 phosphorylation is dependent on the Snf1 signalling cascade (Hahn & Thiele, 2004). We further assessed expression changes of 267 strictly growth rate-dependent genes extracted from Fazio et al. (2008) which followed the observed transient $Y_{X/S}$ reduction implied by Figure 3A. In contrast, the cell cycle gene set was not affected significantly during the non-adapted time series, even though Figure 8B indicated a steady gene expression decline of Swi4 targets. However, this cell cycle regulator reportedly plays a role in the induction of several stress-responsive genes under the control of the Xbp1 promoter (Mai & Breeden, 1997). Altogether, we anticipate that stress-sensing networks dominated the transfer of non-adapted cells to a defensive state. We rule out mere growth rate sensing as an effector since μ correlated genes surged after 4.5 min, while the first significant reduction in $Y_{X/S}$ was observed 1 h post-s-LSL stimulus.

Remarkably, the adapted DS-culture predominately followed the same course of transcriptional dynamics of the mid-term s-LSL response after 20–40 min. In this phase, the *S. cerevisiae* transcriptome ramped up growth-associated genes and repressing stress-responsive genes. Regarding metabolic gene sets a pronounced difference emerged: The non-adapted response showed expression changes of gene sets representing glycolysis, gluconeogenesis and fatty acid oxidation coordinated by their respective TFs Adr1 and Cat8 (Young et al., 2003). In contrast, the DS-phenotype showed down-regulated glycolytic/gluconeogenic genes, but no sign of Adr1 or Cat8 regulation. Instead, Cat8 targets were constantly differentially expressed within adapted LSL-cycling. Another regulatory program with persistent temporal activity during DS was controlled by Bas1, a control mechanism for ATP homeostasis (Pinson et al., 2019).
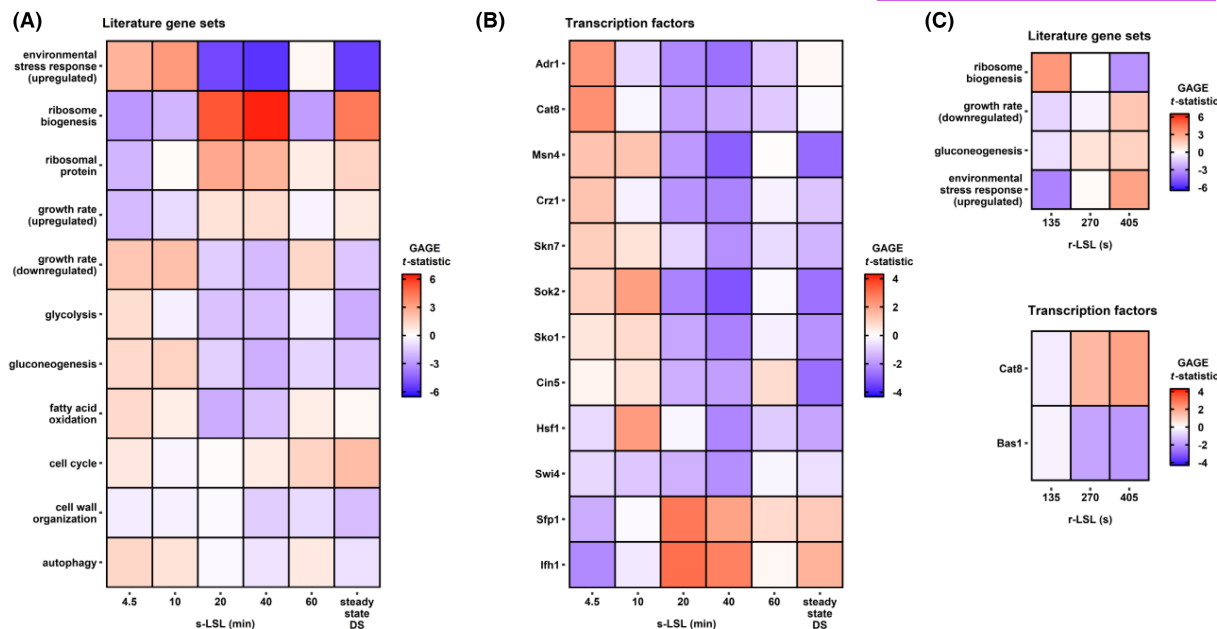
FIGURE 8 Gene set enrichment analysis (GSEA) of pre-defined gene lists from literature and transcription factor target lists. The reported *t*-statistic implies the strength and direction of coordinated differential gene expression of a given set. GSEA was performed comparing the single (s) LSL time series and steady-state DS (A and B) on the one hand, and the dynamics within the repeated (r) LSL cycles (C) on the other hand. Only gene sets with significant enrichment during at least one sample point (FDR <0.05) are reported in this figure.

Figure 8C further indicates additional short-term dynamics of ESR-associated gene expression, although to a lesser extent, compared to the time series after a single famine stimulus. Notably, only RiBi, not RP genes, were differentially expressed in concert with the ESRi group.

DISCUSSION

The impact of famine zones in industrial bioreactors

Gradients of limiting nutrients occur when reaction times of microbial activity match or exceed mean circulation times (Haringa et al., 2018; Lara et al., 2006). This correlation causes the appearance of carbon starvation regimes during the growth (Nadal-Rey et al., 2021) or production phase of C-limited fed-batch processes. We imposed a single famine stimulus on steady-state yeast cultures to investigate the influence of this scale-up effect on strain performance when starvation zones start to build up. The population which was already adapted to glucose limitation apparently perceived the exposure to glucose starvation as a warning signal, which immediately triggered facets of the ESR (Gasch et al., 2000). Even though optimal conditions were restored within 76 s, *S. cerevisiae* CEN.PK 113-7D obviously lacks the regulatory capability to stop the initiated program efficiently. Instead, the stressed cells shifted into a 'panic mode' which is characterized by frequent switching

on/off of regulatory genes that caused increased ATP expenditure and impaired growth. Understanding the underlying regulatory mechanisms is paramount to engineer robust strains and guided this study.

Several studies anticipate that the initiation of the ESR following acute glucose starvation is dominated by cAMP-dependent PKA signalling (De Wever et al., 2005; Görner et al., 2002; Martínez-Pastor et al., 1996). PKA, in turn, controls the ESRi regulon through activation of the transcriptional inducers Msn2/Msn4 and inactivation of the repressors Sko1 and Sok2 (Gutin et al., 2015). A characteristic property of these and other stress-related TFs such as Crz1 is their oscillating translocation between nucleus and cytoplasm (Zadrąg-Tęcza et al., 2018). Gutin et al. (2019) reported that Msn2/Msn4 activate two successive bursts of transcription upon exposure to osmotic stress: First, PKA dephosphorylates Msn2/Msn4 causing their translocation to the nucleus to initiate quick but weak transcriptional changes within 10 min. Strong transcriptional changes require a pulsatile translocation of Msn2/Msn4 between nucleus and cytoplasm, during which nuclear export is mediated by Msn5. Thus, we reason that the non-adapted response examined in this work displayed the initiation phase but not the second progression phase, potentially explaining the mild log-fold changes compared to others (Causton et al., 2001; Gasch, 2007). Recently, Wu et al. (2021) inferred that Msn4, but not Msn2, is regulated by an incoherent feedforward loop (IFFL), including the intermediate regulator kinase

Yak1. Since the purpose of IFFLs is to accelerate response time and execute oscillatory behaviour (Reeves, 2019) we interpret the absence of significant Msn2 regulation (Figure 7B) as further support for an early ESR retraction mechanism.

Recent research concerning the ESR identified strong counter-correlated gene expression between the ESRi and RP/RiBi clusters. The latter, sometimes referred to as the ESRr (ESR repressed) cluster, is mediated by the regulatory activity of Sfp1, Ihf1/Fhl1 and the general activator/repressor TF Rap1 (Gasch et al., 2017; MacGilvray et al., 2020). Our experiment confirmed the mutual relationship between ESRi and ESRr, even though transcriptional control of RP and RiBi genes was executed exclusively via Sfp1 and Ifh1. Both TFs are inducers of proliferative capacity as Sfp1 binds the RiBi-associated PAC promoter while Ifh1 positively controls RP gene expression through a currently unknown promoter architecture (Cipollina et al., 2008; Schawalder et al., 2004). Either TORC1 or PKA retains their active state during optimal growth. Sudden downshift of nutrients, however, induces PKA-coordinated ESRr down-regulation, which can be explained by cytosolic localization of Sfp1 and Ifh1 alone (Shore et al., 2021; Zencir et al., 2020). This exclusively stress-specific role of Sfp1 and Ifh1 is mediated through their antagonizing TFs Dot6/Tod6 and Stb3 respectively (Huber et al., 2011; Plank, 2022).

Taken together, the observed retraction and overshooting gene expression originated from the TORC1/PKA circuitry since both nodes tune the temporal and local displacement of overlapping TFs. Acute glucose exhaustion signals PKA to execute its feedforward role to rapidly respond to the stimulus and override the steady-state controller TORC1 (Kunkel et al., 2019). Similarly, PKA remains dominant when glucose levels elevate, leading to overshooting regulation until TORC1 regains control. It is somewhat surprising that the overshoot amplitude matches the initial response. Combined with the feedforward role of PKA, multiple feedback mechanisms exist with the potential to act as signal amplifiers. For instance, Ashe et al. (2000) reported severe inhibition of translation initiation within 30–60 s after glucose depletion, which can induce rapid RiBi and RP mRNA degradation (Huch & Nissan, 2014). In our experiment, ample nutrient conditions 2 min after the start of the s-LSL cycle superimposed the initiated decay of translation-associated genes. The phenotype may be explained by consequent disparate sensing of expected versus actual growth rates that may prompt yeasts to boost transcription of growth-associated mRNAs causing the observed overshoot (Shore et al., 2021). Regarding the regulation of energy homeostasis, the Snf1 kinase is activated upon AEC drops by as narrow as 0.1 causing inhibition of TORC1 (González & Hall, 2017; Oakhill et al., 2012) and co-phosphorylation of stress-responsive PKA targets (De Wever et al., 2005).

Once activated, Snf1 co-activated specific gene expression programs via crosstalk with the TOR/PKA node. Furthermore, the TFs Adr1 and Cat8 are amplified but not Mig1 (Busti et al., 2010). Besides Snf1, Mig1 is dependent on further activation through hexose kinase 2 and represents one branch of dual control over the carbon catabolite repression (CCR) regulon. The second branch integrates extracellular glucose signals through the sensory Rgt2/Snf3-PKB system (Busti et al., 2010; Kim, Roy, et al., 2013). Since we did not observe any differentially expressed CCR genes, we reason that Snf1 regulation is solely AEC driven. Consequently, the strictly glucose-related Rgt2/Snf3-PKB pathway was not implicated in the non-adapted response. Short-term energy deprivation further induced changes in mitochondrial translation (see Figure 5 cluster 5). Yi et al. (2017) reported that Snf1 associates with the mitochondrial membrane to support respiratory activity for 10 h of glucose starvation—a prerequisite to sustain autophagy during arrested growth. We hypothesize the existence of a preparative program that was aborted in early stage in analogy to the observed ESR dynamics: Genes encoding translational capacities might have been differentially expressed as a preparatory measure to alter mitochondrial respiration. Nevertheless, the cascade was shut down promptly after return to steady-state conditions.

The transcriptional response mirroring frequent glucose starvation

Once famine zones are established during industrial fermentations, yeast cells require adaptation to withstand the repeated exposure to the starvation conditions that request regime transitions. Our experimental design enabled the investigation of the growth phenotype and the transcriptional strategy during oscillatory glucose availability by imposing an intermittent feeding regime. On a macroscopic level, the cellular mode of operation mimicked that of a faster-growing population, *that is*, reduced carbon storage pools, increased rRNA content and ribosomal gene expression, decreased ESR expression levels, down-regulated glycolytic genes and up-regulated cell cycle genes (Brauer et al., 2008; Nissen et al., 1997; Regenberg et al., 2006; Silljé et al., 1999; Xia et al., 2022).

Processing of dynamic environmental inputs can cause repeated decoupling of the growth rate from the expected μ-specific transcriptome (Levy & Barkai, 2009; Zakrzewska et al., 2011; Zaman et al., 2009). Dedicated studies assigned this dissonance predominantly to high PKA activity, which is in agreement with our DS dataset: Strong ESRi repression and RiBi induction, backed by increased expression levels of PKA pathway components are opposed to relatively weak RP induction, owing to

the TORC1-dependency of the latter (see summarizing Figure 9) (Huber et al., 2011). Under the investigated conditions, however, cells did not shut down rapid translation initiation control mechanisms, which is also reflected by dynamic ESRi/RiBi patterns during the adapted time series. This finding may surprise as the yeast's ability to decelerate translation upon glucose scarcity may be regarded as a persistent 'first line of defence' (Hershey et al., 2012). Instead, cells apparently enable growth by benefitting from higher ribosome abundance as it was observed in other studies (Metzl-Raz et al., 2017; Young & Bungay, 1973). This seems to be an evolutionarily conserved principle since bacterial cells elevate ribosome content for accelerating growth after relieving from various stresses (Bergen et al., 2021). However, despite amplifying genes encoding ribosomal proteins, yeasts further backed ribosomal biogenesis and configuration to maximize growth capacities. In this context, Parenteau et al. (2015) reported that perturbed growth can induce the expression of different subunits including gene paralogues which increase fitness and which are repressed under normal growth. Likely, de-repressed RP paralogues do not exert stress-specific functions but may enable atypical gene overexpression. In our study, however, we could not draw any conclusion if and to which extent differentially expressed paralogue genes actually contributed to the observed phenotype.

Furthermore, even though still under debate, increased RiBi expression supposedly indirectly promotes progression over START during the cell cycle through Whi5 inactivation (Bernstein et al., 2007; Polymenis & Aramayo, 2015; Schmoller et al., 2015). Eased START passaging leads to reduced time within the G0/G1 phase and decreased trehalose and glycogen pools (Brauer et al., 2008; Paalman et al., 2003). Hence, we argue that the cell cycle aligned with the PKA-guided shaping of the translational machinery following the environmental signal as a feedback mechanism (Müller et al., 2003). Transcriptome analysis revealed added regulatory rearrangements that point towards a preference for PKA activity over TORC1 control. Down-regulation of non-relevant stress signalling cascades was observed, such as the

osmo-responsive MAPK cascade—a constitutive inhibitor of PKA (Mace et al., 2020). In terms of energy homeostasis, elevated translational capacity is ATP-costly and might have contributed to the increased AEC difference during the LSL transition in DS. A more pronounced drop of the AEC, in turn, could potentially amplify the earlier discussed Snf1-guided energy signal integration with positive feedback for PKA and repression of TORC1 targets. In conclusion, exposure to recurring regime transitions shifted the regulatory response of *S. cerevisiae* into a mode of dominating PKA signalling. The kinase constantly overrides the steady-state controller TORC1 and is amplified by several feedback mechanisms, the consequence of which is a cellular tuning to enable efficient growth acceleration based on the adapted ribosome portfolio.

Potential transfer of knowledge for industrial strain engineering

Understanding how cells adapt to substrate heterogeneities in industrial bioreactors is important for bioprocess optimization. The trade-off between stress-response and internal growth capacity turned out as a key mechanism to explain cellular performance under recurring glucose starvation. If biomass itself is the product, maintaining a high growth rate is a favourable trait. However, for exploiting metabolic production capacities the prioritization of re-installing high growth rates may deteriorate the supply of carbon, reduction factors, and energy for the targeted product formation. This conflict may arise for metabolic products as well as for heterologous proteins. For the latter, ribosome buildup could potentially reduce the product yield and *vice versa* (Birnbaum & Bailey, 1991). Yet, predicting the impact of competing resource allocations influenced by environmental signalling is not a trivial task (Kafri et al., 2016). For instance, Wright et al. (2020) reported increased insulin production from *S. cerevisiae* in a two-compartment scale-down approach with a remarkable conformity to the results presented here: Environmental heterogeneity enforced the translational machinery and repressed stress-responsive networks, which proved to
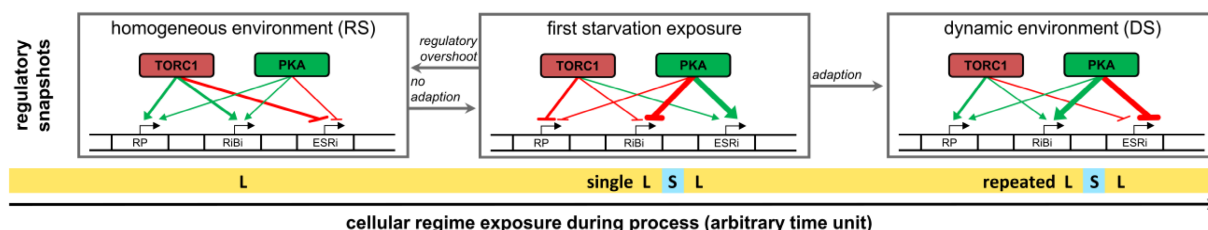

FIGURE 9 Key regulatory elements comprising target of rapamycin 1 (TORC1) and protein kinase A (PKA) signalling. DS, dynamic steady state; ESRi, induced environmental stress response genes; L, C-limitation; RiBi, ribosome biogenesis genes; RP, ribosome protein genes; RS, reference steady state; S, C-starvation.

be beneficiary for insulin productivity. In consequence, we propose two use cases for our dataset.

First, the deployed scale-down approach can enable strain engineers to streamline industrial hosts. For instance, we observed a presumably unnecessary induction of the ESRi cluster upon first-time glucose withdrawal as it was actively repressed during repeated glucose oscillations. Thus, deleting Msn2/4 could potentially save unwanted resource expenditure. This proposal is supported by the work of Ashe et al. (2000), who prove that *msn2/4Δ* strains abolished the induction of the stress response program while maintaining a normal growth phenotype. Likewise, our dataset suggests wasteful gene expression induced via Hsf1 and Crz1. Indeed, altering nuances of the regulatory response via TF engineering gains popularity as relatively minor changes in the genetic background can improve strain performance significantly (Mohedano et al., 2022). For instance, several studies achieved increased ethanol yield through the atypical expression of just a single transcription factor (Michael et al., 2016; Samakkarn et al., 2021; Watanabe et al., 2017).

Second, this and other work supports the finding that glucose availability, but also other industrially relevant heterogeneities, converge mainly on the level of PKA signaling (de Lucena et al., 2015; De Melo et al., 2010; Norbeck & Blomberg, 2000; Zaman et al., 2009; Zhao et al., 2015). To conclude, we would like to formulate a somewhat alternative, maybe even provocative scale-down route. If mere activation/inhibition dynamism of PKA shapes the corpus of adaptation effects during industrial fermentations, wouldn't triggering PKA according to process-relevant stimuli suffice as the most simplistic scale-down experiment? Instead of trying to mimic physicochemical perturbations by wet-lab approaches as close to reality as possible, it might be sufficient to characterize the frequency and amplitude of relevant stimuli a priori, for instance, by means of CFD simulations. Consequentially, the simulation output should be translated into an input signal for the PKA hub. Tools to control PKA activity on relevant scales are already available, such as optogenetic switches (Hepp et al., 2020; Stewart-Ornstein et al., 2017). Ultimately, this approach could empower rational scale-down by providing a fast and easy method to estimate the impact of extracellular signal fluctuations on strain performance.

CONCLUSIONS

This study revealed that perception of extracellular glucose concentration alone can induce pronounced biological scale-up effects. Industrially relevant glucose gradients with regime transitions between carbon limitation and starvation were set in a chemostat with intermittent feeding. The single most prominent observation, irrespective of the adaptation status, was the adjustment of internal resources following a growth–stress response tradeoff. Interpretation of transcriptomic data allowed us to identify the implication of several regulatory circuits, all centred around protein kinase A. In consequence, we were able to define engineering propositions with the potential to (i) improve strain performance in an industrial setting and (ii) simplify classical scale-down. Here, a growth scenario was investigated with the laboratory *S. cerevisiae* strain CEN.PK113-7D. Comparative experiments carried out under the same premise with industrial production hosts, especially considering polyploid strains, could shed further light on the general applicability of the demonstrated approach.

AUTHOR CONTRIBUTIONS
Steven Minden: Conceptualization (lead); data curation (lead); formal analysis (lead); investigation (lead); methodology (lead); writing – original draft (lead); writing – review and editing (equal). **Maria Aniolek:** Formal analysis (supporting). **Henk Noorman:** Project administration (equal); writing – review and editing (equal). **Ralf Takors:** Funding acquisition (lead); project administration (equal); resources (lead); supervision (lead); writing – review and editing (equal).

CONFLICT OF INTEREST
The authors declare no conflict of interest.

DATA AVAILABILITY STATEMENT

The data that support the findings of this study are available from https://dataverse.nl/dataverse/minden-microbialbiotechnology.

ORCID

Steven Minden https://orcid.org/0000-0001-5130-8556
Ralf Takors https://orcid.org/0000-0001-5837-6906

REFERENCES

Afgan, E., Baker, D., Batut, B., Van Den Beek, M., Bouvier, D., Ech, M. et al. (2018) The Galaxy platform for accessible, reproducible and collaborative biomedical analyses: 2018 update. *Nucleic Acids Research*, 46(W1), W537–W544. Available from: https://doi.org/10.1093/nar/gky379

An, H. & Harper, J.W. (2020) Ribosome abundance control via the ubiquitin–proteasome system and autophagy. *Journal of Molecular Biology*, 432(1), 170–184. Available from: https://doi.org/10.1016/j.jmb.2019.06.001

Andrews, S. (2010) *FastQC: a quality control tool for high throughput sequence data*. Available from: http://www.bioinformatics.babraham.ac.uk/projects/fastqc/

Aon, J.C., Sun, J., Leighton, J.M. & Appelbaum, E.R. (2016) Hypoxia-elicited impairment of cell wall integrity, glycosylation precursor synthesis, and growth in scaled-up high-cell density fed-batch cultures of Saccharomyces cerevisiae. *Microbial Cell Factories*, 15(1), 1–16. Available from: https://doi.org/10.1186/s12934-016-0542-3

Ashe, M.P., De Long, S.K. & Sachs, A.B. (2000) Glucose depletion rapidly inhibits translation initiation in yeast. *Molecular Biology of the Cell*, 11, 833–848.

Ball, W.J. & Atkinson, D.E. (1975) Adenylate energy charge in *Saccharomyces cerevisiae* during starvation. *Journal of Bacteriology*, 121(3), 975–982.

Benjamini, Y. & Hochberg, Y. (1995) Controlling the false discovery rate: a practical and powerful approach to multiple testing. *Journal of the Royal Statistical Society*, 57(1), 289–300.

Bergen, A.C., Hose, J., McClean, M. & Gasch, A.P. (2021) Integrating multiple single-cell phenotypes links stress acclimation to prior life history in yeast. *BioRxiv*. Available from: https://www.biorxiv.org/content/10.1101/2021.09.08.459442v1.abstract

Bernstein, K.A., Bleichert, F., Bean, J.M., Cross, F.R. & Baserga, S. (2007) Ribosome biogenesis is sensed at the start cell cycle checkpoint. *Molecular Biology of the Cell*, 18, 953–964. Available from: https://doi.org/10.1091/mbc.E06-06-0512

Birnbaum, S. & Bailey, J.E. (1991) Plasmid presence changes the relative levels of many host cell proteins and ribosome components in recombinant *Escherichia coli*. *Biotechnology and Bioengineering*, 37(8), 736–745. Available from: https://doi.org/10.1002/bit.260370808

Bisschops, M.M.M., Luttik, M.A.H., Doerr, A., Verheijen, P.J.T., Bruggeman, F., Pronk, J.T. et al. (2017) Extreme calorie restriction in yeast retentostats induces uniform non-quiescent growth arrest. *Biochimica et Biophysica Acta – Molecular Cell Research*, 1864(1), 231–242. Available from: https://doi.org/10.1016/j.bbamcr.2016.11.002

Blomberg, A. (2000) Metabolic surprises in Saccharomyces cerevisiae during adaptation to saline conditions: questions, some answers and a model. *FEMS Microbiology Letters*, 182(1), 1–8. Available from: https://doi.org/10.1016/S0378-1097(99)00531-5

Bolger, A.M., Lohse, M. & Usadel, B. (2014) Trimmomatic: a flexible trimmer for Illumina sequence data. *Bioinformatics*, 30(15), 2114–2120. Available from: https://doi.org/10.1093/bioinformatics/btu170

Bonawitz, N.D., Chatenay-Lapointe, M., Pan, Y. & Shadel, G.S. (2007) Reduced TOR signaling extends chronological life span via increased respiration and upregulation of mitochondrial gene expression. *Cell Metabolism*, 5(4), 265–277. Available from: https://doi.org/10.1016/j.cmet.2007.02.009

Branzei, D. & Foiani, M. (2006) The Rad53 signal transduction pathway: replication fork stabilization, DNA repair, and adaptation. *Experimental Cell Research*, 312(14), 2654–2659. Available from: https://doi.org/10.1016/j.yexcr.2006.06.012

Brauer, J.M., Huttenhower, C., Airoldi, E.M., Rosenstein, R., Matese, J.C., Gresham, D. et al. (2008) Coordination of growth rate, cell cycle, stress response, and metabolic activity in yeast. *Molecular Biology of the Cell*, 19, 308–317. Available from: https://doi.org/10.1091/mbc.E07

Brion, C., Pflieger, D., Souali-Crespo, S., Friedrich, A. & Schacherer, J. (2016) Differences in environmental stress response among yeasts is consistent with species-specific lifestyles. *Molecular Biology of the Cell*, 27(10), 1694–1705. Available from: https://doi.org/10.1091/mbc.E15-12-0816

Busti, S., Coccetti, P., Alberghina, L. & Vanoni, M. (2010) Glucose signaling-mediated coordination of cell growth and cell cycle in Saccharomyces Cerevisiae. *Sensors*, 10(6), 6195–6240. Available from: https://doi.org/10.3390/s100606195

Causton, H.C., Ren, B., Koh, S.S., Harbison, C.T., Kanin, E., Jennings, E.G. et al. (2001) Remodeling of yeast genome expression in response to environmental changes. *Molecular Biology of the Cell*, 12(2), 323–337. Available from: https://doi.org/10.1091/mbc.12.2.323

Chen, E.Y., Tan, C.M., Kou, Y., Duan, Q., Wang, Z., Meirelles, G.V. et al. (2013) Enrichr: interactive and collaborative HTML5 gene list enrichment analysis tool. *BMC Bioinformatics*, 14, 128. Available from: https://doi.org/10.1186/1471-2105-14-128

Cipollina, C., van den Brink, J., Daran-Lapujade, P., Pronk, J.T., Porro, D. & de Winde, J.H. (2008) Saccharomyces cerevisiae SFP1: at the crossroads of central metabolism and ribosome biogenesis. *Microbiology*, 154(6), 1686–1699. Available from: https://doi.org/10.1099/mic.0.2008/017392-0

Coccetti, P., Nicastro, R. & Tripodi, F. (2018) Conventional and emerging roles of the energy sensor Snf1/AMPK in *Saccharomyces cerevisiae*. *Microbial Cell*, 5(11), 482–494. Available from: https://doi.org/10.15698/mic2018.11.655

Couvillion, M.T., Soto, I.C., Shipkovenska, G. & Churchman, L.S. (2016) Synchronized mitochondrial and cytosolic translation programs. *Nature*, 533(7604), 499–503. Available from: https://doi.org/10.1038/nature18015

Crater, J.S. & Lievense, J.C. (2018) Scale-up of industrial microbial processes. *FEMS Microbiology Letters*, 365(13), 1–5. Available from: https://doi.org/10.1093/femsle/fny138

de Alteriis, E., Cartenì, F., Parascandola, P., Serpa, J. & Mazzoleni, S. (2018) Revisiting the Crabtree/Warburg effect in a dynamic perspective: a fitness advantage against sugar-induced cell death Elisabetta. *Cell Cycle*, 17(6), 688–701. Available from: https://doi.org/10.1080/15384101.2018.1442622

De La Fuente, I.M., Cortés, J.M., Valero, E., Desroches, M., Rodrigues, S., Malaina, I. et al. (2014) On the dynamics of the adenylate energy system: homeorhesis vs homeostasis. *PLoS One*, 9(10), e108676. Available from: https://doi.org/10.1371/journal.pone.0108676

de Lucena, R.M., Elsztein, C., de Barros Pita, W., de Souza, R.B., de Sá Leitão Paiva Júnior, S. & de Morais Junior, M.A. (2015) Transcriptomic response of Saccharomyces cerevisiae for its adaptation to sulphuric acid-induced stress. *Antonie van Leeuwenhoek, International Journal of General and Molecular Microbiology*, 108(5), 1147–1160. Available from: https://doi.org/10.1007/s10482-015-0568-2

De Melo, H.F., Bonini, B.M., Thevelein, J., Simões, D.A. & Morais, M.A. (2010) Physiological and molecular analysis of the stress response of *Saccharomyces cerevisiae* imposed by strong

164

MICROBIAL
BIOTECHNOLOGY

Applied
Microbiology
International

RESEARCH ARTICLE

inorganic acid with implication to industrial fermentations. *Journal of Applied Microbiology*, 109(1), 116–127. Available from: https://doi.org/10.1111/j.1365-2672.2009.04633.x

De Wever, V., Reiter, W., Ballarini, A., Ammerer, G. & Brocard, C. (2005) A dual role for PP1 in shaping the Msn2-dependent transcriptional response to glucose starvation. *The EMBO Journal*, 24(23), 4115–4123. Available from: https://doi.org/10.1038/sj.emboj.7600871

Delvigne, F. & Goffin, P. (2014) Microbial heterogeneity affects bioprocess robustness: dynamic single-cell analysis contributes to understanding of microbial populations. *Biotechnology Journal*, 9(1), 61–72. Available from: https://doi.org/10.1002/biot.201300119

Delvigne, F. & Noorman, H. (2017) Scale-up/scale-down of microbial bioprocesses: a modern light on an old issue. *Microbial Biotechnology*, 10(4), 685–687. Available from: https://doi.org/10.1111/1751-7915.12732

Diderich, J.A., Schepper, M., Van Hoek, P., Luttik, M.A.H., Van Dijken, J.P., Pronk, J.T. et al. (1999) Glucose uptake kinetics and transcription of HXT genes in chemostat cultures of *Saccharomyces cerevisiae*. *Journal of Biological Chemistry*, 274(22), 15350–15359. Available from: https://doi.org/10.1074/jbc.274.22.15350

Enfors, S.O., Jahic, M., Rozkov, A., Xu, B., Hecker, M., Jürgen, B. et al. (2001) Physiological responses to mixing in large scale bioreactors. *Journal of Biotechnology*, 85(2), 175–185. Available from: https://doi.org/10.1016/S0168-1656(00)00365-5

Fazio, A., Jewett, M.C., Daran-Lapujade, P., Mustacchi, R., Usaite, R., Pronk, J.T. et al. (2008) Transcription factor control of growth rate dependent genes in *Saccharomyces cerevisiae*: a three factor design. *BMC Genomics*, 9, 1–14. Available from: https://doi.org/10.1186/1471-2164-9-341

François, J. & Parrou, J.L. (2001) Reserve carbohydrates metabolism in the yeast *Saccharomyces cerevisiae*. *FEMS Microbiology Reviews*, 25(1), 125–145. Available from: https://doi.org/10.1016/S0168-6445(00)00059-0

Gaikwad, S., Ghobakhlou, F., Young, D.J., Visweswaraiah, J., Zhang, H. & Hinnebusch, A.G. (2021) Reprogramming of translation in yeast cells impaired for ribosome recycling favors short, efficiently translated mRNAs. *eLife*, 10, 1–38. Available from: https://doi.org/10.7554/eLife.64283

Gasch, A.P. (2007) Comparative genomics of the environmental stress response in ascomycete fungi. *Yeast*, 24, 169–177. Available from: https://doi.org/10.1002/yea

Gasch, A.P., Spellman, P.T., Kao, C.M., Carmel-Harel, O., Eisen, M.B., Storz, G. et al. (2000) Genomic expression programs in the response of yeast cells to environmental changes. *Molecular Biology of the Cell*, 11(12), 4241–4257. Available from: https://doi.org/10.1091/mbc.11.12.4241

Gasch, A.P., Yu, F.B., Hose, J., Escalante, L.E., Place, M., Bacher, R. et al. (2017) Single-cell RNA sequencing reveals intrinsic and extrinsic regulatory heterogeneity in yeast responding to stress. *PLoS Biology*, 15(12), 1–28. Available from: https://doi.org/10.1371/journal.pbio.2004050

George, S., Larsson, G., Olsson, K. & Enfors, S.-O. (1998) Comparison of the Baker's yeast process performance in laboratory and production scale. *Bioprocess Engineering*, 18, 135–142. Available from: https://doi.org/10.1007/PL00008979

Goddard, M.R. & Greig, D. (2015) *Saccharomyces cerevisiae*: a nomadic yeast with no niche? *FEMS Yeast Research*, 15(3), 1–6. Available from: https://doi.org/10.1093/femsyr/fov009

González, A. & Hall, M.N. (2017) Nutrient sensing and TOR signaling in yeast and mammals. *The EMBO Journal*, 36(4), 397–408. Available from: https://doi.org/10.15252/embj.201696010

Görner, W., Durchschlag, E., Wolf, J., Brown, E.L., Ammerer, G., Ruis, H. et al. (2002) Acute glucose starvation activates the nuclear localization signal of a stress-specific yeast transcription factor. *The EMBO Journal*, 21(1–2), 135–144. Available from: https://doi.org/10.1093/emboj/21.1.135

Gower, J.C. (1966) Some distance properties of latent root and vector methods used in multivariate analysis. *Biometrika*, 53(3/4), 325. Available from: https://doi.org/10.2307/2333639

Gross, A.S. & Graef, M. (2020) Mechanisms of autophagy in metabolic stress response. *Journal of Molecular Biology*, 432(1), 28–52. Available from: https://doi.org/10.1016/j.jmb.2019.09.005

Gutin, J., Joseph-Strauss, D., Sadeh, A., Shalom, E. & Friedman, N. (2019) Genetic screen of the yeast environmental stress response dynamics uncovers distinct regulatory phases. *Molecular Systems Biology*, 15(8), 1–16. Available from: https://doi.org/10.15252/msb.20198939

Gutin, J., Sadeh, A., Rahat, A., Aharoni, A. & Friedman, N. (2015) Condition-specific genetic interaction maps reveal crosstalk between the cAMP/PKA and the HOG MAPK pathways in the activation of the general stress response. *Molecular Systems Biology*, 11(10), 829. Available from: https://doi.org/10.15252/msb.20156451

Hahn, J.S. & Thiele, D.J. (2004) Activation of the *Saccharomyces cerevisiae* heat shock transcription factor under glucose starvation conditions by Snf1 protein kinase. *Journal of Biological Chemistry*, 279(7), 5169–5176. Available from: https://doi.org/10.1074/jbc.M311005200

Haringa, C., Deshmukh, A.T., Mudde, R.F. & Noorman, H. (2017) Euler-Lagrange analysis towards representative down-scaling of a 22 m3 aerobic *S. cerevisiae* fermentation. *Chemical Engineering Science*, 170, 653–669. Available from: https://doi.org/10.1016/j.ces.2017.01.014

Haringa, C., Mudde, R.F. & Noorman, H. (2018) From industrial fermentor to CFD-guided downscaling: what have we learned? *Biochemical Engineering Journal*, 140, 57–71. Available from: https://doi.org/10.1016/j.bej.2018.09.001

Haringa, C., Tang, W., Deshmukh, A.T., Xia, J., Reuss, M., Heijnen, J. et al. (2016) Euler-Lagrange computational fluid dynamics for (bio)reactor scale down: an analysis of organism lifelines. *Engineering in Life Sciences*, 16(7), 652–663. Available from: https://doi.org/10.1002/elsc.201600061

Hepp, S., Trauth, J., Hasenjäger, S., Bezold, F., Essen, L.O. & Taxis, C. (2020) An optogenetic tool for induced protein stabilization based on the *Phaeodactylum tricornutum* aureochrome 1a light–oxygen–voltage domain. *Journal of Molecular Biology*, 432, 1880–1900. Available from: https://doi.org/10.1016/j.jmb.2020.02.019

Hershey, J.W.B., Sonenberg, N. & Mathews, M.B. (2012) Principles of translational control: an overview. *Cold Spring Harbor Perspectives in Biology*, 4(12), 1–10. Available from: https://doi.org/10.1101/cshperspect.a009829

Ho, P., Täuber, S., Stute, B., Grünberger, A. & von Lieres, E. (2022) Microfluidic reproduction of dynamic bioreactor environment based on computational lifelines. *Frontiers in Chemical Engineering*, 4, 1–15. Available from: https://doi.org/10.3389/fceng.2022.826485

Howe, K.L., Achuthan, P., Allen, J., Allen, J., Alvarez-Jarreta, J., Ridwan Amode, M. et al. (2021) Ensembl 2021. *Nucleic Acids Research*, 49(D1), D884–D891. Available from: https://doi.org/10.1093/nar/gkaa942

Huber, A., French, S.L., Tekotte, H., Yerlikaya, S., Stahl, M., Perepelkina, M.P. et al. (2011) Sch9 regulates ribosome biogenesis via Stb3, Dot6 and Tod6 and the histone deacetylase complex RPD3L. *The EMBO Journal*, 30(15), 3052–3064. Available from: https://doi.org/10.1038/emboj.2011.221

Huch, S. & Nissan, T. (2014) Interrelations between translation and general mRNA degradation in yeast. *Wiley Interdisciplinary Reviews. RNA*, 5(6), 747–763. Available from: https://doi.org/10.1002/wrna.1244

Johnston, N.R., Nallur, S., Gordon, P.B., Smith, K.D. & Strobel, S.A. (2020) Genome-wide identification of genes involved in general

acid stress and fluoride toxicity in *Saccharomyces cerevisiae*. *Frontiers in Microbiology*, 11, 1–11. Available from: https://doi.org/10.3389/fmicb.2020.01410

Junker, B.H. (2004) Scale-up methodologies for *Escherichia coli* and yeast fermentation processes. *Journal of Bioscience and Bioengineering*, 97(6), 347–364.

Kafri, M., Metzl-Raz, E., Jona, G. & Barkai, N. (2016) The cost of protein production. *Cell Reports*, 14(1), 22–31. Available from: https://doi.org/10.1016/j.celrep.2015.12.015

Kim, D., Pertea, G., Trapnell, C., Pimentel, H., Kelley, R. & Salzberg, L. (2013) TopHat2: accurate alignment of transcriptomes in the presence of insertions, deletions and gene fusions. *Genome Biology*, 14(1–13), 957–961. Available from: https://doi.org/10.1186/gb-2013-14-4-r36

Kim, J.-H., Roy, A., Jouandot, D., II & Cho, K.H. (2013) The glucose signaling network in yeast. *Biochimica et Biophysica Acta*, 1830(11), 5204–5210. Available from: https://doi.org/10.1016/j.bbagen.2013.07.025

Kresnowati, M.T.A.P., Van Winden, W.A., Almering, M.J.H., Ten Pierick, A., Ras, C., Knijnenburg, T.A. et al. (2006) When transcriptome meets metabolome: fast cellular responses of yeast to sudden relief of glucose limitation. *Molecular Systems Biology*, 2, 49. Available from: https://doi.org/10.1038/msb4100083

Kuleshov, M.V., Diaz, J.E.L., Flamholz, Z.N., Keenan, A.B., Lachmann, A., Wojciechowicz, M.L. et al. (2019) modEnrichr: a suite of gene set enrichment analysis tools for model organisms. *Nucleic Acids Research*, 47(W1), W183–W190. Available from: https://doi.org/10.1093/nar/gkz347

Kunkel, J., Luo, X. & Capaldi, A.P. (2019) Integrated TORC1 and PKA signaling control the temporal activation of glucose-induced gene expression in yeast. *Nature Communications*, 10(1), 1–11. Available from: https://doi.org/10.1038/s41467-019-11540-y

Kuschel, M. & Takors, R. (2020) Simulated oxygen and glucose gradients as a prerequisite for predicting industrial scale performance a priori. *Biotechnology and Bioengineering*, 117(9), 2760–2770. Available from: https://doi.org/10.1002/bit.27457

Lapin, A., Müller, D. & Reuss, M. (2004) Dynamic behavior of microbial populations in stirred bioreactors simulated with Euler–Lagrange Methods: traveling along the lifelines of single cells. *Industrial & Engineering Chemistry Research*, 43(16), 4647–4656. Available from: https://doi.org/10.1021/ie030786k

Lara, A.R., Galindo, E., Ramírez, O.T. & Palomares, L.A. (2006) Living with heterogeneities in bioreactors. *Molecular Biotechnology*, 34(3), 355–381. Available from: https://doi.org/10.1385/mb:34:3:355

Levy, S. & Barkai, N. (2009) Coordination of gene expression with growth rate: a feedback or a feed-forward strategy? *FEBS Letters*, 583(24), 3974–3978. Available from: https://doi.org/10.1016/j.febslet.2009.10.071

Levy, S., Ihmels, J., Carmi, M., Weinberger, A., Friedlander, G. & Barkai, N. (2007) Strategy of transcription regulation in the budding yeast. *PLoS One*, 2(2), e250. Available from: https://doi.org/10.1371/journal.pone.0000250

Liao, Y., Smyth, G.K. & Shi, W. (2014) FeatureCounts: an efficient general purpose program for assigning sequence reads to genomic features. *Bioinformatics*, 30(7), 923–930. Available from: https://doi.org/10.1093/bioinformatics/btt656

López-Maury, L., Marguerat, S. & Bähler, J. (2008) Tuning gene expression to changing environments: from rapid responses to evolutionary adaptation. *Nature Reviews Genetics*, 9(8), 583–593. Available from: https://doi.org/10.1038/nrg2398

Love, M.I., Huber, W. & Anders, S. (2014) Moderated estimation of fold change and dispersion for RNA-seq data with DESeq2. *Genome Biology*, 15(12), 1–21. Available from: https://doi.org/10.1186/s13059-014-0550-8

Luo, W., Friedman, M.S., Shedden, K., Hankenson, K.D. & Woolf, P.J. (2009) GAGE: generally applicable gene set enrichment for pathway analysis. *BMC Bioinformatics*, 10, 1–17. Available from: https://doi.org/10.1186/1471-2105-10-161

Mace, K., Krakowiak, J., El-Samad, H. & Pincus, D. (2020) Multi-kinase control of environmental stress responsive transcription. *PLoS One*, 15(3), 1–21. Available from: https://doi.org/10.1371/journal.pone.0230246

MacGilvray, M.E., Shishkova, E., Place, M., Wagner, E.R., Coon, J.J. & Gasch, A.P. (2020) Phosphoproteome response to dithiothreitol reveals unique versus shared features of *Saccharomyces cerevisiae* stress responses. *Journal of Proteome Research*, 19(8), 3405–3417. Available from: https://doi.org/10.1021/acs.jproteome.0c00253

Mai, B. & Breeden, L. (1997) Xbp1, a stress-induced transcriptional repressor of the *Saccharomyces cerevisiae* Swi4/Mbp1 family. *Molecular and Cellular Biology*, 17(11), 6491–6501. Available from: https://doi.org/10.1128/mcb.17.11.6491

Martínez-Pastor, M.T., Marchler, G., Schüller, C., Marchler-Bauer, A., Ruis, H. & Estruch, F. (1996) The *Saccharomyces cerevisiae* zinc finger proteins Msn2p and Msn4p are required for transcriptional induction through the stress response element (STRE). *The EMBO Journal*, 15(9), 2227–2235. Available from: https://doi.org/10.1002/j.1460-2075.1996.tb00576.x

Metzl-Raz, E., Kafri, M., Yaakov, G., Soifer, I., Gurvich, Y. & Barkai, N. (2017) Principles of cellular resource allocation revealed by condition-dependent proteome profiling. *eLife*, 6, 1–21. Available from: https://doi.org/10.7554/eLife.28034

Michael, D.G., Maier, E.J., Brown, H., Gish, S.R., Fiore, C., Brown, R.H. et al. (2016) Model-based transcriptome engineering promotes a fermentative transcriptional state in yeast. *Proceedings of the National Academy of Sciences of the United States of America*, 113(47), E7428–E7437. Available from: https://doi.org/10.1073/pnas.1603577113

Miller, C., Schwalb, B., Maier, K., Schulz, D., Dümcke, S., Zacher, B. et al. (2011) Dynamic transcriptome analysis measures rates of mRNA synthesis and decay in yeast. *Molecular Systems Biology*, 7, 458. Available from: https://doi.org/10.1038/msb.2010.112

Minden, S., Aniolek, M., Sarkizi, C., Hajian, S., Teleki, A., Zerrer, T. et al. (2022) Monitoring intracellular metabolite dynamics in *Saccharomyces cerevisiae* during industrially relevant famine stimuli. *Metabolites*, 12(263), 1–26. Available from: https://doi.org/10.3390/metabo12030263

Mohedano, M.T., Konzock, O. & Chen, Y. (2022) Strategies to increase tolerance and robustness of industrial microorganisms. *Synthetic and Systems Biotechnology*, 7(1), 533–540. Available from: https://doi.org/10.1016/j.synbio.2021.12.009

Monteiro, P.T., Oliveira, J., Pais, P., Antunes, M., Palma, M., Cavalheiro, M. et al. (2020) YEASTRACT+: a portal for cross-species comparative genomics of transcription regulation in yeasts. *Nucleic Acids Research*, 48(D1), D642–D649. Available from: https://doi.org/10.1093/nar/gkz859

Müller, D., Exler, S., Aguilera-Vázquez, L., Guerrero-Martín, E. & Reuss, M. (2003) Cyclic AMP mediates the cell cycle dynamics of energy metabolism in *Saccharomyces cerevisiae*. *Yeast*, 20(4), 351–367. Available from: https://doi.org/10.1002/yea.967

Nadal-Rey, G., McClure, D.D., Kavanagh, J.M., Cassells, B., Cornelissen, S., Fletcher, D.F. et al. (2021) Development of dynamic compartment models for industrial aerobic fed-batch fermentation processes. *Chemical Engineering Journal*, 420(P3), 130402. Available from: https://doi.org/10.1016/j.cej.2021.130402

Nielsen, J. (2019) Yeast systems biology: model organism and cell factory. *Biotechnology Journal*, 14(9), 1–9. Available from: https://doi.org/10.1002/biot.201800421

Nijkamp, J.F., van den Broek, M., Datema, E., de Kok, S., Bosman, L., Luttik, M.A.H. et al. (2012) De novo sequencing, assembly and analysis of the genome of the laboratory strain *Saccharomyces*

cerevisiae CEN.PK113-7D, a model for modern industrial biotechnology. *Microbial Cell Factories*, 11, 36. Available from: https://doi.org/10.1186/1475-2859-11-36

Nissen, T.L., Schulze, U., Nielsen, J. & Villadsen, J. (1997) Flux distributions in anaerobic, glucose-limited continuous cultures of *Saccharomyces cerevisiae*. *Microbiology*, 143(1), 203–218. Available from: https://doi.org/10.1099/00221287-143-1-203

Norbeck, J. & Blomberg, A. (2000) The level of cAMP-dependent protein kinase A activity strongly affects osmotolerance and osmo-instigated gene expression changes in *Saccharomyces cerevisiae*. *Yeast*, 16(2), 121–137. Available from: https://doi.org/10.1002/(SICI)1097-0061(20000130)16:2<121::AID-YEA511>3.0.CO;2-A

Oakhill, J.S., Scott, J.W. & Kemp, B.E. (2012) AMPK functions as an adenylate charge-regulated protein kinase. *Trends in Endocrinology and Metabolism*, 23(3), 125–132. Available from: https://doi.org/10.1016/j.tem.2011.12.006

Paalman, J.W.G., Verwaal, R., Slofstra, S.H., Verkleij, A.J., Boonstra, J. & Verrips, C.T. (2003) Trehalose and glycogen accumulation is related to the duration of the G1 phase of *Saccharomyces cerevisiae*. *FEMS Yeast Research*, 3(3), 261–268. Available from: https://doi.org/10.1016/S1567-1356(02)00163-0

Pardo, B., Crabbé, L. & Pasero, P. (2017) Signaling pathways of replication stress in yeast. *FEMS Yeast Research*, 17(2), 1–11. Available from: https://doi.org/10.1093/femsyr/fow101

Parenteau, J., Lavoie, M., Catala, M., Malik-Ghulam, M., Gagnon, J. & Abou Elela, S. (2015) Preservation of gene duplication increases the regulatory spectrum of ribosomal protein genes and enhances growth under stress. *Cell Reports*, 13(11), 2516–2526. Available from: https://doi.org/10.1016/j.celrep.2015.11.033

Parrou, J.L. & Francois, J. (1997) A simplified procedure for a rapid and reliable assay of both glycogen and trehalose in whole yeast cells. *Analytical Biochemistry*, 248, 186–188. Available from: https://doi.org/10.1556/aarch.59.2008.2.28

Penia Kresnowati, M.T.A., Van Winden, W.A. & Heijnen, J.J. (2005) Determination of elasticities, concentration and flux control coefficients from transient metabolite data using linlog kinetics. *Metabolic Engineering*, 7(2), 142–153. Available from: https://doi.org/10.1016/j.ymben.2004.12.002

Petrenko, N., Chereji, R.V., McClean, M.N., Morozov, A.V. & Broach, J.R. (2013) Noise and interlocking signaling pathways promote distinct transcription factor dynamics in response to different stresses. *Molecular Biology of the Cell*, 24(12), 2045–2057. Available from: https://doi.org/10.1091/mbc.E12-12-0870

Pinson, B., Ceschin, J., Saint-Marc, C. & Daignan-Fornier, B. (2019) Dual control of NAD+ synthesis by purine metabolites in yeast. *eLife*, 8, 1–23. Available from: https://doi.org/10.7554/eLife.43808

Plank, M. (2022) Interaction of TOR and PKA signaling in *S. cerevisiae*. *Biomolecules*, 12(2), 210. Available from: https://doi.org/10.3390/biom12020210

Polymenis, M. & Aramayo, R. (2015) Translate to divide: control of the cell cycle by protein synthesis. *Microbial Cell*, 2(4), 94–104. Available from: https://doi.org/10.15698/mic2015.04.198

R Core Team. (2021) R: a language and environment for statistical computing. Available from: https://www.r-project.org/

Reeves, G.T. (2019) The engineering principles of combining a transcriptional incoherent feedforward loop with negative feedback. *Journal of Biological Engineering*, 13(1), 1–11. Available from: https://doi.org/10.1186/s13036-019-0190-3

Regenberg, B., Grotkjær, T., Winther, O., Fausbøll, A., Åkesson, M., Bro, C. et al. (2006) Growth-rate regulated genes have profound impact on interpretation of transcriptome profiling in *Saccharomyces cerevisiae*. *Genome Biology*, 7(11), R-107. Available from: https://doi.org/10.1186/gb-2006-7-11-r107

Ritchie, M.E., Phipson, B., Wu, D., Hu, Y., Law, C.W., Shi, W. et al. (2015) Limma powers differential expression analyses for RNA-sequencing and microarray studies. *Nucleic Acids Research*, 43(7), e47. Available from: https://doi.org/10.1093/nar/gkv007

Samakkarn, W., Ratanakhanokchai, K. & Soontorngun, N. (2021) Reprogramming of the ethanol stress response in *Saccharomyces cerevisiae* by the transcription factor znf1 and its effect on the biosynthesis of glycerol and ethanol. *Applied and Environmental Microbiology*, 87(16), 1–26. Available from: https://doi.org/10.1128/AEM.00588-21

Sarkizi Shams Hajian, C., Haringa, C., Noorman, H. & Takors, R. (2020) Predicting by-product gradients of Baker's yeast production at industrial scale: a practical simulation approach. *PRO*, 8(1554), 19. Available from: https://doi.org/10.3390/pr8121554

Sasano, Y., Kariya, T., Usugi, S., Sugiyama, M. & Harashima, S. (2017) Molecular breeding of *Saccharomyces cerevisiae* with high RNA content by harnessing essential ribosomal RNA transcription regulator. *AMB Express*, 7(1), 32. Available from: https://doi.org/10.1186/s13568-017-0330-4

Schawalder, S.B., Kabani, M., Howald, I., Choudhury, U., Werner, M. & Shore, D. (2004) Growth-regulated recruitment of the essential yeast ribosomal protein gene activator Ifh1. *Nature*, 432(7020), 1058–1061. Available from: https://doi.org/10.1038/nature03200

Schmoller, K.M., Turner, J.J., Kõivomägi, M. & Skotheim, J.M. (2015) Dilution of the cell cycle inhibitor Whi5 controls budding-yeast cell size. *Nature*, 526(7572), 268–272. Available from: https://doi.org/10.1038/nature14908

Sheu, Y.-J., Kawaguchi, R.K., Gillis, J. & Stillman, B. (2021) Prevalent and dynamic binding of the cell cycle checkpoint kinase Rad53 to gene promoters. *BioRxiv*. Available from: https://www.biorxiv.org/content/10.1101/2021.05.23.445333v2.abstract

Shore, D., Zencir, S. & Albert, B. (2021) Transcriptional control of ribosome biogenesis in yeast: links to growth and stress signals. *Biochemical Society Transactions*, 49(4), 1589–1599. Available from: https://doi.org/10.1042/BST20201136

Silljé, H.H.W., Paalman, J.W.G., Ter Schure, E.G., Olsthoorn, S.Q.B., Verkleij, A.J., Boonstra, J. et al. (1999) Function of trehalose and glycogen in cell cycle progression and cell viability in *Saccharomyces cerevisiae*. *Journal of Bacteriology*, 181(2), 396–400. Available from: https://doi.org/10.1128/jb.181.2.396-400.1999

Skoneczny, M. (2018) In: Skoneczny, M. (Ed.) *Stress response mechanisms in fungi*. Cham, Switzerland: Springer Nature. Available from: https://doi.org/10.1007/978-3-030-00683-9

Stasyk, O.G. & Stasyk, O.V. (2019) Glucose sensing and regulation in yeasts. In: Sibirny, A. (Ed.) *Non-conventional yeasts: from basic research to application*. Basel: Springer Cham, pp. 477–519. Available from: https://doi.org/10.1007/978-3-030-21110-3_14

Stewart-Ornstein, J., Chen, S., Bhatnagar, R., Weissman, J.S. & El-Samad, H. (2017) Model-guided optogenetic study of PKA signaling in budding yeast. *Molecular Biology of the Cell*, 28(1), 221–227. Available from: https://doi.org/10.1091/mbc.E16-06-0354

Straathof, A.J.J., Wahl, S.A., Benjamin, K.R., Takors, R., Wierckx, N. & Noorman, H. (2019) Grand research challenges for sustainable industrial biotechnology. *Trends in Biotechnology*, 37(10), 1042–1050. Available from: https://doi.org/10.1016/j.tibtech.2019.04.002

Suarez-Mendez, C. A. (2015). *Dynamics of storage carbohydrates metabolism in Saccharomyces cerevisiae: a quantitative*. Delft: TU Delft Repos.

Suarez-Mendez, C.A., Ras, C. & Wahl, S.A. (2017) Metabolic adjustment upon repetitive substrate perturbations using dynamic13C-tracing in yeast. *Microbial Cell Factories*, 16(1), 1–14. Available from: https://doi.org/10.1186/s12934-017-0778-6

Suhm, T., Kaimal, J.M., Dawitz, H., Peselj, C., Masser, A.E., Hanzén, S. et al. (2018) Mitochondrial translation efficiency controls cytoplasmic protein homeostasis. *Cell Metabolism*, 27(6), 1309–1322.e6. Available from: https://doi.org/10.1016/j.cmet.2018.04.011

Sung, M.K., Reitsma, J.M., Sweredoski, M.J., Hess, S. & Deshaies, R.J. (2016) Ribosomal proteins produced in excess are degraded by the ubiquitin-proteasome system. *Molecular Biology of the Cell*, 27(17), 2642–2652. Available from: https://doi.org/10.1091/mbc.E16-05-0290

Takors, R. (2016) Editorial: How can we ensure the successful transfer from lab- to large-scale production? *Engineering in Life Sciences*, 16(7), 587. Available from: https://doi.org/10.1002/elsc.201670073

Theobald, U. (1995) *Untersuchungen zur Dynamik des Crabtree-Effektes* (Reihe 17). Düsseldorf: Fortschrittberichte/VDI.

Theobald, U.M., Mailinger, W., Baltes, M., Rizzi, M. & Reuss, M. (1997) In vivo analysis of metabolic dynamics in *Saccharomyces cerevisiae*: I. Experimental observations. *Biotechnology & Bioengineering*, 55, 305–316.

Uhl, V.W. & Von Essen, J.A. (1986) Scale-up of equipment for agitating liquids. In: Uhl, V.W., & Gray, J.B. (Eds.) *Mixing* (Vol. III). Cambridge, Massachusetts: Academic Press Inc. Available from: https://doi.org/10.1016/b978-0-12-706603-5.50007-6

Van Den Brink, J., Canelas, A.B., Van Gulik, W.M., Pronk, J.T., Heijnen, J.J., De Winde, J.H. et al. (2008) Dynamics of glycolytic regulation during adaptation of *Saccharomyces cerevisiae* to fermentative metabolism. *Applied and Environmental Microbiology*, 74(18), 5710–5723. Available from: https://doi.org/10.1128/AEM.01121-08

Verduyn, C., Postma, E., Scheffers, W.A. & van Dijken, J.P. (1992) Effect of benzoic acid on metabolic fluxes in yeasts. *Yeast*, 8(1992), 501–517. Available from: https://doi.org/10.1007/BF00270792

Verhagen, K.J.A., Eerden, S.A., Sikkema, B.J., Wahl, S.A. & Martin, A.J. (2022) Predicting metabolic adaptation under dynamic substrate conditions using a resource-dependent kinetic model: a case study using *Saccharomyces cerevisiae*, 9, 1–12. Available from: https://doi.org/10.3389/fmolb.2022.863470

Verma, M., Zakhartsev, M., Reuss, M. & Westerhoff, H.V. (2013) "Domino" systems biology and the "A" of ATP. *Biochimica et Biophysica Acta – Bioenergetics*, 1827(1), 19–29. Available from: https://doi.org/10.1016/j.bbabio.2012.09.014

Wang, G., Haringa, C., Noorman, H., Chu, J. & Zhuang, Y. (2020) Developing a computational framework to advance bioprocess scale-up. *Trends in Biotechnology*, 38(8), 846–856. Available from: https://doi.org/10.1016/j.tibtech.2020.01.009

Warner, J.R. (1999) The economics of ribosome biosynthesis in yeast. *Trends in Biochemical Sciences*, 24, 437–440.

Watanabe, D., Kaneko, A., Sugimoto, Y., Ohnuki, S., Takagi, H. & Ohya, Y. (2017) Promoter engineering of the *Saccharomyces cerevisiae* RIM15 gene for improvement of alcoholic fermentation rates under stress conditions. *Journal of Bioscience and Bioengineering*, 123(2), 183–189. Available from: https://doi.org/10.1016/j.jbiosc.2016.08.004

Wehrs, M., Tanjore, D., Eng, T., Lievense, J., Pray, T.R. & Mukhopadhyay, A. (2019) Engineering robust production microbes for large-scale cultivation. *Trends in Microbiology*, 27(6), 524–537. Available from: https://doi.org/10.1016/j.tim.2019.01.006

Weibel, K.E., Mor, J.R. & Fiechter, A. (1974) Rapid sampling of yeast cells and automated assays of adenylate, citrate, pyruvate and glucose-6-phosphate pools. *Analytical Biochemistry*, 58(1), 208–216. Available from: https://doi.org/10.1016/0003-2697(74)90459-X

Woolford, J.L. & Baserga, S.J. (2013) Ribosome biogenesis in the yeast *Saccharomyces cerevisiae*. *Genetics*, 195(3), 643–681. Available from: https://doi.org/10.1534/genetics.113.153197

Wright, N.R., Wulff, T., Palmqvist, E.A., Jørgensen, T.R., Workman, C.T., Sonnenschein, N. et al. (2020) Fluctuations in glucose availability prevent global proteome changes and physiological transition during prolonged chemostat cultivations of *Saccharomyces cerevisiae*. *Biotechnology and Bioengineering*, 117(7), 2074–2088. Available from: https://doi.org/10.1002/bit.27353

Wu, L., Schipper, D., Kresnowati, P., Proell, A.M., Ras, C. & Heijnen, J.J. (2006) Short-term metabolome dynamics and carbon, electron, and ATP balances in chemostat-grown. *Society*, 72(5), 3566–3577. Available from: https://doi.org/10.1128/AEM.72.5.3566

Wu, Y., Wu, J., Deng, M. & Lin, Y. (2021) Yeast cell fate control by temporal redundancy modulation of transcription factor paralogs. *Nature Communications*, 12(1), 1–13. Available from: https://doi.org/10.1038/s41467-021-23425-0

Wullschleger, S., Loewith, R. & Hall, M.N. (2006) TOR signaling in growth and metabolism. *Cell*, 124(3), 471–484. Available from: https://doi.org/10.1016/j.cell.2006.01.016

Xia, J., Sánchez, B.J., Chen, Y. & Nielsen, J. (2022) Proteome allocations change linearly with the specific growth rate of *Saccharomyces cerevisiae* under glucose limitation. *Nature Communications*, 13(2819), 1–12. Available from: https://doi.org/10.1038/s41467-022-30513-2

Yi, C., Tong, J., Lu, P., Wang, Y., Zhang, J., Sun, C. et al. (2017) Formation of a Snf1-Mec1-Atg1 module on mitochondria governs energy deprivation-induced autophagy by regulating mitochondrial respiration. *Developmental Cell*, 41(1), 59–71.e4. Available from: https://doi.org/10.1016/j.devcel.2017.03.007

Young, E.T., Dombek, K.M., Tachibana, C. & Ideker, T. (2003) Multiple pathways are co-regulated by the protein kinase Snf1 and the transcription factors Adr1 and Cat8. *Journal of Biological Chemistry*, 278(28), 26146–26158. Available from: https://doi.org/10.1074/jbc.M301981200

Young, T.B. & Bungay, H.R. (1973) Dynamic analysis of a microbial process: a systems engineering approach. *Biotechnology and Bioengineering*, 15(2), 377–393. Available from: https://doi.org/10.1002/bit.260150212

Zadrąg-Tęcza, R., Maślanka, R., Bednarska, S. & Kwolek-Mirek, M. (2018) Stress response mechanisms in fungi: theoretical and practical aspects. In: *Stress response mechanisms in fungi*. Basel: Springer Nature Switzerland AG. Available from: https://doi.org/10.1007/978-3-030-00683-9

Zakrzewska, A., Van Eikenhorst, G., Burggraaff, J.E.C., Vis, D.J., Hoefsloot, H., Delneri, D. et al. (2011) Genome-wide analysis of yeast stress survival and tolerance acquisition to analyze the central trade-off between growth rate and cellular robustness. *Molecular Biology of the Cell*, 22(22), 4435–4446. Available from: https://doi.org/10.1091/mbc.E10-08-0721

Zaman, S., Lippman, S.I., Schneper, L., Slonim, N. & Broach, J.R. (2009) Glucose regulates transcription in yeast through a network of signaling pathways. *Molecular Systems Biology*, 5(245), 1–14. Available from: https://doi.org/10.1038/msb.2009.2

Zencir, S., Dilg, D., Rueda, M.P., Shore, D. & Albert, B. (2020) Mechanisms coordinating ribosomal protein gene transcription in response to stress. *Nucleic Acids Research*, 48(20), 11408–11420. Available from: https://doi.org/10.1093/nar/gkaa852

Zhao, H., Chen, J., Liu, J. & Han, B. (2015) Transcriptome analysis reveals the oxidative stress response in *Saccharomyces cerevisiae*. *RSC Advances*, 5(29), 22923–22934. Available from: https://doi.org/10.1039/c4ra14600j

Zieringer, J. & Takors, R. (2018) In silico prediction of large-scale microbial production performance: constraints for getting proper data-driven models. *Computational and Structural Biotechnology Journal*, 16, 246–256. Available from: https://doi.org/10.1016/j.csbj.2018.06.002

Zou, K., Rouskin, S., Dervishi, K., McCormick, M.A., Sasikumar, A., Deng, C. et al. (2020) Life span extension by glucose restriction is abrogated by methionine supplementation: cross-talk between glucose and methionine and implication of methionine as a key regulator of life span. *Science Advances*, 6(32), eaba130. Available from: https://doi.org/10.1126/sciadv.aba1306

SUPPORTING INFORMATION

Additional supporting information can be found online in the Supporting Information section at the end of this article.

Mimicked Mixing-Induced Heterogeneities of Industrial Bioreactors Stimulate Long-Lasting Adaption Programs in Ethanol-Producing Yeasts

Steven Minden [1] [iD]**, Maria Aniolek** [1]**, Henk Noorman** [2,3] **and Ralf Takors** [1,*] [iD]

1 Institute of Biochemical Engineering, University of Stuttgart, 70569 Stuttgart, Germany
2 Royal DSM, 2613 AX Delft, The Netherlands
3 Department of Biotechnology, Delft University of Technology, 2628 CD Delft, The Netherlands
* Correspondence: takors@ibvt.uni-stuttgart.de

Abstract: Commercial-scale bioreactors create an unnatural environment for microbes from an evolutionary point of view. Mixing insufficiencies expose individual cells to fluctuating nutrient concentrations on a second-to-minute scale while transcriptional and translational capacities limit the microbial adaptation time from minutes to hours. This mismatch carries the risk of inadequate adaptation effects, especially considering that nutrients are available at optimal concentrations on average. Consequently, industrial bioprocesses that strive to maintain microbes in a phenotypic sweet spot, during lab-scale development, might suffer performance losses when said adaptive misconfigurations arise during scale-up. Here, we investigated the influence of fluctuating glucose availability on the gene-expression profile in the industrial yeast Ethanol Red™. The stimulus–response experiment introduced 2 min glucose depletion phases to cells growing under glucose limitation in a chemostat. Even though Ethanol Red™ displayed robust growth and productivity, a single 2 min depletion of glucose transiently triggered the environmental stress response. Furthermore, a new growth phenotype with an increased ribosome portfolio emerged after complete adaptation to recurring glucose shortages. The results of this study serve a twofold purpose. First, it highlights the necessity to consider the large-scale environment already at the experimental development stage, even when process-related stressors are moderate. Second, it allowed the deduction of strain engineering guidelines to optimize the genetic background of large-scale production hosts.

Keywords: scale-up; scale-down; bioreactor; stimulus–response experiment; substrate gradient; *Saccharomyces cerevisiae*; Ethanol Red™; transcriptomics

1. Introduction

Microbial fitness is determined by the ability to maintain internal homeostasis in view of external heterogeneity. Complex sensory systems allow microorganisms to adapt to the resource availability in a given habitat for survival and enabling growth [1]. Stress-response mechanisms take over if environmental conditions turn for the worse. Depending on the severity of external stress, a growing organism might reduce proliferation, enter a quiescent state or even undergo self-induced cell death [2]. Nonetheless, the early response usually involves a transcriptional adjustment that represses growth capacities to save resources for adequate adaptation. This program is a conserved feature across species, commonly referred to as the stringent response or environmental stress response (ESR) in prokaryotes and eukaryotes, respectively [3,4]. Upon initiation, the transcriptional information propagates towards phenotypic change, which is well-aligned with the environmental shift.

In industrial fermentation development, in the lab the microbial habitat is that of a tightly regulated bioreactor. Several variables, such as pH, temperature, dissolved oxygen and substrate concentration, are kept at optimal levels to maintain the microbial host in

the physiological state of optimal productivity. Still, many bioprocesses suffer unforeseen performance losses when engineers transfer a process from the homogeneous lab environment to the industrial scale [5]. So-called biological scale-up effects occur when transport limitations in large tanks prevent proper mixing, cooling and mass transfer needs of the broth rendering the environment heterogeneous [6,7]. Often, limiting substrate concentrations are set during production phases to ensure that microbial activities still cope with the technical limits of aeration, heat exchange, etc. Such limiting substrate supply defines substrate-to-product conversion yields, and cellular and volumetric productivities. Gradients of said substrates evolve as their reaction time is typically shorter than the mean circulation time in industrially-sized tanks [8]. Therefore, a fluctuating physicochemical environment clashes with a complex biological sensory system. Understanding the systematic incompatibility helps to understand why biological scale-up effects occur and guide rational strain engineering efforts [9].

Saccharomyces cerevisiae, a widely adopted host in the biotech industry, is equipped with the sensory abilities to adapt to the entire spectrum of substrate concentrations it may encounter in a fermentation process. Backed by large-scale process data, simulation studies confirmed the existence of glucose concentration gradients spanning several metabolic regimes in a glucose-limited fed-batch production of baker's yeast [10–12]. For instance, highly concentrated feed solutions may locally introduce glucose concentrations above respiratory capacities, potentially triggering carbon catabolite repression. Distant from the feed inlet, in turn, the substrate becomes depleted triggering starvation-like signals. However, minute-to-hour adaptation times typically exceed the second-to-minute exposure times in the stirred bioreactor space [13]. Thus, cells are prompted to initiate adaptive or even stress-responsive programs, and either their execution or trimming causes unnecessary resource expenditure that might even lead to phenotypic heterogeneity [13,14].

Following the scale-down route, researchers aim to use insights from physical large-scale studies to investigate the physiological response against realistic gradients. Especially in high-cell density processes, the influence of carbon starvation zones draws more and more attention [15–18]. Dedicated experiments with prokaryotic hosts revealed redundant induction and repression of the stringent response when cells were repeatedly withheld from the limiting substrate [19,20]. Derived knowledge on the gene-regulation level ultimately guided rational strain engineering approaches to increase microbial robustness [21,22]. In a recent study, we investigated the transcriptional profile of respiring *S. cerevisiae* against short-term transitions between glucose limitation and starvation in an analogous approach [23]. First-time exposure to acute glucose depletion elicited the ESR prematurely in a non-adapted culture, while it was globally repressed in a 'stand-by mode' enabling dynamic response once the population was adapted to the signals. We concluded that regulatory elements of the ESR, such as the involved transcriptional activators Msn2/4, might be promising targets for strain engineering approaches. However, both the culture conditions and the applied haploid CEN.PK 113-7D strain has little to no relevance in industrial fermentation processes. In addition, this strain harbors several non-synonymous mutations in its cAMP signaling system, the primary mediator of ESR activity [24]. Consequently, we set out to replicate the experiment with the diploid industrial Ethanol Red™ strain under anaerobic, ethanol-producing conditions.

2. Materials and Methods

2.1. Strain, Maintenance and Seed Culture

The commercial, MATa/MATα diploid *S. cerevisiae* strain Ethanol Red™, currently marketed by Fermentis (Lesaffre, Marcq-en-Barśul, France), was kindly provided by Royal DSM N.V. (Delft, The Netherlands). Cells were preserved in 30% (*v*/*v*) glycerol at −70 °C and grown on yeast extract peptone dextrose (YPD) agar plates for two days before starting the aerobic seed cultures. First, a 10 mL glass vial with 5 mL of YPD broth was inoculated with a single colony and incubated at +30 °C on an orbital shaker operated at 120 rpm for 6–8 h. Subsequently, the whole volume was pelleted and used to inoculate 110 mL of a

synthetic medium in a 1000 mL baffled shake flask and grown under identical conditions overnight until the stationary phase was reached. The medium was designed to support approximately 5.0 g·L^{-1} biomass during carbon-limited growth with 50 g·L^{-1} glucose and contained 10 g·L^{-1} ammonium sulfate, 6.0 g·L^{-1} monopotassium phosphate, 1.0 mg·L^{-1} magnesium sulfate heptahydrate, 19.1 mg·L^{-1} ethylenediaminetetraacetic, 4.5 mg·L^{-1} zinc sulfate heptahydrate, 1.0 mg·L^{-1} manganese(II) chloride tetrahydrate, 0.3 mg·L^{-1} cobalt(II) chloride hexahydrate, 0.3 mg·L^{-1} copper(II) sulfate pentahydrate, 0.4 mg·L^{-1} sodium molybdate dihydrate, 4.5 mg·L^{-1} calcium chloride, 3.0 mg·L^{-1} iron(II) sulfate heptahydrate, 1.0 mg·L^{-1} boric acid, 0.1 mg·L^{-1} potassium iodide, 0.05 mg·L^{-1} D-biotin, 1.0 mg·L^{-1} calcium pantothenate, 1.0 mg·L^{-1} nicotinic acid, 25.0 mg·L^{-1} myo-inositol, 1.0 mg·L^{-1} thiamine HCl, 1.0 mg·L^{-1} pyridoxine HCl, 0.2 mg·L^{-1} para-aminobenzoic acid, 0.42 g·L^{-1} tween 80, 10 mg·L^{-1} ergosterol and 0.2 g·L^{-1} Struktol J 674 antifoam (Schill und Seilacher, Hamburg, Germany). The same medium was used for seed, batch and continuous cultures.

2.2. Chemostat Setup

Anaerobic cultivation experiments were carried out in a stainless-steel benchtop bioreactor (Bioengineering, Wald, Switzerland) with a liquid working volume of 1.7 l under a 0.3 bar overpressure. The reactor system and its rapid sampling device were operated as previously described [15,23] with the following modifications: (i) silicone tubing was replaced by oxygen-impermeable tubing (Norprene, Cole Parmer, Vernon Hills, IL, USA), (ii) anaerobiosis was maintained with a sterile nitrogen supply of 0.425 vvm and (iii) no antifoam agent was supplied as it was already present in the medium. Furthermore, the headspace of the feed casket was kept flushed with sterile nitrogen throughout the experiment.

The reactor was aseptically inoculated with 100 mL of seed culture and operated in batch mode until a decrease in CO_2 emission indicated glucose exhaustion. Subsequently, the chemostat was initiated via continuous medium influx and broth efflux at net rates of 2.83 mL·min^{-1} to yield a dilution rate (D) of 0.10 h^{-1}. During stimulus–response experiments (SREs), the system was operated as an intermittently fed chemostat. The feeding pump was set to 0.00 mL·min^{-1} for two minutes while the harvest pump control was inactive. In the case of repeated perturbation cycles (2 min feed off, 7 min feed on), the feed rate was set to 3.64 mL·min^{-1} to maintain the same net D.

2.3. Stimulus–Response Design

Three biologically independent fermentation experiments were carried out according to the process design depicted in Figure 1. Each chemostat operated for 5 residence times (τ) of constant $q_{\text{carbon dioxide}}$ to sample the reference steady state (RS). Thereafter, a single limitation–starvation–limitation (s-LSL) stimulus was imposed to track the non-adapted response as a time series of up to six hours. Subsequently, the mode of operation changed to an intermittent feeding regime. After five τ of repeated cycling, the new, dynamic steady state (DS) was established. The adapted response was sampled as a time series during repetitive cycles (r-LSL) and thus limited to one representative nine-minute series. Dynamic steady state values were expressed as cycle averages.
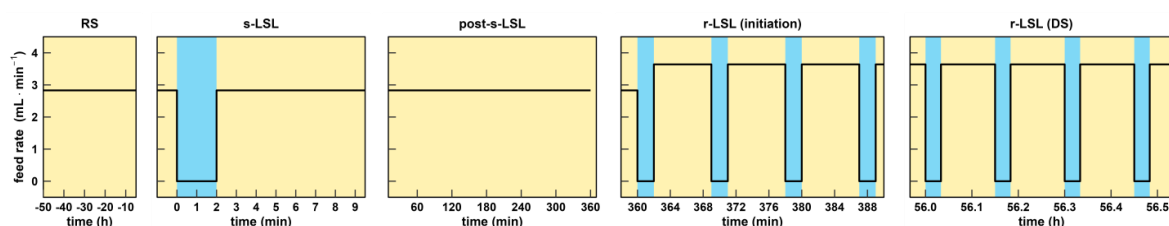

Figure 1. Process design of the chemostat experiment. DS, dynamic steady state; RS, reference steady state; r-LSL, repeated limitation–starvation–limitation transition; s-LSL, single limitation–starvation–limitation transition.

2.4. Analytical Procedures

Sample processing and analysis are thoroughly reported in [15,23]. In brief, biomass, expressed as dry matter of biomass (*DMB*), was determined gravimetrically. All extracellular metabolites were determined with UV-based enzymatic kits (r-biopharm AG, Darmstadt, Germany). Intracellular carbohydrate and RNA pools were assessed according to the original protocols from Parrou and Sasano, respectively [25,26]. Unknown carbon in the supernatant was determined by subtracting the molar carbon concentrations of the antifoam agent and all quantified extracellular metabolites except CO_2 from the total organic carbon concentration in the broth supernatant. We assumed no uptake of the antifoam agent, which has a carbon mass fraction of 61% (w/w) [27]. Total organic carbon was measured indirectly with a multi-N/C 2100 S composition analyzer (Analytik Jena, Jena, Germany) by reducing the inorganic carbon fraction from the total carbon fraction of the supernatant. We estimated a 4.8% loss of ethanol due to stripping which was accounted for in the carbon balance and parameter calculation ($Y_{\text{ethanol/glucose}}$, and q_{ethanol}). Ethanol stripping was estimated based on the approach by Löser and colleagues [28] and is described in detail in Supporting Information A1.

2.5. Processing of Next-Generation Sequencing Samples

We used the Quick-RNA Fungal/Bacterial Miniprep Kit (R2014, Zymo Research, Freiburg, Germany) for total RNA extraction with the following changes to the manufacturer's instructions: 0.5 mL of the biosuspension was sampled directly into a ZR BashingBead™ lysis tubes, pre-loaded with 0.5 mL of a lysis buffer. After the sample was withdrawn, the whole tube was instantly flash-frozen in liquid nitrogen and stored at $-70\,^{\circ}$C. The extraction protocol was resumed by thawing the samples halfway (5–10 min at room temperature) before performing the homogenization step in a Precellys 24 tissue homogenizer (Bertin Technologies, Montigny-le-Bretonneux, France) twice for 20 s at maximum speed with a 10 s break in between. At the end of the protocol, total RNA was eluted with 60 μL DNase/RNase-free H_2O and stored at $-70\,^{\circ}$C.

One 30 μL aliquot from each sample was shipped for mRNA sequencing to AZENTA/ GENEWIZ (Leipzig, Germany). The contractor performed an initial quality check using Agilent 2100 BioAnalyzer (Agilent, Santa Clara, CA, USA) which revealed a heterogeneous RIN (RNA integrity number) value distribution ranging from 2.2–9.9 for all samples. After personal communication with the contractor, it was decided that the project would be commenced since the heterogeneous RIN values were a result of non-uniform rRNA peaks, even though the cause for this effect was unknown. Peaks for nucleotides of <1500 nt including mRNA, however, showed uniform distribution. Next, polyA-selected cDNA libraries were synthesized and sequenced as 150 bp paired-end reads on a NovaSeq 6000 platform (Illumina, CA, USA) with a sequencing depth of 2×10^7 reads.

2.6. Gene Expression Analysis

A sequencing output in the form of *.fastqsanger* files was uploaded on a local Galaxy platform [29] followed by a quality check using *FastQC* v. 0.72 [30]. Sequence files were subsequently aligned with *TopHat* v. 2.1.1 [31] against the phylogenetically closely related *S. cerevisiae* S288C reference genome [32] (GCA 000146045.2-2011), which was accessed from the ENSEMBL database [33]. The overall alignment rate ranged between 83 and 92%. Genes were annotated to *S. cerevisiae.R64-1-1.50.gtf* (from ENSEMBL) and counted using *featureCounts* v. 1.6.4 [34]. From here, count tables were extracted from the Galaxy platform and merged into a *data.frame* object for further processing in the R environment v. 1.4.1106 (R Core Team 2021).

Differentially expressed genes (DEGs) were computed using *DESeq2* v. 1.32.0 [35], applying the likelihood-ratio test with threshold values for |log$_2$-fold change| and a false discovery rate (FDR) [36] of 1.0 and 1×10^{-3}, respectively. More detail is provided in Supporting Information A3 and the experimental design matrix is reported in Supporting Information B (sheet 1). Time series data was clustered with the *kmeans* function

from the *stats* (v. 4.1.0) package and functional annotations were derived from the web implementation of *YeastEnrichr* [37,38]. The raw enrichment analysis output can be accessed in Supporting Information B. Gene set enrichment analysis (GSEA) was carried out using *GAGE* (v. 2.42.0) [39] with $\log_2$-scaled count tables (Supporting Information B, sheet 19) and pre-defined literature data sets (sheet 20) or transcription factor (TF) target sets (sheet 21), which were downloaded from the *Yeastract* database [40]. The results in Figure 6 were reduced to sets showing statistical significance (FDR $< 1 \times 10^{-3}$) during at least one condition in the SRE. Multiple set intersections of DEG lists were computed using the package *SuperExactTest* (v 1.1.0) which uses the combinatorial theory to provide the statistical significance of intersections [41].

3. Results

3.1. Characterization of Extracellular Glucose Profile

The showcasing stimulus–response experiment enabled the observation of transcriptional feedback mechanisms of the industrial yeast Ethanol Red™ (ScER) after intermittent carbon supply. After anaerobically growing cells were adapted to strict glucose limitation for five residence times in a chemostat, the glucose feed was stopped for two minutes to establish a single limitation–starvation–limitation (s-LSL) cycle. A sharp, uptake-driven drop of the glucose concentration from 0.86 mmol·L^{-1} to 0.28 mmol·L^{-1} occurred, which restored to previous steady-state levels within eight minutes after feed resumption (Figure 2, left panel). The biomass-specific glucose uptake rate ($q_{glucose}$) ramped down from 45% to 21% of the maximum capacities (for $q_{glucose,max}$, see Table 1). Glucose uptake kinetics remained also for cells that were completely adapted to repeated LSL cycling for five residence times (r-LSL, Figure 2, right panel). Notably, the perturbation never challenged cellular maintenance demands since the minimum $q_{glucose}$ of 2.5 mmol·g$_{DMB}^{-1}$·h^{-1} stayed 5-fold above the maintenance rate of 0.5 mmol$_{glucose}$·g$_{DMB}^{-1}$·h^{-1} [42].
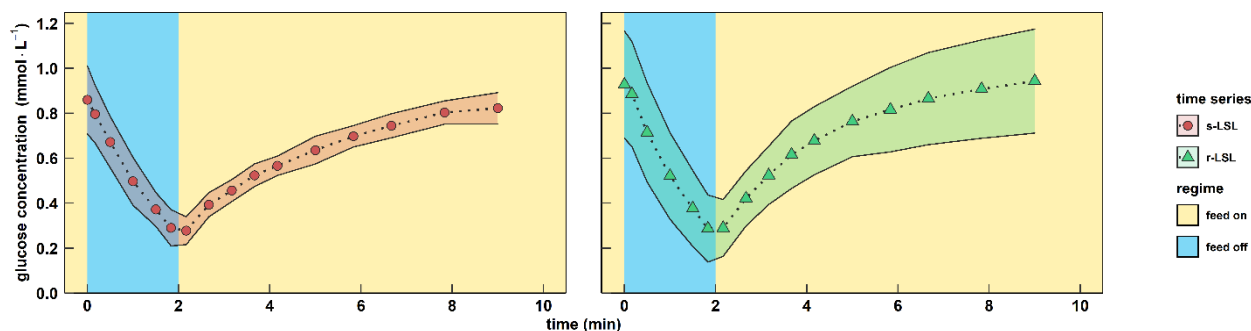

Figure 2. Characterization of the famine stimulus. Extracellular glucose concentrations during the course of one perturbation cycle are shown. Red circles indicate dynamics following a single (s) LSL transition ("feed off" phase) and green triangles indicate trends over a representative repetitive (r) LSL cycle during the DS. Time point 0 min of the s-LSL response is the equivalent of the RS. All values indicate means ± standard deviation of three biological replicates.

3.2. The Physiology of Dynamic and Steady-State Adaptation toward Short-Lived Famine Stimuli

The biomass-substrate yield remained for three hours after the s-LSL cycle indicating the absence of growth-arresting measures by the non-adapted yeast culture (Figure 3A). Steadiness of growth was backed by constant intracellular RNA levels (Figure 3D, *p*-Value > 0.05) that may also serve as a surrogate parameter for ribosomal content [43]. Regarding primary metabolism, substrate shortage was propagated through glycolysis causing a transitory reduction of carbon dioxide emission from 7.8 ± 0.2 mmol·g$_{DMB}^{-1}$·h^{-1} to 5.8 ± 0.2 mmol·g$_{DMB}^{-1}$·h^{-1} (Figure 3B). We reason that the inertness of the off-gas measurement caused the five-minute delay between both minima of glucose uptake and CO_2 emission. A similar observation was reported in a previous study with the same bioreactor system [15]. In addition, an acutely decreased glycolytic flux along the s-LSL trajectory

caused the short-term mobilization of trehalose (*p*-Value 0.06–0.11), but not glycogen, during the first six minutes.

Table 1. Process parameters comparing the reference steady state (RS) against the dynamic steady state (DS). RS parameter values are the means ± standard deviation of three biological replicates. The DS indicates averaged parameter values over one 9 min perturbation cycle of three biological replicates. *D*, dilution rate; *DMB*, dry matter of biomass; $Y_{i/j}$, yield of compound i from j; q_i, biomass specific rate of compound i; c_i, concentration of compound i; n.a., not applicable; n.s., not significant (*p*-Value > 0.05).

Parameter	Dimension	Steady State RS	Steady State DS	% Change	Welch Test (*p*-Value)
D	h^{-1}	0.098 ± 0.003	0.099 ± 0.003	$+0.5$	n.s.
DMB	$g \cdot l^{-1}$	5.06 ± 0.04	4.72 ± 0.17	-6.8	n.s.
$Y_{DMB/glucose}$	$mol_C \cdot mol_C^{-1}$	0.114 ± 0.001	0.106 ± 0.003	-6.9	0.05
$q_{glucose}$	$mmol_C \cdot g_{DMB}^{-1} \cdot h^{-1}$	32.1 ± 0.8	34.7 ± 1.2	$+8.0$	0.04
$q_{glucose,max}$ [1]	$mmol_C \cdot g_{DMB}^{-1} \cdot h^{-1}$	71.50	64.80	-9.4	n.a.
K_S [1]	$mmol_C \cdot l^{-1}$	6.19	5.47	-11.6	n.a.
$Y_{ethanol/glucose}$	$mol_C \cdot mol_C^{-1}$	0.488 ± 0.033	0.468 ± 0.026	-4.0	n.s.
$q_{ethanol}$	$mmol_C \cdot g_{DMB}^{-1} \cdot h^{-1}$	16.7 ± 1.3	17.3 ± 1.4	$+3.6$	n.s.
$q_{carbon\ dioxide}$	$mmol_C \cdot g_{DMB}^{-1} \cdot h^{-1}$	7.68 ± 0.25	8.47 ± 0.18	$+10.3$	0.01
$q_{glycerole}$	$mmol_C \cdot g_{DMB}^{-1} \cdot h^{-1}$	2.70 ± 0.09	2.99 ± 0.12	$+11$	n.s.
$q_{acetic\ acid}$	$mmol_C \cdot g_{DMB}^{-1} \cdot h^{-1}$	0.04 ± 0.00	0.04 ± 0.00	-2.1	0.03
$q_{succinic\ acid}$	$mmol_C \cdot g_{DMB}^{-1} \cdot h^{-1}$	$2.9 \times 10^{-2} \pm 4.7 \times 10^{-3}$	$3.6 \times 10^{-2} \pm 1.4 \times 10^{-3}$	$+25.7$	n.s.
$q_{unknown\ carbon}$	$mmol_C \cdot g_{DMB}^{-1} \cdot h^{-1}$	1.06 ± 0.53	1.81 ± 0.91	$+71.2$	n.s.
$c_{glycogen}$	$mmol_C \cdot g_{DMB}^{-1}$	2.87 ± 0.16	1.65 ± 0.12	-42	1.0×10^{-3}
$c_{trehalose}$	$mmol_C \cdot g_{DMB}^{-1}$	1.84 ± 0.19	1.25 ± 0.52	-32	n.s.
c_{RNA}	$mg \cdot g_{DMB}^{-1}$	64.3 ± 2.5	80.7 ± 3.1	$+25$	2.0×10^{-3}
C-recovery	$mol_C \cdot mol_C^{-1}$	0.98 ± 0.02	0.98 ± 0.02		

[1] Estimated parameters (see Supporting Information A2 for details).

After the s-LSL cycle, repeated (r) r-LSL stimuli were performed during the second phase of the experiment. A single r-LSL cycle was analyzed using averaged data, the so-called dynamic steady state (DS). Therewith, distinct adaptations of ScER resource management were unraveled that mimicked cellular efforts to cope with the fluctuating substrate environment (Table 1). Supported by closing carbon recoveries, the biomass-substrate yield ($Y_{DMB/glucose}$) dropped by 6.9% whereas the net dilution rate and glucose feed remained. Consequentially, an equal rise of biomass-specific glucose uptake occurred. Relative to the reference steady state (RS), the surplus of the glycolytic input was channeled towards CO_2 emission. From the trend, increased ethanol production and glycerol secretion were also found, which agrees with stoichiometric expectations. The DS population released 71.2% more unknown carbon products than the reference state. Even though this value possesses low statistical confidence, the trend supports the slightly reduced $Y_{DMB/glucose}$ and might point to elevated cell lysis [44]. Intracellular resource allocation changes made up the most pronounced r-LSL adaptations. We observed glycogen and trehalose pool size reductions of 42% and 32%, respectively. They were accompanied by increased intracellular RNA concentrations from 64.3 ± 2.5 mg$\cdot$g$_{DMB}^{-1}$ to 80.7 ± 3.1 mg$\cdot$g$_{DMB}^{-1}$. Even though it is a well-known tendency of *S. cerevisiae* to counter-

balance ribosome abundance with the degradation of glycogen reserves, the correlation is anticipated to be growth-rate-dependent only [45].
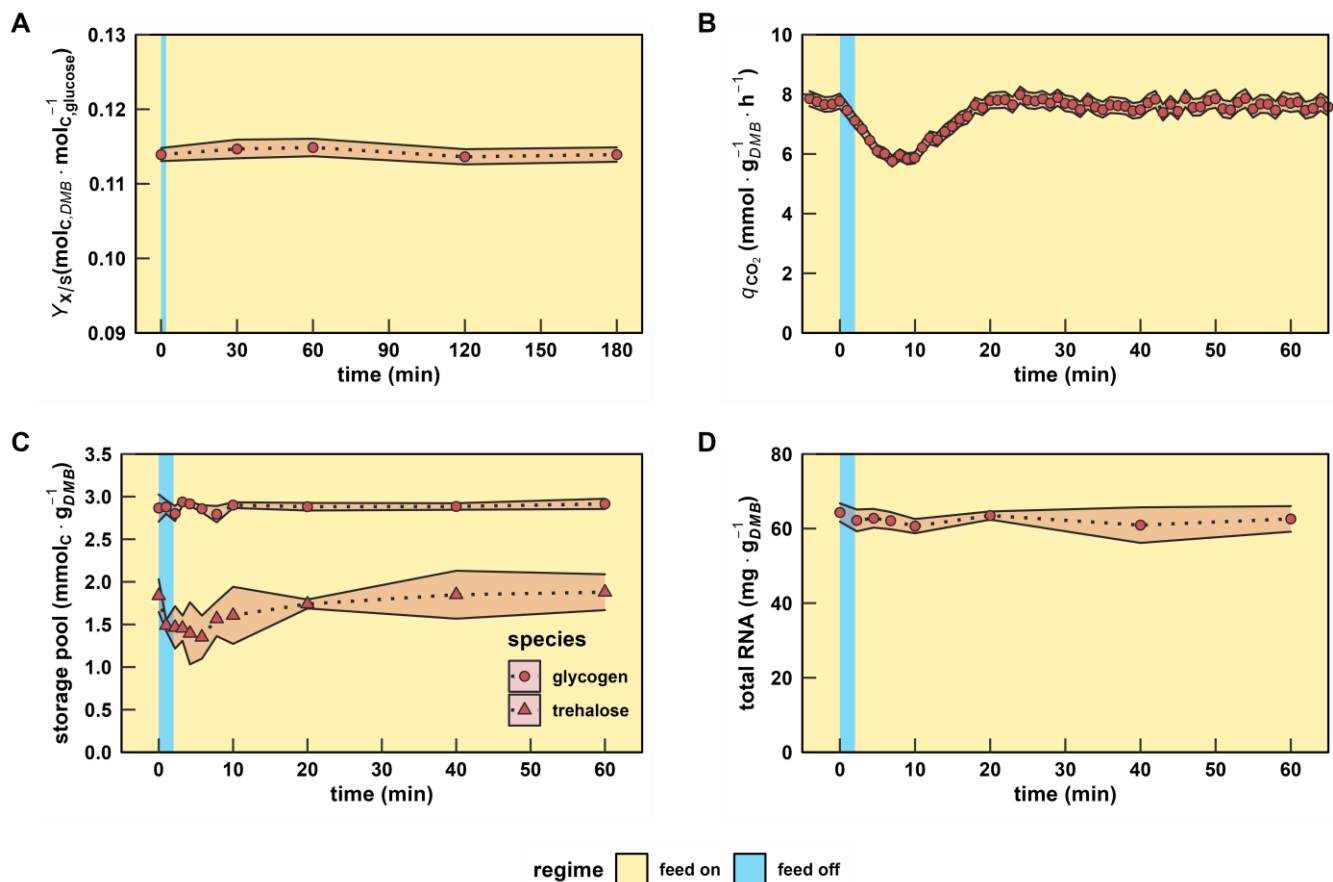

Figure 3. Characterization of macroscopic readouts after a single LSL stimulus. (**A**) Biomass-substrate yield up to 180 min. (**B**) Biomass-specific carbon dioxide production rate, (**C**) intracellular carbon storage, and (**D**) total RNA pool dynamics up to 60 min. The time series indicates dynamics following a single transition into the starvation phase ("feed off" phase). Time point 0 min is equal to the reference steady state. All values indicate means ± standard deviation of three biological replicates.

In consequence, we set out to investigate whether or not the sensing of the dynamic extracellular environment triggered cascading effects that propagated through the ScER regulatory network in a manner that was independent on the growth rate.

3.3. The Transcriptional Response to Single Starvation Exposure (s-LSL)

The post-s-LSL cycle monitoring of ScER cells that operated at the steady state with an industrially representative production rate [46] revealed a differential expression of 1053 genes (Figure 4). Co-regulated mRNAs were grouped into seven clusters containing 66 to 211 genes before characterizing them through functional enrichment. This non-adapted feedback peaked between 10–20 min and entirely relaxed 60 min after the stimulus added.

Clusters 1 and 2 followed a similar repression/de-repression trajectory with a strong amplitude of cluster 1 before RS levels were restored. Both clusters were significantly enriched with genes of the ribosome biogenesis (RiBi) ontology, which were further specified as sub-ontologies such as rRNA processing or subunit maturation. Notably, the observed expression changes did not result in a detectable correlation with total intracellular RNA levels (Figure 3D). Cytoplasmic translation was also enriched in the steadily induced cluster 4 opposing the downregulation trend of clusters 1 and 2 during early responses. Cluster 4 contains 29 of 37 differentially expressed ribosome subunits. Thus, the s-LSL response

elicited 27% of all 135 ribosome proteins (RPs). However, the remaining majority responded only in a dampened manner according to the analysis of RiBi-associated gene expressions.
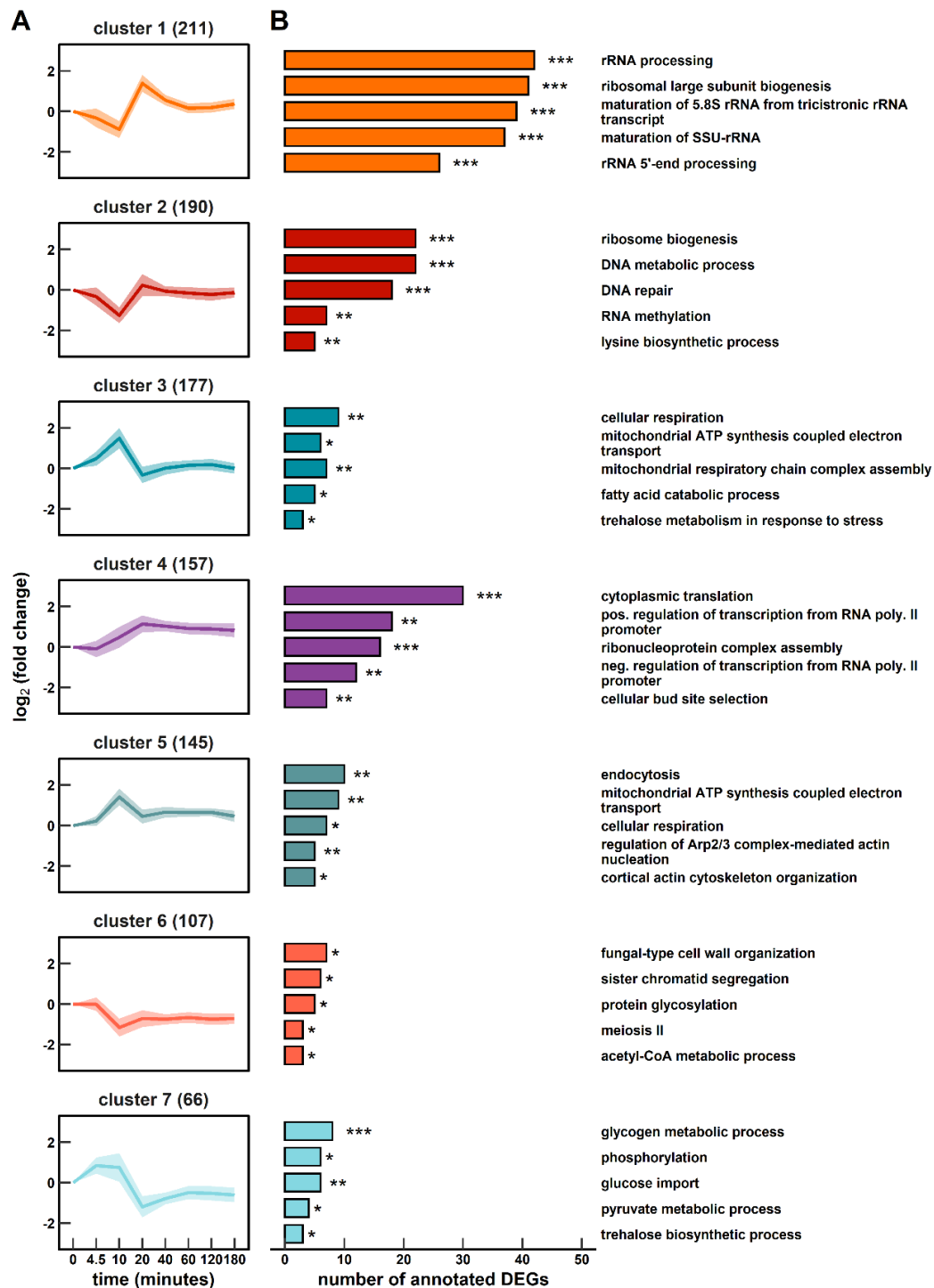

Figure 4. Gene expression dynamics following the single-LSL stimulus up to 180 min. (**A**) Seven k-means clustered groups of co-expressed genes are shown with the number of corresponding genes in brackets. (**B**) Corresponding gene ontology (GO) enrichment analysis. The false discovery rate (FDR) is indicated by asterisks for each GO term (* $1 \times 10^{-5} \leq$ FDR $< 5 \times 10^{-2}$; ** $1 \times 10^{-10} \leq$ FDR $< 1 \times 10^{-5}$; *** FDR $< 1 \times 10^{-10}$).

In addition to the well-equilibrated response of protein formation, we observed evidence of the transiently reduced production of cell cycle-related transcripts. Cluster 2

covers DNA metabolic and repair mechanisms while cluster 6 comprises sister chromatid segregation and the term "meiosis II". Even though industrial diploid strains such as ScER should exhibit high mitotic stability [47], meiotic events especially during nutrient starvation are not uncommon [48]. In addition, the three genes leading to the significant call of "meiosis II", namely *IRC15*, *IML3* and *IPL1*, are involved in both mitotic and meiotic processes [49].

Clusters 3 and 5 somewhat mirror the trends of clusters 1 and 2 in an opposite manner. As they comprise a significant proportion of genes encoding respiratory capacities, this is unexpected given the strictly anaerobic environment. However, factoring in other functional enrichments, the picture of an acutely energy scavenging population evolves. Upregulated mRNAs coding for both endocytic functions and related regulatory elements such as Arp2/3-mediated actin nucleation are well-studied responses of acute glucose withdrawal [50]. Furthermore, the joint analysis of clusters 3 and 7 reveals the induced metabolic activity of the major carbon storage compounds glycogen, trehalose, and fatty acids. Rapid trehalose mobilization was accompanied by a 1.2-fold induction of the neutral trehalase encoding transcript *NTH1* in agreement with the literature [51]. Conversely, glycogen mRNAs in cluster 7 were mainly involved in glycogen buildup (*GAC1*, *GIP2*, *GLC3*, *GLG1*, *GSY1*, *GSY2* and *UGP1*) whereas the respective polymer level remained constant. A functional dependency on the strategic upregulation of the respiratory apparatus becomes evident in genes that make up the "fatty acid catabolic process" ontology. In fact, products of transcripts such as *FOX2*, *ECI1*, *POT1* and *IDP3* catalyze the O_2-dependent β-oxidation of fatty acids [52]. Glucose import was equally tuned by inducing three high-affinity facilitators (Hxt4/17/13) and two of three hexokinases (Hxk1 and Glk1) [53].

In essence, the cellular transcriptional program prepared the population for carbon scarcity. The reset occurred after the glucose availability improved again. Interestingly, even though the transcriptome was deemed to be fully relaxed after 60 min, clusters 4, 6, and 7 did not re-install RS levels.

3.4. The Transcriptional Response to r-LSL

Next, we set out to investigate the adaptation status of ScER in the permanently dynamic environment. We assessed the steady-state gene expression profile of the DS versus RS. Thereof, we uncovered 332 induced and 265 repressed genes that were characterized using gene ontology and pathway enrichment (Figure 5A,B). In addition, 141 transcripts remained responsive, as they were repeatedly upregulated and downregulated within r-LSL cycles (Figure 5C,D).

Completely DS-adapted yeast cells revealed a strategy of increasing their internal translation capacities against recurring starvation signals. Significant overrepresentation of related gene ontologies such as "cytoplasmic translation" and "ribosome biogenesis" further indicated that this strategy occurred for two sub-groups: transcripts coding for ribosome subunits and their maintenance apparatus. Notably, 45 RPs of the total 57 RPs revealed permanent amplification. In contrast to the observations for the s-LSL cycle, r-LSL gene expression changes were backed by a 25% increase in the intracellular RNA content (Table 1). Pathway ontologies further indicated the marked upregulation of "translation factors" including the initiation factors eIF1, eIF2β, eIF4A, eIF4E, and eIF6. Notably eIF4A (also known as TIF2), which was induced 2.2-fold, plays a pivotal role in the early response of yeast towards acute glucose shortage by dissociating from the 48S pre-initiation complex [54]. Dissociated eIF4A caused the instant stalling of translation initiation, which appeared to be alleviated through its upregulation under the given conditions. Figure 5C,D further indicates the persistent short-term regulatory responses of gene products involved in ribosome biogenesis and more particular, rRNA processing in cluster 2. This functional group accounts for 25% of the steadily upregulated and downregulated portion of the transcriptome.
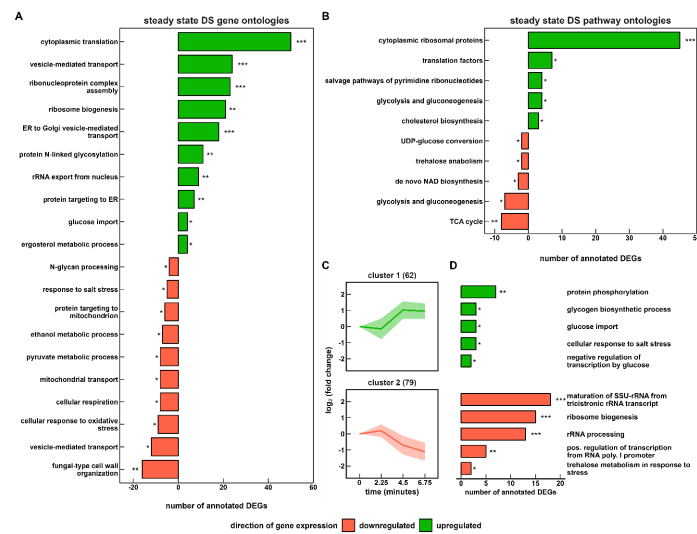
Figure 5. Functional enrichment analysis of DS based on (**A**) biological function and (**B**) pathway annotations. Short-term gene expression changes during the repeated (r) LSL cycles are shown in (**C**). Two k-means clustered groups of co-expressed genes are shown with the number of corresponding genes in brackets (**D**) representing the corresponding enrichment analysis of biological function. The false discovery rate (FDR) is indicated by asterisks for each category (* $1 \times 10^{-5} \leq$ FDR $< 5 \times 10^{-2}$; ** $1 \times 10^{-10} \leq$ FDR $< 1 \times 10^{-5}$; *** FDR $< 1 \times 10^{-10}$).

In addition to protein synthesis, we observed a highly significant differential expression of several genes annotated to protein modification and trafficking. The upregulated group "protein targeting to the endoplasmic reticulum (ER)" contains all four subunits of the signal peptidase complex (SPC), which is involved in cleaving signal peptides of secretory and membrane proteins during translocation into the ER [55]. Regarding protein processing activity in the ER, significant upregulation of *N*-linked glycosylation genes occurred, such as the asparagine-linked glycosylation (ALG) group (*alg5/6/8*) and the oligosaccharyltransferase (OST) complex (*ost2/4/5/6*). Induction of genes that are involved in the formation of GPI anchors was observed, too (see Supporting Information B, sheet 12).

Next, anterograde transport from the ER to the Golgi apparatus was stimulated through the induction of several coat protein complex II (COPII) elements, such as the GTPase Sar1 and the ER vesicle genes *erv29*, *erv41*, *erv14*, and *erv15*. COPII-coated vesicles transport membrane-bound proteins to the Golgi apparatus for the maturation of *N*- and *O*-linked glycosylation [56]. Despite the strong upregulation of 22 Golgi-transport genes, downregulated mannosyltransferase transcripts, represented by the ontology "*N*-glycan processing", were the only significantly enriched DEGs with a Golgi-located protein modification function. At the end of the secretory pathway, we found upregulated sterol biosynthetic genes in both the gene ontology and pathway enrichment. This observation, however, seems rather counter-intuitive given that sterol synthesis is oxygen-dependent, rendering *S. cerevisiae* auxotrophic for this essential cell membrane component in anaerobic cultivations. In addition, a pronounced repression of "fungal-type cell wall organization" occurred, which included a set of genes such as the cell wall mannoproteins *cwp1*, *cwp2*, *tip1*, *tir3*, and *ccw12*—all functionally related to the downregulated mannosyltransferase capacities.

Yeast cells reportedly maintain branched tricarboxylic acid cycle (TCA) activity under anaerobic conditions to supply building blocks for growth [57], which was reflected by the small amounts of extracellular succinic acid (Table 1). Moreover, respiratory abilities are preserved in the absence of oxygen, too [58,59]. Here, we observed a significant downregulation of these auxiliary functions of respiratory pathways, such as mRNAs involved in the reductive (*MDH1*, *MDH2*, and *FUM1*) and oxidative (*ACO1*) TCA branches and repressed "cellular respiration", "mitochondrial transport", and "TCA cycle" ontologies. Regarding central carbon metabolism, repression also occurred on the level of pyruvate and ethanol

metabolism. Gene-level investigation revealed that TCA influx mainly was hampered through pyruvate dehydrogenase (*PDA1*), pyruvate decarboxylase (*PDC6*), and aldehyde dehydrogenase (*ALD4*). This coincided with amplified fluxes towards fermentative pathways upstream of TCA. For instance, *ADH5*, which supports ethanol production [60], was induced 5.2-fold. Glucose uptake was also re-arranged to cope with decreasing extracellular availability through increased expression levels of the high-affinity transporter mRNA *HXT2/6/7* and the hexokinase 2. Non-glucose hexose transporters, such as mannitol and sorbitol scavenging Hxt13/17 were found to be dynamically expressed/repressed in cluster 1 during r-LSL transitioning.

Taken together, the adaption towards short-term limitation–starvation cycling encompassed the marked restructuring measures taken to aim at fostering growth. Translation-related genes were amplified at the expense of sacrificing reserve respiratory abilities and some non-specific stress response mechanisms, such as the "cellular response to oxidative stress" and the "response to salt stress". As indicated in the gene expression profiles, the ATP-demanding formation of ribosomes was additionally supported by fostering ATP generation through ethanol fermentation.

3.5. Comparing Transcriptional Responses of s-LSL and r-LSL

Regulatory information was deduced from gene set enrichment analysis (GSEA) to uncover the dynamics of literature-derived sets [61,62] (Figure 6A) and more nuanced transcription factor (TF)-mediated regulons (Figure 6B). The analysis was conducted on s-LSL, r-LSL and DS data while restricting the output to gene sets with statistically significant enrichment in at least one sample point across all conditions. Figure 7 serves as a visual summary of the involved regulatory elements and reported interactions.
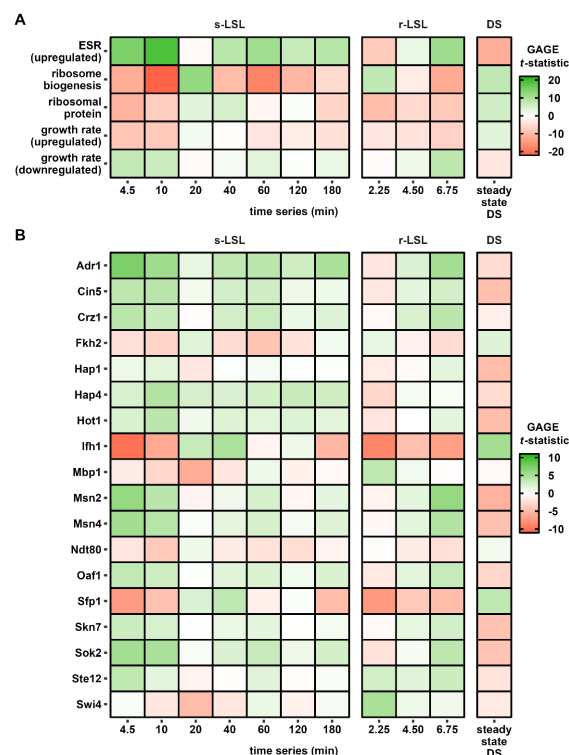

Figure 6. Gene set enrichment analysis (GSEA) of pre-defined gene lists from the literature (**A**) and transcription factor target lists (**B**). The reported *t*-statistic implies the strength and direction of the coordinated differential gene expression of a given set. GSEA was performed comparing the single (s) LSL time series against the reference steady state. Furthermore, the repeated (r) LSL time series was compared against its internal time point 0 min. The DS is a contrast between the reference steady state and all r-LSL sample points. Only gene sets with significant enrichment in at least one sample point (FDR < 1×10^{-3}) are shown.
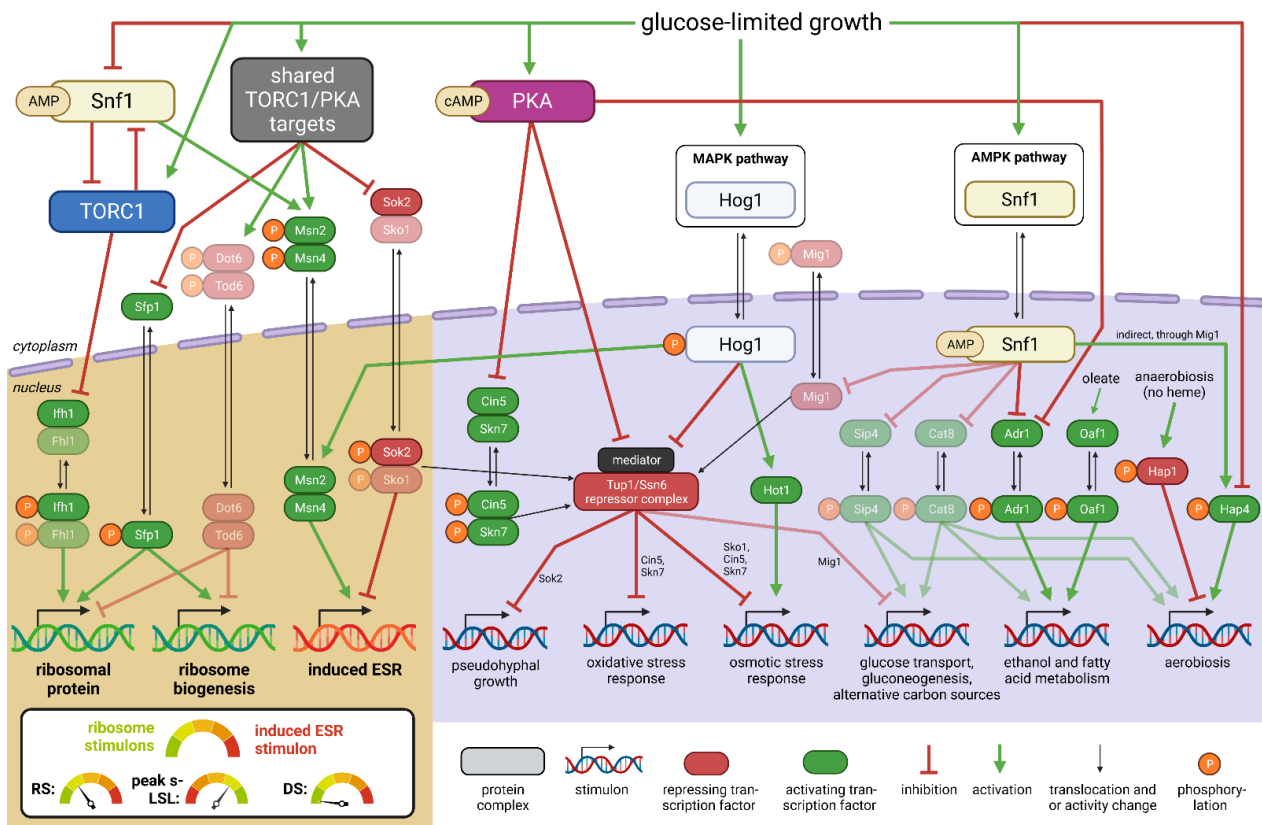
Figure 7. Regulatory kinase and transcription factor network active under the given experimental conditions. The brown background highlights the main ESR-associated stimulons. The violet background depicts observed co-induced stimulons. The simplified schematic network is limited to transcription factors (TFs) with significant calls in the GSEA and their known upstream effectors. Transparent TFs were either not significant or not part of the analytical pipeline but still included due to the reported implication in the given network. For simplification, not all pathway components, connections, and alternative functions are illustrated. The shown network is based on [63–71].

ScER perceived the transient first-time exposure to starvation as an elicitor of the environmental stress response (ESR). As is typical for this program, the early induction of the ESR stimulon coincided with repression of ribosome stimulons represented by the RiBi and RP sets. Strictly growth-rate-dependent sets were considered to discriminate between the onset of the ESR program and mere adjustments of the growth rate. Since amplitudes measured after 10 min of s-LSL exposure of the ESR and RiBi sets showed 2–3-fold larger $|t$-statistic$|$ values than those of the growth-rate-dependent sets, we concluded that the observed response was dominated by the ESR. This was also backed by constant $Y_{DMB/\text{glucose}}$ throughout the non-adapted time-series. Similarly to the responses to the s-LSL cycle, r-LSL transcript dynamics reveal dampened oscillations, which are also visible in TF targets. Examples are the Msn2/Msn4 pair and the de-repression through Sok2 target genes. Further examples are also given regarding the repressed ESR branch with Ifh1-guided RP repression and Sfp1 control over both RP and RiBi genes [62,67].

Thus, a stress response–growth trade-off emerges, which is primarily balanced via the upstream effector target of rapamycin 1 (TORC1) and the protein kinase A (PKA). Our results further revealed additional signal input through the stress-activated signaling hubs, such as the mitogen activated kinase (MAPK) cascade or the glucose de-repression program [1]. One example is the osmo-responsive mitogen-activated Hog1 kinase as it is involved in both the direct induction of the osmotic stress response and fine-tuning of the ESR [67,72]. Hog1 activity was confirmed though the significant regulation of Hot1, a mediator of the osmo-specific gene expression program of this kinase. Closely related

are the activators Cin5 and Skn7 and the repressor Sok2, which are stress-responsive recruiter molecules for the Tup1-Ssn6 repressor complex [73]. Tup1-Ssn6, in turn, interacts with the mediator complex—a coordinator of PKA and Hog1 signal integration under environmental stress [67]. Tup1-Ssn6 recruitment is not the only role of Skn7 as it further stabilizes the calcineurin-dependent transcription factor Crz1 [72]. Thus, it may not be surprising that both gene sets displayed almost identical expression dynamics. Another TF under MAPK control with a similar profile is Ste12, which regulates mainly mating and filamentous growth clusters [74]. Typical glucose de-repression signatures were observed by the deregulation of Snf1downstream targets, such as TFs Adr1, Hap4 and putatively Oaf1 [68,75]. Their activity can be observed in the transient induction of cluster 3 in Figure 4 with the enriched ontologies "cellular respiration" and "fatty acid catabolic process".

GSEA further uncovered four active cell cycle-related transcription factors, two of which make up one partner of the heterodimeric SBF (Swi4) and MBF (Mbp1) factors that induce gene expression during the G_1-to-S transition [76]. The forkhead homolog Fkh2 co-regulates genes which are active during both the mitotic and meiotic G_2-to-M transition [77]. On the other hand, Ndt80 is a strictly meiotic regulator [78]. Apparently, cell cycle-related regulation followed a repressive pattern following the single stimulus. More precisely, the G_2/M-related regulatory effects were found to be associated with the repressed dynamics of the ESR while regulation during G_1/S took effect in a delayed manner, peaking after 20 min.

In conclusion, the transcriptional response to the s-LSL cycle comprised the transient expression of global regulatory programs, including the ESR and growth repression. DS-adapted yeasts showed the opposite gene expression pattern—namely, the repression of stress-induced gene sets and induction of growth-associated genes. Interestingly, there was still residual transcriptional activity of the same regulatory groups during the r-LSL time series. This result suggests that the short-term responsiveness of the regulatory circuitry controlling the adapted and non-adapted phenotypes was not entirely shut down during the DS.

3.6. Comparing Different Strain Backgrounds and Production Scenarios to the Same Stimulus

Transcriptional responses of ScER were compared to the likewise stimulated haploid MATa strain CEN.PK 113-7D [23] that was growing under aerobic conditions (Figure 8). Except for different $|\log_2$-fold change$|$ thresholds, the same analytical pipeline was used in both studies.

In essence, commonly found key regulation features are (i) the trade-off between stress response and growth abilities and (ii) the re-allocation of intracellular carbon storage and RNA pools. Whereas CEN.PK 113-7D revealed the reduction of $Y_{DMB/\text{glucose}}$ to a single LSL exposure, ScER merely limited responses to the transcriptional level. However, ScER significantly reduced its biomass yield after complete adaptation (r-LSL), which was not the case for CEN.PK 113-7D. Other differences were found for transcriptional relaxation times after single perturbation: ScER restored pre-perturbation conditions almost entirely within one hour. For comparison, the process lasted up to three hours within dampening amplitudes for CEN.PK 113-7D.

One-third of differentially expressed genes (350) of the non-adapted response was shared between both strains, indicating the presence of a highly conserved regulatory program. Shared genes in this core response were primarily enriched for RiBi mRNAs during the s-LSL cycle. Moreover, RiBi genes that were repressed initially upon unprecedented glucose exhaustion were upregulated later during the DS. This led to several overlaps of functionally related GO enrichments between the s-LSL cycle and upregulated DS sets of both strains. Eisosome assembly emerged as another conserved mechanism that is positively correlated to the ESR. The finding is in agreement with that of a recent study linking endocytosis to nutrient-scavenging activity in a nutrient-depleted environment [79]. As an analogy, "glycogen metabolic process" was found to be significantly enriched in overlapping gene sets of the non-adapted response and repression during DS. Stress pro-

grams with an unobvious role in surviving famine exposure, such as the oxidative and salt stress response, were observed to be downregulated during the DS in both strains, but only actively induced during the s-LSL cycle in ScER.
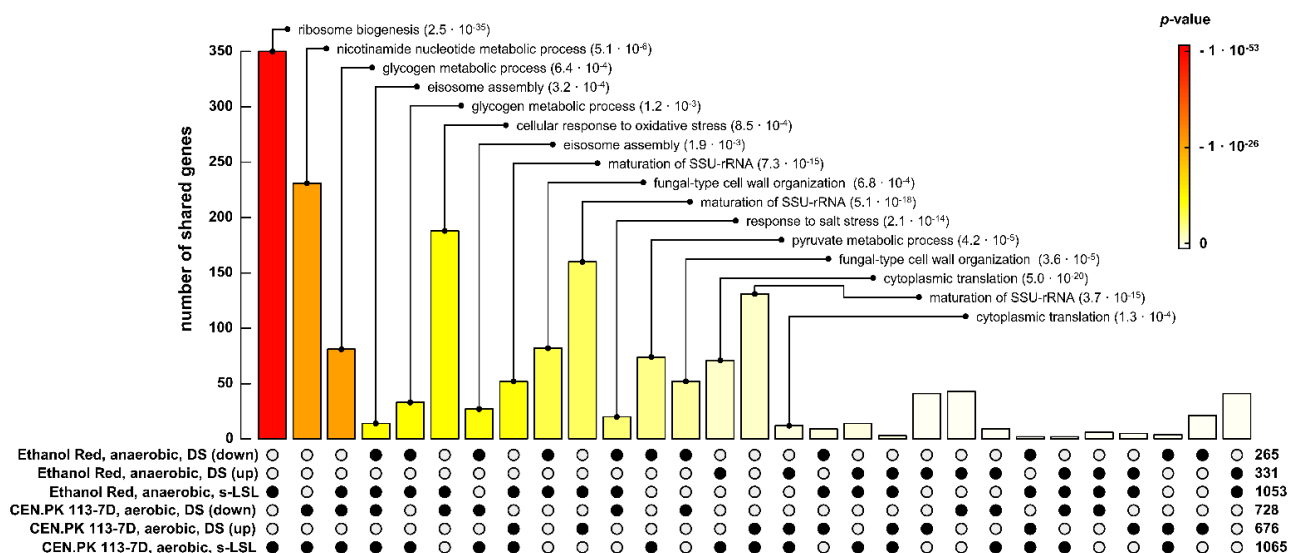

Figure 8. Shared sets of differentially expressed genes under anaerobic (this study) and aerobic [23] conditions in LSL-cycling chemostats. Black dots in the matrix indicate the considered DEG sets, the bar above represents the respective intersection size and the color gradient illustrates significance. The number of genes included in each set is reported on the right. Gene ontologies of the intersection sets are only reported if both the intersection and GO enrichment were significant (FDR $< 1 \times 10^{-3}$).

Peculiar CEN.PK 113-7D-specific gene expression changes occurred on the metabolic level as the ontology "nicotinamide nucleotide metabolic process" was mainly made up of glycolytic genes. Eighty-two genes were exclusively found in the s-LSL cycle and repressed DS datasets of ER and were functionally enriched for "fungal type cell wall organization". Taken together, we interpret the overall sparsity of common gene sets across conditions per strain as further evidence of a highly conserved transcriptional regulation circuitry, which operates at the glucose limitation–starvation junction.

4. Discussion

4.1. Fluctuating Glucose Supply—Threat or Not?

Conditions of limiting glucose availability may frequently occur in large-scale fermentation processes [16–18,80] and are not restricted to aerobic cultivations [81–83]. In the present study, we cultivated ScER in a tightly controlled steady-state environment to investigate the effect of sudden glucose shortage. Since the stimulus was not strong enough to induce metabolic regime changes or to compete with maintenance demands, the observed signals may have mimicked the immediate cellular response to the environmental perturbations.

Apparently, the rapid ramp-down of the primary substrate supply instantly triggered the defensive transcriptional program, the so-called environmental stress response ESR [84], in the previously unstressed ScER strain. Thus, the first-time occurrence of glucose shortage was perceived as a 'threat'. The primary task of the ESR is to save resources by ramping down growth capacities to invest in defensive precaution measures. Given the absent growth rate reduction and the relatively quick relaxation of the transcriptome changes, we reason that the ER efficiently shut down this program. Otherwise, said consequences would have been much more pronounced [1,23,85,86]. Comparing with CEN.PK 113-7D, trehalose mobilization, or the lack thereof, might contribute to this difference. The strain ScER instantly mobilized trehalose pools when the glucose influx decreased, likely to support energetic homeostasis [51]. Contrarily, CEN.PK 113-7D failed to maintain glycolytic flux as trehalose and glycogen pools remained stable during the stimulation (see Supporting

Information A4). As a consequence, ATP reduction occurred in CEN.PK 113-7D, which further induced the ESR signaling cascade [23,87] through the energy-sensory Snf1 kinase. However, the role of trehalose in preventing energetic imbalances still remains somewhat elusive, though divergent short-term metabolic reactions to rapid changes in glucose concentration seem to cause strain-specific adaptation mechanisms. Glucose pulse experiments with *Escherichia coli*, *S. cerevisiae*, *Aspergillus niger* and *Penicillium chrysogenum* showcased this dependency [88].

Recurring glucose shortages did negatively affect the biomass-substrate yield. Even though biomass-specific ethanol production seemed to increase, the overall reduction in $Y_{DMB/\text{glucose}}$ superimposed this effect and caused a net loss of the ethanol yield on glucose. Apparently, the regulatory modules involved during the peak ESR also controlled the DS phenotype since the same regulatory targets were affected in an inverse manner. Interestingly, these results showed high conformity with the operational mode of fast-growing yeasts, in which decreased carbon reserve pools enable increased anabolic demands to sustain enforced ribosomal machinery [45,89]. In an independent study, Metzl-Raz and colleagues confirmed that environmental sensing rather than internal feedback from the actual growth rate controls ribosome abundance [90]. Increased resource allocation for translation finally helps to accelerate growth after stress relief—a mechanism that displays an evolutionary advantage [91], especially in the selective environment of a chemostat.

Taken together, transient glucose depletion did not prove to be detrimental to the productivity of ScER. Nevertheless, we observed the presence of conserved regulation phenomena, such as increased transcriptional activity during ESR execution, which may cause unnecessary metabolic investments when stressful conditions arise [4,92]. Moreover, sustained transcriptional stimulation–repression dynamics after adaptation identifies a non-optimally operating biocatalytic host, and enables an understanding of the underlying regulatory mechanisms that motivated this study.

4.2. Not a Threat, but Still a New Habitat—How LSL Transitions Induce a New Growth Phenotype

The environmental stress response is a highly conserved gene expression program in *S. cerevisiae* [93,94]. Thus, it may not come as a surprise that different yeasts operating in different environments elicit strikingly conforming differential gene expression patterns when exposed to the same stimulus. The corpus of the induced ESR branch under acute stress, including glucose depletion, is driven by the feed-forward role of cAMP-dependent PKA signaling against the same targets primarily controlled by TORC1 under steady-state conditions [23,87,95–97]. When cAMP levels drop, PKA de-phosphorylates of the paralogue TFs Msn2 and Msn4 cause their nuclear translocation, during which they bind the so-called stress response elements within promoters to induce downstream expression [96]. In addition to the dual TORC1-PKA circuit, Msn2/4 regulation is fine-tuned in a condition-specific manner either upstream by the concerted activity of cross-talking kinases, such as PCK, Pho85, Hog1, and Snf1 or intersecting TFs, such as the repressors Sko1 and Sok2 [67,98].

Indeed, our transcriptomic analysis revealed the involvement of Hog1 through the significant activity of its osmo-specific transcription activator Hot1. This mitogen-activated kinase induces various mechanisms that converge for Msn2/4 regulation, including protection against temperature [99,100] and oxygen [101] shifts. The latter, especially, displays a high degree of coaction with the program induced by Hog1, even under anaerobic conditions [102,103]. Krantz et al. observed a dampened transcriptional response of osmotic and oxidative stress genes following a 0.5 M NaCl shock in anaerobic versus aerobic yeast cultures [102]. The authors inferred from their experiments that the glycerol production necessary to maintain NADH redox homeostasis in anaerobic cultures is the main driver of negative feedback for Hog1 phosphorylation. Conversely, this negative feedback does not exist in respiring, glucose-limited yeast cultures. Thus, the more stringent regulation of Hog1 during anaerobic growth might partially explain the more efficient ESR shutdown of non-adapted ScER compared to the dampened dynamic of CEN.PK113-7D during

the s-LSL cycle. Consistent with this line of reasoning is the occurrence of overshooting Hog1 activity under aerobic conditions upon transient glucose withdrawal reported in an independent study [104].

The AMP-activated Snf1 cross-talk could not be characterized based on the dynamics of its actuating parameter, the adenylate energy charge, even though a rapid decrease was described under experimental conditions [105]. Upon glucose depletion, however, the Snf1 kinase acts as a cooperative modulator of the PKA pathway, with shared targets such as Msn2/4 and Adr1 [70], a direct regulator of glucose de-repression [70,106,107]. The role of Snf1 in the latter is thoroughly described in the literature to be involved during the diauxic shift when glucose is depleted in batch cultures [108–110]. During the s-LSL response, we observed a significant regulation of Adr1 and genes involved in ethanol metabolism and fatty acid degradation, a typical feature of the diauxic shift. Moreover, this transitionary phase usually encompasses the induction of respiratory, high-glucose-affinity, and alternative carbon assimilation activities [70]. Although we observed a differential expression of genes involved in said activities, our data lacked statistical significance for the strictly Snf1-dependent TFs Cat8, Sip4, and Mig1 [70,111]. A potential explanation might be the presence of Snf1 bypassing regulation through either PKA in the case of Adr1 or the heme-activated protein (Hap) complex. The Hap complex is also involved in glucose de-repression [112,113] but displays Snf1- and PKA-independent transcriptional regulation of respiratory genes [71,107].

Past studies concluded the same negative correlation between the induced ESR and repressed ribosome stimulons observed in this study during a s-LSL cycle [62,114]. Regarding the regulatory hierarchy, both stimulons are controlled by the overriding PKA activity under acute stress and both RiBi and RP genes are repressed through the de-phosphorylation of the master repressor pair Dot6/Tod6. A study by Lippman and Broach suggested that only Dot6 is a substrate of PKA under carbon source stress [107]. We were, however, not able to test for significant Dot6/Tod6 regulation as the target gene sets available from the Yeastract database were not rich enough to include the TFs in our analytical pipeline. Nonetheless, we identified significant regulation of the Dot6-antagonizing activators Sfp1 and Ifh1 [115]. The somewhat weakened response of the RP versus RiBi sets creates room for speculation as several potentially overlapping mechanisms might become relevant during the investigated perturbation. Both the Sfp1 and Ihf1 TFs target different promoter architectures. Nuclear exit causes Sfp1 release from RiBi-associated RRPE and PAC promoter elements while Ifh1 dissociates from an as-yet-unknown RP-specific promoter [115,116]. Acute glucose withdrawal further post-transcriptionally inhibits translation initiation [117], partly causing mRNAs to aggregate in so-called processing bodies or stress granules. Growth-associated transcripts are withdrawn from translation or actively degraded once located in said agglomerates [118,119]. Bresson et al. provide additional evidence that RiBi and RP genes are specifically flagged for TRAMP-mediated mRNA degradation following glucose withdrawal, with both gene sets exhibiting different degradation dynamics [120]. High PKA activity reportedly inhibits p-body and stress granule formation [121] and more remarkably, the assembly of these structures is independent of TORC1 or Snf1 signaling [122].

The results thus far indicate that cAMP-dependent PKA signaling is at the core of adaption toward dynamic glucose availability. Clearly, specific stress-responsive stimulons and the ESR were repressed while ribosome-associated mRNAs were induced. This emerging "high-growth" phenotype in the DS showed striking resemblance with the conditions of other experimental scenarios, all having high PKA activity in common [87,96,107,121,123,124]. Our experimental design, however, involved the same dilution rate during the DS compared to the RS, implying merely transiently downshifting and upshifting signals for protein kinase A. This was indeed reflected by the dynamic fraction of the transcriptome during the r-LSL cycle, especially with respect to the RiBi genes, which possess high transcriptional turnover [125]. However, the global transcriptional pattern displayed an overall elevated differential expression of PKA targets during the DS. Several feedback mechanisms may play a role when the PKA hub controls transcriptional responses.

We recently speculated that during the LSL transition, disparate sensing of internal growth rate feedback and environmental substrate availability causes a boost of growth-related mRNAs at the end of the perturbation, also explaining the regulatory overswing that occurs during a s-LSL cycle [23,115]. When the population adapts to transitions in a recurring manner, a scenario might occur in which the molecular transmitter, cAMP, accumulates due to an asymmetry in production and decay [126,127], finally causing its levels to gradually ramp up during r-LSL adaptation. In conclusion, our data strongly suggest that PKA is the dominant factor that shapes the cellular fate in response to external glucose fluctuations in an industrial bioreactor setting in a highly conserved manner across different strain and bioprocess backgrounds.

4.3. Take-Away Message for Industrial Strain Engineers

We understand the obtained results to be fundamental proof that large-scale insight should be used in early-stage strain development. Here, even moderate environmental oscillations shifted the production host's regulatory configuration. The resulting "large-scale-phenotype" might lead to non-optimal operational decisions given that most growth-coupled production processes are optimized based on the relationship between the biomass-specific production rate and the growth rate [128]. Obviously, an increased ribosome portfolio can impose a substantial metabolic burden on a cell, especially when the product is a heterologous protein [129]. In this specific context, strain performance seems rather unpredictable as neither prokaryotic nor eukaryotic hosts unanimously possess a linear correlation between ribosome content and protein productivity [130,131].

ScER was proven to be particularly robust under the investigated conditions. Nevertheless, its gene expression profile revealed the presence of futile stress-responsive mechanisms. The induced ESR branch during the s-LSL cycle and the repeatedly triggered RiBi cluster during the r-LSL cycle depict appealing targets for constructing a streamlined universal production chassis. For instance, Msn2/4 deletion could reduce induced ESR expression when cells adapt to emerging famine zones during fed-batch processes, whereas the antagonizing TFs Sko1 and Sok2 still repress the ESR in the adapted state. Likewise, we observed several cross-talking transcription factors activating non-specific stress responses such as the activation of the osmotic stress response or the activation of oxygen-dependent energy scavenging. Hot1 or Hap proteins could be targeted to reduce said expression programs and further enable safe transcriptional expenditures, even though the latter should be restricted to anaerobic production strains. More globally, the stabilization of Tup1/Ssn6-guided repression carries the potential to avoid premature glucose de-repression with possible metabolic impacts. Examples of the beneficial impacts of TF modulation on bioprocesses exist in the literature. For instance, Hap4 deletion increased fermentative capacity during cellobiose fermentation [132], and similar results were obtained through Cat8 deletion [133]. However, the cited studies reasoned that metabolic rerouting rather than gene expression savings caused the boosted productivity.

Here, we propose a valorization of the generated data centered around the idea that the ESR and other transcriptional stress response programs aggravate a variety of production scenarios, all induced by PKA activity (reviewed in [134,135]). In a bottom-up strategy, all TFs that are involved in futile or non-specific transcriptional stress responses such as Msn2/4, Hot1, or Hap4 should be individually tested for their potential to abolish said responses. Finally, such a procedure could lead to a stepwise optimization of the yeast's regulatory landscape and ultimately reduce the maintenance demands made upon the introduction of short-term stimuli.

Author Contributions: Funding acquisition, R.T.; investigation, S.M.; conceptualization, S.M.; stimulus–response experiments, S.M. and M.A.; transcriptome analysis, S.M.; methodology, S.M.;

References

1. López-Maury, L.; Marguerat, S.; Bähler, J. Tuning Gene Expression to Changing Environments: From Rapid Responses to Evolutionary Adaptation. *Nat. Rev. Genet.* **2008**, *9*, 583–593. [CrossRef] [PubMed]
2. Skoneczny, M. (Ed.) *Stress Response Mechanisms in Fungi*; Springer: Berlin/Heidelberg, Germany, 2018. [CrossRef]
3. Boutte, C.C.; Crosson, S. Bacterial Lifestyle Shapes Stringent Response Activation. *Trends Microbiol.* **2013**, *21*, 174–180. [CrossRef] [PubMed]
4. Gasch, A.P. The Environmental Stress Response: A Common Yeast Response to Diverse Environmental Stresses. *Yeast Stress Responses* **2007**, *1*, 11–70. [CrossRef]
5. Takors, R. Editorial: How Can We Ensure the Successful Transfer from Lab- to Large-Scale Production? *Eng. Life Sci.* **2016**, *16*, 587. [CrossRef]
6. Crater, J.S.; Lievense, J.C. Scale-up of Industrial Microbial Processes. *FEMS Microbiol. Lett.* **2018**, *365*, fny138. [CrossRef]
7. Enfors, S.O.; Jahic, M.; Rozkov, A.; Xu, B.; Hecker, M.; Jürgen, B.; Krüger, E.; Schweder, T.; Hamer, G.; O'Beirne, D.; et al. Physiological Responses to Mixing in Large Scale Bioreactors. *J. Biotechnol.* **2001**, *85*, 175–185. [CrossRef]
8. Fowler, J.D.; Dunlop, E.H. Effects of Reactant Heterogeneity and Mixing on Catabolite Repression in Cultures of *Saccharomyces cerevisiae*. *Biotechnol. Bioeng.* **1989**, *33*, 1039–1046. [CrossRef]
9. Wehrs, M.; Tanjore, D.; Eng, T.; Lievense, J.; Pray, T.R.; Mukhopadhyay, A. Engineering Robust Production Microbes for Large-Scale Cultivation. *Trends Microbiol.* **2019**, *27*, 524–537. [CrossRef]
10. George, S.; Larsson, G.; Olsson, K.; Enfors, S.-O. Comparison of the Baker's Yeast Process Performance in Laboratory and Production Scale. *Bioprocess Eng.* **1998**, *18*, 135–142. [CrossRef]
11. Sarkizi Shams Hajian, C.; Haringa, C.; Noorman, H.; Takors, R. Predicting By-Product Gradients of Baker's Yeast Production at Industrial Scale: A Practical Simulation Approach. *Processes* **2020**, *8*, 1554. [CrossRef]
12. Haringa, C.; Deshmukh, A.T.; Mudde, R.F.; Noorman, H. Euler-Lagrange Analysis towards Representative down-Scaling of a 22 M3 Aerobic *S. cerevisiae* Fermentation. *Chem. Eng. Sci.* **2017**, *170*, 653–669. [CrossRef]
13. Delvigne, F.; Goffin, P. Microbial Heterogeneity Affects Bioprocess Robustness: Dynamic Single-Cell Analysis Contributes to Understanding of Microbial Populations. *Biotechnol. J.* **2014**, *9*, 61–72. [CrossRef]
14. Gutin, J.; Joseph-Strauss, D.; Sadeh, A.; Shalom, E.; Friedman, N. Genetic Screen of the Yeast Environmental Stress Response Dynamics Uncovers Distinct Regulatory Phases. *Mol. Syst. Biol.* **2019**, *15*, 1–16. [CrossRef] [PubMed]
15. Minden, S.; Aniolek, M.; Sarkizi, C.; Hajian, S.; Teleki, A.; Zerrer, T.; Delvigne, F.; van Gulik, W.; Deshmukh, A.; Noorman, H.; et al. Monitoring Intracellular Metabolite Dynamics in *Saccharomyces cerevisiae* during Industrially Relevant Famine Stimuli. *Metabolites* **2022**, *12*, 263. [CrossRef] [PubMed]
16. Ho, P.; Täuber, S.; Stute, B.; Grünberger, A.; von Lieres, E. Microfluidic Reproduction of Dynamic Bioreactor Environment Based on Computational Lifelines. *Front. Chem. Eng.* **2022**, *4*, 27. [CrossRef]
17. Kuschel, M.; Takors, R. Simulated Oxygen and Glucose Gradients as a Prerequisite for Predicting Industrial Scale Performance a Priori. *Biotechnol. Bioeng.* **2020**, *117*, 2760–2770. [CrossRef] [PubMed]
18. Nadal-Rey, G.; McClure, D.D.; Kavanagh, J.M.; Cassells, B.; Cornelissen, S.; Fletcher, D.F.; Gernaey, K.V. Development of Dynamic Compartment Models for Industrial Aerobic Fed-Batch Fermentation Processes. *Chem. Eng. J.* **2021**, *420*, 130402. [CrossRef]
19. Löffler, M.; Simen, J.D.; Jäger, G.; Schäferhoff, K.; Freund, A.; Takors, R. Engineering, *E. coli* for Large-Scale Production—Strategies Considering ATP Expenses and Transcriptional Responses. *Metab. Eng.* **2016**, *38*, 73–85. [CrossRef]

20. Ankenbauer, A.; Schäfer, R.A.; Viegas, S.C.; Pobre, V.; Voß, B.; Arraiano, C.M.; Takors, R. Pseudomonas Putida KT2440 Is Naturally Endowed to Withstand Industrial-Scale Stress Conditions. *Microb. Biotechnol.* **2020**, *13*, 1145–1161. [CrossRef]

21. Michalowski, A.; Siemann-Herzberg, M.; Takors, R. *Escherichia coli* HGT: Engineered for High Glucose Throughput Even under Slowly Growing or Resting Conditions. *Metab. Eng.* **2017**, *40*, 93–103. [CrossRef]

22. Ziegler, M.; Zieringer, J.; Döring, C.L.; Paul, L.; Schaal, C.; Takors, R. Engineering of a Robust *Escherichia coli* Chassis and Exploitation for Large-Scale Production Processes. *Metab. Eng.* **2021**, *67*, 75–87. [CrossRef] [PubMed]

23. Minden, S.; Aniolek, M.; Noorman, H.; Takors, R. Performing in Spite of Starvation: How *Saccharomyces cerevisiae* Maintains Robust Growth When Facing Famine Zones in Industrial Bioreactors. *Microb. Biotechnol.* **2023**, *16*, 148–168. [CrossRef]

24. Nijkamp, J.F.; van den Broek, M.; Datema, E.; de Kok, S.; Bosman, L.; Luttik, M.A.H.; Dalen, J.P.; Vongsangnak, W.; Nielsen, J.; Heijne, W.H.M.; et al. De Novo Sequencing, Assembly and Analysis of the Genome of the Laboratory Strain *Saccharomyces cerevisiae* CEN.PK113-7D, a Model for Modern Industrial Biotechnology. *Microb. Cell Factories* **2012**, *11*, 36. [CrossRef] [PubMed]

25. Parrou, J.L.; Francois, J. A Simplified Procedure for a Rapid and Reliable Assay of Both Glycogen and Trehalose in Whole Yeast Cells. *Anal. Biochem.* **1997**, *248*, 186–188. [CrossRef]

26. Sasano, Y.; Kariya, T.; Usugi, S.; Sugiyama, M.; Harashima, S. Molecular Breeding of *Saccharomyces cerevisiae* with High RNA Content by Harnessing Essential Ribosomal RNA Transcription Regulator. *AMB Express* **2017**, *7*, 32. [CrossRef] [PubMed]

27. Buchholz, J. Development, Characterization, and Application of a Novel Scale-Down Apparatus for the Investigation of the Scale-Up Dependent CO_2/HCO_3—Stimulus in Corynebacterium Glutamicum. Ph.D. Thesis, University of Stuttgart, Stuttgart, Germany, 2015. Volume 278. [CrossRef]

28. Löser, C.; Schröder, A.; Deponte, S.; Bley, T. Balancing the Ethanol Formation in Continuous Bioreactors with Ethanol Stripping. *Eng. Life Sci.* **2005**, *5*, 325–332. [CrossRef]

29. Afgan, E.; Baker, D.; Batut, B.; Van Den Beek, M.; Bouvier, D.; Ech, M.; Chilton, J.; Clements, D.; Coraor, N.; Grüning, B.A.; et al. The Galaxy Platform for Accessible, Reproducible and Collaborative Biomedical Analyses: 2018 Update. *Nucleic Acids Res.* **2018**, *46*, W537–W544. [CrossRef]

30. RTSF–Michigan State University. FastQC Tutorial & FAQ. Available online: https://rtsf.natsci.msu.edu/genomics/tech-notes/fastqc-tutorial-and-faq/ (accessed on 18 May 2022).

31. Kim, D.; Pertea, G.; Trapnell, C.; Pimentel, H.; Kelley, R.; Salzberg, L. TopHat2: Accurate Alignment of Transcriptomes in the Presence of Insertions, Deletions and Gene Fusions. *Genome Biol.* **2013**, *14*, 957–961. [CrossRef]

32. Gronchi, N.; De Bernardini, N.; Cripwell, R.A.; Treu, L.; Campanaro, S.; Basaglia, M.; Foulquié-Moreno, M.R.; Thevelein, J.M.; Van Zyl, W.H.; Favaro, L.; et al. Natural *Saccharomyces cerevisiae* Strain Reveals Peculiar Genomic Traits for Starch-to-Bioethanol Production: The Design of an Amylolytic Consolidated Bioprocessing Yeast. *Front. Microbiol.* **2022**, *12*, 4226. [CrossRef]

33. Howe, K.L.; Achuthan, P.; Allen, J.; Allen, J.; Alvarez-Jarreta, J.; Ridwan Amode, M.; Armean, I.M.; Azov, A.G.; Bennett, R.; Bhai, J.; et al. Ensembl 2021. *Nucleic Acids Res.* **2021**, *49*, D884–D891. [CrossRef]

34. Liao, Y.; Smyth, G.K.; Shi, W. FeatureCounts: An Efficient General Purpose Program for Assigning Sequence Reads to Genomic Features. *Bioinformatics* **2014**, *30*, 923–930. [CrossRef] [PubMed]

35. Love, M.I.; Huber, W.; Anders, S. Moderated Estimation of Fold Change and Dispersion for RNA-Seq Data with DESeq2. *Genome Biol.* **2014**, *15*, 389–393. [CrossRef] [PubMed]

36. Benjamini, Y.; Hochberg, Y. Controlling the false discovery rate: A practical and powerful approach to multiple testing. *J. R. Stat. Soc. Ser. B Methodol.* **1995**, *57*, 289–300. [CrossRef]

37. Chen, E.Y.; Tan, C.M.; Kou, Y.; Duan, Q.; Wang, Z.; Meirelles, G.V.; Clark, N.R.; Ma'ayan, A. Enrichr: Interactive and Collaborative HTML5 Gene List Enrichment Analysis Tool. *BMC Bioinform.* **2013**, *14*, 128. [CrossRef] [PubMed]

38. Kuleshov, M.V.; Diaz, J.E.L.; Flamholz, Z.N.; Keenan, A.B.; Lachmann, A.; Wojciechowicz, M.L.; Cagan, R.L.; Ma'ayan, A. ModEnrichr: A Suite of Gene Set Enrichment Analysis Tools for Model Organisms. *Nucleic Acids Res.* **2019**, *47*, W183–W190. [CrossRef] [PubMed]

39. Luo, W.; Friedman, M.S.; Shedden, K.; Hankenson, K.D.; Woolf, P.J. GAGE: Generally Applicable Gene Set Enrichment for Pathway Analysis. *BMC Bioinform.* **2009**, *10*, 161. [CrossRef]

40. Monteiro, P.T.; Oliveira, J.; Pais, P.; Antunes, M.; Palma, M.; Cavalheiro, M.; Galocha, M.; Godinho, C.P.; Martins, L.C.; Bourbon, N.; et al. YEASTRACT+: A Portal for Cross-Species Comparative Genomics of Transcription Regulation in Yeasts. *Nucleic Acids Res.* **2020**, *48*, D642–D649. [CrossRef]

41. Wang, M.; Zhao, Y.; Zhang, B. Efficient Test and Visualization of Multi-Set Intersections. *Sci. Rep.* **2015**, *5*, 16923. [CrossRef]

42. Boender, L.G.M.; De Hulster, E.A.F.; van Maris, A.J.A.; Dalen, J.P.; Pronk, J.T. Quantitative Physiology of *Saccharomyces cerevisiae* at Near-Zero Specific Growth Rates. *Appl. Environ. Microbiol.* **2009**, *75*, 5607–5614. [CrossRef]

43. Warner, J.R. The Economics of Ribosome Biosynthesis in Yeast. *Trends Biochem. Sci.* **1999**, *24*, 437–440. [CrossRef]

44. Wang, G.; Wu, B.; Zhao, J.; Haringa, C.; Xia, J.; Chu, J.; Zhuang, Y.; Zhang, S.; Heijnen, J.J.; van Gulik, W.; et al. Power Input Effects on Degeneration in Prolonged Penicillin Chemostat Cultures: A Systems Analysis at Flux, Residual Glucose, Metabolite, and Transcript Levels. *Biotechnol. Bioeng.* **2018**, *115*, 114–125. [CrossRef]

45. Nissen, T.L.; Schulze, U.; Nielsen, J.; Villadsen, J. Flux Distributions in Anaerobic, Glucose-Limited Continuous Cultures of *Saccharomyces cerevisiae*. *Microbiology* **1997**, *143*, 203–218. [CrossRef] [PubMed]

46. Pais, T.M.; Foulquié-Moreno, M.R.; Hubmann, G.; Duitama, J.; Swinnen, S.; Goovaerts, A.; Yang, Y.; Dumortier, F.; Thevelein, J.M. Comparative Polygenic Analysis of Maximal Ethanol Accumulation Capacity and Tolerance to High Ethanol Levels of Cell Proliferation in Yeast. *PLoS Genet.* **2013**, *9*, e1003548. [CrossRef] [PubMed]

47. Steensels, J.; Snoek, T.; Meersman, E.; Nicolino, M.P.; Voordeckers, K.; Verstrepen, K.J. Improving Industrial Yeast Strains: Exploiting Natural and Artificial Diversity. *FEMS Microbiol. Rev.* **2014**, *38*, 947–995. [CrossRef]

48. HERSKOWITZ, I. Life Cycle of the Budding Yeast *Saccharomyces cerevisiae* IRA. *Microbiol. Rev.* **1988**, *52*, 536–553. [CrossRef] [PubMed]

49. Cherry, J.M.; Hong, E.L.; Amundsen, C.; Balakrishnan, R.; Binkley, G.; Chan, E.T.; Christie, K.R.; Costanzo, M.C.; Dwight, S.S.; Engel, S.R.; et al. Saccharomyces Genome Database: The genomics resource of budding yeast. *Nucleic Acids Res.* **2012**, *40*, D700–D705. [CrossRef] [PubMed]

50. Lang, M.J.; Martinez-Marquez, J.Y.; Prosser, D.C.; Ganser, L.R.; Buelto, D.; Wendland, B.; Duncan, M.C. Glucose Starvation Inhibits Autophagy via Vacuolar Hydrolysis and Induces Plasma Membrane Internalization by Down-Regulating Recycling. *J. Biol. Chem.* **2014**, *289*, 16736–16747. [CrossRef]

51. Thevelein, J.M. Regulation of Trehalose Mobilization in Fungi. *Microbiol. Rev.* **1984**, *48*, 42–59. [CrossRef]

52. Kohlwein, S.D.; Veenhuis, M.; van der Klei, I.J. Lipid Droplets and Peroxisomes: Key Players in Cellular Lipid Homeostasis or a Matter of Fat-Store'em up or Burn'em Down. *Genetics* **2013**, *193*, 1–50. [CrossRef]

53. Herrero, P.; Galíndez, J.; Ruiz, N.; Martínez-Campa, C.; Moreno, F. Transcriptional Regulation of the *Saccharomyces cerevisiae* HXK1, HXK2 and GLK1 Genes. *Yeast* **1995**, *11*, 137–144. [CrossRef]

54. Castelli, L.M.; Lui, J.; Campbell, S.G.; Rowe, W.; Zeef, L.A.H.; Holmes, L.E.A.; Hoyle, N.P.; Bone, J.; Selley, J.N.; Sims, P.F.G.; et al. Glucose Depletion Inhibits Translation Initiation via EIF4A Loss and Subsequent 48S Preinitiation Complex Accumulation, While the Pentose Phosphate Pathway Is Coordinately up-Regulated. *Mol. Biol. Cell* **2011**, *22*, 3379–3393. [CrossRef] [PubMed]

55. Antonin, W.; Meyer, H.-A.; Hartmann, E. Interactions between Spc2p and Other Components of the Endoplasmic Reticulum Translocation Sites of the Yeast*Saccharomyces cerevisiae*. *J. Biol. Chem.* **2000**, *275*, 34068–34072. [CrossRef] [PubMed]

56. Sutterlin, C.; Doering, T.L.; Schimmoller, F.; Schroder, S.; Riezman, H. Specific Requirements for the ER to Golgi Transport of GPI-Anchored Proteins in Yeast. *J. Cell Sci.* **1997**, *110*, 2703–2714. [CrossRef] [PubMed]

57. Rodrigues, F.; Ludovicio, P.; Leao, C. Sugar Metabolism in Yeasts: An Overview of Aerobic and Anaerobic Glucose Catabolism. *Biodivers. Ecophysiol. Yeasts* **2006**, *62*, 101–122.

58. Helbig, A.O.; De Groot, M.J.L.; Van Gestel, R.A.; Mohammed, S.; De Hulster, E.A.F.; Luttik, M.A.H.; Daran-Lapujade, P.; Pronk, J.T.; Heck, A.J.R.; Slijper, M. A Three-Way Proteomics Strategy Allows Differential Analysis of Yeast Mitochondrial Membrane Protein Complexes under Anaerobic and Aerobic Conditions. *Proteomics* **2009**, *9*, 4787–4798. [CrossRef]

59. David, P.S.; Poyton, R.O. Effects of a Transition from Normoxia to Anoxia on Yeast Cytochrome c Oxidase and the Mitochondrial Respiratory Chain: Implications for Hypoxic Gene Induction. *Biochim. Biophys. Acta Bioenerg.* **2005**, *1709*, 169–180. [CrossRef]

60. Sazegari, S.; Niazi, A.; Zinati, Z.; Eskandari, M.H. Mining Transcriptomic Data to Identify *Saccharomyces cerevisiae* Signatures Related to Improved and Repressed Ethanol Production under Fermentation. *PLoS ONE* **2022**, *17*, e259476. [CrossRef]

61. Fazio, A.; Jewett, M.C.; Daran-Lapujade, P.; Mustacchi, R.; Usaite, R.; Pronk, J.T.; Workman, C.T.; Nielsen, J. Transcription Factor Control of Growth Rate Dependent Genes in *Saccharomyces cerevisiae*: A Three Factor Design. *BMC Genom.* **2008**, *9*, 341. [CrossRef] [PubMed]

62. Gasch, A.P.; Yu, F.B.; Hose, J.; Escalante, L.E.; Place, M.; Bacher, R.; Kanbar, J.; Ciobanu, D.; Sandor, L.; Grigoriev, I.V.; et al. Single-Cell RNA Sequencing Reveals Intrinsic and Extrinsic Regulatory Heterogeneity in Yeast Responding to Stress. *PLoS Biol.* **2017**, *15*, e2004050. [CrossRef]

63. Gutin, J.; Sadeh, A.; Rahat, A.; Aharoni, A.; Friedman, N. Condition-specific Genetic Interaction Maps Reveal Crosstalk between the CAMP/PKA and the HOG MAPK Pathways in the Activation of the General Stress Response. *Mol. Syst. Biol.* **2015**, *11*, 829. [CrossRef]

64. Hohmann, S. Osmotic Stress Signaling and Osmoadaptation in Yeasts. *Microbiol. Mol. Biol. Rev.* **2002**, *66*, 300–372. [CrossRef]

65. Hanlon, S.E.; Rizzo, J.M.; Tatomer, D.C.; Lieb, J.D.; Buck, M.J. The Stress Response Factors Yap6, Cin5, Phd1, and Skn7 Direct Targeting of the Conserved Co-Repressor Tup1-Ssn6 in *S. cerevisiae*. *PLoS ONE* **2011**, *6*, e29590. [CrossRef]

66. Bardwell, L.; Cook, J.G.; Voora, D.; Baggott, D.M.; Martinez, A.R.; Thorner, J. Repression of Yeast Ste12 Transcription Factor by Direct Binding of Unphosphorylated Kss1 MAPK and Its Regulation by the Ste7 MEK. *Genes Dev.* **1998**, *12*, 2887–2898. [CrossRef]

67. Ratnakumar, S.; Kacherovsky, N.; Arms, E.; Young, E.T. Snf1 Controls the Activity of Adr1 through Dephosphorylation of Ser230. *Genetics* **2009**, *182*, 735–745. [CrossRef] [PubMed]

68. Livas, D.; Almering, M.J.H.; Daran, J.M.; Pronk, J.T.; Gancedo, J.M. Transcriptional Responses to Glucose in *Saccharomyces cerevisiae* Strains Lacking a Functional Protein Kinase A. *BMC Genomics* **2011**, *12*, 405. [CrossRef] [PubMed]

69. Iyer, V.R.; Horak, C.E.; Scafe, C.S.; Botstein, D.; Snyder, M.; Brown, P.O. Genomic Binding Sites of the Yeast Cell-Cycle Transcription Factors SBF and MBF. *Nature* **2001**, *409*, 533–538. [CrossRef] [PubMed]

70. Murakami, H.; Aiba, H.; Nakanishi, M.; Murakami-Tonami, Y. Regulation of Yeast Forkhead Transcription Factors and FoxM1 by Cyclin-Dependent and Polo-like Kinases. *Cell Cycle* **2010**, *9*, 3233–3242. [CrossRef]

71. Tsuchiya, D.; Yang, Y.; Lacefield, S. Positive Feedback of NDT80 Expression Ensures Irreversible Meiotic Commitment in Budding Yeast. *PLoS Genet.* **2014**, *10*, e1004398. [CrossRef] [PubMed]

72. Huber, A.; French, S.L.; Tekotte, H.; Yerlikaya, S.; Stahl, M.; Perepelkina, M.P.; Tyers, M.; Rougemont, J.; Beyer, A.L.; Loewith, R. Sch9 Regulates Ribosome Biogenesis via Stb3, Dot6 and Tod6 and the Histone Deacetylase Complex RPD3L. *EMBO J.* **2011**, *30*, 3052–3064. [CrossRef]

73. Lempiäinen, H.; Shore, D. Growth Control and Ribosome Biogenesis. *Curr. Opin. Cell Biol.* **2009**, *21*, 855–863. [CrossRef]

74. Shenhar, G.; Kassir, Y. A Positive Regulator of Mitosis, Sok2, Functions as a Negative Regulator of Meiosis in *Saccharomyces cerevisiae*. *Mol. Cell. Biol.* **2001**, *21*, 1603–1612. [CrossRef] [PubMed]

75. Charizanis, C.; Juhnke, H.; Krems, B.; Entian, K.-D. The Oxidative Stress Response Mediated via Pos9/Skn7 Is Negatively Regulated by the Ras/PKA Pathway in *Saccharomyces cerevisiae*. *Mol. Gen. Genet. MGG* **1999**, *261*, 740–752. [CrossRef] [PubMed]

76. Broach, J.R. Nutritional Control of Growth and Development in Yeast. *Genetics* **2012**, *192*, 73–105. [CrossRef] [PubMed]

77. Busti, S.; Coccetti, P.; Alberghina, L.; Vanoni, M. Glucose Signaling-Mediated Coordination of Cell Growth and Cell Cycle in *Saccharomyces cerevisiae*. *Sensors* **2010**, *10*, 6195–6240. [CrossRef] [PubMed]

78. Zhang, T.; Bu, P.; Zeng, J.; Vancura, A. Increased Heme Synthesis in Yeast Induces a Metabolic Switch from Fermentation to Respiration Even under Conditions of Glucose Repression. *J. Biol. Chem.* **2017**, *292*, 16942–16954. [CrossRef]

79. Johnston, N.R.; Nallur, S.; Gordon, P.B.; Smith, K.D.; Strobel, S.A. Genome-Wide Identification of Genes Involved in General Acid Stress and Fluoride Toxicity in *Saccharomyces cerevisiae*. *Front. Microbiol.* **2020**, *11*, 1410. [CrossRef]

80. Haringa, C.; Tang, W.; Deshmukh, A.T.; Xia, J.; Reuss, M.; Heijnen, J.; Mudde, R.F.; Noorman, H. Euler-Lagrange Computational Fluid Dynamics for (Bio)Reactor Scale down: An Analysis of Organism Lifelines. *Eng. Life Sci.* **2016**, *16*, 652–663. [CrossRef]

81. Bergdahl, B.; Heer, D.; Sauer, U.; Hahn-Hägerdal, B.; Van Niel, E.W. Dynamic Metabolomics Differentiates between Carbon and Energy Starvation in Recombinant *Saccharomyces cerevisiae* Fermenting Xylose. *Biotechnol. Biofuels* **2012**, *5*, 34. [CrossRef]

82. Saini, P.; Beniwal, A.; Kokkiligadda, A.; Vij, S. Response and Tolerance of Yeast to Changing Environmental Stress during Ethanol Fermentation. *Process Biochem.* **2018**, *72*, 1–12. [CrossRef]

83. Osiro, K.O.; Brink, D.P.; Borgström, C.; Wasserstrom, L.; Carlquist, M.; Gorwa-Grauslund, M.F. Assessing the Effect of D-Xylose on the Sugar Signaling Pathways of *Saccharomyces cerevisiae* in Strains Engineered for Xylose Transport and Assimilation. *FEMS Yeast Res.* **2018**, *18*, fox096. [CrossRef]

84. Gasch, A.P.; Spellman, P.T.; Kao, C.M.; Carmel-Harel, O.; Eisen, M.B.; Storz, G.; Botstein, D.; Brown, P.O. Genomic Expression Programs in the Response of Yeast Cells to Environmental Changes. *TMolecular Biol. Cell* **2000**, *11*, 4241–4257. [CrossRef] [PubMed]

85. Brauer, J.M.; Huttenhower, C.; Airoldi, E.M.; Rosenstein, R.; Matese, J.C.; Gresham, D.; Boer, V.M.; Troyanskaya, O.G.; Botstein, D. Coordination of Growth Rate, Cell Cycle, Stress Response, and Metabolic Activity in Yeast. *Mol. Biol. Cell* **2008**, *19*, 308–317. [CrossRef] [PubMed]

86. De Nadal, E.; Ammerer, G.; Posas, F. Controlling Gene Expression in Response to Stress. *Nat. Rev. Genet.* **2011**, *12*, 833–845. [CrossRef]

87. De Wever, V.; Reiter, W.; Ballarini, A.; Ammerer, G.; Brocard, C. A Dual Role for PP1 in Shaping the Msn2-Dependent Transcriptional Response to Glucose Starvation. *EMBO J.* **2005**, *24*, 4115–4123. [CrossRef] [PubMed]

88. Wang, S.; Liu, P.; Shu, W.; Li, C.; Li, H.; Liu, S.; Xia, J.; Noorman, H. Dynamic Response of *Aspergillus niger* to Single Pulses of Glucose with High and Low Concentrations. *Bioresour. Bioprocess.* **2019**, *6*, 16. [CrossRef]

89. Woolford, J.L.; Baserga, S.J. Ribosome Biogenesis in the Yeast *Saccharomyces cerevisiae*. *Genetics* **2013**, *195*, 643–681. [CrossRef]

90. Metzl-Raz, E.; Kafri, M.; Yaakov, G.; Soifer, I.; Gurvich, Y.; Barkai, N. Principles of Cellular Resource Allocation Revealed by Condition-Dependent Proteome Profiling. *Elife* **2017**, *6*, e28034. [CrossRef]

91. Remigi, P.; Ferguson, G.C.; McConnell, E.; De Monte, S.; Rogers, D.W.; Rainey, P.B. Ribosome Provisioning Activates a Bistable Switch Coupled to Fast Exit from Stationary Phase. *Mol. Biol. Evol.* **2019**, *36*, 1056–1070. [CrossRef]

92. Mattanovich, D.; Gasser, B.; Hohenblum, H.; Sauer, M. Stress in Recombinant Protein Producing Yeasts. *J. Biotechnol.* **2004**, *113*, 121–135. [CrossRef]

93. Gasch, A.P. Comparative Genomics of the Environmental Stress Response in Ascomycete Fungi. *Yeast* **2007**, *24*, 961–976. [CrossRef]

94. Brion, C.; Pflieger, D.; Souali-Crespo, S.; Friedrich, A.; Schacherer, J. Differences in Environmental Stress Response among Yeasts Is Consistent with Species-Specific Lifestyles. *Mol. Biol. Cell* **2016**, *27*, 1694–1705. [CrossRef] [PubMed]

95. Kunkel, J.; Luo, X.; Capaldi, A.P. Integrated TORC1 and PKA Signaling Control the Temporal Activation of Glucose-Induced Gene Expression in Yeast. *Nat. Commun.* **2019**, *10*, 3558. [CrossRef] [PubMed]

96. Görner, W.; Durchschlag, E.; Wolf, J.; Brown, E.L.; Ammerer, G.; Ruis, H.; Schüller, C. Acute Glucose Starvation Activates the Nuclear Localization Signal of a Stress-Specific Yeast Transcription Factor. *EMBO J.* **2002**, *21*, 135–144. [CrossRef]

97. Martínez-Pastor, M.T.; Marchler, G.; Schüller, C.; Marchler-Bauer, A.; Ruis, H.; Estruch, F. The *Saccharomyces cerevisiae* Zinc Finger Proteins Msn2p and Msn4p Are Required for Transcriptional Induction through the Stress Response Element (STRE). *EMBO J.* **1996**, *15*, 2227–2235. [CrossRef]

98. Plank, M. Interaction of TOR and PKA Signaling in *S. cerevisiae*. *Biomolecules* **2022**, *12*, 210. [CrossRef]

99. Winkler, A.; Arkind, C.; Mattison, C.P.; Burkholder, A.; Knoche, K.; Ota, I. Heat Stress Activates the Yeast High-Osmolarity Glycerol Mitogen-Activated Protein Kinase Pathway, and Protein Tyrosine Phosphatases Are Essential under Heat Stress. *Eukaryot. Cell* **2002**, *1*, 163–173. [CrossRef]

100. Panadero, J.; Pallotti, C.; Rodríguez-Vargas, S.; Randez-Gil, F.; Prieto, J.A. A Downshift in Temperature Activates the High Osmolarity Glycerol (HOG) Pathway, Which Determines Freeze Tolerance in *Saccharomyces cerevisiae*. *J. Biol. Chem.* **2006**, *281*, 4638–4645. [CrossRef]

101. Bilsland, E.; Molin, C.; Swaminathan, S.; Ramne, A.; Sunnerhagen, P. Rck1 and Rck2 MAPKAP Kinases and the HOG Pathway Are Required for Oxidative Stress Resistance. *Mol. Microbiol.* **2004**, *53*, 1743–1756. [CrossRef]

102. Krantz, M.; Nordlander, B.; Valadi, H.; Johansson, M.; Gustafsson, L.; Hohmann, S. Anaerobicity Prepares *Saccharomyces cerevisiae* Cells for Faster Adaptation to Osmotic Shock. *Eukaryot. Cell* **2004**, *3*, 1381–1390. [CrossRef] [PubMed]

103. James, T.C.; Campbell, S.; Donnelly, D.; Bond, U. Transcription Profile of Brewery Yeast under Fermentation Conditions. *J. Appl. Microbiol.* **2003**, *94*, 432–448. [CrossRef]

104. Sharifian, H.; Lampert, F.; Stojanovski, K.; Regot, S.; Vaga, S.; Buser, R.; Lee, S.S.; Koeppl, H.; Posas, F.; Pelet, S.; et al. Parallel Feedback Loops Control the Basal Activity of the HOG MAPK Signaling Cascade. *Integr. Biol.* **2015**, *7*, 412–422. [CrossRef]

105. Ball, W.J.; Atkinson, D.E. Adenylate Energy Charge in *Saccharomyces cerevisiae* during Starvation. *J. Bacteriol.* **1975**, *121*, 975–982. [CrossRef] [PubMed]

106. Caligaris, M.; Nicastro, R.; Hu, Z.; Tripodi, F.; Hummel, J.E.; Deprez, M.-A.; Winderickx, J.; Rospert, S.; Coccetti, P.; Dengjel, J.; et al. Snf1/AMPK Fine-Tunes TORC1 Signaling in Response to Glucose Starvation. *Elife* **2022**, *12*, e84319. [CrossRef]

107. Zaman, S.; Lippman, S.I.; Schneper, L.; Slonim, N.; Broach, J.R. Glucose Regulates Transcription in Yeast through a Network of Signaling Pathways. *Mol. Syst. Biol.* **2009**, *5*, 245. [CrossRef] [PubMed]

108. Shashkova, S.; Welkenhuysen, N.; Hohmann, S. Molecular Communication: Crosstalk between the Snf1 and Other Signaling Pathways. *FEMS Yeast Res.* **2015**, *15*, fov026. [CrossRef]

109. Nicastro, R.; Tripodi, F.; Gaggini, M.; Castoldi, A.; Reghellin, V.; Nonnis, S.; Tedeschi, G.; Coccetti, P. Snf1 Phosphorylates Adenylate Cyclase and Negatively Regulates Protein Kinase A-Dependent Transcription in *Saccharomyces cerevisiae*. *J. Biol. Chem.* **2015**, *290*, 24715–24726. [CrossRef] [PubMed]

110. Hardie, D.G.; Ross, F.A.; Hawley, S.A. AMPK: A Nutrient and Energy Sensor That Maintains Energy Homeostasis. *Nat. Rev. Mol. Cell Biol.* **2012**, *13*, 251–262. [CrossRef] [PubMed]

111. Coccetti, P.; Nicastro, R.; Tripodi, F. Conventional and Emerging Roles of the Energy Sensor Snf1/AMPK in *Saccharomyces cerevisiae*. *Microb. Cell* **2018**, *5*, 482–494. [CrossRef]

112. Zampar, G.G.; Kümmel, A.; Ewald, J.; Jol, S.; Niebel, B.; Picotti, P.; Aebersold, R.; Sauer, U.; Zamboni, N.; Heinemann, M. Temporal System-Level Organization of the Switch from Glycolytic to Gluconeogenic Operation in Yeast. *Mol. Syst. Biol.* **2013**, *9*, 651. [CrossRef]

113. Knijnenburg, T.A.; de Winde, J.H.; Daran, J.-M.; Daran-Lapujade, P.; Pronk, J.T.; Reinders, M.J.T.; Wessels, L.F.A. Exploiting Combinatorial Cultivation Conditions to Infer Transcriptional Regulation. *BMC Genom.* **2007**, *8*, 25. [CrossRef]

114. MacGilvray, M.E.; Shishkova, E.; Place, M.; Wagner, E.R.; Coon, J.J.; Gasch, A.P. Phosphoproteome Response to Dithiothreitol Reveals Unique Versus Shared Features of *Saccharomyces cerevisiae* Stress Responses. *J. Proteome Res.* **2020**, *19*, 3405–3417. [CrossRef]

115. Shore, D.; Zencir, S.; Albert, B. Transcriptional Control of Ribosome Biogenesis in Yeast: Links to Growth and Stress Signals. *Biochem. Soc. Trans.* **2021**, *49*, 1589–1599. [CrossRef]

116. Cipollina, C.; van den Brink, J.; Daran-Lapujade, P.; Pronk, J.T.; Porro, D.; de Winde, J.H. *Saccharomyces cerevisiae* SFP1: At the Crossroads of Central Metabolism and Ribosome Biogenesis. *Microbiology* **2008**, *154*, 1686–1699. [CrossRef]

117. Ashe, M.P.; De Long, S.K.; Sachs, A.B. Glucose Depletion Rapidly Inhibits Translation Initiation in Yeast. *Mol. Biol. Cell* **2000**, *11*, 833–848. [CrossRef] [PubMed]

118. Huch, S.; Nissan, T. Interrelations between Translation and General MRNA Degradation in Yeast. *Wiley Interdiscip. Rev. RNA* **2014**, *5*, 747–763. [CrossRef]

119. Brengues, M.; Parker, R. Accumulation of Polyadenylated MRNA, Pab1p, EIF4E, and EIF4G with P-Bodies in *Saccharomyces cerevisiae*. *Mol. Biol. Cell* **2007**, *18*, 2592–2602. [CrossRef] [PubMed]

120. Bresson, S.; Tuck, A.; Staneva, D.; Tollervey, D. Nuclear RNA Decay Pathways Aid Rapid Remodeling of Gene Expression in Yeast. *Mol. Cell* **2017**, *65*, 787–800.e5. [CrossRef]

121. Barraza, C.E.; Solari, C.A.; Rinaldi, J.; Ojeda, L.; Rossi, S.; Ashe, M.P.; Portela, P. A Prion-like Domain of Tpk2 Catalytic Subunit of Protein Kinase A Modulates P-Body Formation in Response to Stress in Budding Yeast. *Biochim. Biophys. Acta Mol. Cell Res.* **2021**, *1868*, 118884. [CrossRef]

122. Ramachandran, V.; Shah, K.H.; Herman, P.K. The CAMP-Dependent Protein Kinase Signaling Pathway Is a Key Regulator of P Body Foci Formation. *Mol. Cell* **2011**, *43*, 973–981. [CrossRef] [PubMed]

123. Cannon, J.F.; Tatchell, K. Characterization of *Saccharomyces cerevisiae* Genes Encoding Subunits of Cyclic AMP-Dependent Protein Kinase. *Mol. Cell. Biol.* **1987**, *7*, 2653–2663. [CrossRef] [PubMed]

124. Müller, D.; Exler, S.; Aguilera-Vázquez, L.; Guerrero-Martín, E.; Reuss, M. Cyclic AMP Mediates the Cell Cycle Dynamics of Energy Metabolism in *Saccharomyces cerevisiae*. *Yeast* **2003**, *20*, 351–367. [CrossRef]

125. Pelechano, V.; Chávez, S.; Pérez-Ortín, J.E. A Complete Set of Nascent Transcription Rates for Yeast Genes. *PLoS ONE* **2010**, *7*, e15442. [CrossRef]

126. Beullens, M.; Mbonyi, K.; Geerts, L.; Gladines, D.; Detremerie, K.; Jans, A.W.H.; Thevelein, J.M. Studies on the Mechanism of the Glucose-induced CAMP Signal in Glycolysis and Glucose Repression Mutants of the Yeast *Saccharomyces cerevisiae*. *Eur. J. Biochem.* **1988**, *172*, 227–231. [CrossRef]

127. Botman, D.; O'Toole, T.G.; Goedhart, J.; Bruggeman, F.J.; van Heerden, J.H.; Teusink, B. A New FRET Biosensor Enlightens CAMP Signalling in Budding Yeast. *bioRxiv* **2019**. [CrossRef]

128. Peebo, K.; Neubauer, P. Application of Continuous Culture Methods to Recombinant Protein Production in Microorganisms. *Microorganisms* **2018**, *6*, 56. [CrossRef] [PubMed]

129. Wu, G.; Yan, Q.; Jones, J.A.; Tang, Y.J.; Fong, S.S.; Koffas, M.A.G. Metabolic Burden: Cornerstones in Synthetic Biology and Metabolic Engineering Applications. *Trends Biotechnol.* **2016**, *34*, 652–664. [CrossRef] [PubMed]

130. Birnbaum, S.; Bailey, J.E. Plasmid Presence Changes the Relative Levels of Many Host Cell Proteins and Ribosome Components in Recombinant *Escherichia coli*. *Biotechnol. Bioeng.* **1991**, *37*, 736–745. [CrossRef] [PubMed]

131. Wright, N.R.; Wulff, T.; Palmqvist, E.A.; Jørgensen, T.R.; Workman, C.T.; Sonnenschein, N.; Rønnest, N.P.; Herrgård, M.J. Fluctuations in Glucose Availability Prevent Global Proteome Changes and Physiological Transition during Prolonged Chemostat Cultivations of *Saccharomyces cerevisiae*. *Biotechnol. Bioeng.* **2020**, *117*, 2074–2088. [CrossRef] [PubMed]

132. Lin, Y.; Chomvong, K.; Acosta-Sampson, L.; Estrela, R.; Galazka, J.M.; Kim, S.R.; Jin, Y.-S.; Cate, J.H. Leveraging Transcription Factors to Speed Cellobiose Fermentation by *Saccharomyces cerevisiae*. *Biotechnol. Biofuels* **2014**, *7*, 126. [CrossRef]

133. Michael, D.G.; Maier, E.J.; Brown, H.; Gish, S.R.; Fiore, C.; Brown, R.H.; Brent, M.R. Model-Based Transcriptome Engineering Promotes a Fermentative Transcriptional State in Yeast. *Proc. Natl. Acad. Sci. USA* **2016**, *113*, E7428–E7437. [CrossRef] [PubMed]

134. Ribeiro, R.A.; Bourbon-Melo, N.; Sá-Correia, I. The Cell Wall and the Response and Tolerance to Stresses of Biotechnological Relevance in Yeasts. *Front. Microbiol.* **2022**, *13*, 1–25. [CrossRef] [PubMed]

135. Creamer, D.R.; Hubbard, S.J.; Ashe, M.P.; Grant, C.M. Yeast Protein Kinase A Isoforms: A Means of Encoding Specificity in the Response to Diverse Stress Conditions? *Biomolecules* **2022**, *12*, 958. [CrossRef] [PubMed]

136. Soetaert, K.; Petzoldt, T.; Setzer, R.W. Solving Differential Equations in R: Package DeSolve. *J. Stat. Softw.* **2010**, *33*, 1–25. [CrossRef]

137. Ritchie, M.E.; Phipson, B.; Wu, D.; Hu, Y.; Law, C.W.; Shi, W.; Smyth, G.K. Limma Powers Differential Expression Analyses for RNA-Sequencing and Microarray Studies. *Nucleic Acids Res.* **2015**, *43*, e47. [CrossRef]